UTS UNIVERSITY OF TECHNOLOGY SYDNEY

Development of Anion Transport-Based Mitochondrial Uncouplers as Anticancer Agents

by Edward York

Thesis submitted in fulfilment of the requirements for the degree of

Doctor of Philosophy

under the supervision of
Tristan Rawling and Andrew McDonagh

University of Technology Sydney
Faculty of Science

August 2024

Certificate of Original Authorship

I, Edward, declare that this thesis is submitted in fulfilment of the requirements for the award of Doctor of Philosophy, in the School of Mathematical and Physical Sciences at the University of Technology Sydney. This thesis is wholly my own work unless otherwise referenced or acknowledged. In addition, I certify that all information sources and literature used are indicated in this thesis. This document has not been submitted for qualifications at any other academic institution. This research is supported by the Australian Government Research Training Program.

Edward York 22/08/24

COVID-19 Impact Statement

Experimental work for this thesis began in 2020 and was impacted by the COVID-19 pandemic, particularly through 2020 and 2021. The laboratory-based activities required by this project were unable to be fully transitioned to an online format. As a result, research progress was delayed during this period due to reduced access to laboratories (from full access to just 4-6 hours per week) in accordance with New South Wales Health COVID-19 policies, and increased delivery times for chemical reagents and laboratory consumables (which shifted from weeks to months). In response to this challenge, the project's scope was adjusted to ensure that the core aims could still be addressed, despite the extended timelines.

Contents

List of Figures

List of Tables

List of Schemes

Abbreviations

ADMET	absorption, distribution, metabolism, excretion, and toxicity
ADP	adenosine diphosphate
ANT	adenine nucleotide translocase
ANOVA	analysis of variance
ATCC	American type culture collection
ATP	adenosine triphosphate
BRAF	v-raf murine sarcoma viral oncogene homolog B1
BSA	bovine serum albumin
BSSE	basis set superposition error
CCCP	carbonyl cyanide m-chlorophenylhydrazone
$CDCl_3$	deuterated chloroform
CDI	1,1'-carbonyldiimidazole
COMU	(1-Cyano-2-ethoxy-2-oxoethylidenaminooxy)dimethylamino- morpholinocarbenium hexafluorophosphate
CO_2	carbon dioxide
CTL	control
DCM	dichloromethane
DCVC	dry column vacuum chromatography
DMSO	dimethyl sulfoxide
DMSO-d_6	deuterated dimethyl sulfoxide
DMEM	Dulbecco's modified eagle medium
DMF	dimethyl formamide
DNP	2,4-dinitrophenol
dPBS	Dulbecco's phosphate buffered saline
EC_{50}	half maximal effective concentration
ECAR	extracellular acidification rate
EDC	1,2-dichloroethylene

EDTA	ethylenediaminetetraacetic acid
ESI	electrospray ionisation
EtOAc	ethyl acetate
ETC	electron transport chain
$FADH_2$	flavin adenine dinucleotide
FCCP	carbonyl cyanide-4-(trifluoromethoxy)phenylhydrazone
H^+	proton
$HCOONH_4$	ammonium formate
HEPES	4-(2-hydroxyethyl)-1-piperazineethanesulfonic acid
HRMS	high-resolution mass spectrometry
HPTS	8-hydroxypyrene-1,3,6-trisulfonic acid
IC	internal calibrant
IC_{50}	half maximal inhibitory concentration
I_F	fractional fluorescence intensity
IUPAC	international union of pure and applied chemistry
JC-1	5,5',6,6'-tetrachloro-1,1',3,3'-tetraethylbenzimidazolylcarbocyanine chloride
KOH	potassium hydroxide
LDH	lactate dehydrogenase
LUV	large unilamellar vesicles
MIM	inner mitochondrial membrane
MTS	3-(4,5-dimethylthiazol-2-yl)-5-(3-carboxymethoxyphenyl)-2-(4-sulfophenyl)-2H-tetrazolium
NADH	nicotinamide adenine dinucleotide
NaOH	sodium hydroxide
NMR	nuclear magnetic resonance
OA	oleic acid
OCR	oxygen consumption rate
OH^-	hydroxide
OXPHOS	oxidative phosphorylation

Pd/C	palladium on carbon
P_i	inorganic phosphate
pK_a	acid dissociation constant (Logarithmic form)
π	hydrophobicity constant
Q-TOF LCMS	quadropole time-of-flight liquid chromatography/mass spectrometry
r^2	correlation coefficient
ROS	reactive oxygen species
SAR	structure activity relationship
SEM	standard error of the mean
SMD	solvation model based on density
SR4	N,N'-bis(3,5-dichlorophenyl)urea
σ	Hammett substituent constant
TBAOAc	tetrabutylammonium acetate
THF	tetrahydrofuran
TLC	thin layer chromatography
UCP	uncoupling protein
$\Delta\Psi_m$	mitochondrial membrane potential

Equations

$$I_F = \frac{R_t - R_0}{R_d - R_0}$$

$$y = y_0 + (y_{max} - y_0)\frac{x^n}{k^n + x^n}$$

$$EC_{50} = k\left(\frac{0.5}{y_1 - y_0}\right)^{1/n}$$

$$Purity_t = \frac{integral\ area_t \times MW_t \times mass_t}{integral\ area_{IC} \times MW_{IC} \times mass_{IC}} \times Purity_{IC}$$

$$Y = Bottom + \frac{Top - Bottom}{1 + 10^{(LogIC_{50} - X)} \times HillSlope}$$

Acknowledgements

Completing this project has been a journey worth pursuing because of the incredible people who have supported, guided, and inspired me along the way.

I want to express my gratitude to my supervisor and mentor Tristan Rawling, who gave me the tools to pursue and express a science story with clarity and purpose. Your generosity—both in giving your time and expertise when I needed it, and in allowing me the space to figure things out on my own—has been truly invaluable. To my research group, Ritik Roy, Meryem-Nur Duman, Ethan Pacchini, Freddy Ha and Phoenix Chick thank you for winging it through the unknown together, for sharing our wins and our losses, and for fostering a culture of enthusiasm, shared responsibility, and good lab citizenship.

To the old guard—Matthew Phillips, Camilla Gazzana, Hugh Hiscocks, Mika Tham Westerhausen, Iurii Bodachivskyi, and Callum Clarke—thank you for your love of chemistry and for all that you taught me. To my cohort—Siobhan Peters, Tom Lockwood, David Gertner, Jacob Merecic, Dylan Johnson, Anjar Asmara and Tom Goulden—thank you for always being in my corner, for hearing me and for your friendship.

I am also thankful to my collaborators, particularly Daniel McNaughton, who generously stepped in to test my compound's mechanism and later taught me how to do the same. Your combined expertise and willingness to help has made me a better scientist and were key to this project's success.

To my partner Helen, thank you for everything you have given me in these past two years, I truly couldn't have done this without you. You inspired me with your fire, pushed me to be better, and showed me the way forward even when I could not see it. You were my rock during the most challenging times and I will always cherish the happiness you have brought into my life.

And finally, to my family, thank you for your unwavering support throughout this journey. I would like to dedicate this thesis to my late mother Ruth Elizabeth York, whose light has guided me more profoundly than I ever realised.

List of Publications Included

Structure−Activity Relationship and Mechanistic Studies of Bisaryl Urea Anticancer Agents Indicate Mitochondrial Uncoupling by a Fatty Acid-Activated Mechanism

York, E., McNaughton, D.A., Roseblade, A., Cranfield, C.G., Gale, P.A. & Rawling, T. 2022, 'Structure–Activity Relationship and Mechanistic Studies of Bisaryl Urea Anticancer Agents Indicate Mitochondrial Uncoupling by a Fatty Acid-Activated Mechanism', *ACS Chemical Biology*, vol. 17, no. 8, pp. 2065-73. https://doi.org/10.1021/acschembio.1c00807.

Fatty Acid-Activated Proton Transport by Bisaryl Anion Transporters Depolarises Mitochondria and Reduces the Viability of MDA-MB-231 Breast Cancer Cells

York, E., McNaughton, D.A., Duman, M.-N., Gale, P.A. & Rawling, T. 2023, 'Fatty Acid-Activated Proton Transport by Bisaryl Anion Transporters Depolarises Mitochondria and Reduces the Viability of MDA-MB-231 Breast Cancer Cells', *Biomolecules (Basel, Switzerland)*, vol. 13, no. 8, p. 1202. https://doi.org/10.3390/biom13081202

Expanding the π-system of Fatty Acid-Anion Transporter Conjugates Modulates Their Mechanism of Proton Transport and Mitochondrial Uncoupling Activity

York, E., McNaughton, D.A., Gertner, D.S., Gale, P.A., Murray, M. & Rawling, T., 'Expanding the π- system of Fatty Acid-Anion Transporter Conjugates Modulates Their Mechanism of Proton Transport and Mitochondrial Uncoupling Activity', *Chemistry – A European Journal*, e202400931. https://doi.org/10.1002/chem.202400931.

Abstract

Respiring mitochondria generate a proton gradient across the inner mitochondrial membrane (MIM) to drive adenosine triphosphate (ATP) production. Mitochondrial uncouplers, which are typically weak acid protonophores, disrupt this process by inducing proton leak across the MIM, dissipating the membrane potential and leading to futile cycles of nutrient oxidation without ATP synthesis. Mitochondrial uncouplers are currently being explored as therapeutic agents in a range of applications. Emerging evidence suggests that mitochondrial uncouplers may be an attractive platform for the development of anticancer agents due to the unique characteristics of cancer cell mitochondria.

Mitochondrial uncouplers are generally weak acids, however in 2016 Gale *et al.* discovered a synthetic anion transporter that transports protons via a novel mechanism that involves their interaction with deprotonated free fatty acids in lipid bilayers. This thesis explores the use of anion transporters as mitochondrial uncouplers and their capacity to serve as novel anticancer agents. In Chapter Two the bisaryl urea **SR4**, an experimental anticancer agent and nonacidic mitochondrial uncoupler, was investigated for its proton transport mechanism and anticancer activity against MDA-MB-231 breast cancer cells. Vesicular proton transport assays demonstrated that **SR4**-mediated proton transport was enhanced in the presence of free fatty acids, indicating that **SR4**-mediated proton transport occurs via the fatty acid-activated proton transport mechanism. A library of bisaryl ureas was synthesised with various aromatic substituents for structure-activity relationship and *in vitro* cell studies. These revealed that substitution with lipophilic electron withdrawing groups enhanced proton transport activity, and the most active compound **U1**, uncoupled mitochondria, reduced cell viability, and inhibited ATP production with greater potency than **SR4**.

In Chapter Three, the urea anion binding motif of the compounds studied in Chapter Two was replaced with squaramide, amide, and diurea groups and the proton transport and mitochondrial actions of these compounds were evaluated against MDA-MB-231 cells. Substitution of the bisaryl rings with

lipophilic electron withdrawing groups remained key to antiproliferative and uncoupling activity, and these compounds were also found to mediate proton transport by the fatty acid-activated mechanism. The mitochondrial actions and proton transport capacity of the new bisaryl squaramide, amide and diurea analogues were less pronounced than their bisaryl urea counterparts, indicating the urea motif is better suited for mitochondrial uncoupling by this mechanism.

The bisaryl ureas presented in Chapter Two promote fatty acid-activated proton transport due to their capacity to delocalise the anionic charge of deprotonated fatty acids. In Chapter Four these insights were used to enhance the proton transport and uncoupling activity of aryl urea substituted fatty acids, a new class of uncoupler that relies on intermolecular urea-carboxylate interactions to mediate proton transport. It was anticipated that incorporating a second (proximal) ring into the aryl urea substituted fatty acid scaffold would enhance proton transport by increasing urea NH hydrogen bond donor strength and providing a larger π-system for charge delocalisation. A library of diphenyl urea substituted fatty acids were synthesised and their proton transport activity was assessed in cell and vesicle-based assays. It was revealed that *meta*-linked but not *para*-linked proximal rings enhanced proton transport in vesicles, which was attributed to steric factors that inhibit the *para*-linked analogues from forming membrane permeable complexes. Overall, the inclusion of *meta*-linked proximal rings greatly enhanced uncoupling activity in MDA-MB-231 cells, although this did not result in enhancement of their antiproliferative activity compared to the parent aryl ureas.

Collectively, this thesis provides new mechanistic insights into the mitochondrial effects of the experimental anticancer agent **SR4** and defines structure-activity relationships that describe how aromatic substitution and various anion receptors impact the protonophoric and anticancer actions of anion transport-based mitochondrial uncouplers. The promising mitochondrial and anticancer actions of the most potent bisaryl ureas and diphenyl urea substituted fatty acids warrant further testing to evaluate their use as mitochondria-targeted anticancer agents.

Chapter One: Introduction to Mitochondrial Uncouplers

1.1 Mitochondrial structure and function

Mitochondria are rod-shaped organelles found in the cytosol of eukaryotic cells and play a critical role in the generation of metabolic energy, earning their culturally celebrated moniker "the power-house of the cell". Mitochondria consist of a folded mitochondrial inner membrane (MIM) encased within an ovoid outer membrane (Figure 1) that divides the organelle into the mitochondrial matrix (inner core) and the intermembrane space (outer mantle).[1,2] The MIM is impermeable to most ionic species, as they cannot diffuse across the lipophilic core of the phospholipid bilayer. The asymmetric accumulation of protons between the mitochondrial matrix and the intermembrane space generates a high membrane potential across the MIM (termed the $\Delta\Psi_M$). This electrochemical potential functions as the direct link between nutrient oxidation and mitochondrial energy production in the form of ATP.

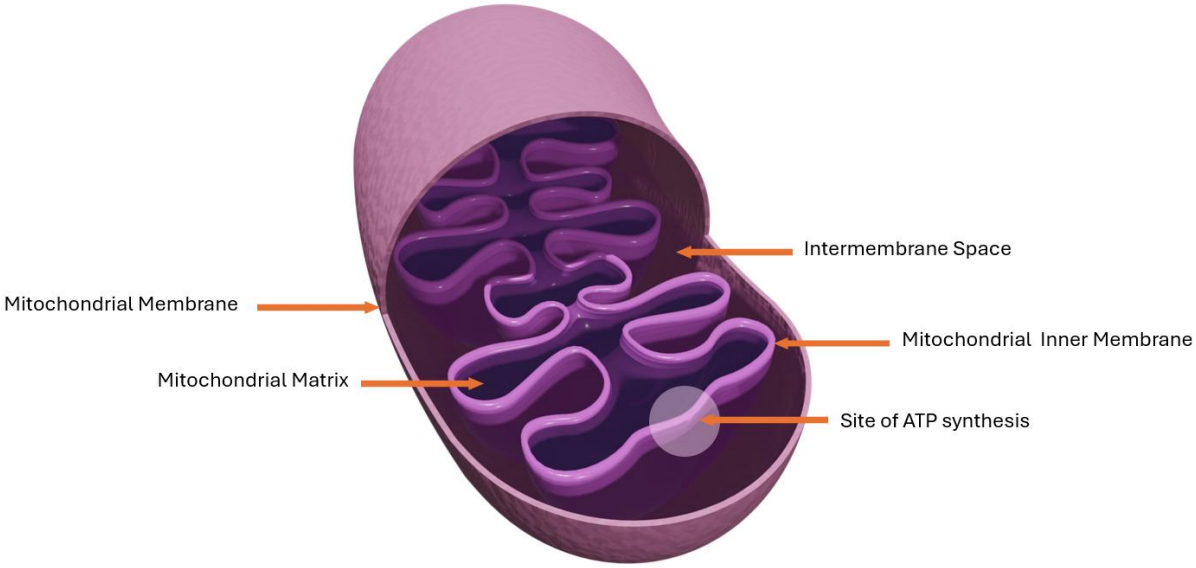

Figure 1. Diagram displaying the double-membrane structure of the mitochondria.

1.2 Mitochondrial ATP production: Oxidative Phosphorylation

Mitochondria generate the $\Delta\Psi_M$ and produce ATP through a process called oxidative phosphorylation (OXPHOS, Figure 2). Nutrients are transported from the cytosol and catabolised in the mitochondrial matrix via the citric acid cycle to produce reduced electron carriers NADH and $FADH_2$.[3-5] These high energy species then fuel a cascade of redox reactions mediated by the electron transport chain (ETC),

a series of protein complexes embedded in the MIM.[4,5] The energy released in this oxidative process powers the active transport of protons (H^+) from the mitochondrial matrix into the intermembrane space, generating a mitochondrial membrane potential ($\Delta\Psi_M$) of about – 140 mV across the MIM.[4-6] The $\Delta\Psi_M$ drives protons back into the mitochondrial matrix through the MIM-embedded protein ATP synthase. As protons flow through ATP synthase the protein catalyses the formation of ATP from inorganic phosphate (P_i) and adenosine diphosphate (ADP). Nutrient oxidation is therefore coupled to ATP synthesis via the $\Delta\Psi_M$. [3-5]

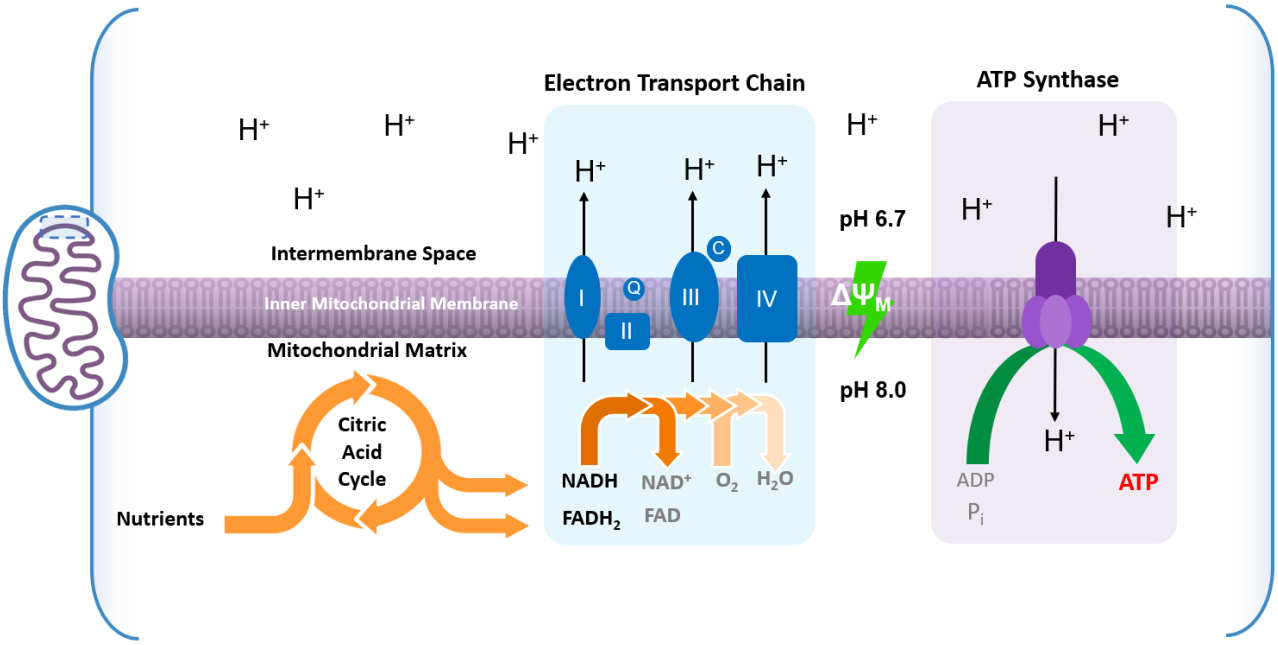

Figure 2. Synthesis of ATP through OXPHOS in the mitochondria. Nutrient oxidation is coupled to ATP synthesis through the generation of an electrochemical potential across the MIM.

1.2.1 Mitochondrial Uncoupling

Mitochondrial uncoupling is a process that disconnects nutrient oxidation from ATP synthesis by disrupting the $\Delta\Psi_m$. Uncoupling was first encountered when brown adipose tissue was found to generate heat in response to cold exposure. These observations led researchers to investigate the mechanism behind this phenomenon, ultimately resulting in the identification of the first uncoupling protein in 1978.[7] It was subsequently found that uncoupling proteins are expressed in the MIM of all cells and dissipate energy stored in the $\Delta\Psi_M$ as heat by allowing protons to flow from the intermembrane space

back into the matrix, bypassing ATP synthase. This apparent inefficiency was first thought to be dysfunctional, but further research demonstrates that mitochondrial uncoupling is a highly adaptive regulatory mechanism with keys roles in thermogenesis, metabolism and cell signalling.[8] As a result of these discoveries mitochondrial uncoupling has garnered significant interest for its physiological implications in both ageing and disease.[8,9]

1.3 Mitochondrial Uncouplers and the Protonophoric Cycle

Chemical agents that uncouple oxidative phosphorylation are known as mitochondrial uncouplers. The crucial feature of uncouplers is their ability to promote the passage of protons from the intermembrane space into the matrix without the involvement of ATP synthase. This biochemical "short-circuit" collapses the $\Delta\Psi_m$, thus removing the driving force for ATP production and creating futile cycles of energy expenditure.[10] Typically, this is achieved through the protonation and subsequent deprotonation of an acidic functional group on the uncoupler molecule, which sits in the MIM and cycles between the matrix and intermembrane space to shuttle protons via the protonophoric cycle (Figure 3).[11]

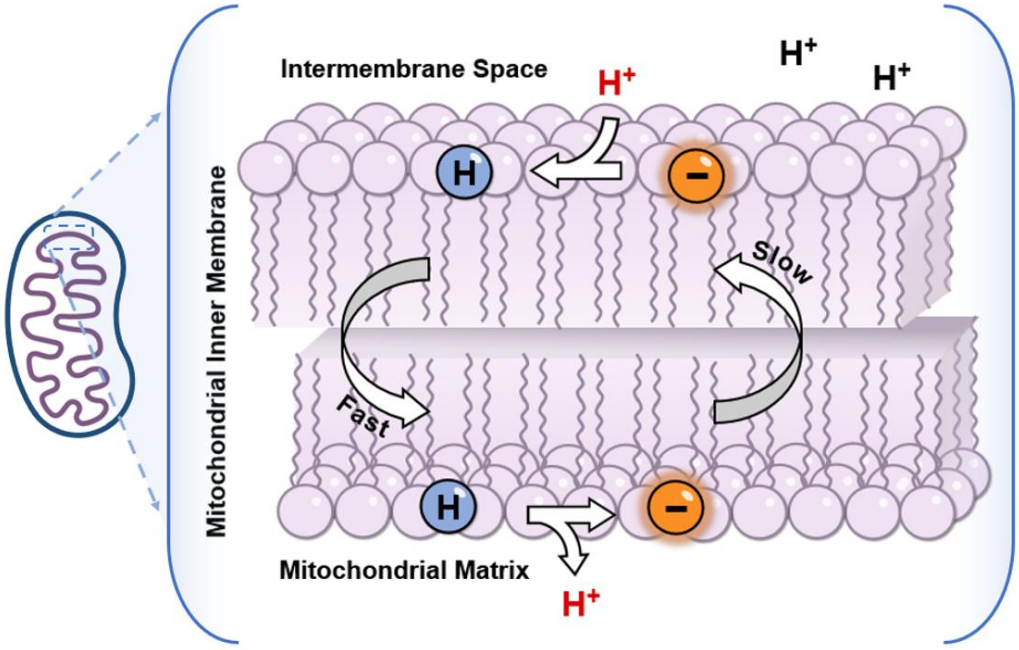

Figure 3. Mitochondrial uncouplers dissipate the $\Delta\Psi_m$ via the protonophoric cycle.

In the protonophoric cycle the deprotonated uncoupler (A-) first accepts a proton in the acidic intermembrane space to generate a neutral species (A-H). The neutral uncoupler (A-H) readily diffuses

through the MIM where it is subsequently deprotonated in the alkaline mitochondrial matrix (pH ~8).[12] This results in the transport of one proton across the MIM. The resultant anion (A^-) must then return to the intermembrane space to be protonated again to establish a continuous cycle.[13] However, transport of the negatively charged uncoupler back to the intermembrane space is hindered by the MIM's lipophilic core, which is relatively impermeable to ions.[13] Sufficiently lipophilic anions can overcome this barrier and passively diffuse the MIM, but others must rely on active transport by uncoupling proteins embedded in the MIM to complete the protonophoric cycle.[14,15]

1.3.1 Protein-dependent mitochondrial uncouplers

Free fatty acids such as palmitate are examples of protein-dependent mitochondrial uncouplers because they rely on active transport to translocate the anion across the MIM. Several dedicated uncoupling proteins (UCP1 i.e. thermogenin, and UCP2-UCP5)[16,17] have been identified as well as mitochondrial carriers such as adenine nucleotide translocase (ANT) that exhibit concomitant uncoupling activity.[18,19] The uncoupling activities of UCP1,[19,20] UCP2,[21] UCP3,[22] UCP4/5[23] and ANT[18,19] are activated in the presence of free fatty acids, which are physiological substrates present in the MIM (most commonly palmitate, stearate, and oleate[24]). Multiple theories have been proposed to explain the precise mechanism of fatty acid-activation.[25] However, it has been demonstrated that UCP1 transports laurate, UCP2 transports palmitate and ANT transports arachidonate in proteoliposomes.[20,21,26] Without protein assistance, transbilayer movement of anionic fatty acids is extremely slow due to their high charge density.[27] Together this indicates that uncoupling proteins mediate proton transport *indirectly* by catalysing the transbilayer movement ("flip-flop") of anionic fatty acids, providing the missing link for free fatty acids to complete the protonophoric cycle (see Figure 4b).

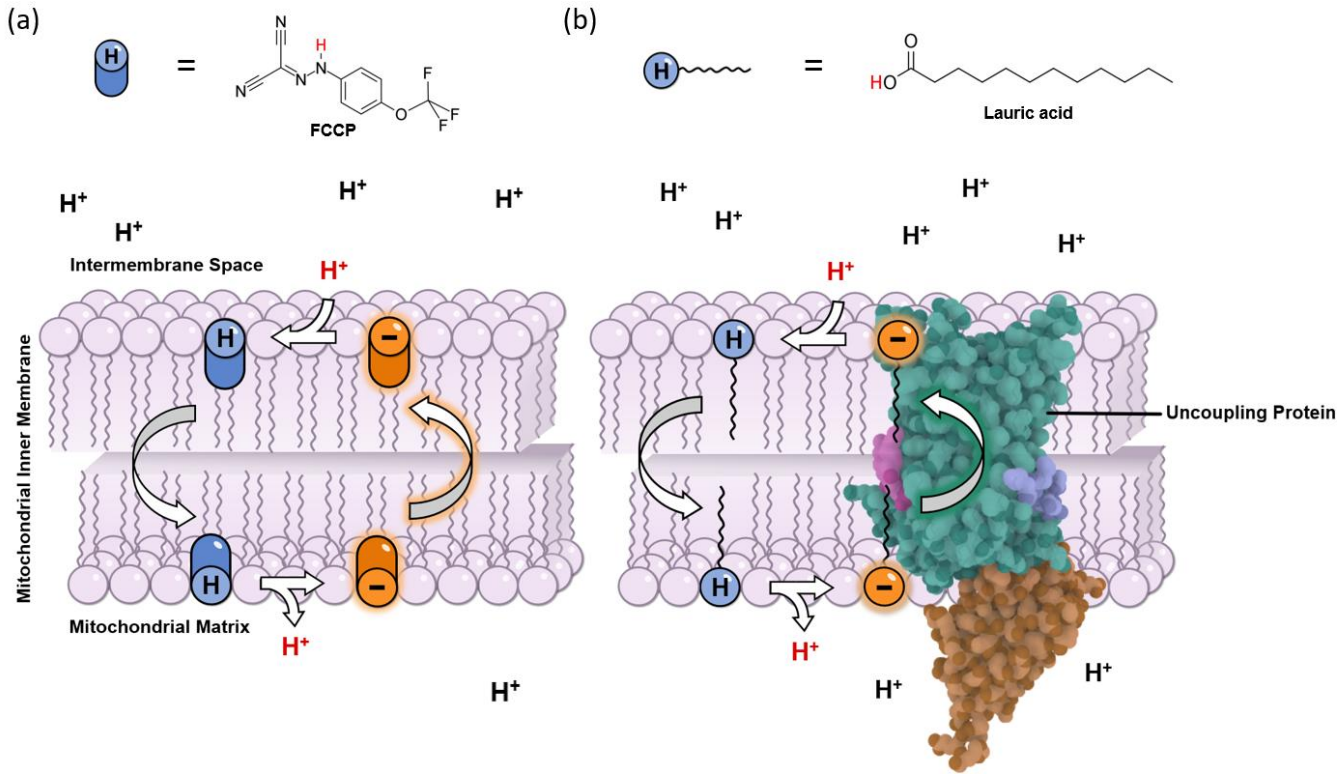

Figure 4. (a) Protein-Independent mitochondrial uncouplers such as FCCP possess extended π systems conjugated to their acidic group, allowing them to make MIM-permeable anions and complete the protonophoric cycle without active transport. (b) Protein-dependent mitochondrial uncouplers such as lauric acid do not form MIM-permeable anions, and instead rely on active transport by uncoupling proteins to complete the protonophoric cycle. UCP1 shown as representative uncoupling protein, structure elucidated by electron microscopy[28] and available free of charge at https://doi.org/10.2210/pdb8HBV/pdb.

1.3.2 Protein-independent mitochondrial uncouplers

Mitochondrial uncouplers that form MIM-permeable anions can complete the cycle and disrupt the $\Delta\Psi_M$ without protein involvement. Typically, these uncouplers are lipophilic weak acids that possess extended π-systems conjugated to their acidic group. These features delocalise the anions negative charge over a large area to promote anion lipophilicity (see Figure 4a). FCCP (Carbonyl cyanide-4-(trifluoromethoxy)phenylhydrazone) is an example of a protonophore. The FCCP anion disperses its

negative charge across the hydrazone and aromatic π-systems that flank its acidic NH group, allowing the anion to move through the MIM unassisted.[13]

1.4 Applications of mitochondrial uncouplers

1.4.1 Weight loss treatment

The ability for mitochondrial uncouplers to dissipate nutrient-derived energy and bypass ATP synthesis has generated significant interest in uncouplers as a treatment for weight loss.[10] The potential and dangers of this approach was demonstrated in the early 20th century, when the protein-independent uncoupler 2,4-dinitrophenol (DNP) was used to treat obesity. Historically, DNP was used in the preparation of explosives in World War One, where French factory workers exposed to DNP experienced significant weight loss and in some cases death (symptoms vividly described in Figure 5). This ultimately lead to the discovery of DNP as a mitochondrial uncoupler, and was clinically used in the 1930s as a weight loss drug due to its ability to significantly increase basal metabolic rate.[29] Patients on DNP reported weight losses of up to 1.5 kg per week on calorie unrestricted diets, however severe side effects and a number of fatalities lead the withdrawal of DNP in 1938. However, research into mitochondrial uncouplers as weight-loss agents remains active, with efforts focused on developing compounds with less pronounced mitochondrial effects and thus a larger therapeutic window.

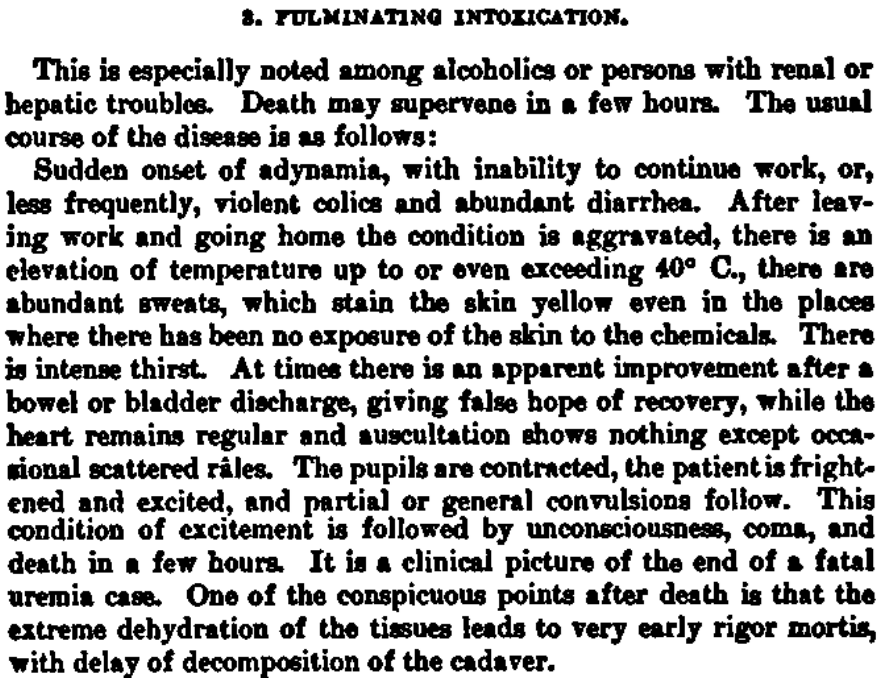

3. FULMINATING INTOXICATION.

This is especially noted among alcoholics or persons with renal or hepatic troubles. Death may supervene in a few hours. The usual course of the disease is as follows:

Sudden onset of adynamia, with inability to continue work, or, less frequently, violent colics and abundant diarrhea. After leaving work and going home the condition is aggravated, there is an elevation of temperature up to or even exceeding 40° C., there are abundant sweats, which stain the skin yellow even in the places where there has been no exposure of the skin to the chemicals. There is intense thirst. At times there is an apparent improvement after a bowel or bladder discharge, giving false hope of recovery, while the heart remains regular and auscultation shows nothing except occasional scattered râles. The pupils are contracted, the patient is frightened and excited, and partial or general convulsions follow. This condition of excitement is followed by unconsciousness, coma, and death in a few hours. It is a clinical picture of the end of a fatal uremia case. One of the conspicuous points after death is that the extreme dehydration of the tissues leads to very early rigor mortis, with delay of decomposition of the cadaver.

Figure 5. Excerpt from 1919 public health report describing the effects of DNP exposure on French munition workers[30]

1.4.2 Spinal Cord injury and neurodegenerative diseases

Mitochondrial uncouplers also have therapeutic potential in the treatment of spinal cord injury and some neurodegenerative diseases. Neurons damaged by physical trauma and other triggers of glutamate excitotoxicity accumulate harmful levels of Ca^{2+} in their cytosol that activates many pro-apoptotic enzymes. In an apparent attempt to mitigate harm, neurons sequester excess Ca^{2+} in their mitochondria, but in doing so increase production of reactive oxygen species (ROS).[31,32] Increased ROS can overwhelm antioxidant defences, causing oxidative stress that destabilises mitochondria and can lead to cell death. Mitochondrial uncoupling by DNP has been shown to decrease ROS production in many tissues including brain, highlighting its potential as a treatment for spinal cord injury and some neurodegenerative diseases.[33,34] For example, pretreatment of rodents with spinal cord contusions with DNP reduced ROS, protein oxidation and lipid peroxidation levels, which was found to ameliorate loss of function and conserved 23% more white matter than control six weeks following injury.[35]

1.4.3 Mitochondrial Uncouplers as anticancer agents

Cancer is a complex disease that occurs when cells stop responding appropriately to normal cellular signals and begin to proliferate uncontrollably, forming abnormal growths called tumours that spread to and disrupt the function of vital organs.[36,37] This disease poses enormous health, economic and societal burdens to the global community, and is the leading cause of death in Australia accounting for 29% of all registered death in 2018.[38] Considering Australia's ageing population and that improvements in cancer mortality rates trail behind that of other disease modalities (Figure 6),[39] the impact of cancer is set to intensify with 43% of Australians anticipated to be diagnosed by 85.[40] These sobering numbers underline the increasingly urgent need for new anticancer treatments that improve the survival rates of cancer patients.

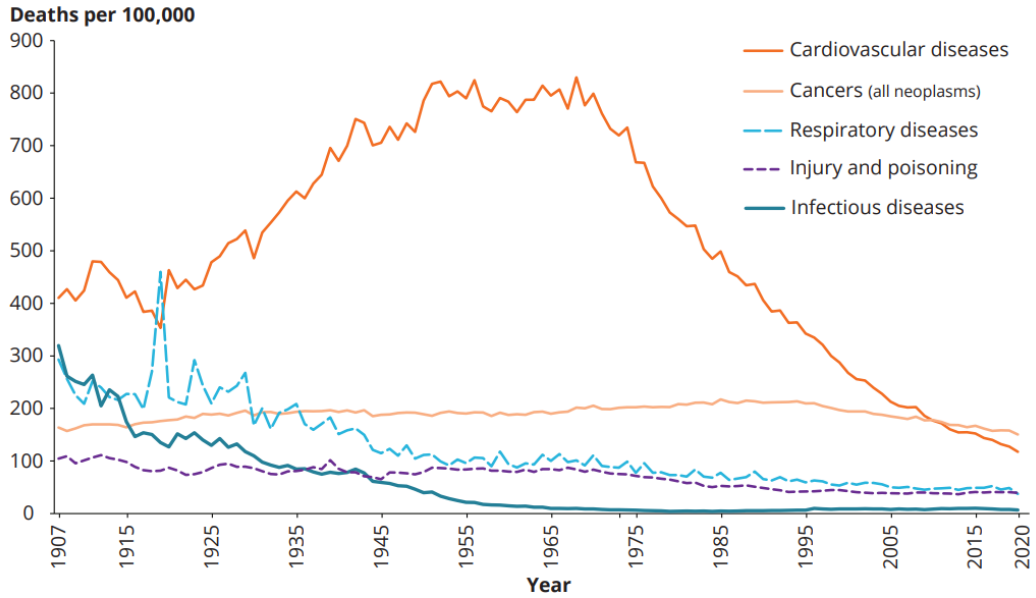

Figure 6. Age-standardised mortality rates by cause of death in Australia from 1907-2020.[39]

The genetic mutations that induce malignant transformation and cause cancer can occur in any cell in the body, and as a result the characteristics and behaviour of cancerous cells are very diverse.[41] Even cancerous cells arising from the same tumour exhibit genetic diversity.[42] However, the fundamental structure and biology of cancerous cells are still analogous to noncancerous cells. Thus, the body's immune system struggles to recognise and destroy cancer cells in the same way it does for foreign pathogens such as bacteria. Consequently, cancers evade immune surveillance and treatment relies

on medical interventions such as surgical removal of tumours, and pharmaceutical and radiotherapeutic treatments.[43] Pharmaceuticals or chemotherapies have become an increasingly important tool for cancer treatment, however the cellular characteristics of cancer cells make the development of effective and well-tolerated drugs challenging. Most anticancer agents are only effective against specific cancers due to tumour heterogeneity. Furthermore, because of the similarities between cancer and non-cancerous cells, most anticancer agents have poor selectivity towards cancer cells. This lack of selectivity leads to poorly tolerated drugs that damage cancer and noncancer cells alike resulting in severe side effects. For example, the widely used chemotherapy Paclitaxel (Taxol) indiscriminately disrupts cell division by preventing mitotic spindle disassembly during mitosis; ultimately leading to life threatening side effects such as hypotension, myelosuppression and peripheral neuropathy.[44] Adverse side effects like these severely narrow the therapeutic window for many cancer treatments, spurring efforts to identify novel drug mechanisms that selectively target the unique characteristics cancerous cells.

Cancerous cells have greater energy and biomass demands than non-cancerous cells to produce the elevated quantities of carbohydrates, nucleic acids, proteins and lipids to divide rapidly.[45] To accommodate for this, cancer cells exhibit an altered metabolism, leading to mitochondria that are structurally and functionally distinct to those found in non-cancerous cells.[46,47] Rather than generating ATP through mitochondrial OXPHOS, cancer cells generate ATP predominately through "fermenting" glucose to lactate in the cytosol, a less efficient pathway typically only used in oxygen deficient environments.[45,48,49] This metabolic shift, termed the Warburg Effect, was first thought to be caused by genetic defects that impaired mitochondrial ATP production. However, it has been found that cancer cell mitochondria are functional and integral to cell survival,[50-52] but glycolytic metabolism may be better suited to the needs of rapidly proliferating cells. This can be attributed to the feature that aerobic glycolysis accumulates biomass quickly, conserving all six glucose carbons but netting only two ATP molecules.[49] Alternatively, OXPHOS fully oxidises glucose to CO_2, producing up to 36 ATP molecules but leaving no biomass. In agreement with this hypothesis, another argument poses that cancer

cells divert resources usually devoted to OXPHOS-related protein expression into biosynthetic pathways to maintain their rapid proliferation at the expense of efficient ATP synthesis. As cell growth and division is highly dependent on biomass and rarely limited by ATP demand,[53,54] both these phenotypes confer a significant proliferative advantage to cancerous cells. Thus, the Warburg Effect is thought to develop evolutionarily (via cancer selection) due to the selective pressures exerted by its host environment in competition with other cancer cells to proliferate rapidly.[55]

Interestingly, the Warburg Effect causes cancer cell mitochondria to exhibit an increased $\Delta\Psi_M$ compared to non-cancerous cells.[48,56,57] For example A549 (lung), M059K (glioblastoma), and MCF-7 (breast) cancer cells exhibit elevated $\Delta\Psi_M$ compared to non-cancerous fibroblasts, respiratory epithelium and arterial smooth muscle cells.[56] Some studies have suggested that the more invasive and aggressive the cancer, the greater the Warburg effect and the $\Delta\Psi_M$,[58-60] presumably due to increased glycolytic demand to meet biomass requirements. For example, the fast growing, hypoxia resistant breast cancer cell line Neu4145 carries a $\Delta\Psi_M$ of –210 mV,[61] 50% greater than the –140 mV found typically in non-cancerous cells.[4,62,63]

This feature provides a promising platform for the development of chemotherapies that specifically target the hyperpolarised mitochondria found in cancerous cells. Indeed, several reported uncouplers induce apoptotic cell death in cancerous cell lines and demonstrate antitumour activity in animal models. The direct mechanism between mitochondrial uncoupling and cancerous cell death is still being explored, but accumulating evidence suggests the initiation of apoptosis is closely associated with the dissipation of the $\Delta\Psi_M$ by mitochondrial uncouplers.[64-66] Table 1 lists mitochondrial uncouplers with anticancer activity in different human cell lines and/or xenograft mouse models.

Table 1. Reported uncouplers with anticancer activity in human cell lines and/or xenograft mouse models.

Mitochondrial Uncoupler	Model/Methods	Effects	Comments
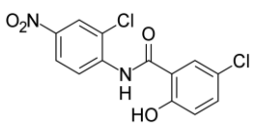 **Niclosamide**	*In vitro:* HeLa, A549 and HT29 cells lines[67]	IC_{50} = 0.25 μM (HeLa) IC_{50} = 3.0 μM (A549) IC_{50} = 7.2 μM (HT29)	72 h MTT assay 72 h MTT assay 72 h MTT assay
	In vivo: MC38 xenografts in NSG mice[68]	Reduced tumour volume by >90% of control and number of hepatic metasteses from 10 to 4.	NSG mice fed chow containing 2000 ppm NEN for 3 weeks.
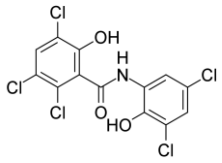 **Oxyclonazide**	*In vitro:* MC38, HCT116 and C2C12 cell lines[68]	increased oxygen consumption rate (C2C12) and reduced mitochondrial membrane potential (MC38 and HCT116)	Seahorse XF analyser 2 h TMRE assay
	In vivo: MC38 xenografts in NSG mice[68]	Reduced tumour volume by >90% of control and number of heptatic metasteses from 10 to 3.	NSG mice fed chow containing 800 ppm oxyclonazide for 3 weeks.
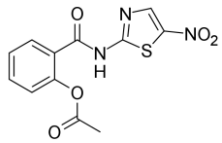 **Nitazoxanide**	*In vitro:* HT-29, DLD-1, SW403 and SW480[69]	IC_{50} = 1.93 μM (HT-29) IC_{50} = 2.15 μM (DLD-1) IC_{50} = 2.76 μM (SW403) IC_{50} = 2.29 μM (SW480)	48 h CCK8 assay 48 h CCK8 assay 48 h CCK8 assay 48 h CCK8 assay
	In vivo: HCT116 xenografts in NMRI nu/nu mice[70]	Reduced tumour volume by 80% of control when treated in combination with Irinotecan.	Mice admininstered 100 mg/kg nitazoxanide twice daily, and 40 mg/kg irinotecan twice weekly for 4 weeks.
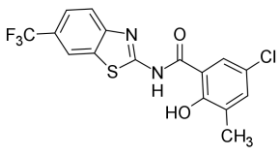 **MB1-47**	*In vitro:* MIA PACA-2, BxPC3, Panc1, CF-Pac1, Capan2, Pan02, and AsPC1 cell lines.[71]	All eight pancreatic cancer cell lines reduced cell viability with IC_{50}s between 0.5-1.0 μM.	48 h SRB assay
	In vivo: Panc02 xenografts in male NSG mice.[71]	Reduced tumour growth by >60% of control.	NSG mice fed chow containing 750 ppm MB1-47 for 2 weeks.
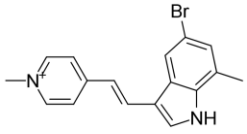 **5BMF**	*In vitro:* MDA-MB-231 and U87MG cell lines.[72]	IC_{50} = 4.15 μM (MDA-MB-231) IC_{50} = 0.36 μM (U87MG)	72 h direct cell counting 72 h direct cell counting
	In vivo:		

	Glioblastoma U87MG xenografts in female nu/nu mice.[72]	Reduced tumour volume by 90% of control.	15 mg/kg 5BMF administered intravenously for 3 weeks.
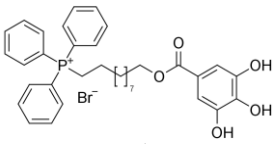 **TPP^+C_{10}**	*In vitro:* TA3/Ha, TA3-MTX-R, CCRF-CEM cell lines.[73] *In vivo:* TA3/Ha xenografts in CAF1-Jax mice. [74]	IC_{50} = 0.40 µM (TA3/Ha) IC_{50} = 0.38 µM (TA3-MTX-R) IC_{50} = 1.65 µM (CCRF-CEM) Reduced tumour volume by 80% of control	48 h neutral red assay 48 h neutral red assay 48 h neutral red assay Mice treated with 10mg/Kg TPP^+C_{10} intraperitoneally every 48h for 28 days.
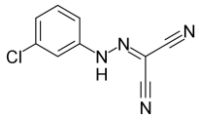 **CCCP**	*In vitro:* HL-60 and SH-SY5Y cell lines.[75]	20 µM CCCP induced apoptosis in 80% HL-60 cells after 24 h treatment. IC_{50} = ~10 µM (SH-SY5Y)	Morphological Hoechst 3332 staining.
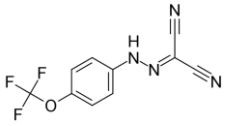 **FCCP**	*In vitro:* HepG2, A2058 and H358 cell lines.[76]	IC_{50} = 11 µM (HepG2) IC_{50} = ~4 µM (A2058) IC_{50} = ~6.5 µM (H358)	48 h MTT assay 48 h MTT assay 48 h MTT assay
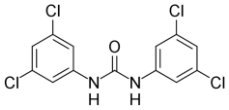 **SR4**	*In vitro:* HepG2, A2058 and H358 cell lines.[76] *In vivo:* A375 xenografts in athymic nu/nu mice.[77]	IC_{50} = 3.5 µM (HepG2) IC_{50} = ~2 µM (A2058) IC_{50} = ~2.5 µM (H358) Reduced tumour volume and weight by >90% compared to vehicle control.	48 h MTT assay 48 h MTT assay 48 h MTT assay Mice fed chow containing 10 mg/kg **SR4** for 3 weeks.
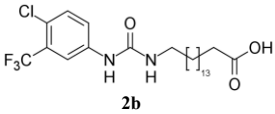 **2b**	*In vitro:* MDA-MB-231 cell line.[78] *In vivo:* MDA-MB-231 xenografts in female Balb/c nu/nu mice. [79]	Treatment with 10 µM reduced intracellular ATP by ~65%. Reduced tumour volume by ~50% compared to vehicle control.	24 h CellTiter-Glo ATP assay Mice treated with 40 mg/kg administered intraperitoneally six days a week for 38 days.
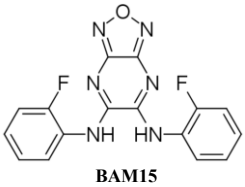 **BAM15**	*In vitro:* MCF-7, A375 and MeWo cell lines.[80] *In vivo:* C1498 leukemia allografts in C57BL/6N mice.[81]	In vitro: Reduced colony formation by >70% when treated in combination with MEK and BRAF inhibitor. Reduced leukocyte counts by 80% and significantly reduced spleen and liver weight compared to control after 20 days.	24 h treatment then colorimetric clonogenic assay seven days later. Mice treated with 5 mg/kg intraperitoneally every two days for three weeks.

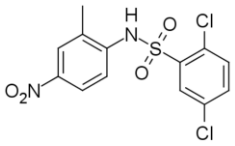 **FH535**	*In vitro:* LCSC, HuH7, Hep3B, PLC cell lines.[82] *In vivo:* Hepatocarcinoma HuH7 xenografts in athymic nu/nu mice.[83]	IC_{50} = 13.8 µM (LCSC) IC_{50} = 10.9 µM (HuH7) IC_{50} = 9.25 (Hep3B) IC_{50} = 6.6 (PLC) Reduced tumour volume by 60% compared to vehicle control after 10 days.	72 h ^{3}H-thymidine incorporation assay. 72 h ^{3}H-thymidine incorporation assay. 72 h ^{3}H-thymidine incorporation assay. 72 h ^{3}H-thymidine incorporation assay. Mice administered 15 mg/kg subcutaneously every second day.

In 2015 Figarola *et al.* reported the discovery of an experimental anticancer drug **SR4** (N,N'-*bis*(3,5-dichlorophenyl)urea, Figure 7a), which functions as a protein-independent mitochondrial uncoupler and causes dose-dependent apoptotic cell death in *in vitro* and animal models of cancer.[76,84-86] For example in xenograft mice carrying human A375 $BRAF^{V600E}$ melanomas, **SR4** showed superior activity to the BRAF inhibitor Vemurafenib, suppressing tumour growth (95% vs 82%, Figure 7b) and reducing tumour mass (94% vs 72%) after 3 weeks treatment.[77] **SR4** also outperformed another uncoupler in the study, niclosamide, and has demonstrated superior antiproliferative activity in cancerous liver (HepG2), skin (A2058) and lung (H358) cell lines compared to the classical protonophore FCCP (Figure 7),[76] highlighting its therapeutic promise over other reported mitochondrial uncouplers.

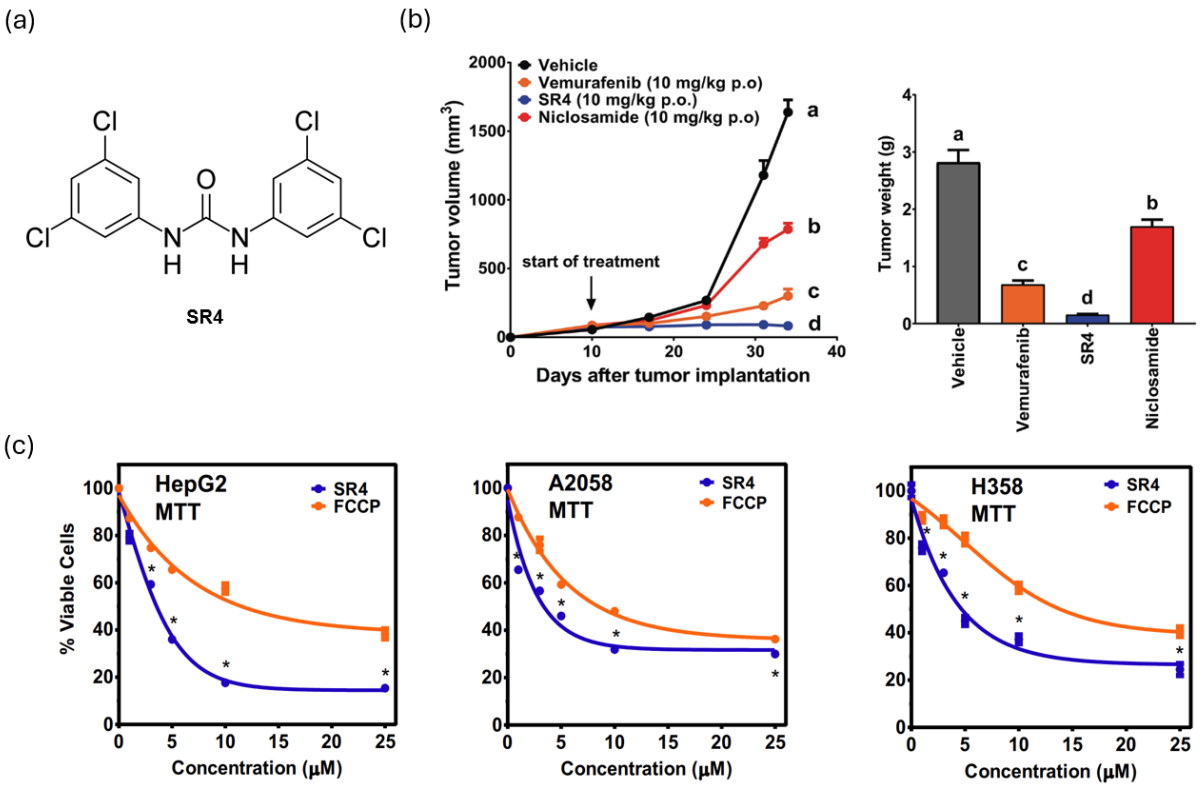

Figure 7. (a) Chemical structure of **SR4** (IUPAC name: N,N'-bis(3,5-dichlorophenyl)urea). (b) Tumour volume time course and final tumour weight in athymic nu/nu mice bearing A375(BRAF^{V600E} mutant melanoma) xenografts treated with **SR4**, niclosamide or vemurafib.[77] (c) Cell viability (MTT assay) following 48 h treatment with **SR4** or FCCP on HepG2 liver carcinoma, A2058 melanoma and H358 lung carcinoma.[76]

Despite its impressive activity, further development of **SR4** and its bisaryl urea scaffold has not been reported. This may be attributed to a lack of clarity surrounding the mechanism by which **SR4** mediates uncoupling. While **SR4** possesses an extended π-system, it lacks the acidic functional group needed to act as a protonophore. Indeed, calculated[87] and experimental[88] pK_a values of bisaryl ureas bearing electron withdrawing substituents range from 14 to 18, which is well above those of previously reported protonophores (pK_a values range from 4 to 8)[10] and too high to allow appreciable protonation / deprotonation at mitochondrial pH. This apparent contradiction was noted by Figarola *et al.*,[76] and without a detailed understanding of the uncoupling mechanism of **SR4**, a rational approach to the optimisation is not possible.

1.5 Synthetic anion transporters

Synthetic anion transporters are small lipophilic molecules that facilitate the passive transport of anionic species such as Cl^- and HCO_3^- across phospholipid bilayers. Transporters can mediate anion flux by disrupting bilayer integrity to form defects, assembling into ion channels, or acting as mobile carriers that ferry individual anions across the membrane. Transporters that operate as mobile carriers possess anion recognition motifs e.g. urea, thiourea and squaramide that reversibly bind their guest anion through non-covalent interactions on one side of the membrane. Dispersal of the anionic charge within these assemblies allows the complex to diffuse across the bilayer and translocate the anion. Synthetic anion transporters have received significant research attention due to their potential therapeutic applications,[89,90] which include treating cystic fibrosis by restoring HCO_3^- and Cl^- permeability in epithelia,[91] and inducing cancer cell death by perturbing intracellular anion concentrations.[92,93]

1.5.1 Synthetic anion transporter uncoupling protein mimics: fatty acid-activated mitochondrial uncoupling

In 2016 Wu and Gale made the surprising discovery that anion transporters can facilitate the movement of protons across lipid bilayers via their interaction with free fatty acids. As described previously, free fatty acids by themselves make poor protonophores because they do not make membrane permeable anions. It was found that anion transporters such as thiourea **T1** can overcome this barrier by hydrogen bonding to the fatty acid anion and ferrying it across the membrane as a mobile carrier (see Figure 8 for chemical structure and full mechanism). This mechanism mimics the function of uncoupling proteins in the MIM and allows for continuous cycles of proton transport. First the fatty acid carboxylate ($RCOO^-$) is protonated in the acidic space and permeates the membrane in its neutral form (RCOOH). The fatty acid is then deprotonated in the alkaline environment, resulting in the transport of one proton. To complete the cycle, thiourea **T1** then binds to and translocates the fatty acid carboxylate via hydrogen bonding with its thiourea NHs, which disperses the anions negative

charge and produces a membrane-permeable complex. Subsequent protonation regenerates the neutral fatty acid and frees the thiourea, allowing for repeated cycles of proton transport.

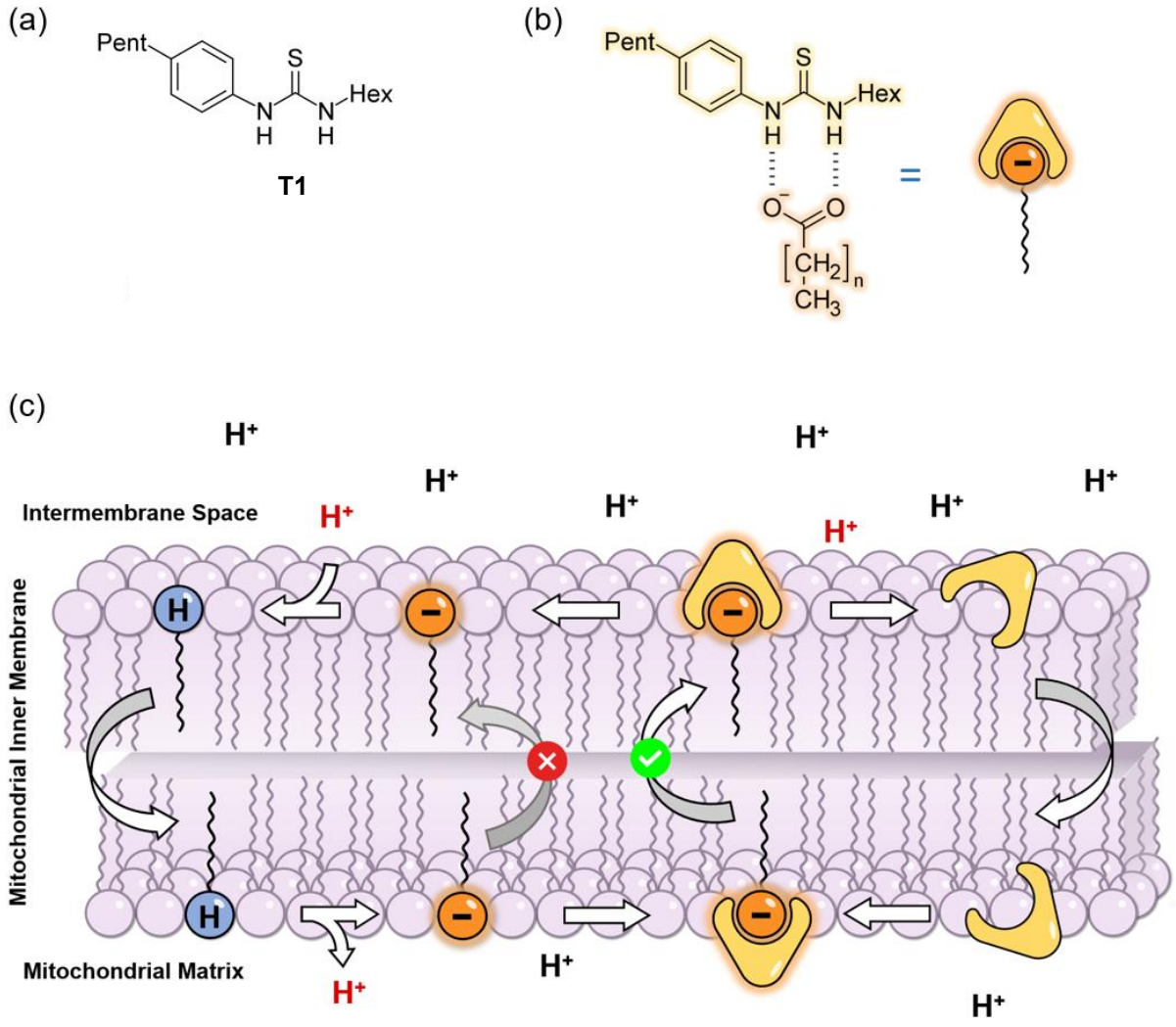

Figure 8. (a) Chemical structure of the thiourea-based fatty acid-activated proton transporter **T1**. (b) Thiourea **T1** bound to deprotonated fatty acid by parallel hydrogen bonds (c) Fatty acid-activated proton transport mechanism. After deprotonation of the fatty acid in the mitochondrial matrix, the thiourea-based anion transporter binds carboxylate and masks its charge to facilitate fatty acid flip-flop and proton transport across the MIM.

1.6 Project aims and thesis structure

This thesis sought to investigate the fatty acid-activated protonophoric and mitochondrial uncoupling activity of anion transporters in vesicles and cells. It is divided into three experimental chapters (Chapters Two, Three and Four), the general conclusions of which are summarised in Chapter Five and accompanied by suggestions for future work.

The first aim was to provide experimental evidence that **SR4** utilises fatty acid-activated proton transport, and to investigate the effect of aromatic substitution on uncoupling and anticancer activity. Chapter Two presents an investigation of the proton transport mechanism of **SR4**, and uses the insights gained to assess how aromatic substitution on the bisaryl urea scaffold impacts proton transport and mitochondrial actions in MDA-MB-231 breast cancer cells.

The second aim was to investigate the effects of replacing the urea group with alternative anion-binding motifs on proton transport and mitochondrial uncoupling activity. Chapter Three presents the synthesis of bisaryl squaramide, amide, and diurea analogues, and investigates the capacity for these compounds to operate via the fatty acid-activated proton transport mechanism and uncouple mitochondria in MDA-MB-231 cells.

The third and final aim was to enhance the proton transport and uncoupling activity of aryl urea substituted fatty acids, a new class of uncoupler that also rely on intermolecular urea-carboxylate interactions. The bisaryl ureas investigated in Chapter Two transport deprotonated fatty acids by dispersing their negative charge across an extended π-system. Based on this insight Chapter Four presents a library of diphenyl urea substituted fatty acids that incorporate an additional phenyl substituent into the scaffold, and investigates the effect of this expanded π-system on proton transport and mitochondrial actions in MDA-MB-231 cells.

Chapter Two: Characterisation and Development of Bisaryl Urea Mitochondrial Uncouplers as Fatty Acid-Activated Proton Transporters

Chapter Two Preamble

The initial papers that reported the activity of **SR4** provided extensive assay data to establish that **SR4** is a protein-independent mitochondrial uncoupler, but the full mechanism was not determined as **SR4** lacked an acidic functional group, which is a central feature of uncouplers. Given that **SR4** is structurally similar to thiourea **T1**, that aryl ureas are known anion receptors and transporters,[89,94-96] and because the MIM contains free fatty acids,[24,97,98] it was hypothesised that **SR4**-mediated proton transport operates via the fatty acid-activated mechanism. Proton transport by **SR4** was studied in the vesicle-based HPTS assay. This assay provides mechanistic data and can be conducted with varying levels of free fatty acids, and was used to establish the fatty acid-dependence of **SR4**-mediated proton transport. Next, the effect of aromatic substitution was assessed. A library of fourteen bisaryl ureas bearing various aromatic substituents was synthesised and the proton transport and mitochondrial actions of these compounds were evaluated against MDA-MB-231 breast cancer cells. This work resulted in the following chapter which was published in the journal *ACS Chemical Biology*, entitled 'Structure–Activity Relationship and Mechanistic Studies of Bisaryl Urea Anticancer Agents Indicate Mitochondrial Uncoupling by a Fatty Acid-Activated Mechanism'.

Declaration of Authorship Contributions

The following chapter is an accepted manuscript published in *ACS Chemical Biology (ACS Chem. Biol.)*. I, Edward York, was the principal investigator and author of this work with key contributions from Daniel A. McNaughton, direct training from Ariane Roseblade and supervision and guidance from Charles G. Cranfield, Philip A. Gale and Tristan Rawling. Daniel A. McNaughton performed the HPTS proton transport assays and assisted in writing the results and discussion for this data. All other experimental data was collected by myself.

Author	Contribution (CRediT)	Signature
Edward York	Conceptualisation, methodology, investigation, formal analysis, validation, visualisation, writing – original draft, writing – review and editing	Production Note: Signature removed prior to publication.
Daniel A McNaughton	Methodology, investigation, formal analysis, validation, visualisation, writing-original draft	Production Note: Signature removed prior to publication.
Ariane Roseblade	Methodology, Supervision	Production Note: Signature removed prior to publication.
Charles G Cranfield	Supervision, writing – review and editing	Production Note: Signature removed prior to publication.
Philip A Gale	Supervision, writing – review and editing	Production Note: Signature removed prior to publication.
Tristan Rawling	Conceptualisation, methodology, supervision, writing - review and editing	Production Note: Signature removed prior to publication.

ACS chemical biology

pubs.acs.org/acschemicalbiology Articles

Structure–Activity Relationship and Mechanistic Studies of Bisaryl Urea Anticancer Agents Indicate Mitochondrial Uncoupling by a Fatty Acid-Activated Mechanism

Edward York,[a] Daniel A. McNaughton,[b] Ariane Roseblade, [a] Charles G. Cranfield,[c] Philip A. Gale[b,c] and Tristan Rawling [a]

[a] School of Mathematical and Physical Sciences, Faculty of Science, University of Technology Sydney, Sydney, NSW 2007, Australia ;
[b] School of Chemistry, The University of Sydney, Sydney, NSW 2006, Australia ;
[c] School of Life Sciences, Faculty of Science, University of Technology Sydney, Sydney, NSW 2007, Australia ;
[d] The University of Sydney Nano Institute (SydneyNano), The University of Sydney, Sydney, NSW 2006, Australia;

Abstract: Targeting the cancer cell mitochondrion is a promising approach for developing novel anticancer agents. The experimental anticancer agent **SR4** (*N*,*N*'-bis(3,5-dichlorophenyl) urea) induces apoptotic cell death in several cancer cell lines by uncoupling mitochondrial oxidative phosphorylation (OXPHOS) using a protein free mechanism. However, the precise mechanism by which **SR4** depolarises mitochondria is unclear because **SR4** lacks an acidic functional group typically found in protein-independent uncouplers. Recently it was shown that structurally related thioureas can facilitate proton transport across lipid bilayers by a fatty acid-activated mechanism, in which the fatty acid acts as the site of protonation/deprotonation and the thiourea acts as an anion transporter that shuttles deprotonated fatty acids across the phospholipid bilayer to enable proton leak. In this paper we show that **SR4**-mediated proton transport is enhanced by the presence of free fatty acids in the lipid bilayer, indicating that **SR4** uncouples mitochondria through the fatty acid-activated mechanism. This mechanistic insight was used to develop a library of substituted bisaryl ureas for structure-activity relationship (SAR) studies and subsequent cell testing. It was found that lipophilic

electron-withdrawing groups on bisaryl ureas enhanced electrogenic proton transport via the fatty acid-activated mechanism, and capacity to depolarise mitochondria and reduce the viability of MDA-MB-231 breast cancer cells. The most active compound in the series reduced cell viability with greater potency than **SR4**, and was more effective at inhibiting ATP production.

Introduction

The discovery of cytotoxic agents that selectively target cancer cells is critical to the development of well-tolerated anticancer therapeutics. Cancer cell mitochondrion have emerged as a promising anticancer drug target because they are structurally and functionally distinct from mitochondria in non-cancerous cells and because of their central role in cellular metabolism and apoptosis.[47] Mitochondria are the site of oxidative phosphorylation (OXPHOS), a process that converts nutrients into ATP. OXPHOS commences in the mitochondrial matrix, the central region of mitochondria enclosed by the mitochondrial inner membrane (MIM), where nutrients are oxidised to form NADH and $FADH_2$. NADH and $FADH_2$ feed high energy electrons into the electron transport chain (ETC), a series of proteins embedded in the MIM. As electrons pass through the ETC protons are pumped from the matrix and into the intermembrane space, generating a proton gradient across the MIM. The resultant mitochondrial membrane potential ($\Delta\Psi_M$) drives the flow of protons back into the matrix through the MIM-embedded protein ATP synthase, which catalyses the formation of ATP.[2,4,5] Thus, nutrient oxidation is coupled to ATP formation by the $\Delta\Psi_M$. In cancer cells, deregulated mitochondrial metabolism results in a shift towards glycolysis and an increased mitochondrial $\Delta\Psi_M$ compared to non-cancerous cells.[99] Indeed, hyperpolarization of the MIM is a universal feature of cancer cells, and targeting $\Delta\Psi_M$ may produce novel drugs that selectively target cancer cells.[48,56,59]

Mitochondrial uncouplers are compounds that uncouple nutrient oxidation from ATP production by collapsing the $\Delta\Psi_M$.[10] The most common uncouplers are protonophores, which are lipophilic weak acids that can shuttle protons across membranes such as the MIM via the protonophoric cycle

(Figure 9a). The deprotonated uncoupler (A^-) accepts a proton in the intermembrane space and diffuses across the MIM in its neutral form (A-H). Deprotonation of the protonophore in the relatively alkaline matrix results in the transport of one proton across the MIM. For the cycle to continue the deprotonated protonophore (A^-) must permeate the MIM and return to the intermembrane space, however this step is inhibited by the MIM's lipophilic core, which is relatively impermeable to anions.[12,13] Thus, the acidic groups in protonophores are conjugated to extended π-systems, which provide a large surface area for delocalization of the anionic charge. Charge delocalization enhances the lipophilicity and MIM-permeability of the anionic protonophore and allows the cycle to continue.[100] Fatty acids such as palmitic acid are weak acids but poor protonophores because insufficient charge delocalization prevents the fatty acid carboxylate from permeating the MIM.[101,102]

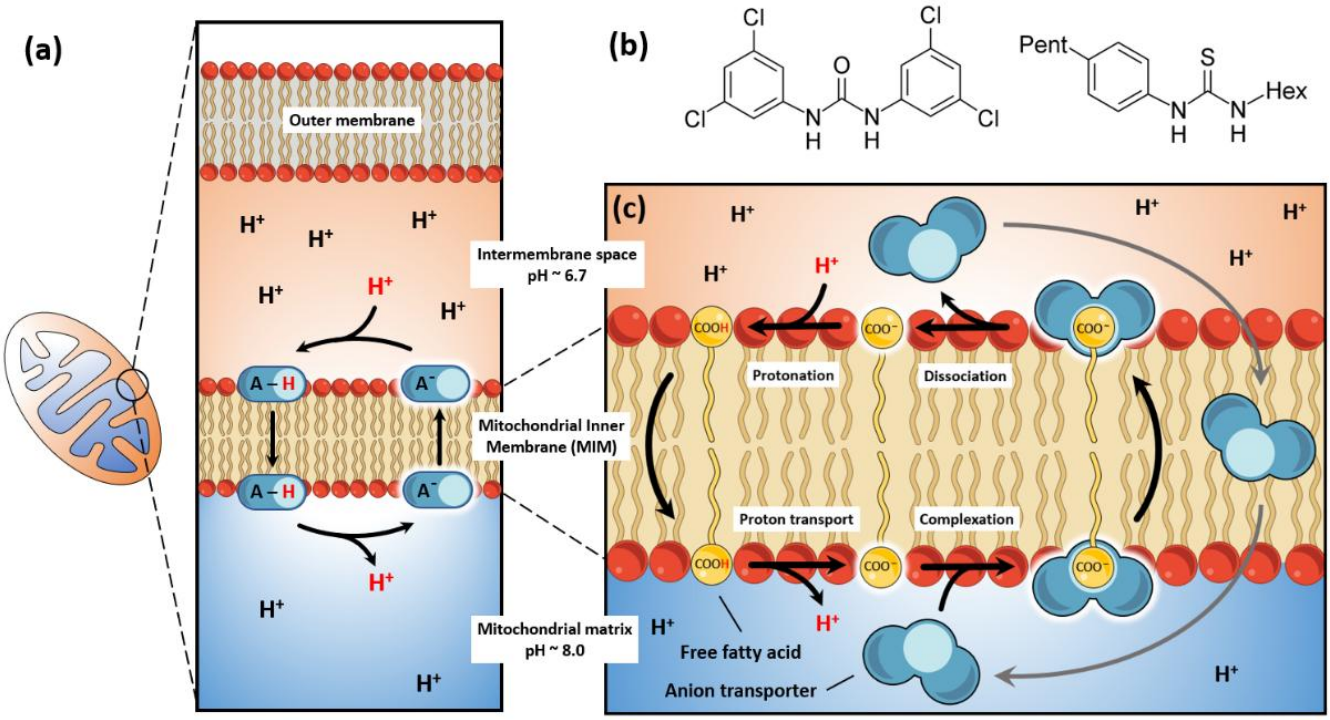

Figure 9. Proton transport and mitochondrial uncoupling by protonophoric and fatty acid-activated mechanisms. (a) Mitochondrial uncoupling by classical protonophores. The protonophoric cycle that results in the transport of protons across the MIM and mitochondrial uncoupling. The rate determining step is diffusion of the anionic species across the MIM. To complete this step the negative charge is delocalised across an extended π-system to produce a MIM permeable anion. (b) Chemical structures

of **SR4** and structurally related fatty acid-activated thiourea proton transporter respectively. (c) Fatty acid-activated proton transport mechanism. After deprotonation of the fatty acid in the mitochondrial matrix the thiourea-based anion transporter binds carboxylate and masks the charge to facilitate fatty acid flip-flop and proton transport across the MIM.

The anticancer actions of mitochondrial uncouplers has been increasingly recognised as several uncouplers have been shown to selectively kill cancer cells.[100] One such compound is **SR4** (Figure 9b), a chlorinated bisaryl urea reported by Figarola *et al.* to induce apoptotic cell death in leukaemia (HL-60), liver (HepG2) and lung (H358) cancer cells line *in vitro*.[76,85,86] **SR4** also induces apoptosis in naïve and drug resistant melanoma (A375, SK-MEL-28) cell lines,[77] and inhibits tumour growth in mouse models of cancer.[77,86,103] Rigorous mechanistic studies established that **SR4** induces cell death through uncoupling of cancer cell mitochondria, and that uncoupling occurs by a protein-independent mechanism. However the precise mechanism by which **SR4**-mediated uncoupling occurs has not been determined because **SR4** lacks an acidic functional group required for protonophoric activity. Indeed, calculated and experimental pK_a values of substituted bisaryl ureas range from 14 to 18,[87] which is well above that of previously reported protonophores (pK_a values range from 4-8),[10] and too high to allow protonation/deprotonation at mitochondrial pHs.

In 2016 Wu and Gale reported that thiourea-based anion receptors can mediate proton transport across lipid bilayers by a fatty acid-activated mechanism (Figure 8c), shown using unilamellar vesicles that model the MIM.[104] Similar to the protonophoric cycle, the fatty acid carboxylate is protonated in the intermembrane space and permeates the MIM as a neutral species. Once in the alkaline matrix the fatty acid is deprotonated, which results in the transport of one proton and the formation of a fatty acid carboxylate that must diffuse back across the MIM. The thiourea next binds to the fatty acid carboxylate group through parallel hydrogen bonds with the thiourea NH groups, which masks the anionic charge to produce a complex that is sufficiently lipophilic to diffuse through the lipid bilayer. Dissociation in the intermembrane space liberates the fatty acid and thiourea, allowing further proton transport to occur. Given that **SR4** is structurally similar to the thiourea-based anion

receptors and aryl ureas are known anion receptors and transporters,[89,94-96] and because the MIM contains free fatty acids,[97,98] we suspected that **SR4** may uncouple mitochondria by the same fatty acid-activated mechanism. In this paper we show using a HPTS proton transport assay that **SR4**-mediated proton transport is enhanced by free fatty acids in the bilayer, indicating that **SR4** uncouples mitochondria through the fatty acid-activated mechanism. This insight was used to develop a library of substituted bisaryl ureas for structure-activity relationship (SAR) studies and subsequent cell testing. The resulting SAR demonstrated that lipophilic electron-withdrawing groups enhance fatty acid-activated proton transport, and analogues bearing these groups were found to effectively depolarise mitochondria and reduce cell viability in MDA-MB-231 breast cancer cells. The most potent transporter in the series (compound **3**) maintained the cellular actions of **SR4** and was found to uncouple mitochondrial OXPHOS and impair ATP production.

RESULTS AND DISCUSSION

SR4-mediated proton transport is enhanced in phospholipid bilayers containing oleic acid

To determine if **SR4** can participate in the fatty acid-activated proton transport mechanism identified by Wu and Gale[104] we used a similar HPTS fluorescence assay to measure electrogenic proton transport in large unilamellar 1-palmitoyl-2-oleoyl-sn-glycero-3-phosphocholine (POPC) vesicles (200 nm) in HEPES-buffered potassium gluconate (100 mM) (Figure 10a, see Supplementary Information for details).[105] In this system a pH gradient is established between the interior and exterior environments of the vesicles and proton transport is measured by monitoring the increase in intravesicular pH using the pH-sensitive fluorescent probe 8-hydroxypyrene-1, 3, 6-trisulfonic acid (HPTS). **SR4**-mediated proton transport was tested under three conditions, in untreated POPC vesicles, vesicles pretreated with bovine serum albumin (BSA, 1 mol%) and vesicles pretreated with both BSA (1 mol%) and oleic acid (OA, 10 mol%, corresponding to 4 mol% free concentration after BSA binding). Pretreatment with BSA removes contaminating fatty acids present in POPC to detect proton transport via protonophoric cycling (i.e. classical protonophores). The addition of OA reintroduces the fatty

acid-activated mechanism of proton transport, and any enhancement in activity can be assigned to this pathway.

As shown in Figure 10b, **SR4**-mediated proton transport is diminished in vesicles containing BSA compared to untreated vesicles, demonstrating that direct protonophoric cycling cannot explain the observed proton transport facilitated by **SR4**. This was anticipated because **SR4** lacks a functional group sufficiently acidic for deprotonation at mitochondrial pHs, and the slight efflux observed may be attributed to the traces of fatty acids that remain in the membrane after BSA treatment.[104] Further, proton transport was enhanced in the presence of OA suggesting a fatty acid-dependent pathway. Combined these data indicate **SR4**-mediated proton transport across lipid bilayers is enhanced by free fatty acids, and is consistent with the hypothesis that **SR4** can act as a fatty acid-activated proton transporter.

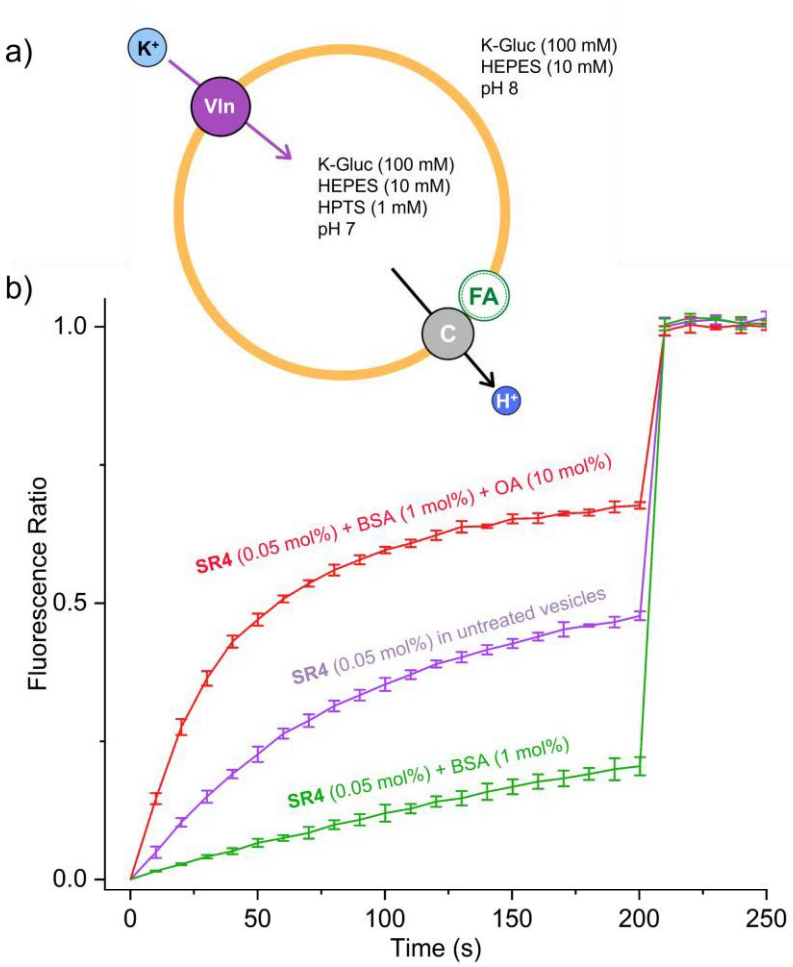

Figure 10. a) Schematic of the HTPS proton transport assay, monitored by HPTS fluorescence, outlining the conditions of the experiment and b) the proton transport induced by **SR4** under the various assay conditions. Vesicles were lysed at 200 s to provide a 100% dissipation reading for calibration purposes. Compound concentrations are represented as compound-to-lipid molar ratios.

Compound library design and synthesis

We next prepared a series of symmetrically substituted bisaryl ureas to determine if the observed SAR was consistent with the fatty acid-activated proton transport mechanism. Under this mechanism, the urea-based anion receptor promotes transbilayer movement ("flip-flop") of anionic fatty acids by binding to and masking the carboxylate charge through parallel hydrogen bonds with the urea N-H groups, producing a complex that is sufficiently lipophilic to permeate lipid bilayers. It was anticipated that electron-withdrawing substituents on the bisaryl urea rings would enhance the carboxylate affinity of the urea binding group, promoting complexation and thus proton transport

activity. It was also anticipated that lipophilic substituents would increase complex lipophilicity and improve activity. To test this a series of symmetrically substituted bisaryl ureas bearing substituents with various electron-withdrawing and donating capacities (determined from Hammett substituent constant, σ) and lipophilic properties (determined from hydrophobicity constant, π) were synthesised (Table 2). The compounds were synthesised in one step by reaction of *N,N'*-carbonyldiimidazole (CDI) with appropriately substituted anilines.

Table 2. Chemical structures, aromatic substituent constants, HPTS (200 s) EC_{50} concentrations and Hill coefficients in untreated POPC vesicles, MTS (72 h) and JC-1 (1 h) absolute IC_{50} concentrations measured in MDA-MB-231 breast cancer cells.

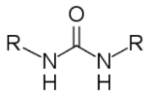

Compound	R	σ_{total}[a]	π_{total}[a]	HPTS EC_{50} (mol%)	Hill (n)	MTS IC_{50} (μM)	JC-1 IC_{50} (μM)
1	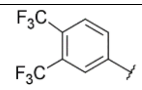	1.94	3.52	0.022 ± 0.001	0.91 ± 0.06	0.51 ± 0.1	1.80 ± 0.3
2	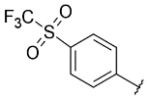	1.92	1.10	0.044 ± 0.002	1.38 ± 0.06	0.44 ± 0.1	2.34 ± 0.2
3	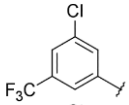	1.60	3.18	0.0046 ± 0.0004	0.82 ± 0.07	0.37 ± 0.1	0.26 ± 0.1
SR4	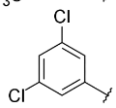	1.48	2.84	0.015 ± 5 x 10^{-4}	1.01 ± 0.04	1.10 ± 0.3	0.45 ± 0.1
5	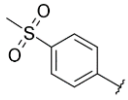	1.44	-3.26	-[b]	-[b]	-[d]	-[d]
6	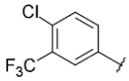	1.32	3.18	0.010 ± 9 x 10^{-4}	0.81 ± 0.1	0.68 ± 0.1	1.24 ± 0.3
7	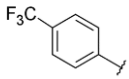	1.08	1.76	0.023 ± 0.001	1.16 ± 0.06	0.84 ± 0.1	2.26 ± 0.4
8	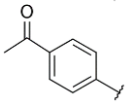	1.00	-1.10	1.61 ± 0.04	1.15 ± 0.05	>100[c]	22.9 ± 0.4
9	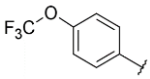	0.70	2.08	0.028 ± 0.005	1.33 ± 0.3	>100[c]	>100[c]
10	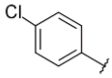	0.46	1.42	0.11 ± 0.03	2.00 ± 0.6	-[d]	>100[c]
11		0	0	-[b]	-[b]	>100[c]	>100[c]
12	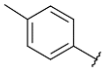	-0.34	1.12	-[b]	-[b]	-[d]	-[d]
13	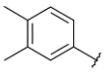	-0.48	2.24	-[b]	-[b]	-[d]	-[d]
14	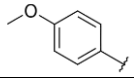	-0.54	-0.04	-[b]	-[b]	-[d]	-[d]

[a] Aromatic substituent constants were taken from published values.[106] [b] Did not exceed 50 % efflux after 200 s at a loading of 10 mol%. [c] Produced moderate activity at 100 μM but insufficient for absolute IC_{50} determination. [d] No activity observed at the maximum test concentration of 100 μM

Bisaryl ureas mediate proton transport by a fatty acid-activated mechanism

We first studied the ability of bisaryl ureas **1–14** to mediate electrogenic proton transport using the HPTS proton transport assay as performed for **SR4**. Dose-response studies and Hill analyses were performed for compounds **1−14** under three test conditions. An EC_{50} value, which represents the concentration required to facilitate 50% of the maximum transport, and a Hill coefficient (n), which provides an indication of the stoichiometry of test compound required for the transport process, was calculated for each compound. Initially, the proton transport capability of compounds **1–14** were assessed in untreated vesicles to establish an SAR for the series (Table 2). Subsequently, dose-response studies were performed in the presence of BSA (1 mol%) or in the presence of both BSA (1 mol%) and OA (10 mol%) (Table 3).

Bisaryl ureas **1–SR4** and **6–10** achieved appreciable proton transport below 10 mol% loadings (compound-to-lipid molar ratio) such that EC_{50} values could be calculated. The remaining compounds at commensurate concentrations did not exhibit significant activity, and higher loadings caused the compounds to precipitate out of aqueous media during experimental runs, meaning EC_{50} values for the remaining compounds could not be calculated and were considered as inactive.

The SAR elicited from the HPTS assay data of the compounds in untreated vesicles indicates that lipophilic and electron-withdrawing substituents enhance electrogenic proton transport activity. The impact of electron-withdrawing capacity is highlighted clearly as compounds possessing electron-withdrawing substituents all showed appreciable activity apart from urea **5**, whereas compounds bearing electron-donating substituents (**12**, **13** and **14**), as well as the unsubstituted urea **11**, lacked activity. The importance of lipophilicity can be seen by comparison of urea **2** and **5**. Both compounds share similar electronic and steric properties, but differ substantially in lipophilicity. Bisaryl urea **2** is substituted with lipophilic trifluoromethylsulfonyl groups and exhibited an EC_{50} of 0.044 mol%. In contrast, while the hydrophilic methanesulfonyl groups of **5** are sufficiently electron-withdrawing, urea **5** lacked activity; presumably because it does not form fatty acid complexes with the lipophilicity required to permeate the lipid bilayer. That polar substituents reduce activity is also

supported by urea **8**, which has electron-withdrawing but polar acetyl substituents and was found to be the least potent of the active compounds with an EC_{50} of 1.61 mol%.

Compounds with two substituents generally outperformed those with a single *para* positioned electron-withdrawing group. Bisaryl urea **3** was the most potent proton transporter of the series, with an EC_{50} value of 0.0046 mol%. **3** closely resembles the structure of **SR4**, bearing a trifluoromethyl group in place of a chlorine, however, its three-fold greater transport activity highlight that modest changes in lipophilic and electronic properties have significant effects on transport activity. However, notably urea **1** was less effective in the HPTS assays than compounds **3** and **6**, despite the replacement of a second chlorine with another trifluoromethyl substituent. Previous studies by the Gale group and others have highlighted that an optimal degree of lipophilicity is crucial for efficient transport activity.[107,108] Compounds that are too lipophilic tend to localise in the non-polar interior of the lipid bilayer and struggle to diffuse into the aqueous phase to complete the transport cycle, resulting in diminished activity.

The EC_{50} values determined under the BSA and BSA + OA experimental conditions are displayed in Table 3. Enhancement of transport activity in the presence of fatty acid was quantified using an activation factor, calculated by dividing the EC_{50} in the presence of BSA by the EC_{50} in the presence of both BSA and OA.[104] An activation factor greater than 1 was returned for all compounds with appreciable activity, indicating that dissipation of the proton gradient is enhanced in the presence of fatty acid and, therefore, that the fatty acid-activated mechanism is the dominant pathway of proton transport for the active bisaryl urea compounds.

Table 3. HPTS EC_{50} (200 s) concentrations and Hill coefficients in POPC vesicles in the presence of BSA and both BSA and OA.

Compound	EC_{50} (BSA)	n (BSA)	EC_{50} (OA)	n (OA)	Activation Factor [a]
1	0.065 ± 0.003	1.06 ± 0.05	0.014 ± 0.002	0.55 ± 0.1	4.64
2	0.044 ± 0.003	1.26 ± 0.2	0.033 ± 0.001	1.55 ± 0.05	1.33
3	0.06 ± 0.004	1.24 ± 0.09	0.003 ± 1 x 10^{-4}	0.80 ± 0.04	20.00
SR4	0.075 ± 0.009	1.32 ± 0.2	0.00512 ± 4 x 10^{-4}	1.36 ± 0.30	14.65
5	-[b]	-[b]	-[b]	-[b]	-[c]
6	0.098 ± 0.004	1.04 ± 0.1	0.0040 ± 1 x 10^{-4}	1.03 ± 0.03	24.50
7	0.13 ± 0.02	2.00 ± 0.4	0.012 ± 7 x 10^{-4}	1.04 ± 0.03	10.83
8	-[b]	-[b]	0.63 ± 0.07	1.05 ± 0.10	-[c]
9	0.35 ± 0.05	1.56 ± 0.3	0.019 ± 3 x 10^{-4}	1.27 ± 0.03	18.42
10	-[b]	-[b]	0.042 ± 0.004	1.46 ± 0.20	-[c]
11	-[b]	-[b]	-[b]	-[b]	-[c]
12	-[b]	-[b]	-[b]	-[b]	-[c]
13	-[b]	-[b]	-[b]	-[b]	-[c]
14	-[b]	-[b]	-[b]	-[b]	-[c]
CCCP[21]	0.0013	0.97	0.0014	0.99	0.93

[a] EC_{50} in the presence of BSA divided by EC_{50} in the presence of both BSA and OA. [b] Did not exceed 50% efflux after 200 s at a loading of 10 mol%. [c] Activation factor could not be calculated.

For comparison, the activation factor previously reported for carbonyl cyanide m-chloro-phenyl hydrazone (CCCP), a classical protonophore, has been included in Table 3.[104] The activation factor for CCCP is close to one, demonstrating that proton transport facilitated by this compound occurs independently of fatty acids present in the membrane. Notably, urea **2** exhibited only mild activation in the presence of OA and was 10 times less potent than **3**, which may be attributed to its markedly lower lipophilicity compared to **3**. Hill analyses of compounds **8** and **10** for the HPTS assay in the presence of BSA could not be completed due to a lack of transport activity below 10 mol% loading. However, EC_{50} values could be determined in the presence of OA, and were much lower than the 10 mol% thresholds (0.63 and 0.042 mol%, respectively). This further emphasises the

contribution of the fatty acid-activated mechanism as the main proton transport mode of this compound series.

Mitochondrial actions of bisaryl ureas 1-14

We next assessed the capacity of bisaryl ureas **1–14** to transport protons across the MIM and depolarise mitochondria in MDA-MB-231 cells using the JC-1 assay. JC-1 is a fluorescent cationic dye that partitions between the mitochondrial matrix and the cytosol according to the $\Delta\Psi_M$. In polarised mitochondria with high $\Delta\Psi_M$, JC-1 accumulates in the matrix and forms aggregates that fluoresce red. Upon dissipation of $\Delta\Psi_M$ by mitochondrial uncouplers, JC-1 diffuses into the cytosol and disaggregates into monomers that fluoresce green. Thus, the JC-1 red : green fluorescence ratio is proportional to the proton gradient across the MIM. JC-1 IC_{50} concentrations for the ureas were determined from dose-response curves as the concentration required to shift the red : green fluorescence ratio by 50% of control (Table 2). One hour treatments were used to distinguish the direct actions of the bisaryl ureas on the MIM from the collapse of the $\Delta\Psi_M$ that occurs during apoptotic cell death.

The observed JC-1 activity was consistent with the SAR established from the HPTS assay. Analogues that induced mitochondrial depolarization with the lowest JC-1 IC_{50} concentrations (**1**, **2**, **3**, **6**, **7** and **SR4**) were substituted with lipophilic and electron-withdrawing groups. Polar electron-withdrawing substituents reduced JC-1 activity, as reflected by the inactive urea **5** and urea **8**, which had a relatively high IC_{50} of 22.9 ± 0.4 μM. The JC-1 results for these analogues follow the HPTS activity trends, and bivariate analysis using log reciprocal transformations of JC-1 IC_{50} and HTPS EC_{50} concentrations demonstrates a strong positive relationship ($r^2 = 0.87$, Supplementary Figure S2). Ureas **9** and **10**, which both possess moderately electron-withdrawing substituents ($\sigma_{total} \leq 0.70$) in *para* positions, lacked sufficient activity when tested at their solubility limits to calculate JC-1 IC_{50} concentrations. These analogues were active in HPTS assays, and the differences may arise from confounding factors (plasma membrane permeability, metabolic stability etc.) in cell-based assays that are not present in the cell free HPTS assay. Unsubstituted urea **11** and ureas substituted with electron-donating groups (**12**, **13** and **14**) had poor or no observable activity in both JC-1 and HPTS

assays. Taken together, these data support the hypothesis that, like **SR4**, active bisaryl ureas depolarise mitochondria by the fatty acid-activated mechanism.

Proton transport across the MIM by **SR4** leads to mitochondrial uncoupling and reductions in intracellular ATP. To confirm that the most potent urea **3** also produces these actions, we examined each one of these steps.

First we established that **3** was a mitochondrial uncoupler using the Seahorse Mito Stress test, which measures the oxygen consumption rate (OCR) of MDA-MB-231 cells. Treatment of the cells with the ATP synthase inhibitor oligomycin reduces electron flow through the ETC and lowers OCR. Addition of an uncoupler in these conditions collapses the proton gradient across the MIM and allows unimpeded ETC activity that is observed as an increase in OCR.[109] As shown in Figure 11, addition of **3** (5 μM), **SR4** (5 μM) and the classical uncoupler FCCP (0.5 μM) increased OCR in MDA-MB-231 cells treated with oligomycin, indicating that **3**, like **SR4** and FCCP, is a mitochondrial uncoupler. In contrast, urea **12** (10 μM) failed to increase OCR, which was anticipated based on its inactivity in the HPTS and JC-1 assays.

Interestingly, the initial spike in OCR caused by **3** was followed by a steady decline, a pattern not observed for **SR4** or FCCP, but has been previously shown for FCCP when tested at higher concentrations (> 5 μM).[76] High concentrations of FCCP have also been found to inhibit oxidation of NADH and $FADH_2$ by complex I and II,[110] which would counteract the increase in OCR caused by uncoupling. Since FCCP and **3** produce similar responses despite being structurally unrelated, it is possible that excessive uncoupling activity inhibits complexes I and II by matrix acidification, which could induce conformational changes in their matrix-exposed domains and/or disfavour the equilibria for nutrient oxidation.

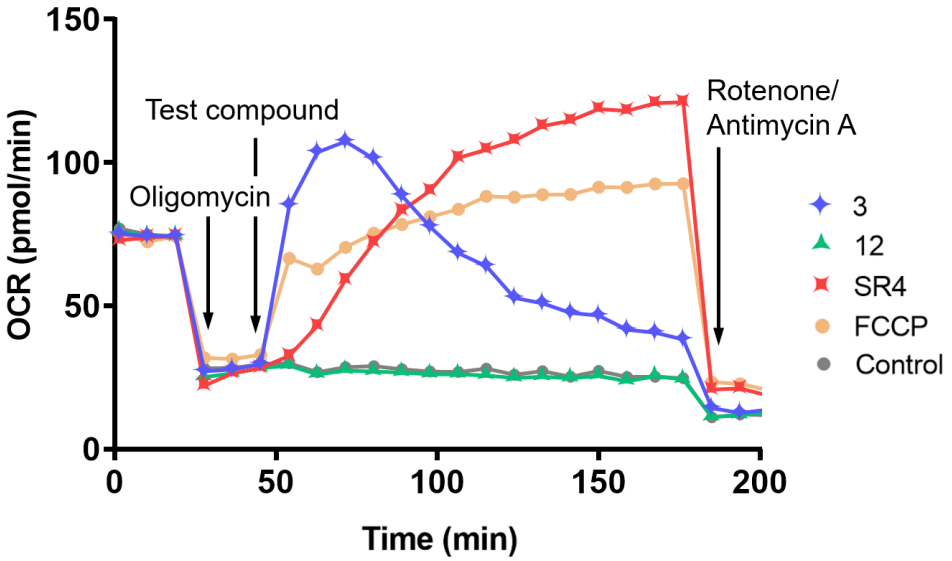

Figure 11. OCR in MDA-MB-231 cells treated sequentially with the ATP synthase inhibitor oligomycin (1 μM), a test compound (5 μM **SR4**, 5 μM **3** or 10 μM **12**), and the ETC complex inhibitors rotenone / antimycin A (1 μM). Test compounds were compared against the classical protonophore FCCP (0.5 μM) and a 0.1% DMSO vehicle containing no test compound as control.

ATP production by OXPHOS is dependent on the proton gradient across the MIM, and collapse of the $\Delta\Psi_M$ by mitochondrial uncouplers inhibits ATP production. We therefore assessed the effects of **SR4** and **3** on intracellular ATP levels in MDA-MB-231 cells. The uncoupler FCCP was included for comparison. Similar to previous observations in liver carcinoma (HepG2) and melanoma (A375 and MeWo) cell lines,[76,77] **SR4** and FCCP both reduced intracellular ATP levels to ~85% of DMSO-treated control cells over eight hours (Figure 12). Urea **3** had the largest impact on intracellular ATP and reduced ATP levels to 60% of control after eight hours. The higher activity of **3** in this assay is consistent with the higher potencies observed for **3** in the HPTS and JC-1 assays. To confirm that the observed decreases in intracellular ATP were not a result of cell death LDH release assays were performed. These assays showed that **SR4** and **3** did not increase LDH release in MDA-MB-231 cells compared to control following 8 hours treatment (Supplementary Figure S6), supporting the conclusion that **SR4** and **3** inhibit ATP production. Taken together, these data demonstrate that urea **3** produces similar cellular actions to **SR4** in MDA-MB-231 cells by depolarizing mitochondria, uncoupling OXPHOS and inhibiting ATP production.

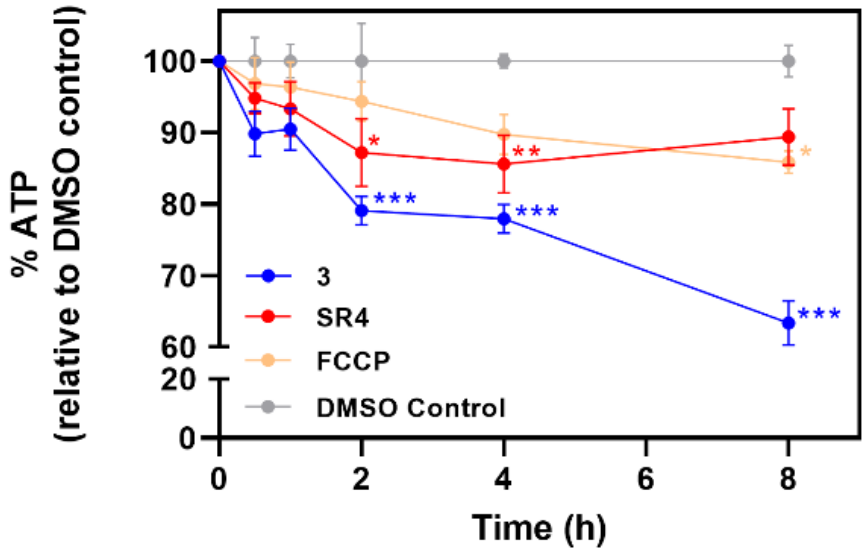

Figure 12. Total intracellular ATP levels in MDA-MB-231 cells following treatment with 5 µM of **SR4**, **3**, FCCP or vehicle (DMSO) control. ATP levels are expressed as percentage of time-matched DMSO control. Different from DMSO-treated control: (*) $P < 0.05$, (**) $P < 0.01$, (***) $P < 0.001$.

Effects of bisaryl ureas 1-14 on MDA-MB-231 cell viability

Mitochondrial uncoupling by **SR4** is reported to lead to reduction in cancer cell viability,[15,18] so we last assessed the effects of **1**-**14** on MDA-MB-231 cell viability using MTS assays, and compared the findings to the observed SAR from the HPTS and JC-1 data. Dose-response curves (Supplementary Figure S3) were constructed from three independent repeats and used to calculate absolute IC_{50} concentrations (Table 2). **SR4** reduced MDA-MB-231 cell viability with an IC_{50} of 1.1 ± 0.3 µM after 72 hours treatment, which is comparable to IC_{50} concentrations reported against human HL-60 (1.2 µM, 72 h MTT), HepG2 (3.5 µM, 48 h MTT) and A2058 (5.0 µM, 96 h MTT) cancer cell lines.[76,85,86] Analogues **1**, **2**, **3**, **6** and **7** reduced MDA-MB-231 cell viability with absolute IC_{50} concentrations between 0.3–1 µM. Ureas **8** and **9** reduced cell viability at concentrations above 10 mM, however absolute IC_{50} concentrations could not be calculated for these compounds as they failed to reduce cell viability to below 50% of control. This activity could indicate these analogues impact cell viability by affecting progression through the cell cycle, an effect that has been demonstrated for

SR4.[76,85] All other bisaryl ureas were essentially inactive, with **11** producing only a moderate reduction in cell viability at the highest test concentration of 100 μM.

Unlike the HPTS data, the MTS IC_{50} concentrations calculated for the active compounds were all tightly grouped between 0.37 and 1.10 μM, and the correlation observed between the JC-1 and HPTS results was not found between MTS IC_{50} data and HPTS EC_{50} data (Supplementary Figure S4). One possible explanation is that some of the ureas in the series may be capable of inducing cell death by a second mechanism. For example, pyrimidine-based synthetic anion transporters transport chloride across cellular membranes, and have been shown to disrupt intracellular ion homeostasis and induce apoptotic cell death in HeLa and A549 cancer cell lines.[93] Despite this, broad similarities between HPTS and MTS activity remain. All analogues that displayed sufficient activity to calculate absolute MTS IC_{50} concentrations (**1**, **2**, **3**, **6**, **7** and **SR4**) were substituted with lipophilic electron-withdrawing groups and exhibited proton transport activity in the HPTS assays. Urea **3** was the most active in the series in HPTS, JC-1 and MTS assays and was ~2–3 fold more active than **SR4** across all three assays. All analogues that lacked proton transport activity in HPTS assays (**5**, **11–14**) did not significantly reduce cell viability, and were unsubstituted or substituted with polar and/or electron-donating substituents.

Taken together, the data presented in this paper indicate that bisaryl ureas substituted with lipophilic electron-withdrawing groups uncouple mitochondria by the fatty acid-activated mechanism first identified by Wu and Gale,[104] and that this uncoupling contributes to the ability of these compounds to reduce cancer cell viability.

Conclusions

In this paper we provide experimental evidence that **SR4** uncouples mitochondria by a fatty acid-activated proton transport mechanism first identified by Wu and Gale. Lipophilic and electron-withdrawing substituents on the bisaryl urea scaffold were shown to enhance electrogenic proton transport using this mechanism, promoting mitochondrial depolarization and reducing cell viability in MDA-MB-231 cells. The SAR is consistent with the proposed fatty acid-activated proton transport

mechanism whereby bisaryl ureas facilitate fatty acid flip-flop by binding to fatty acid carboxylate groups to form MIM-permeable complexes. The most potent analogue **3**, like **SR4**, was shown to uncouple mitochondrial OXPHOS and inhibit ATP formation in MDA-MB-231 breast cancer cells.

METHODS

Chemistry

CDI, 4-chloro-3-(trifluoromethyl) and 4-(methylsulfonyl)aniline was purchased from Fluorochem, aniline from Univar and 3,4-bis(trifluoromethyl)aniline from Combiblocks. The remaining substituted anilines were purchased from Sigma Aldrich. Reactions were monitored using TLC on Merck silica gel 60 F_{254} aluminium backed plates. ^{1}H NMR (500 MHz) and ^{13}C NMR (125 MHz) spectra were recorded using an Agilent 500 MHz NMR spectrometer. Spectra were referenced internally to residual solvent (DMSO-d_6: ^{1}H δ 2.50, ^{13}C δ 39.52). Melting point determination was performed using a Gallenkamp melting point apparatus. High resolution mass spectra (HRMS) were recorded on an Agilent Technologies 6510 Q-TOF LCMS. The purity of all test compounds was confirmed to be >95% by absolute quantitative NMR spectroscopy (Supplementary Table S1).

General bisaryl urea synthesis

N,N'-carbonyldiimidazole (1.0 mmol) was added to a solution of substituted aniline (2.0 mmol) in anhydrous dichloromethane (DCM, 5 ml) under a nitrogen atmosphere. The solution was refluxed until TLC indicated complete consumption of the aniline (6-48 hours). The products were purified by one of the following methods:

Method A: The product formed a precipitate in the reaction mixture that was isolated by vacuum filtration and washed with DCM. Any unreacted aniline was then removed by trituration with 1M HCl (3 x 5 ml).

Method B: The reaction mixture was washed with brine, dried over $MgSO_4$ and concentrated under reduce pressure. The resulting solid was triturated with 1M HCl (3 x 5 ml).

Method C: The reaction mixture was washed with brine, dried over $MgSO_4$ and concentrated under reduced pressure. The crude solid was purified by dry column vacuum chromatography (DCVC) using gradient elution's of DCM/EtOAc (100:0 to 85:15).

N,N'-bis[3,4-bis(trifluoromethyl)phenyl]urea (1)

Purified by method B. Yield: 0.172 g, 32%; Melting point = 221-222°C. ^{1}H NMR: (500 MHz, DMSO-d_6) δ 9.76 (s, 2H), 8.22 (s, 2H), 7.95 (d, J = 8.5 Hz, 2H), 7.89 (d, J = 9 Hz, 2H). ^{13}C NMR: (125 MHz, DMSO-d_6) δ 152.1 (1C), 143.5 (2C), 129.5 (q, J = 6 Hz, 2C), 127.0 (q, J = 34 Hz, 2C), 123.1 (q, J = 271 Hz, 2C), 122.7 (q, J = 272 Hz, 2C), 118.8 (q, J = 33 Hz, 2C), 117.2 (q, J = 7 Hz, 2C). HRMS (ESI) *m/z* $[M+H]^+$ calcd for $C_{17}H_9F_{12}N_2O$ 485.0518, found 485.0512.

N,N'-bis[4-(trifluoromethylsulfonyl)phenyl]urea (2)

Purified by method B. Yield: 0.120 g, 25%; Melting point = 304-306°C. ^{1}H NMR: (500 MHz, DMSO-d_6) δ 9.91 (s, 2H), 8.06 (m, J = 9.0 Hz, 4H), 7.90 (m, J = 9.0, 2.5 Hz, 4H). ^{13}C NMR: (125 MHz, DMSO-d_6) δ 151.7 (1C), 147.7 (2C), 132.5 (4C), 120.8 (2C), 119.6 (q, J = 324 Hz, 2C), 118.9 (4C). HRMS (ESI) *m/z* $[M+H]^+$ calcd for $C_{15}H_{11}F_6N_2O_5S_2$ 477.0008, found 477.0002.

N,N'-bis[3-chloro-5-(trifluoromethyl)phenyl]urea (3)

Purified by method B. Yield: 0.273 g, 56%; Melting point = 210-211°C. ^{1}H NMR: (500 MHz, DMSO-d_6) δ 9.53 (s, 2H), 7.84 (s, 2H), 7.83 (s, 2H), 7.42 (s, 2H).^{13}C NMR: (125 MHz, DMSO-d_6) δ 152.2 (1C), 141.6 (2C), 134.2 (2C), 131.1 (q, J = 32 Hz, 2C), 123.3 (q, J = 271 Hz, 2C), 121.6 (2C), 118.3 (2C), 113.5 (q, J = 4 Hz, 2C). HRMS (ESI) *m/z* $[M+H]^+$ calcd for $C_{15}H_9Cl_2F_6N_2O$ 416.9991 , found 416.9985.

N,N'-bis[3,5-dichlorophenyl]urea (SR4)

Purified by method A. Yield: 0.190 g, 35%. ^{1}H and ^{13}C NMR, mp, and HRMS are in agreement with previously reported data.[103,111]

N,N'-bis[4(methylsulfonyl)phenyl]urea (5)

Purified by method A. Yield: 0.100 g, 20%, Melting point = 301-303°C. ^{1}H and ^{13}C NMR and HRMS are in agreement with previously reported data.[112]

N,N'-bis[4-chloro-3-(trifluoromethyl)phenyl]urea (6)

Purified by method B. Yield: 0.266 g, 41%; Melting point = 231-232°C. ^{1}H and ^{13}C NMR and HRMS are in agreement with previously reported data.[113]

N,N'-bis[4-(trifluoromethyl)phenyl]urea (7)

Purified by method C. Yield: 0.211 g, 43%. ^{1}H and ^{13}C NMR, mp, and HRMS are in agreement with previously reported data.[114]

N,N'-bis(4-acetylphenyl)urea (8)

Reaction volume was increased to 20 ml to accommodate for the low solubility of the **8** carbamoylimidazole intermediate. Purified by method A. Yield: 0.162 g, 33%. ^{1}H and ^{13}C NMR, mp, and HRMS are in agreement with previously reported data.[115]

N,N'-bis[4-(trifluoromethoxy)phenyl]urea (9)

Purified by method A. Yield: 0.191 g, 36%. ^{1}H and ^{13}C NMR, mp, and HRMS are in agreement with previously reported data.[116]

N,N'-bis[4-chlorophenyl]urea (10)

Purified by method A. Yield: 0.383 g, 70%, ^{1}H and ^{13}C NMR, mp, and HRMS are in agreement with previously reported data.[117]

N,N'-diphenylurea (11)

Purified by method A. Yield: 0.340 g, 60%, ^{1}H and ^{13}C NMR, mp, and HRMS are in agreement with previously reported data.[114]

N,N'-bis(3,4-dimethylphenyl)urea (12)

Purified by method A. Yield: 0.363 g, 65%; ^{1}H and ^{13}C NMR, mp, and HRMS are in agreement with previously reported data.[117]

N,N-bis(3,4-dimethylphenyl)urea (13)

Purified by method A. Yield: 0.212 g, 42%; ^{1}H and ^{13}C NMR, mp, and HRMS are in agreement with previously reported data.[118]

N,N-bis(4-methoxyphenyl)urea (14)

Purified by method A. Yield: 0.265 g, 48%, ^{1}H and ^{13}C NMR, mp, and HRMS are in agreement with previously reported data.[117]

Cell-based assays

General

Human MDA-MB-231 breast cancer cells were obtained from ATCC. Cells were cultures in Dulbecco's Modified Eagle Medium containing 10% (v/v) fetal bovine serum (Thermo Fischer Scientific) and 1% (v/v) penicillin/streptomycin (Sigma-Aldrich), referred to as complete media, and incubatedat 37°C in a humidified atmosphere of 5% CO_2. Confluent cells (80-90%) were harvested with trypsin/EDTA after washing in dulbecco's phosphate-buffered saline (dPBS, Sigma-Aldrich). Cells were treated with various concentrations of the test compounds in DMSO (final concentration 0.1% v/v); control cells were treated with DMSO alone.

JC-1

MDA-MB-231 cells were seeded in triplicate in black wall 96 well plates ($1.5x10^4$ cells per well) in complete media 24 h before treatment. Media was removed and cells were treated with various drug concentrations in complete media and incubated for one hour. Cells were incubated with JC-1 in media for 20 minutes, washed with dPBS and read using a Tecan Infinite M1000 Pro plate reader to evaluate red (535 nm) and green (595 nm) fluorescence using excitation wavelengths of 485 and 535 nm respectively (JC-1 Mitochondrial Membrane Potential Assay Kit; Cayman Chemical).

Seahorse Xfe24 Mito Stress Test

Mitochondrial function was measured by determining the oxygen consumption rate (OCR) of cells with a Seahorse XF24 extracellular flux analyser (Seahorse Bioscience) according to the manufacturer's protocol. MDA-MB-231 cells were seeded in Seahorse XF24 well cell culture microplates ($2.0x10^4$ cells per well) in complete media, allowed to adhere for three hours at room temperature and incubated overnight. Well media was replaced with 500 µL XF media (1 mM pyruvate, 2 mM glutamine and 10mM glucose Seahorse XF DMEM medium, pH 7.4 with 5 mM HEPES), placed in a non-CO_2 incubator (37ºC, humidified) for one hour, and then OCR was measured utilising an XF Cell Mito Stress Test Kit (Seahorse Bioscience, MA, USA). Oligomycin (final concentration 1 µM), FCCP (final concentration 0.5 µM) or test compounds (final concentration 5 µM or 10 µM), and rotenone/antimycin A (final concentrations 0.5 µM each) were added to the sensor cartridge, and the OCR was measured using a modified cycling program on Agilent Seahorse Wave Desktop software.

Intracellular ATP

MDA-MB-231 cells were seeded in triplicate in 96 well plates ($1.0x10^4$ cells per well) in complete media 24 h before treatment. At different timepoints, media was removed and cells were treated with test compounds (5 µM) and incubated for the duration of the experiment. Cells were incubated with CellTiter-Glo® 2.0 in complete media, mixed on an orbital shaker for two minutes, left at room temperature in dark conditions for 10 minutes and luminescence was read on a Tecan Infinite M1000 Pro plate reader (CellTiter-Glo® 2.0 Luminescent Cell Viability Assay).

LDH release

MDA-MB-231 cells well seeded in triplicate in 96 well plates ($1.0x10^4$ cells per well) in complete media 24 h before treatment. Media was removed and cells were treated with test compounds (5 µM) or vehicle control and incubated for 8 hours. Well media was homogenised gently, sampled, diluted in LDH storage buffer and stored at -20˚C, including wells containing vehicle control treated with 0.2% (v/v) Triton X-100 (Sigma-Aldrich) and incubated for 15 minutes prior to sampling to obtain a maximum LDH release value. Samples were thawed, incubated with LDH detection reagent

in a black wall plate at room temperature for one hour and luminescence was measured on a Tecan infinite M1000 Pro plate reader (LDH-Glo™ Cytotoxicity Assay, Promega).

MTS

MDA-MB-231 cells were seeded in triplicate in 96 well plates ($3.5x10^3$ cells per well) in complete media and incubated for 24 h before treatment. Media was removed and cells were treated with various drug concentrations in complete media and incubated for 72 hours. Cells were then incubated with CellTiter MTS 96® Aqueous MTS Reagent Powder (Promega) and phenazine ethosulfate (Sigma-Aldrich) in dark conditions for approximately three hours. Absorbance of each well at 490 nm was measured using Tecan Infinite M1000 Pro plate reader to evaluate cell viability (CellTiter 96® Aqueous Non-Radioactive Cell Proliferation Assay, Promega).

Statistical Analysis

All data are expressed throughout as means ± SEM from three independent experiments (N=3). Dose-response curves were constructed using log(inhibitor) vs response, variable slope (4 parameters) non-linear regressions on GraphPad Prism 8. Equation: *Y=Bottom* + (*Top-Bottom*)/(1+10^((Log*IC50-X*)**HillSlope*)). Absolute IC50 concentrations were interpolated from these normalised curves (data normalised to DMSO vehicle control) with the top constrained to 100%. ATP and Apoptosis data are expressed as mean percentage of time-matched DMSO control. (*) $P < 0.05$, (**) $P < 0.01$, (***) $P < 0.001$ versus time-matched control by two-way ANOVA with Dunnett's multiple comparison test. Seahorse data normalised to baseline OCR prior to oligomycin addition.

Supplementary Information

Supplementary Information available: This material is available free of charge via the internet at http://pubs.acs.org.

HPTS proton transport assay protocol, bisaryl urea absolute quantitative ^{1}H NMR purity determination, representative JC-1 / MTS dose-response curves, ATP assay data distribution, LDH release cytotoxicity assay, bisaryl urea ^{1}H and ^{13}C NMR spectra, HPTS dose-response and Hill Analyses

Acknowledgments

The author acknowledges H. Macdermott-Opeskin for his assistance in preparing the manuscript. D. McNaughton and P. Gale acknowledge and pay respect to the Gadigal people of the Eora Nation, the traditional owners of the land on which we research, teach, and collaborate at the University of Sydney. P. Gale thanks the University of Sydney and the Australian Research Council (DP200100453) for funding.

*Correspondence: Dr Tristan Rawling, School of Mathematical and Physical Sciences, Faculty of Science, University of Technology Sydney, Ultimo, NSW 2007, Australia. Tel: (61-2)-9514-7956, Email: Tristan.Rawling@uts.edu.au

Chapter Three: Expansion of Fatty Acid-Activated Proton Transporters to Squaramide, Amide and Diurea Anion Transport Motifs

Chapter Three Preamble

Demonstrating that bisaryl ureas mediate proton flux across the MIM by a fatty acid-activated proton transport mechanism challenges the perception that mitochondrial uncouplers must possess an acidic functional group. Based off this mechanistic insight and the promising activity of bisaryl urea **3**, I sought to assess the anticancer and mitochondrial activities of other bisaryl-based anion transporters by incorporating different anion binding motifs. Amide, squaramide and diurea binding groups were used, and the new scaffolds were substituted with lipophilic electron withdrawing groups, as these groups were key to bisaryl urea activity. Characterising the mitochondrial and anticancer actions of these compounds was a key aim of my thesis and resulted in the following chapter, which was published in the *MDPI Biomolecules* special issue 'Proton and Proton-Coupled Transport' and is entitled 'Fatty Acid-Activated Proton Transport by Bisaryl Anion Transporters Depolarises Mitochondria and Reduces the Viability of MDA-MB-231 Breast Cancer Cells'. For consistency the aromatic substitution patterns in this chapter follow the same numbering system as used in Chapter Two, but are prefixed with U, S, A, or D to denote the urea, squaramide, amide or diurea motif respectively.

Declaration of Authorship Contributions

The following chapter is an accepted manuscript published in *MDPI Biomolecules*. I, Edward York, was the principal investigator and author of this work with key contributions from Daniel A. McNaughton and Meryem-Nur Duman, with guidance from Philip A. Gale and Tristan Rawling. Daniel A. McNaughton performed the HPTS proton transport assays and Meryem-Nur Duman performed MTS assays on BEAS-2B lung epithelial cells (supplementary information). All other experimental data was collected by myself.

Certificate of Authorship

Author	Contribution (CRediT)	Signature
Edward York	Conceptualisation, methodology, investigation, formal analysis, validation, visualisation, writing – original draft, writing – review and editing	Production Note: Signature removed prior to publication.
Daniel A McNaughton	Methodology, investigation, formal analysis, validation, visualisation, writing-original draft	Production Note: Signature removed prior to publication.
Meyrem-Nur Duman	Investigation, validation	Production Note: Signature removed prior to publication.
Philip A Gale	Methodology, supervision, writing – review and editing	Production Note: Signature removed prior to publication.
Tristan Rawling	Conceptualisation, methodology, supervision, writing - review and editing	Production Note: Signature removed prior to publication.

biomolecules

MDPI

Article

Fatty Acid-Activated Proton Transport by Bisaryl Anion Transporters Depolarises Mitochondria and Reduces the Viability of MDA-MB-231 Breast Cancer Cells

Edward York,[a] Daniel A. McNaughton,[a,b] Meryem-Nur Duman, [a] Philip A. Gale[a,b,c] and Tristan Rawling [a]

[a] School of Mathematical and Physical Sciences, Faculty of Science, University of Technology Sydney, Sydney, NSW 2007, Australia ;
[b] School of Chemistry, The University of Sydney, Sydney, NSW 2006, Australia ;
[c] The University of Sydney Nano Institute (SydneyNano), The University of Sydney, Sydney, NSW 2006, Australia;

Abstract: In respiring mitochondria, the proton gradient across the inner mitochondrial membrane is used to drive ATP production. Mitochondrial uncouplers, which are typically weak acid protonophores, can disrupt this process to induce mitochondrial dysfunction and apoptosis in cancer cells. We have shown that bisaryl urea-based anion transporters can also mediate mitochondrial uncoupling through a novel fatty acid-activated proton transport mechanism, where the bisaryl urea promotes the transbilayer movement of deprotonated fatty acids and proton transport. In this paper, we investigated the impact of replacing the urea group with squaramide, amide and diurea anion binding motifs. Bisaryl squaramides were found to depolarise mitochondria and reduce MDA-MB-231 breast cancer cell viability to similar extents as their urea counterpart. Bisaryl amides and diureas were less active and required higher concentrations to produce these effects. For all scaffolds, the substitution of the bisaryl rings with lipophilic electron-withdrawing groups was required for activity. An investigation of the proton transport mechanism in vesicles showed that active compounds participate in fatty acid-activated proton transport, except for a squaramide analogue, which was sufficiently acidic to act as a classical protonophore and transport protons in the absence of free fatty acids.

Introduction

Targeting mitochondria is a promising approach to the development of new anticancer agents, as cancer cell mitochondria are structurally and functionally distinct from those in noncancerous cells, and because mitochondria play pivotal roles in cellular metabolism and cell survival.[47,100] Importantly, mitochondria use nutrients to synthesise ATP via oxidative phosphorylation (OXPHOS), where nutrient oxidation feeds electrons into the electron transport chain (ETC), a series of proteins embedded in the inner mitochondrial membrane (MIM). Electron flow through the ETC pumps protons from the mitochondrial matrix into the intermembrane space, generating a proton gradient across the MIM. The resulting membrane potential ($\Delta\Psi_M$) is used to drive protons back into the matrix through ATP synthase, which converts ADP to ATP.[2,5] Nutrient oxidation is therefore coupled to ATP synthesis by the proton gradient across the MIM. Mitochondrial uncouplers are compounds that disrupt OXPHOS by inducing proton leakage across the MIM, creating a futile cycle of energy expenditure that diminishes the $\Delta\Psi_m$ and ATP synthesis.[10] The most common uncouplers are lipophilic weak acids, such as 2,4-dinitrophenol (DNP), which transport protons across the MIM via a protonophoric cycle that involves the direct protonation and deprotonation of the acidic group. A growing body of evidence indicates that mitochondrial uncouplers can selectively kill cancer cells,[77,119,120] which has focused attention on their potential use as new anticancer agents.[100]

While most protonophores are weak acids, we have recently shown that synthetic anion transporters can also facilitate the movement of protons across lipid bilayers via a fatty acid-activated mechanism.[104] Anion transporters possess an anion binding motif that can form reversible intermolecular interactions with various anions, producing a lipophilic complex that facilities the passive transport of the anion across lipid bilayers.[89] Anion transporters promote transbilayer proton movement by interacting with free fatty acids within the membrane (see Figure 13).[104] In the first step, the anionic form of the fatty acid accepts a proton from the relatively acidic solution and permeates the membrane as a neutral species. The fatty acid is deprotonated in the relatively alkaline solution, resulting in the transport of one proton and the regeneration of the membrane-impermeable carboxylate

species. Next, the anion transporter binds to the carboxylate group through parallel hydrogen bonds to produce a lipophilic complex that is capable of diffusing through the bilayer. The dissociation of the complex is followed by the protonation of the fatty acid and further proton transport cycles.

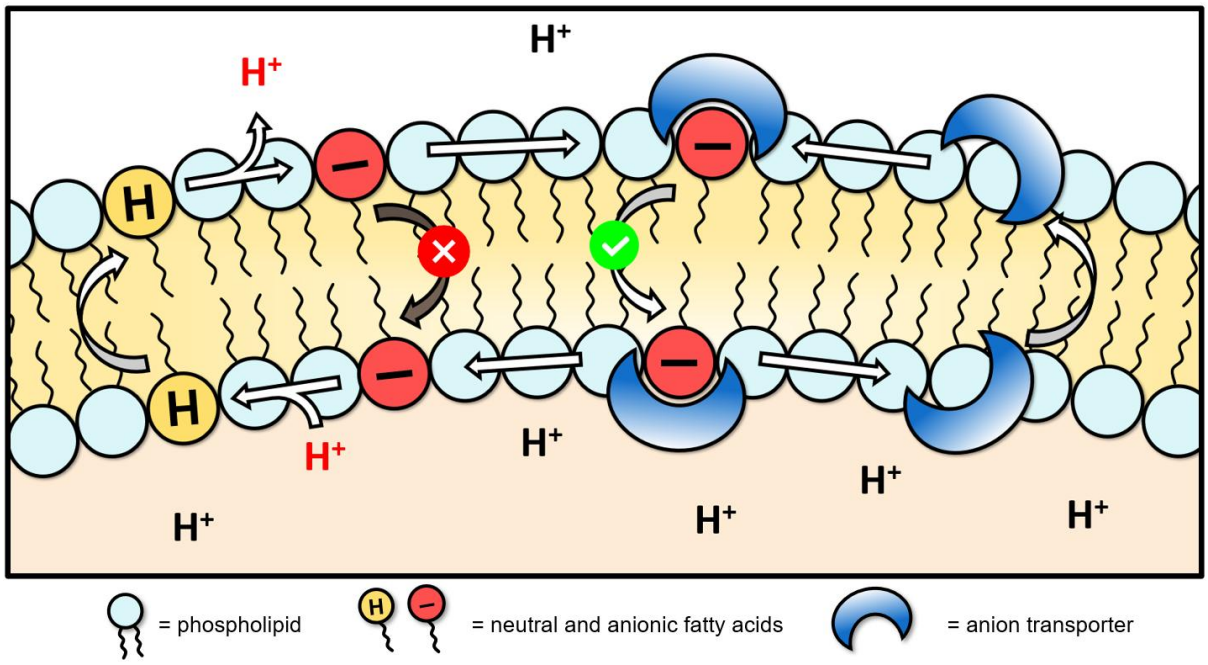

Figure 13. Fatty acid-activated proton transport mechanism via anion transporters in large unilamellar vesicles.[104] The anion transporter binds fatty acid carboxylates, masking their anionic charge to facilitate fatty acid flip-flop and proton transport across the membrane.

The discovery of the fatty acid-activated proton transport mechanism was made using large unilamellar vesicles (LUVs), and we subsequently showed that the same mechanism can operate in the mitochondria of intact cells[121] by utilising free fatty acids that are present in the MIM.[98,122] Thus, the treatment of MDA-MB-231 breast cancer cells with bisaryl urea-based synthetic anion transporters collapsed the proton gradient across the MIM and uncoupled OXPHOS, leading to a loss of cell viability.[121] The substitution of the bisaryl urea scaffold with lipophilic electron-withdrawing groups enhanced electrogenic proton transport using the fatty acid-activated mechanism, as well as the mitochondrial and cellular effects.[121] This structure–activity relationship (SAR) aligns with the proposed transport mechanism as electron-withdrawing groups increase the urea N-H hydrogen bond donor

strength and complexation with fatty acid anions, and lipophilic groups enhance the membrane permeability of the resulting complex.

In this paper we replaced the anion binding motif in the bisaryl urea scaffold with squaramide,[114,123] amide and diurea[124] groups (Figure 14) and studied the proton transport and mitochondrial uncoupling activities of these compounds. Bisaryl amides and diureas substituted with lipophilic electron-withdrawing groups showed enhanced proton transport by the fatty acid-activated mechanism, consistent with the established SAR. Bisaryl squaramides bearing these groups also show enhanced proton transport, but participated as both anion transporters and as classical protonophores, presumably due to the higher acidity of the squaramide motif. The analogues with the greatest proton transport activity uncoupled mitochondria, disrupting OXPHOS and reducing cell viability in MDA-MB-231 breast cancer cells.

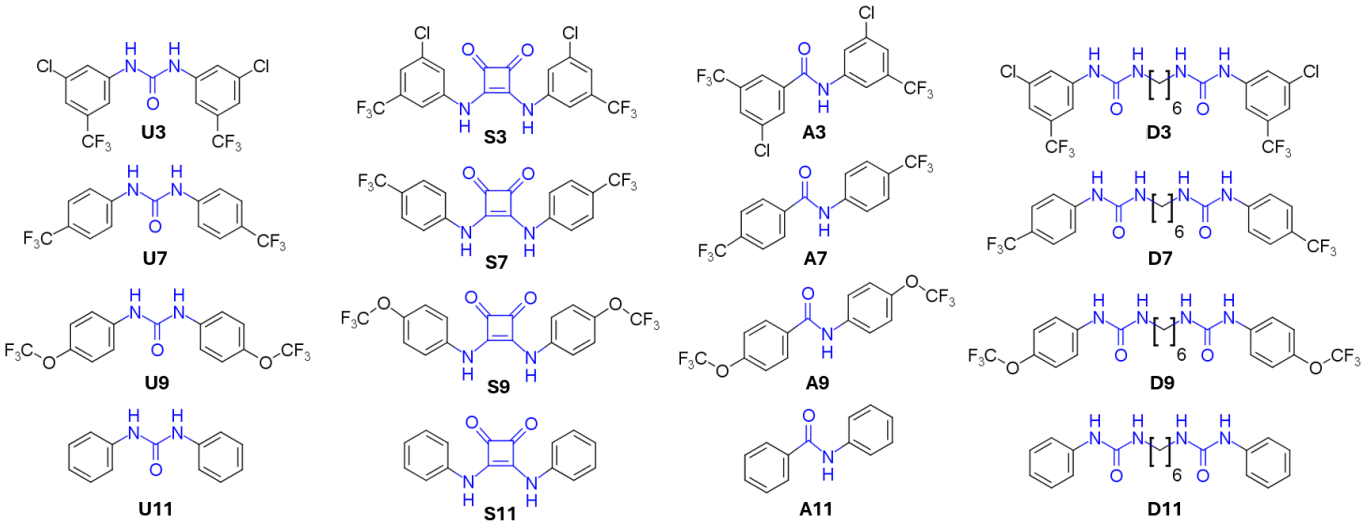

Figure 14. Chemical structures of bisaryl urea, squaramide, amide and diurea anion transporters studied in this work.

2. Materials and Methods

2.1. Chemistry

U3–**11** were synthesised by the procedure in the literature.[121] 3-Chloro-5-(trifluoromethyl)benzoic acid, 4-(trifluoromethoxy)benzoic acid, 3,4-diethoxycyclobut-3-ene-1,2-dione and COMU were purchased from Fluorochem Limited (Hadfield, UK). The remaining reagents were purchased from

Merck (Darmstadt, Germany). Reactions were monitored using TLC on Merck silica gel 60 F_{254} aluminium-backed plates. Reaction products were purified as required with dry column vacuum chromatography on silica gel using gradient elutions. NMR spectra were recorded using a Bruker 400 MHz and an Agilent 500 MHz NMR spectrometer, at operating frequencies of 400 and 500 MHz for ^{1}H and 100 and 125 MHz for ^{13}C spectra, respectively. Spectra were referenced internally to the residual solvent ($CDCl_3$: ^{1}H δ 7.26, ^{13}C δ 77.16. DMSO-d_6: ^{1}H δ 2.50, ^{13}C δ 39.52. CD_3OD: ^{1}H δ 3.31, ^{13}C δ 49.00). Multiplicity was assigned as *s* (singlet), *d* (doublet), *t* (triplet), *q* (quartet), *qu* (quintet) and *m* (multiplet). High resolution mass spectra (HRMS) were recorded on an Agilent Technologies 6510 Q-TOF LCMS. The purity of all test compounds was confirmed to be >95% using absolute quantitative NMR spectroscopy (Supplementary Information, Table S2).[125]

2.1.1. General Procedure for the Synthesis of Bisaryl Squaramides

To a solution of an appropriately substituted aniline (0.338 g, 2.1 mmol, 2.1 equiv.) in 2 mL 19:1 toluene:dimethyl formamide (DMF) was added the diethyl squarate ester (3,4-diethoxycyclobut-3-ene-1,2-dione, 0.170 g, 1.0 mmol, 1 equiv.) and zinc triflate (0.073 g, 0.2 mmol, 0.2 equiv.), and the resultant mixture was stirred for 18 h at 100 °C in a 10 mL sealed pressure tube. The desired squaramide products were found to precipitate out of the solution upon formation. The reaction mixture was pelleted via centrifugation and the supernatant was discarded, and then the crude solid was washed with 5 × 5 mL methanol using successive resuspension and centrifugation to give the desired products as white/yellow solids.

2.1.2. General Procedure for the Synthesis of Bisaryl Amides

To a mixture of COMU ((1-cyano-2-ethoxy-2-oxoethylidenaminooxy)dimethylamino morpholino-carbenium hexafluorophosphate, 1.028 g, 2.4 mmol, 1.2 equiv.), triethylamine (0.405 g, 4.0 mmol, 2 equiv.) and an appropriately substituted benzoic acid (0.449 g, 2.0 mmol, 1.0 equiv.) in 5 mL DMF was added the corresponding substituted aniline (0.430 g, 2.2 mmol, 1.1 equiv.), and it was stirred for 24 h at room temperature under nitrogen. The resultant reaction mixtures were diluted ten-

fold with water, extracted with 3 × 20 mL ethyl acetate and then washed with 3 × 20 mL of 1M hydrochloric acid followed by 3 × 20 mL saturated sodium bicarbonate. Crude solids were isolated with rotary evaporation and then purified via dry column vacuum chromatography (DCVC) using a gradient elution of Hexane/EtOAc (100:0 to 70:30).

2.1.3. General Procedure for the Synthesis of Bisaryl Diureas

N,N'-Carbonyldiimidazole (1.14 g, 7 mmol, 1.4 equiv.) was added to a solution of an appropriately substituted aniline (0.466 g, 5 mmol, 1.0 equiv.) in anhydrous 1,2-dichloroethane (EDC, 7 mL) under N_2. After stirring for 18 h, the resulting suspension was cooled on ice for 1 h, then filtered and washed with 1,2-dichloroethane to give the *N*-carbamoyl imidazole intermediate as a white solid. Next, the *N*-carbamoyl imidazole (0.562 g, 3.0 mmol, 3 equiv.) was resuspended in dichloromethane, hexamethylene diamine (0.116 g, 1 mmol, 1 equiv.) was added and it was stirred at room temperature for 18 h. The resultant suspension was filtered, and the solid obtained was washed with 10 mL dichloromethane. Residual aniline and the bisaryl urea byproduct were removed as required by trituration with 2 × 10 mL ethyl acetate.

Bis({[3-chloro-5-(trifluoromethyl)phenyl]amino})cyclobut-3-ene-1,2-dione (**S3**). ^{1}H NMR (500 MHz, CD_3OD) δ 7.78 (s, 2H), 7.71 (s, 2H), 7.37 (s, 2H). ^{13}C NMR (125 MHz, CD_3OD) δ 184.2 (2C), 167.2 (2C), 142.2 (2C), 137.1 (2C), 134.1 (q, J = 33 Hz, 2C), 124.5 (q, J = 271 Hz, 2C), 123.2 (2C), 121.0 (2C), 115.1 (q, J = 4 Hz, 2C). HRMS (ESI): m/z $[M + H]^+$ calculated for $C_{18}H_8Cl_2F_6N_2O_2$: 468.9940, found: 468.9937.

Bis({[4-(trifluoromethyl)phenyl]amino})cyclobut-3-ene-1,2-dione (**S7**). 1H and 13C NMR and HRMS are in agreement with previously reported data.[114,126]

Bis({[4-(trifluoromethoxy)phenyl]amino})cyclobut-3-ene-1,2-dione (**S9**). ^{1}H NMR (500 MHz, DMSO-d_6) δ 10.5 (br s, 2H), 7.59 (d, J = 8.5 Hz, 4H), 7.35 (d, J = 8 Hz, 4H) ^{13}C NMR (125 MHz, DMSO-d_6) δ 181.7 (2C), 165.7 (2C), 143.8 (2C), 137.9 (2C), 122.2 (4C), 120.1 (q, J = 255 Hz, 2H), 120.0 (4C). HRMS (ESI): m/z $[M + H]^+$ calculated for $C_{18}H_{10}F_6N_2O_4$: 433.0618, found: 433.0623.

Bis(phenylamino)cyclobut-3-ene-1,2-dione (**S11**). ^{1}H and ^{13}C NMR are in agreement with previously reported data.[114] HRMS (ESI): *m*/*z* $[M + H]^+$ calculated for $C_{16}H_{12}N_2O_2$: 265.0972, found: 265.0958.

3-Chloro-N-[3-chloro-5-(trifluoromethyl)phenyl]-5-(trifluoromethyl)benzamide (**A3**). ^{1}H NMR (500 MHz, $CDCl_3$) δ 8.10 (br s, 1H), 8.04 (s, 1H), 7.99 (s, 1H), 7.98 (s, 1H), 7.82 (s, 1H), 7.77 (s, 1H), 7.43 (s, 1H). ^{13}C NMR (125 MHz, $CDCl_3$) δ 163.1 (1C), 138.8 (1C), 136.5 (1C), 136.1 (1C), 135.8 (1C), 133.1 (q, *J* = 34 Hz, 1C), 132.8 (q, *J* = 33 Hz, 1C), 130.8 (1C), 129.3 (q, *J* = 4 Hz, 1C), 123.47 (1C), 123.46 (1C), 122.9 (q, *J* = 271 Hz, 1C), 122.7 (q, *J* = 272 Hz, 1C), 122.1 (m, 2C), 115.3 (q, *J* = 4 Hz, 1C). HRMS (ESI): *m*/*z* $[M + H]^+$ calculated for $C_{15}H_7Cl_2F_6NO$: 401.9882 found: 401.9883.

4-(Trifluoromethyl)-N-[4-(trifluoromethyl)phenyl]benzamide (**A7**). ^{1}H and ^{13}C NMR and HRMS are in agreement with previously reported data.[127]

4-(Trifluoromethoxy)-N-[4-(trifluoromethoxy)phenyl]benzamide (**A9**). ^{1}H NMR (500 MHz, DMSO-d_6) δ 10.53 (s, 1H), 8.08 (AA'BB', 2H), 7.88 (AA'BB', 2H), 7.54 (d, *J* = 9 Hz, 2H), 7.38 (d, *J* = 9 Hz, 2H). ^{13}C NMR (125 MHz, DMSO-d_6) δ 164.5 (1C), 151.9 (1C), 145.7 (1C), 136.2 (1C), 132.9 (1C), 129.0 (2C), 121.9 (2C), 121.5 (2C), 120.8 (2C), 120.4 (q, *J* = 256 Hz, 1C), 120.3 (q, *J* = 257 Hz, 1C). HRMS (ESI): *m*/*z* $[M + H]^+$ calculated for $C_{15}H_9F_6NO_3$: 366.0559 found: 366.0562.

N-Phenylbenzamide (**A11**). ^{1}H and ^{13}C NMR and HRMS are in agreement with previously reported data [19].

3-[3-Chloro-5-(trifluoromethyl)phenyl]-1-[6-({[3-chloro-5-(trifluoromethyl)phenyl]carbamoyl}camino)hexyl]urea (**D3**). ^{1}H NMR (400 MHz, DMSO-d_6) δ 8.97 (s, 2H), 7.76 (s, 2H), 7.75 (s, 2H), 7.27 (s, 2H), 6.40 (t, *J* = 5.6 Hz, 2H), 3.08 (q, *J* = 6.2 Hz, 4H), 1.44 (m, 4H), 1.29 (m, 4H). ^{13}C NMR (100 MHz, DMSO-d_6) δ 154.7 (2C), 143.0 (2C), 134.1 (2C), 130.9 (q, *J* = 32 Hz, 2C), 123.4 (q, *J* = 271 Hz, 2C), 120.3 (2C), 116.7 (2C), 112.3 (2C), 39.1 (2C), 29.6 (2C), 26.1 (2C). HRMS (ESI): *m*/*z* $[M - H]^-$ calculated for $C_{22}H_{22}Cl_2F_6N_4O_2$: 557.0953 found: 557.0953.

3-[4-(Trifluoromethyl)phenyl]-1-[6-({[4-(trifluoromethyl)phenyl]carbamoyl}amino)hexyl]urea (**D7**). ^{1}H NMR (400 MHz, DMSO-d_6) δ 8.86 (s, 2H), 7.58 (d, *J* = 8.9 Hz, 4H), 7.54 (d, *J* = 8.9 Hz,

4H), 6.30 (t, *J* = 5.5 Hz, 2H), 3.09 (q, *J* = 6.6 Hz, 4H), 1.43 (m, 4H), 1.31 (m, 4H). ^{13}C NMR (100 MHz, DMSO-d_6) δ 154.8 (2C), 144.3 (2C), 125.9 (2C), 124.7 (q, *J* = 269 Hz, 2C), 120.8 (q, *J* = 32 Hz, 2C), 117.1 (2C), 39.0 (2C), 29.6 (2C), 26.1 (2C). HRMS (ESI): *m*/*z* [M − H]$^-$ calculated for $C_{22}H_{24}F_6N_4O_2$: 489.1732 found: 489.1727.

3-[4-(Trifluoromethoxy)phenyl]-1-[6-({[4-(trifluoromethoxy)phenyl]carbamoyl}amino)hexyl]urea (**D9**). ^{1}H NMR (400 MHz, DMSO-d_6) δ 8.60 (s, 2H), 7.47 (d, *J* = 9.2 Hz, 4H), 7.19 (d, *J* = 8.4 Hz, 4H), 6.18 (t, *J* = 5.6 Hz, 2H), 3.07 (q, *J* = 6.7 Hz, 4H), 1.43 (m, 4H), 1.30 (m, 4H). ^{13}C NMR (100 MHz, DMSO-d_6) δ 155.2 (2C), 142.0 (2C), 140.0 (2C), 121.6 (2C), 120.3 (q, *J* = 254 Hz, 2C), 118.7 (2C), 39.1 (2C), 29.7 (2C), 26.2 (2C). HRMS (ESI): *m*/*z* [M − H]$^-$ calculated for $C_{22}H_{24}F_6N_4O_4$: 521.1629 found: 521.1630.

3-Phenyl-1-{6-[(phenylcarbamoyl)amino]hexyl}urea (**D11**). 1H and 13C NMR and HRMS are in agreement with previously reported data.[128]

2.2. Biology

2.2.1. Cell Lines and Culture Conditions

Human MDA-MB-231 breast cancer cells and BEAS-2B lung epithelial cells (ATCC) were cultured in Dulbecco's Modified Eagle Medium containing 1% (*v*/*v*) penicillin/streptomycin (Merck) and 10% (*v*/*v*) foetal bovine serum (Thermo Fisher Scientific), referred to as complete media. Cells were cultured at 37 °C in a humidified atmosphere of 5% CO_2 and harvested at 80-90% confluency using trypsin/EDTA after washing with Dulbecco's phosphate-buffered saline (dPBS, Merck). Test compounds were administered to cells using a DMSO vehicle (final concentration 0.1% *v*/*v*) and were compared against cells treated with DMSO alone (vehicle-only control).

2.2.2. MTS Cell Viability Assay

Cell viability following 72 h drug treatment was assayed by measuring the conversion of MTS (3-(4,5-dimethylthiazol-2-yl)-5-(3-carboxymethoxyphenyl)-2-(4-sulfophenyl)-2H-tetrazolium) to

formazan via dehydrogenase enzymes in metabolically active cells. In a 96-well plate, cells were seeded in triplicate in complete media at a density of 3.5×10^3 cells per well and incubated for 24 h. Well media were removed and replaced with complete media containing various drug concentrations and incubated for 72 h. Cells were then incubated with CellTiter MTS 96 Aqueous MTS Reagent Powder (Promega) and phenazine ethosulfate (Merck) under dark conditions for approximately 3 h. The absorbance of each well at 490 nm was measured using a Tecan Infinite M1000 Pro plate reader to evaluate cell viability (CellTiter 96 Aqueous Non-Radioactive Cell Proliferation Assay, Promega).

2.2.3. JC-1 Mitochondrial Membrane Potential Assay

The ability of the test compounds to depolarise the inner mitochondrial membrane was measured using the JC-1 assay. MDA-MB-231 cells were seeded in triplicate in black wall 96-well plates (1.5×10^4 cells per well) in complete media 24 h before treatment. Media were removed and cells were treated with various drug concentrations in complete media and incubated for one hour. Cells were incubated with JC-1 in media for 20 min, washed with dPBS and read using a Tecan Infinite M1000 Pro plate reader to evaluate red (535 nm) and green (595 nm) fluorescence using excitation wavelengths of 485 and 535 nm, respectively (JC-1 Mitochondrial Membrane Potential Assay Kit; Cayman Chemical).

2.2.4. Seahorse XFe24 Analyser Assay

Mitochondrial function was measured by determining the oxygen consumption rate (OCR) and extracellular acidification rate (ECAR) of cells with a Seahorse XFe24 extracellular flux analyser (Seahorse Bioscience) according to the manufacturer's protocol. MDA-MB-231 cells were seeded in Seahorse XF24 well cell culture microplates (2.0×10^4 cells per well) in complete media, allowed to adhere for 3 h at room temperature, and incubated overnight. Wells were washed and media were replaced with 500 µL of XF media (1 mM pyruvate, 2 mM glutamine, and 10 mM glucose Seahorse XF DMEM, pH 7.4 with 5 mM HEPES) and placed in a non-CO_2 incubator (37 °C, humidified) for 1 h, and then the OCR was measured utilizing an XF Cell Mito Stress Test kit (Seahorse Bioscience,

MA, USA). Following sensor calibration and baseline measurements, test compounds were added and changes to the oxygen consumption rate (OCR) and extracellular acidification rate (ECAR) were monitored using a modified cycling program on Agilent Seahorse Wave Desktop software.

2.2.5. Statistical Analysis

All IC_{50} concentration values are expressed as means ± SEM from three independent experiments (N = 3). Data were normalised to the DMSO vehicle control, and dose−response curves were constructed on GraphPad Prism 8 using log(inhibitor) versus response, variable slope (four parameters) nonlinear regressions. Equation: Y = Bottom + (Top−Bottom)/(1 + 100[(Log IC50-X)*HillSlope)]. Absolute IC_{50} concentrations were then interpolated from these normalised curves, and the top constrained to 100%. Seahorse measurements were normalised to the OCR/ECAR of DMSO vehicle wells prior to the test compound addition.

3. Results and Discussion

3.1. Compound Library Design and Synthesis

Bisaryl ureas are comprised of a urea anion binding group covalently attached to two substituted aromatic rings. To investigate the capacity of alternative anion binding motifs to function as fatty acid-activated mitochondrial uncouplers, we designed a library of bisaryl squaramide (**S3**–**11**), amide (**A3**–**11**), and diurea (**D3**–**11**) transporters bearing various aromatic substituents (Figure 14) and compared their activities to their previously reported[121] urea counterparts, **U3**–**11**. Amides and squaramides are well-known anion binding groups that have previously been used in anion transporters.[124,129,130] Squaramides typically have stronger anion affinity than amides, as squaramides can form two convergent hydrogen bonds to host anions via their N-H groups, and have been explored using a variety of scaffolds.[131] Diureas **D3**–**11** were included as multi-armed anion transporters and can have superior anion transport to their mono-derivatives.[89] All bisaryl anion transporters were prepared as unsubstituted analogues (series **11**), and bearing lipophilic electron-withdrawing substituents, which we have previously shown to enhance fatty acid-activated proton transport and the cytotoxicity of

bisaryl ureas.[121] Three different substitution patterns were included, based on electron-withdrawing strength (determined from their Hammet's substituent constants, σ_{total}).[106] These included 3-chloro 5-trifluoromethyl- (series **3**, $\sigma_{total} = 0.80$), 4-trifluoromethyl- (series **7**, $\sigma_{total} = 0.54$) and 4-trifluoromethoxy- (series **9**, $\sigma_{total} = 0.35$) substitution.

The synthesis of the compound library is shown in Scheme 1. Bisaryl squaramides **S3**–**11** were prepared via Lewis-acid-promoted condensation reactions of appropriately substituted anilines with squarate esters. A $Zn(OTf)_2$ Lewis acid catalyst was preferred to minimise the formation of unwanted squaramide monoester and squaraine side products[132] and the squaramide products precipitated from the reaction mixture and isolated by filtration. Bisaryl amides **A3**–**11** were synthesised by COMU-based coupling reactions of the corresponding substituted anilines and benzoic acids with two equivalents of triethylamine.[133] Bisaryl diurea derivatives **D3**–**11** were synthesised by first reacting appropriately substituted anilines with *N,N*-carbonyldiimidazole (CDI) to give the corresponding *N*-carbamoylimidazoles, which were then reacted with hexamethylenediamine to give the disubstituted product.

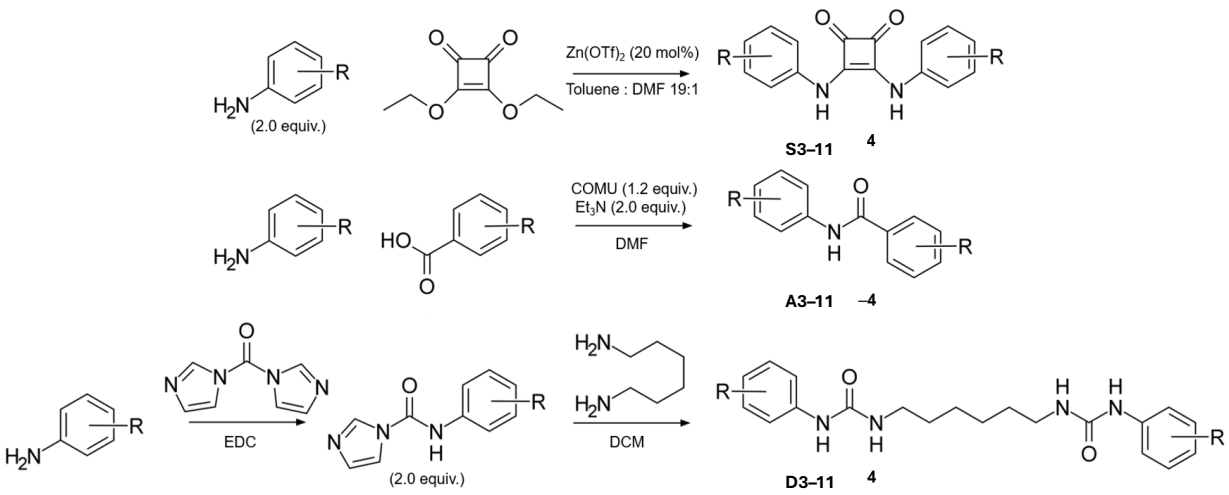

Scheme 1. Synthesis of bisaryl squaramide (S3–11), amide (A3–11) and diurea (D3–11) anion transporters.

3.2. Bisaryl Anion Transporter Effects in MDA-MB-231 Cells

We first determined the ability of the bisaryl anion transporters to reduce the viability of MDA-MB-231 cells using the MTS assay (Table 4 and Figure S67). The urea-based anion transporters were the most active in the series, with **U3** and **U7** reducing MDA-MB-231 cell viability with IC_{50} concentrations below 1 μM. The corresponding squaramides **S3** and **S7** were the next most active, and reduced cell viability with IC_{50} concentrations of 4.15 ± 1.4 and 7.28 ± 0.9 μM, respectively. Within the diurea and amide series, only the di-substituted analogues **D3** and **A3** affected cell viability, although **A3** lacked sufficient activity and solubility to produce an IC_{50} concentration. Neither **D7** nor **A7** had an impact on cell viability. The MTS data also indicated that substitution with electron-withdrawing groups was required, as no unsubstituted anion transporters (series **11**) had an effect on cell viability, while those bearing the strongest electron-withdrawing substituents (series **3**) were the most active. It was also found that the MTS activity decreased as the electron-withdrawing capacity of the substituents decreased. For example, **U9** ($\sigma_{total} = 0.35$) failed to reduce cell viability to below 50% at 100 μM, while **U3** and **U7** ($\sigma_{total} > 0.54$) reduced MDA-MB-231 cell viability with IC_{50} concentrations below 1 μM. The exception to this trend was **A3**, which was the most active in the amide series, although it contains relatively weakly electron-withdrawing trifluoromethoxy substituents (series **3** substitution). It is noteworthy that **A3** did not affect mitochondrial polarisation (as reflected by the JC-1 assay), as this suggests that **A3** reduces cell viability via a different mechanism that does not involve mitochondrial targeting.

To confirm that the MTS data reflected reductions in the number of viable cells, phase contrast images of MDA-MB-231 cells treated with the active compounds **U3**, **U7**, **S3**, **S7**, **A9** and **D3** at their IC_{50} concentrations were recorded (Figure S68 in the Supplementary Material). Vehicle (DMSO) control cells and cells treated with the inactive compound **U11** were included for comparison. The images revealed that the MTS active compounds (but not inactive **U11**) reduced the number of cells and altered their morphology compared to control, which is consistent with the MTS data. We also assessed the antiproliferative activity of **U3**, **U7**, **S3**, **S7**, **A9** and **D3** against BEAS-2B lung epithelial

cells in MTS assays to obtain an indication of the selectivity of these compounds towards cancer cells. As shown in Figure S69 of the Supplementary Material, **U3**, **U7** and **S3** preferentially reduced MDA-MB-231 cell viability, while **A9** had no effect on BEAS-2B cells. In contrast, diurea **D3** and squaramide **S7** had similar effects on the viability of both cell lines.

Table 4. Chemical structures, MTS (72 h) and JC-1 (1 h) IC_{50} concentrations measured in MDA-MB-231 breast cancer cells.

		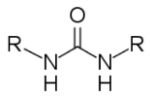 **U3–11**		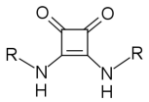 **S3–11**		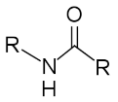 **A3–11**		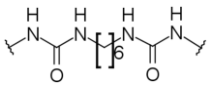 **D3–11**	
Substitution Pattern	**R**	**IC_{50} (µM)**		**IC_{50} (µM)**		**IC_{50} (µM)**		**IC_{50} (µM)**	
		MTS	**JC-1**	**MTS**	**JC-1**	**MTS**	**JC-1**	**MTS**	**JC-1**
Series 3	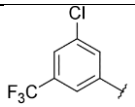	0.37 ± 0.1	0.26 ± 0.1	4.15 ± 1.4	1.73 ± 0.1	>20 [a]	7.30 ± 1.0	10.5 ± 1.1	8.1 ± 1.2
Series 7	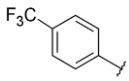	0.84 ± 0.1	2.26 ± 0.4	7.28 ± 0.9	3.34 ± 0.9	- [b]	19.7 ± 5.9	- [b]	>50 [a]
Series 9	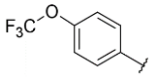	>100 [a]	>100 [a]	- [b]	- [b]	5.64 ± 1.1	- [b]	- [b]	>50 [a]
Series 11		- [b]	>100 [a]	- [b]	- [b]	- [b]	- [b]	- [b]	>100 [a]

[a] Produced moderate activity at maximum test concentration but insufficient for absolute IC_{50} determination. [b] No significant activity observed at the maximum test concentration.

We next assessed the capacity of the analogues to transport protons across the MIM and depolarise mitochondria in MDA-MB-231 cells using JC-1 assays. JC-1 is a cationic, fluorescent dye that partitions between the mitochondrial matrix and the cytosol according to the $\Delta\Psi_M$. In polarised mitochondria with high $\Delta\Psi_M$, JC-1 forms aggregates in the matrix that fluoresce red. When mitochondrial depolarisation occurs, JC-1 is released into the cytosol and disaggregates into monomers that fluoresce green. Thus, the JC-1 red/green fluorescence ratio reflects the proton gradient across the MIM. JC-1 IC_{50} concentrations were determined for the bisaryl analogues from dose–response curves

(Figure S70), which were defined as the concentration required to shift the red/green fluorescence ratio by 50% of the control (Table 4). Cells were treated for one hour to discriminate between direct mitochondrial uncoupling activity and the mitochondrial depolarisation that occurs during apoptosis. Similar to the trends observed from the MTS data, the urea-based **U3** was the most active (IC_{50} = 0.26 ± 0.1) anion transporter with series **3** substitution, followed by squaramide **S3** (IC_{50} = 1.73 ± 0.1), and then the amide and diurea analogues **A3** and **D3**. The dependence on electron-withdrawing substituents for activity was also observed, as JC-1 IC_{50} concentrations tended to increase moving from series **3** to series **7** to series **9** substitution patterns, with all unsubstituted analogues (series **11**) lacking sufficient JC-1 activity to determine IC_{50} concentrations. The broad similarities between the observed MTS and JC-1 data indicate that the active anion transporters depolarise mitochondria, which leads to a loss of cell viability. This finding is consistent with previous studies, which have shown that the collapse of the proton gradient across the MIM by mitochondrial uncouplers leads to cancer cell death.[100,121,131]

To further investigate the mitochondrial actions of the anion transporters, we measured the capacity of series **3** (3-Cl 5-CF_3) and **11** (unsubstituted) analogues to increase the oxygen consumption rate (OCR) and extracellular acidification rate (ECAR) of MDA-MB-231 cells using a seahorse analyser (see Figure 14). Proton transport across the MIM by mitochondrial uncouplers reduces OXPHOS efficiency, leading to an increase in oxygen consumption and a shift to glycolysis (proportional to ECAR) to meet energy demands.[77] Anion transporters that were JC-1 active were anticipated to produce the same metabolic shifts, and were tested at concentrations two-fold higher than their JC-1 IC_{50} concentrations.

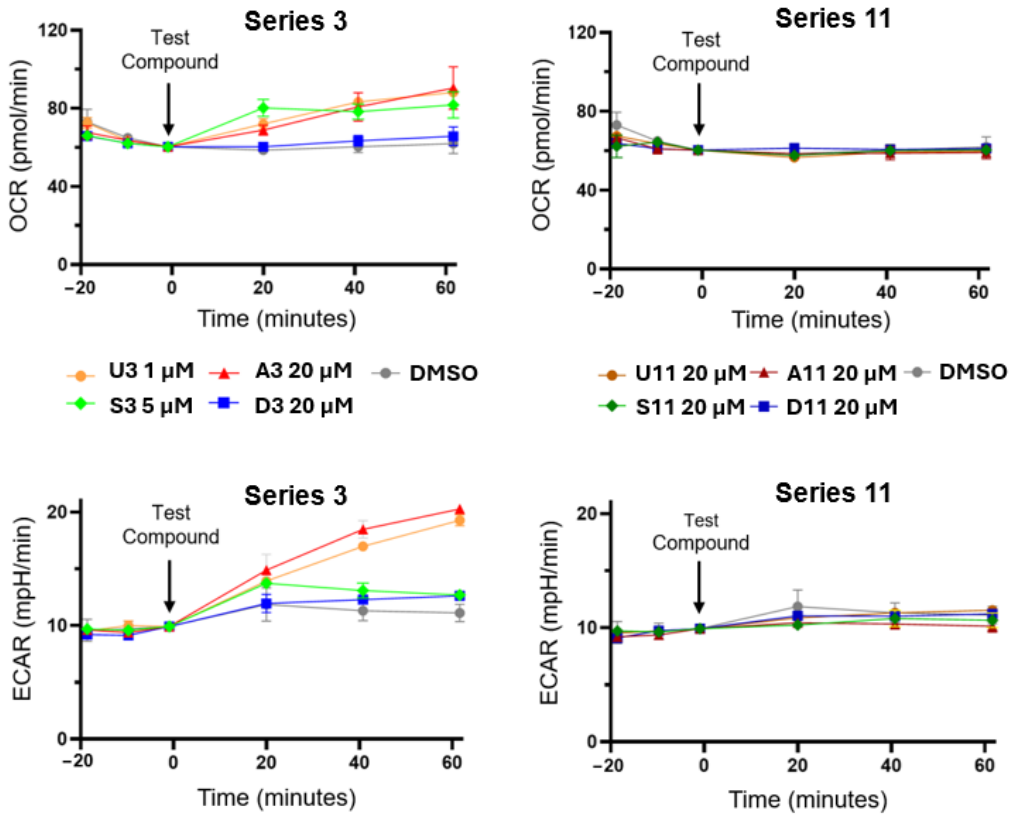

Figure 15. OCR and ECAR in MDA-MB-231 cells treated with series **3** and **11** test compounds as measured using a Seahorse XFe24 flux analyser. Measurements normalised to the OCR and ECAR of DMSO vehicle wells prior to test compound addition.

As anticipated, the JC-1 active anion transporters **U3**, **S3** and **A3** increased OCR and ECAR in MDA-MD-231 cells, which is consistent with their activity as mitochondrial uncouplers, and JC-1 inactive anion transporters **U11**, **S11**, **A11** and **D11** failed to impact OCR and ECAR (Figure 15). Diurea **D3** had the smallest impact on OCR and ECAR, which may reflect its lack of potency in JC-1 assays.

3.3. HPTS Proton Transport Assay

The cellular data suggest that bisaryl anion transporters substituted with electron withdrawing substituents (series **3**) can transport protons across the MIM in MDA-MB-231 cells, leading to mitochondrial uncoupling and a loss of cell viability, while unsubstituted (series **11**) transporters lack activity. We therefore studied the proton transport mechanisms of the series **3** and **11** anion transporters using the cell-free 8-hydroxy-1,3,6-pyrene trisulfonic acid (HPTS) proton transport assay to

identify the underlying proton transport mechanisms.[104] Our previous work determined that bisaryl urea **U3** operated predominantly via the fatty acid-facilitated proton transport mechanism rather than directly cycling protons in a unimolecular process. The strong binding affinity of the urea group towards the carboxylate head groups, and the efficient shuttling across the membrane due to the presence of multiple lipophilic groups, were noted as contributing factors to its high proton transport activity.[121]

Large unilamellar 1-palmitoyl-2-oleoyl-*sn*-glycero-3-phosphocholine vesicles (POPC, 200 nm) were prepared in a solution of potassium gluconate (100 mM) and HEPES buffer (10 mM). HPTS, a pH-sensitive fluorescent probe, was encapsulated inside the vesicles and used to measure the intravesicular pH (see Supplementary Material for full details).[105] Once a pH gradient had been established by the addition of a base pulse to the extravesicular medium, dissipation across the membrane occurred via proton transport facilitated by the target compound.

Initially, dose–response studies were conducted for each compound in untreated POPC vesicles to establish their proton transport activity. Synthetic POPC contains trace amounts of fatty acid impurities (palmitic and oleic acid), which means that transport under these conditions may be partially facilitated by the fatty acid flip-flop mechanism.[134,135] Therefore, the studies were then repeated with vesicles treated with bovine serum albumin (BSA, 1 mol%). This protein binds to free fatty acids present in the membrane and removes them, meaning that proton transport under these conditions is a consequence of direct proton cycling, akin to classical protonophores such as CCCP.[10] The fatty acid impurities present in synthetic POPC are found at a significantly lower concentration than the quantity of BSA added to the vesicles, meaning we can safely assume that all fatty acid impurities are removed upon treatment with BSA. A final set of studies involved the addition of oleic acid (OA, 10 mol%) to the BSA-treated vesicles, which saturated the remaining BSA binding sites and resulted in a 4 mol% concentration of fatty acid present in the membrane (see Figure 16 for representative plots). An enhancement in transport activity under these conditions, compared to the results of the BSA-treated vesicles, can be attributed to proton transport facilitated by a fatty acid-activated mechanism.

Transport activity was quantified by fitting the dose–response curve to an adapted Hill equation and calculating an EC_{50} value (the transport concentration required to facilitate 50% proton efflux after 200 s) under each of the experimental conditions. The Hill coefficient, *n*, provides an indication of the transporter/anion stoichiometry of the transmembrane transport event. These values, under each of the experimental conditions, are presented in Table 5.

Table 5. HPTS (200 s) EC_{50} concentrations and Hill coefficients in untreated (Utd) POPC vesicles, BSA-treated POPC vesicles and OA-treated vesicles.

Compound [a]	EC_{50} (Utd, mol%)	n (Utd)	EC_{50} (BSA, mol%)	n (BSA)	EC_{50} (OA, mol%)	n (OA)	Activation Factor
U3	$0.0046 \pm 4 \times 10^{-4}$	0.82 ± 0.07	0.06 ± 0.004	1.24 ± 0.09	$0.003 \pm 1 \times 10^{-4}$	0.8 ± 0.04	20
A3	$0.02 \pm 2 \times 10^{-4}$	2.00 ± 0.07	0.12 ± 0.005	1.74 ± 0.08	0.02 ± 0.001	1.44 ± 0.2	6
D3	0.04 ± 0.003	0.91 ± 0.08	0.15 ± 0.02	0.58 ± 0.05	0.04 ± 0.001	0.66 ± 0.05	3.75
S3	$0.007 \pm 6 \times 10^{-5}$	1.63 ± 0.02	0.02 ± 0.001	1.38 ± 0.11	0.01 ± 0.001	1.24 ± 0.01	2
S11	0.15 ± 0.006	1.09 ± 0.09	0.89 ± 0.009	1.67 ± 0.05	0.13 ± 0.008	0.74 ± 0.04	6.85

[a] Anion transporters **U11**, **A11** and **D11** lacked activity in HPTS assays and are not shown.

In general, the results of the studies on untreated POPC vesicles correlate well with the in vitro findings. **U3** was the most active protonophore in the series ($EC_{50} = 0.0046 \pm 4 \times 10^{-4}$), followed by squaramide **S3**, amide **A3** and then diurea **D3**. This same ordering of activities was observed in MTS and JC-1 assays. Unsubstituted anion transporters **U11**, **A11** and **D11** were inactive in the HPTS assay, and also lacked MTS and JC-1 activity. Squaramide **S11** was the only unsubstituted derivative to display transport activity; however, it was approximately 21 times less active than substituted squaramide **S3**, reflecting the poor electron-withdrawing ability of this substituent. Compounds bearing

the series **11** substitution were less likely to bind to carboxylate groups and facilitate fatty acid-facilitated transport, or acidify the hydrogen donor effectively enough to enable direct proton cycling. The low proton transport capacity of **S11** likely accounts for its lack of significant activity in cell-based assays.

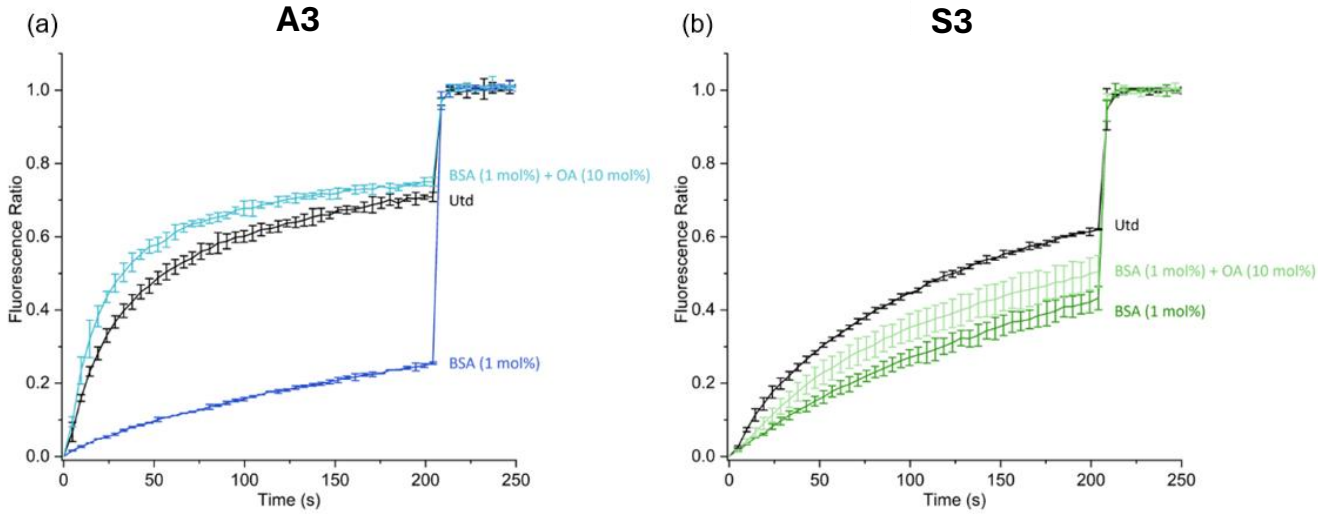

Figure 16. (**a**) The proton transport induced in the HPTS assay by **A3** at a molar-to-lipid concentration of 0.1 mol%, under various experimental conditions. Black represents untreated vesicles, dark blue represents BSA-treated vesicles, and light blue represents OA-treated vesicles. (**b**) The proton transport induced in the HPTS assay by **S3** at a molar-to-lipid concentration of 0.02 mol%, under various experimental conditions. Black represents untreated vesicles, dark green represents BSA-treated vesicles, and light green represents OA-treated vesicles.

An activation factor was calculated for each transport by dividing the EC_{50} value of the BSA-treated vesicles by the EC_{50} value of the OA-treated vesicles. A value greater than 1.0 reflects an enhancement in transport activity in the presence of free fatty acids, and that a fatty acid-facilitated mechanism is the predominant mode of proton transport. **A3** and **D3** returned activation factors of 6.00 and 3.75, respectively. These were lower than the activation factor of **U3**, but still suggest that binding to carboxylate head groups is a key mechanism of proton transport. Interestingly, the Hill coefficients for these compounds suggest a transport stoichiometry which matches a fatty acid-facilitated process. The *n* values for **A3** were all greater than 1.0, and a value of exactly $n = 2.00$ was

reported in the studies using untreated vesicles. This suggests that amide donor motifs from two independent molecules were involved in binding to a single carboxylate group to facilitate its movement across the membrane. The *n* values for **D3** were less than 1.0, and *n* was close to 0.50 in the case of the OA-treated vesicles. This stoichiometry reflects a potential transport pathway where the two urea groups of a single unit of **D3** coordinate to two separate carboxylate head groups and facilitate their transport simultaneously. Proton transport purely via the classical proton cycling pathway would return a Hill coefficient closer to 1.0.

The only unsubstituted anion transporter with HPTS activity was **S11**, and the activation factor suggested that a fatty acid-facilitated mechanism was the active pathway. This may be due to the enhanced hydrogen bond donor capacity of squaramide protons and the smaller bite-angle of this donor leading to greater contributions to binding by the *ortho*-CH protons.[136] With these properties under consideration, we would therefore expect to see enhanced fatty acid-facilitated transport for **S3** compared to **U3**. However, **S3** in untreated POPC vesicles is 1.5 times less active than its urea analogue. Moreover, **S3** returned the lowest activation factor of the series, and instead exhibited the greatest potency in BSA-treated vesicles (Figure 16), indicating that a fatty acid-facilitated mechanism is not the preferred mechanism of proton transport for this squaramide. It is possible that the coordination of this molecule to carboxylate head groups is very strong, resulting in a reduced tendency to decomplex after the translocation of the carboxylate through the membrane—a vital step in the fatty acid "flip-flop" cycle depicted in Figure 13. Furthermore, the enhanced acidity of squaramides compared to urea groups and the delocalisation of the charge around the squarate system, coupled with the increase in lipophilicity provided by the bis-trifluoromethyl groups, means that compound **S3** can most likely facilitate proton transport by a classical proton cycling mechanism. This would account for the low activation factor calculated for compound **S3**.

The results of these experiments verify that a number of hydrogen bond donor motifs can facilitate proton transport via a fatty acid-activated mechanism. The anion transporters with electron-withdrawing substituents (series **3**) all demonstrated enhanced activity over their unsubstituted analogues;

however, the results for compound **S3** suggest that bisaryl squaramides appended with multiple electron-withdrawing substituents are sufficiently acidic to function as classical protonophores. This means that a combination of hydrogen bond donor species and aryl substituents must be considered to maximise proton transport via the fatty acid-activated pathway.

4. Conclusions

In this paper, we replaced the anion binding motif of bisaryl urea mitochondrial uncouplers with squaramide, amide and diurea groups, and investigated the capacity of these compounds to uncouple mitochondria via fatty acid-activated proton transport. Bisaryl squaramide-based anion transporters were found to uncouple mitochondria and reduce MDA-MB-231 cell viability with similar potency to their urea counterparts, while amide and diurea scaffolds were less active. LUV studies found that lipophilic electron-withdrawing groups on the amide and diurea scaffolds were essential for fatty acid-activated proton transport. However, the same substituents reduced fatty acid dependency in bisaryl squaramides, instead favouring proton transport as a classical protonophore via direct deprotonation.

Supplementary Materials: The following supporting information can be downloaded at: https://www.mdpi.com/article/10.3390/biom13081202/s1. Table S2. Library absolute quantitative ^{1}H NMR purity determination; Figure S67. Representative MTS dose–response curves; Figure S68. MDA-MB-231 cell images; Figure S69. MDA-MB-231 and BEAS-2B MTS data; Figure S70. Representative JC-1 dose–response curves; Figures S71–93. Library ^{1}H and ^{13}C NMR spectra; Figures S94–S107: HPTS dose–response and Hill plot analyses.

Author Contributions: Conceptualisation, E.Y. and T.R.; Methodology, E.Y., D.A.M., M.-N.D., P.A.G. and T.R.; Investigation, E.Y., D.A.M. and M.-N.D.; Formal Analysis, E.Y., D.A.M., M.-N.D., P.A.G. and T.R.; Validation, E.Y., D.A.M. and M.-N.D.; Visualisation, E.Y. and D.A.M.; Writing—original draft, E.Y. and D.A.M.; Writing—review and editing, E.Y., D.A.M., P.A.G. and T.R.; Supervision, P.A.G. and T.R. All authors have read and agreed to the published version of the manuscript.

Funding: P.A.G. thanks the Australian Research Council (DP200100453) and the University of Technology Sydney for funding.

Acknowledgments: E.Y., D.A.M., M.-N.D., P.A.G. and T.R. acknowledge and pay respect to the Gadigal people of the Eora Nation, the traditional owners of the land on which we research, teach, and collaborate at the University of Technology Sydney.

Institutional Review Board Statement: Not applicable.

Informed Consent Statement: Not applicable.

Data Availability Statement: All data are available in the main text or the Supplementary Materials.

Conflicts of Interest: The authors declare no conflicts of interest.

Chapter Four: Expanding the π-system of Aryl Urea Substituted Fatty Acids to Promote Proton Transport Activity

Chapter Four preamble

Another class of urea-based anion transporters are aryl urea substituted fatty acids (termed 'aryl ureas' in this chapter), which possess promising anticancer activity in MDA-MB-231 xenografts in mice and were demonstrated in 2020 by Rawling *et al.* to function as protein-independent mitochondrial uncouplers.[78] These molecules possess an aryl-urea anion receptor and fatty acid moiety separated by a long alkyl chain, and thus their acidic group is not conjugated to an extended π-system (See Figure 17a). This deviates from classical protonophores like FCCP, which has lead to an investigation of the aryl urea uncoupling mechanism. Upon deprotonation of the fatty acid group in the mitochondrial matrix, the aryl ureas were found to self-assemble into lipophilic dimers that diffuse across the MIM, allowing for continued protonophoric cycling (see Figure 17c for full mechanism). The uncoupling actions of these compounds has spurred interest in aryl ureas as mitochondria-targeted anticancer agents, but despite demonstrating promising activity *in vitro* and *in vivo*, these compounds lack overall potency. The crucial feature enabling membrane transport is the formation of intermolecular hydrogen bonds between the carboxylate and urea groups, a similar interaction to that of fatty acid-activated proton transporters presented in Chapters Two and Three. Given these mechanistic similarities, and because of the superior transport activity of bisaryl ureas compared to the aryl ureas, it was anticipated that introduction of a second aromatic ring would enhance aryl urea proton transport activity by enhancing the urea NH hydrogen bond donor strength and providing a larger π-system for charge delocalisation. A library of diphenyl urea substituted fatty acids were designed and synthesised to test this hypothesis and evaluate the uncoupling and antiproliferative actions of these compounds against MDA-MB-231 breast cancer cells. This investigation resulted in the following chapter, which was published in *Chemistry – A European Journal* and titled 'Expanding the π-system of Fatty Acid-Anion Transporter Conjugates Modulates Their Mechanism of Proton Transport and Mitochondrial Uncoupling Activity'.

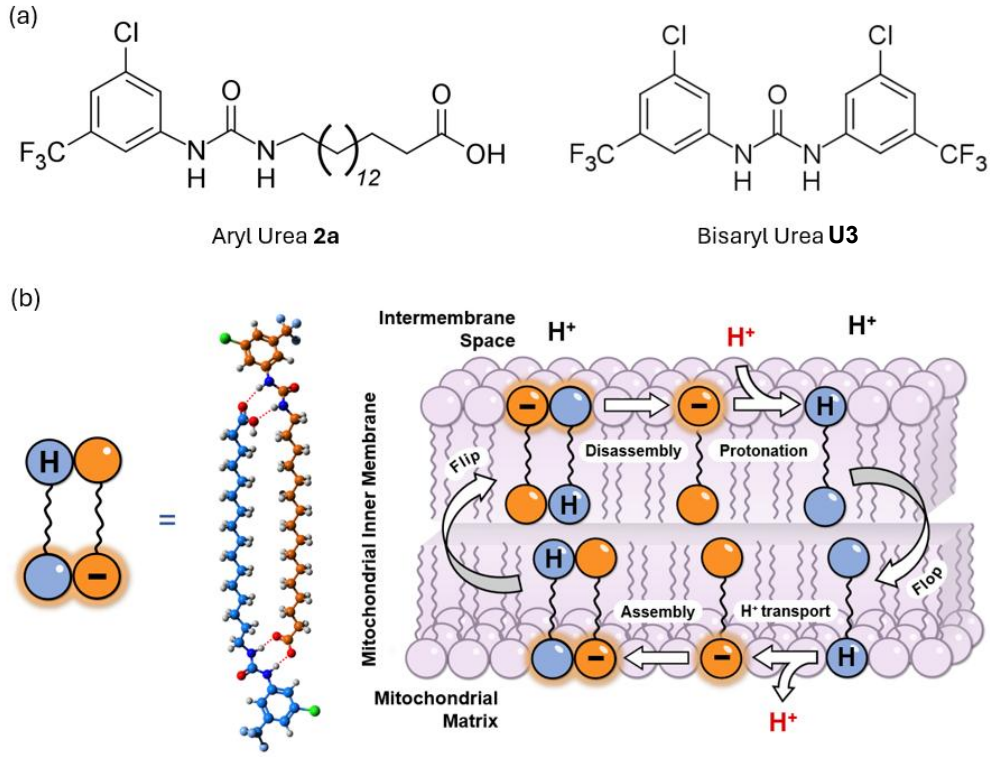

Figure 17**.** (a) aryl urea substituted fatty acid **2a** and bisaryl urea **U3** (b) The acidic group of aryl ureas is separated from its extended π-system by a long alkyl chain. On deprotonation, the aryl ureas mediate proton transport by self-assembling into lipophilic dimers that are stabilised by intermolecular hydrogen bonds between the carboxylate and urea groups.

Declaration of Authorship Contributions

The following chapter is an accepted manuscript published in *Chemistry – A European Journal*. I, Edward York, was the principal investigator and author of this work with direct contributions from David S Getner, training from Daniel A McNaughton, and guidance and conceptualisation from Philip A. Gale, Michael Murray and Tristan Rawling. David S Gertner determined computational binding enthalpies of the aryl urea and diphenyl urea library. Daniel A Naughton trained me to prepare large unilamellar vesicles and perform the HPTS proton transport assays. All other experimental data was collected by myself.

Author	Contribution (CRediT)	Signature
Edward York	Conceptualisation, methodology, investigation, formal analysis, validation, visualisation, writing – original draft, writing – review and editing	Production Note: Signature removed prior to publication.
Daniel A McNaughton	Methodology, resources, formal analysis, validation, visualisation, writing-original draft	Production Note: Signature removed prior to publication.
David S Gertner	Investigation, formal analysis, visualisation, writing – review and editing	Production Note: Signature removed prior to publication.
Michael Murray	Conceptualisation	Production Note: Signature removed prior to publication.
Philip A Gale	Methodology, resources, supervision, writing – review and editing	Production Note: Signature removed prior to publication.
Tristan Rawling	Conceptualisation, methodology, supervision, writing - review and editing	Production Note: Signature removed prior to publication.

Chemistry–A European Journal
Research Article
doi.org/10.1002/chem.202400931
Chemistry Europe
European Chemical Societies Publishing
www.chemeurj.org

Expanding the π-system of Fatty Acid-Anion Transporter Conjugates Modulates Their Mechanism of Proton Transport and Mitochondrial Uncoupling Activity

Edward York,[a] Daniel A. McNaughton,[a] David S. Gertner,[a] Philip A. Gale,[a] Michael Murray[b][c] and Tristan Rawling*[a]

[a] E. York, Dr. D.A. McNaughton, Dr. D. S. Gertner, Prof. P.A. Gale, Assoc. Prof. Tristan Rawling
School of Mathematical and Physical Sciences
University of Technology Sydney
Sydney, NSW 2007, Australia
E-mail: Tristan.Rawling@uts.edu.au

[b] Prof. M. Murray
Sydney Pharmacy School, Faculty of Medicine and Health
University of Sydney
Sydney, NSW 2000, Australia

[c] Prof. M. Murray
Woolcock Institute of Medical Research
Macquarie University
Macquarie Park, NSW 2113, Australia

Supporting information for this article is given via a link at the end of the document.

Abstract: Disrupting proton gradients across mitochondrial inner membranes by mitochondrial uncouplers is a promising strategy for developing novel anticancer agents. Recently, aryl urea substituted fatty acids (aryl ureas) have been identified as a new class of protonophoric mitochondrial uncoupler with promising anticancer activity. The molecules consist of a distal aryl-urea anion receptor and fatty acid motif that, when deprotonated, mediate proton transport via self-assembly into lipophilic dimers. Intermolecular hydrogen bonds between the carboxylate and aryl-urea anion receptor delocalise the negative charge across the aromatic π-system and promote membrane permeability. In this work, we extend the aromatic π-system by introducing a second phenyl substituent to the aryl urea scaffold and compare the proton transport mechanisms and mitochondrial uncoupling actions of these compounds against their monoarylated analogues. It was found that incorporation of *meta*-linked phenyl substituents into the aryl urea scaffold enhanced proton transport in vesicles and demonstrated superior capacity to depolarise mitochondria, inhibit ATP production and reduce the viability of MDA-MB-231 breast cancer cells. In contrast, diphenyl ureas linked through a 1,4-distribution across the phenyl ring displayed diminished proton transport activity, despite both diphenyl urea isomers possessing similar binding affinities for carboxylates. Mechanistic studies suggest that

these compounds transport protons via a competing mechanism that relies on free fatty acids in the phospholipid bilayer, presumably due to steric factors that impose higher energy penalties for dimer formation.

Introduction

Cancer cell mitochondria have emerged as a promising target for new anticancer agents due to their key roles in regulating metabolism and cell survival, and because mitochondria in cancerous and noncancerous cells are structurally and functionally distinct.[47,100] In respiring mitochondria, energy derived from nutrient oxidation is used by the electron transport chain (ETC) to pump protons across the mitochondrial inner membrane (MIM) and into the intermembrane space. The resultant mitochondrial membrane potential ($\Delta\Psi_M$) drives proton flow through the MIM-embedded enzyme ATP synthase, which harnesses this energy to synthesise adenosine triphosphate (ATP).[2,5] Thus, nutrient oxidation is coupled to ATP synthesis via the $\Delta\Psi_M$. Mitochondrial uncoupling occurs when protons flow back across the MIM independent of ATP synthase, which dissipates the $\Delta\Psi_M$ and creates a futile cycle of nutrient expenditure without ATP production. Mitochondrial uncoupling can be mediated by MIM-embedded proteins or small molecule mitochondrial uncouplers. Most classical small molecule uncouplers are weakly acidic protonophores that transport protons across the MIM by transmembrane flip-flop of the protonated species followed by deprotonation in the relatively alkaline interior of mitochondria, called the mitochondrial matrix (Figure 18c).[10] For repeated proton shuttling to occur the resulting anion must diffuse across the MIM back into the intermembrane space. To achieve this, the acidic functional group of protonophores is conjugated to a π-system that delocalises the negative charge, generating a lipophilic anion that can permeate through the non-polar core of the MIM. For example, the classical protonophore carbonyl cyanide-4-(trifluoromethoxy)phenylhydrazone (FCCP, **1**, Figure 18a) forms MIM-permeable anions by distributing its negative charge across the hydrazone and aromatic π-systems adjacent to its acidic NH group.[13]

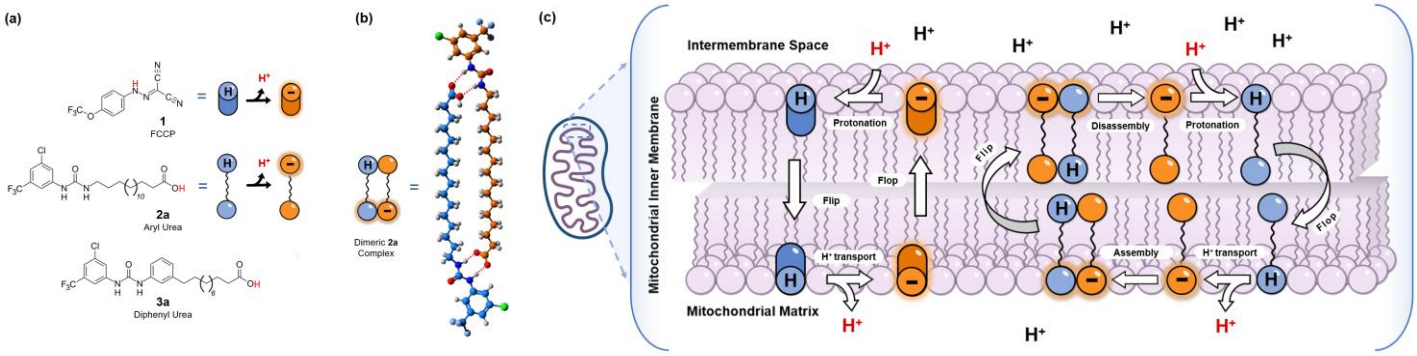

Figure 18. (a) Chemical structures of classical protonophore FCCP (**1**), aryl urea substituted fatty acid (**2a**) and representative diphenyl urea (**3a**) investigated in this work. (b) Ball-and-stick model showing optimised geometry of a monoanionic **2a** dimer calculated at the M062X/6-31+G(d) level of theory in n-pentadecane, hydrogen bonds shown as red dashed lines. (c) Mechanism of proton transport across the mitochondrial inner membrane (MIM) mediated by FCCP (left) and aryl urea substituted fatty acids (right). The rate determining step is diffusion of the anionic species across the MIM. Left: the acidic group in FCCP is attached to a π-system that delocalises the negative charge to produce a MIM-permeable anion. Right: the acidic group in aryl urea **2a** is separated from its extended π-system by a long alkyl chain, and instead self-assembles into MIM-permeable dimers stabilised by intermolecular hydrogen bonds between the carboxylate and urea moieties. Arrows labelled with "flip" and "flop" denote the transbilayer flip-flop motion of compounds in the MIM as part of the protonophoric cycle.

We recently reported the discovery of aryl urea substituted fatty acids (termed aryl ureas, Figure 18a) as a new class of protonophoric mitochondrial uncoupler[78] in which the acidic group is not conjugated to an extended π-system. These compounds utilise an aryl-urea anion receptor to form membrane-permeable dimers that allow for continued protonophoric cycling. As shown in Figure 18c, the carboxylate group of an aryl urea accepts a proton in the intermembrane space and diffuses across MIM as a neutral species. Deprotonation in the alkaline matrix results in the transport of one proton and generation of an anionic species. The aryl urea then self-assembles into a dimer via intermolecular hydrogen bonds between the carboxylate and urea-based anion receptor (Figure 18b). The MIM-permeable dimer can re-enter the intermembrane space to facilitate further protonophoric cycling. In

Figure 18c deprotonation and dimer formation are shown as two distinct events, but it should be noted that these processes may occur in a concerted manner where dimer formation simultaneously drives deprotonation of the acid.

Given their protonophoric activity, the aryl ureas have been assessed as mitochondria-targeted anti-cancer agents. In cell-based assays the aryl ureas were shown to reduce the viability of several breast cancer cell lines (MDA-MB-231, T47D, MDA-MB-468, and MCF-7), as well as reduce tumour volume in nude mice carrying MDA-MB-231 xenografts.[79] Although the aryl ureas possess promising anticancer actions they lack potency and we have undertaken structural modifications of the scaffold to enhance activity, attention has focused on the aryl urea-based anion receptor due to its central role in facilitating dimer formation and charge delocalisation across the π-system. Substitution of the aromatic ring with lipophilic electron withdrawing groups (see **2a** in Figure 18a) was found to enhance protonophoric activity by promoting dimer formation and charge delocalisation by through-bond propagation of electron density.[78] Replacement of the anion binding urea group with carbamate groups afforded a series of analogues with similar but not superior activity to the parent aryl ureas.[137]

In this paper we explore the impact of extending the π-system on protonophoric and anticancer activity. To achieve this a series of diphenyl urea substituted fatty acids (termed diphenyl ureas) were synthesised that possess an additional aromatic ring between the alkyl chain and urea binding group (referred to as proximal ring, Figure 18a). The proton transport capacity, mitochondrial actions and anticancer activity of the diphenyl ureas were evaluated and compared to the parent aryl ureas. It was anticipated that extending the aromatic π-system of the urea anion receptor would promote protonophoric activity by increasing the hydrogen bond acidity of the NH groups and the overall surface area available for charge delocalisation. From these studies it emerged that incorporation of *meta*-linked but not *para*-linked proximal rings enhanced proton transport in cell-free HPTS vesicle studies, and the most active compounds depolarised mitochondria, inhibited ATP production and reduced viability

of MDA-MB-231 cells with greater potency than their aryl urea counterparts. Using experimental and computational approaches we show that *para*-linked diphenyl ureas transport protons by a competing fatty acid-activated mechanism due to steric factors that misalign the carboxylate and urea moieties for optimal dimerisation.

Results and Discussion

Compound Library Design

To extend the π-systems of aryl ureas **2a** and **2b** we designed analogues that incorporated a second proximal aromatic ring between the urea and alkyl linker groups (Figure 19). Analogues **3a** and **3b** were designed with alkyl chains connected at the *meta*-position of the proximal ring. Relative to an unsubstituted phenyl ring, in this position the alkyl chain was expected to donate electron density towards the urea group, which may hinder anion binding and dimer formation.[121] The **4** and **5** series analogues possess ether linkages in the *meta*- and *para*-positions, respectively. Ether substituents provide an electron withdrawing effect in the *meta*-position and a donating effect in the *para*-position.[106] It was therefore anticipated that the urea groups in the **4** series would have higher anion affinity for carboxylates and thus superior protonophoric activity than the **3** and **5** series analogues.

To evaluate the impact of the proximal ring the activities of **3a–5b** were directly compared to the parent compounds **2a** and **2b.** However, introduction of a second ring also increases compound lipophilicity, which is known to affect anion transport activity.[108] To exclude the role of lipophilicity the length of the alkyl chains in compounds **3a–5b** were shortened to provide compounds with similar calculated LogP (cLogP) values to **2a** and **2b**.

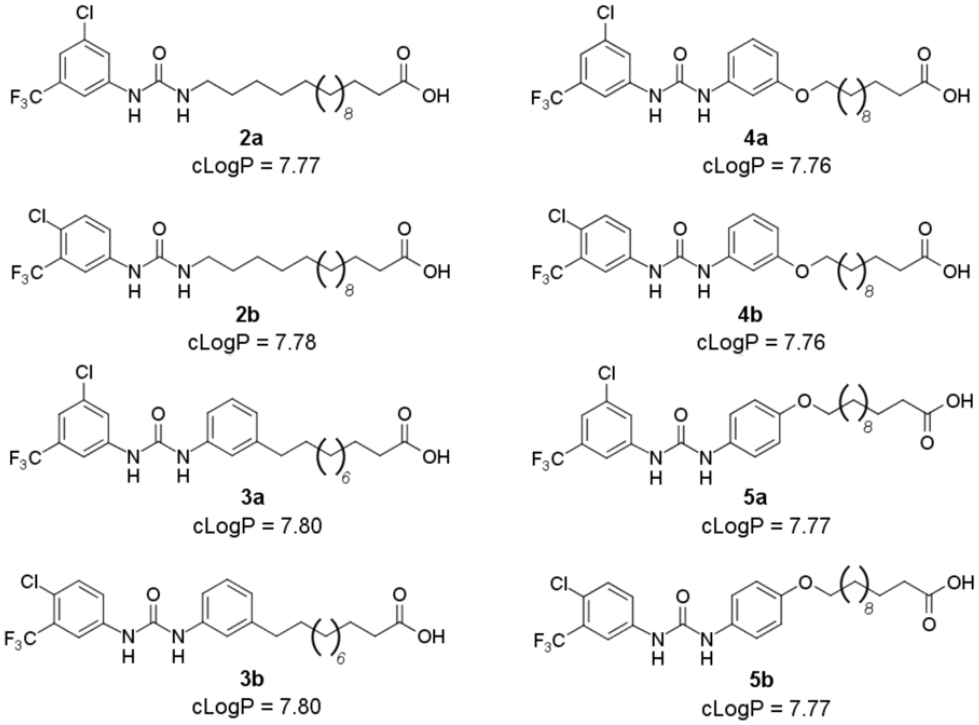

Figure 19. Chemical structures and cLogP values of the aryl and diphenyl ureas studied in this work. The partition coefficient shown represents the average cLogP value obtained using freely available ALOGPS 2.1, XLOGP2 and MiLogP web tools as well as Marvin Consensus software.

Diphenyl ureas **3-5a** and **3-5b** were synthesised as shown in Scheme 2. Important intermediates in the syntheses were anilines **3-5x**, which could be reacted with carbamoylimidazoles **23a** and **23b** to form the diphenyl urea groups. Ether-linked intermediates **4x** and **5x** were synthesised from bromo-fatty acids **12** and **13**, which were sourced commercially or synthesised from the corresponding alcohol (**11**) using HBr in good yield (87%). The carboxylic acid groups of **12** and **13** were esterified using acetyl chloride in ethanol to give **14** (88%) and **15** (85%), which were then reacted with Boc-protected anilines **19** and **20** under Williamson conditions to yield ethers **Boc4** (40%) and **Boc5** (91%) respectively. The aniline groups of **17** and **18** were Boc protected prior to Williamson reactions to prevent N-alkylation side reactions. **17** was readily Boc-protected by reaction with Boc anhydride in anhydrous dichloromethane, however reactions with **18** under the same conditions gave a mixture of both *N*- and *O*-Boc-protected products. Selective Boc protection of **18** was instead achieved using

Amberlyst 15 as a catalyst, affording **20** (87%) in high yield.[138] Finally, trifluoroacetic acid was used to remove the Boc groups of **Boc4** and **Boc5** to provide key ether intermediates **4x** (98%) and **5x** (91%) in excellent yields.

A different pathway was needed to produce alkyl intermediate **3x**, which relied on the synthesis of aldehyde **10**. To access **10** the aldehyde group of **6** was first acetal-protected to give **7** in excellent yield (97%). The exposed nitro group was then reduced with Pd/C + $HCOONH_4$ to give aniline **8** (78%). *N*-Boc protection was achieved in anhydrous dichloromethane under argon to form **9** (71%), followed by selective hydrolysis of the acetal protecting group with Amberlyst 15, at last affording aldehyde **10** (94%). **3x** was then synthesised in four steps from **14**. In the first step, phosphonium **16** (78%) was synthesised by reaction of **14** with triphenylphosphine. A Wittig reaction between aldehyde **10** and phosphonium **16** with sodium bis(trimethylsilyl)amide was used to prepare olefin **21** (80%),[139] which was reduced to **Boc3** (99%) and then reacted with trifluoracetic acid to remove the Boc group and afford anilino fatty acid ester **3x** (98%).

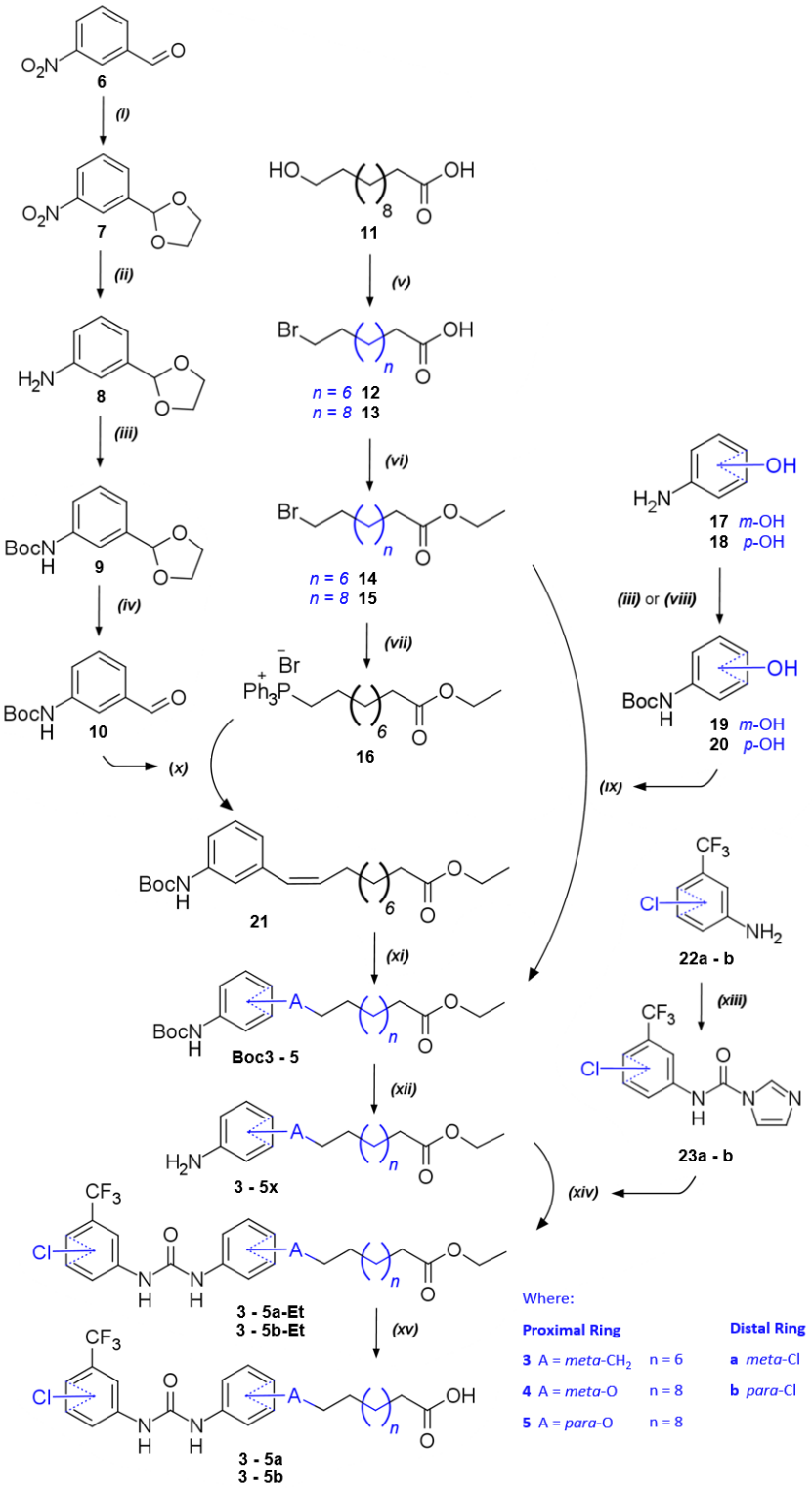

Scheme 2. Synthesis of Diphenyl ureas **3-5a** and **3-5b**. Curved arrows represent convergent syntheses. Reagents and conditions: (i) toluene, ethylene glycol, cat. TsOH, Dean-Stark trap, reflux, 18 h;

(ii) absolute ethanol, palladium/charcoal, $HCOONH_4$, 0°C to 35°C, 1 h; (iii) anhydrous dichloromethane under argon, Boc anhydride, 40°C 18 h; (iv) acetone/water, Amberlyst 15, rt, 3.5 h; (v) 1:4 98% H_2SO_4 : 48% HBr, reflux, 16 h (vi) absolute ethanol, acetyl chloride, rt, 4 h; (vii) neat, Ph_3P, 120°C, 20 h; (viii) 95% ethanol, Boc anhydride, Amberlyst 15, rt, 15 min; (ix) anhydrous dimethylformamide under argon, K_2CO_3, 100°C, 24 h; (x) anhydrous tetrahydrofuran, $NaN(TMS)_2$, 0°C to -78°C to rt, 2 h; (xi) absolute ethanol, palladium/charcoal, $HCOONH_4$, 0°C to 35°C, 1 h; (xii) anhydrous dichloromethane, trifluoroacetic acid, rt, 4 h; (xiii) 1,2-dichloroethylene under nitrogen, carbonyldiimidazole, 50°C, 24 h (xiv) anhydrous dichloromethane under argon, rt, 24 h; (xv). 95% ethanol, NaOH, 40°C, 3 h.

Following the successful synthesis of key intermediates **3-5x** formation of the diphenyl urea groups was achieved using **23a** and **23b**, which were prepared by reactions of substituted anilines **22a** and **22b** with *N,N'*-carbonyldiimidazole. In solution **23a** and **23b** dissociate into imidazole and isocyanate species,[140] thus serving as masked isocyanates that were reacted with anilino fatty acid esters **3-5x** to give diphenyl urea fatty acid esters **3–5a-Et** and **3–5b-Et** in varying yields (40-90%). In the final step base-catalysed hydrolysis of the ester protecting groups afforded the final acid products **3-5a** and **3-5b** as solids in excellent yields (>90%).

HPTS Proton Transport Assay

The capacity for diphenyl urea fatty acids **3a–5b** to mediate proton transport was assessed using a cell-free 8-hydroxy-1,3,6-pyrene trisulfonic acid (HPTS) vesicular proton transport assay. The results were compared against the activity of aryl ureas **2a** and **2b** to investigate the influence of the proximal ring on transmembrane transport. Large unilamellar 1-palmitoyl-2-oleoyl-*sn*-glycero-3-phosphocholine vesicles (POPC, 200 nm) containing the pH-sensitive fluorophore HPTS were prepared in 4-(2-hydroxyethyl)-1-piperazineethanesulfonic acid (HEPES, 10 mM)-buffered potassium gluconate (100 mM) (see Supporting Information for full experimental details). To initiate the experiment, an

addition of base to the extravesicular environment establishes a pH gradient across the membrane before addition of the test molecule. In this system the increase in intravesicular pH by proton transporters can be measured by monitoring the ratio of HPTS fluorescence emission intensity at different excitation wavelengths. Transporter dose-response curves were used to fit an adapted Hill equation and calculate an EC_{50} value for each compound (representing the transporter concentration required to facilitate 50% proton efflux after 200 s). The Hill coefficient, *n*, indicating the stoichiometry of the transport event, was also calculated, and both are presented in Table 6. We note that in this assay proton efflux and hydroxide influx appear identical, which can obscure efforts to identify the transported ion. In 2016 Wu *et al*. suggested that symmetrical bisaryl ureas likely transport OH^- via hydrogen bonds because they lack an acidic group for protonophoric transport.[141] However, the diphenyl ureas studied in this work possess an acidic group, which on deprotonation would anchor the compound to one membrane leaflet and prevent the urea moiety from successfully transporting hydroxide. Consequently, the HPTS transport data was interpreted as extravesicular proton transport. This is supported by the mitochondrial uncoupling activity of the compounds (see following subsection), which requires the transport of protons across the MIM.

Several structure-activity relationships can be gained from the EC_{50} data. Firstly, the **3**- and **4**-series diphenyl ureas are approximately two-fold more potent than parent aryl ureas **2a** and **2b**, while the **5**-series diphenyl ureas were less active. These data indicate that extension of the π-system via proximal ring inclusion can promote proton transport activity, although only when the ring is *meta*-substituted. The data also indicate that 3,5-substitution of the distal ring (**a**-series) is preferred to 3,4-substitution (**b**-series) as the **a-**series diphenyl ureas consistently outperformed their 3,4-substituted counterparts. These trends in activity may be attributed to substituent electronic effects. Due to their substitution pattern the chloro and trifluoromethyl substituents in the **a**-series provide a greater electron

withdrawing effect than in the **b**-series (σ_{total} = 0.80 for **a**-series and 0.66 for **b**-series),[106] which may influence the anion affinity of the urea NHs. Similarly, the reduced activity of **5a** and **5b** may be attributed to the electron donating effect provided by the *para*-ether group on the proximal ring. It should be noted however that the *meta*-alkyl chain of the **3**-series analogues also provides an electron donating effect, but this did not translate to inferior activity compared to the *meta*-ether-linked **4**-series analogues. Alternatively, the diminished activity of **5a** and **5b** could also be due to the subtle shape change between the *meta*- and *para*-linked analogues, which misaligns the carboxylate and urea moieties against favourable dimerisation.

Table 6. HPTS (200 s) EC_{50} concentrations and Hill coefficients in Corden Pharma POPC vesicles, acetate binding affinities determined by ^{1}H NMR titrations with tetrabutylammonium acetate (TBAOAc) in DMSO / 0.5% H_2O, JC-1 (1 h) and MTS (48 h) absolute IC_{50} concentrations measured in MDA-MB-231 breast cancer cells.

	HPTS EC_{50} (mol%)	Hill (n)	AcO^- Binding Affinity (M^{-1})	JC-1 IC_{50} (μM)	MTS IC_{50} (μM)
2a	0.016 ± 0.003	2.00 ± 0.38	1159 ± 1.4% [a]	2.07 ± 0.05	3.48 ± 0.45
2b	0.021 ± 0.002	1.72 ± 0.25	548 ± 0.8% [b]	2.98 ± 0.10	5.76 ± 0.52
3a	0.008 ± 5 x 10^{-4}	0.93 ± 0.05	7201 ± 4.8% [b]	0.26 ± 0.05	2.96 ± 0.39
3b	0.013 ± 6 x 10^{-4}	0.82 ± 0.01	6761 ± 3.8% [b]	0.48 ± 0.04	5.00 ± 0.70
4a	0.008 ± 7 x 10^{-4}	1.32 ± 0.08	7388 ± 0.7% [b]	0.31 ± 0.01	2.96 ± 0.38
4b	0.011 ± 3 x 10^{-4}	1.00 ± 0.03	6128 ± 4.1% [b]	0.51 ± 0.06	3.99 ± 0.50
5a	0.023 ± 0.003	1.15 ± 0.09	5077 ± 1.2% [b]	1.75 ± 0.09	5.00 ± 0.90
5b	0.035 ± 0.001	1.33 ± 0.06	6991 ± 4.4% [b]	1.96 ± 0.02	6.95 ± 0.65

[a] Methyl ester tested; [b] Ethyl ester tested.

To determine if substituent electronic effects significantly alter the favourability of intermolecular urea-carboxylate interaction, we determined acetate (AcO^-) binding constants using ^1H NMR titrations in DMSO-d_6 / 0.5% H_2O with tetrabutylammonium acetate. The methyl or ethyl ester precursors of each compound were used to eliminate competing interactions from their carboxylic acid group. The chemical shifts of the urea NHs were recorded and fit a 1:1 (host:guest) binding model (see Supporting Information for details). Consistent with the EC_{50} data and Hammett substituent constants, **2a**, **3a** and **4a** had higher acetate affinities than their **b**-series counterparts, suggesting the greater electron withdrawing effect of the 3,5-substitution pattern promotes dimerisation and proton transport. However, **5b** bound acetate more strongly than **5a** but exhibited inferior transport activity, opposing this trend. Similarly, the relationship between EC_{50}, Hammett substituent constant and anion affinity was less clear in comparing the **4**- and **5**-series. It was found that all diphenyl ureas bound acetate more strongly than their aryl urea counterparts, but the **5**-series compounds did not have consistently lower anion affinities than the **4**-series despite the electron donating character of the *para*-ether substituent. Taken together, these data indicate that binding affinity alone cannot explain the diminished transport activity of **5a** and **5b,** indicating that the proton transport event is influenced by additional factors.

Interestingly, the HPTS Hill coefficients for the compounds suggest that the proton transport stoichiometry for diphenyl ureas differ from their aryl urea analogues. **2a** and **2b** returned *n* values close to 2 (2.00 and 1.72 respectively). This aligns with previous molecular dynamics simulations that observed **2a** dimer formation between one protonated and one deprotonated **2a** molecule (monoanionic complex),[78] resulting in the transmembrane transport of a single proton. In contrast, the diphenyl ureas returned *n* values between 0.82-1.33, which may reflect that these compounds favour the co-transport of two deprotonated molecules bound at each end (dianionic complex), resulting in a two-

proton transport event to give a transport stoichiometry of one. Alternatively, this could indicate that diphenyl ureas transport protons monomerically via intramolecular urea-carboxylate interactions, and/or rely on free fatty acids present in the membrane to facilitate transport. For example, symmetrical bisaryl urea anion transporters have been shown to facilitate proton transport by a fatty acid-activated mechanism, where the transporter shuttles a deprotonated fatty acid across the membrane to enable protonophoric cycling.[104,121] The POPC lipids used for the previous HPTS studies (purchased from Corden Pharma) contain high levels of free fatty acids (up to 2 mol%). Deprotonation of the urea groups in the diphenyl ureas,[142] rather than the carboxylic acid, could also be responsible for their proton transport stoichiometry, however this is unlikely. Calculated[87] and experimental[88] pK_a values of symmetrical bisaryl ureas substituted with electron withdrawing groups range from 14 to 18, which is significantly higher than known protonophores (pK_a values range from 4 to 8)[10] and indicates that the urea NHs are not sufficiently acidic to allow protonation/deprotonation in HPTS assays and at mitochondrial pH.

To investigate the contribution of the fatty acid-activated mechanism to diphenyl urea proton transport, additional HPTS assays were performed on all compounds using low fatty acid content POPC (purchased from Avanti Polar Lipids) in the presence and absence of oleic acid (OA, at 2 and 4 mol%, see Figure 20). Compounds were tested under each condition at concentrations close to their original EC_{50}. Remarkably, the addition of OA reduced proton transport by all compounds, except for **5a** and **5b**, which showed a sharp increase with the addition of OA. This confirms that **5a** and **5b** transport protons partially by a fatty acid-activated mechanism, which may account for their inferior transport activity. The dual mechanism may stem from steric factors that incur a higher energy penalty for the complexation of *para*-linked analogues and expose the urea group to the approach of free fatty acids.

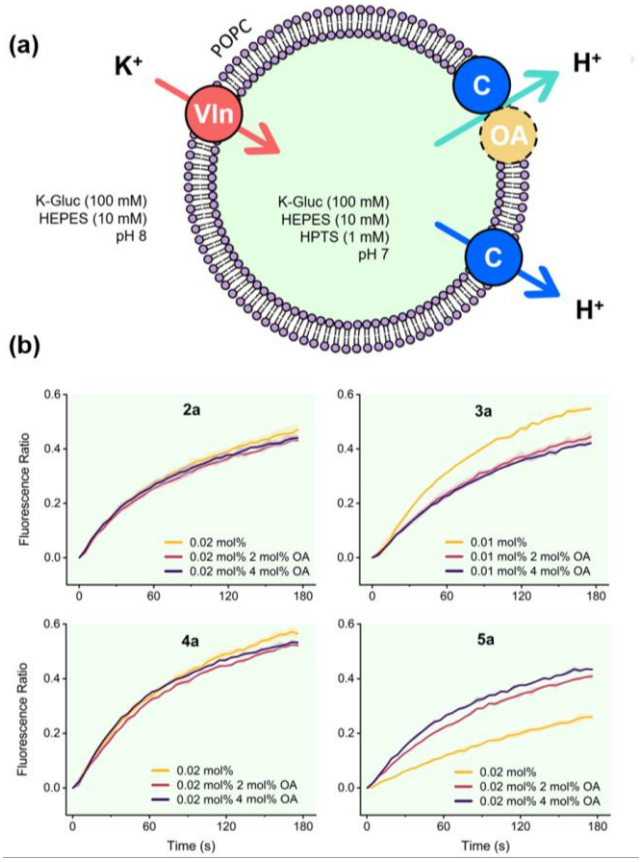

Figure 20. (a) Schematic of the HPTS proton transport assay performed using low fatty acid POPC to determine transporter (C) fatty acid-dependency and (b) the proton transport induced by **2a**, **3a**, **4a** and **5a** in low fatty acid content POPC with and without OA (2 and 4 mol%) (see Supporting Information for **b**-series proton transport plots).

To examine this, binding free energies were calculated for the complexation of deprotonated **2a–5a** molecules at the M062X/6-31+G(d) level of theory in *n*-pentadecane to estimate the relative stability of the dimeric and monomeric species in a low dielectric environment such as the MIM (see Supporting Information for details).[143] Notably, deprotonated **5a** molecules dimerised less favourably (−278.5 kJ/mol) compared to *meta*-linked analogue **4a** (−300.2 kJ/mol), and the same trend was observed for the formation of monomeric species (−283.8 kJ/mol and −321.0 kJ/mol respectively). This indicates that the subtle shape change of *para*-linked **5a** and **5b** does hinder intra- and intermolecular binding. Both dimerisation and intramolecular complexation was identified as favourable for all diphenyl

ureas **3a–5a** and aryl urea **2a** (Supporting Information, Table S4 and Figure S125), although it should be noted that intramolecular complexation was not observed in previous molecular dynamics simulations of **2a** in DOPC membranes. Instead, the exclusion of the carboxylate group from the bilayer interior favoured linear bilayer packing and the formation of head-to-tail dimers and multimers.[78]

Interestingly, OA addition reduced proton transport for the **3**-series more than the **2**- and **4**-series analogues. HPTS assay Hill analysis of **3a** and **3b** returned the lowest *n* values, which may suggest these compounds exhibit a stricter preference for co-transport as a dianionic complex. This could account for the effect of OA on **3a** and **3b**, as increased competition for urea binding sites would hinder formation of dianionic dimers over cyclic monomers or monoanionic dimers that only require one urea-carboxylate binding event. Taken together, these studies show that the diphenyl ureas operate by different transport mechanisms to the aryl ureas. In contrast to the aryl ureas, all diphenyl ureas transport one proton per molecule. The change in transport stoichiometry may result from the preference of the diphenyl ureas to form dianionic dimers, intramolecularly bound monomeric complexes or complexation to free fatty acids in the membrane, the latter of which is more likely for *para*-linked analogues **5a** and **5b**.

Mitochondrial Effects of Diphenyl Ureas

We next sought to evaluate the capacity of diphenyl ureas to transport protons across the MIM and depolarise mitochondria in MDA-MB-231 cells. Mitochondrial depolarisation was measured using JC-1, a cationic fluorophore that forms aggregates in energised mitochondria (that possess a high $\Delta\Psi_M$) that fluoresce red.[144] Dissipation of the $\Delta\Psi_M$ by mitochondrial uncouplers releases JC-1 into the cytosol as monomers that fluoresce green. Dose-response curves (Supporting Information, Figure S126) were constructed for all aryl and diphenyl ureas and JC-1 IC_{50} concentrations were determined as the concentration required to shift the red/green fluorescence ratio by 50% of control. Cells were

exposed to test compounds for 1 h to distinguish direct mitochondrial uncoupling actions from the characteristic mitochondrial depolarisation that occurs during apoptosis.

As shown in Table 6, all test compounds were active in JC-1 assays. Diphenyl ureas **3a–4b** were the most active compounds in JC-1 assays and shifted the JC-1 red/green fluorescence ratio with IC_{50} concentrations below 1 μM. *Para*-ether-linked diphenyl ureas **5a** and **5b**, and aryl ureas **2a** and **2b** had similar levels of activity with JC-1 IC_{50} concentrations between 1.75 and 2.98 μM. All **a**-series compounds bearing 3,5-substituted distal rings outperformed their 3,4-substituted **b**-series counterparts. The activity trends observed in JC-1 assays reflect those found in HPTS assays, which indicates that proton transport capacities measured in the vesicle-based HPTS proton transport assay translates into depolarisation of the MIM in live cell mitochondria. Indeed and bivariate analysis of JC-1 and HPTS activity demonstrates a strong positive association ($r^2 = 0.77$, Supporting Information, Figure S128).

Mitochondria utilise the proton gradient across the MIM for ATP production, so we measured ATP levels in MDA-MB-231 cells treated with each compound at the common concentration of 5 μM (see Figure 21). All **3**- and **4**-series compounds, which have submicromolar JC-1 IC_{50} concentrations, reduced intracellular ATP levels to ~ 80% of time-matched control. Decreased intracellular ATP can result from reduced cell viability rather than direct effects on mitochondrial function, so LDH release assays were conducted to detect cell death. It was found that **3a–4b** (5 μM) did not increase LDH release over 6 h treatment (Supporting Information, Figure S129), thus confirming direct inhibition of ATP synthesis by these compounds. In contrast, aryl urea **2b** and the **5**-series diphenyl ureas failed to reduce ATP production, while **2a** had a modest effect on ATP levels at 4 h only. These compounds

all had reduced capacity to depolarise mitochondria in JC-1 assays and their failure to inhibit ATP production at 5 μM is likely to be a result of their diminished proton transport capacity.

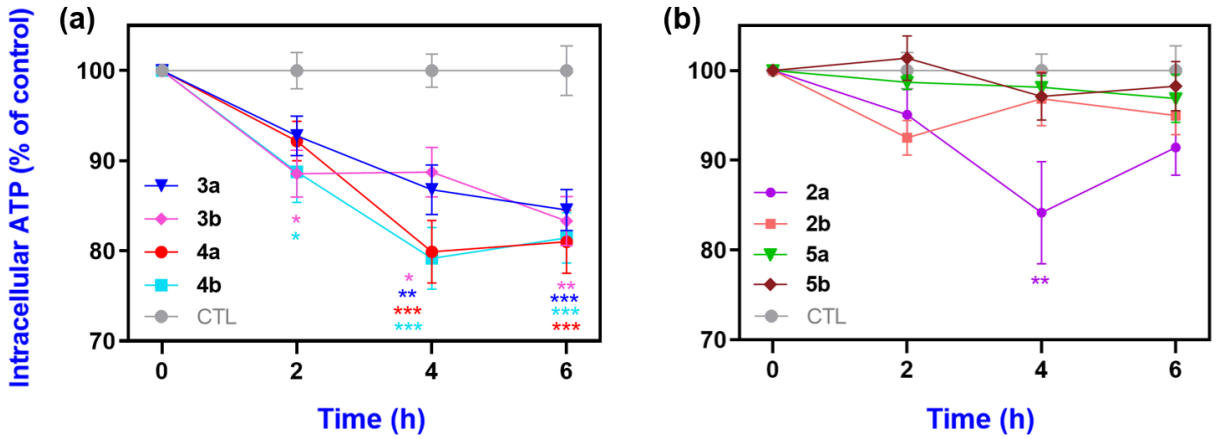

Figure 21. Total intracellular ATP levels in MDA-MB-231 cells following treatment with (a) **3-**, **4-** and (b) **5-**series diphenyl ureas and parent aryl ureas **2a** and **2b** (5 μM). ATP levels are expressed as the percentage of time-matched DMSO control. Different from DMSO-treated control: (*) $P < 0.05$, (**) $P < 0.01$, (***) $P < 0.001$.

Finally, we performed Seahorse Mito Stress Tests using MDA-MB-231 cells treated with the **a**-series compounds to confirm their mitochondrial uncoupling activity. This assay measures the oxygen consumption rate (OCR) of the ETC in MDA-MB-231 cells. Cells are first treated with the ATP synthase inhibitor Oligomycin, which blocks the flow of protons through ATP synthase. As a consequence electron flow through the ETC is inhibited, which is detected as a decrease in OCR. Introducing a protonophoric uncoupler under these conditions reestablishes proton flow across the MIM, leading to unimpeded ETC activity and an increase in OCR.[145]Seahorse assays were carried out using **2a**, **3a**, **4a**, **5a** (5 μM) and the classical protonophore **1** (FCCP, 1 μM) for comparison. As shown in Figure 22, **3a** produced an increase in OCR that exceeded that produced by **1**. **4a** and **2a** also increased OCR while compound **5a** showed no effect compared to control. The observed OCR trace for **3a** is similar

to that observed for FCCP[76] and compound **3** in Chapter Two, and may be attributed to the inhibition of ETC complexes I and II due to matrix acidification caused by excessive uncoupling.

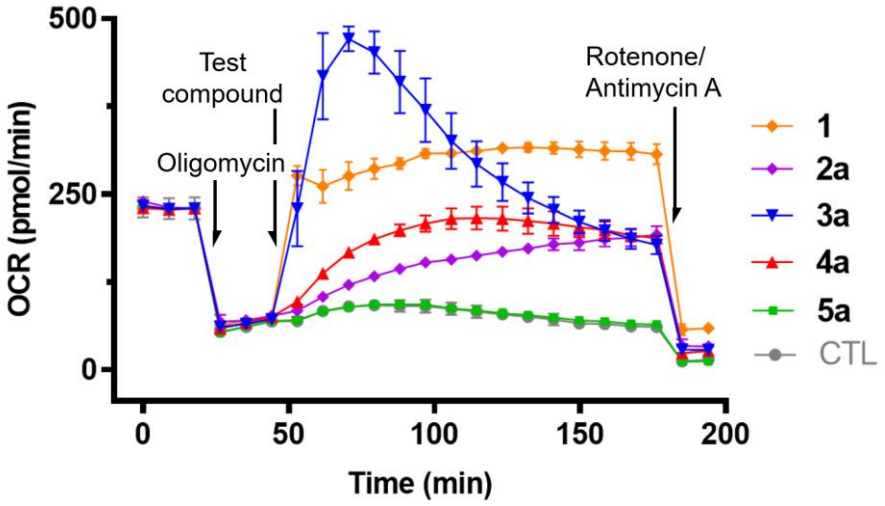

Figure 22. OCR in MDA-MB-231 cells treated sequentially with the ATP synthase inhibitor oligomycin (1 μM), a test compound (5 μM **2a**, **3a**, **4a** or **5a**), and the ETC complex inhibitors rotenone/antimycin A (1 μM). Test compounds were compared against classical protonophore **1** (FCCP, 1 μM) and a 0.1% DMSO vehicle containing no test compound as control (CTL).

Effects of Diphenyl Ureas on MDA-MB-231 Cell Viability

Mitochondrial uncouplers have been shown to induce cancer cell death so MTS assays were performed to investigate the effect of diphenyl ureas on MDA-MB-231 cell viability. Cells were treated with the test compounds for 48 h over a wide concentration range, and dose-response curves (Supporting Information, Figure S127) were used to calculate absolute IC_{50} concentrations (Table 6). Consistent with the other assays, the **a**-series analogues were more active than their **b**-series counterparts. Bivariate analysis of the HPTS and MTS data exhibits a strong positive association ($r^2 = 0.79$, Supporting Information, Figure S128), although it should be noted that the changes in MTS activities across the test series were minor compared to those seen in JC-1 and HPTS assays. For example, diphenyl urea **3a** was >2-fold more active than **2a** in JC-1 and HPTS assays, but both compounds

reduced MDA-MB-231 cell viability with similar IC_{50} concentrations of 2.96 ± 0.39 and 3.48 ± 0.45 μM, respectively.

Taken together, the data presented here demonstrates that incorporation of a *meta*- but not *para*- linked proximal ring into the aryl urea scaffold promotes proton transport capacity in vesicles and live cell mitochondria, but this does not translate into a significant increase in cytotoxicity.

Conclusion

In this paper we extended the π-systems of aryl urea-substituted fatty acids by introduction of a second phenyl group to the scaffold and evaluated the impact on proton transport and mitochondrial uncoupling actions. Incorporation of *meta*-linked proximal rings into the aryl urea scaffold enhanced proton transport in vesicle studies, indicating improved charge delocalisation by the urea anion binding group to produce membrane-permeable complexes. The most active compounds in the series depolarised mitochondria, inhibited ATP production and reduced cell viability with greater potency than the parent aryl urea analogues. In contrast, diphenyl ureas linked through a 1,4-distribution across the proximal ring showed diminished proton transport and cellular activity, despite both *meta*- and *para*-linked isomers possessing similar binding affinities for carboxylates. Mechanistic testing and computational binding enthalpies indicate that *para*-linked diphenyl ureas form monomeric and dimeric complexes less favourably due to steric factors and instead transport protons by a competing fatty acid-activated mechanism.

Supporting Information

The authors have cited additional references within the Supporting Information.[105,125,146-149]

Acknowledgements

The author acknowledges C. Clarke for his assistance in developing the fatty acid chemistry used in this synthesis, and H. Zeng for her assistance accessing high performance computing workstations for quantum chemistry simulations. E.Y., D.A.M., D.S.G., P.A.G. and T.R. acknowledge and pay

respect to the Gadigal people of the Eora Nation, the traditional owners of the land on which we research, teach, and collaborate at the University of Technology Sydney.

Keywords: mitochondrial uncoupling • anion transporter • proton transport • dimer • anticancer

Chapter Five: General Conclusions and Future Directions

5.1 General Conclusions

The anticancer bisaryl urea **SR4** exhibits mitochondrial uncoupling activity but lacks the acidic group of classical protonophores, an apparent contradiction that has hindered further development of the drug scaffold as an anticancer agent. Informed by the discovery thiourea **T1**, an anion transporter that mediates proton transport by a novel fatty acid-activated mechanism, this project sought to assess the capacity for **SR4** and other anion transporters to operate using the same mechanism, and to optimise the mitochondrial uncoupling and antiproliferative activity of these compounds towards MDA-MB-231 breast cancer cells.

In Chapter Two, vesicular proton transport assays were performed that provided experimental evidence that **SR4**-mediated proton transport occurs via the fatty acid-activated mechanism. Based off this finding, a library of bisaryl ureas was synthesised bearing various aromatic substituents for structure-activity relationship studies and subsequent testing in MDA-MB-231 breast cancer cells. These studies revealed that substitution with lipophilic electron withdrawing groups enhanced proton transport activity, which correlated with their capacity to induce mitochondrial dysfunction in MDA-MB-231 cells. The most active compound in the series, bisaryl urea **U3**, uncoupled mitochondria, reduced cell viability and inhibited ATP production with greater potency than **SR4**.

In Chapter Three the urea anion binding motif was replaced with squaramide, amide and diurea groups, and the capacity for these compounds to uncouple mitochondria, reduce MDA-MB-231 cell viability and transport protons via fatty acid-activated proton transport was evaluated. Bisaryl squaramide, amide and diurea-based transporters depolarised mitochondria and reduced MDA-MB-231 cell viability, but with lower potency than their urea counterparts. Proton transport studies revealed that lipophilic electron withdrawing substituents were essential for the bisaryl amide and diurea scaffolds to participate in fatty acid-activated proton transport. However, the same substituents reduced

fatty acid dependence in bisaryl squaramides. This was attributed to the enhanced acidity of the squaramide motif, that when coupled with electron withdrawing aromatic substituents, favoured proton transport by direct deprotonation of the squaramide NHs.

In Chapter Four this anion transporter knowledge was translated to enhance the activity of aryl urea substituted fatty acids, a new class of mitochondrial uncoupler that also rely on intermolecular urea-carboxylate interactions. Due to the superior transport activity of bisaryl ureas compared to the aryl ureas, it was anticipated that incorporating a second (proximal) ring into the aryl urea scaffold would enhance proton transport by increasing urea NH hydrogen bond donor strength and providing a larger π-system for charge delocalisation. As expected, introduction of *meta*-linked proximal rings into the scaffold enhanced proton transport in vesicles, consistent with improved binding and charge delocalisation. In contrast, the inclusion of *para*-linked proximal rings diminished proton transport and cellular effects, despite possessing similar carboxylate binding affinities as the *meta*-linked analogues. Interestingly, mechanistic studies demonstrated that *para*-linked diphenyl ureas transport protons partially by the fatty acid-activated mechanism, which was attributed to steric factors that hinder these compounds from forming monomeric and dimeric complexes. Overall, the inclusion of *meta*-linked proximal rings approximately doubled the proton transport activity for these compounds, and greatly enhanced their ability to depolarise mitochondria. However, this only translated to a minor enhancement in antiproliferative activity towards MDA-MB-231 cells compared to the parent aryl ureas.

Taken together, these studies demonstrate the fatty acid-activated proton transport activity of a range of different anion transporters and provide the first experimental evidence of this mechanism operating in live cells to induce mitochondrial uncoupling. These effects were also shown to reduce the viability of MDA-MB-231 breast cancer cells, indicating that these compounds may represent a promising class of anticancer agents. SARs derived from this project provide useful insight into how various anion transport motifs and aromatic substitution patterns can be tuned to optimise carboxylate

binding and proton transport. These findings are important for the development of new classes of mitochondrial uncouplers and their application as mitochondria-targeted anticancer agents.

5.2 Future Directions

This thesis was primarily concerned with demonstrating the mechanisms of anion transport-mediated uncoupling, but an integral feature of well tolerated anticancer agents is their selectivity towards cancer cells. Consequently, more research is needed to better assess the efficacy of lead compounds such as **U3** and **3a** as potential anticancer agents for clinical use. Firstly, the cytotoxicity of **U3** and **3a** was only assessed against one cancer cell line (MDA-MB-231 cells), and should be tested on an array of cancerous and noncancerous cells lines to elucidate their anticancer selectivity. Additionally, the limited data on the ADMET (absorption, distribution, metabolism, excretion and toxicity) properties of these scaffolds precludes these compounds from clinical use. To begin addressing systemic human toxicity, off-target pharmacological profiling could be performed for the lead compounds using *in vitro* ligand binding assays such as Eurofins Discovery SafetyScreen87^{TM} and SpectrumScreen® Panels. Finally, in recognition of the promising activity of parent compounds **SR4** and aryl urea **2b** in xenograft mouse models, **U3** and diphenyl urea **3a** should be tested *in vivo* to evaluate whether their superior proton transport and *in vitro* biological actions translate to improved antitumour activity.

The biological features that govern the anticancer activity of these compounds could be elucidated further. There is evidence suggesting that charged species such as delocalised lipophilic cations can selectively accumulate in cancer cell mitochondria due to their elevated $\Delta\Psi_M$,[150] but accumulation of uncouplers into cancer cell mitochondria has not been demonstrated. It is likely that the mitochondrial uncouplers studied in this project disrupt OXPHOS in both cancerous and noncancerous cells, but these effects are more poorly tolerated by cancerous cells due to their unique energy demands and abnormal metabolism. Alternatively, the rate of uncoupling may be accelerated in hyperpolarised

mitochondria, causing a greater perturbation of OXPHOS in cancer cells. The elevated $\Delta\Psi_M$ is attributed to higher proton flux across the MIM and thus a greater ΔpH, and would drive favourable equilibria for deprotonation in the matrix and protonation in the intermembrane space. Further, diffusion of the anionic species across the MIM, which is considered the rate-limiting step of the cycle,[151] would be accelerated in mitochondria with elevated $\Delta\Psi_M$ due to the increased electrostatic forces experienced by the anion.

Importantly, the characterisation of anion transport-based mitochondrial uncoupling in this project, coupled with the superior anticancer activity of **SR4** compared to classical protonophores such as niclosamide and FCCP,[76,77] may suggest that fatty acid-activated uncoupling has improved selectivity and/or toxicity towards cancer cell mitochondria. The crucial difference between this mechanism and classical protonophoric cycling is the involvement of endogenous free fatty acids in the MIM.

One possibility is that the pK_a's of free fatty acids, which are approximately 4.8,[152] are uniquely suited for the acid-base equilibria present in cancer cell mitochondria. While pK_a determinations of small molecules in biological membranes differ from those measured in water,[153,154] the pK_a's of reported protonophores vary between 4 to 8.[10] This broad range suggests that free fatty acids do not possess unique acid-base properties, and indicates that the protonation and deprotonation events in the transport cycle are non-rate-limiting.

Alternatively, selectivity could instead arise because there are more free fatty acids in the MIM of cancerous cells, leading to increased uncoupling of OXPHOS by fatty acid-activated proton transport. A metabolic hallmark of cancer cells is the abnormal activation of de novo fatty acid synthesis and β-oxidation of fatty acids for ATP, leading to increased transport of free fatty acids to mitochondria.[155] Further, the highly folded structure of the MIM is organised in part by phospholipases, which hydrolyse phospholipids into free fatty acids and are upregulated in numerous cancers including lung,

prostate, colon, and breast.[156] These hypotheses are informed by the findings of this thesis but extend beyond its scope, and serve to stimulate new research avenues into the kinetics of fatty acid-activated proton transport, the levels of free fatty acids in the MIM of cancerous and noncancerous cells, and the development of new anticancer agents that function as fatty acid-activated mitochondrial uncouplers.

Finally, demonstrating that uncouplers like **U3** selectively transport deprotonated fatty acids over other physiologically relevant anions is important to directly link their biological actions to the fatty acid-activated mechanism. The physicochemical properties that make these molecules effective anion transporters for carboxylates would enhance their affinity for other anions too. As such the observed anticancer activity of this compounds could arise in part from the transport of other anions that are critical to cell viability. For example the squaramide-based synthetic anion transporter **S7** has been shown to induce apoptosis and disrupt autophagy in cancerous liver cells by facilitating chloride transport across membranes.[92] To explore the contribution of this pathway to the observed biological effects, future studies should be performed to determine whether these compounds can transport chloride in cancer cells at concentrations corresponding to their MTS IC_{50} values. If these compounds perturb chloride levels and uncouple mitochondria at similar concentrations, they could be considered as multitarget anticancer agents that enhances their therapeutic potential.

Appendices

Supplementary Information for Chapter Two

S2.1 HPTS proton transport assay

Vesicle Preparation

HPTS assays were conducted using POPC LUVs (200 nm diameter) vesicles loaded with an internal solution containing pH-sensitive fluorescent dye HPTS (1 mM), HEPES buffer (10 mM) and potassium gluconate (100 mM). An external solution of HEPES buffer (10 mM) and potassium gluconate (100 mM) was also prepared, and both solutions were buffered to pH 7.[105]

Unilamellar vesicles were prepared following a procedure outlined previously by the Gale group.[105] A chloroform solution of POPC (37.5 mM, 4 mL) was transferred to a pre-weighed round-bottom flask, and the solvent was removed using a rotary evaporator. The pressure was lowered slowly to ensure the formation of a smooth lipid film. Subsequently, the film was dried in vacuo for 4−24 h, and the mass of lipid was recorded. The lipids were rehydrated with 4 mL of internal solution (this number should correspond to the volume of POPC solution used initially) and vortexed until all lipids were removed from the sides of the flask and were suspended in solution. The lipids were subjected to 9 cycles of freeze-thaw by freezing using a dry ice/acetone bath and thawing in lukewarm water. Following this, the vesicles were left to rest at room temperature for 30 min. The lipids were extruded through a 200 nm polycarbonate membrane 25 times to form monodisperse vesicles. Only 1 mL of solution was extruded at a time before being collected. Finally, any residual unencapsulated salt from the internal solution was removed using a B19 column packed with hydrated G-25 Sephadex®, which had been pre-saturated with the respective external solution. The lipid suspensions were diluted with the external solution to afford a stock solution (10 mL) of a known concentration.

When fatty acid removal by BSA was required, fatty acid-free BSA was dissolved in the vesicle stock suspension to a final BSA concentration of 1 mol% (with respect to lipid). The BSA-containing vesicle stock suspension was stirred for 20 min before being used for membrane transport studies.

HPTS Assay

For a given experiment, the prepared vesicles were diluted to a concentration of 0.1 mM in a 4.5 mL plastic cuvette. A pH gradient is required to drive transport through the vesicle membrane in these experiments before the transporter is added. An aliquot of aqueous NaOH solution (25 μL, 0.5 M) was added to increase the pH of the external solution by approx. one pH unit to pH 8.0. For experiments requiring the addition of Oleic Acid (5 μL of 5 mM DMSO solution, 10 mol%, corresponding to ∼4 mol% free concentration after BSA binding) was added before NaOH. Following this, valinomycin (5 μL of 25 μM DMSO solution, 0.05 mol%) was added to each cuvette. Transport was initiated with the addition of the transporter as a DMSO solution (5 μL) and ended with the addition of detergent (Triton X-100 (10% v/v in water), 25 μL) was added at t = 200 s to lyse the vesicles, and a final fluorescence intensity reading was recorded at t = 300 s to signify 100% proton efflux.

Experiments were conducted under three conditions: i) Untreated vesicles (NaOH and valinomycin addition); ii) BSA-treated vesicles (NaOH and valinomycin addition); iii) BSA-treated vesicles with OA addition (OA, NaOH and valinomycin addition).

Dose-Response Hill Analysis

The changes in the fluorescent activity of intravesicular HPTS were used to detect pH changes during the experiments, and hence represent proton efflux. The acidic and basic forms of the HPTS probe were excited at λ_{ex} = 403 nm and λ_{ex} = 460 nm, respectively, and the fluorescence emission of

both forms recorded at λ_{em} = 510 nm. The intensity ratio of basic form to acidic form was determined, and the fractional fluorescence intensity (I_F) was calculated using the equation:

$$I_F = \frac{R_t - R_0}{R_d - R_0}$$

Where R_t is the ratiometric fluorescence value at a given time (t), R_0 is the ratiometric fluorescence value at t = 0 s and R_d is the fluorescence ratiometric value recorded at t = 280 s following the addition of detergent.

Dose-response experiments were performed at a minimum of five transporter concentrations plus a blank DMSO control run. The fractional fluorescence intensity (I_F) was plotted as a function of transporter concentration (mol%, with respect to lipid concentration). The I_F value at t = 200 s for each tested transporter concentration was fit to an adapted Hill Equation, using Origin 2021b (Academic), given as:

$$y = y_0 + (y_{max} - y_0)\frac{x^n}{k^n + x^n}$$

where y_0 is the I_F value at t = 200 s for the DMSO blank run, y_{max} is the maximum I_F value, n is the Hill coefficient, and k is a derived parameter.

A derived equation was used to calculate the EC_{50} value, the transporter concentration required to facilitate 50% proton efflux, given as:

$$EC_{50} = k\left(\frac{0.5}{y_1 - y_0}\right)^{1/n}$$

where k and n are the derived parameters from the Hill equation, y_0 is the percentage proton efflux at t = 0 s, and y_1 is the percentage proton efflux at t = 280 s. The dose-response Hill analyses for **1**–**14** under each test condition can be found in section 1.8 in this document.

S2.2 Purity testing of 1-14 through qNMR

The purity of all test compounds was confirmed to be >95% by absolute quantitative NMR spectroscopy according to the protocol outlined by the Journal of Medicinal Chemistry.[125] This technique determines purity by comparing the NMR signals of a given analyte against an internal calibrant (IC) of known purity. DMSO-d_6 was spiked with a known mass of the internal calibrant 1,3,5-trioxane (99.5% purity) to give a final IC concentration of approximately 3 mg/ml. Approximately 5 mg of each test compound was accurately weighed on a 5-decimal place analytical balance (0.01 mg accuracy). The sample was then dissolved in 600 µL of IC spiked DMSO-d_6 administered via mechanical pipette, then transferred to 5 mm NMR tubes. Collection and processing of NMR spectra, and calculation of purity, were performed according to the procedure described by the Journal of Medicinal Chemistry. The final calculated purities are shown in Table S1.

Table S1. Bisaryl urea qNMR table

Compound	Purity (%)
1	100.7
2	95.9
3	96.0
SR4	98.8
5	96.0
6	100.7
7	99.7
8	100.7
9	98.9
10	99.1
11	101.9
12	100.2
13	96.9
14	100.9

S2.3 JC-1 Representative dose-response curves

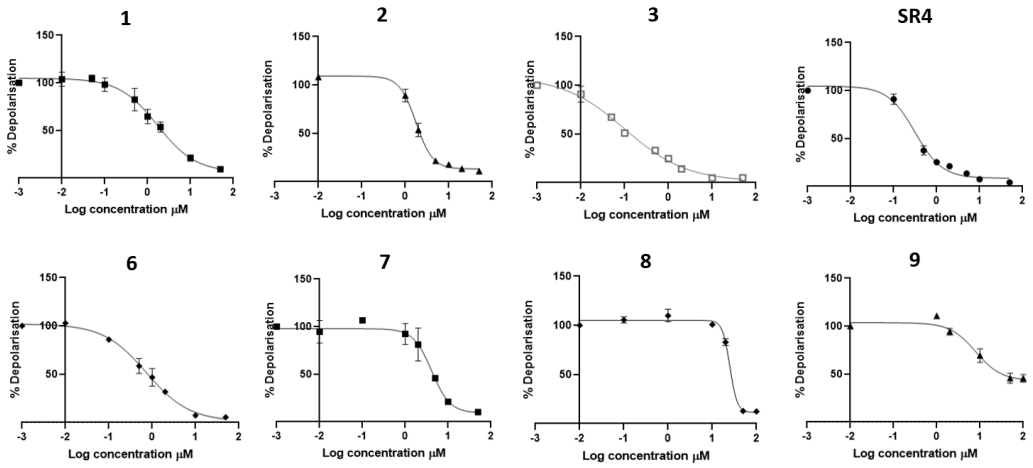

Figure S1 – Representative dose-response curves showing the effects of bisaryl ureas **1**, **2**, **3**, **6**, **7, 8, 9** and **SR4** on the JC-1 red:green fluorescence ratio in MDA-MB-231 breast cancer cells after 1 hour treatment with the test compound. Dose-response curves were constructed using log(inhibitor) vs response, variable slope (4 parameters) nonlinear regressions on GraphPad Prism 8 . Absolute IC50 concentrations were interpolated from these normalised curves (data normalised to DMSO vehicle control) with the top constrained to 100%. Equation: Y=Bottom + (Top-Bottom)/(1+10^((LogIC50-X)*HillSlope)).

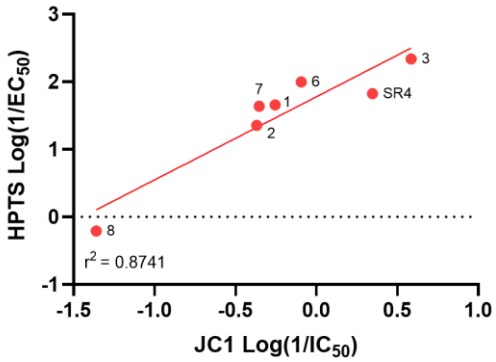

Figure S2 – Correlation plot of HPTS Log(1/EC_{50}) against JC-1 Log(1/IC_{50}) for **1**–**SR4** and **6**–**8**.

S2.4 MTS representative dose-response curves

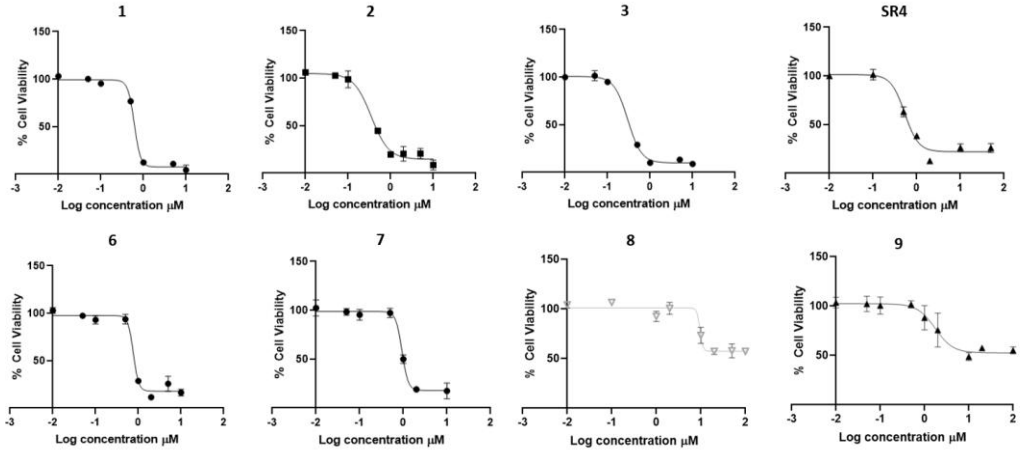

Figure S3 – Representative Dose-response curves showing the antiproliferative effects of bisaryl ureas **1**, **2**, **3**, **6**, **7, 8, 9** and **SR4** in MDA-MB-231 cells in a 72 h MTS cell viability assay. Dose-response curves were constructed using log(inhibitor) vs response, variable slope (4 parameters) non-linear regressions on GraphPad Prism 8. Absolute IC50 concentrations were interpolated from these normalised curves (data normalised to DMSO vehicle control) with the top constrained to 100%. Equation: Y=Bottom + (Top-Bottom)/(1+10^((LogIC50-X)*HillSlope)).

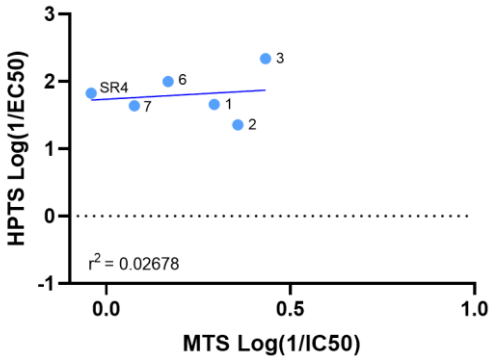

Figure S4 – Correlation plot of HPTS Log($1/EC_{50}$) against MTS Log($1/IC_{50}$) for **1**–**SR4**, **6** and **7**.

S2.5 ATP assay data distribution

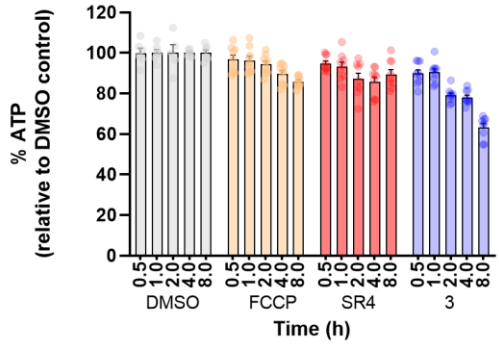

Figure S5 – Total intracellular ATP assay bar chart describing the mean, SEM and individual data points from three independent experiments.

S2.6 LDH Release Cytotoxicity Assay

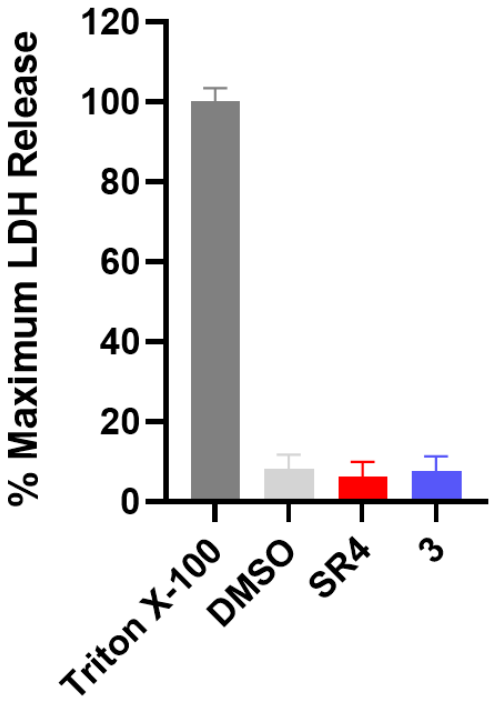

Figure S6 – LDH release assay data displaying cytotoxicity of **SR4** and **3** vs DMSO vehicle control following 8 hours treatment. Maximum LDH release determined from a positive control consisting of cells treated with 0.2% Triton X-100 and incubated for 15 minutes prior to sample collection.

S2.7 1-14 ^{1}H NMR and ^{13}C NMR Spectra

N,N'-bis[3,4-bis(trifluoromethyl)phenyl]urea (1)

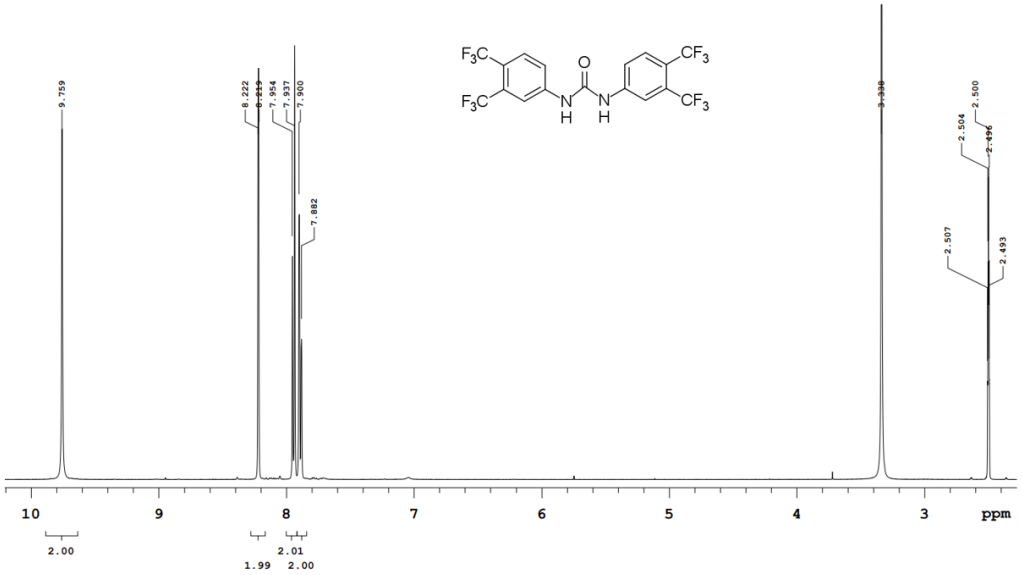

Figure S7. ^{1}H NMR spectrum of **1**

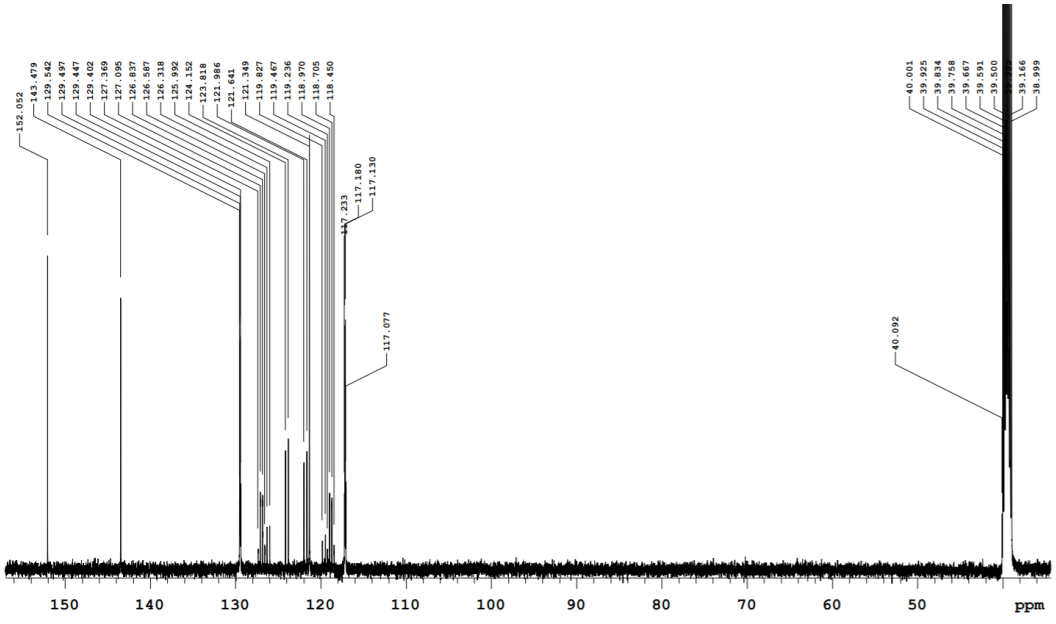

Figure S8. ^{13}C NMR spectrum of **1**

N,N'-bis[4-(trifluoromethylsulfonyl)phenyl]urea (2)

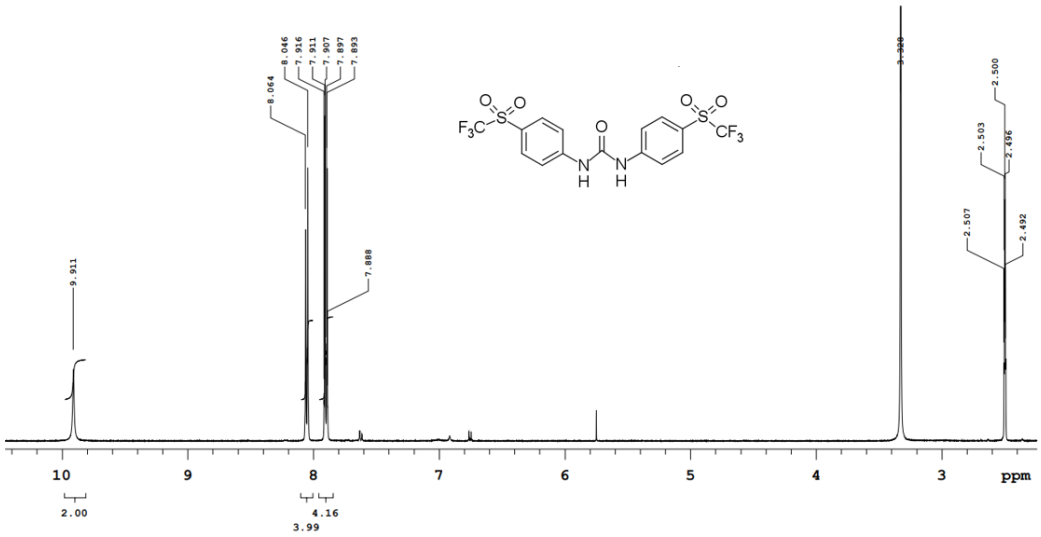

Figure S9. ^{1}H NMR spectrum of **2**

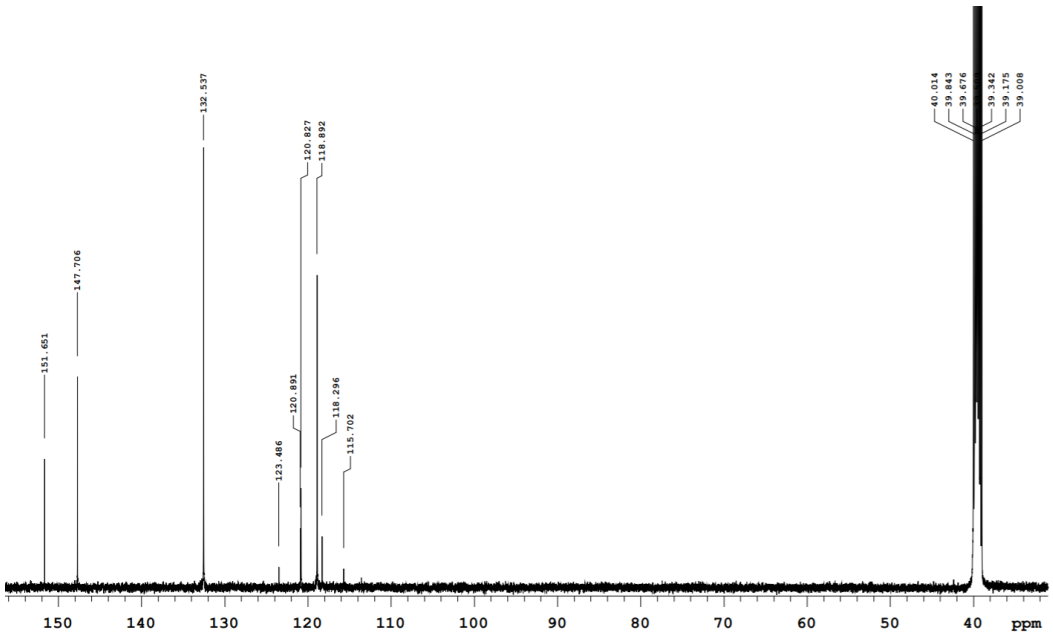

Figure S10. ^{13}C NMR spectrum of **2**

N,N'-bis[3-chloro-5-(trifluoromethyl)phenyl]urea (3)

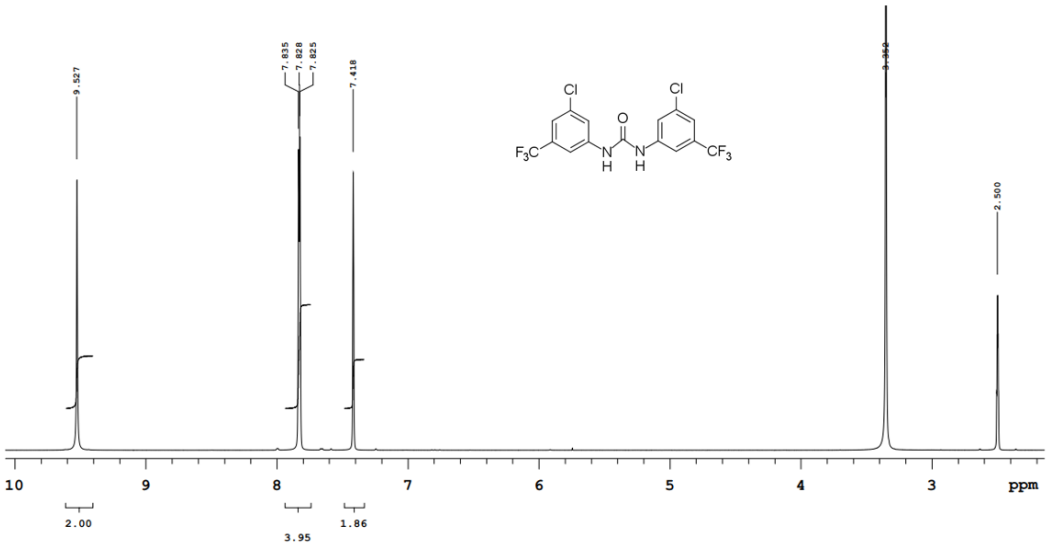

Figure S11. ^{1}H NMR spectrum of **3**

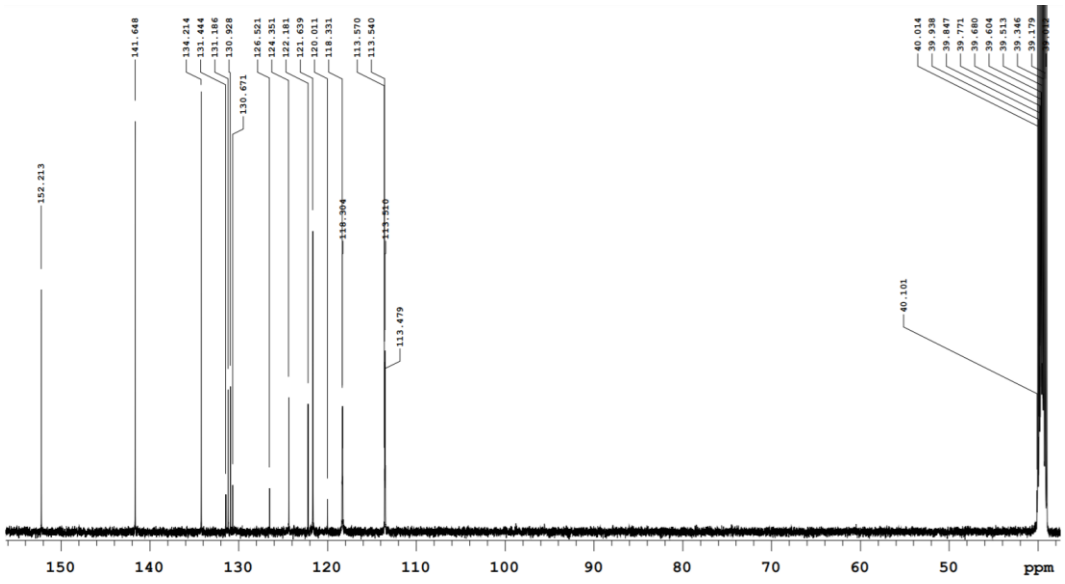

Figure S12. ^{13}C NMR spectrum of **3**

N,N'-bis[3,5-dichlorophenyl]urea (SR4)

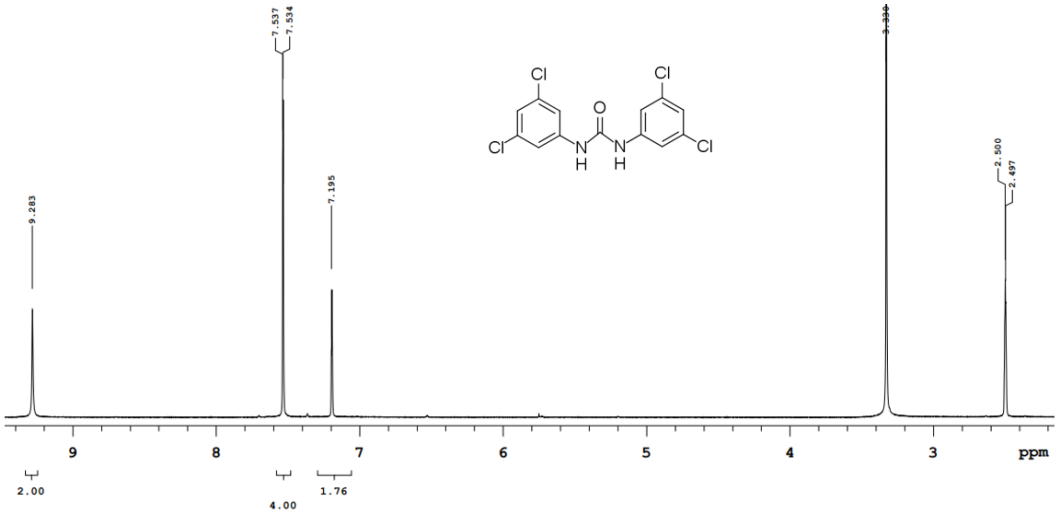

Figure S13. ^{1}H NMR spectrum of **SR4**

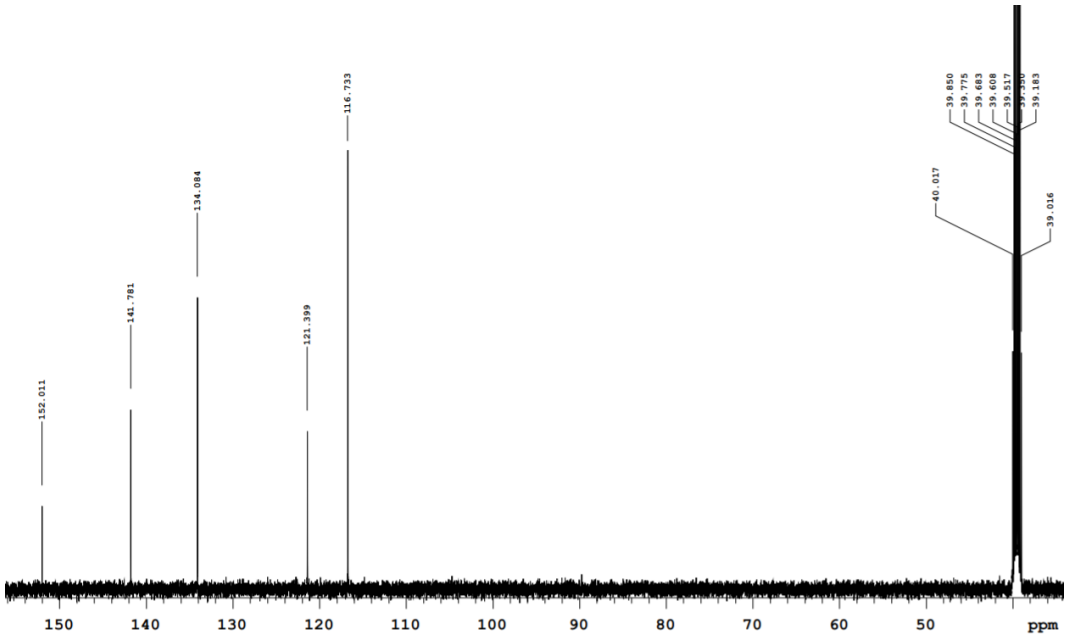

Figure S14. ^{13}C NMR spectrum of **SR4**

N,N'-bis[4(methylsulfonyl)phenyl]urea (5)

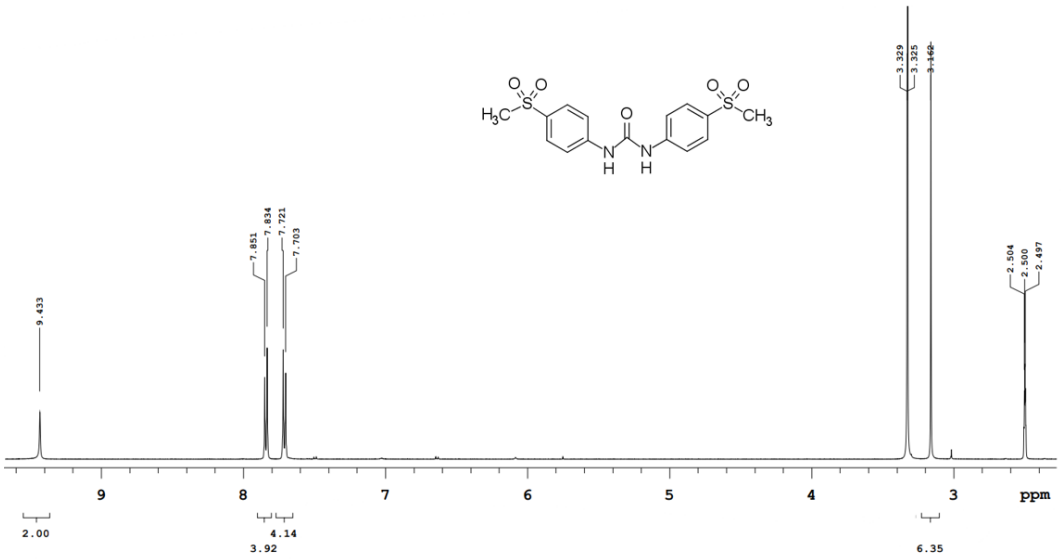

Figure S15. ^{1}H NMR spectrum of **5**

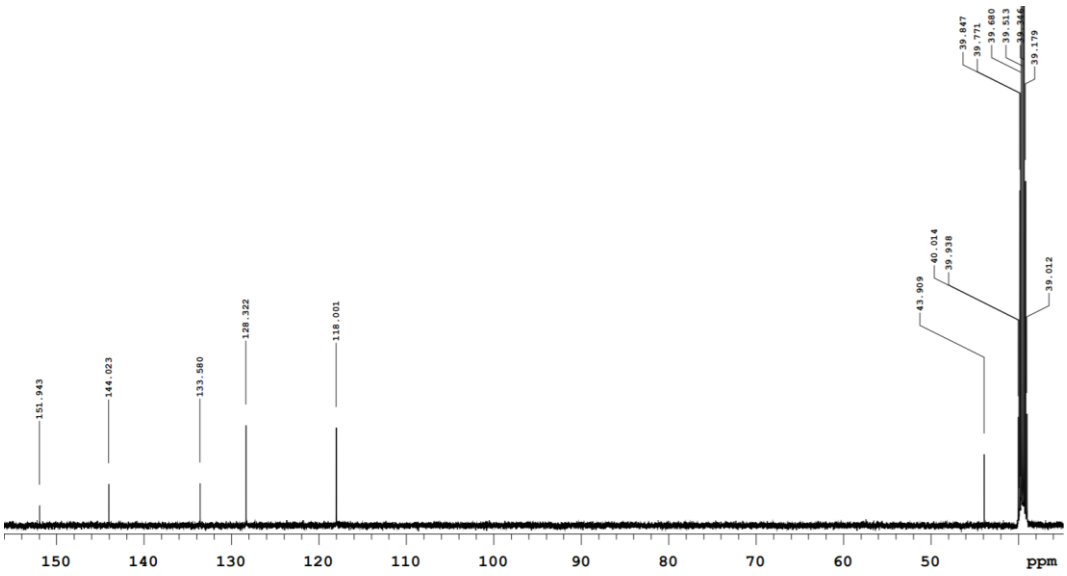

Figure S16. ^{13}C NMR spectrum of **5**

N,N'-bis[4-chloro-3-(trifluoromethyl)phenyl]urea (6)

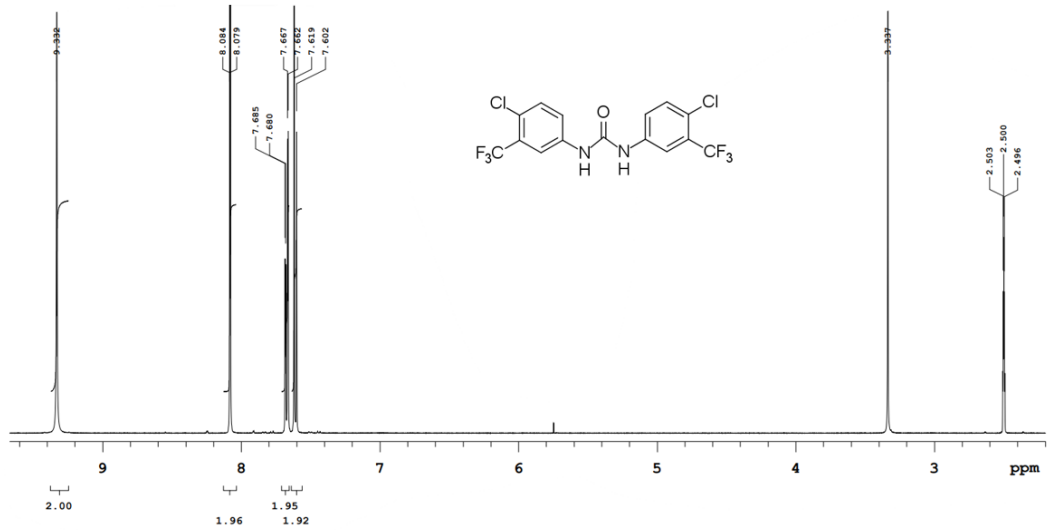

Figure S17. ^{1}H NMR spectrum of **6**

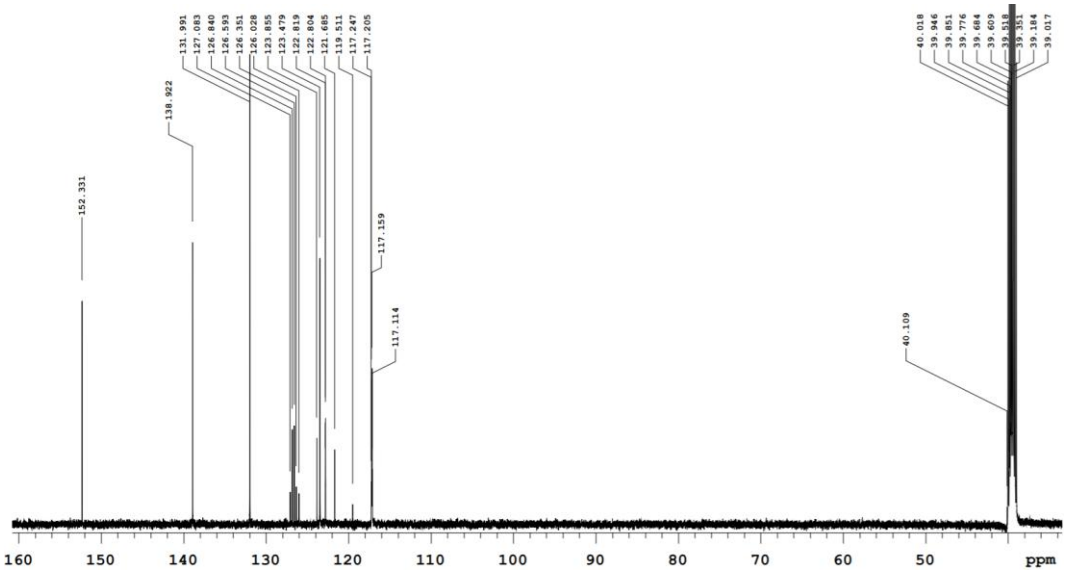

Figure S18. ^{13}C NMR spectrum of **6**

N,N'-bis[4-(trifluoromethyl)phenyl]urea (7)

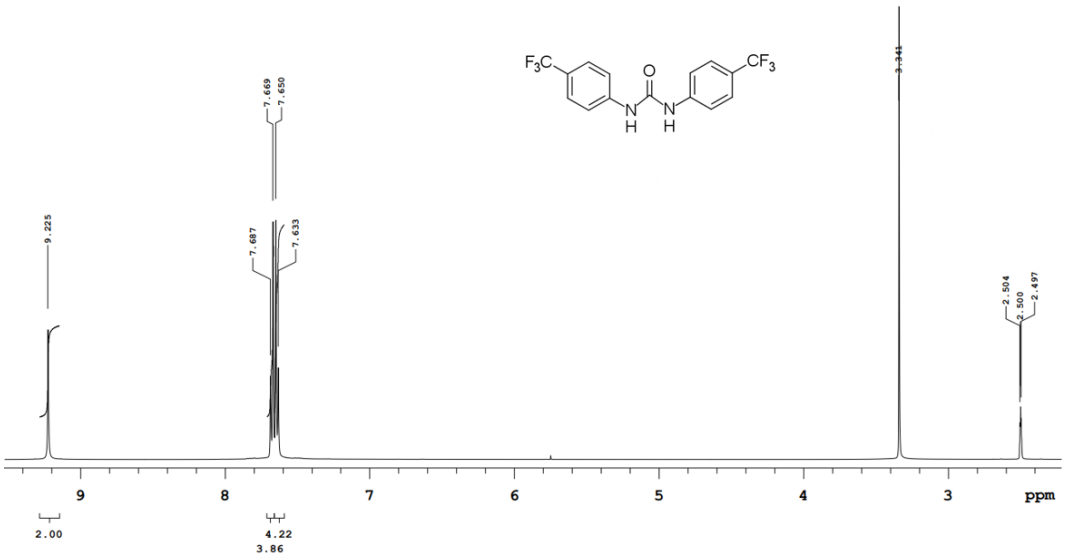

Figure S19. ^{1}H NMR spectrum of **7**

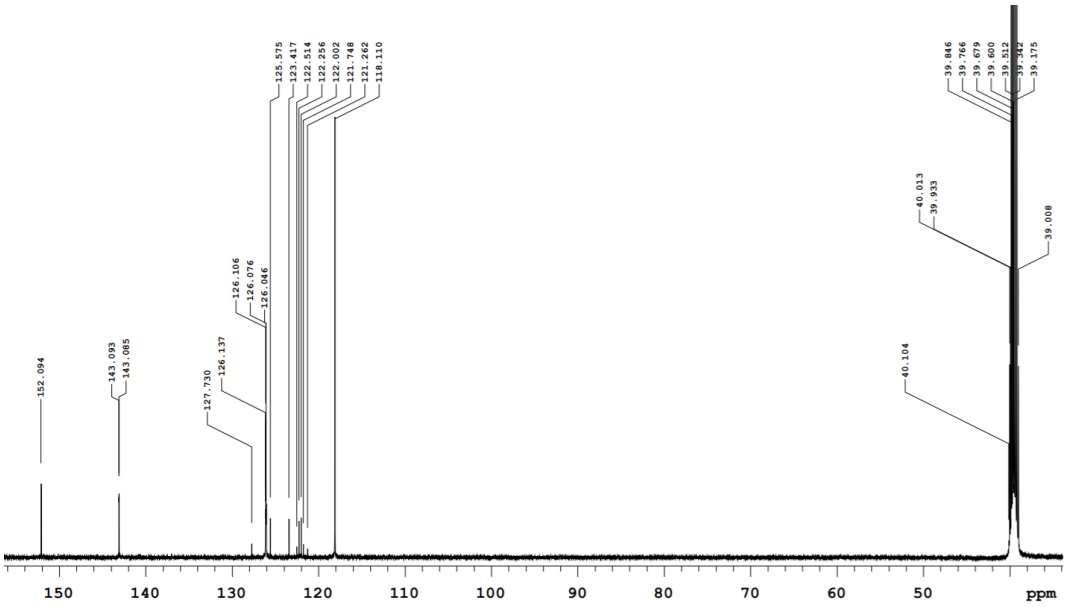

Figure S20. ^{13}C NMR spectrum of **7**

N,N'-bis(4-acetylphenyl)urea (8)

Figure S21. ^{1}H NMR spectrum of **8**

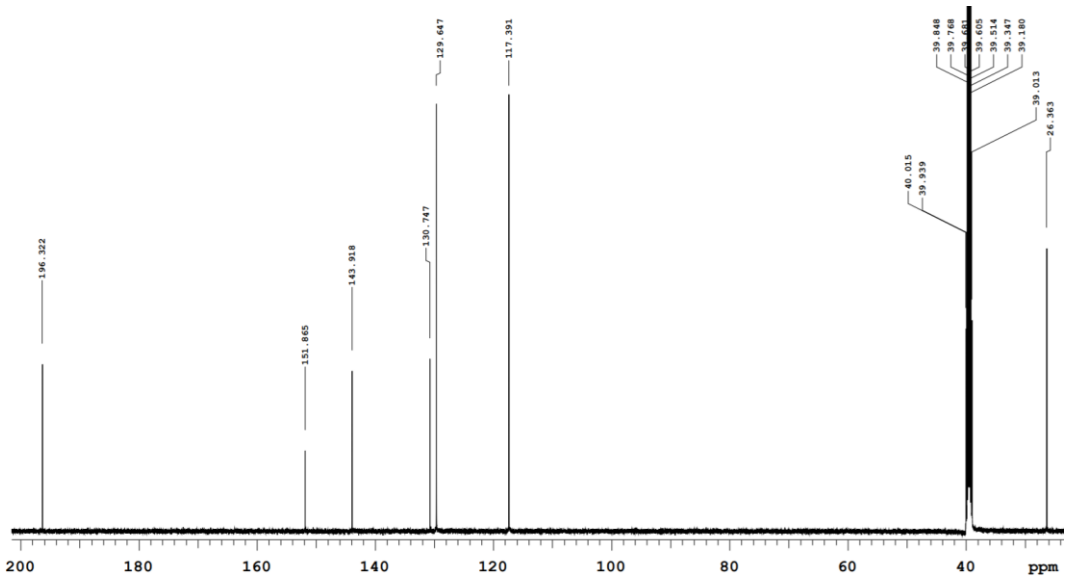

Figure S22. ^{13}C NMR spectrum of **8**

N,N'-bis[4-(trifluoromethoxy)phenyl]urea (9)

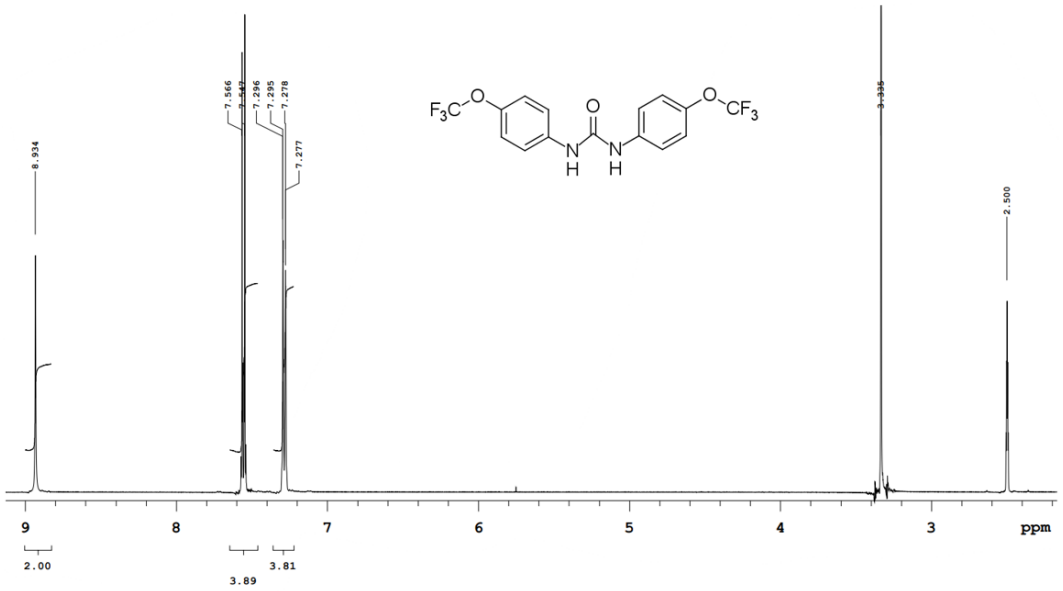

Figure S23. ^{1}H NMR spectrum of **9**

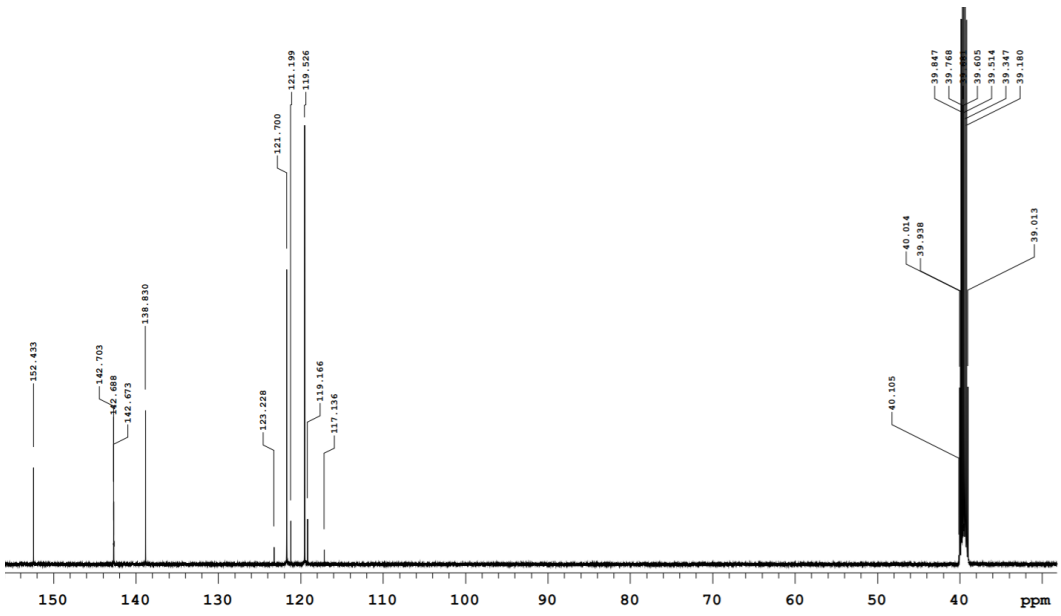

Figure S24. ^{13}C NMR Spectrum of **9**

N,N'-bis[4-chlorophenyl]urea (10)

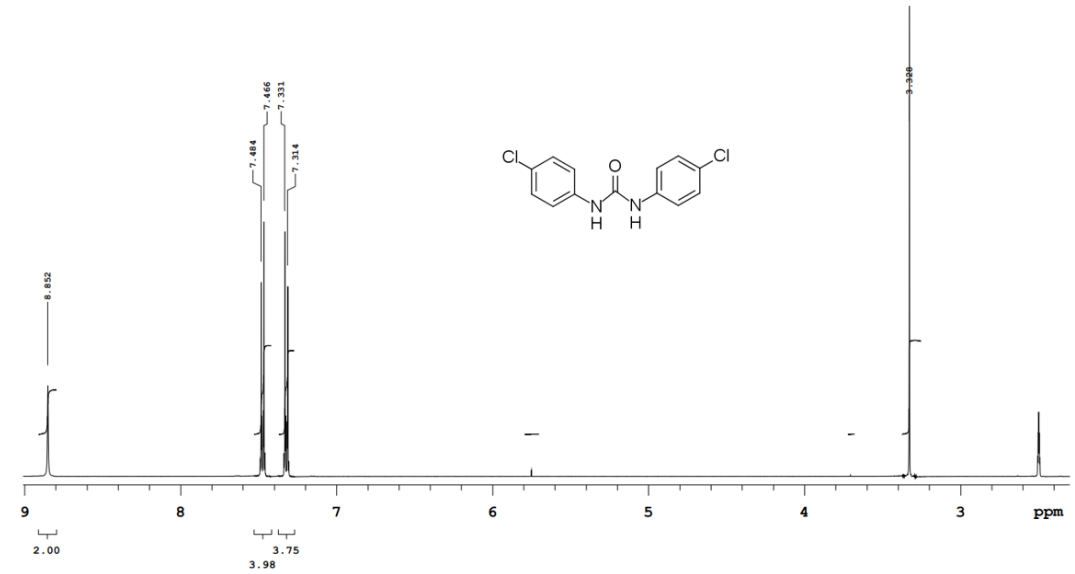

Figure S25. ^{1}H NMR spectrum of **10**

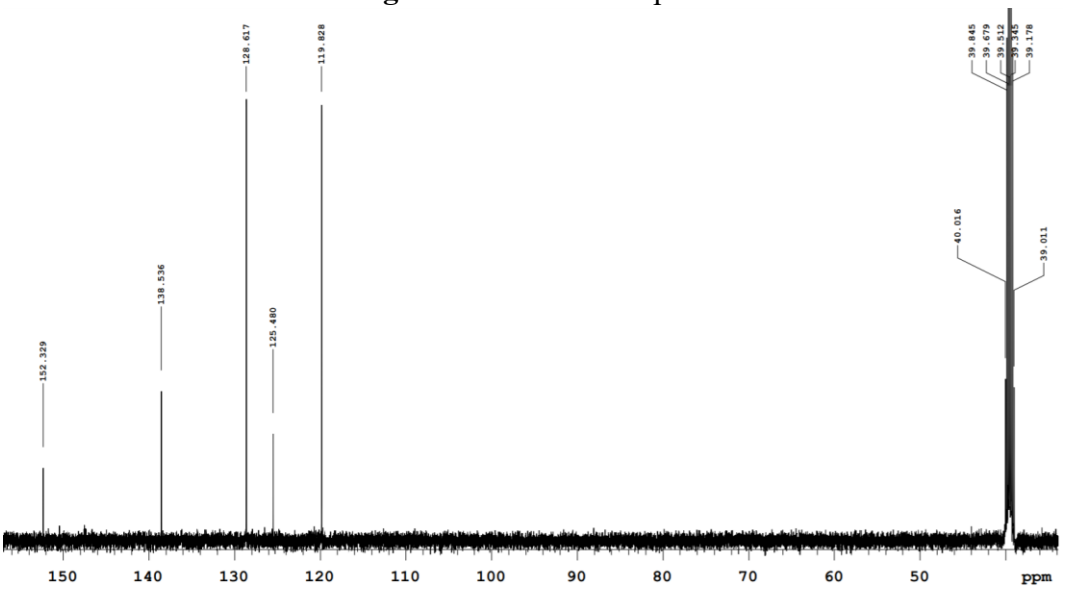

Figure S26. ^{13}C NMR spectrum of **10**

N,N'-diphenylurea (11)

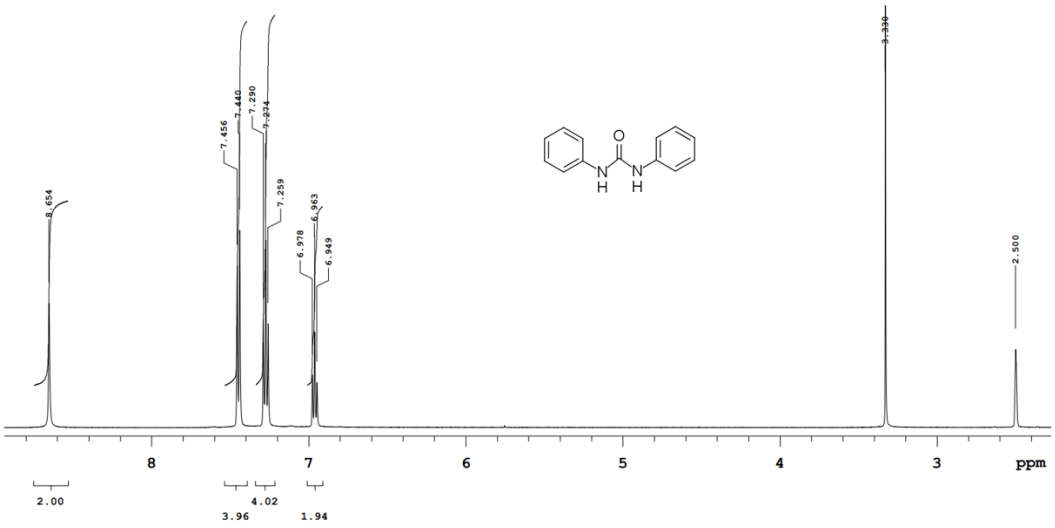

Figure S27. ^{1}H NMR spectrum of **11**

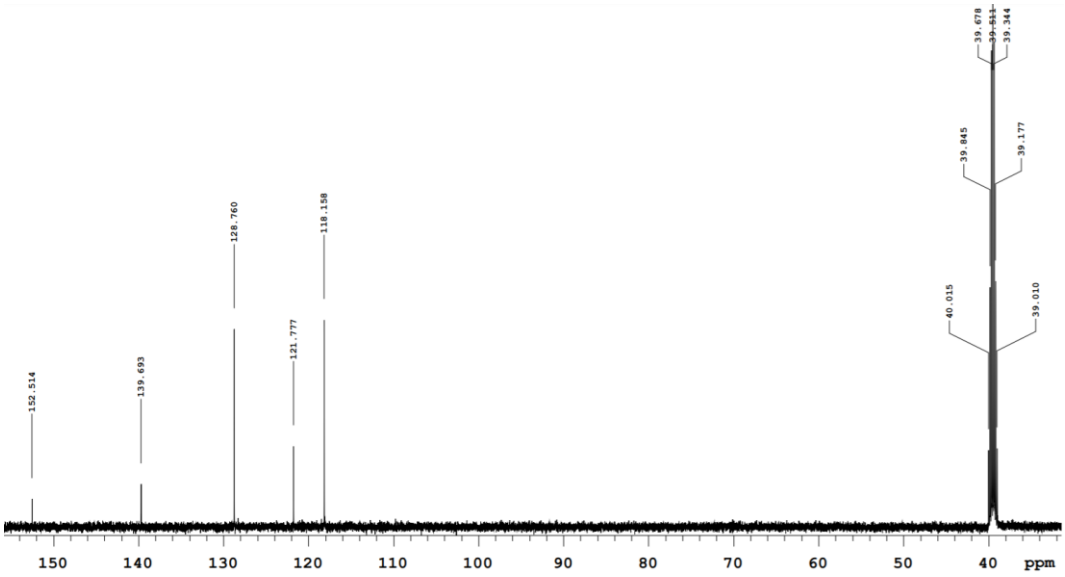

Figure S28. ^{13}C NMR spectrum of **11**

N,N'-bis(4-methylphenyl)urea (12)

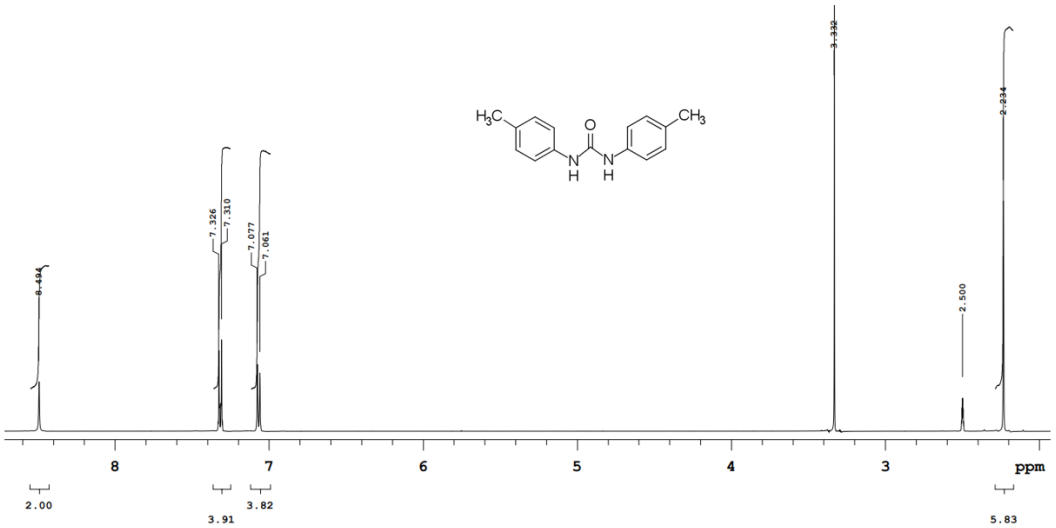

Figure S29. ^{1}H NMR spectrum of **12**

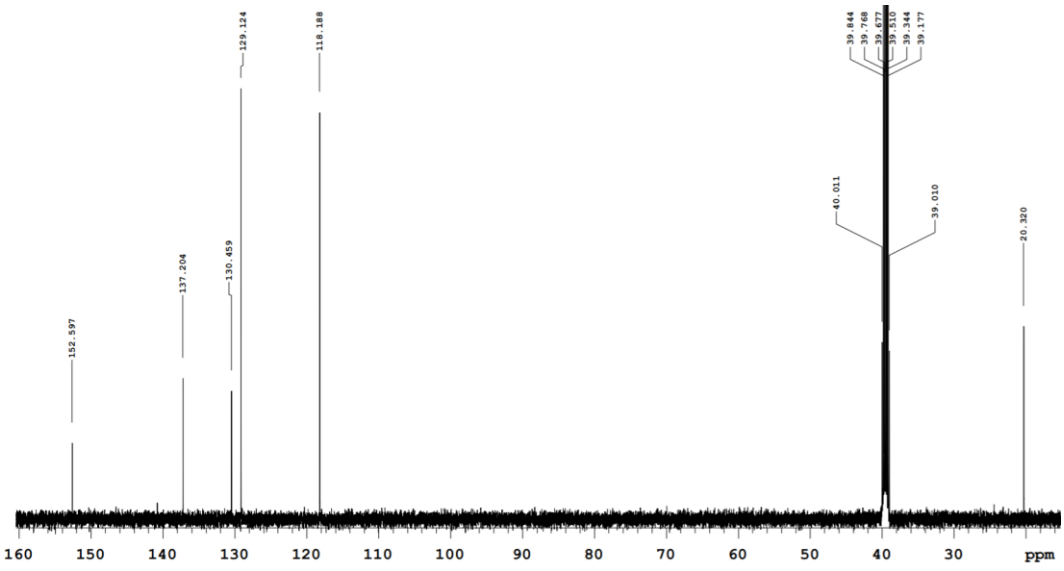

Figure S30. ^{13}C NMR spectrum of **12**

N,N-bis(3,4-dimethylphenyl)urea (13)

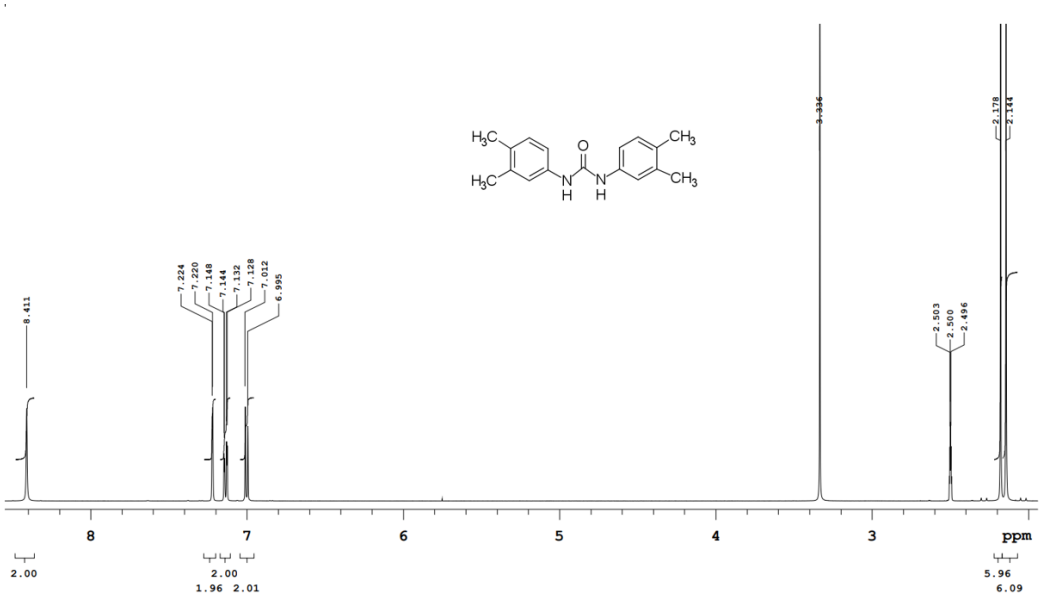

Figure S31. ^{1}H NMR spectrum of **13**

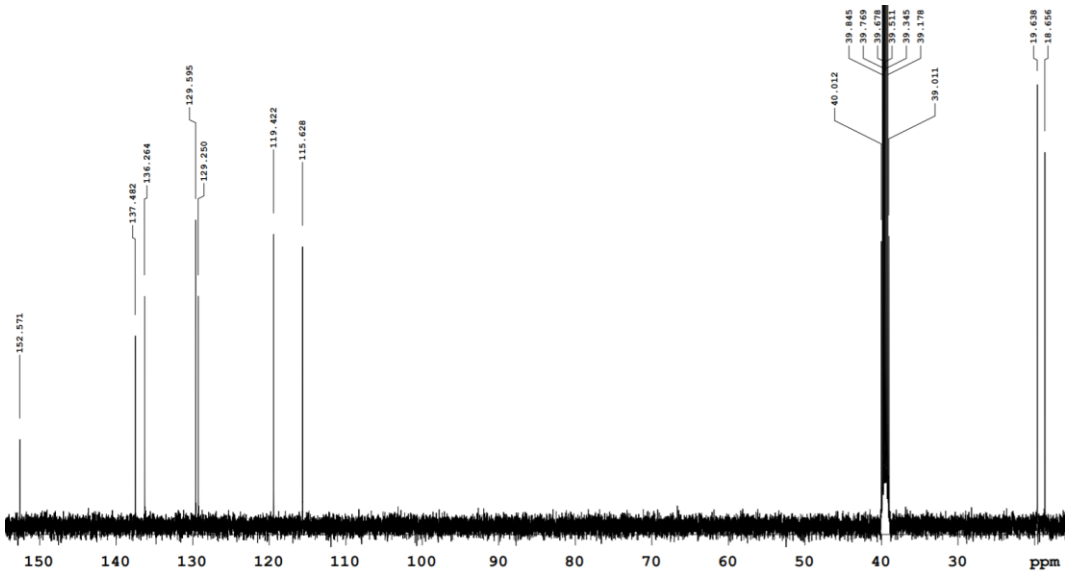

Figure S32. ^{13}C NMR spectrum of **13**

N,N-bis(4-methoxyphenyl)urea (14)

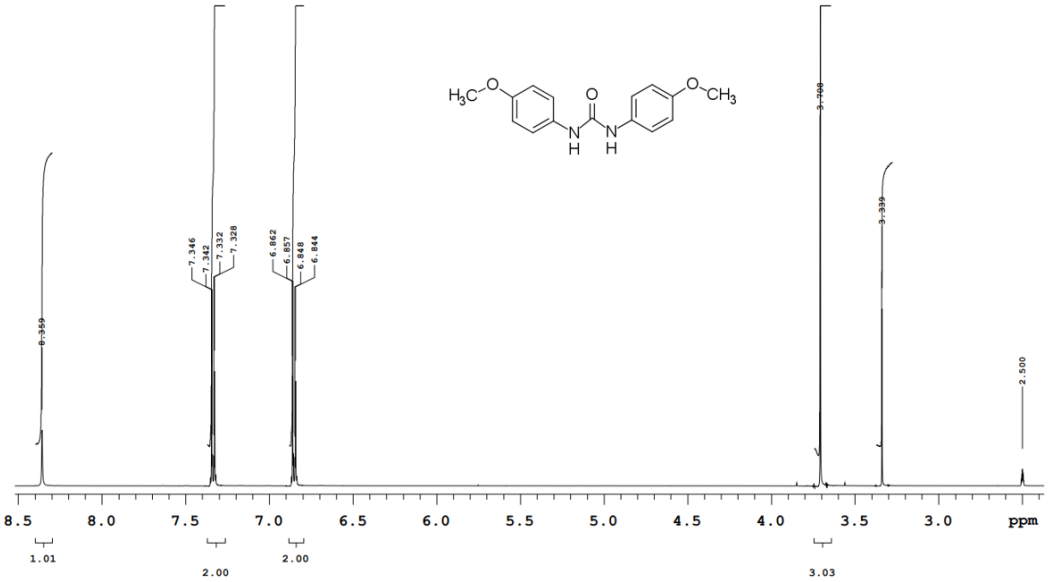

Figure S33. ^{1}H NMR spectrum of **14**

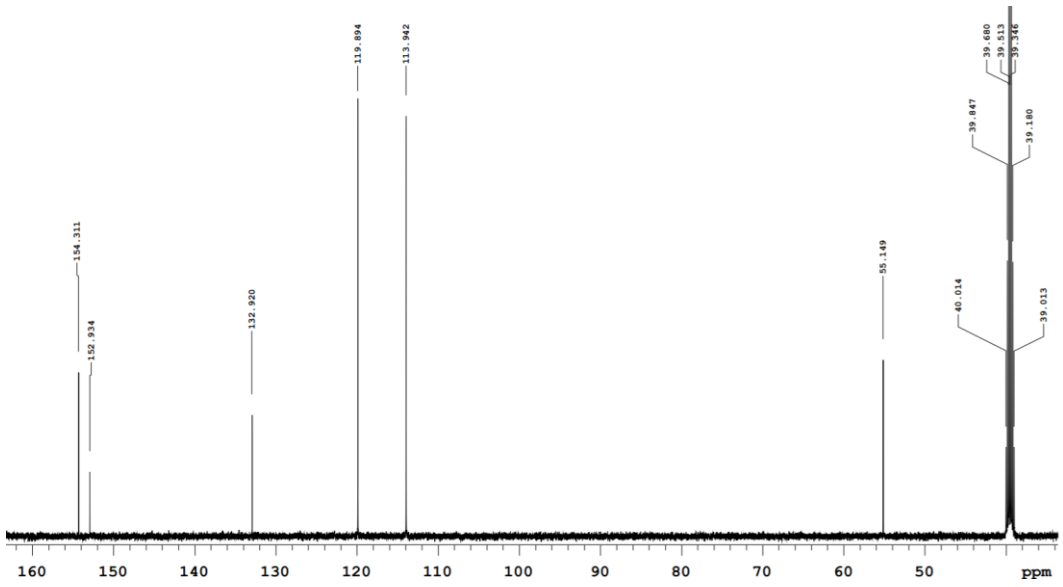

Figure S34. ^{13}C NMR spectrum of **14**

S2.8 1–14 HPTS Dose-response Hill Analyses

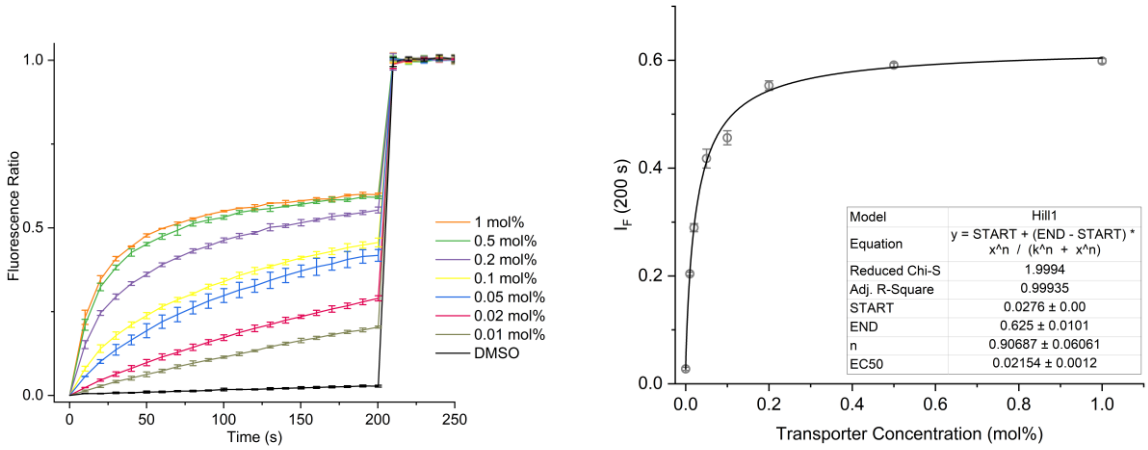

Figure S35 – Hill plot analysis of H^+/OH^- transport facilitated by compound **1** measured using the KGluc assay. NaOH (5 mM) and valinomycin (0.05 mol%) were added to the vesicles before the addition of **1** at 0 s. Detergent was added at 200 s to lyse the vesicles. Compound concentrations are shown as compound-to-lipid molar ratios. Error bars represent standard deviations from at least two repeats.

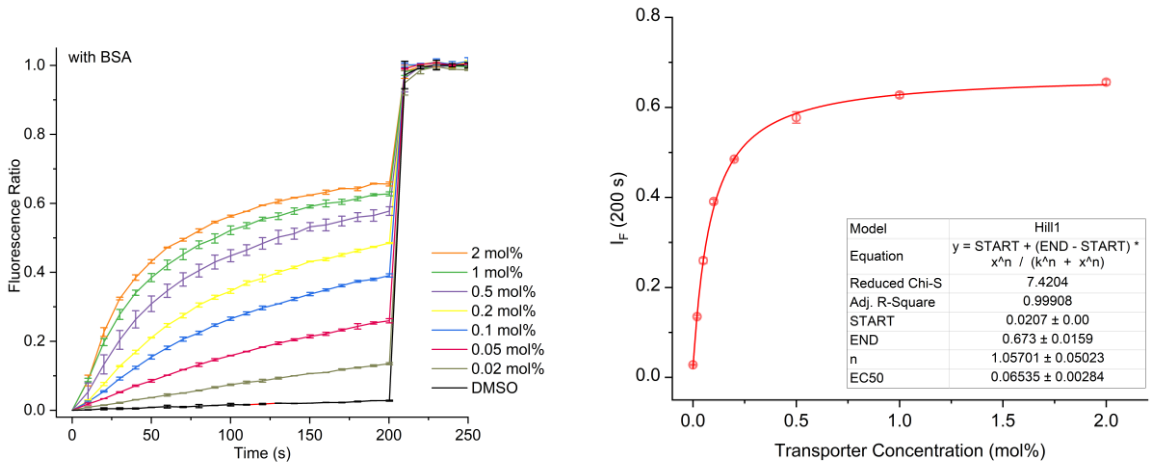

Figure S36 – Hill plot analysis of H^+/OH^- transport facilitated by compound **1** measured using the KGluc assay. The vesicles were pre-treated with BSA (1 mol%). NaOH (5 mM) and valinomycin (0.05 mol%) were added to the vesicles before the addition of **1** at 0 s. Detergent was added at 200 s

to lyse the vesicles. Compound concentrations are shown as compound-to-lipid molar ratios. Error bars represent standard deviations from at least two repeats.

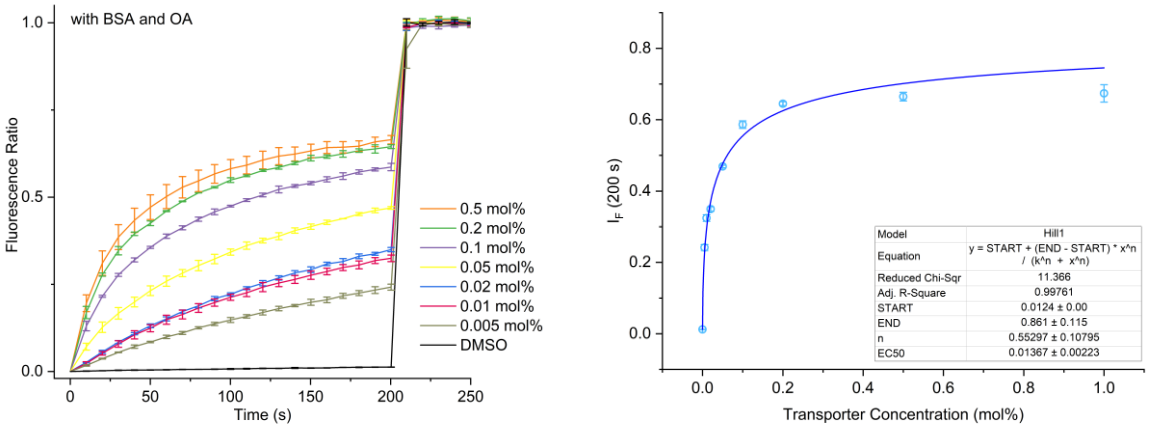

Figure S37 – Hill plot analysis of H^+/OH^- transport facilitated by compound **1** measured using the KGluc assay. The vesicles were pre-treated with BSA (1 mol%). OA (10 mol%), NaOH (5 mM) and valinomycin (0.05 mol%) were added to the vesicles before the addition of **1** at 0 s. Detergent was added at 200 s to lyse the vesicles. Compound concentrations are shown as compound-to-lipid molar ratios. Error bars represent standard deviations from at least two repeats.

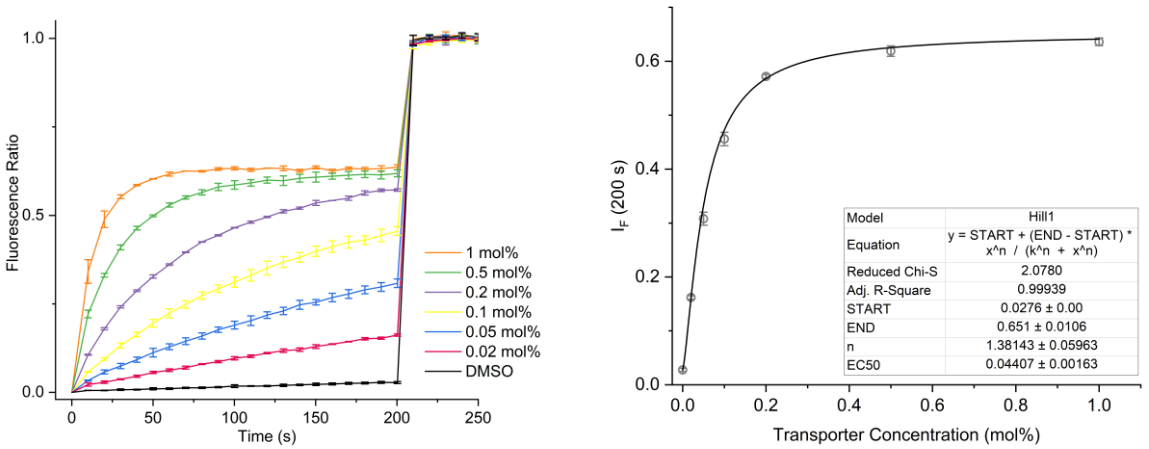

Figure S38 – Hill plot analysis of H^+/OH^- transport facilitated by compound **2** measured using the KGluc assay. NaOH (5 mM) and valinomycin (0.05 mol%) were added to the vesicles before the addition of **2** at 0 s. Detergent was added at 200 s to lyse the vesicles. Compound concentrations are

shown as compound-to-lipid molar ratios. Error bars represent standard deviations from at least two repeats.

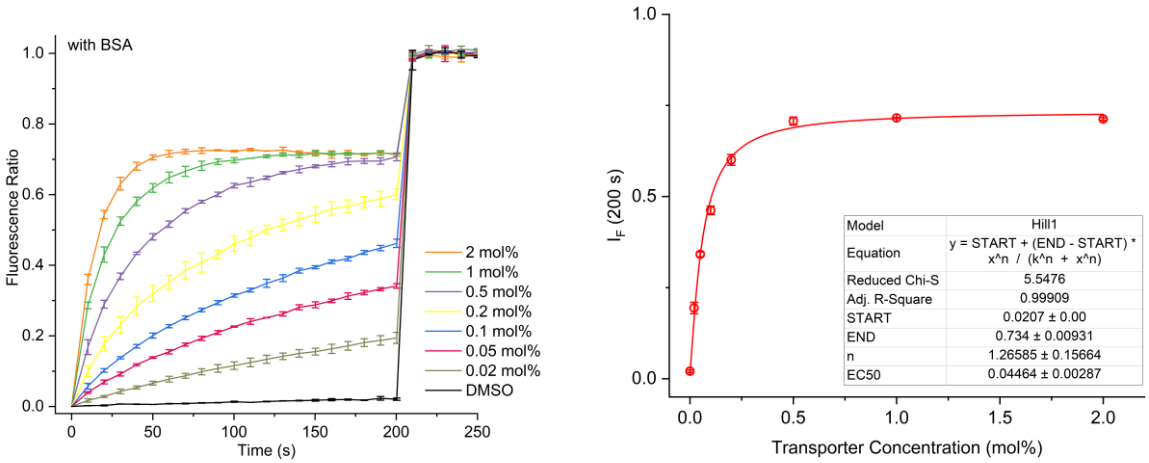

Figure S39 – Hill plot analysis of H^+/OH^- transport facilitated by compound **2** measured using the KGluc assay. The vesicles were pre-treated with BSA (1 mol%). NaOH (5 mM) and valinomycin (0.05 mol%) were added to the vesicles before the addition of **2** at 0 s. Detergent was added at 200 s to lyse the vesicles. Compound concentrations are shown as compound-to-lipid molar ratios. Error bars represent standard deviations from at least two repeats.

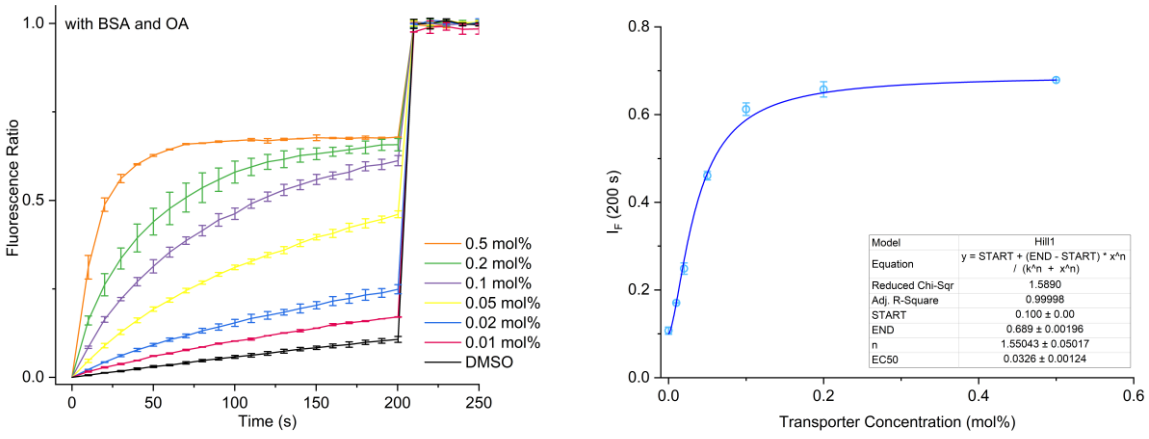

Figure S40 – Hill plot analysis of H^+/OH^- transport facilitated by compound **2** measured using the KGluc assay. The vesicles were pre-treated with BSA (1 mol%). OA (10 mol%), NaOH (5 mM) and

valinomycin (0.05 mol%) were added to the vesicles before the addition of **2** at 0 s. Detergent was added at 200 s to lyse the vesicles. Compound concentrations are shown as compound-to-lipid molar ratios. Error bars represent standard deviations from at least two repeats.

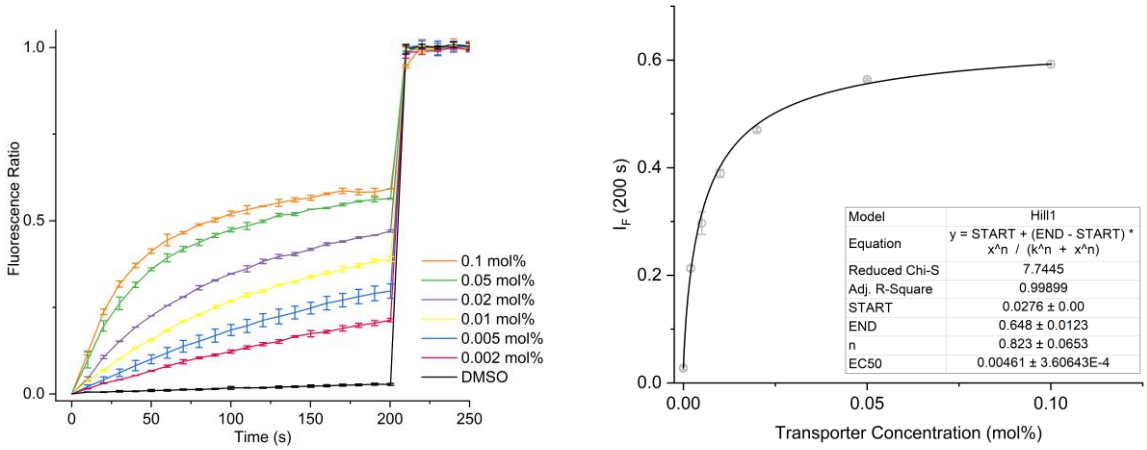

Figure S41 – Hill plot analysis of H^+/OH^- transport facilitated by compound **3** measured using the KGluc assay. NaOH (5 mM) and valinomycin (0.05 mol%) were added to the vesicles before the addition of **3** at 0 s. Detergent was added at 200 s to lyse the vesicles. Compound concentrations are shown as compound-to-lipid molar ratios. Error bars represent standard deviations from at least two repeats.

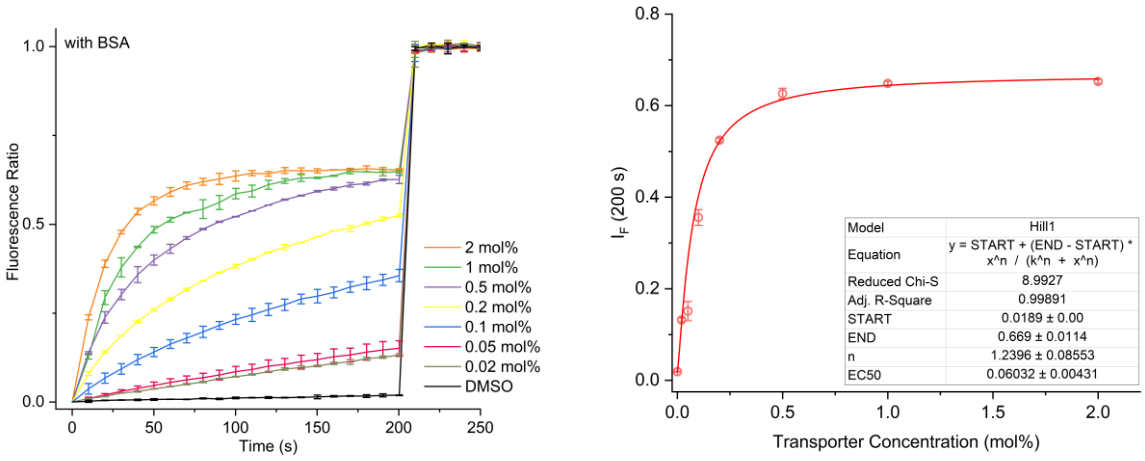

Figure S42 – Hill plot analysis of H^+/OH^- transport facilitated by compound **3** measured using the KGluc assay. The vesicles were pre-treated with BSA (1 mol%). NaOH (5 mM) and valinomycin (0.05 mol%) were added to the vesicles before the addition of **3** at 0 s. Detergent was added at 200 s to lyse the vesicles. Compound concentrations are shown as compound-to-lipid molar ratios. Error bars represent standard deviations from at least two repeats.

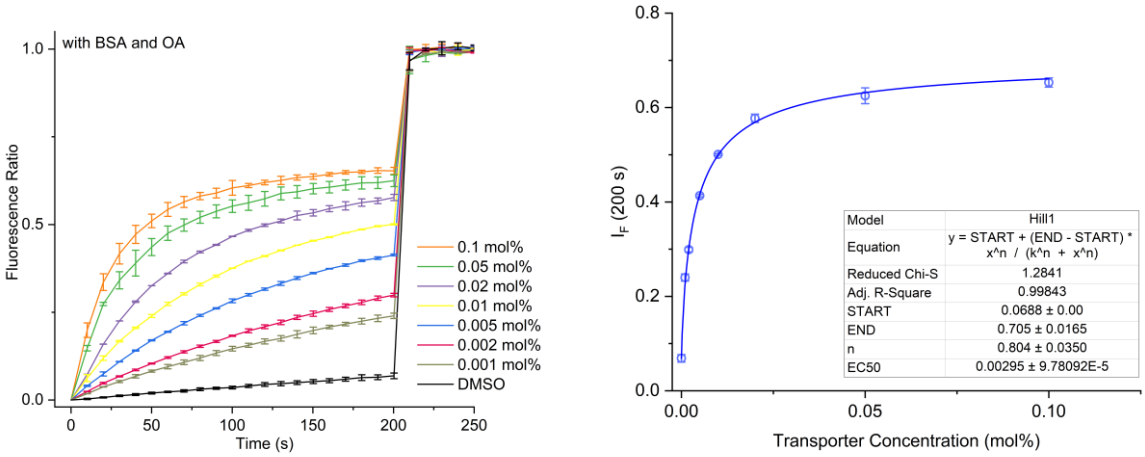

Figure S43 – Hill plot analysis of H^+/OH^- transport facilitated by compound **3** measured using the KGluc assay. The vesicles were pre-treated with BSA (1 mol%). OA (10 mol%), NaOH (5 mM) and valinomycin (0.05 mol%) were added to the vesicles before the addition of **3** at 0 s. Detergent was added at 200 s to lyse the vesicles. Compound concentrations are shown as compound-to-lipid molar ratios. Error bars represent standard deviations from at least two repeats.

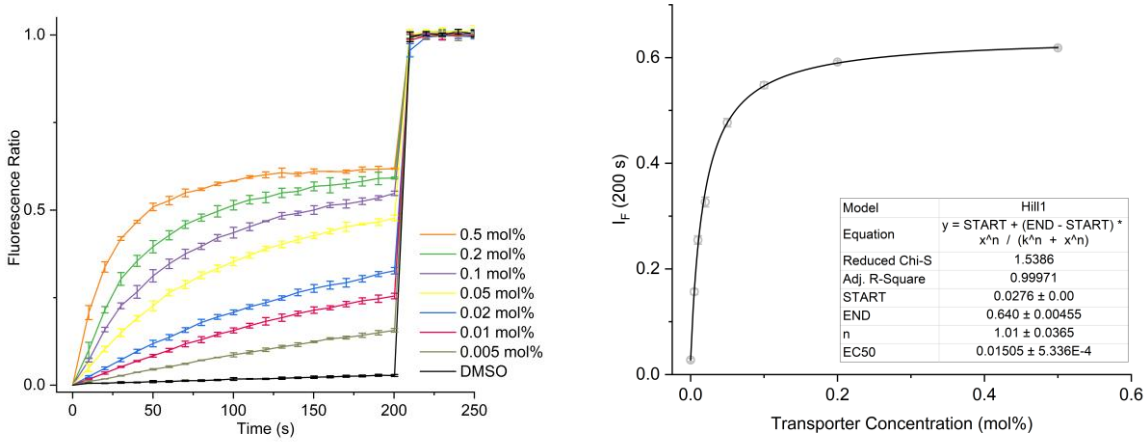

Figure S44 – Hill plot analysis of H^+/OH^- transport facilitated by compound **4** measured using the KGluc assay. NaOH (5 mM) and valinomycin (0.05 mol%) were added to the vesicles before the addition of **4** at 0 s. Detergent was added at 200 s to lyse the vesicles. Compound concentrations are shown as compound-to-lipid molar ratios. Error bars represent standard deviations from at least two repeats.

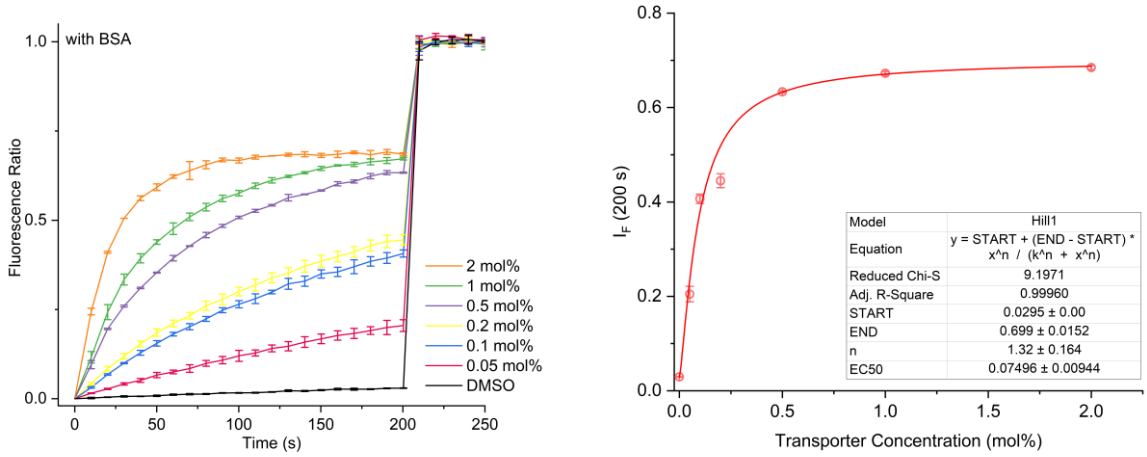

Figure S45 – Hill plot analysis of H^+/OH^- transport facilitated by compound **4** measured using the KGluc assay. The vesicles were pre-treated with BSA (1 mol%). NaOH (5 mM) and valinomycin (0.05 mol%) were added to the vesicles before the addition of **4** at 0 s. Detergent was added at 200 s to lyse the vesicles. Compound concentrations are shown as compound-to-lipid molar ratios. Error bars represent standard deviations from at least two repeats.

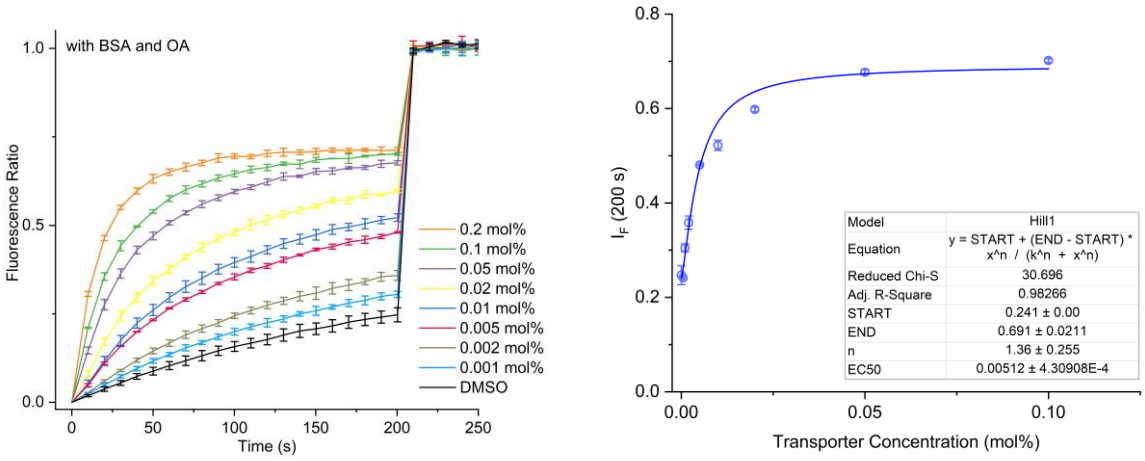

Figure S46 – Hill plot analysis of H^+/OH^- transport facilitated by compound **4** measured using the KGluc assay. The vesicles were pre-treated with BSA (1 mol%). OA (10 mol%), NaOH (5 mM) and valinomycin (0.05 mol%) were added to the vesicles before the addition of **4** at 0 s. Detergent was added at 200 s to lyse the vesicles. Compound concentrations are shown as compound-to-lipid molar ratios. Error bars represent standard deviations from at least two repeats.

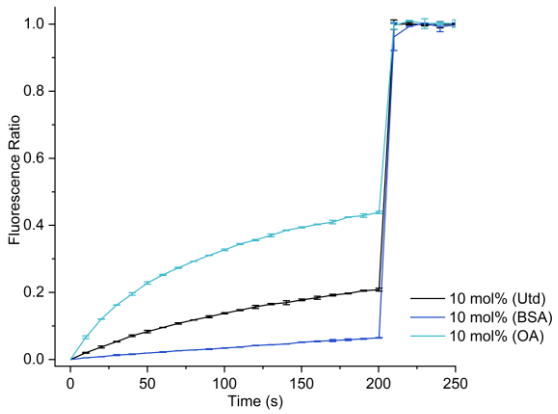

Figure S47 – Efflux plots of H^+/OH^- transport facilitated by compound **5** measured using the KGluc assay. A 10 mol% compound-to-lipid molar ratio of **5** was added to the vesicles at 0 s under the three conditions outlined above (Untreated, BSA treated, BSA and OA treated), and detergent was added at 200 s to lyse the vesicles. Error bars represent standard deviations from at least two repeats. H^+/OH^- efflux did not exceed 50% after 200 s under any of the conditions tested.

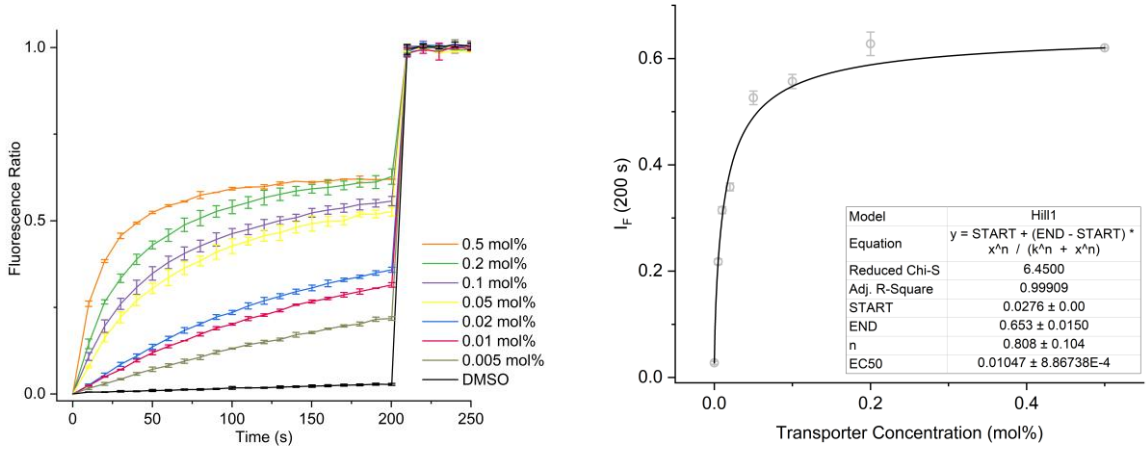

Figure S48 – Hill plot analysis of H^+/OH^- transport facilitated by compound **6** measured using the KGluc assay. NaOH (5 mM) and valinomycin (0.05 mol%) were added to the vesicles before the addition of **6** at 0 s. Detergent was added at 200 s to lyse the vesicles. Compound concentrations are shown as compound-to-lipid molar ratios. Error bars represent standard deviations from at least two repeats.

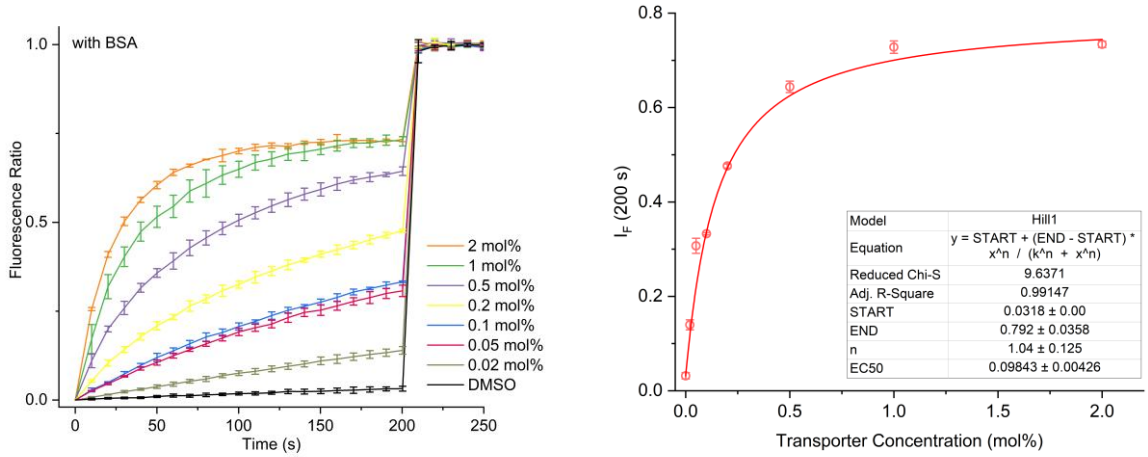

Figure S49 – Hill plot analysis of H^+/OH^- transport facilitated by compound **6** measured using the KGluc assay. The vesicles were pre-treated with BSA (1 mol%). NaOH (5 mM) and valinomycin (0.05 mol%) were added to the vesicles before the addition of **6** at 0 s. Detergent was added at 200 s to lyse the vesicles. Compound concentrations are shown as compound-to-lipid molar ratios. Error bars represent standard deviations from at least two repeats.

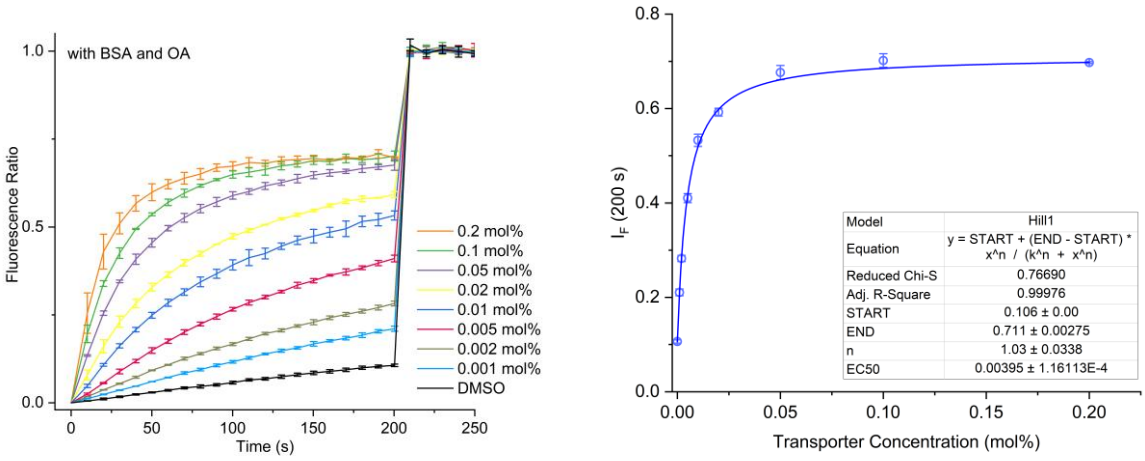

Figure S50 – Hill plot analysis of H^+/OH^- transport facilitated by compound **6** measured using the KGluc assay. The vesicles were pre-treated with BSA (1 mol%). OA (10 mol%), NaOH (5 mM) and valinomycin (0.05 mol%) were added to the vesicles before the addition of **6** at 0 s. Detergent was added at 200 s to lyse the vesicles. Compound concentrations are shown as compound-to-lipid molar ratios. Error bars represent standard deviations from at least two repeats.

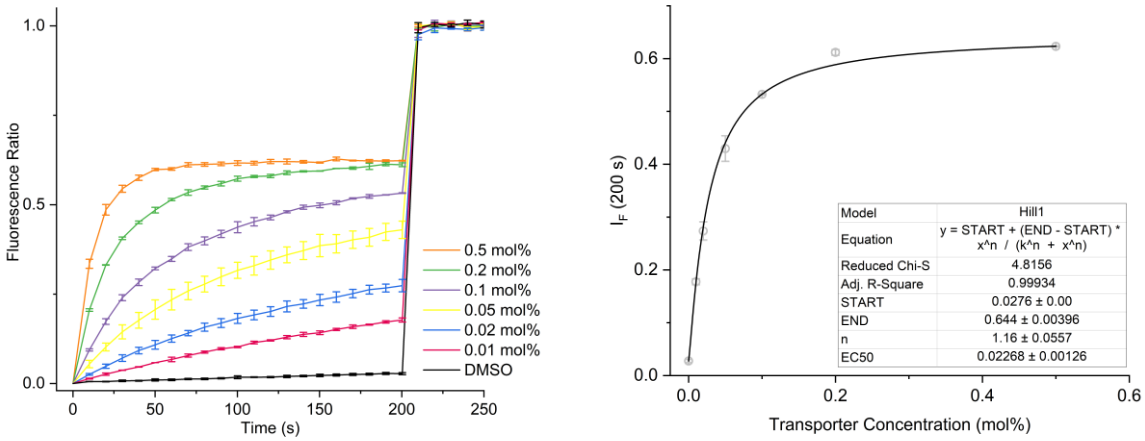

Figure S51 – Hill plot analysis of H^+/OH^- transport facilitated by compound **7** measured using the KGluc assay. NaOH (5 mM) and valinomycin (0.05 mol%) were added to the vesicles before the addition of **7** at 0 s. Detergent was added at 200 s to lyse the vesicles. Compound concentrations are shown as compound-to-lipid molar ratios. Error bars represent standard deviations from at least two repeats.

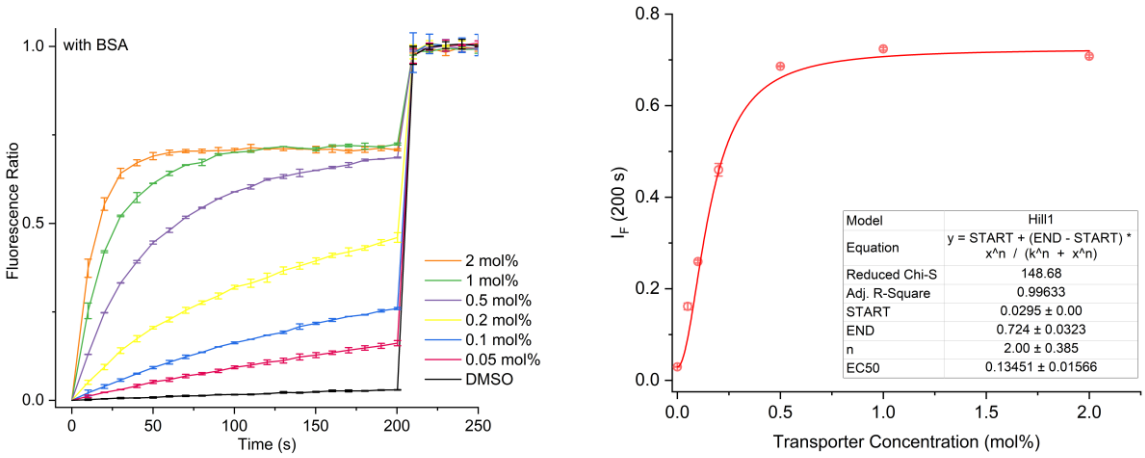

Figure S52 – Hill plot analysis of H^+/OH^- transport facilitated by compound **7** measured using the KGluc assay. The vesicles were pre-treated with BSA (1 mol%). NaOH (5 mM) and valinomycin (0.05 mol%) were added to the vesicles before the addition of **7** at 0 s. Detergent was added at 200 s to lyse the vesicles. Compound concentrations are shown as compound-to-lipid molar ratios. Error bars represent standard deviations from at least two repeats.

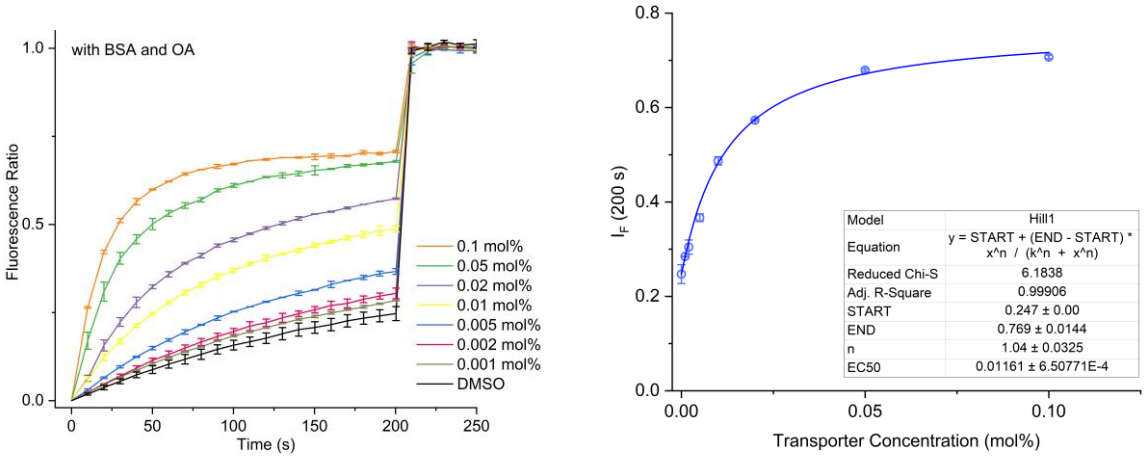

Figure S53 – Hill plot analysis of H^+/OH^- transport facilitated by compound **7** measured using the KGluc assay. The vesicles were pre-treated with BSA (1 mol%). OA (10 mol%), NaOH (5 mM) and valinomycin (0.05 mol%) were added to the vesicles before the addition of **7** at 0 s. Detergent was added at 200 s to lyse the vesicles. Compound concentrations are shown as compound-to-lipid molar ratios. Error bars represent standard deviations from at least two repeats.

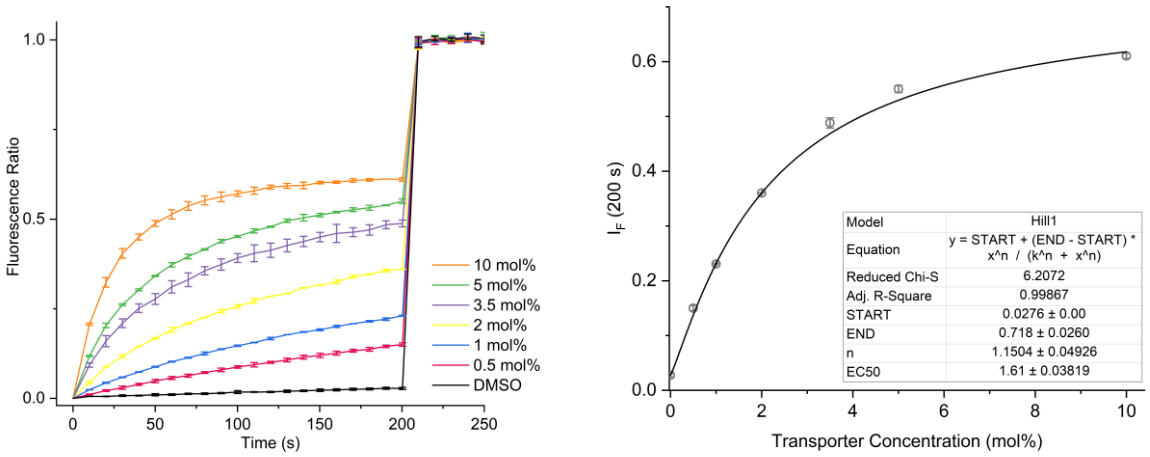

Figure S54 – Hill plot analysis of H^+/OH^- transport facilitated by compound **8** measured using the KGluc assay. NaOH (5 mM) and valinomycin (0.05 mol%) were added to the vesicles before the addition of **8** at 0 s. Detergent was added at 200 s to lyse the vesicles. Compound concentrations are shown as compound-to-lipid molar ratios. Error bars represent standard deviations from at least two repeats.

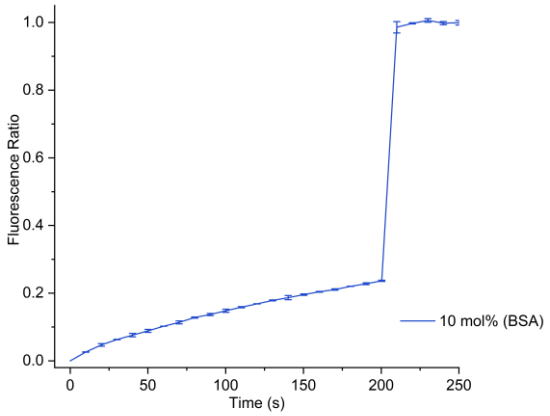

Figure S55 – Efflux plot of H^+/OH^- transport facilitated by compound **8** measured using the KGluc assay. The vesicles were pre-treated with BSA (1 mol%). NaOH (5 mM) and valinomycin (0.05 mol%) were added to the vesicles before the addition of a 10 mol% solution of **8** at 0 s. Detergent was added at 200 s to lyse the vesicles. Compound concentrations are shown as compound-to-lipid

molar ratios. Error bars represent standard deviations from at least two repeats. H^+/OH^- efflux did not exceed 50% after 200 s under the conditions tested.

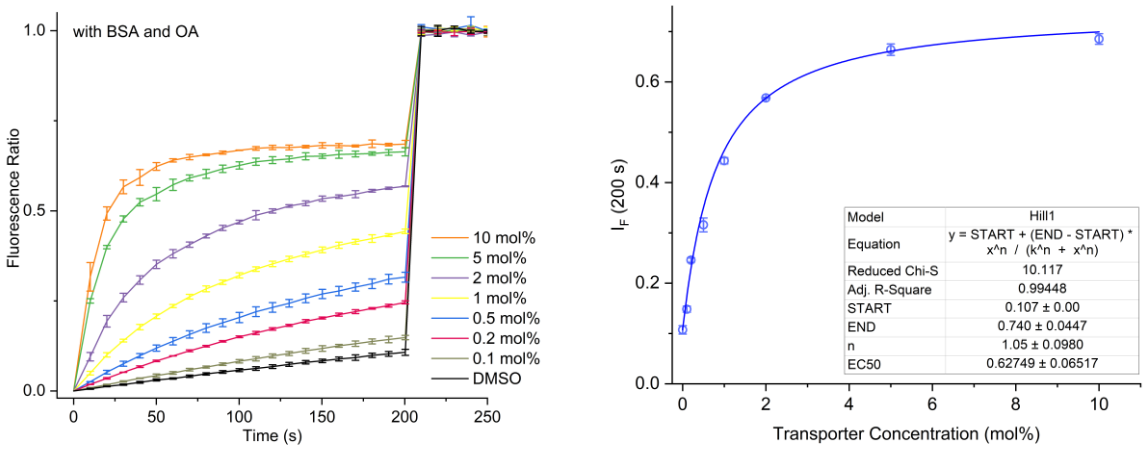

Figure S56 – Hill plot analysis of H^+/OH^- transport facilitated by compound **8** measured using the KGluc assay. The vesicles were pre-treated with BSA (1 mol%). OA (10 mol%), NaOH (5 mM) and valinomycin (0.05 mol%) were added to the vesicles before the addition of **8** at 0 s. Detergent was added at 200 s to lyse the vesicles. Compound concentrations are shown as compound-to-lipid molar ratios. Error bars represent standard deviations from at least two repeats.

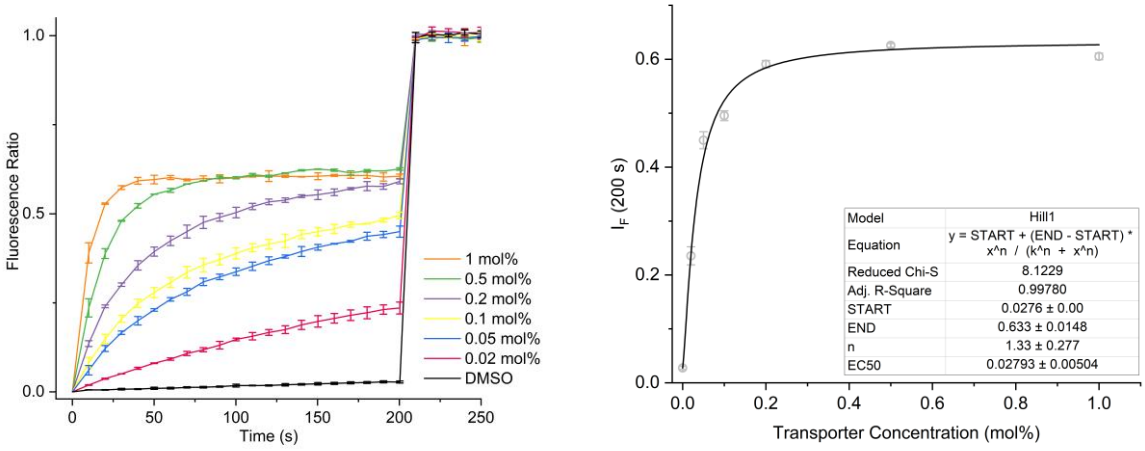

Figure S57 – Hill plot analysis of H^+/OH^- transport facilitated by compound **9** measured using the KGluc assay. NaOH (5 mM) and valinomycin (0.05 mol%) were added to the vesicles before the

addition of **9** at 0 s. Detergent was added at 200 s to lyse the vesicles. Compound concentrations are shown as compound-to-lipid molar ratios. Error bars represent standard deviations from at least two repeats.

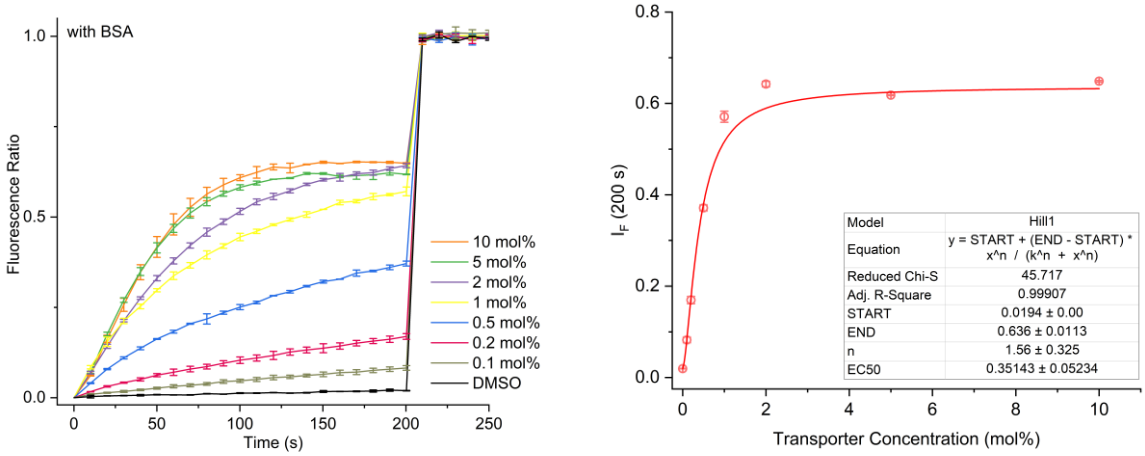

Figure S58 – Hill plot analysis of H^+/OH^- transport facilitated by compound **9** measured using the KGluc assay. The vesicles were pre-treated with BSA (1 mol%). NaOH (5 mM) and valinomycin (0.05 mol%) were added to the vesicles before the addition of **9** at 0 s. Detergent was added at 200 s to lyse the vesicles. Compound concentrations are shown as compound-to-lipid molar ratios. Error bars represent standard deviations from at least two repeats.

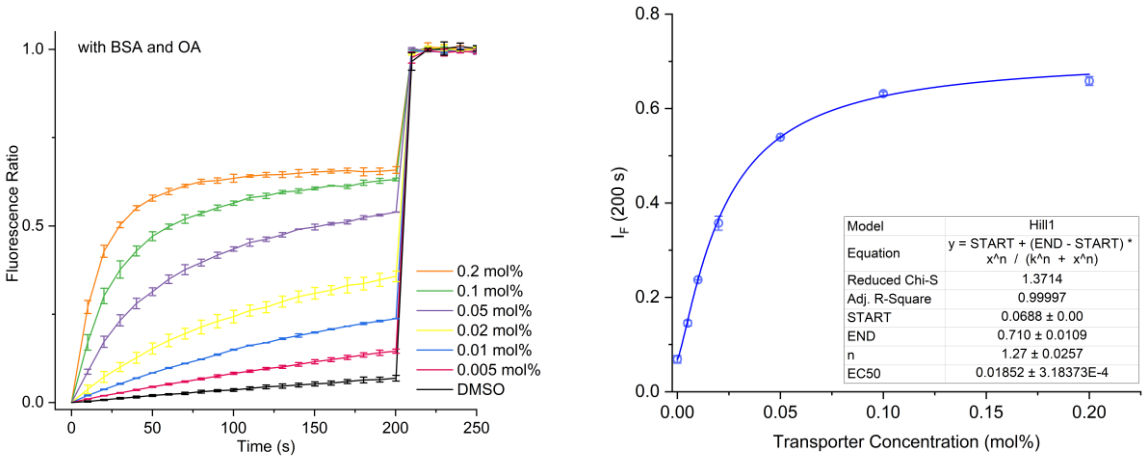

Figure S59 – Hill plot analysis of H^+/OH^- transport facilitated by compound **9** measured using the KGluc assay. The vesicles were pre-treated with BSA (1 mol%). OA (10 mol%), NaOH (5 mM) and valinomycin (0.05 mol%) were added to the vesicles before the addition of **9** at 0 s. Detergent was added at 200 s to lyse the vesicles. Compound concentrations are shown as compound-to-lipid molar ratios. Error bars represent standard deviations from at least two repeats.

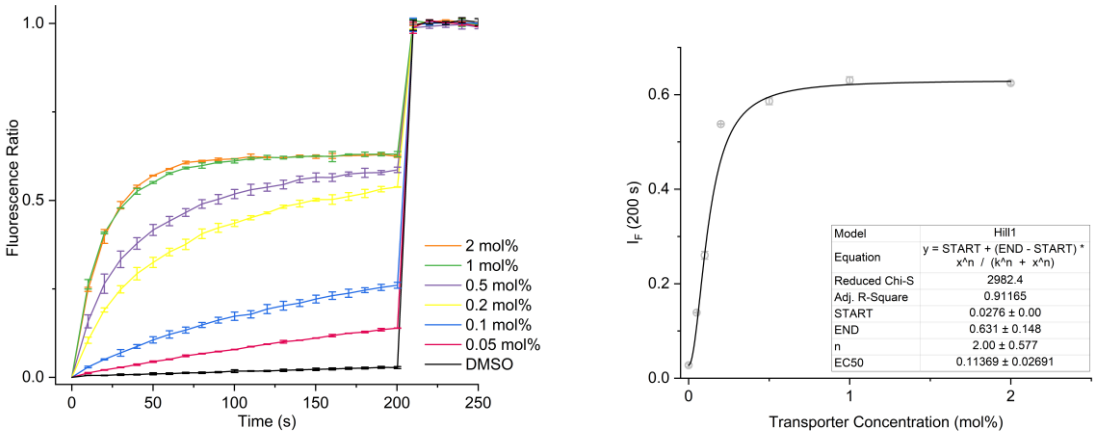

Figure S60 – Hill plot analysis of H^+/OH^- transport facilitated by compound **10** measured using the KGluc assay. NaOH (5 mM) and valinomycin (0.05 mol%) were added to the vesicles before the addition of **10** at 0 s. Detergent was added at 200 s to lyse the vesicles. Compound concentrations are shown as compound-to-lipid molar ratios. Error bars represent standard deviations from at least two repeats.

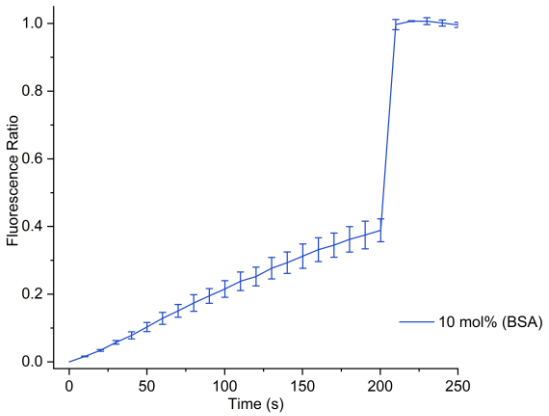

Figure S61 – Efflux plot of H^+/OH^- transport facilitated by compound **10** measured using the KGluc assay. The vesicles were pre-treated with BSA (1 mol%). NaOH (5 mM) and valinomycin (0.05 mol%) were added to the vesicles before the addition of a 10 mol% solution of **10** at 0 s. Detergent was added at 200 s to lyse the vesicles. Compound concentrations are shown as compound-to-lipid molar ratios. Error bars represent standard deviations from at least two repeats. H^+/OH^- efflux did not exceed 50% after 200 s under the conditions tested

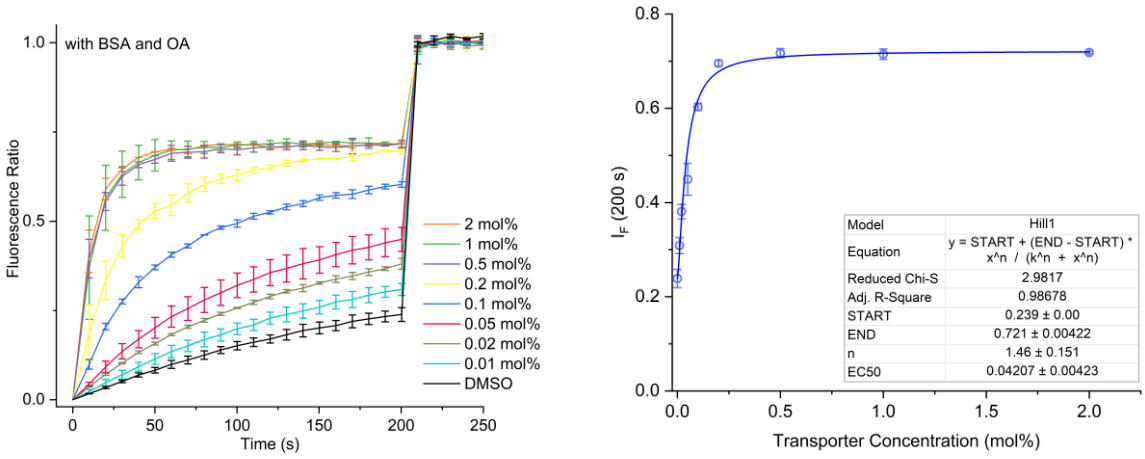

Figure S62 – Hill plot analysis of H^+/OH^- transport facilitated by compound **10** measured using the KGluc assay. The vesicles were pre-treated with BSA (1 mol%). OA (10 mol%), NaOH (5 mM) and valinomycin (0.05 mol%) were added to the vesicles before the addition of **10** at 0 s. Detergent was

added at 200 s to lyse the vesicles. Compound concentrations are shown as compound-to-lipid molar ratios. Error bars represent standard deviations from at least two repeats.

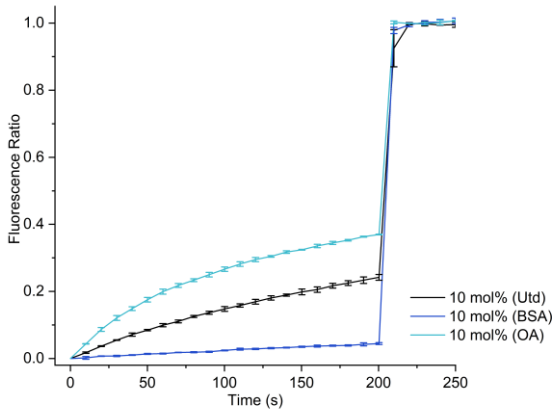

Figure S63 – Efflux plots of H^+/OH^- transport facilitated by compound **11** measured using the KGluc assay. A 10 mol% compound-to-lipid molar ratio of **11** was added to the vesicles at 0 s under the three conditions outlined above (Untreated, BSA treated, BSA and OA treated), and detergent was added at 200 s to lyse the vesicles. Error bars represent standard deviations from at least two repeats. H^+/OH^- efflux did not exceed 50% after 200 s under any of the conditions tested.

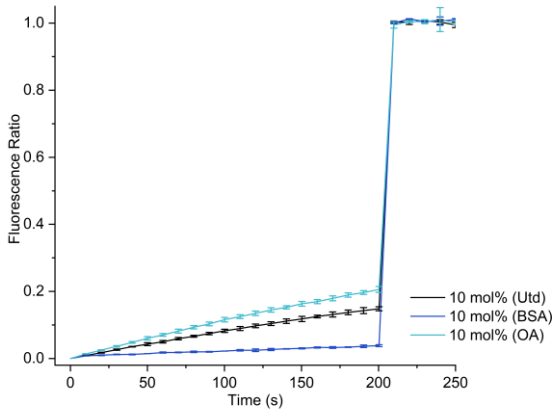

Figure S64 – Efflux plots of H^+/OH^- transport facilitated by compound **12** measured using the KGluc assay. A 10 mol% compound-to-lipid molar ratio of **12** was added to the vesicles at 0 s under the three conditions outlined above (Untreated, BSA treated, BSA and OA treated), and detergent was added

at 200 s to lyse the vesicles. Error bars represent standard deviations from at least two repeats. H^+/OH^- efflux did not exceed 50% after 200 s under any of the conditions tested.

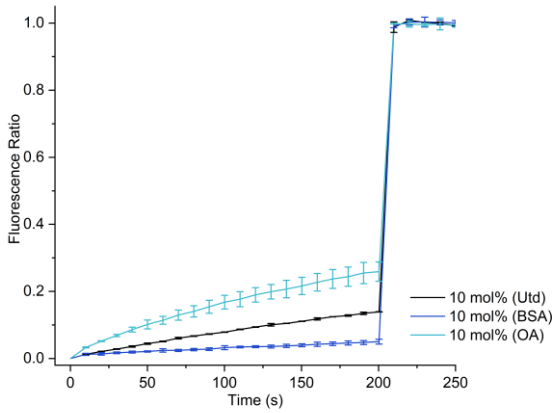

Figure S65 – Efflux plots of H^+/OH^- transport facilitated by compound **13** measured using the KGluc assay. A 10 mol% compound-to-lipid molar ratio of **13** was added to the vesicles at 0 s under the three conditions outlined above (Untreated, BSA treated, BSA and OA treated), and detergent was added at 200 s to lyse the vesicles. Error bars represent standard deviations from at least two repeats. H^+/OH^- efflux did not exceed 50% after 200 s under any of the conditions tested.

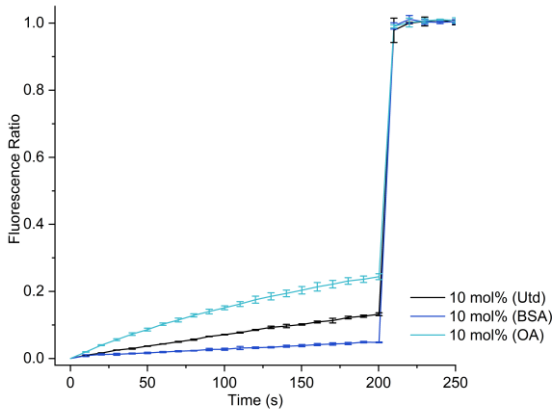

Figure S66 – Efflux plots of H^+/OH^- transport facilitated by compound **14** measured using the KGluc assay. A 10 mol% compound-to-lipid molar ratio of **14** was added to the vesicles at 0 s under the three conditions outlined above (Untreated, BSA treated, BSA and OA treated), and detergent was added

at 200 s to lyse the vesicles. Error bars represent standard deviations from at least two repeats. H^+/OH^- efflux did not exceed 50% after 200 s under any of the conditions tested.

Supplementary Information for Chapter Three

S3.1 H^+/OH^- transport assay in vesicles

Vesicle Preparation

HPTS assays were conducted using POPC LUVs (200 nm diameter) vesicles loaded with an internal solution containing pH-sensitive fluorescent dye HPTS (1 mM), HEPES buffer (10 mM) and potassium gluconate (100 mM). An external solution of HEPES buffer (10 mM) and potassium gluconate (100 mM) was also prepared, and both solutions were buffered to pH 7.

Unilamellar vesicles were prepared following a procedure outlined previously by the Gale group.[1] A chloroform solution of POPC (37.5 mM, 4 mL) was transferred to a pre-weighed round-bottom flask, and the solvent was removed using a rotary evaporator. The pressure was lowered slowly to ensure the formation of a smooth lipid film. Subsequently, the film was dried in vacuo for 4−24 h, and the mass of lipid was recorded. The lipids were rehydrated with 4 mL of internal solution (this number should correspond to the volume of POPC solution used initially) and vortexed until all lipids were removed from the sides of the flask and were suspended in solution. The lipids were subjected to 9 cycles of freeze-thaw by freezing using a dry ice/acetone bath and thawing in lukewarm water. Following this, the vesicles were left to rest at room temperature for 30 min. The lipids were extruded through a 200 nm polycarbonate membrane 25 times to form monodisperse vesicles. Only 1 mL of solution was extruded at a time before being collected. Finally, any residual unencapsulated salt from the internal solution was using a B19 column packed with hydrated G-25 Sephadex®, which had been pre-saturated with the respective external solution. The lipid suspensions were diluted with the external solution to afford a stock solution (10 mL) of a known concentration.

When fatty acid removal by BSA was required, fatty acid-free BSA was dissolved in the vesicle stock suspension to a final BSA concentration of 1 mol% (with respect to lipid). The BSA-

containing vesicle stock suspension was stirred for 20 min before being used for membrane transport studies.

HPTS Assay

For a given experiment, the prepared vesicles were diluted to a concentration of 0.1 mM in a 4.5 mL plastic cuvette. A pH gradient is required to drive transport through the vesicle membrane in these experiments before the transporter is added. An aliquot of aqueous KOH solution (25 μL, 0.5 M) was added to increase the pH of the external solution by approx. one pH unit to pH 8.0. For experiments requiring the addition of Oleic Acid (5 μL of 5 mM DMSO solution, 10 mol%, corresponding to ~4 mol% free concentration after BSA binding) was added before KOH. Following this, valinomycin (5 μL of 25 μM DMSO solution, 0.05 mol%) was added to each cuvette. Transport was initiated with the addition of the transporter as a DMSO solution (5 μL) and ended with the addition of detergent (Triton X-100 (10% v/v in water), 25 μL) was added at t = 205 s to lyse the vesicles, and a final fluorescence intensity reading was recorded at t = 300 s to signify 100% proton efflux.

Experiments were conducted under three conditions: i) Untreated vesicles (KOH and valinomycin addition); ii) BSA-treated vesicles (KOH and valinomycin addition); iii) BSA-treated vesicles with OA addition (OA, KOH and valinomycin addition).

Dose-Response Hill Analysis

The changes in the fluorescent activity of intravesicular HPTS were used to detect pH changes during the experiments, and hence represent proton efflux. The acidic and basic forms of the HPTS probe were excited at λex = 403 nm and λex = 460 nm, respectively, and the fluorescence emission of both forms recorded at λem = 510 nm. The intensity ratio of basic form to acidic form was determined, and the fractional fluorescence intensity (IF) was calculated using the equation:

$$I_F = \frac{R_t - R_0}{R_d - R_0}$$

Where R_t is the ratiometric fluorescence value at a given time (t), R_0 is the ratiometric fluorescence value at t = 0 s and R_d is the fluorescence ratiometric value recorded at t = 280 s following the addition of detergent.

Dose-response experiments were performed at a minimum of five transporter concentrations plus a blank DMSO control run. The fractional fluorescence intensity (I_F) was plotted as a function of transporter concentration (mol%, with respect to lipid concentration). The I_F value at t = 200 s for each tested transporter concentration was fit to an adapted Hill Equation, using Origin 2021b (Academic), given as:

$$y = y_0 + (y_{max} - y_0)\frac{x^n}{k^n + x^n}$$

where y_0 is the I_F value at t = 200 s for the DMSO blank run, y_{max} is the maximum I_F value, n is the Hill coefficient, and k is a derived parameter.

A derived equation was used to calculate the EC_{50} value, the transporter concentration required to facilitate 50% chloride efflux, given as:

$$EC_{50} = k\left(\frac{0.5}{y_1 - y_0}\right)^{1/n}$$

where k and n are the derived parameters from the Hill equation, y_0 is the percentage chloride efflux at t = 0 s, and y_1 is the percentage chloride efflux at t = 280 s.

S3.2 Absolute quantitative ^{1}H NMR purity determination of S3-11, A3-11 and D3-11

The purity of all test compounds was confirmed to be >95% by absolute quantitative NMR spectroscopy according to the protocol outlined by the Journal of Medicinal Chemistry.[125] This technique determines purity by comparing the NMR signals of a given analyte against an internal calibrant (IC) of known purity. DMSO-$d_6$was spiked with a known mass of the internal calibrant 1,3,5-trioxane (99.5% purity) to give a final IC concentration of approximately 1.5 mg/ml. Approximately 5 mg of each test compound was accurately weighed on a 5-decimal place analytical balance (0.01 mg accuracy). The sample was then dissolved in 600 µL of IC spiked DMSO-d_6 administered via mechanical pipette, then transferred to 5 mm NMR tubes. Collection and processing of NMR spectra, and calculation of purity, were performed according to the procedure described by the Journal of Medicinal Chemistry. The final calculated purities are shown in Table S2.

Table S2. Bisaryl anion transporter qNMR table

Compound	Purity (%)
S3	98.0
S7	100.5
S9	99
S11	96.5
A3	99.4
A7	100.6
A9	100.6
A11	100.6
D3	97.1
D7	95.3
D9	99.7
D11	96.8

S3.3 Representative MTS dose-response curves

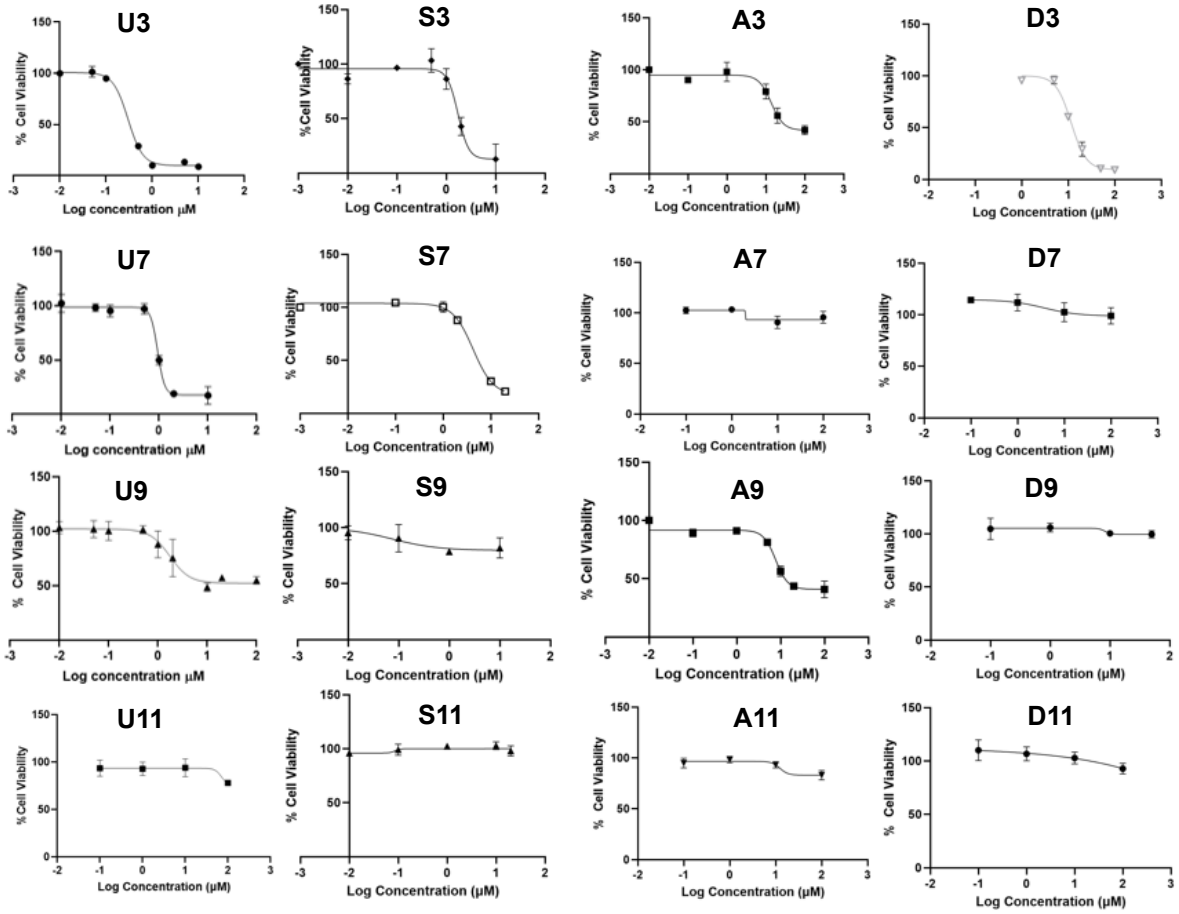

Figure S67. Representative Dose-response curves showing the antiproliferative effects of **U3-11**, **S3-11**, **A3-11** and **D3-11** in MDA-MB-231 cells in a 72 h MTS cell viability assay. Dose-response curves were constructed using log(inhibitor) vs response, variable slope (4 parameters) nonlinear regressions on GraphPad Prism 8. Absolute IC50 concentrations were interpolated from these normalised curves (data normalised to DMSO vehicle control) with the top constrained to 100%. Equation: Y=Bottom + (Top-Bottom)/(1+10^((LogIC50-X)*HillSlope)).

S3.4 MDA-MB-231 Cell Imaging

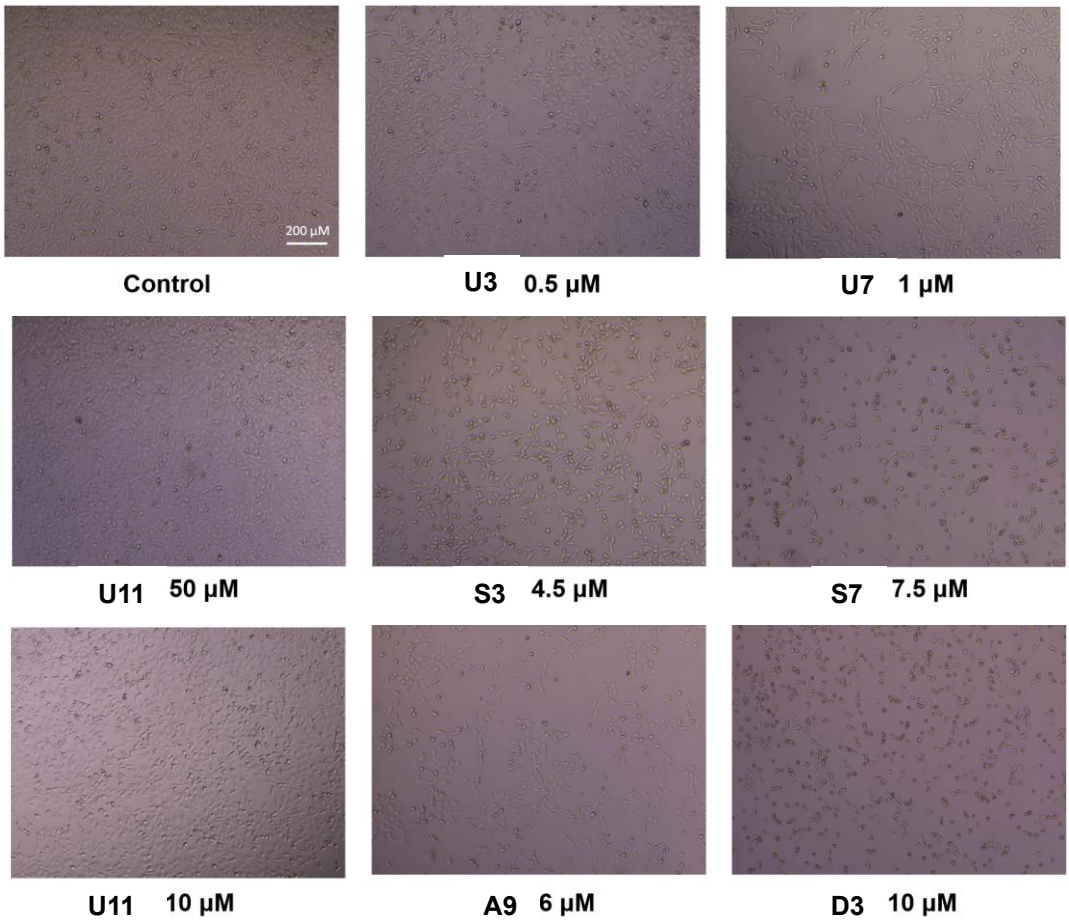

Figure S68. Images of MDA-MB-231 cells treated with **U3**, **U7**, **S3**, **S7**, **A9** and **D3** for 72 hours at their corresponding MTS IC_{50} concentration. Inactive compound **U11** (10 µM, 50 µM) and DMSO vehicle control shown for comparison. Cells were seeded in 12-well plates (2.5 x 10^4 cells/well) and imaged following treatment at 40X magnification using a Lumenera Infinity 1-2CB microscope camera.

S3.5 MDA-MB-231 and Beas-2B MTS cell viability

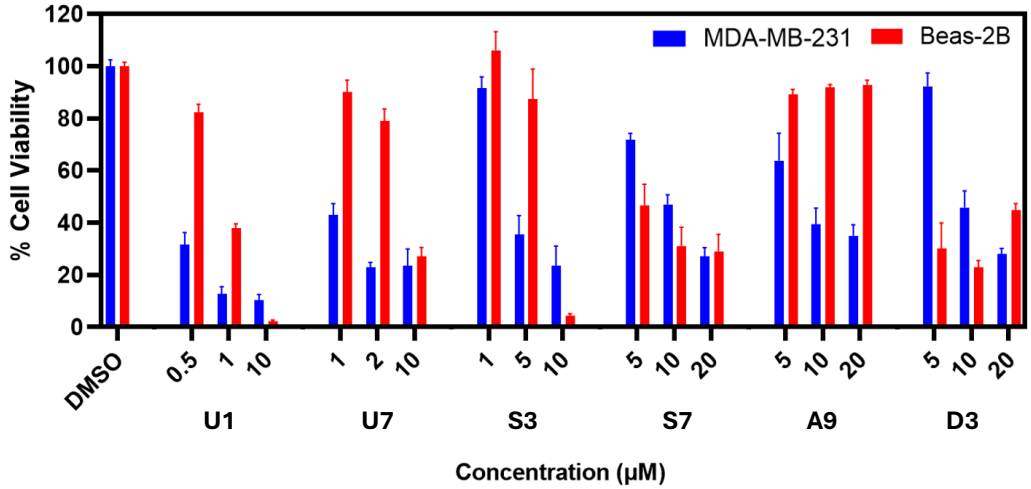

Figure S69. Effects of **U3**, **U7**, **S3**, **S7**, **A9** and **D3** on MDA-MB-231 and Beas-2B cell viability measured by 72 h MTS assays. Compounds with MTS activity in MDA-MB-231 cells were tested in Beas-2B cells at three common concentrations near and above their corresponding IC_{50} concentrations to indicate selectivity between cell lines. Beas-2B MTS assays performed as described in the main text.

S3.6 Representative JC-1 dose-response curves

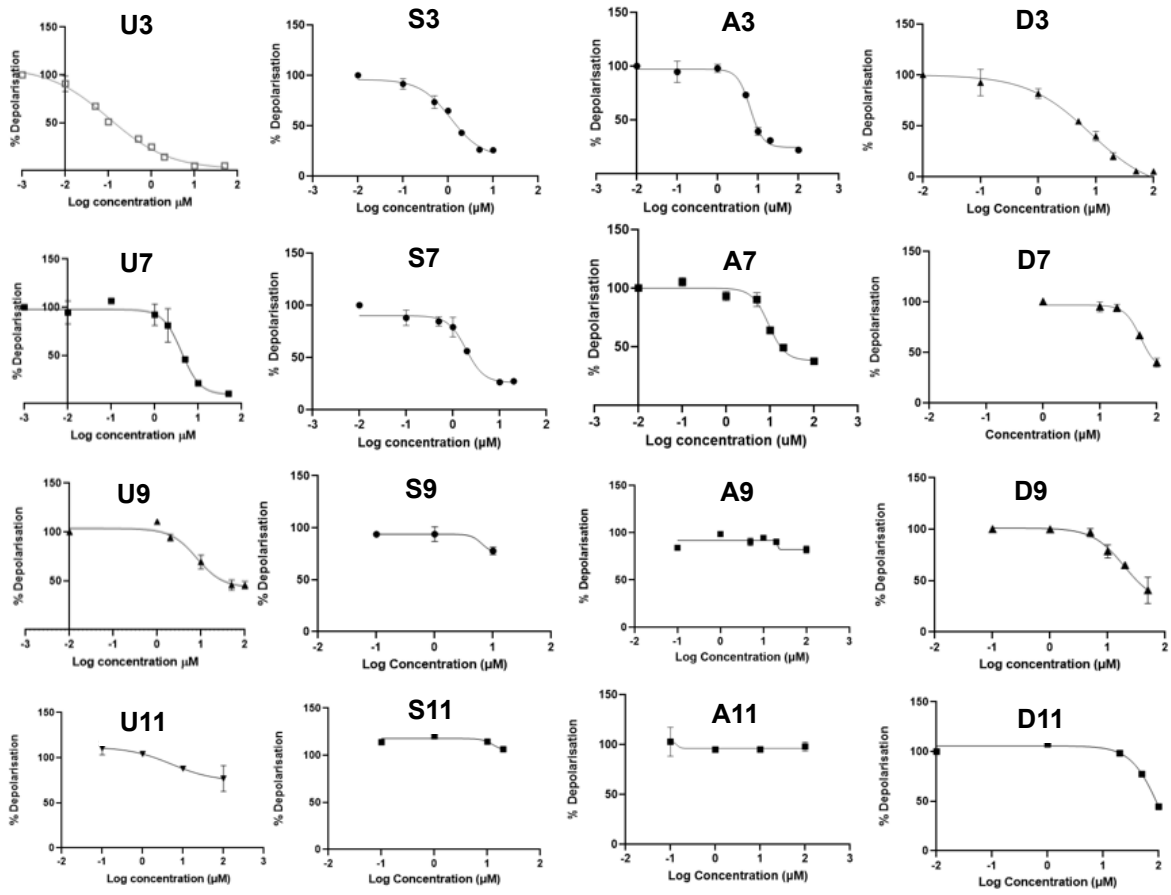

Figure S70. Representative dose-response curves showing the effects of **U3-11**, **S3-11**, **A3-11** and **D3-11** on the JC-1 red:green fluorescence ratio in MDA-MB-231 breast cancer cells after 1 hour treatment with the test compound. Dose-response curves were constructed using log(inhibitor) vs response, variable slope (4 parameters) nonlinear regressions on GraphPad Prism 8. Absolute IC50 concentrations were interpolated from these normalised curves (data normalised to DMSO vehicle control) with the top constrained to 100%. Equation: Y=Bottom + (Top-Bottom)/(1+10^((LogIC50-X)*HillSlope)).

S3.7 ^{1}H NMR and ^{13}C NMR Spectra

Bis({[3-chloro-5-(trifluoromethyl)phenyl]amino})cyclobut-3-ene-1,2-dione (S3)

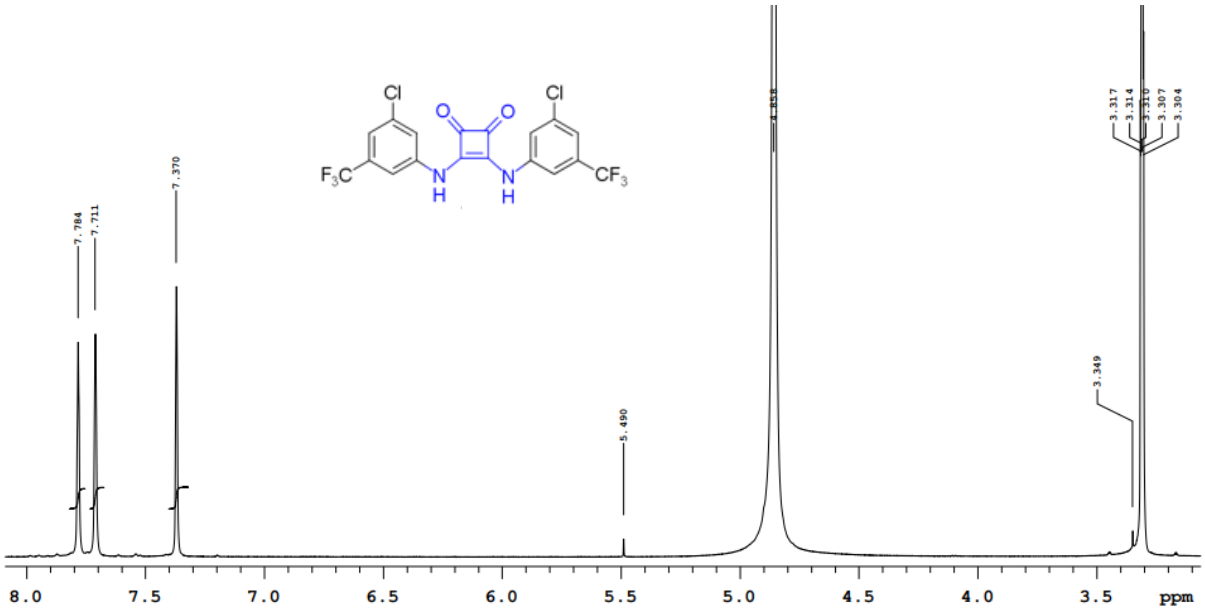

Figure S71. 500 MHz ^{1}H NMR spectrum of **S3**

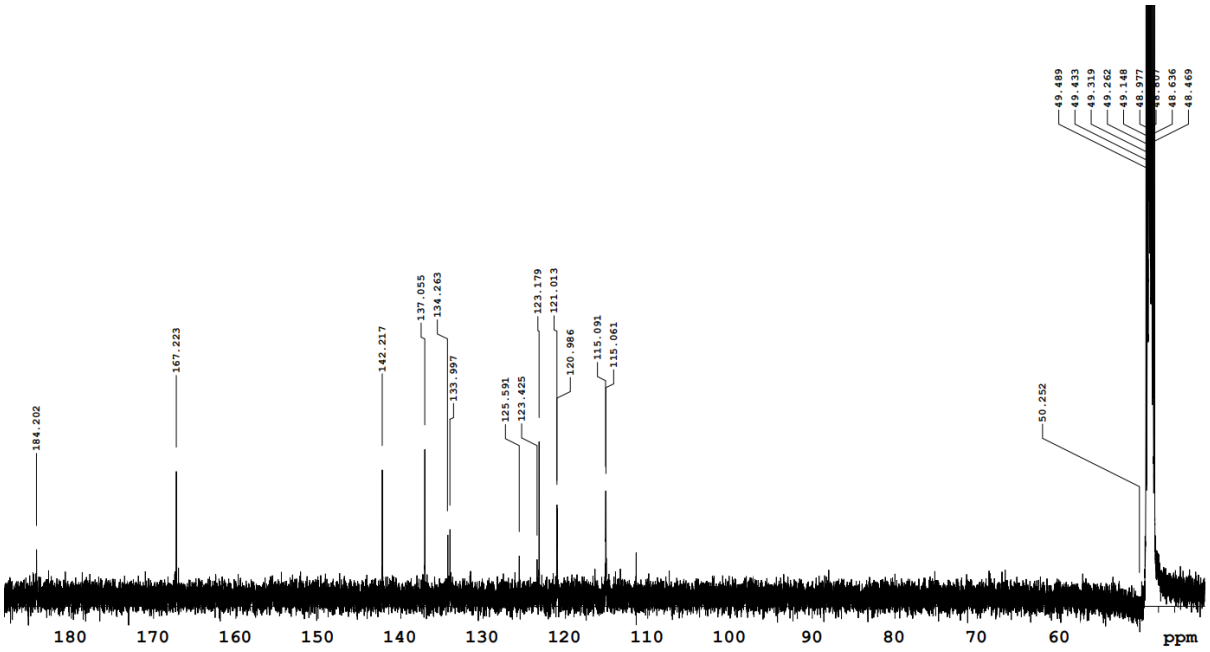

Figure S72. 125 MHz ^{13}C NMR spectrum of **S3**

Bis({[4-(trifluoromethyl)phenyl]amino})cyclobut-3-ene-1,2-dione (S7)

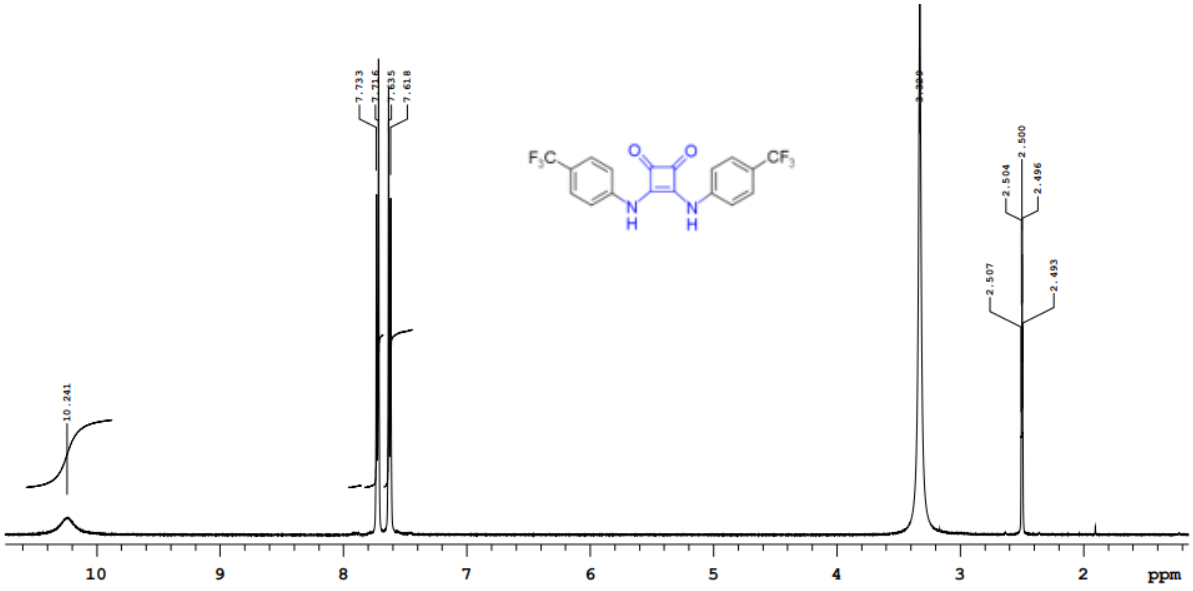

Figure S73. 500 MHz ^{1}H NMR spectrum of **S7**

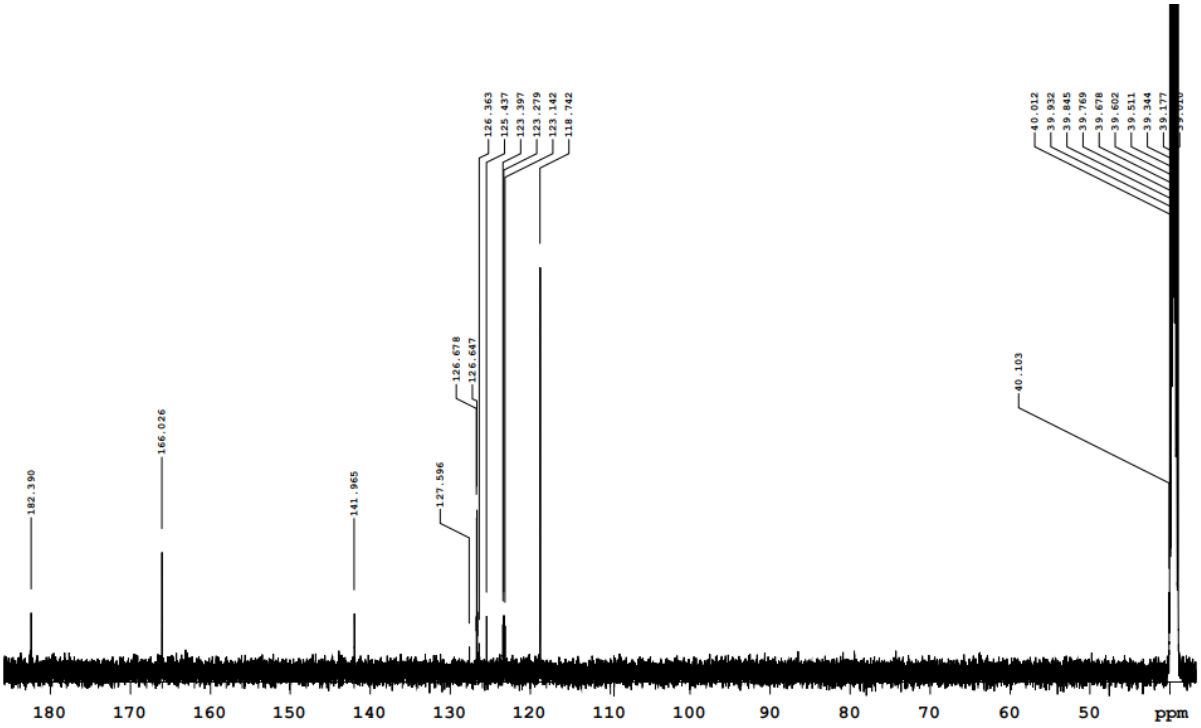

Figure S74. 125 MHz ^{13}C NMR spectrum of **S7**

Bis({[4-(trifluoromethoxy)phenyl]amino})cyclobut-3-ene-1,2-dione (S9)

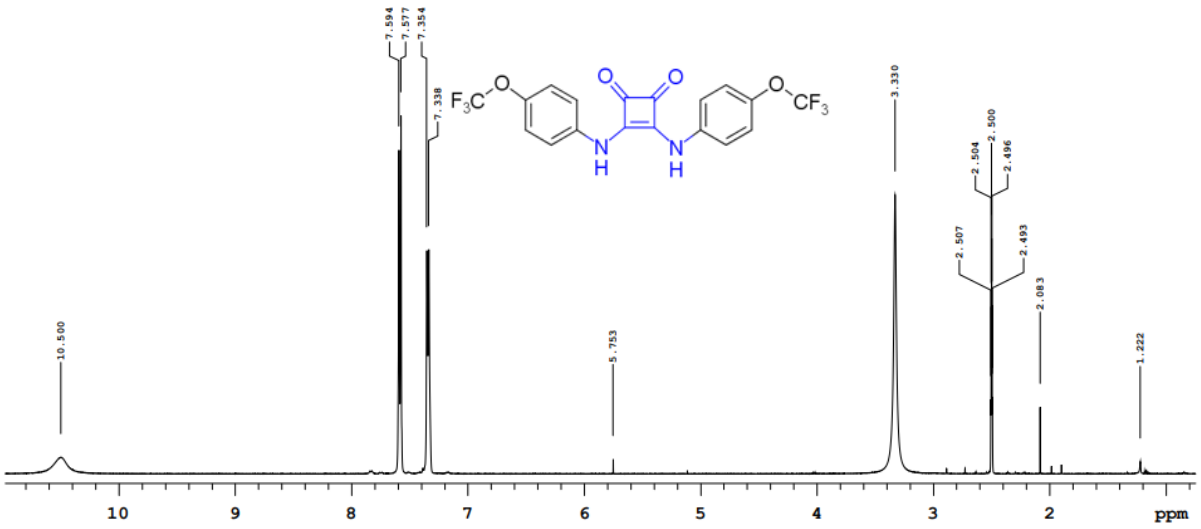

Figure S75. 500 MHz ^{1}H NMR spectrum of **S9**

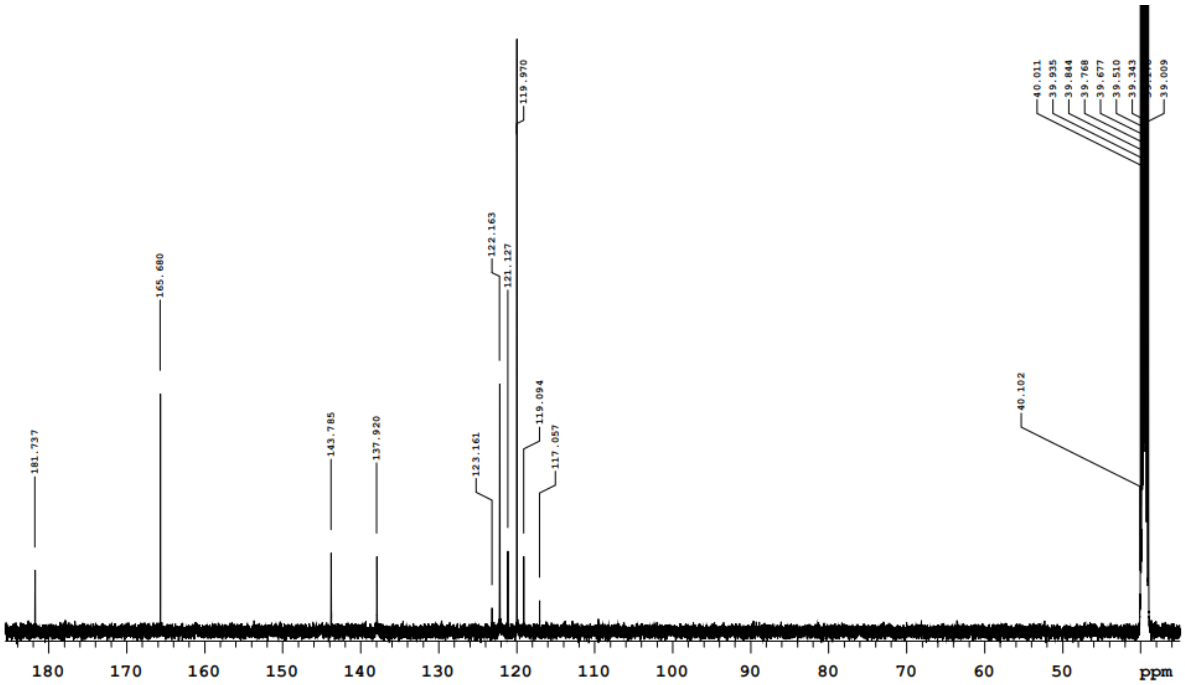

Figure S76. 125 MHz ^{13}C NMR spectrum of **S9**

Bis(phenylamino)cyclobut-3-ene-1,2-dione (S11)

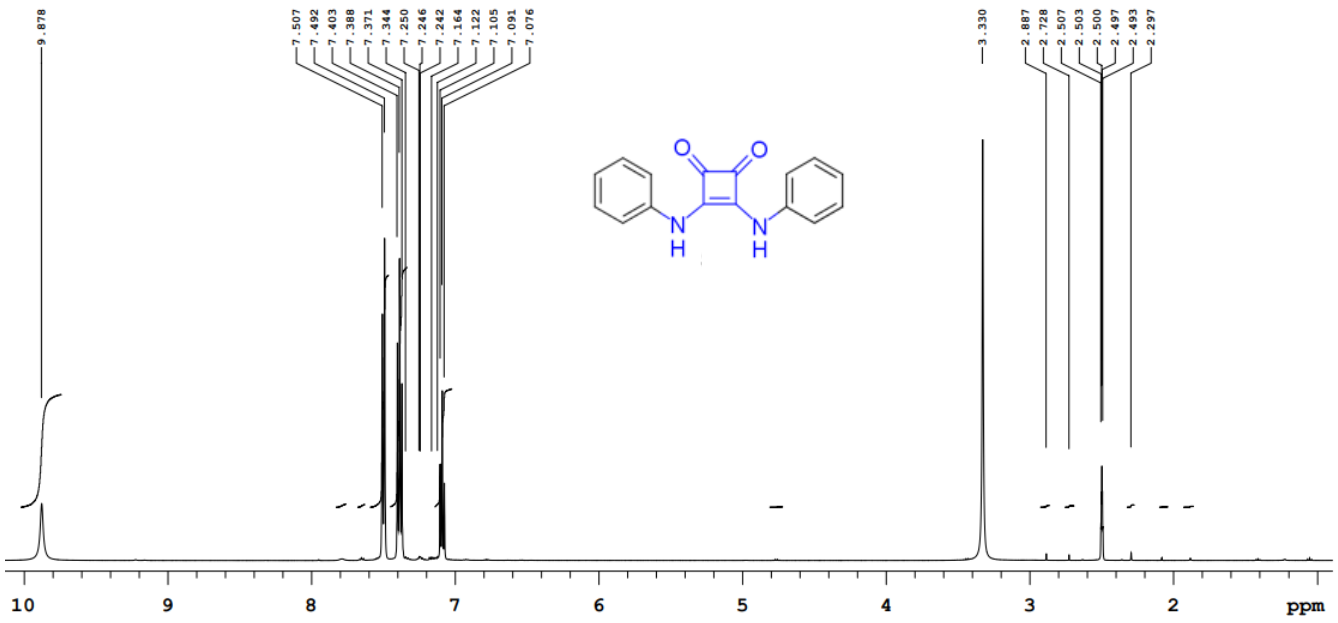

Figure S77. 500 MHz ^{1}H NMR spectrum of **S11**

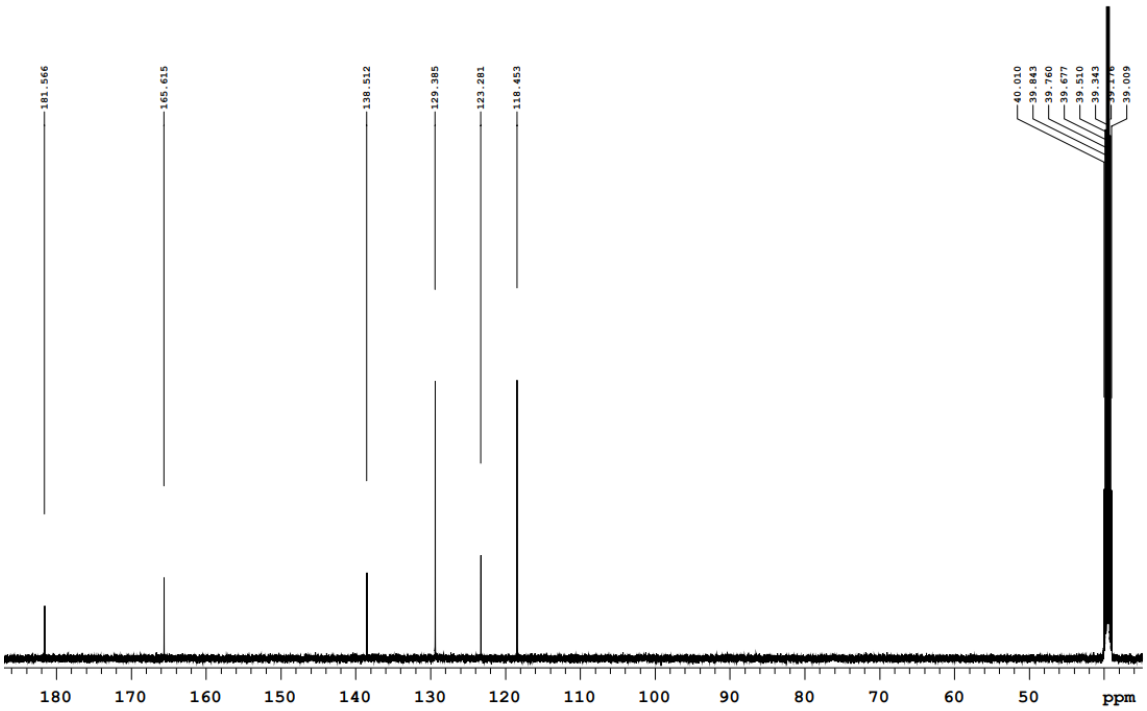

Figure S78. 125 MHz ^{13}C NMR spectrum of **S11**

3-chloro-N-[3-chloro-5-(trifluoromethyl)phenyl]-5-(trifluoromethyl)benzamide (A3)

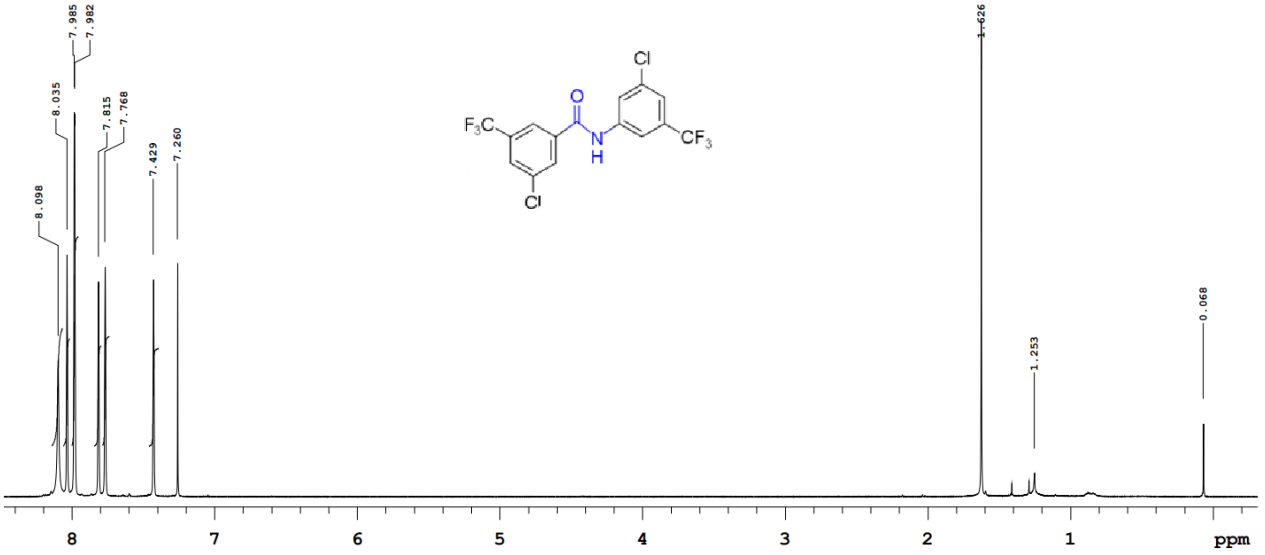

Figure S79. 500 MHz ^{1}H NMR spectrum of **A3**

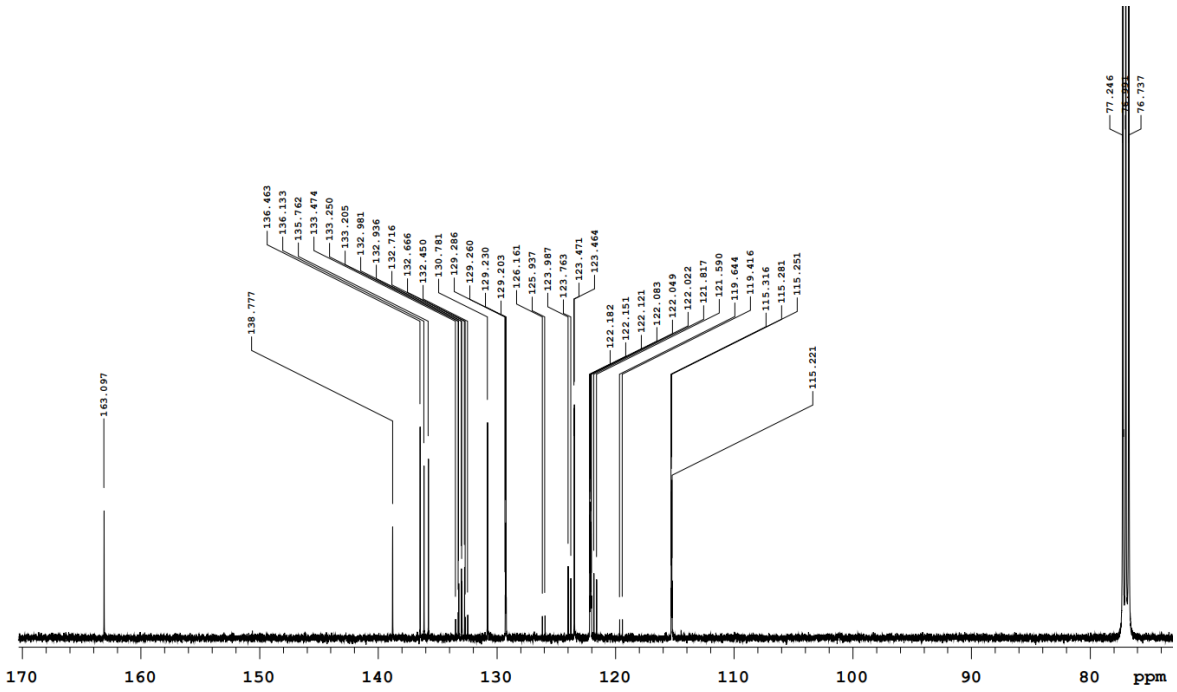

Figure S80. 125 MHz ^{13}C NMR spectrum of **A3**

4-(trifluoromethyl)-N-[4-(trifluoromethyl)phenyl]benzamide (A7)

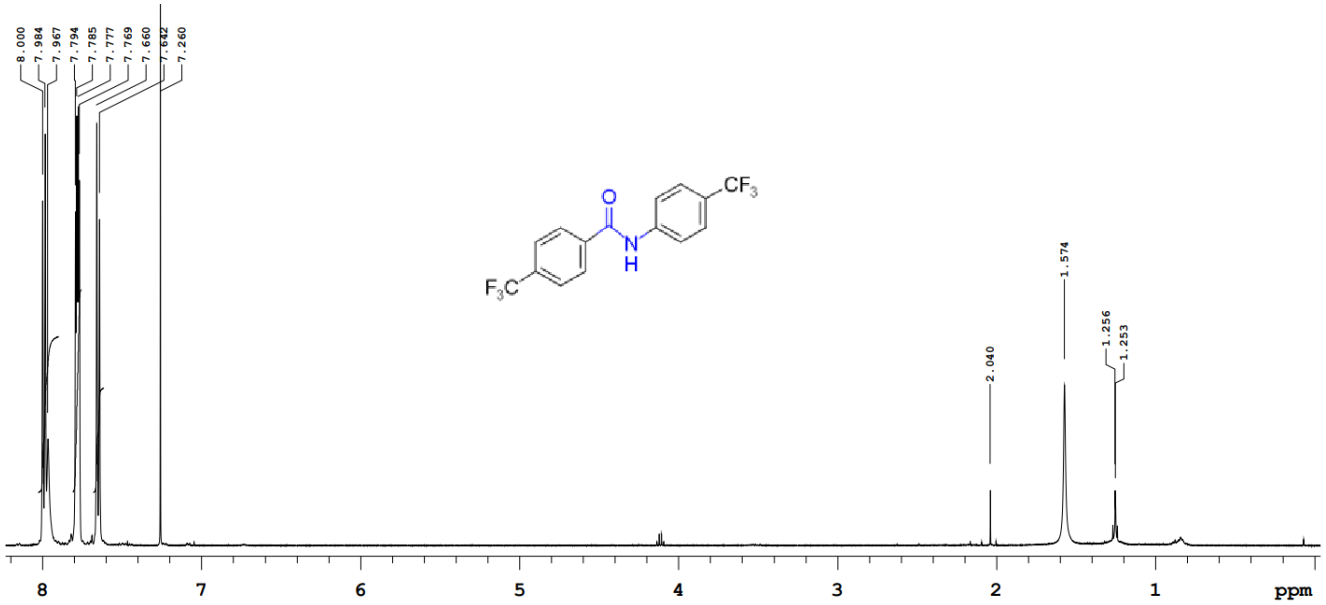

Figure S81. 500 MHz ^{1}H NMR spectrum of **A7**

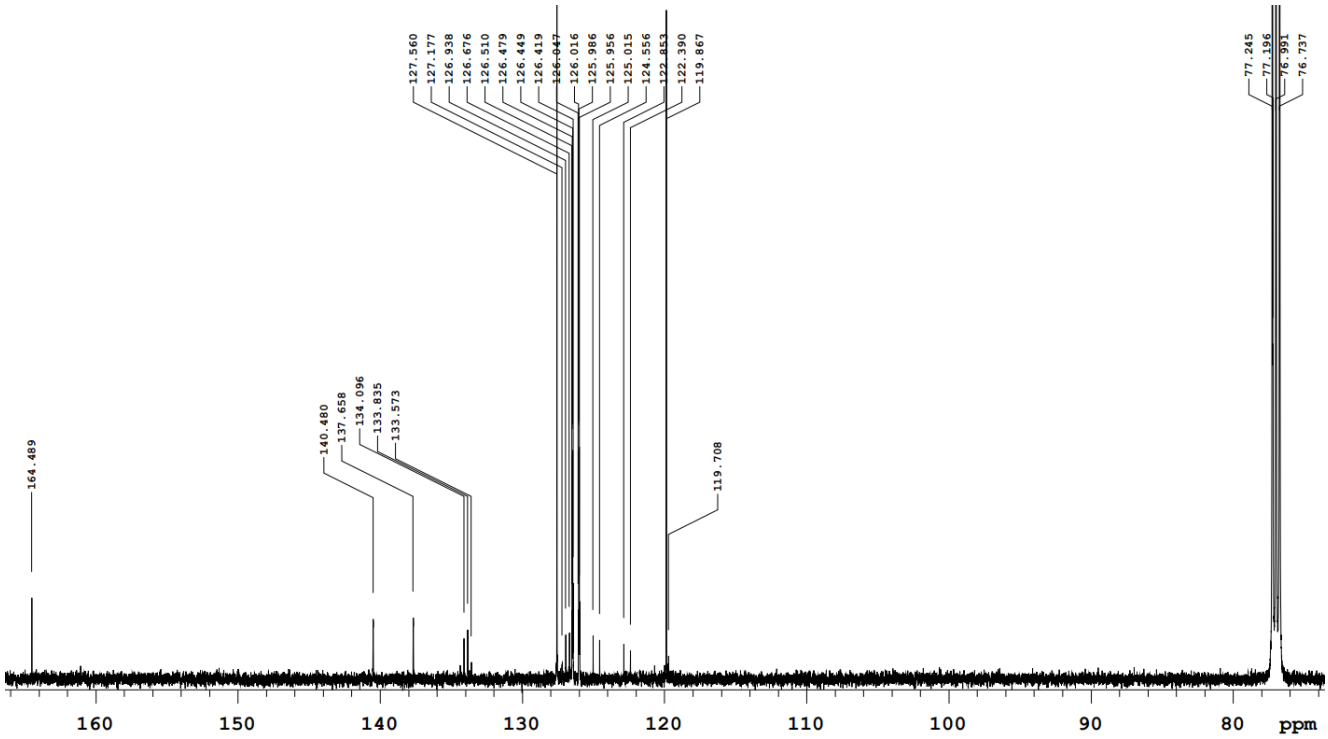

Figure S82. 125 MHz ^{13}C NMR spectrum of **A7**

4-(trifluoromethoxy)-N-[4-(trifluoromethoxy)phenyl]benzamide (A9)

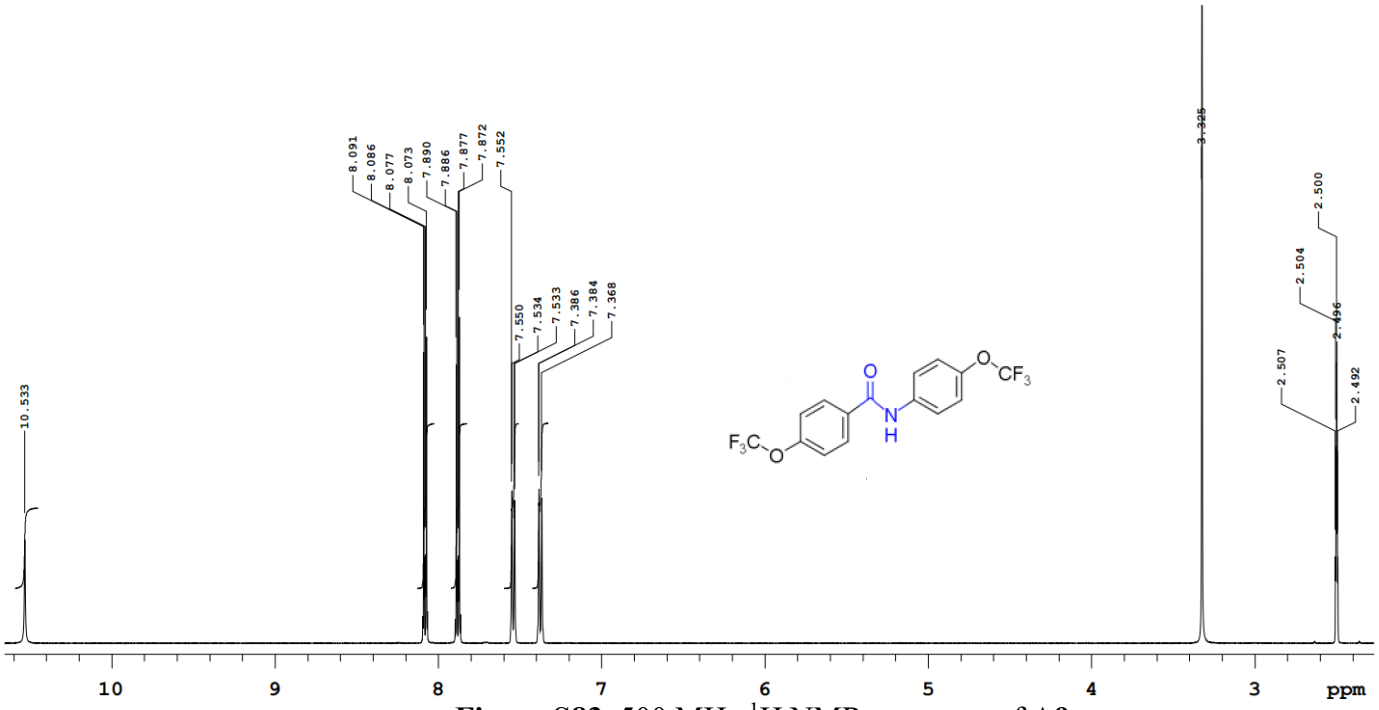

Figure S83. 500 MHz ^{1}H NMR spectrum of **A9**

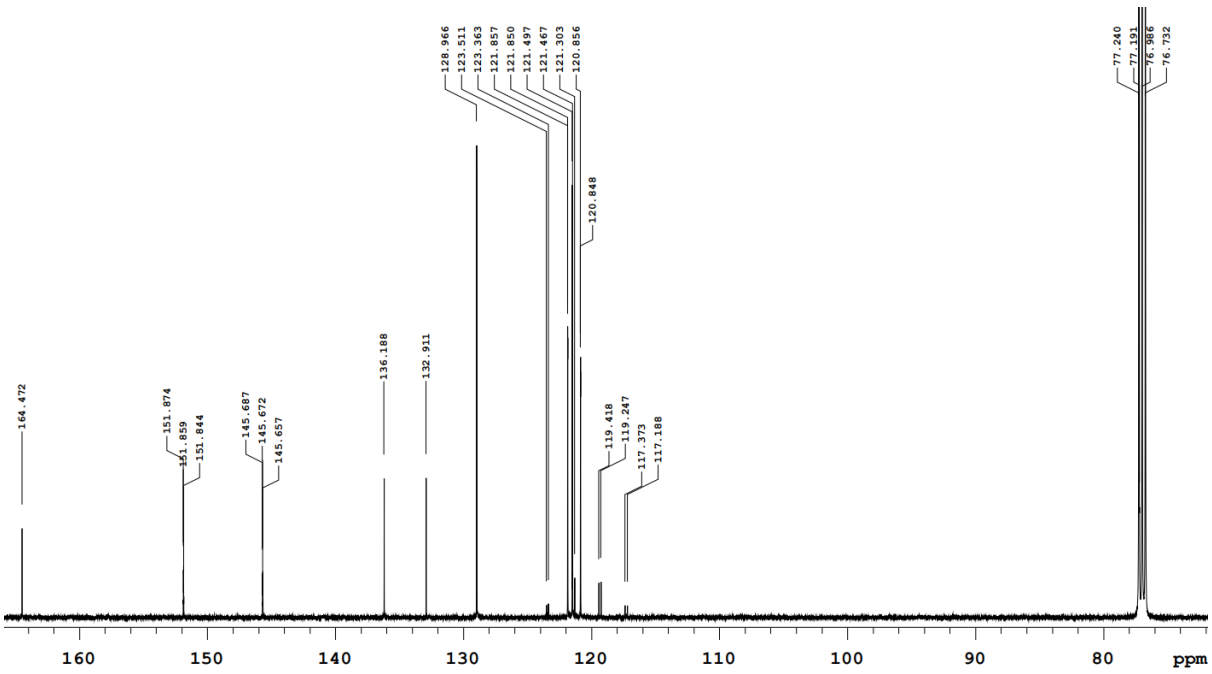

Figure S84. 125 MHz ^{13}C NMR spectrum of **A9**

N-phenylbenzamide (A11)

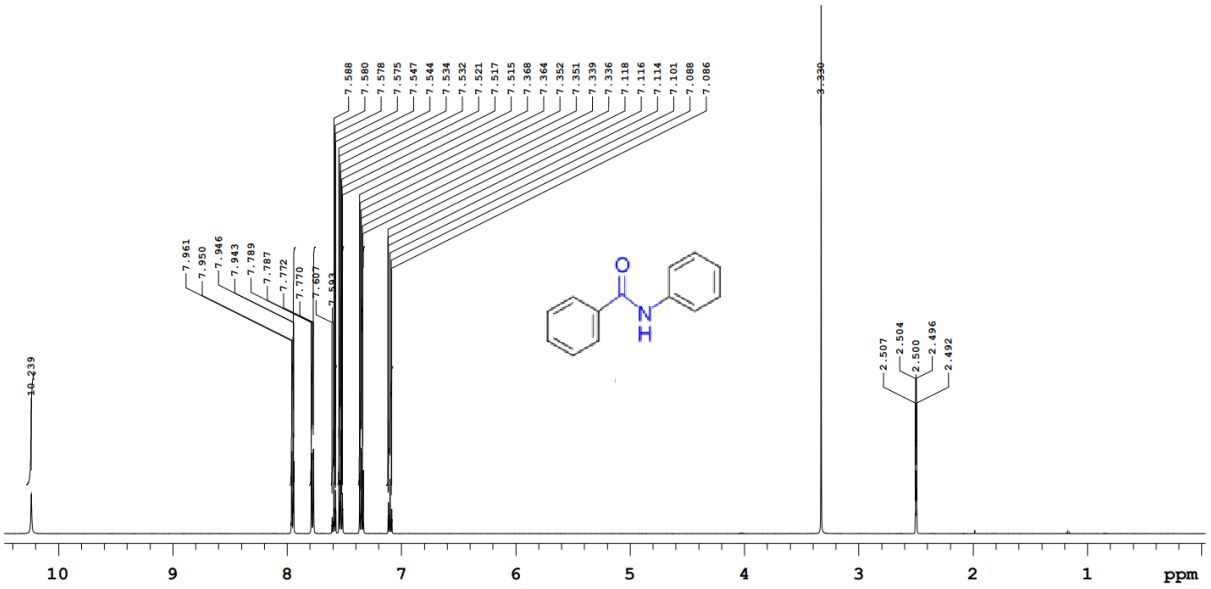

Figure S85. 500 MHz ^{1}H NMR spectrum of **A11**

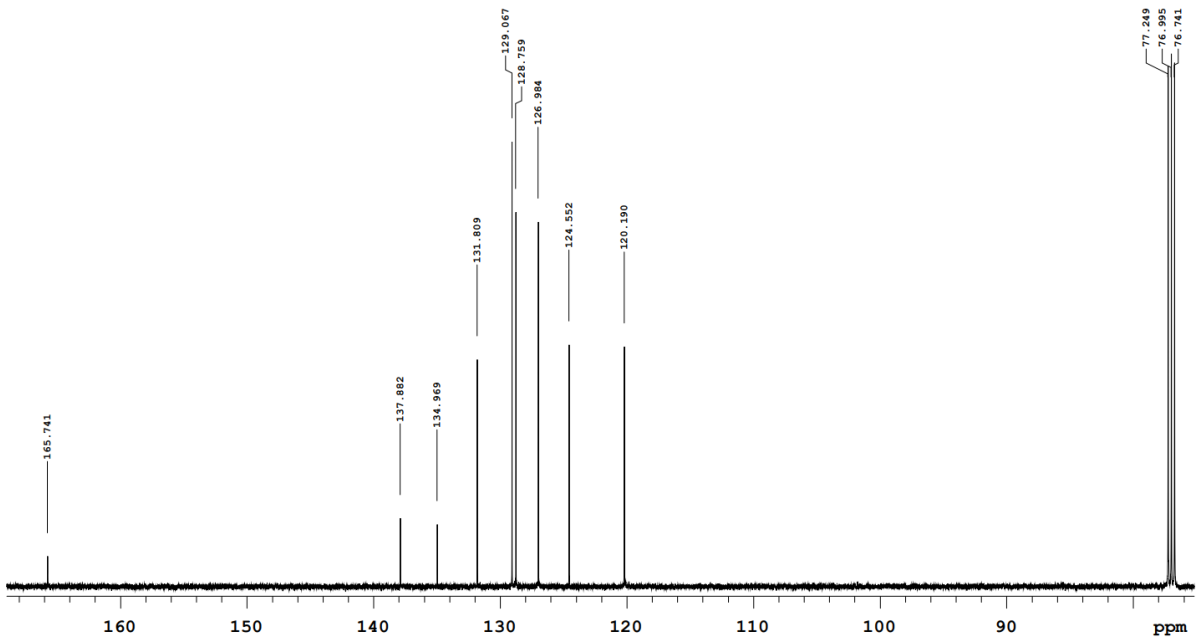

Figure S86. 125 MHz ^{13}C NMR spectrum of **A11**

3-[3-chloro-5-(trifluoromethyl)phenyl]-1-[6-({[3-chloro-5-(trifluoromethyl)phenyl]carbamoyl}amino)hexyl]urea (D3)

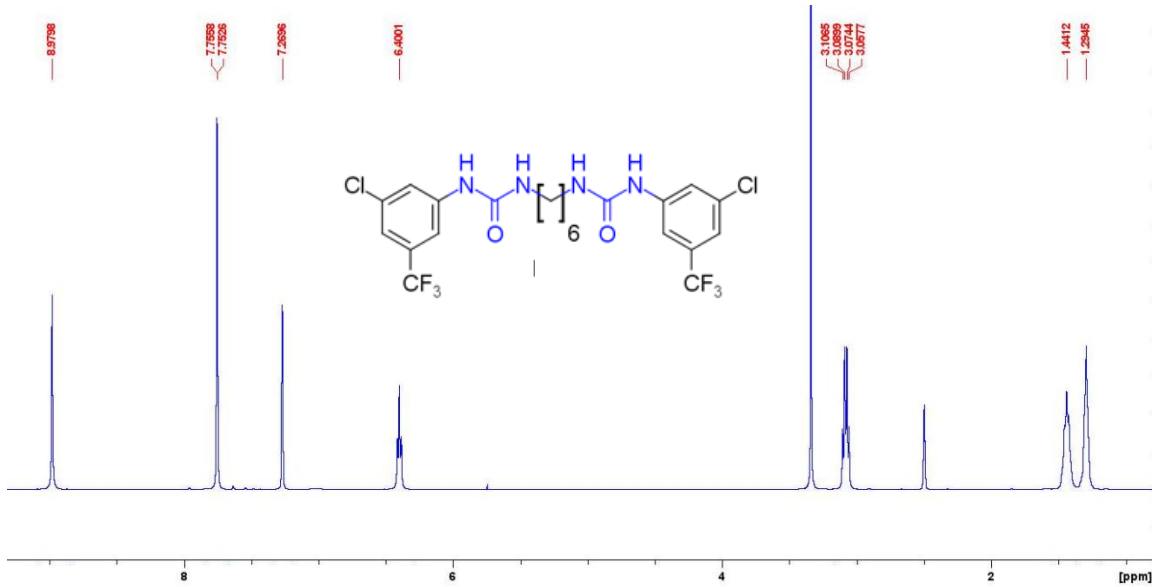

Figure S87. 400 MHz ^{1}H NMR spectrum of **D3**

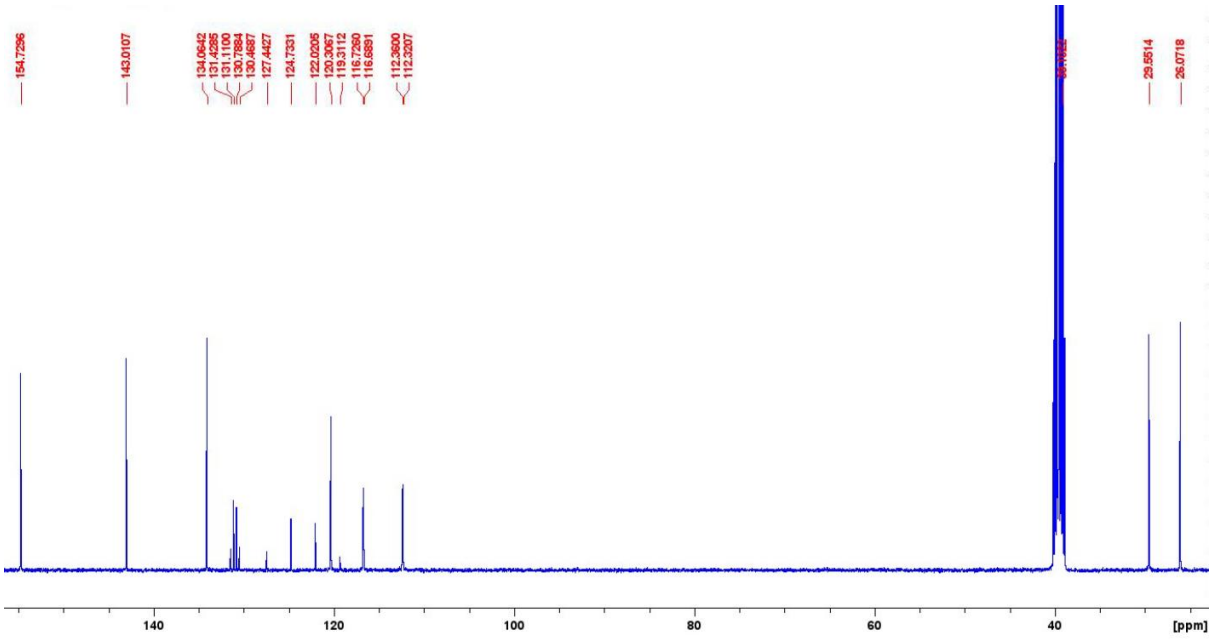

Figure S88. 100 MHz ^{13}C NMR spectrum of **D3**

3-[4-(trifluoromethyl)phenyl]-1-[6-({[4-(trifluoromethyl)phenyl]carbamoyl}amino)hexyl]urea (D7)

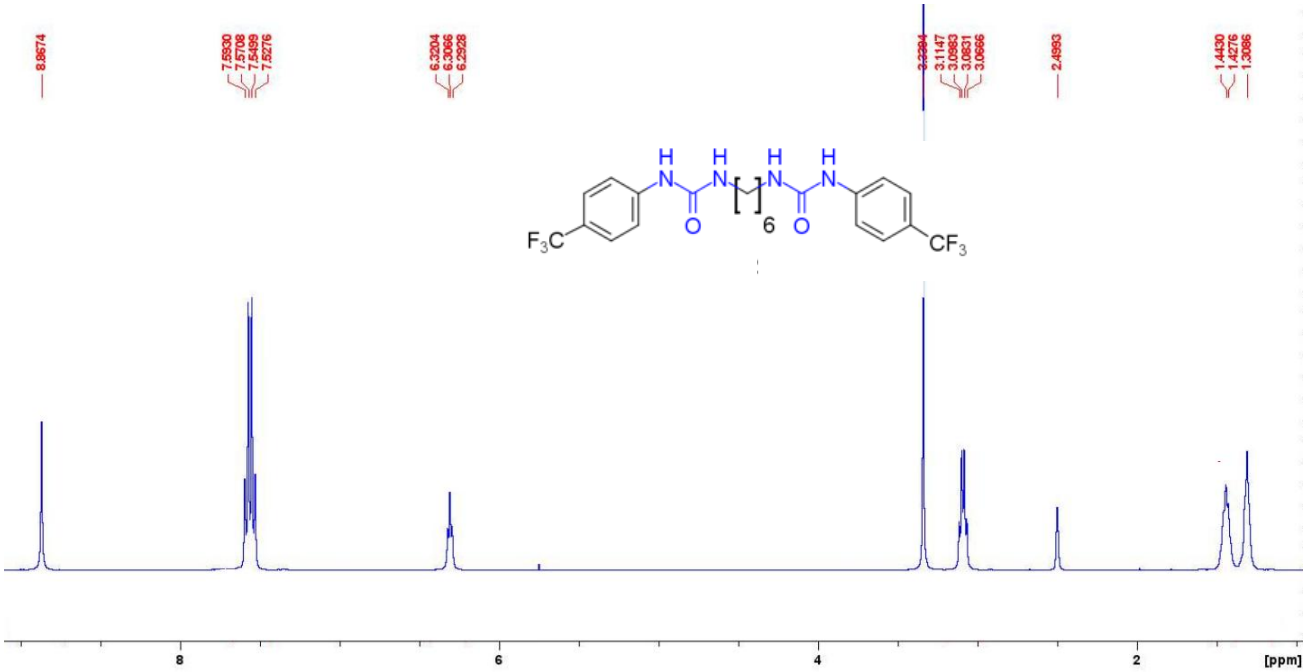

Figure S89. 400 MHz ^{1}H NMR spectrum of **D7**

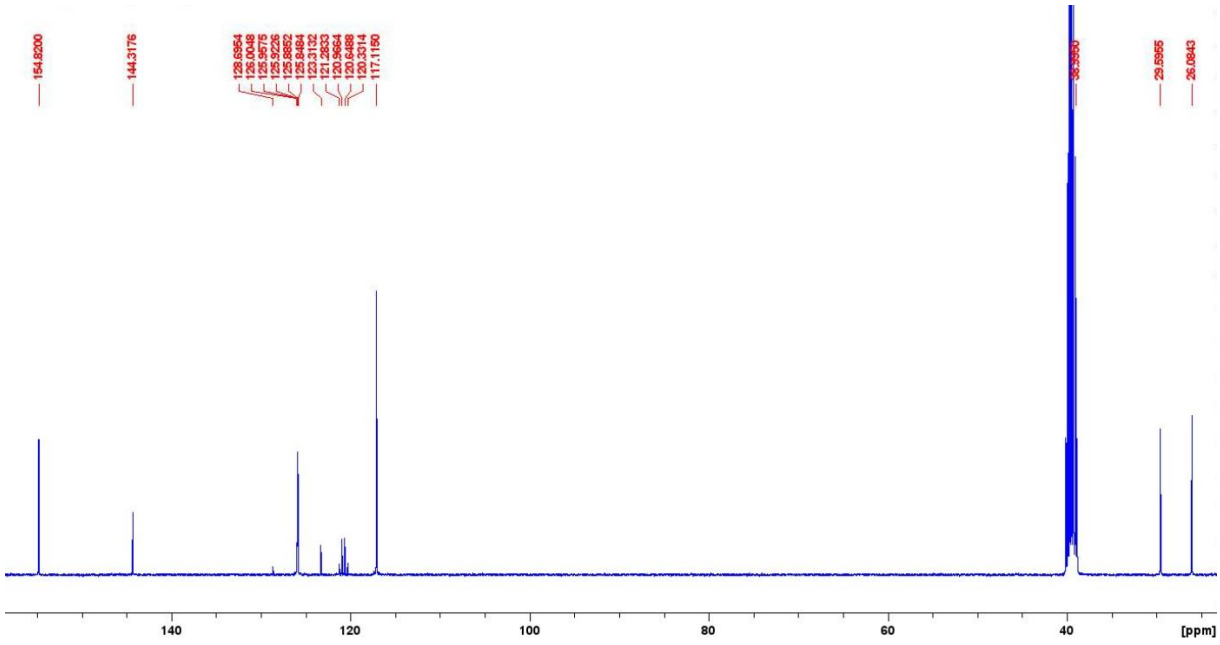

Figure S90. 100 MHz ^{13}C NMR spectrum of **D7**

3-[4-(trifluoromethoxy)phenyl]-1-[6-({[4-(trifluoromethoxy)phenyl]carbamoyl}amino)hexyl]urea (D9)

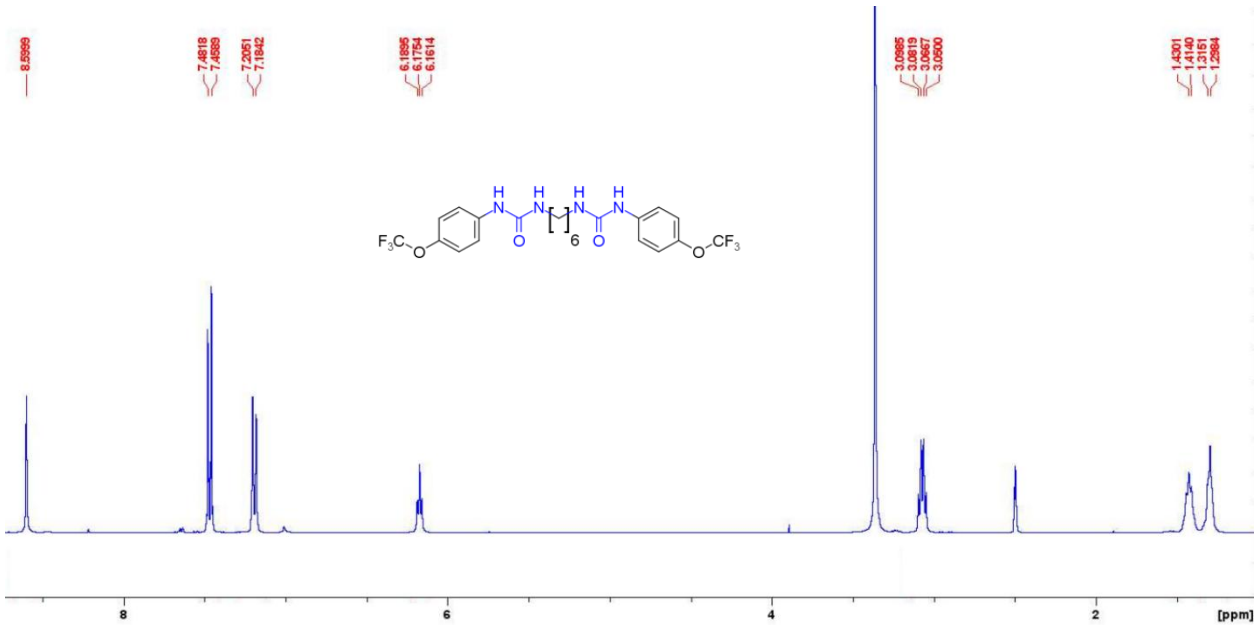

Figure S91. 400 MHz ^{1}H NMR spectrum of **D9**

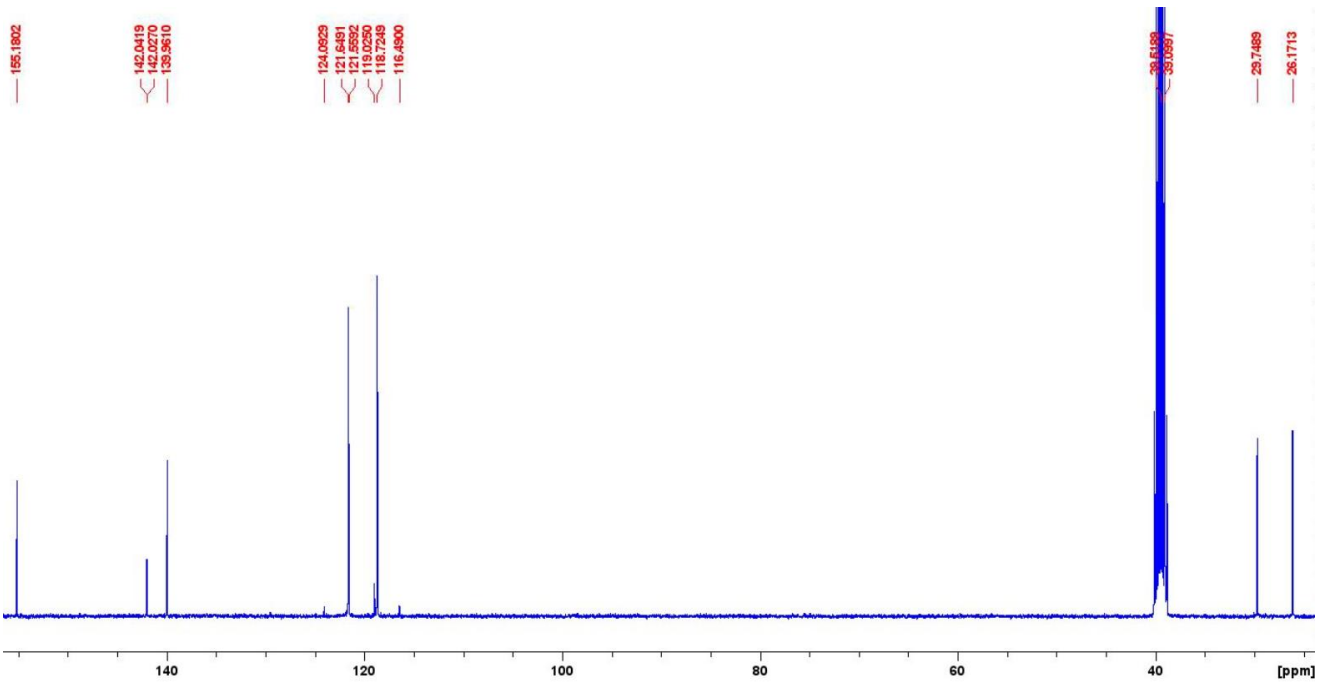

Figure S92. 100 MHz ^{13}C NMR spectrum of **D9**

3-phenyl-1-{6-[(phenylcarbamoyl)amino]hexyl}urea (D11)

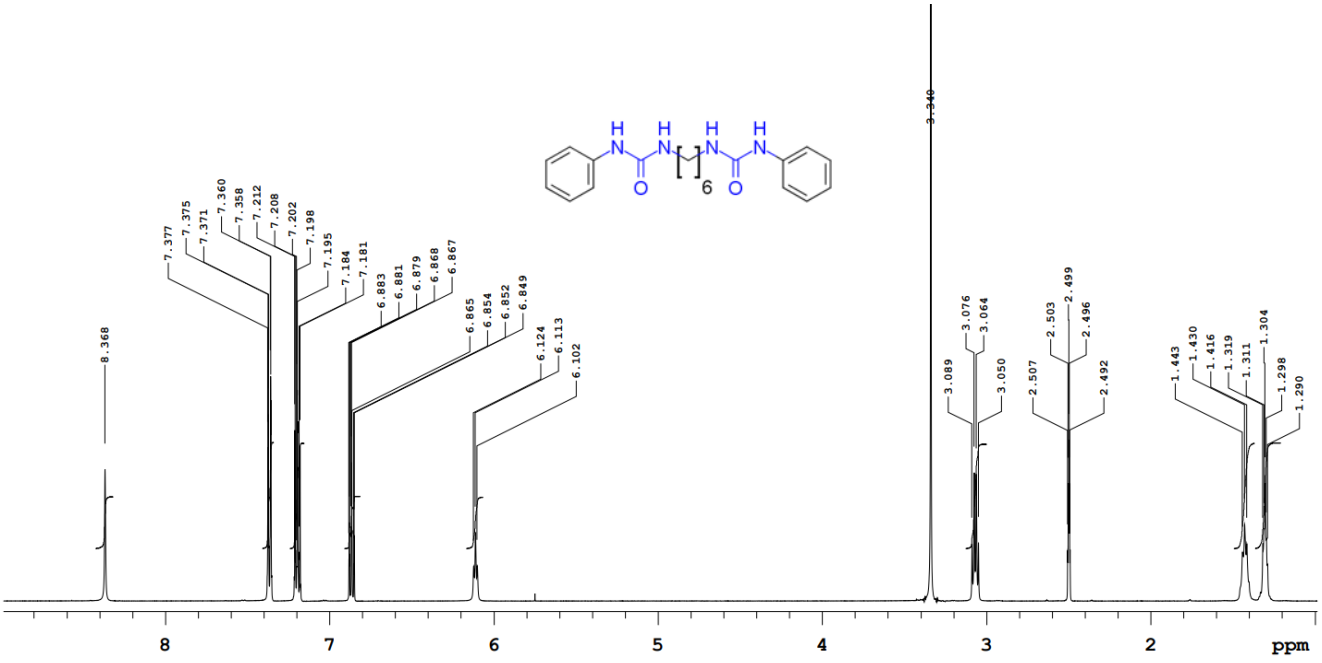

Figure S93. 500 MHz ^{1}H NMR spectrum of **D11**

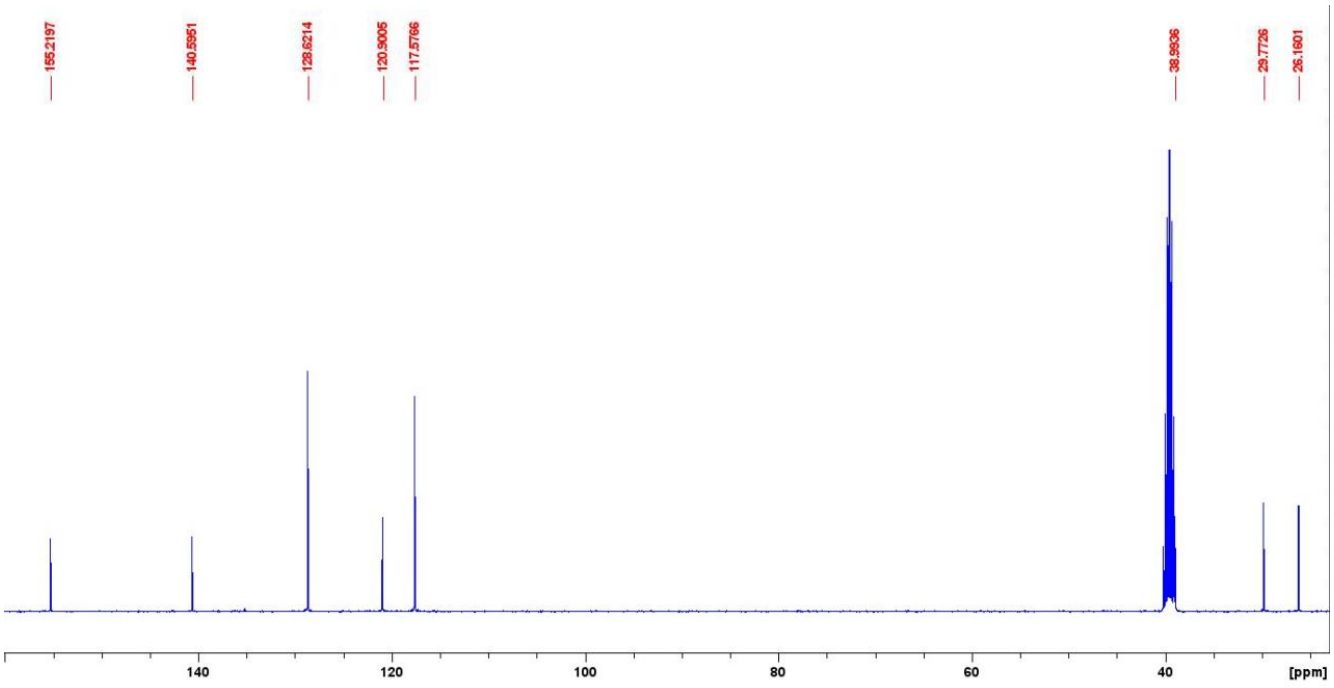

Figure S94. 100 MHz ^{13}C NMR spectrum of **D11**

S3.8 S1/S4, A1/A4, D1/D4 HPTS Dose-Response Hill Analyses

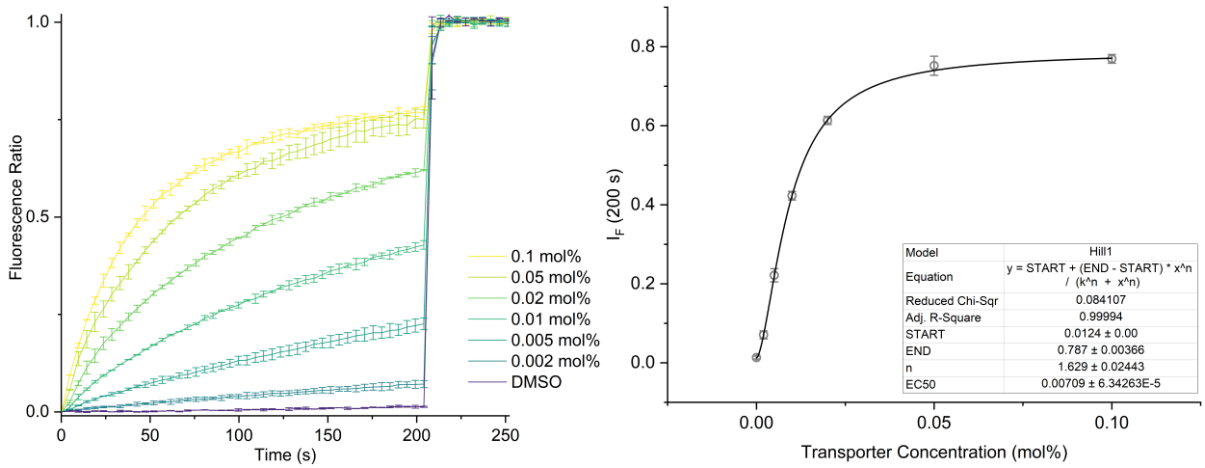

Figure S95. Hill plot analysis of H^+/OH^- transport facilitated by compound **S3** measured using the KGluc assay. NaOH (5 mM) and valinomycin (0.05 mol%) were added to the vesicles before the addition of **S3** at 0 s. Detergent was added at 205 s to lyse the vesicles. Compound concentrations are shown as compound-to-lipid molar ratios. Error bars represent standard deviations from at least two repeats.

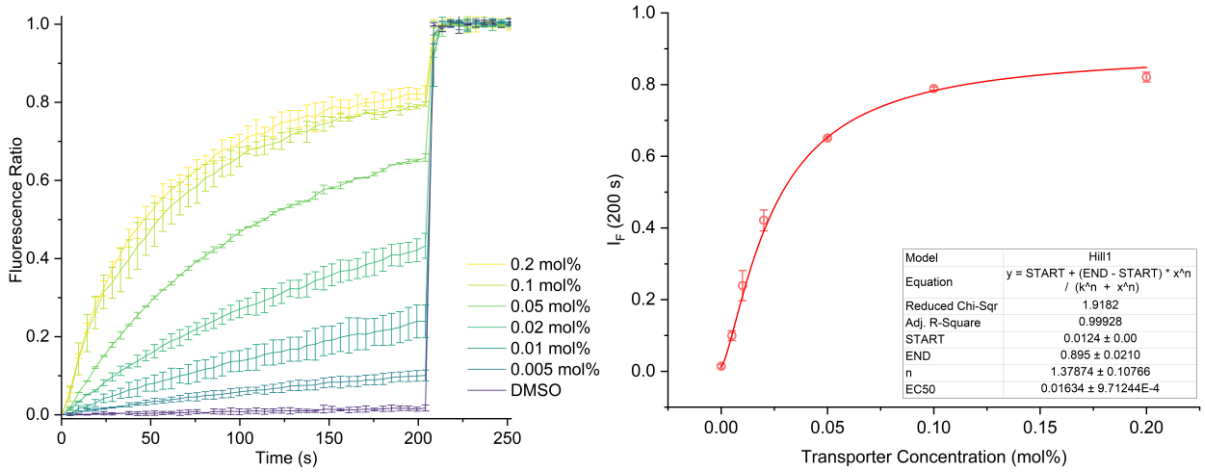

Figure S96. Hill plot analysis of H^+/OH^- transport facilitated by compound **S3** measured using the KGluc assay. The vesicles were pre-treated with BSA (1 mol%). NaOH (5 mM) and valinomycin (0.05 mol%) were added to the vesicles before the addition of **S3** at 0 s. Detergent was added at 205 s to lyse the vesicles. Compound concentrations are shown as compound-to-lipid molar ratios. Error bars represent standard deviations from at least two repeats.

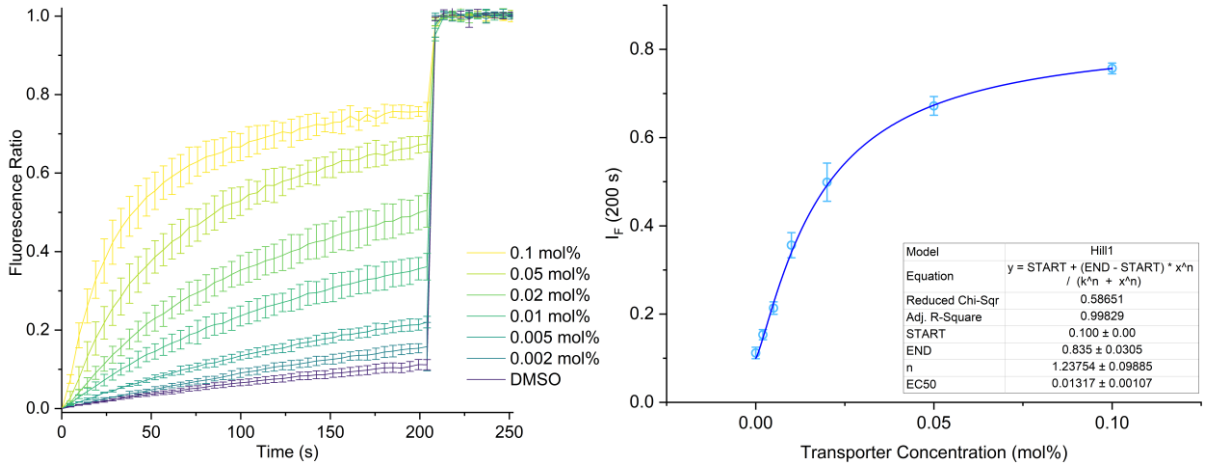

Figure S97. Hill plot analysis of H^+/OH^- transport facilitated by compound **S3** measured using the KGluc assay. The vesicles were pre-treated with BSA (1 mol%). OA (10 mol%), NaOH (5 mM) and valinomycin (0.05 mol%) were added to the vesicles before the addition of **S3** at 0 s. Detergent was added at 205 s to lyse the vesicles. Compound concentrations are shown as compound-to-lipid molar ratios. Error bars represent standard deviations from at least two repeats.

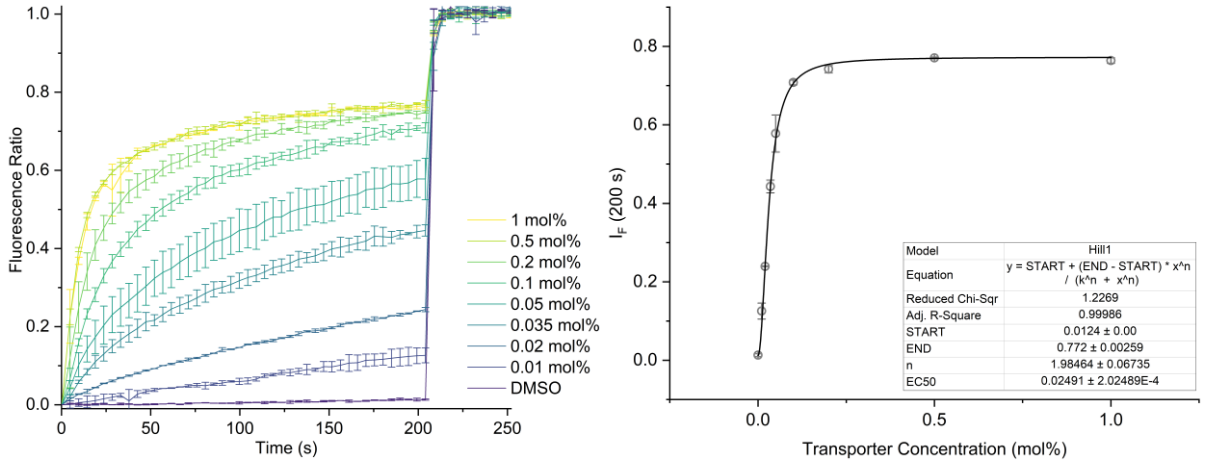

Figure S98. Hill plot analysis of H^+/OH^- transport facilitated by compound **A3** measured using the KGluc assay. NaOH (5 mM) and valinomycin (0.05 mol%) were added to the vesicles before the addition of **A3** at 0 s. Detergent was added at 205 s to lyse the vesicles. Compound concentrations are shown as compound-to-lipid molar ratios. Error bars represent standard deviations from at least two repeats.

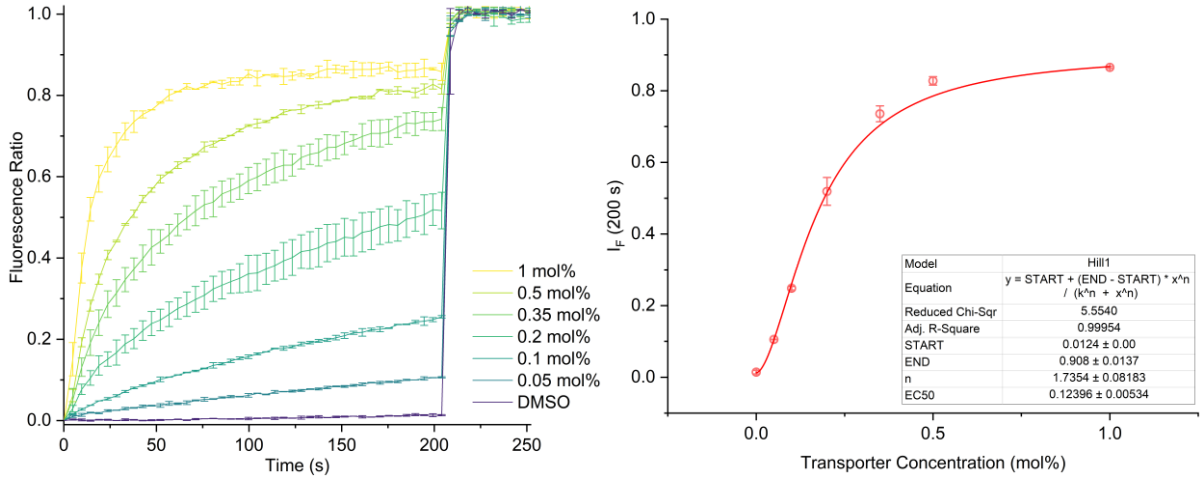

Figure S99. Hill plot analysis of H^+/OH^- transport facilitated by compound **A3** measured using the KGluc assay. The vesicles were pre-treated with BSA (1 mol%). NaOH (5 mM) and valinomycin (0.05 mol%) were added to the vesicles before the addition of **A3** at 0 s. Detergent was added at 205 s to lyse the vesicles. Compound concentrations are shown as compound-to-lipid molar ratios. Error bars represent standard deviations from at least two repeats.

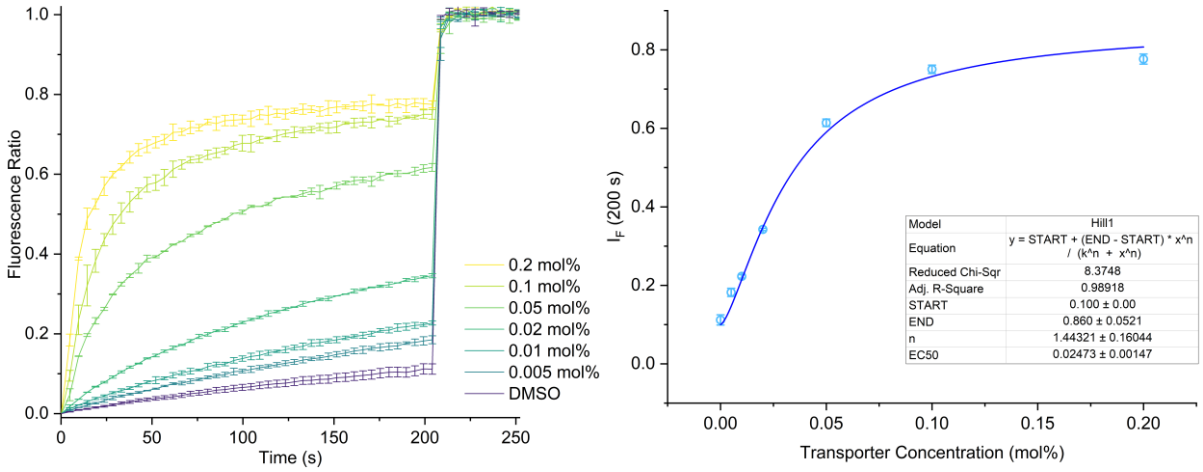

Figure S100. Hill plot analysis of H^+/OH^- transport facilitated by compound **A3** measured using the KGluc assay. The vesicles were pre-treated with BSA (1 mol%). OA (10 mol%), NaOH (5 mM) and valinomycin (0.05 mol%) were added to the vesicles before the addition of **A3** at 0 s. Detergent was added at 205 s to lyse the vesicles. Compound concentrations are shown as compound-to-lipid molar ratios. Error bars represent standard deviations from at least two repeats.

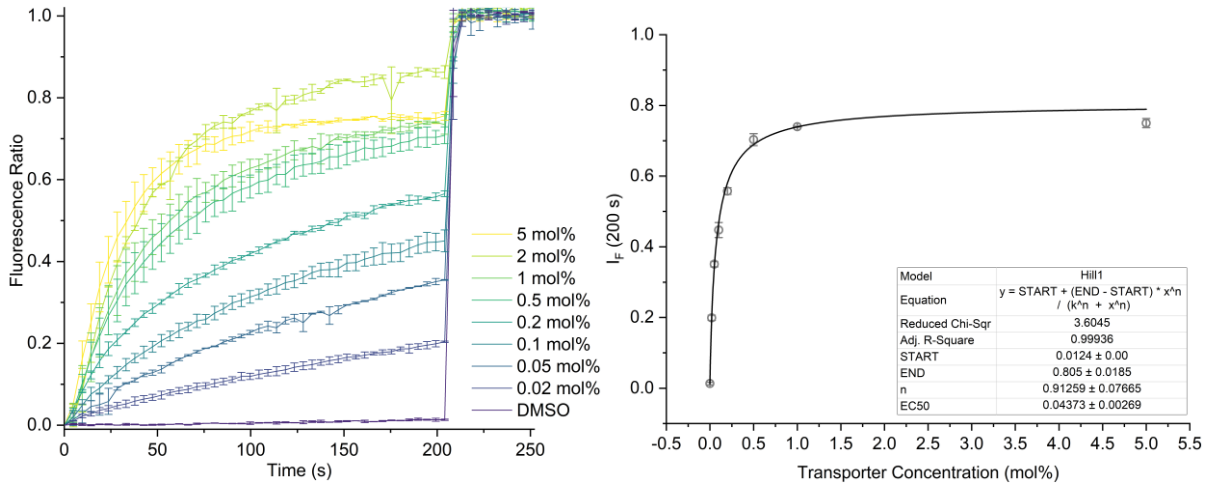

Figure S101. Hill plot analysis of H^+/OH^- transport facilitated by compound **D3** measured using the KGluc assay. NaOH (5 mM) and valinomycin (0.05 mol%) were added to the vesicles before the addition of **D3** at 0 s. Detergent was added at 205 s to lyse the vesicles. Compound concentrations are shown as compound-to-lipid molar ratios. Error bars represent standard deviations from at least two repeats.

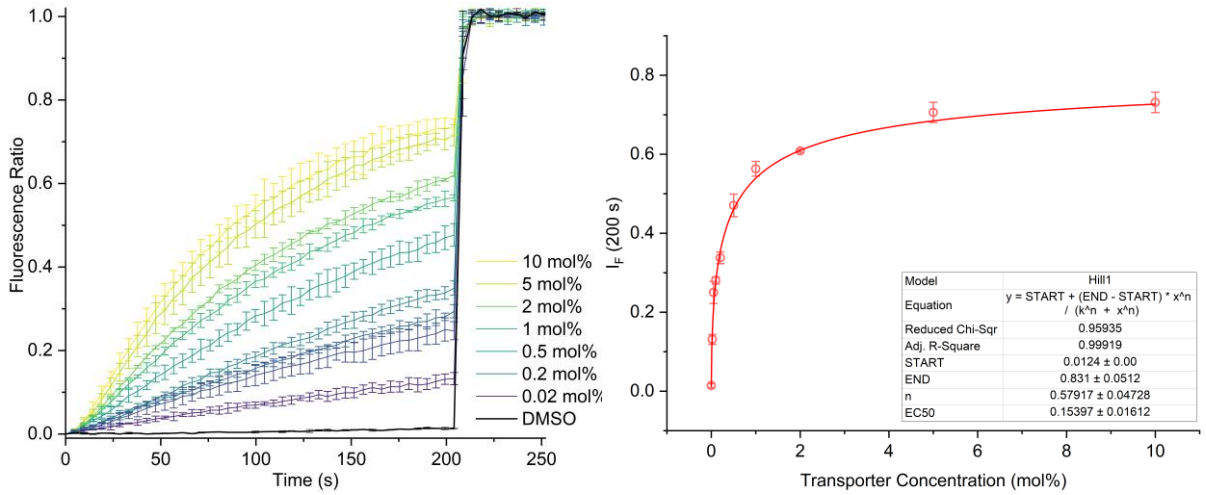

Figure S102. Hill plot analysis of H^+/OH^- transport facilitated by compound **D3** measured using the KGluc assay. The vesicles were pre-treated with BSA (1 mol%). NaOH (5 mM) and valinomycin (0.05 mol%) were added to the vesicles before the addition of **D3** at 0 s. Detergent was added at 205 s to lyse the vesicles. Compound concentrations are shown as compound-to-lipid molar ratios. Error bars represent standard deviations from at least two repeats.

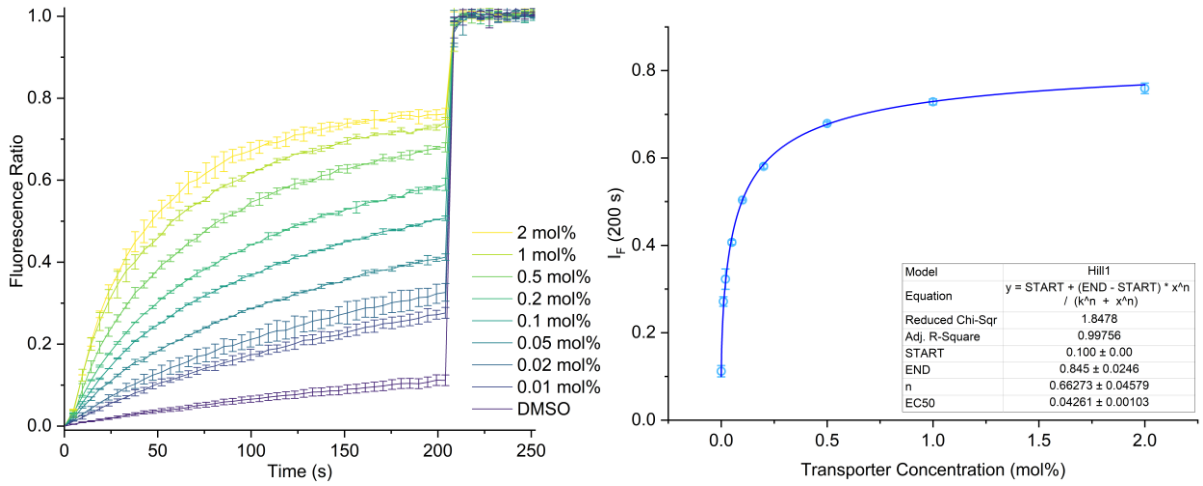

Figure S103. Hill plot analysis of H^+/OH^- transport facilitated by compound **D3** measured using the KGluc assay. The vesicles were pre-treated with BSA (1 mol%). OA (10 mol%), NaOH (5 mM) and valinomycin (0.05 mol%) were added to the vesicles before the addition of **D3** at 0 s. Detergent was added at 205 s to lyse the vesicles. Compound concentrations are shown as compound-to-lipid molar ratios. Error bars represent standard deviations from at least two repeats.

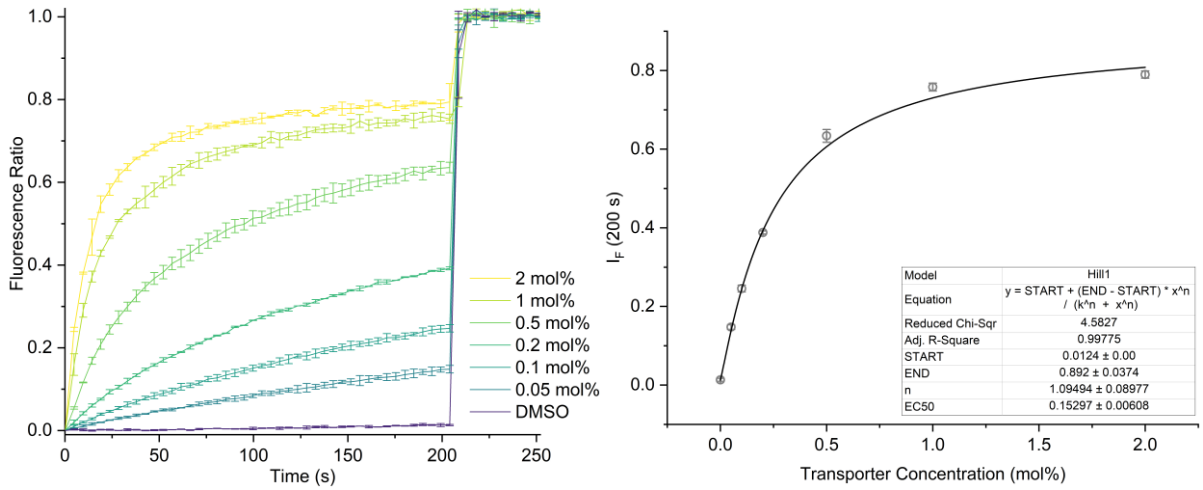

Figure S104. Hill plot analysis of H^+/OH^- transport facilitated by compound **S11** measured using the KGluc assay. NaOH (5 mM) and valinomycin (0.05 mol%) were added to the vesicles before the addition of **S11** at 0 s. Detergent was added at 205 s to lyse the vesicles. Compound concentrations are shown as compound-to-lipid molar ratios. Error bars represent standard deviations from at least two repeats.

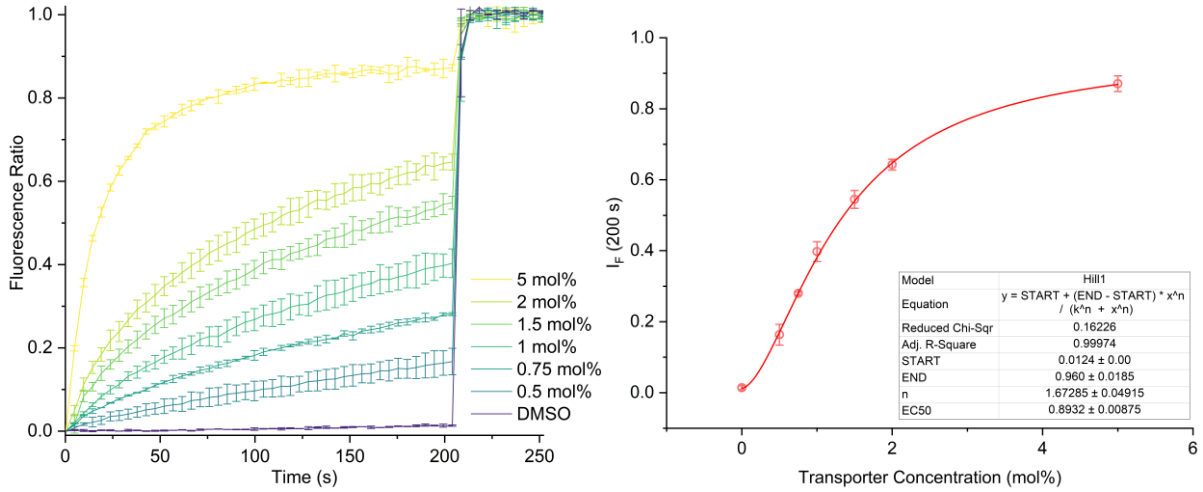

Figure S105. Hill plot analysis of H^+/OH^- transport facilitated by compound **S11** measured using the KGluc assay. The vesicles were pre-treated with BSA (1 mol%). NaOH (5 mM) and valinomycin (0.05 mol%) were added to the vesicles before the addition of **S11** at 0 s. Detergent was added at 205 s to lyse the vesicles. Compound concentrations are shown as compound-to-lipid molar ratios. Error bars represent standard deviations from at least two repeats.

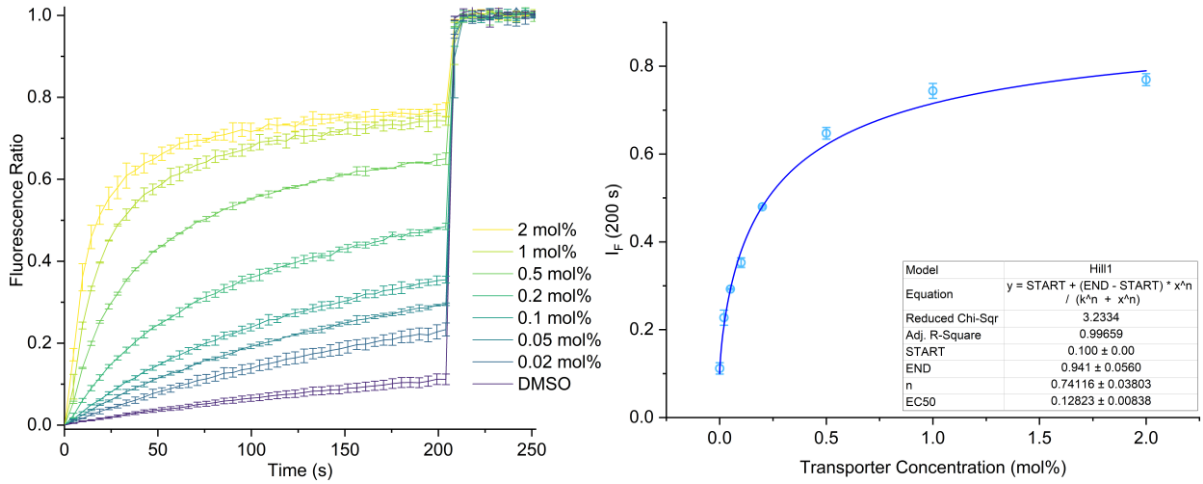

Figure S106. Hill plot analysis of H^+/OH^- transport facilitated by compound **S11** measured using the KGluc assay. The vesicles were pre-treated with BSA (1 mol%). OA (10 mol%), NaOH (5 mM) and valinomycin (0.05 mol%) were added to the vesicles before the addition of **S11** at 0 s. Detergent was added at 205 s to lyse the vesicles. Compound concentrations are shown as compound-to-lipid molar ratios. Error bars represent standard deviations from at least two repeats.

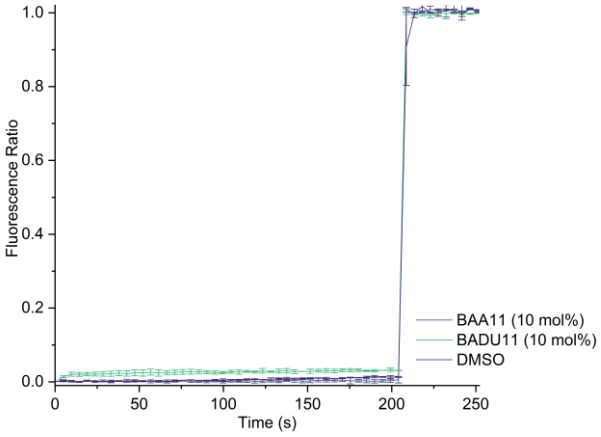

Figure S107. Efflux plots of H^+/OH^- transport facilitated by compound **A11** and **D11** measured using the KGluc assay. A 10 mol% compound-to-lipid molar ratio of either compound was added to the vesicles at 0 s and detergent was added at 205 s to lyse the vesicles. Error bars represent standard deviations from at least two repeats. H^+/OH^- efflux did not exceed 10% after 200 s under the conditions tested.

Supporting Information for Chapter Four

S4.1 Chemistry

2a and **2b** were synthesised by the procedure in the literature.[8] 3-chloro-5-(trifluoromethyl)aniline and 4-chloro-3-(trifluoromethyl)aniline were purchased from Fluorochem Limited (Hadfield, UK). The remaining reagents were purchased from Merck (Darmstadt, Germany). TLC reaction monitoring was performed using Merck silica gel 60 F254 aluminium-backed plates. Reaction products were purified as required with dry column vacuum chromatography on silica gel using gradient elutions. NMR spectra were recorded using a Bruker 400 MHz spectrometer operating at 400 MHz for ^{1}H and 100 MHz for ^{13}C spectra. Spectra were referenced internally to the residual solvent ($CDCl_3$: ^{1}H δ 7.26, ^{13}C δ 77.16. DMSO-d_6: ^{1}H δ 2.50, ^{13}C δ 39.52). Multiplicity was assigned as s (singlet), d (doublet), t (triplet), q (quartet), quintet and m (multiplet). High resolution mass spectra (HRMS) were recorded on an Agilent Technologies 6510 Q-TOF LCMS. The purity of all test compounds was confirmed to be >95% using absolute quantitative NMR spectroscopy.[24]

S4.2 Synthesis and Characterisation data

Synthesis of 3-nitrobenzaldehyde dioxolane acetal (7)

3-nitrobenzaldehyde (10.0 g, 66 mmol, 1 equiv.) was added 250 ml toluene, then ethylene glycol (8.2 g, 132 mmol, 2 equiv.) and *para*-toluenesulfonic acid (0.375 g, 2.2 mmol, 3.3 mol%). Reaction mixture was heated and stirred to reflux with Dean-Stark trap and water-cooled condenser. Flask and dean-stark trap required heat insulation with foil and rubber tubing to encourage distillation. Following 18 hours reflux, reaction mixture was cooled to room temperature then washed with 3 x 100 ml saturated sodium bicarbonate solution. Mixture was then dried over sodium sulfate, solvent removed under vacuo to give 3-nitrobenzaldehyde dioxolane acetal (12.5 g) in quantitative yield as a colourless viscous oil.

Characterisation data for 3-nitrobenzaldehyde dioxolane acetal (7)

Colourless Oil; Yield: 12.5 g, 98%; mp = N/A. ^{1}H NMR (400 MHz, $CDCl_3$): δ 8.35 (*s*, 1H), 8.23 (d, J = 8.2 Hz, 1H), 7.80 (d, J = 7.7 Hz, 1H), 7.55 (t, J = 7.9 Hz, 1H), 5.88 (s, 1H), 3.95-4.20 (m, 4H). ^{13}C NMR (100 MHz, $CDCl_3$): δ 148.4 (1C), 140.5 (1C), 132.8 (1C), 129.5 (1C), 124.1 (1C), 121.8 (1C), 102.3 (1C), 65.6 (2C). HRMS (ESI) m/z: $[M + H]^+$ calcd for $C_9H_9NO_4$, 196.0604; found, 196.0590.

Synthesis of 3-aminobenzaldehyde dioxolane acetal (8)

3-nitrobenzaldehyde dioxolane acetal (2.928 g, 15 mmol, 1 equiv.) was added slowly to a suspension of Pd/C (0.146 mg, 5% w/w) in 40 ml absolute Ethanol (distilled from 95% Ethanol over KOH) with cooling in an ice-water bath. Ammonium formate (3.784 g, 60 mmol, 4 equiv.) was then added in one portion, reaction stirred and gently heated to maintain steady evolution of gas and reaction stirred for one hour. At one hour, the reaction was filtered through celite and solvent removed under vacuo. Added 30 ml of deionised water and extracted three times with 30 ml dichloromethane. The combined

extracts were dried over sodium sulfate and solvent removed under vacuo to give as 3-aminobenzaldehyde dioxolane acetal (1.921 g, 78%) as a brown oil.

Characterisation data for 3-aminobenzaldehyde dioxolane acetal (8)

Brown oil; Yield: 1.921 g, 78%; mp = N/A. ^{1}H NMR (400 MHz, $CDCl_3$): δ 7.16 (t, J = 7.7 Hz, 1H), 6.87 (d, J = 7.6 Hz, 1H), 6.80 (s, 1H), 6.68 (d, J = 7.9 Hz, 1H), 5.74 (s, 1H), 3.95-4.20 (m, 4H), 3.69 (br s, 2H). ^{13}C NMR (100 MHz, $CDCl_3$): δ 146.6 (1C), 139.2 (1C), 129.5 (1C), 116.7 (1C), 116.0 (1C), 112.9 (1C), 103.8 (1C), 65.3 (1C). HRMS (ESI) m/z: $[M + H]^+$ calcd for $C_9H_{11}NO_2$, 166.0863; found, 166.0860.

Synthesis of Boc-3-aminobenaldehyde dioxolane acetal (9)

3-aminobenzaldehyde dioxolane acetal (0.330 g, 2 mmol, 1 equiv.) was dissolved in 8 mL anhydrous dichloromethane under an argon atmosphere. Boc anhydride (0.873 g, 4 mmol, 2 equiv.) was added and stirred at 40°C. Following 18 hours, reaction was cooled to room temperature and 50 mL deionised water was added. Mixture was extracted three times with 20 mL dichloromethane. Combined organic extracts were washed with 50 mL brine then dried over sodium sulfate, filtered and solvent removed under vacuo. The resultant oil was purified by dry column vacuum chromatography using gradient elutions of EtOAc/Hexane (0:100 to 30:70) to isolate Boc-3-aminobenzaldehyde dioxolane acetal (0.377 g, 71%) as a pale green/colourless oil.

Characterisation data for Boc-3-aminobenaldehyde dioxolane acetal (9)

Colourless oil; Yield: 0.377 g, 71%; mp = N/A. ^{1}H NMR (400 MHz, $CDCl_3$): δ 7.47 (s, 1H), 7.37 (d, J = 8.1 Hz, 1H), 7.29 (t, J = 7.7 Hz, 1H), 7.14 (d, J = 7.5 Hz, 1H), 6.51 (br s, 1H), 5.78 (s, 1H), 3.95-4.20 (m, 4H), 1.51 (s, 9H). ^{13}C NMR (100 MHz, $CDCl_3$): δ 152.8 (1C), 139.0 (1C), 138.6 (1C), 129.1 (1C), 121.1 (1C), 119.3 (1C), 116.6 (1C), 103.6 (1C), 80.6 (1C), 65.4 (3C). HRMS (ESI) m/z: $[M + H]^+$ calcd for $C_{14}H_{19}NO_4$, 266.1387; found, 266.1387.

Synthesis of Boc-3-aminobenzaldehyde (10)

Boc-3-aminobenzaldehyde dioxolane acetal (1.887 g, 7.1 mmol, 1 equiv.) was dissolved in 30 mL acetone and 0.3 mL deionised water. Amberlyst 15 (0.230 g, 12 % w/w) was added and reaction mixture was stirred at room temperature for 3.5 hours. The reaction mixture was filtered through celite and solvent removed under vacuo to give Boc-3-aminobenzaldehyde (1.473 g, 94%) as a white solid.

Characterisation data for Boc-3-aminobenzaldehyde (10)

White solid; Yield: 1.473 g, 94%; mp = 86-88°C. ^{1}H NMR (400 MHz, $CDCl_3$): δ 9.97 (s, 1H), 7.91 (s, 1H), 7.63 (d, J = 8 Hz, 1H), 7.55 (d, J = 7.6 Hz, 1H), 7.45 (t, J = 7.8 Hz, 1H), 6.66 (br s, 1H), 1.53 (s, 9H). ^{13}C NMR (100 MHz, $CDCl_3$): δ 192.2 (1C), 152.7 (1C), 139.5 (1C), 137.3 (1C), 129.8 (1C), 124.3 (1C), 119.4 (1C), 81.3 (1C), 28.4 (3C). HRMS (ESI) m/z: $[M + H]^+$ calcd for $C_{12}H_{15}NO_3$, 222.1125; found, 222.1121.

Synthesis of 12-bromododecanoic acid (13)

10 mL 98% sulfuric acid was added slowly to 40 mL 48% hydrobromic acid in an ice bath with stirring. 12-hydroxydodecanoic acid (1.514 g, 7 mmol, 1 equiv.) was then added and the reaction mixture was heated to reflux for 16 hours. On heating, the 12-hydroxydodecanoic acid melted to give a two phase reaction mixture, two stirrer bars were used to encourage mixing. The reaction was then cooled to room temperature, added to 50 mL deionised water then extracted three times with 40 mL dichloromethane. The combined extracts were then washed with 50 mL brine, dried over sodium sulfate and solvent removed under vacuum to give 12-bromododecanoic acid (1.879 g, 96%) as a beige solid.

Characterisation data for 12-bromododecanoic acid (13)

Beige solid; Yield: 1.879 g, 96%; mp = 53-55 °C; ^{1}H NMR (400 MHz, $CDCl_3$): δ 3.40 (t, J = 6.9 Hz, 2H), 2.35 (t, J = 7.6 Hz, 2H), 1.83 (quintet, J = 7.6 Hz, 2H), 1.63 (quintet, J = 7.4 Hz, 2H), 1.44-1.39 (m, 2H), 1.37-1.25 (m, 12H); ^{13}C NMR (100 MHz, $CDCl_3$): δ 180.1 (1C), 34.2 (1C), 33.0 (1C), 29.6 (2C), 29.52 (1C), 29.49 (1C), 29.3 (1C), 29.2 (1C), 28.9 (1C), 28.3 (1C), 24.8 (1C); HRMS (ESI) m/z: $[M + H]^+$ calcd for $C_{12}H_{23}BrO_2$, 279.0954; found, 279.0947.

Synthesis of ethyl 10-bromodecanoate (14)

Acetyl chloride (1.413 g, 18 mmol, 3 equiv.) was added dropwise to 10-bromodecanoic acid (1.507 g, 6 mmol, 1 equiv.) in 12 mL absolute ethanol and stirred at room temperature. After 4 hours, solvent was removed under vacuo, then solid was dissolved in 30 mL ethyl acetate and washed three times with 20 mL 0.75 M sodium hydroxide solution. Solid sodium chloride added to last wash to aid removal of residual water. Further dried ethyl actate over magnesium sulfate, filtered then solvent was removed under vacuo to give ethyl 10-bromodecanoate (1.477 g, 88%) as a yellow liquid.

Characterisation data for ethyl 10-bromodecanoate (14)

Yellow liquid; Yield: 1.477 g, 88%; mp = N/A; ^{1}H NMR (400 MHz, $CDCl_3$): δ 4.11 (q, J = 7.1 Hz, 2H), 3.39 (t, J = 6.8 Hz, 2H), 2.28 (t, J = 7.6 Hz, 2H), 1.84 (quintet, J = 7.6 Hz, 2H), 1.63-1.58 (m, 2H), 1.43-1.39 (m, 2H), 1.37-1.26 (m, 8H), 1.24 (t, J = 7.1 Hz, 3H); ^{13}C NMR (100 MHz, $CDCl_3$): δ 174.0 (1C), 60.3 (1C), 34.5 (1C), 34.1 (1C), 32.9 (1C), 29.4 (1C), 29.3 (1C), 29.2 (1C), 28.8 (1C), 28.3 (1C), 25.1 (1C), 14.4 (1C); HRMS (ESI) m/z: $[M + H]^+$ calcd for $C_{12}H_{23}BrO_2$, 279.0954; found, 279.0950.

Synthesis of ethyl 12-bromododecanoate (15)

Ethyl 12-bromododecanoate was synthesised following the same procedure as for **14** and was isolated as a yellow liquid (85%).

Characterisation data for ethyl 12-bromododecanoate (15)

Yellow liquid; Yield: 1.735 g, 85%; mp = N/A; ^{1}H NMR (400 MHz, $CDCl_3$): δ 4.12 (q, J = 7.1 Hz, 2H), 3.40 (t, J = 6.9 Hz, 2H), 2.28 (t, J = 7.7 Hz, 2H), 1.85 (quintet, J = 7.6 Hz, 2H), 1.63-1.58 (m, 2H), 1.45-1.35 (m, 2H), 1.30-1.22 (m, 15H); ^{13}C NMR (100 MHz, $CDCl_3$): δ 174.1 (1C), 60.3 (1C), 34.5 (1C), 34.2 (1C), 33.0 (1C), 29.6 (2C), 29.5 (1C), 29.4 (1C), 29.3 (1C), 28.9 (1C), 28.3 (1C), 25.1 (1C), 14.4 (1C); HRMS (ESI) m/z: $[M + H]^+$ calcd for $C_{14}H_{27}BrO_2$, 307.1267; found, 307.1261.

Synthesis of (10-ethoxy-10-oxodecyl)triphenylphosphonium bromide (16)

Triphenylphosphine (3.864 g, 14.7 mmol, 1.4 equiv.) was added to neat ethyl 10-bromodecanoate (2.936 g, 10.5 mmol, 1 equiv.) and stirred at 120°C for 20 hours. The resultant mixture was purified by dry column vacuum chromatography using gradient elutions of Ethanol / Ethyl acetate (0:100 to 60:40) to give (10-ethoxy-10-oxodecyl)triphenylphosphonium bromide (4.481 g, 79%) as a tacky brown gum.

Characterisation data for (10-ethoxy-10-oxodecyl)triphenylphosphonium bromide (16)

Tacky brown resin; Yield: 4.481 g, 78%; mp = N/A; ^{1}H NMR (400 MHz, $CDCl_3$): δ 7.9-7.6 (m, 15H), 4.09 (q, J = 7.1 Hz, 2H), 3.9-3.7 (m, 2H), 2.23 (t, J = 7.6 Hz, 2H), 1.60-1.52 (m, 6H), 1.24-1.15 (m, 11H); ^{13}C NMR (100 MHz, $CDCl_3$): δ 174.0 (1C), 135.1 (1C), 133.8 (d, J = 10 Hz, 6C), 130.6 (d, J = 12.5 Hz, 6C), 118.5 (d, J = 85.2 Hz, 3C), 60.2, 34.4, 30.5, 30.4, 29.2, 29.0, 25.0, 23.1, 22.8, 22.7, 14.3; HRMS (ESI) m/z: $[M + H]^+$ calcd for $C_{30}H_{38}O_2P$, 461.2604; found, 461.2589.

Synthesis of Boc-3-aminophenol (19)

3-aminophenol (0.545 g, 5 mmol, 1 equiv.) was dissolved in 20 mL anhydrous dichloromethane under argon. Boc anhydride (2.183 g, 10 mmol, 2 equiv.) and stirred at 40°C. Following 18 hours, reaction

was cooled to room temperature and 50 mL deionised was added. Mixture was extracted three times with 20 mL dichloromethane. Combined organic extracts were washed with 50 mL brine then dried over sodium sulfate, filtered and solvent removed under vacuo. The resultant oil was purified by dry column vacuum chromatography using gradient elutions of DCM/EtOAc (100:0 to 80:20) to isolate Boc-3-aminophenol (0.641 g, 61%) as a colourless oil that crystallised on hi-vac to give a white solid.

Characterisation data for Boc-3-aminophenol (19)

White solid; Yield: 0.641 g, 61%; mp = 133-136°C; ^{1}H NMR (400 MHz, $CDCl_3$): δ 7.13 (s, 1H), 7.12 (t, J = 8 Hz, 1H), 6.72 (d, J = 8.1 Hz, 1H), 6.52 (d, J = 8.1 Hz, 1H), 6.48 (br s, 1H), 5.27 (br s, 1H), 1.53 (s, 9H); ^{13}C NMR (100 MHz, $CDCl_3$): δ 156.6 (1C), 153.1 (1C), 139.5 (1C), 130.0 (1C), 110.8 (1C), 110.5 (1C), 106.1 (1C), 81.0 (1C), 28.5 (3C); HRMS (ESI) m/z: $[M+Na]^+$ calcd for $C_{11}H_{15}NO_3$, 232.0944; found, 232.0939.

Synthesis of Boc-4-aminophenol (20)

4-aminophenol (0.873 g, 8 mmol, 1 equiv.) was added to a solution of Boc anhydride (1.921 g, 8.8 mmol, 1.1 equiv.) in 10 mL 95% ethanol containing Amberlyst 15 (0.040 g, 10% w/w) and was stirred at room temperature for 15 minutes with evolution of gas. Solvent removed under vacuo, then the resultant solid was resuspended in 10 mL hexane and filtered through celite. Desired solid dissolved in 10 mL ethyl acetate and refiltered to remove amberlyst 15 beads. Solvent removed under vacuo to give Boc-4-aminophenol (1.454 g, 87%) as an off-white solid.

Characterisation data for Boc-4-aminophenol (20)

Off-white solid; Yield: 1.454 g, 87%; mp = 139-142 °C. ^{1}H NMR (400 MHz, $CDCl_3$): δ 7.17 (d, J = 8.5 Hz, 2H), 6.74 (d, J = 8.8 Hz, 2H), 6.33 (br s, 1H), 5.08 (br s, 1H), 1.51 (s, 9H). ^{13}C NMR (100

MHz, $CDCl_3$): δ 153.8 (1C), 152.2 (1C), 131.0 (1C), 121.6 (2C), 115.9 (2C), 80.6 (1C), 28.5 (3C). HRMS (ESI) m/z: $[M + Na]^+$ calcd for $C_{11}H_{15}NO_3$, 232.0944; found, 232.0943.

Synthesis of ethyl (10E)-11-(3-{[(tert-butoxy)carbonyl]amino}phenyl)undec-10-enoate (21)

(10-ethoxy-10-oxodecyl)triphenylphosphonium bromide (4.061 g, 7.5 mmol, 1.5 equiv.) in 25 mL anhydrous tetrahydrofuran at 0°C under argon was slowly added 9.5 mL of 1 M sodium bis(trimethylsilyl)amide solution in THF. The resulting bright orange mixture was stirred at room temperature for 20 minutes. The reaction was then cooled to -78°C, and Boc-3-aminobenzaldehyde (1.106 g, 5 mmol, 1 equiv.) was added dropwise dissolved in 5 mL anhydrous THF. The mixture was stirred for 30 minutes at -78°C after which was allowed to warm to room temperature over 90 minutes. 50 mL saturated ammonium chloride solution was added to quench any unreacted ylide and the mixture was extracted three times with 50 mL ethyl acetate. The combined extracts were washed with 100 mL brine, dried over magnesium sulfate then solvent removed under vacuo. The resultant orange oil was further purified by dry column vacuum chromatography using gradient elutions of ethyl acetate / hexane (0:100 to 30:70) to give ethyl (10E)-11-(3-{[(tert-butoxy)carbonyl]amino}phenyl)undec-10-enoate (1.630 g, 80%) as a colourless liquid.

Characterisation data for ethyl (10E)-11-(3-{[(tert-butoxy)carbonyl]amino}phenyl)undec-10-enoate (21)

Colourless liquid; Yield: 1.630 g, 80%; mp = N/A; ^{1}H NMR (400 MHz, $CDCl_3$): δ 7.25-7.22 (m, 3H), 6.97-6.94 (m, 1H), 6.35 (d, J = 11.6 Hz, 1H), 5.70-5.60 (m, 1H), 4.12 (q, J = 7.1 Hz, 2H), 2.35-2.25 (m, 4H), 1.65-1.55 (m, 2H), 1.52 (s, 9H), 1.45-1.35 (m, 2H), 1.35-1.20 (m, 12H); ^{13}C NMR (100 MHz, $CDCl_3$): δ 174.1 (1C), 152.9 (1C), 138.8 (1C), 138.3 (1C), 133.7 (1C), 128.8 (1C), 128.6 (1C), 123.7 (1C), 119.0 (1C), 116.9 (1C), 80.6 (1C), 60.3 (1C), 34.5 (1C), 30.0 (1C), 29.4 (1C), 29.34 (1C),

29.33 (1C), 29.2 (2C), 28.7 (1C), 28.5 (3C), 25.1 (1C); HRMS (ESI) m/z: $[M + Na]^+$ calcd for $C_{24}H_{37}NO_4$, 426.2615; found, 426.2618.

Synthesis of N-[3-chloro-4-(trifluoromethyl)phenyl]-1H-imidazole-1-carboxamide (23a)

3-chloro-5-(trifluoromethyl)aniline (1.956 g, 10 mmol, 1 equiv.) was added to N,N'-carbonyldiimidazole (2.270 g, 14 mmol, 1.4 equiv.) in 14 mL 1,2-dichloroethylene under nitrogen and stirred at 50°C for 18 hours. After this, the reaction mixture was cooled to room temperature, with an ice bath and then was left to crystallise overnight in -20°C freezer. White N-[4-chloro-3-(trifluoromethyl)phenyl]-1H-imidazole-1-carboxamide (1.912 g, 66%) crystals were isolated by vacuum filtration and were used without characterisation due to their propensity to dissociate in solution into their corresponding isocyanate and imidazole.[18]

Synthesis of N-[4-chloro-3-(trifluoromethyl)phenyl]-1H-imidazole-1-carboxamide (23b)

N-[4-chloro-3-(trifluoromethyl)phenyl]-1H-imidazole-1-carboxamide was synthesised following the same procedure as for **23a** and was isolated as a white crystalline solid (2.840, 98%)

Synthesis of ethyl 11-(3-{[(tert-butoxy)carbonyl]amino}phenyl)undecanoate (Boc3)

Ethyl (10E)-11-(3-{[(tert-butoxy)carbonyl]amino}phenyl)undec-10-enoate (1.009 g, 2.5 mmol, 1 equiv.) and Pd/C (0.050 g, 5 % w/w) were slowly added 30 mL absolute ethanol while cooling in an ice bath. Ice bath was removed and ammonium formate (1.577 g, 25 mmol, 10 equiv.) was added and reaction mixture was heated gently to maintain steady evolution of gas. Following one hour, reaction was cooled to room temperature then filtered through celite and solvent was removed under vacuo. Crude product was added 50 mL deionised water then extracted twice with 40 mL dichloromethane. The combined extracts were washed with 20 mL brine, dried over magnesium sulfate and solvent removed under vacuo to give ethyl 11-(3-{[(tert-butoxy)carbonyl]amino}phenyl)undecanoate (0.997 g, 99%) as a white solid.

Characterisation data for ethyl 11-(3-{[(tert-butoxy)carbonyl]amino}phenyl)undecanoate (Boc3)

White solid; Yield: 0.997 g, 99%; mp = 35-37°C; ^{1}H NMR (400 MHz, $CDCl_3$): δ 7.22 (s, 1H), 7.20 (t, J = 7.8 Hz, 1H), 7.12 (d, J = 8.3 Hz, 1H), 6.44 (br s, 1H), 4.12 (q, J = 7.1 Hz, 2H), 2.56 (t, J = 8.0 Hz, 2H), 2.2807 (t, J = 7.7 Hz, 2H), 1.65-1.55 (m, 4H), 1.51 (s, 9H), 1.30-1.20 (m, 16H); ^{13}C NMR (100 MHz, $CDCl_3$): δ 174.1 (1C), 152.9 (1C), 144.1 (1C), 138.4 (1C), 128.9 (1C), 123.3 (1C), 118.6 (1C), 115.9 (1C), 80.5 (1C), 60.3 (1C), 36.2 (1C), 34.5 (1C), 31.6 (1C), 29.61 (2C), 29.59 (1C), 29.55 (1C), 29.5 (1C), 29.4 (1C), 28.5 (3C), 25.1 (1C), 14.4 (1C); HRMS (ESI) m/z: $[M+Na]^+$ calcd for $C_{24}H_{39}NO_4$, 428.2771; found, 428.2768.

Synthesis of ethyl 11-(3-aminophenyl)undecanoate (3x)

Trifluoroacetic acid (2.25 ml, 29.4 mmol, 15 equiv.) was slowly added to ethyl 11-(3-{[(tert-butoxy)carbonyl]amino}phenyl)undecanoate (0.811 g, 2 mmol, 1 equiv.) in 6 mL anhydrous dichloromethane and stirred at room temperature for 4 hours. 50 mL deionised water was added and the resultant mixture was extracted three times with 25 mL ethyl acetate. The combined organic extracts were washed with 50 mL brine, dried over magnesium sulfate and solvent removed under vacuo to give ethyl 11-(3-aminophenyl)undecanoate (0.600 g, 98%) as a brown oil.

Characterisation data for ethyl 11-(3-aminophenyl)undecanoate (3x)

Brown oil; Yield: 0.600 g, 98%; mp = N/A; ^{1}H NMR (400 MHz, $CDCl_3$): δ 7.06 (t, J = 7.5 Hz, 1H), 6.58 (d, J = 7.5 Hz, 1H), 6.52-6.48 (m, 2H), 4.12 (q, J = 7.1 Hz, 2H), 3.50 (br s, 2H), 2.50 (t, J = 7.9 Hz, 2H), 2.28 (t, J = 7.7 Hz, 2H), 1.65-1.55 (m, 4H), 1.35-1.20 (m, 15H); ^{13}C NMR (100 MHz, $CDCl_3$): δ 174.1 (1C), 146.4 (1C), 144.4 (1C), 129.2 (1C), 119.0 (1C), 115.4 (1C), 112.6 (1C), 60.3 (1C), 36.1 (1C), 34.5 (1C), 31.5 (1C), 31.5 (1C), 29.62 (2C), 29.56 (1C), 29.5 (1C), 29.4 (1C), 29.3 (1C), 25.1 (1C), 14.4 (1C); HRMS (ESI) m/z: $[M + H]^+$ calcd for $C_{19}H_{31}NO_2$, 306.2428; found, 306.2425.

Synthesis of ethyl 12-(3-{[(tert-butoxy)carbonyl]amino}phenoxy)dodecanoate (Boc4)

tert-butyl N-(3-hydroxyphenyl)carbamate (0.502 g, 2.4 mmol, 1.2 equiv.) was added to ethyl 12-bromododecanoate (0.615 g, 2 mmol, 1 equiv.) in 7 mL anhydrous dimethylformamide. Potassium carbonate (0.553 g, 4 mmol, 2 equiv.) was added and the resultant suspension was stirred at 100°C under argon. After 24 hours, the reaction mixture was cooled to room temperature, diluted with 50 mL brine and extracted three times with 50 mL ethyl acetate. The combined organic extracts were washed twice with 50 mL brine, then was dried over magnesium sulfate and solvent removed under vacuum. The crude product was then purified by dry column vacuum chromatography using gradient elutions of hexane / dichloromethane (60:40 to 100:0) to yield ethyl 12-(4-{[(tert-butoxy)carbonyl]-amino}phenoxy)dodecanoate (0.345 g, 40%) as a white solid.

Characterisation data for ethyl 12-(3-{[(tert-butoxy)carbonyl]amino}phenoxy)dodecanoate (Boc4)

White solid; Yield: 0.664 g, 33%; mp = 56-58°C; ^{1}H NMR (400 MHz, $CDCl_3$): δ 7.14 (t, J = 8.2 Hz, 1H), 7.09 (s, 1H), 6.57 (d, J = 8.2 Hz, 1H), 6.48 (br s, 1H), 4.12 (q, J = 7.1 Hz, 2H), 3.93 (t, J = 6.6 Hz, 2H), 2.28 (t, J = 7.7 Hz, 2H), 1.75 (quint, J = 7.9 Hz, 2H), 1.68-1.56 (m, 2H), 1.51 (s, 9H), 1.47 – 1.38 (m, 2H), 1.37-1.22 (m, 15H); ^{13}C NMR (100 MHz, $CDCl_3$): δ 174.1 (1C), 152.9 (1C), 144.1 (1C), 138.4 (1C), 128.9 (1C), 123.3 (1C), 118.6 (1C), 115.9 (1C), 80.5 (1C), 60.3 (1C), 36.2 (1C), 34.5 (1C), 31.6 (1C), 29.61 (2C), 29.59 (1C), 29.55 (1C), 29.5 (1C), 29.4 (1C), 29.3 (1C), 28.5 (3C), 25.1 (1C), 14.4 (1C); HRMS (ESI) m/z: $[M + Na]^+$ calcd for $C_{25}H_{41}NO_5$, 458.2877; found, 458.2881.

Synthesis of ethyl 12-(3-aminophenoxy)dodecanoate (4x)

Ethyl 12-(3-aminophenoxy)dodecanoate was synthesised following the same procedure as for **3x** and was isolated as a beige solid (91%).

Characterisation of ethyl 12-(3-aminophenoxy)dodecanoate (4x)

Beige solid; Yield: 0.386 g, 91%; mp = 54-55°C; ^{1}H NMR (400 MHz, $CDCl_3$): δ 7.04 (t, J = 8 Hz, 1H), 6.31 (dd, J = 8.3, 2.4 Hz, 1H), 6.27 (dd, J = 8, 2.2 Hz, 1H), 6.24 (t, J = 2.2 Hz, 1H), 4.12 (q, J = 7.2 Hz, 2H), 3.90 (t, J = 6.6 Hz, 2H), 3.64 (br s, 2H), 2.28 (t, J = 7.6 Hz, 2H), 1.75 (q, J = 7.9 Hz, 2H), 1.61 (q, J = 7.3 Hz, 2H), 1.47-1.37 (m, 2H), 1.36-1.22 (m, 15H); ^{13}C NMR (100 MHz, $CDCl_3$): δ 174.1 (1C), 160.5 (1C), 147.8 (1C), 130.2 (1C), 107.9 (1C), 104.8 (1C), 101.8 (1C), 67.9 (1C), 60.3 (1C), 34.5 (1C), 29.7 (1C), 29.6 (2C), 29.56 (1C), 29.51 (1C), 29.44 (1C), 29.38 (1C), 29.27 (1C), 26.2 (1C), 25.1 (1C), 14.4 (1C); HRMS (ESI) m/z: $[M + H]^+$ calcd for $C_{20}H_{33}NO_3$, 336.2533; found, 336.2543.

Synthesis of ethyl 12-{3-[(tert-butoxycarbonyl)amino]phenoxy}decanoate (Boc5)

Ethyl 12-{3-[(tert-butoxycarbonyl)amino]phenoxy}decanoate was synthesised following the same procedure as for **Boc4** and was isolated as a white solid (40%).

Characterisation data for ethyl 12-{3-[(tert-butoxycarbonyl)amino]phenoxy}decanoate (Boc5)

White solid; Yield: 0.345 g, 40%; mp = 62-64°C; ^{1}H NMR (400 MHz, $CDCl_3$): δ 7.23 (d, J = 8.5 Hz, 2H), 6.82 (d, J = 9.0 Hz, 2H), 6.33 (br s, 1H), 4.12 (q, J = 7.1 Hz, 2H), 3.91 (t, J = 6.6 Hz, 2H), 2.28 (t, J = 7.6 Hz, 2H), 1.75 (q, J = 7.8 Hz, 2H), 1.65-1.57 (m, 2H), 1.50 (s, 9H), 1.45-1.38 (m, 2H), 1.35-1.20 (m, 15H); ^{13}C NMR (100 MHz, $CDCl_3$): δ 174.1 (1C), 155.4 (1C), 153.3 (1C), 131.4 (1C), 120.6 (2C), 115.0 (2C), 80.4 (1C), 68.5 (1C), 60.3 (1C), 34.5 (1C), 29.7 (1C), 29.6 (2C), 29.5 (2C), 29.42 (1C), 29.38 (1C), 29.27 (1C), 28.5 (3C), 26.1 (1C), 25.1 (1C); HRMS (ESI) m/z: $[M + Na]^+$ calcd for $C_{25}H_{41}NO_5$, 458.2877; found, 458.2880.

***Synthesis of ethyl 12-(4-aminophenoxy)dodecanoate* (5x)**

Ethyl 12-(4-aminophenoxy)dodecanoate was synthesised following the same procedure as for **3x** and was isolated as a brown solid (98%).

***Characterisation data for ethyl 12-(4-aminophenoxy)dodecanoate* (5x)**

Brown solid; Yield: 0.639 g, 98%; mp = 42-45°C; ^{1}H NMR (400 MHz, $CDCl_3$): δ 6.74 (d, J = 8.8 Hz, 2H), 6.63 (d, J = 8.8 Hz, 2H), 4.12 (q, J = 7.2 Hz, 2H), 3.87 (t, J = 6.6 Hz, 2H), 3.40 (br s, 2H), 2.28 (t, J = 7.6 Hz, 2H), 1.73 (quint, J = 8 Hz, 2H), 1.65-1.55 (m, 2H), 1.42 (quint, J = 8 Hz, 2H), 1.36-1.22 (m, 15H); ^{13}C NMR (100 MHz, $CDCl_3$): δ 174.0 (1C), 152.4 (1C), 139.8 (1C), 116.4 (2C), 115.7 (2C), 68.7 (1C), 60.2 (1C), 34.4 (1C), 29.5 (1C), 29.5 (1C), 29.4 (2C), 29.4 (1C), 29.3 (1C), 29.1 (1C); HRMS (ESI) m/z: $[M + H]^+$ calcd for $C_{20}H_{33}NO_3$, 336.2533; found, 336.2529.

Synthesis of ethyl 12-[4-({[3-chloro-5-(trifluoromethyl)phenyl]carbamoyl}amino)phenoxy]dodecanoate (5a-Et)

N-[4-chloro-3-(trifluoromethyl)phenyl]-1H-imidazole-1-carboxamide (0.312 g, 1.1 mmol, 2 equiv.) dissolved in 3 ml anhydrous dichloromethane was added dropwise to a solution of ethyl 12-(4-aminophenoxy)dodecanoate (0.181 g, 0.5 mmol, 1 equiv.) in 3 mL anhydrous dichloromethane. Reaction mixture stirred at room temperature under argon for 24 hours. After this, 50 mL of brine was added and mixture was extracted twice with 50 mL ethyl acetate, then the combined organic extracts were then dried over magnesium sulfate and solvent was removed. The crude product was then purified by dry column vacuum chromatography using gradient elutions of dichloromethane / ethyl acetate (100:0 to 90:10) to give ethyl 12-[4-({[3-chloro-5-(trifluoromethyl)phenyl]-carbamoyl}amino)phenoxy]dodecanoate (0.277 g, 92%) as an off-white solid.

Characterisation data for ethyl 12-[4-({[3-chloro-5-(trifluoromethyl)phenyl]carbamoyl}amino-phenoxy]dodecanoate (5a-Et)

Off-white solid; Yield: 0.277 g, 92%; mp = 112-114°C; ^{1}H NMR (400 MHz, $CDCl_3$): δ 7.63 (s, 1H), 7.43 (s, 1H), 7.24-7.04 (m, 4H), 6.90-6.70 (m, 3H), 4.13 (q, J = 7.1 Hz, 2H), 3.91 (t, J = 6.4 Hz, 2H), 2.30 (t, J = 7.6 Hz, 2H), 1.76 (q, J = 7.8 Hz, 2H), 1.66-1.56 (m, 2H), 1.44 (q, J = 8 Hz, 2H), 1.38-

1.22 (m, 15H); ^{13}C NMR (100 MHz, $CDCl_3$): δ 174.5 (1C), 157.6 (1C), 153.6 (1C), 140.5 (1C), 135.5 (1C), 132.6 (q, J = 33 Hz, 1C), 129.2 (1C), 125.6 (1C), 123.3 (q, J = 271.2 Hz, 1C), 122.3 (2C), 119.9 (q, J = 4 Hz, 1C), 115.7 (2C), 114.2 (q, J = 3.8 Hz, 1C), 68.5 (1C), 60.5 (1C), 34.6 (1C), 29.6 (1C), 29.5 (2C), 29.4 (1C), 29.37 (1C), 29.31 (1C), 29.2 (1C), 26.0 (1C), 25.2 (1C), 14.4 (1C); HRMS (ESI) m/z: $[M + H]^+$ calcd for $C_{28}H_{36}ClF_3N_2O_4$, 557.2388; found, 557.2404.

Synthesis of 12-[4-({[3-chloro-5-(trifluoromethyl)phenyl]carbamoyl}amino)phenoxy] dodecanoic acid (5a)

Ethyl 12-[4-({[3-chloro-5-(trifluoromethyl)phenyl]carbamoyl}amino)phenoxy]dodecanoate (0.100 g, 0.2 mmol, 1 equiv.) in 36 mL 95% ethanol and heated to 40°C with stirring to dissolve. 12 mL 1.5 M sodium hydroxide was then added and reaction mixture was heated and stirred for 3 hours. After this, the solvent volume was reduced by 75% under vacuo and the resultant mixture was acidified with 1 M HCl to pH 1. The mixture was extracted three times with 30 mL ethyl acetate, which was then washed with brine, dried over sodium sulfate and solvent removed under vacuo to give 12-[4-({[3-chloro-5-(trifluoromethyl)phenyl]carbamoyl}amino)phenoxy]dodecanoic acid in quantitative yield as an off-white solid.

Characterisation data for 12-[4-({[3-Chloro-5-(trifluoromethyl)phenyl]carbamoyl}amino)phenoxy]dodecanoic acid (5a)

Off-white solid; Yield: 0.094 g, 99%; mp = 132-134°C; ^{1}H NMR (400 MHz, DMSO-d_6): δ 11.95 (br s, 1H), 9.16 (s, 1H), 8.72 (s, 1H), 7.81 (d, J = 7.1 Hz, 2H), 7.40-7.30 (m, 3H), 6.85 (d, J = 9 Hz, 2H), 3.90 (t, J = 6.6 Hz, 2H), 2.18 (t, J = 7.3 Hz, 2H), 1.68 (q, J = 7.5 Hz, 2H), 1.53-1.33 (m, 4H), 1.32-1.19 (m, 12H). ^{13}C NMR (100 MHz, DMSO-d_6): δ 174.6 (1C), 154.4 (1C), 152.5 (1C), 142.4 (1C), 134.2 (1C), 131.9 (1C), 131.1 (q, J = 32.6 Hz, 1C), 123.3 (q, J = 272.1 Hz, 1C), 121.0 (1C), 120.7 (2C), 117.5 (1C), 114.6 (2C), 112.9 (1C), 67.6 (1C), 33.7 (1C), 29.01 (1C), 28.96 (1C), 28.9 (1C),

28.81 (1C), 28.76 (2C), 28.6 (1C), 25.5 (1C), 24.5 (1C). HRMS (ESI) m/z: $[M + H]^+$ calcd for $C_{26}H_{32}ClF_3N_2O_4$, 529.2075; found, 529.2083.

Synthesis of ethyl 12-[3-({[3-chloro-5 (trifluoromethyl)phenyl]carbamoyl}amino)phenoxy] dodecanoate (4a-Et)

Ethyl 12-[3-({[3-chloro-5(trifluoromethyl)phenyl]carbamoyl}amino)phenoxy]dodecanoate was synthesised following the same procedure as for **5a-Et** and was isolated as an off-white solid (74%).

Characterisation data for Ethyl 12-[3-({[3-chloro-5 (trifluoromethyl)phenyl]carbamoyl} amino)phenoxy]dodecanoate (4a-Et)

Off-white solid; Yield: 0.123 g, 74%; mp = 85-87°C; ^{1}H NMR (400 MHz, $CDCl_3$): δ 7.73 (s, 1H), 7.58 (s, 1H), 7.44-7.38 (m, 2H), 7.21 (s, 1H), 7.15 (t, J = 8.2 Hz, 1H), 6.88 (t, J = 2.1 Hz, 1H), 6.84 (d, J = 7.9 Hz, 1H), 6.61 (dd, J = 8.2, 2.0 Hz, 1H), 4.15 (q, J = 7.2 Hz, 2H), 3.85 (t, J = 6.6 Hz, 2H), 2.32 (t, J = 7.6 Hz, 2H), 1.74-1.58 (m, 4H), 1.44-1.20 (m, 17H); ^{13}C NMR (100 MHz, $CDCl_3$): δ 175.1 (1C), 160.1 (1C), 153.2 (1C), 140.4 (1C), 138.6 (1C), 135.5 (1C), 132.6 (q, J = 33.3 Hz, 1C), 130.2 (1C), 123.3 (q, J = 273 Hz, 1C), 122.5 (1C), 119.9 (1C), 114.3 (1C), 113.3 (1C), 110.7 (1C), 107.9 (1C), 68.1 (1C), 60.7 (1C), 34.7 (1C), 29.41 (2C), 29.38 (2C), 29.3 (1C), 29.23 (2C), 29.18 (1C), 26.0 (1C), 25.2 (1C), 14.3 (1C); HRMS (ESI) m/z: $[M - H]^-$ calcd for $C_{28}H_{36}ClF_3N_2O_4$, 555.2240; found, 555.2244.

Synthesis of 12-[3-({[3-chloro-5-(trifluoromethyl)phenyl]carbamoyl}amino)phenoxy]dodecanoic acid (4a)

12-[3-({[3-chloro-5-(trifluoromethyl)phenyl]carbamoyl}amino)phenoxy]dodecanoic acid was synthesised following the same procedure as for **5a** and was isolated as a beige solid (96%).

Characterisation data for 12-[3-({[3-chloro-5-(trifluoromethyl)phenyl]carbamoyl}amino)phenoxy]dodecanoic acid (4a)

Beige solid; Yield: 0.071 g, 96%; mp = 110-112°C; ^{1}H NMR (400 MHz, DMSO-d_6): δ 11.95 (br s, 1H), 9.24 (s, 1H), 8.93 (s, 1H), 7.84-7.78 (m, 2H), 7.39 (s, 1H), 7.20-7.13 (m, 2H), 6.92 (d, J = 8 Hz, 1H), 6.56 (d, J = 8.3 Hz, 1H), 3.92 (t, J = 6.4 Hz, 2H), 2.17 (t, J = 7.2 Hz, 2H), 1.69 (q, J = 7.5 Hz, 2H), 1.52-1.35 (m, 4H), 1.34-1.20 (m, 12H); ^{13}C NMR (100 MHz, DMSO-d_6): δ 175.5 (1C), 160.1 (1C), 153.2 (1C), 143.1 (1C), 141.3 (1C), 135.2 (1C), 132.0 (q, J = 32.8 Hz, 1C), 130.5 (1C), 124.2 (q, J = 275 Hz, 1C), 122.1 (1C), 118.7 (1C), 114.0 (1C), 111.8 (1C), 109.4 (1C), 105.9 (1C), 68.3 (1C), 34.7 (1C), 30.0 (1C), 29.93 (1C), 29.88 (1C), 29.76 (1C), 29.73 (1C), 29.7 (1C), 29.5 (1C), 26.5 (1C), 25.5 (1C); HRMS (ESI) m/z: $[M - H]^-$ calcd for $C_{26}H_{32}ClF_3N_2O_4$, 527.1930; found, 527.1930.

Synthesis of ethyl 11-[3-({[3-chloro-5-(trifluoromethyl)phenyl]carbamoyl}amino)phenyl]-undecanoate (3a-Et)

Ethyl 11-[3-({[3-chloro-5- (trifluoromethyl)phenyl]carbamoyl}amino)phenyl]undecanoate was synthesised following the same procedure as for **5a-Et** and was isolated as an off-white solid (41%).

Characterisation data for ethyl 11-[3-({[3-chloro-5-(trifluoromethyl)phenyl]carbamoyl}amino)-phenyl]undecanoate (3a-Et)

Off-white solid; Yield: 0.108 g, 41%; mp = 92-93°C; ^{1}H NMR (400 MHz, $CDCl_3$): δ 7.65 (s, 1H), 7.57 (s, 1H), 7.44 (s, 1H), 7.24-7.14 (m, 4H), 7.06 (s, 1H), 6.93 (d, J = 7.2 Hz, 1H), 4.15 (q, J = 7.2 Hz, 2H), 2.53 (t, J = 7.8 Hz, 2H), 2.32 (t, J = 7.6 Hz, 2H), 1.66-1.50 (m, 4H), 1.34-1.18 (m, 15H); ^{13}C NMR (100 MHz, $CDCl_3$): δ 175.1 (1C), 153.1 (1C), 144.6 (1C), 140.6 (1C), 137.3 (1C), 135.5 (1C), 132.6 (q, J = 33 Hz, 1C), 129.4 (1C), 125.2 (1C), 123.2 (q, J = 273 Hz, 1C), 122.3 (1C), 121.6 (1C), 119.8 (q, J = 3.9 Hz, 1C), 118.9 (1C), 114.2 (q, J = 4.1 Hz, 1C), 60.7 (1C), 35.8 (1C), 34.7 (1C),

31.1 (1C), 29.2 (2C), 29.13 (1C), 29.12 (2C), 29.10 (1C), 28.9 (1C), 25.1 (1C); HRMS (ESI) m/z: [M + H]$^+$ calcd for $C_{27}H_{34}ClF_3N_2O_3$, 527.2283; found, 527.2306.

Synthesis of 11-[3-({[3-chloro-5-(trifluoromethyl)phenyl]carbamoyl}amino)phenyl]undecanoic acid (3a)

11-[3-({[3-chloro-5-(trifluoromethyl)phenyl]carbamoyl}amino)phenyl]undecanoic acid was synthesised following the same procedure as for **5a** and was isolated as a cream solid (99%).

Characterisation data for 11-[3-({[3-chloro-5-(trifluoromethyl)phenyl]carbamoyl}amino)phenyl]-undecanoic Acid (3a)

Cream solid; Yield: 0.074 g, 99%; mp = 124-126°C; ^{1}H NMR (400 MHz, DMSO-d_6): δ 11.94 (br s, 1H), 9.21 (s, 1H), 8.87 (s, 1H), 7.83 (s, 1H), 7.81 (s, 1H), 7.39 (s, 1H), 7.33 (s, 1H), 7.24 (d, J = 8.2 Hz, 1H), 7.18 (t, J = 7.9 Hz, 1H), 6.83 (d, J = 7.2 Hz, 1H), 2.56-2.48 (m, 2H), 2.17 (t, J = 7.4 Hz, 1H), 1.60-1.40 (m, 4H), 1.34-1.18 (m, 13H); ^{13}C NMR (100 MHz, DMSO-d_6): δ 174.5 (1C), 152.3 (1C), 143.0 (1C), 142.2 (1C), 139.0 (1C), 134.2 (1C), 131.1 (q, J = 32.6 Hz, 1C), 128.6 (1C), 123.3 (q, J = 272.7 Hz, 1C), 122.5 (1C), 121.1 (1C), 118.6 (1C), 117.7 (q, J = 4 Hz, 1C), 116.1 (1C), 113.0 (q, J = 4.2 Hz, 1C), 35.2 (1C), 33.7 (1C), 30.9 (1C), 29.0 (1C), 28.9 (1C), 28.8 (1C), 28.7 (1C), 28.6 (1C), 28.6 (1C), 24.5 (1C); HRMS (ESI) m/z: [M + H]$^+$ calcd for $C_{25}H_{30}ClF_3N_2O_3$, 499.1970; found, 499.1997.

Synthesis of ethyl 12-[4-({[4-chloro-3-(trifluoromethyl)phenyl]carbamoyl}amino)phenoxy]dodecanoate (5b-Et)

Ethyl 12-[4-({[4-chloro-3-(trifluoromethyl)phenyl]carbamoyl}amino)phenoxy]dodecanoate was synthesised following the same procedure as for **5a-Et** and was isolated as an off-white solid (78%).

Characterisation data for ethyl 12-[4-({[4-chloro-3-(trifluoromethyl)phenyl]carbamoyl}amino)-phenoxy]dodecanoate (5b-Et)

Off-white solid; Yield: 0.105 g, 78%; mp = 98-100°C; ^{1}H NMR (400 MHz, $CDCl_3$): δ 7.56 (s, 1H), 7.50 (d, J = 8.7 Hz, 1H), 7.32 (d, J = 8.7 Hz, 1H), 7.19-7.12 (m, 3H), 6.88-6.81 (m, 3H), 4.13 (q, J = 7.1 Hz, 2H), 3.90 (t, J = 6.5 Hz, 2H), 2.29 (t, J = 7.7 Hz, 2H), 1.75 (q, J = 7.8 Hz, 2H), 1.67-1.55 (m, 2H), 1.43 (q, J = 7.7 Hz, 2H), 1.38-1.22 (m, 15H); ^{13}C NMR (100 MHz, $CDCl_3$): δ 174.5 (1C), 157.4 (1C), 153.9 (1C), 137.6 (1C), 132.0 (2C), 129.4 (1C), 128.7 (q, J = 31.1 Hz, 1C), 125.8 (1C), 125.3 (1C), 123.6 (1C), 122.7 (q, J = 271.8 Hz, 1C), 123.6 (1C), 118.5 (q, J = 5.6 Hz, 1C), 115.5 (2C), 68.4 (1C), 60.5 (1C), 34.6 (1C), 29.6 (1C), 29.6 (1C), 29.5 (1C), 29.4 (2C), 29.3 (1C), 29.2 (1C), 26.0 (1C), 25.2 (1C); HRMS (ESI) m/z: $[M - H]^-$ calcd for $C_{28}H_{36}ClF_3N_2O_4$, 555.2243; found, 555.2248.

Synthesis of 12-[4-({[4-chloro-3-(trifluoromethyl)phenyl]carbamoyl}amino)phenoxy] dodecanoic acid (5b)

12-[4-({[4-Chloro-3-(trifluoromethyl)phenyl]carbamoyl}amino)phenoxy]dodecanoic acid was synthesised following the same procedure as for **5a** and was isolated as a brown solid (99%).

Characterisation data for 12-[4-({[4-Chloro-3-(trifluoromethyl)phenyl]carbamoyl}amino)-phenoxy]dodecanoic acid (5b)

Brown solid; Yield: 0.073 g, 99%; mp = 120-122°C; ^{1}H NMR (400 MHz, DMSO-d_6): δ 11.96 (bs, 1H), 9.09 (s, 1H), 8.63 (s, 1H), 8.09 (s, 1H), 7.65-7.55 (m, 2H), 7.33 (d, J = 9 Hz, 2H), 6.85 (d, J = 9 Hz, 2H), 3.90 (t, J = 6.5 Hz, 2H), 2.18 (t, J = 7.4 Hz, 2H), 1.67 (q, J = 7.8 Hz, 2H), 1.53-1.33 (m, 4H), 1.32-1.20 (m, 12H); ^{13}C NMR (100 MHz, DMSO-d_6): δ 174.5 (1C), 154.2 (1C), 152.6 (1C), 139.6 (1C), 132.0 (1C), 131.9 (1C), 126.7 (q, J = 30.2 Hz, 1C), 122.9 (1C), 122.8 (q, J = 273.1 Hz, 1C), 122.0 (1C), 120.5 (2C), 116.6 (q, J = 5.6 Hz, 1C), 114.6 (2C), 67.6 (1C), 33.7 (1C), 29.0 (1C),

28.95 (1C), 28.90 (1C), 28.8 (1C), 28.7 (2C), 28.6 (1C), 25.5 (1C), 24.5 (1C); HRMS (ESI) m/z: [M + H]$^+$ calcd for $C_{26}H_{32}ClF_3N_2O_4$, 529.2075; found, 529.2094.

Synthesis of ethyl 12-[3-({[4-chloro-3(trifluoromethyl)phenyl]carbamoyl}amino)phenoxy] dodecanoate (4b-Et)

Ethyl 12-[3-({[4-chloro-3(trifluoromethyl)phenyl]carbamoyl}amino)phenoxy]dodecanoate was synthesised following the same procedure as for **5a-Et** and was isolated as a cream solid (81%).

Characterisation data for Ethyl 12-[3-({[4-chloro-3(trifluoromethyl)phenyl]carbamoyl} amino)phenoxy]dodecanoate (4b-Et)

Cream solid; Yield: 0.135 g, 81%; mp = 97-99°C; ^{1}H NMR (400 MHz, $CDCl_3$): δ 7.57-7.50 (m, 3H), 7.32 (d, J = 8.6 Hz, 1H), 7.25 (s, 1H), 7.17 (t, J = 8.1 Hz, 1H), 6.89-6.82 (m, 2H), 6.62 (d, J = 8.3 Hz, 1H), 4.14 (q, J = 7.1 Hz, 2H), 3.87 (t, J = 6.5 Hz, 2H), 2.32 (t, J = 7.6 Hz, 2H), 1.76-1.56 (m, 4H), 1.46-1.36 (m, 2H), 1.35-1.23 (m, 15H); ^{13}C NMR (100 MHz, $CDCl_3$): δ 174.9 (1C), 160.1 (1C), 153.2 (1C), 138.7 (1C), 137.5 (1C), 132.0 (1C), 130.2 (1C), 128.8 (q, J = 31.6 Hz, 1C), 125.9 (1C), 123.6 (1C), 122.7 (q, J = 271.6 Hz, 1C), 118.6 (q, J = 5.6 Hz, 1C), 113.3 (1C), 110.6 (1C), 107.9 (1C), 68.1 (1C), 60.7 (1C), 34.7 (1C), 29.4 (1C), 29.38 (1C), 29.36 (1C), 29.3 (1C), 29.2 (1C), 29.2 (1C), 29.2 (1C), 26.0 (1C), 25.2 (1C), 14.3 (1C); HRMS (ESI) m/z: [M + H]$^+$ calcd for $C_{28}H_{36}ClF_3N_2O_4$, 557.2388; found, 557.2401.

Synthesis of 12-[3-({[4-Chloro-3-(trifluoromethyl)phenyl]carbamoyl}amino)phenoxy] dodecanoic acid (4b)

12-[3-({[4-Chloro-3-(trifluoromethyl)phenyl]carbamoyl}amino)phenoxy]dodecanoic

acid was synthesised following the same procedure as for **5a** and was isolated as a beige solid (95%).

Characterisation data for 12-[3-({[4-Chloro-3-(trifluoromethyl)phenyl]carbamoyl}amino)-phenoxy]dodecanoic acid (4b)

Beige solid; Yield: 0.070 g, 95%; mp = 116-118°C; ^{1}H NMR (400 MHz, DMSO-d_6): δ 11.95 (s, 1H), 9.16 (s, 1H), 8.83 (s, 1H), 8.09 (s, 1H), 7.65-7.57 (m, 2H), 7.19-7.13 (m, 2H), 6.91 (d, J = 8.1 Hz, 1H), 6.55 (d, J = 8.2 Hz, 1H), 3.91 (t, J = 6.6 Hz, 2H), 2.17 (t, J = 7.4 Hz, 2H), 1.69 (q, J = 7.7 Hz, 2H), 1.52-1.35 (m, 4H), 1.34-1.21 (m, 12H); ^{13}C NMR (100 MHz, DMSO-d_6): δ 174.5 (1C), 159.1 (1C), 152.3 (1C), 140.4 (1C), 139.4 (1C), 132.0 (1C), 129.5 (1C), quartet 126.7 (J = 30.5 Hz, 1C), 122.3 (1C), quartet 122.8 (J = 271.4 Hz, 1C), 122.3 (1C), quartet 116.7 (J = 5.8 Hz, 1C), 110.8 (1C), 108.2 (1C), 104.9 (1C), 67.3 (1C), 33.7 (1C), 29.0 (1C), 28.96 (1C), 28.91 (1C), 28.79 (1C), 28.76 (1C), 28.7 (1C), 28.6 (1C), 25.5 (1C), 24.5 (1C); HRMS (ESI) m/z: $[M + H]^+$ calcd for $C_{26}H_{32}ClF_3N_2O_4$, 529.2075; found, 529.2094.

Synthesis of ethyl 11-[3-({[4-chloro-3-(trifluoromethyl)phenyl]carbamoyl}amino)phenyl] undecanoate (3b-Et)

Ethyl 11-[3-({[4-chloro-3-(trifluoromethyl)phenyl]carbamoyl}amino)phenyl]undecanoate was synthesised following the same procedure as for **5a-Et** and was isolated as a beige solid (61%).

Characterisation data for Ethyl 11-[3-({[4-chloro-3-(trifluoromethyl)phenyl]carbamoyl}amino) phenyl]undecanoate (3b-Et)

Beige solid; Yield: 0.162 g, 61%; mp = 82-83°C; ^{1}H NMR (400 MHz, $CDCl_3$): δ 7.59-7.51 (m, 3H), 7.32 (d, J = 8.4 Hz, 1H), 7.24 (s, 1H), 7.19 (t, J = 7.6 Hz, 1H), 7.14 (d, J = 8.4 Hz, 1H), 7.05 (s, 1H), 6.91 (d, J = 7.4 Hz, 1H), 4.15 (q, J = 7.2 Hz, 2H), 2.51 (t, J = 7.8 Hz, 2H), 2.32 (t, J = 7.6 Hz, 2H), 1.66-1.50 (m, 4H), 1.34-1.18 (m, 15H); ^{13}C NMR (100 MHz, $CDCl_3$): δ 175.0 (1C), 153.4 (1C), 144.6 (1C), 137.6 (1C), 137.4 (1C), 132.0 (1C), 129.3 (1C), quartet 128.8 (J = 31.3 Hz, 1C), 125.8 (1C), 125.0 (1C), 123.5 (1C), quartet 122.7 (J = 271.8 Hz, 1C), 121.5 (1C), 118.8 (1C), quartet 118.4 (J =

5.6 Hz, 1C), 60.7 (1C), 35.8 (1C), 34.7 (1C), 31.1 (1C), 29.3 (1C), 29.2 (2C), 29.18 (1C), 29.15 (1C), 29.0 (1C), 25.1 (1C), 14.3 (1C); HRMS (ESI) m/z: $[M + H]^+$ calcd for $C_{27}H_{34}ClF_3N_2O_3$, 527.2283; found, 527.2288.

Synthesis of 11-[3-({[4-chloro-3-(trifluoromethyl)phenyl]carbamoyl}amino)phenyl] undecanoic acid (3b)

11-[3-({[4-Chloro-3-(trifluoromethyl)phenyl]carbamoyl}amino)phenyl]undecanoic acid was synthesised following the same procedure as for **5a** and was isolated as a beige solid (91%).

Characterisation data for 11-[3-({[4-Chloro-3-(trifluoromethyl)phenyl]carbamoyl}amino) phenyl]undecanoic acid (3b)

Beige solid; Yield: 0.068 g, 91%; mp = 101-103°C; ^{1}H NMR (400 MHz, DMSO-d_6): δ 11.95 (s, 1H), 9.14 (s, 1H), 8.77 (s, 1H), 8.10 (s, 1H), 7.65-7.55 (m, 2H), 7.31 (s, 1H), 7.23 (d, J = 8.2 Hz, 1H), 7.17 (t, J = 7.9 Hz, 1H), 6.82 (d, J = 7.4 Hz, 1H), 2.56-2.46 (m, 2H), 2.17 (t, J = 7.4 Hz, 2H), 1.60-1.41 (m, 4H), 1.32-1.18 (m, 12H); ^{13}C NMR (100 MHz, DMSO-d_6): δ 174.6 (1C), 152.4 (1C), 143.0 (1C), 139.4 (1C), 139.1 (1C), 132.0 (1C), 128.6 (1C), quartet 126.7 (J = 30.7 Hz, 1C), 123.0 (1C), quartet 122.9 (J = 271.4 Hz, 1C), 122.4 (1C), 122.2 (1C), 118.5 (1C), quartet 116.7 (J = 5.9 Hz, 1C), 116.0 (1C), 35.3 (1C), 33.7 (1C), 30.9 (1C), 29.0 (1C), 28.91 (1C), 28.86 (1C), 28.7 (1C), 28.7 (1C), 28.6 (1C), 24.5 (1C); HRMS (ESI) m/z: $[M + H]^+$ calcd for $C_{25}H_{30}ClF_3N_2O_3$, 499.1970; found, 499.1974.

S4.3 Absolute quantitative ^1H NMR purity determination of 3-5a and 3-5b

The purity of all test compounds was confirmed to be >95% by absolute quantitative NMR spectroscopy.[24] This technique determines purity by comparing the NMR signals of a given analyte against an internal calibrant (IC) of known purity. DMSO-d_6 was spiked with a known mass of the internal calibrant 1,3,5-trioxane (99.5% purity) to give a final IC concentration of approximately 1.5 mg/ml. Approximately 5 mg of each test compound was accurately weighed on a 5-decimal place analytical balance (0.01 mg accuracy). The sample was then dissolved in 600 µL of IC spiked DMSO-d_6 administered via mechanical pipette, then transferred to 5 mm NMR tubes. Collection and processing of NMR spectra, and calculation of purity, were performed according to the procedure described by the Journal of Medicinal Chemistry.[24] The final calculated purities are shown in Table S3. The purity of compound **5a** was above 100%, and is attributed to the ~1% error associated with manual sample preparation for qNMR experiments.[25]

Table S3. Purity of diphenyl ureas **3a-5b** as determined by qNMR

Compound	Purity (%)
3a	96.9
3b	99.1
4a	98.5
4b	98.1
5a	101.2
5b	99.7

S4.4 H^+/OH^- transport assay in vesicles

Vesicle Preparation

HPTS assays were conducted using POPC LUVs (200 nm diameter) vesicles loaded with an internal solution containing pH-sensitive fluorescent dye HPTS (1 mM), HEPES buffer (10 mM) and potassium gluconate (100 mM). An external solution of HEPES buffer (10 mM) and potassium gluconate (100 mM) was also prepared, and both solutions were buffered to pH 7.

Unilamellar vesicles were prepared following a procedure outlined previously by the Gale group.[26] A chloroform solution of POPC (37.5 mM, 4 mL) was transferred to a pre-weighed round-bottom flask, and the solvent was removed using a rotary evaporator. The pressure was lowered slowly to ensure the formation of a smooth lipid film. Subsequently, the film was dried in vacuo for 4−24 h, and the mass of lipid was recorded. The lipids were rehydrated with 4 mL of internal solution (this number should correspond to the volume of POPC solution used initially) and vortexed until all lipids were removed from the sides of the flask and were suspended in solution. The lipids were subjected to 9 cycles of freeze-thaw by freezing using a dry ice/acetone bath and thawing in lukewarm water. Following this, the vesicles were left to rest at room temperature for 30 min. The lipids were extruded through a 200 nm polycarbonate membrane 25 times to form monodisperse vesicles. Only 1 mL of solution was extruded at a time before being collected. Finally, any residual unencapsulated salt from the internal solution was using a B19 column packed with hydrated G-25 Sephadex®, which had been pre-saturated with the respective external solution. The lipid suspensions were diluted with the external solution to afford a stock solution (10 mL) of a known concentration.

HPTS Assay

For a given experiment, the prepared vesicles were diluted to a concentration of 0.1 mM in a 4.5 mL plastic cuvette. A pH gradient is required to drive transport through the vesicle membrane in these

experiments before the transporter is added. An aliquot of aqueous KOH solution (25 μL, 0.5 M) was added to increase the pH of the external solution by approx. one pH unit to pH 8.0. For experiments requiring the addition of Oleic Acid was added before KOH. Following this, valinomycin (5 μL of 25 μM DMSO solution, 0.05 mol%) was added to each cuvette. Transport was initiated with the addition of the transporter as a DMSO solution (5 μL) and ended with the addition of detergent (Triton X-100 (10% v/v in water), 25 μL) was added at t = 205 s to lyse the vesicles, and a final fluorescence intensity reading was recorded at t = 300 s to signify 100% proton efflux.

Dose-Response Hill Analysis

The changes in the fluorescent activity of intravesicular HPTS were used to detect pH changes during the experiments, and hence represent proton efflux. The acidic and basic forms of the HPTS probe were excited at λ_{ex} = 403 nm and λ_{ex} = 460 nm, respectively, and the fluorescence emission of both forms recorded at λ_{em} = 510 nm. The intensity ratio of basic form to acidic form was determined, and the fractional fluorescence intensity (IF) was calculated using the equation:

$$I_F = \frac{R_t - R_0}{R_d - R_0}$$

Where R_t is the ratiometric fluorescence value at a given time (t), R_0 is the ratiometric fluorescence value at t = 0 s and R_d is the fluorescence ratiometric value recorded at t = 280 s following the addition of detergent.

Dose-response experiments were performed at a minimum of five transporter concentrations plus a blank DMSO control run. The fractional fluorescence intensity (I_F) was plotted as a function of transporter concentration (mol%, with respect to lipid concentration). The I_F value at t = 200 s for each tested transporter concentration was fit to an adapted Hill Equation, using Origin 2021b (Academic), given as:

$$y = y_0 + (y_{max} - y_0)\frac{x^n}{k^n + x^n}$$

where y_0 is the I_F value at t = 200 s for the DMSO blank run, y_{max} is the maximum I_F value, n is the Hill coefficient, and k is a derived parameter.

A derived equation was used to calculate the EC_{50} value, the transporter concentration required to facilitate 50% chloride efflux, given as:

$$EC_{50} = k\left(\frac{0.5}{y_1 - y_0}\right)^{1/n}$$

where k and n are the derived parameters from the Hill equation, y_0 is the percentage chloride efflux at t = 0 s, and y_1 is the percentage chloride efflux at t = 280 s.

S4.5 **2a-5b** *HPTS Dose-Response Hill Analyses*

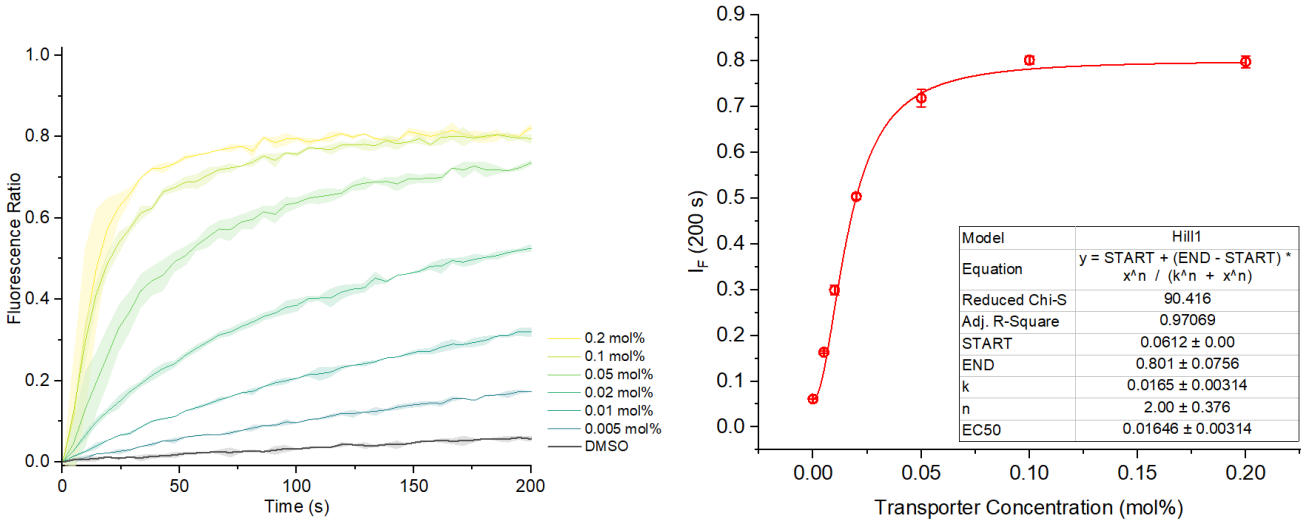

Figure S108. Hill plot analysis of H^+/OH^- transport facilitated by compound **2a** measured using the KGluc assay. KOH (5 mM) and valinomycin (0.05 mol%) were added to the vesicles before the addition of **2a** at 0 s. Detergent was added at 205 s to lyse the vesicles. Compound concentrations are shown as compound-to-lipid molar ratios. Error bars represent standard deviations from at least two repeats.

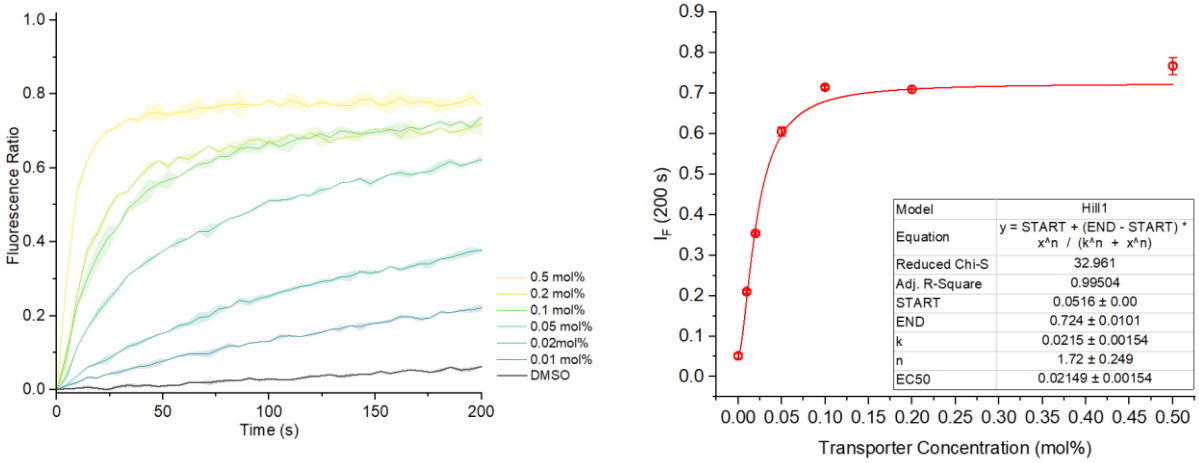

Figure S109. Hill plot analysis of H^+/OH^- transport facilitated by compound **2b** measured using the KGluc assay. KOH (5 mM) and valinomycin (0.05 mol%) were added to the vesicles before the

addition of **2b** at 0 s. Detergent was added at 205 s to lyse the vesicles. Compound concentrations are shown as compound-to-lipid molar ratios. Error bars represent standard deviations from at least two repeats.

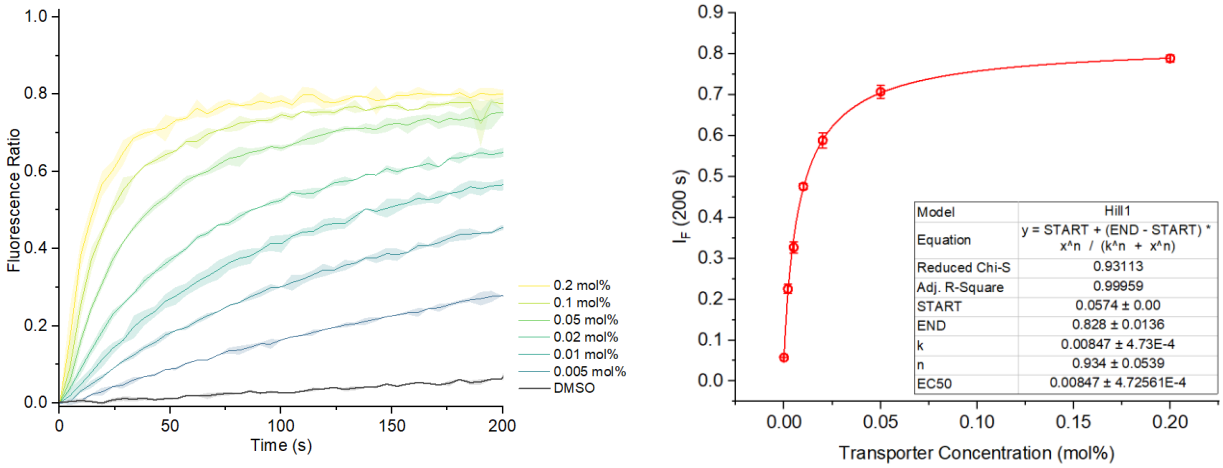

Figure S110. Hill plot analysis of H^+/OH^- transport facilitated by compound **3a** measured using the KGluc assay. KOH (5 mM) and valinomycin (0.05 mol%) were added to the vesicles before the addition of **3a** at 0 s. Detergent was added at 205 s to lyse the vesicles. Compound concentrations are shown as compound-to-lipid molar ratios. Error bars represent standard deviations from at least two repeats.

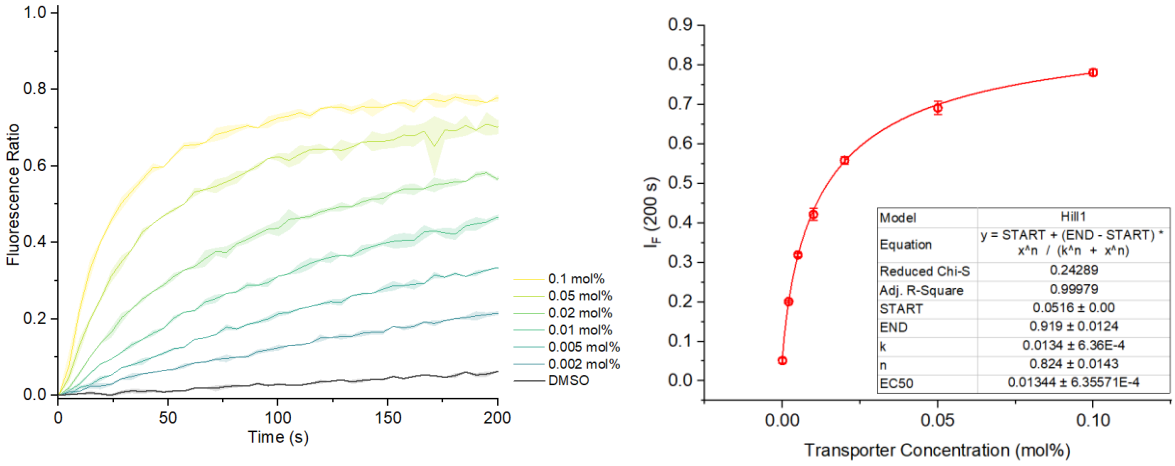

Figure S111. Hill plot analysis of H^+/OH^- transport facilitated by compound **3b** measured using the KGluc assay. KOH (5 mM) and valinomycin (0.05 mol%) were added to the vesicles before the addition of **3b** at 0 s. Detergent was added at 205 s to lyse the vesicles. Compound concentrations are shown as compound-to-lipid molar ratios. Error bars represent standard deviations from at least two repeats.

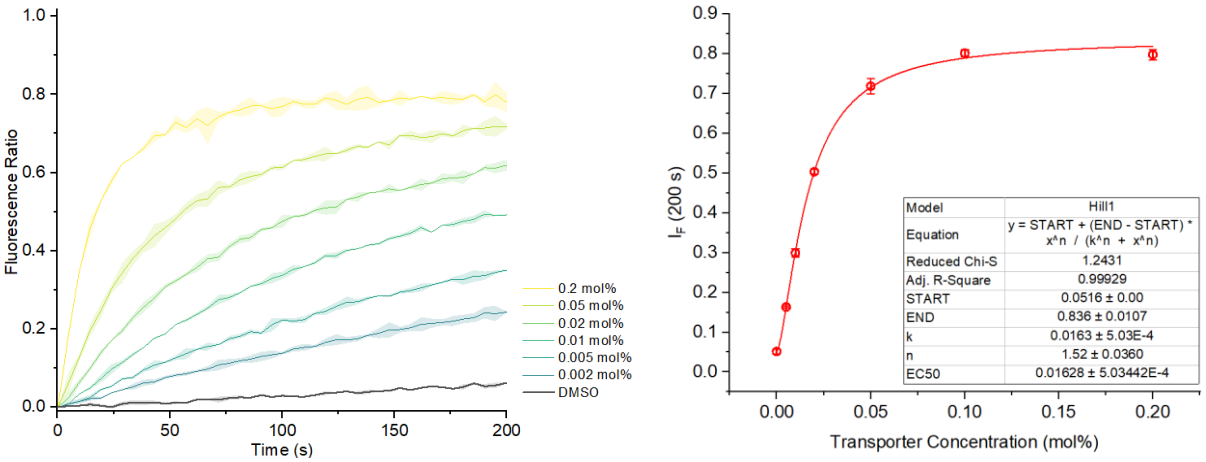

Figure S112. Hill plot analysis of H^+/OH^- transport facilitated by compound **4a** measured using the KGluc assay. KOH (5 mM) and valinomycin (0.05 mol%) were added to the vesicles before the

addition of **4a** at 0 s. Detergent was added at 205 s to lyse the vesicles. Compound concentrations are shown as compound-to-lipid molar ratios. Error bars represent standard deviations from at least two repeats.

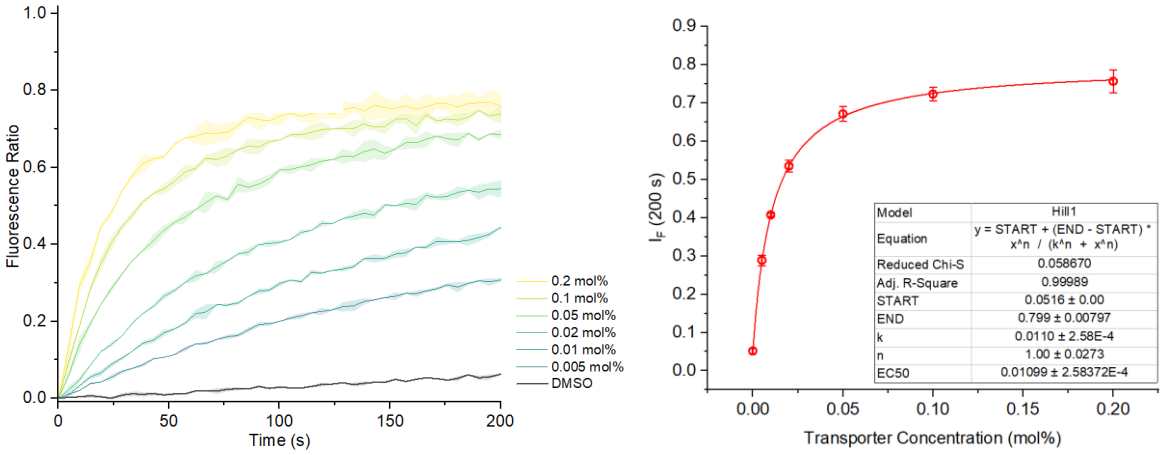

Figure S113. Hill plot analysis of H^+/OH^- transport facilitated by compound **4b** measured using the KGluc assay. KOH (5 mM) and valinomycin (0.05 mol%) were added to the vesicles before the addition of **4b** at 0 s. Detergent was added at 205 s to lyse the vesicles. Compound concentrations are shown as compound-to-lipid molar ratios. Error bars represent standard deviations from at least two repeats.

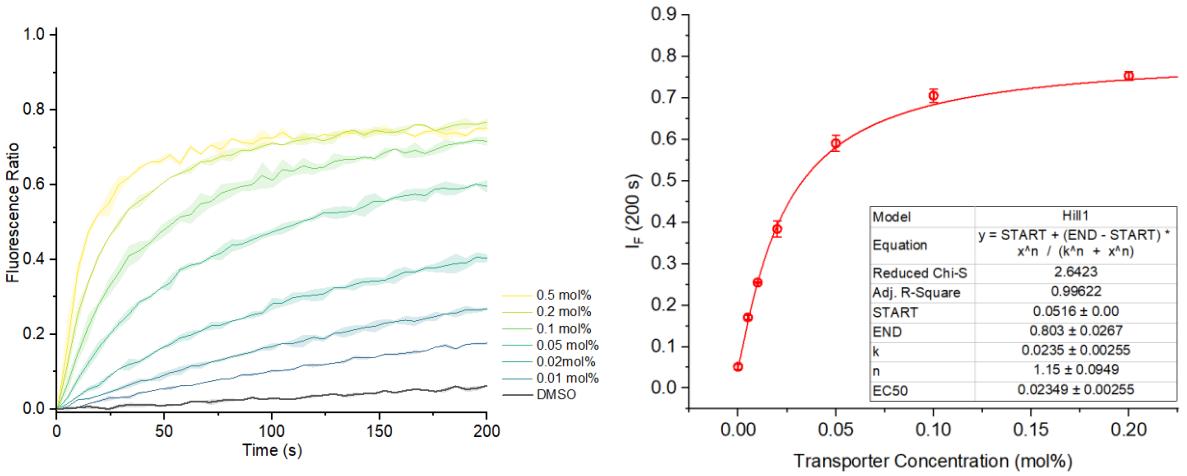

Figure S114. Hill plot analysis of H^+/OH^- transport facilitated by compound **5a** measured using the KGluc assay. KOH (5 mM) and valinomycin (0.05 mol%) were added to the vesicles before the addition of **5a** at 0 s. Detergent was added at 205 s to lyse the vesicles. Compound concentrations are shown as compound-to-lipid molar ratios. Error bars represent standard deviations from at least two repeats.

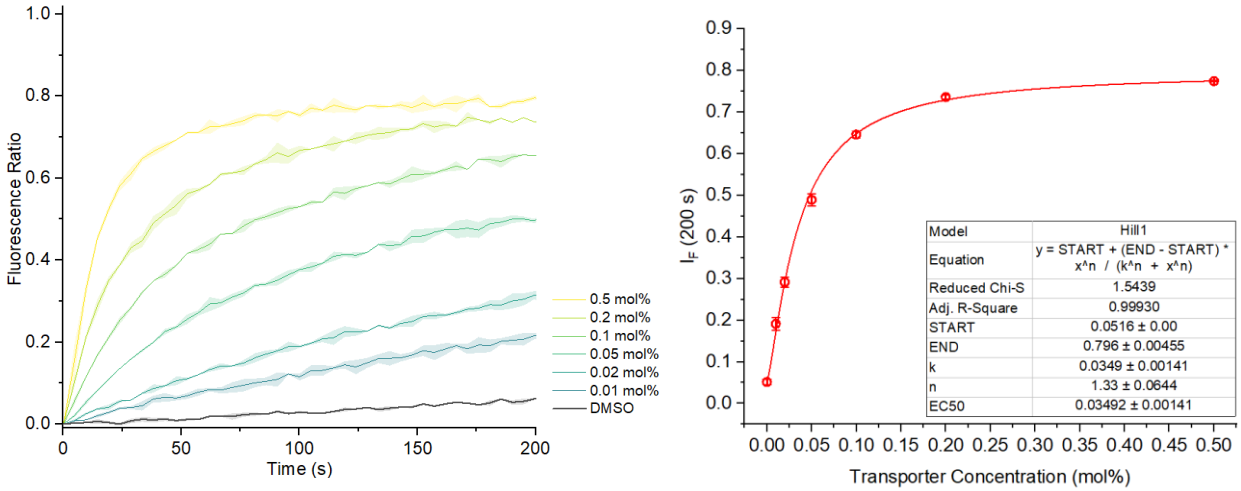

Figure S115. Hill plot analysis of H^+/OH^- transport facilitated by compound **5b** measured using the KGluc assay. KOH (5 mM) and valinomycin (0.05 mol%) were added to the vesicles before the

addition of **5b** at 0 s. Detergent was added at 205 s to lyse the vesicles. Compound concentrations are shown as compound-to-lipid molar ratios. Error bars represent standard deviations from at least two repeats.

S4.6 NMR Studies

Experimental Procedure - Acetate binding studies

^{1}H NMR titration of **2a-Me** and **2a-Et-5b-Et** with tetrabutylammonium acetate (TBAOAc) in DMSO-d_6 / 0.5% H_2O was performed on a Bruker 400 MHz spectrometer at 298 K, using 600 µL of 2.5 mM host solution of DMSO-d_6 / 0.5% H_2O. Stock solutions of TBAOAc (30-100 mM) used as the titrant contained 2.5 mM of the host to prevent host dilution throughout the titration.

[1]H NMR TBAOAc Titration Stack Plots

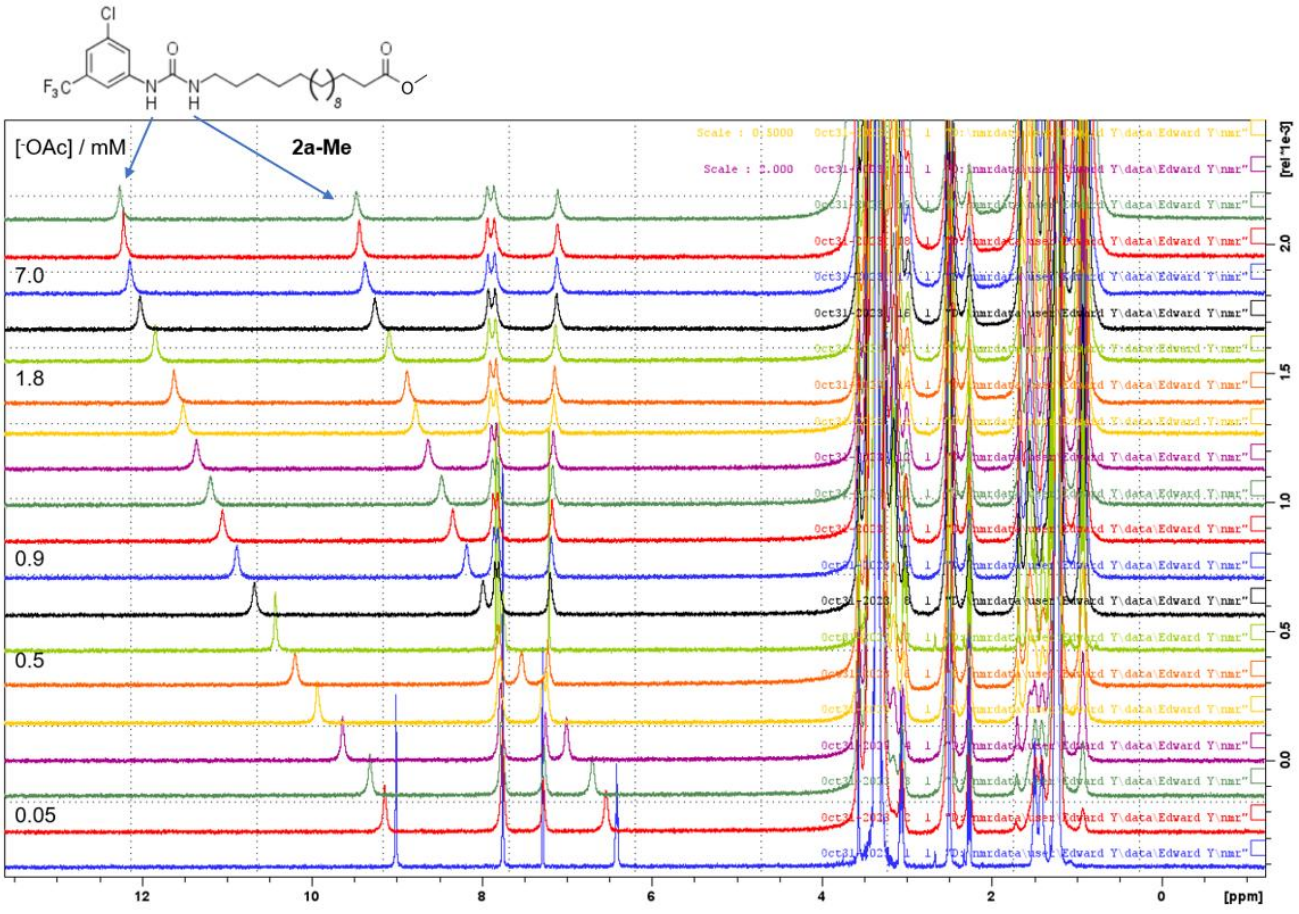

Figure S116. [1]H NMR (400 MHz) titration of **2a-Me** with TBAOAc in DMSO-d_6 / 0.5% H_2O at 298 K. The $^-$OAc binding constant was determined to be 1159 M^{-1} by fitting of the urea NH resonances (downfield shifted from 6.4 to 9.5 and 9 to 12.3 ppm with [$^-$OAc] from 0 to 21 mM / Mm Host. Full plot details published on http://app.supramolecular.org/bindfit/ and can be found using the following link: http://app.supramolecular.org/bindfit/view/d178c9da-37ee-43c7-89c1-15ae813d74d6.

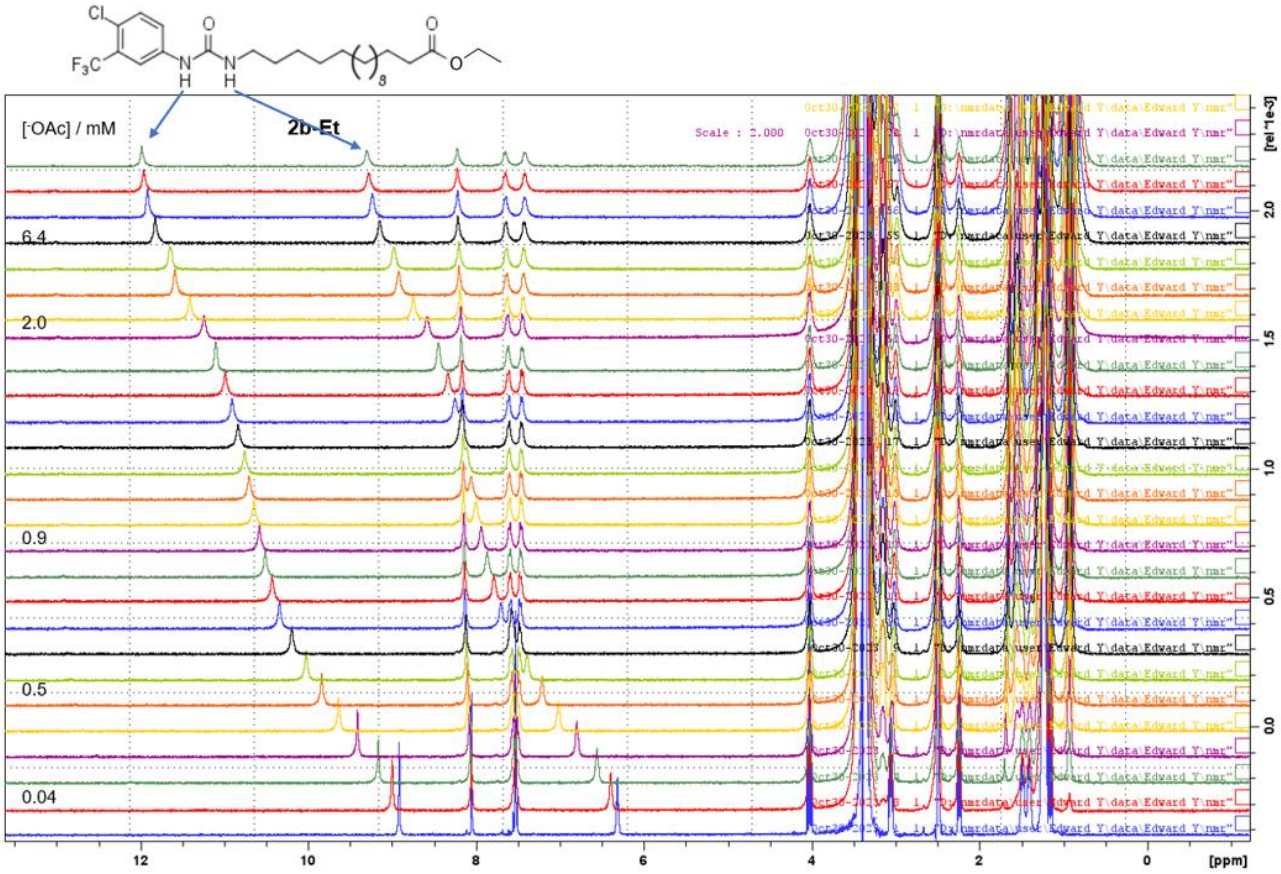

Figure S117. ^{1}H NMR (400 MHz) titration of **2b-Et** with TBAOAc in DMSO-d_6 / 0.5% H_2O at 298 K. The $^{-}$OAc binding constant was determined to be 548 M^{-1} by fitting of the urea NH resonances (downfield shifted from 6.3 to 9.3 and 8.9 to 12.0 ppm with [$^{-}$OAc] from 0 to 21 mM / Mm Host. Full plot details published on http://app.supramolecular.org/bindfit/ and can be found using the following link: http://app.supramolecular.org/bindfit/view/08da0a48-845c-4f13-8df9-04950f08112d.

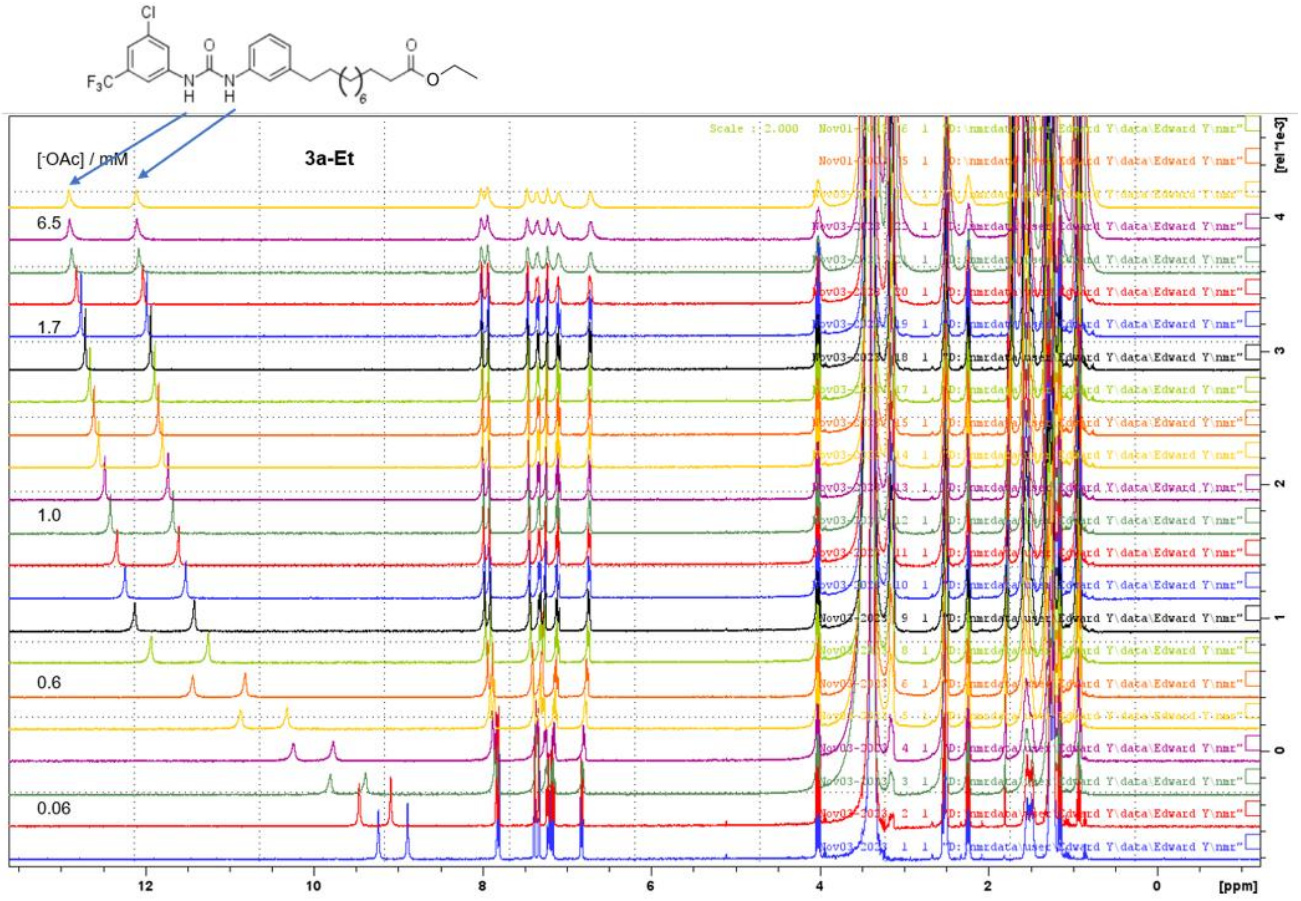

Figure S118. ^{1}H NMR (400 MHz) titration of **3a-Et** with TBAOAc in DMSO-d_6 / 0.5% H_2O at 298 K. The $^{-}$OAc binding constant was determined to be 7201 M^{-1} by fitting of the urea NH resonances (downfield shifted from 8.9 to 12.1 and 9.2 to 12.9 ppm with [$^{-}$OAc] from 0 to 8 mM / Mm Host. Full plot details published on http://app.supramolecular.org/bindfit/ and can be found using the following link: http://app.supramolecular.org/bindfit/view/a9031072-83f0-4122-b0b5-05677ba87d96.

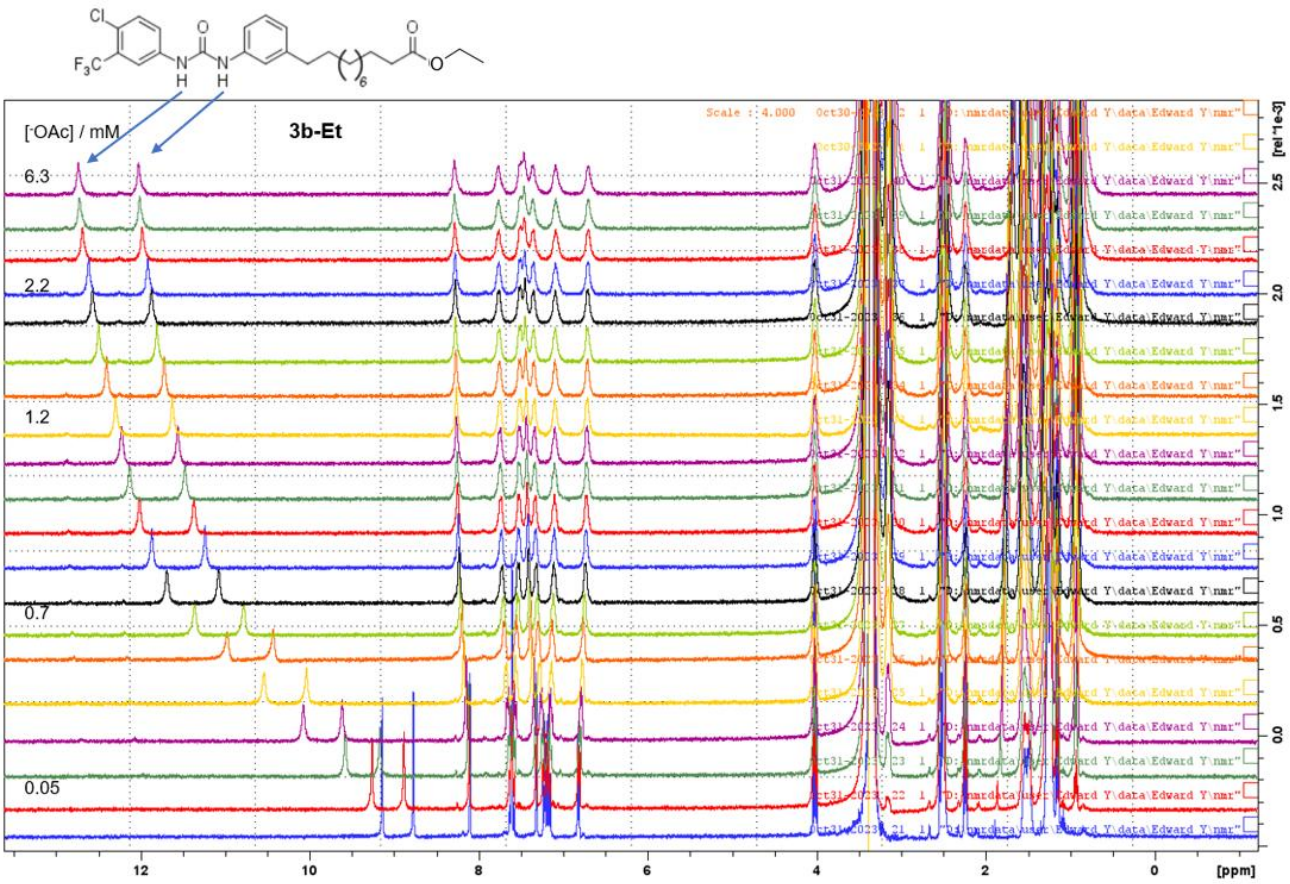

Figure S119. ^{1}H NMR (400 MHz) titration of **3b-Et** with TBAOAc in DMSO-d_6 / 0.5% H_2O at 298 K. The $^{-}$OAc binding constant was determined to be 6761 M^{-1} by fitting of the urea NH resonances (downfield shifted from 8.8 to 12.0 and 9.1 to 12.7 ppm with [$^{-}$OAc] from 0 to 6 mM / Mm Host. Full plot details published on http://app.supramolecular.org/bindfit/ and can be found using the following link: http://app.supramolecular.org/bindfit/view/111644a5-e48a-4fa1-b89b-d772d2a7c849.

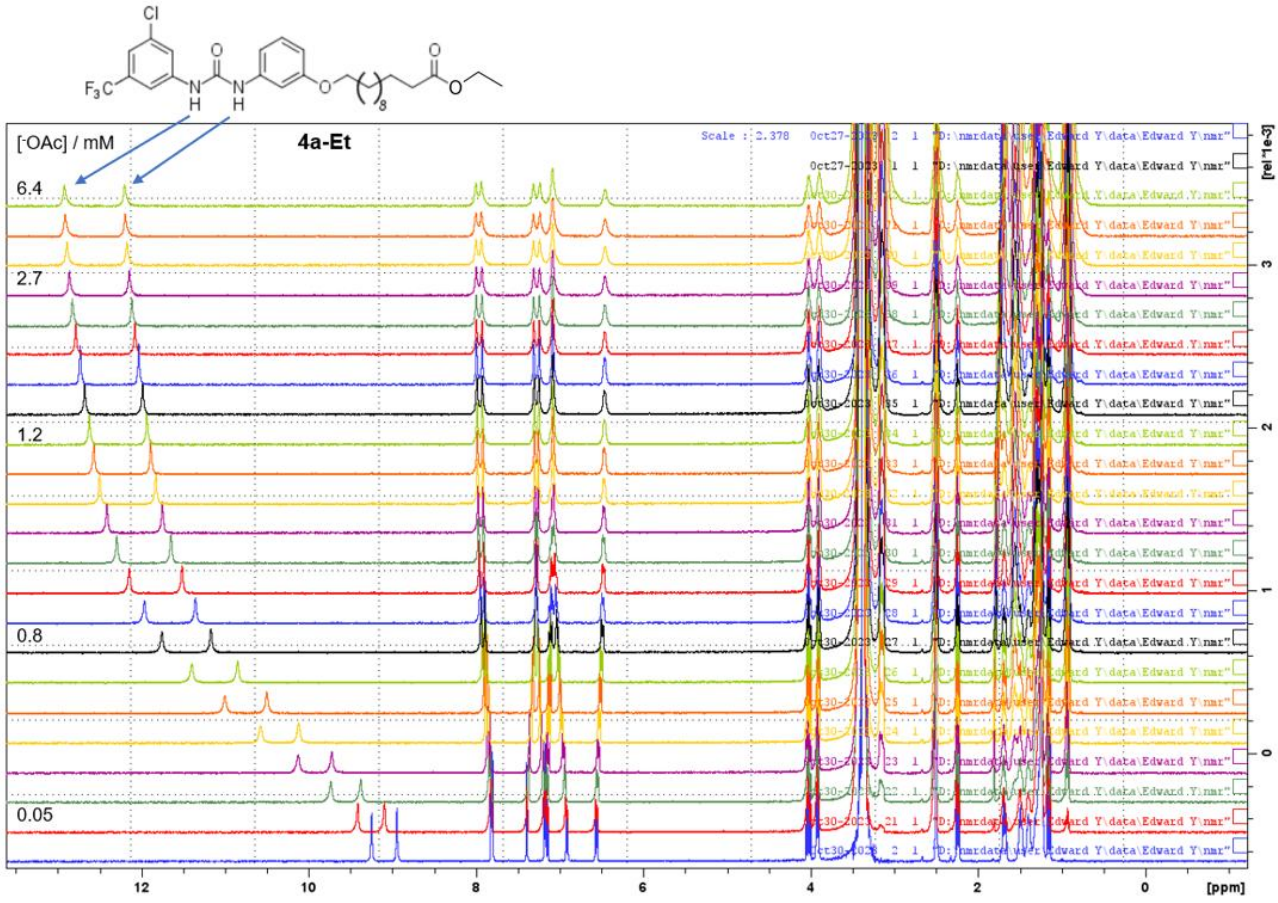

Figure S120. ^{1}H NMR (400 MHz) titration of **4a-Et** with TBAOAc in DMSO-d_6 / 0.5% H_2O at 298 K. The $^{-}$OAc binding constant was determined to be 7388 M^{-1} by fitting of the urea NH resonances (downfield shifted from 8.9 to 12.2 and 9.2 to 12.9 ppm with [$^{-}$OAc] from 0 to 6 mM / Mm Host. Full plot details published on http://app.supramolecular.org/bindfit/ and can be found using the following link: http://app.supramolecular.org/bindfit/view/47d8b6ae-82c0-458b-a03a-79cb2de2f78c.

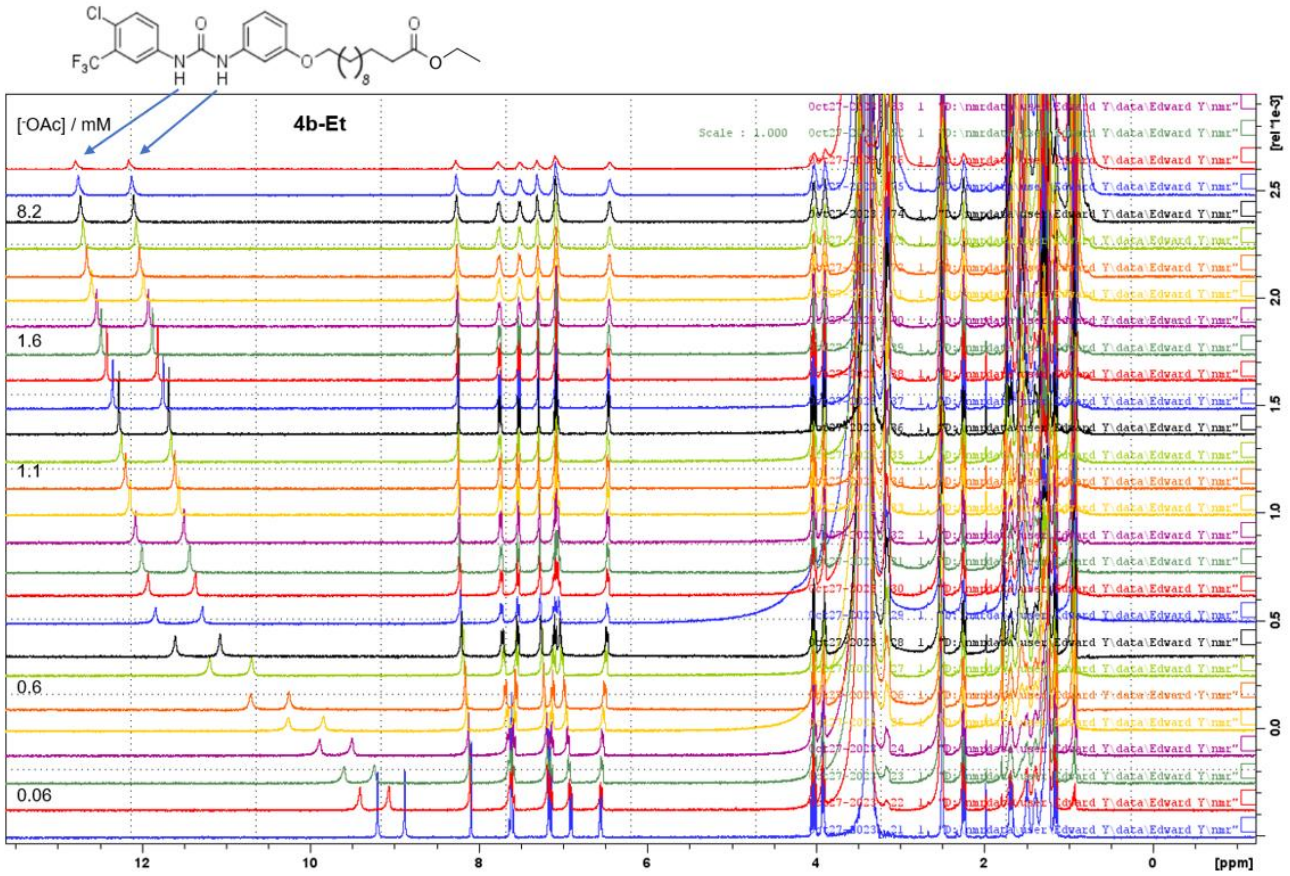

Figure S121. ^{1}H NMR (400 MHz) titration of **4b-Et** with TBAOAc in DMSO-d_6 / 0.5% H_2O at 298 K. The $^{-}$OAc binding constant was determined to be 6128 M^{-1} by fitting of the urea NH resonances (downfield shifted from 8.9.5 to 12.2 and 9.2 to 12.8 ppm with [$^{-}$OAc] from 0 to 37 mM / Mm Host. Full plot details published on http://app.supramolecular.org/bindfit/ and can be found using the following link: http://app.supramolecular.org/bindfit/view/6e5dde39-65a6-48ca-9642-995ee06e6fc3.

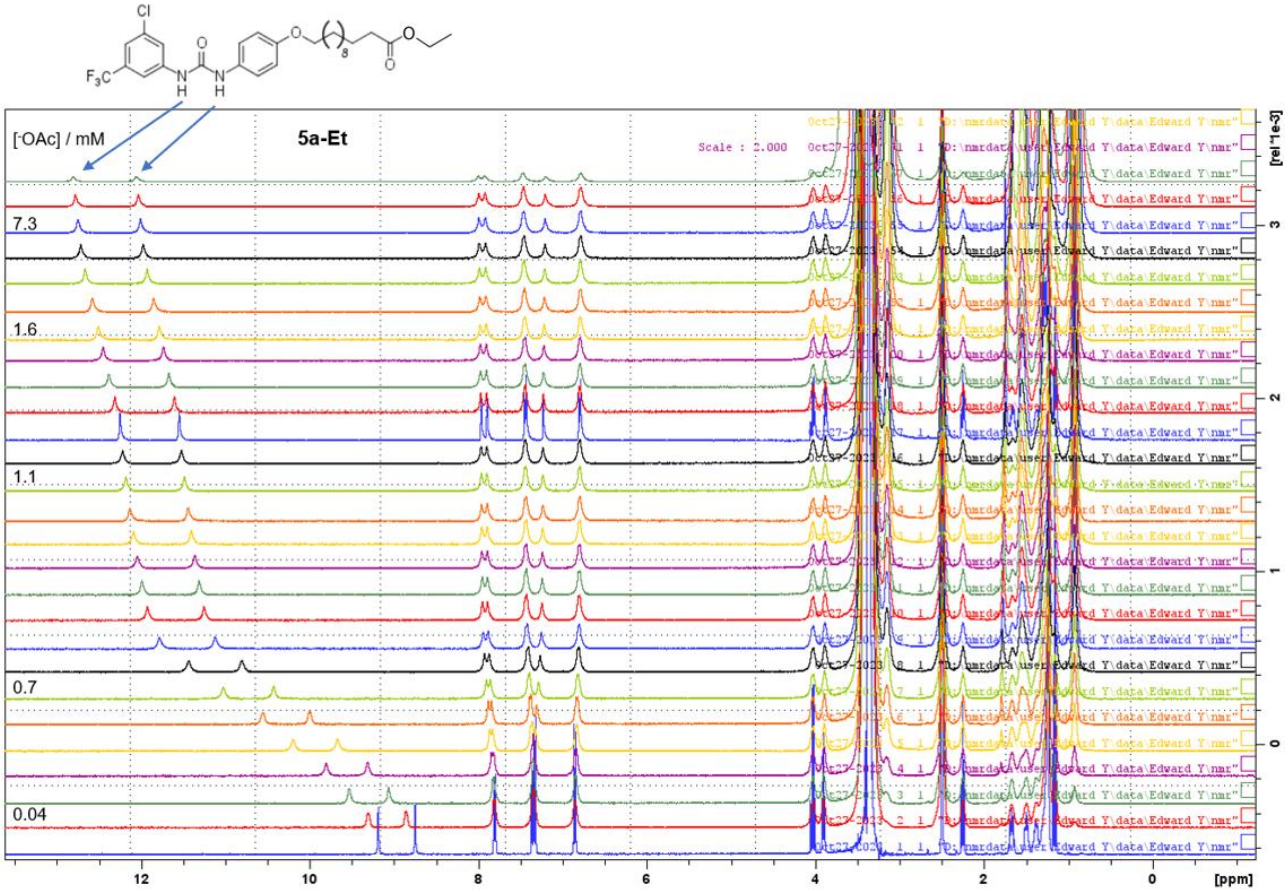

Figure S122. ^{1}H NMR (400 MHz) titration of **5a-Et** with TBAOAc in DMSO-d_6 / 0.5% H_2O at 298 K. The $^{-}$OAc binding constant was determined to be 5077 M^{-1} by fitting of the urea NH resonances (downfield shifted from 8.8 to 12.1 and 9.2 to 12.8 ppm with [$^{-}$OAc] from 0 to 35 mM / Mm Host. Full plot details published on http://app.supramolecular.org/bindfit/ and can be found using the following link: http://app.supramolecular.org/bindfit/view/bb2dead9-8dcb-42ad-a46f-d1b016d3e1c0.

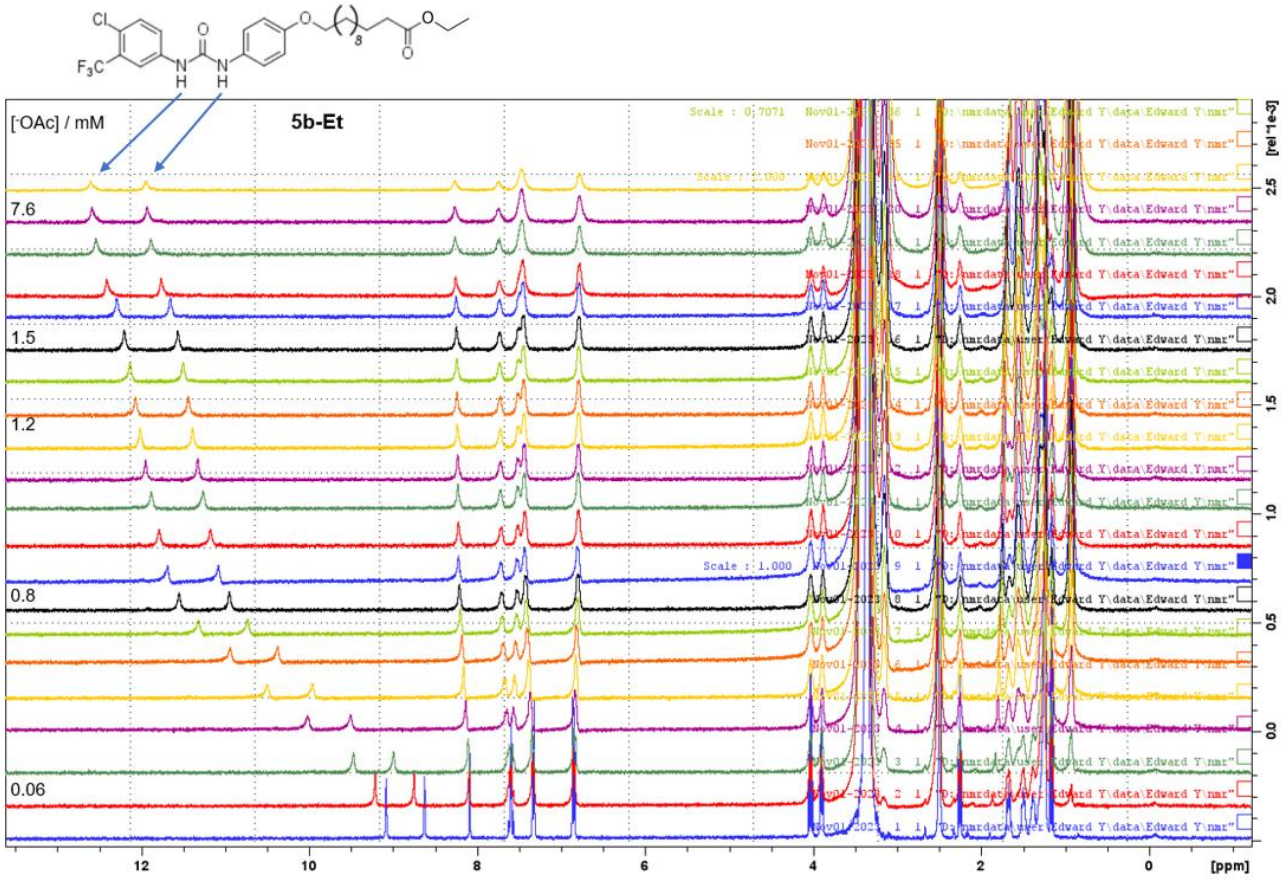

Figure S123. ^{1}H NMR (400 MHz) titration of **5b-Et** with TBAOAc in DMSO-d_6 / 0.5% H_2O at 298 K. The $^{-}$OAc binding constant was determined to be 5077 M^{-1} by fitting of the urea NH resonances (downfield shifted from 8.6 to 12.0 and 9.1 to 12.6 ppm with [$^{-}$OAc] from 0 to 10 mM / Mm Host. Full plot details published on http://app.supramolecular.org/bindfit/ and can be found using the following link: http://app.supramolecular.org/bindfit/view/2ff182e7-b447-4c72-9e15-45e8e6a2e2f8.

S4.7 2b-5b Low Fatty Acid Content POPC HPTS proton transport assay plots

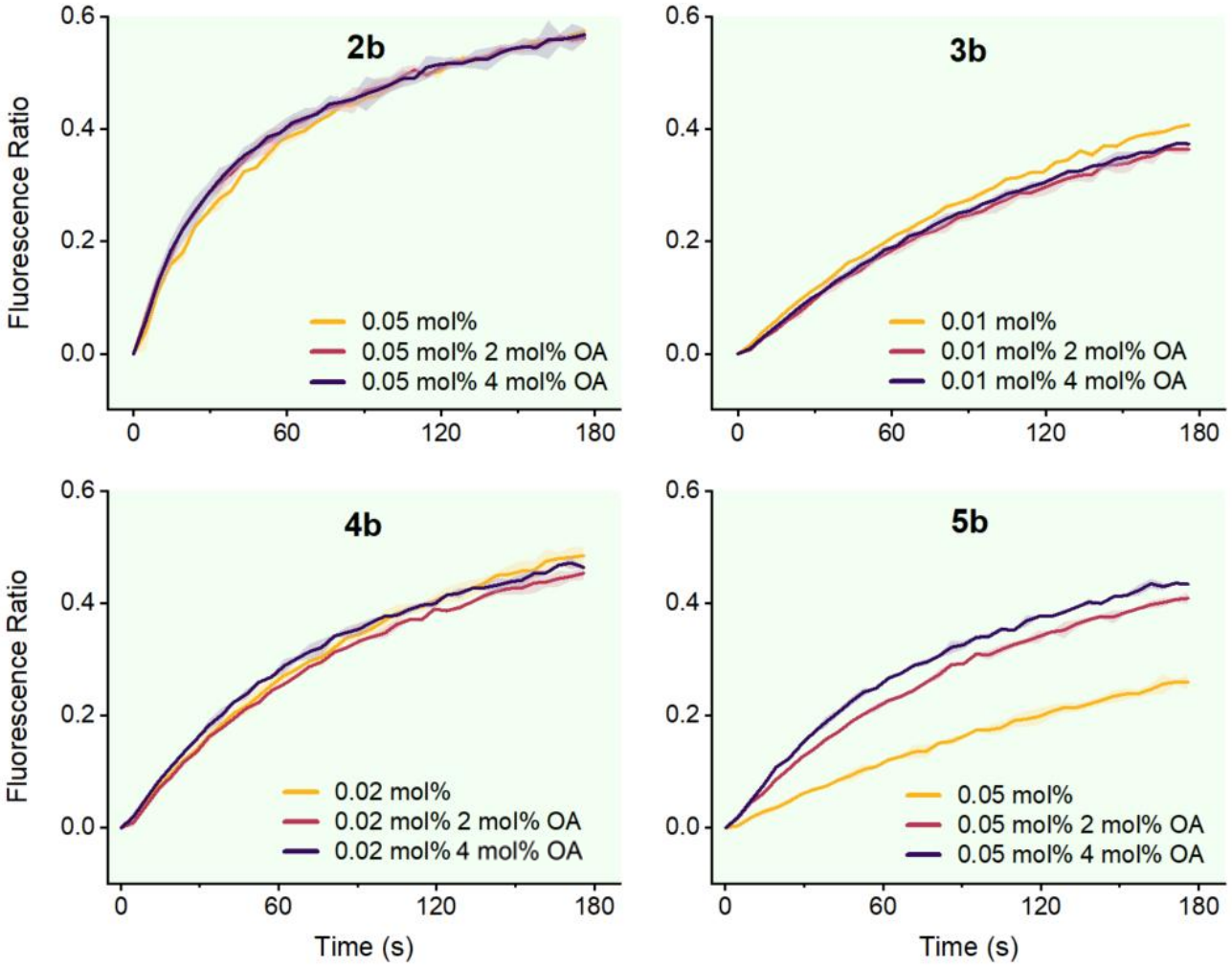

Figure S124. Proton transport induced by **2b**, **3b**, **4b** and **5b** in low fatty acid content POPC with and without OA (2 and 4 mol%) measured using vesicular HPTS proton transport assays.

S4.8 Binding Free Energy calculations for complexation of 2a-5a in n-pentadecane

We performed quantum chemical calculations using the ORCA 5.0.4 software package.[27] Reaction free energies were computed for the complexation of deprotonated **2a-5a** molecules as head-to-tail dimers (ΔE_{dimer}) and cyclic monomers (ΔE_A) using an n-pentadecane SMD continuum solvent model to mimic the low dielectric environment of the MIM. Free energies were calculated using at the M06-2X/6-31+G(d) level of theory, using the Boys-Bernadi counterpoise correction for basis set superposition error (BSSE).[28][29] The resulting free energies are presented in Table S4 and Figure S125.

Table S4. Reaction free energies of **2a-5a** and components of their calculation. Values are shown in Hartree (Eh) unless otherwise specified.

3) ↓ *In optimised geometry for structure 'AA'*

1) *Energy of* $E_{AA}^{AA}(AA)$ ← 4) *Using the basis set for structure 'AA'*

2) ↑ *Molecule 'A'*

Reaction free energies for dianionic dimer (A = deprotonated species)

$$\Delta E_{dimer} = E_{AA}^{AA}(AA) - 2E_{A}^{A}(A) - [2E_{A}^{AA}(AA) - 2E_{A}^{AA}(A)]$$

Compound	ΔE_{dimer} (kJ/mol)	ΔE_{dimer}	$E_{AA}^{AA}(AA)$	$E_{A}^{A}(A)$	$E_{A}^{AA}(AA)$	$E_{A}^{AA}(A)$
2a	−266.4	-0.1015	-4060.115	-2030.000	-2030.000	-2029.994
3a	−292.4	-0.1114	-4129.123	-2064.497	-2064.503	-2064.494
4a	−300.2	-0.1143	-4358.080	-2178.977	-2178.979	-2178.973
5a	−278.5	-0.1061	-4358.066	-2178.975	-2178.972	-2178.967

Reaction free energies for monoanionic dimer (B = protonated species)

$$\Delta E_{dimer}^{*} = E_{AB}^{AB}(AB) - E_{A}^{A}(A) - E_{B}^{B}(B) - [E_{A}^{AB}(AB) - E_{A}^{AB}(A) - E_{B}^{AB}(AB) - E_{B}^{AB}(B)]$$

Compound	ΔE_{dimer}^{*} (kJ/mol)	ΔE_{dimer}^{*}	$E_{AB}^{AB}(AB)$	$E_{A}^{A}(A)$	$E_{B}^{B}(B)$	$E_{A}^{AB}(AB)$	$E_{A}^{AB}(A)$	$E_{B}^{AB}(AB)$	$E_{B}^{AB}(B)$
2a	-192.0	-0.0731	-4060.611	-2030.000	-2030.528	-2030.005	-2029.997	-2030.523	-2030.521
3a	-227.7	-0.0867	-4129.615	-2064.497	-2065.026	-2064.501	-2064.496	-2065.021	-2065.022
4a	-208.9	-0.0796	-4358.575	-2178.977	-2179.512	-2178.981	-2178.975	-2179.507	-2179.507
5a	-216.5	-0.0824	-4358.576	-2178.975	-2179.509	-2178.979	-2178.971	-2179.501	-2179.500

Reaction free energies for cyclic monomer (C = cyclic monomer)

	$\Delta E_A = E_A^A(A) - E_A^C(C)$				$\Delta E_B = E_B^B(B) - E_B^C(C)$			
Compound	ΔE_A (kJ/mol)	ΔE_A	$E_A^A(A)$	$E_A^C(C)$	ΔE_B (kJ/mol)	ΔE_B	$E_B^B(B)$	$E_B^C(C)$
2a	−136.4	-0.0519	-2030.000	-2030.052	−17.3	-0.0066	-2030.528	-2030.534
3a	−176.1	-0.0671	-2064.497	-2064.564	−34.3	-0.0131	-2065.026	-2065.039
4a	−160.5	-0.0611	-2178.977	-2179.038	−12.9	-0.0049	-2179.512	-2179.517
5a	−141.9	-0.0541	-2178.975	-2179.029	−9.6	-0.0037	-2179.509	-2179.612

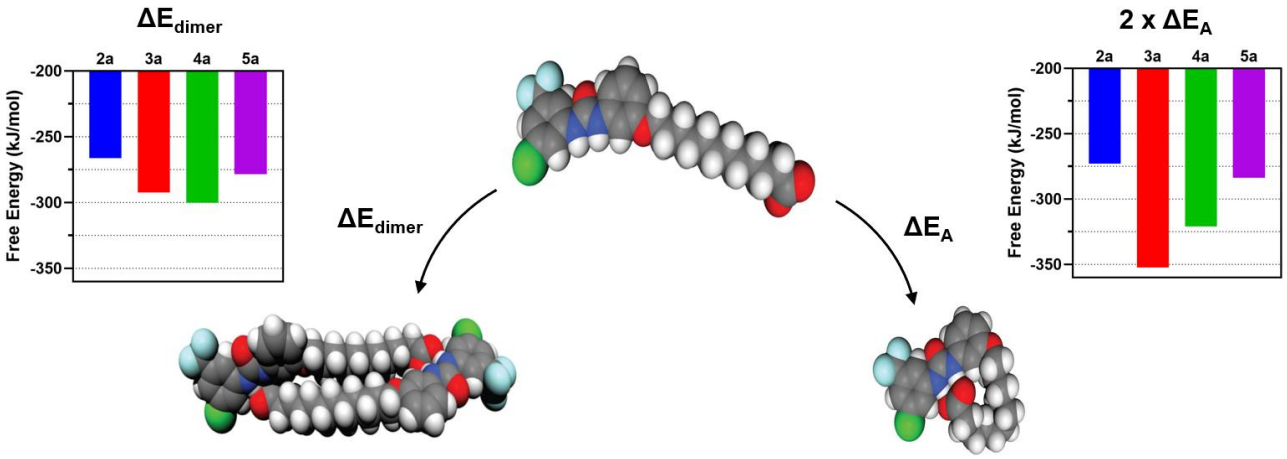

Figure S125. Optimised geometries of deprotonated **4a** molecules in n-pentadecane as linear, dimeric, and cyclic conformers used for single point energy calculations (at M06-2X/6-31+G(d) level of theory, using an SMD continuum solvent model and the Boys-Bernadi counterpoise correction for basis set superposition error (BSSE).

S4.9 Cell Culture and Assay Conditions

Cell Culture Conditions:

Human MDA-MB-231 breast cancer cells (ATCC) were cultured in Dulbecco's Modified Eagle Medium containing 1% (v/v) penicillin/streptomycin (Merck) and 10% (v/v) fetal bovine serum (Thermo Fisher Scientific), referred to as complete media. Cells were cultured at 37°C in a humidified atmosphere of 5% CO_2 and harvested at 80-90% confluency using trypsin/EDTA after washing with Dulbecco's phosphate-buffered saline (dPBS, Merck). Test compounds were administered to cells using a DMSO vehicle (final concentration 0.1% v/v and were compared against cells treated with DMSO alone (vehicle only control).

MTS Cell Viability Assay

Cell viability following 48-hour drug treatment was assayed by measuring the conversion of MTS (3-(4,5-dimethylthiazol-2-yl)-5-(3-carboxymethoxyphenyl)-2-(4-sulfophenyl)-2H-tetrazolium) to formazan by dehydrogenase enzymes in metabolically active cells. In a 96-well plate, MDA-MB-231 cells were seeded in triplicate in complete media at a density of 7.0×10^4 cells per well and incubated for 24 h. After serum starvation for 24 h, media was removed and replaced with serum-free DMEM containing various drug concentrations and incubated for 48 h. Cells were then incubated with CellTiter MTS 96 Aqueous MTS Reagent Powder (Promega) and phenazine ethosulfate (Merck) under dark conditions for approximately 3 h. The absorbance of each well at 490 nm was measured using a Tecan Infinite M1000 Pro plate reader to evaluate cell viability (CellTiter 96 Aqueous Non-Radioactive Cell Proliferation Assay, Promega).

JC-1 Mitochondrial Membrane Potential Assay

The ability of the test compounds to depolarise the inner mitochondrial membrane was

measured using the JC-1 assay. MDA-MB-231 cells were seeded in triplicate in black wall 96-well plates (1.0×10^4 cells per well) in complete media and incubated for 24 h. After serum starvation for 24 h, cells were treated with various drug concentrations in serum-free media and incubated for one hour. Cells were incubated with JC-1 in media for 20 min, washed with dPBS and read using a Tecan Infinite M1000 Pro plate reader to evaluate red (535 nm) and green (595 nm) fluorescence using excitation wavelengths of 485 and 535 nm, respectively (JC-1 Mitochondrial Membrane Potential Assay Kit; Cayman Chemical).

Intracellular ATP Assay

MDA-MB-231 cells were seeded in triplicate in 96-well plates (1.0×10^4 cells per well) in complete media and incubated for 24 h, followed by serum starvation for 24 h. At different timepoints, media were removed, and cells were treated with test compounds (5 μM) in serum-free media and incubated for the duration of the experiment. Cells were incubated with CellTiter-Glo 2.0 in complete media, mixed on an orbital shaker for 2 min, and left at room temperature under dark conditions for 10 min, and luminescence was read on a Tecan Infinite M1000 Pro plate reader (CellTiter-Glo 2.0 Luminescent Cell Viability Assay).

LDH Release Cell Viability Assay

MDA-MB-231 cells well seeded in triplicate in 96-well plates (1.0×10^4 cells per well) in complete media and incubated for 24 h. Following serum starvation for 24 h, well media was removed, and cells were treated with the test compounds (5 μM) or vehicle control in serum-free media and incubated for 6 h. Well media were homogenised gently, sampled, and diluted in LDH storage buffer and stored at −20 °C, including wells containing the vehicle control treated with 0.2% (v/v) Triton X-100 (Sigma-Aldrich) and incubated for 15 min prior to sampling to obtain a maximum LDH release value. Samples were thawed and incubated with LDH

detection reagent in a black-wall plate at room temperature for 1 h, and luminescence was measured on a Tecan infinite M1000 Pro plate reader (LDH-Glo Cytotoxicity Assay, Promega).

Seahorse XFe24 Analyser Assay

Mitochondrial function was measured by determining the oxygen consumption rate (OCR) and extracellular acidification rate (ECAR) of cells with a Seahorse XFe24 extracellular flux analyser (Seahorse Bioscience, North Billerica, MA, USA) according to the manufacturer's protocol. MDA-MB-231 cells were seeded in Seahorse XF24 well cell culture microplates (2.5×10^4 cells per well) in complete media, allowed to adhere for 3 h at room temperature, and incubated overnight. Following serum starvation for 24 h, wells were washed and media were replaced with 500 µL of XF media (1 mM pyruvate, 2 mM glutamine, and 10 mM glucose Seahorse XF DMEM, pH 7.4 with 5 mM HEPES) and placed in a non-CO_2 incubator (37 ◦C, humidified) for 1 h, and then the OCR was measured utilising an XF Cell Mito Stress Test kit (Seahorse Bioscience, MA, USA). Following sensor calibration and baseline measurements, Oligomycin (final concentration: 1 µM), test compounds (final concentration: 5 µM or 20 µM) or FCCP (final concentration: 1 µM), and rotenone/antimycin A (final concentrations: 0.5 µM each) were added to the sensor cartridge. Changes to oxygen consumption rate (OCR) was monitored using a modified cycling program on Agilent Seahorse Wave Desktop software.

Statistical Analysis

All IC_{50} concentration values are expressed as means ± SEM from three independent experiments (N = 3). Data were normalised to the DMSO vehicle control, and dose−response curves were constructed on GraphPad Prism 8 using log(inhibitor) versus response, variable slope (four parameters) nonlinear regressions. Equation: Y = Bottom + (Top − Bottom)/(1 + 100[(Log IC50-X) ∗ HillSlope)]. Intracellular ATP assay data are expressed as mean percentages of the time-matched DMSO control. (*) $P < 0.05$, (**) $P < 0.01$, (***) $P < 0.001$ versus time-matched

control by two-way analysis of variance with Dunnett's multiple comparison test. Absolute IC_{50} concentrations were then interpolated from these normalised curves, and the top constrained to 100%. Seahorse data were normalised to the baseline OCR prior to oligomycin addition.

S4.10 Representative JC-1 dose-response curves

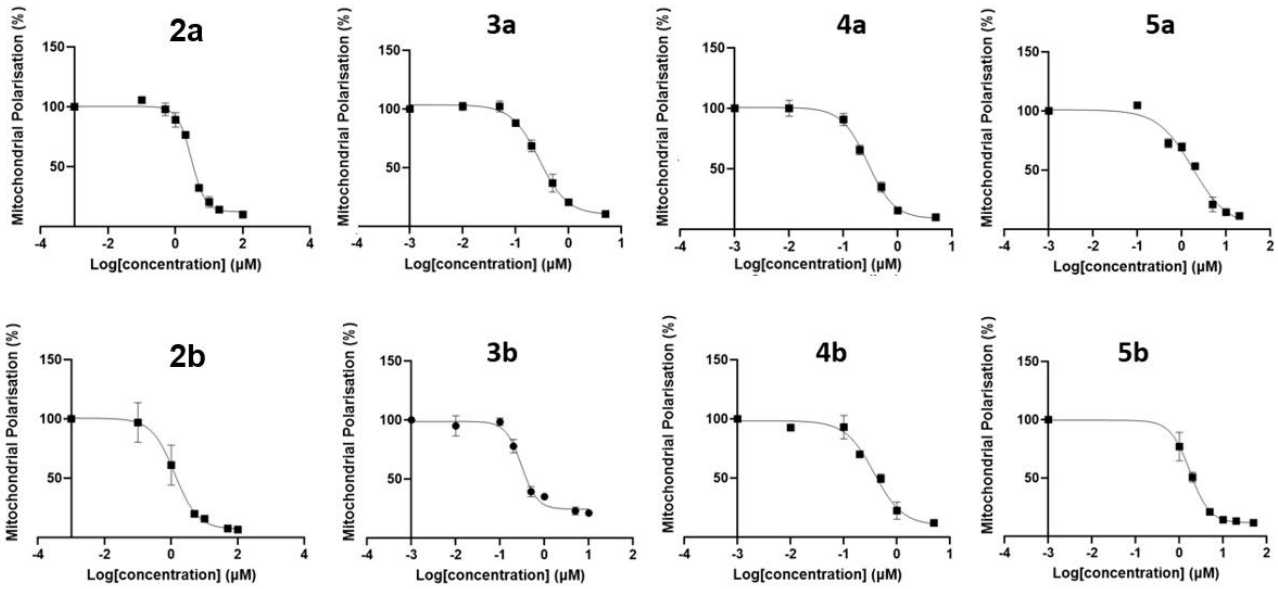

Figure S126. Representative dose-response curves showing the effects of **2a-5b** on the JC-1 red:green fluorescence ratio in MDA-MB-231 breast cancer cells after 1 h treatment with the test compound. Dose-response curves were constructed using log(inhibitor) vs response, variable slope (4 parameters) nonlinear regressions on GraphPad Prism 8. Absolute IC50 concentrations were interpolated from these normalised curves (data normalised to DMSO vehicle control) with the top constrained to 100%. Equation: Y=Bottom + (Top-Bottom)/(1+10^((LogIC50-X)*HillSlope)).

S4.11 Representative MTS dose-response curves

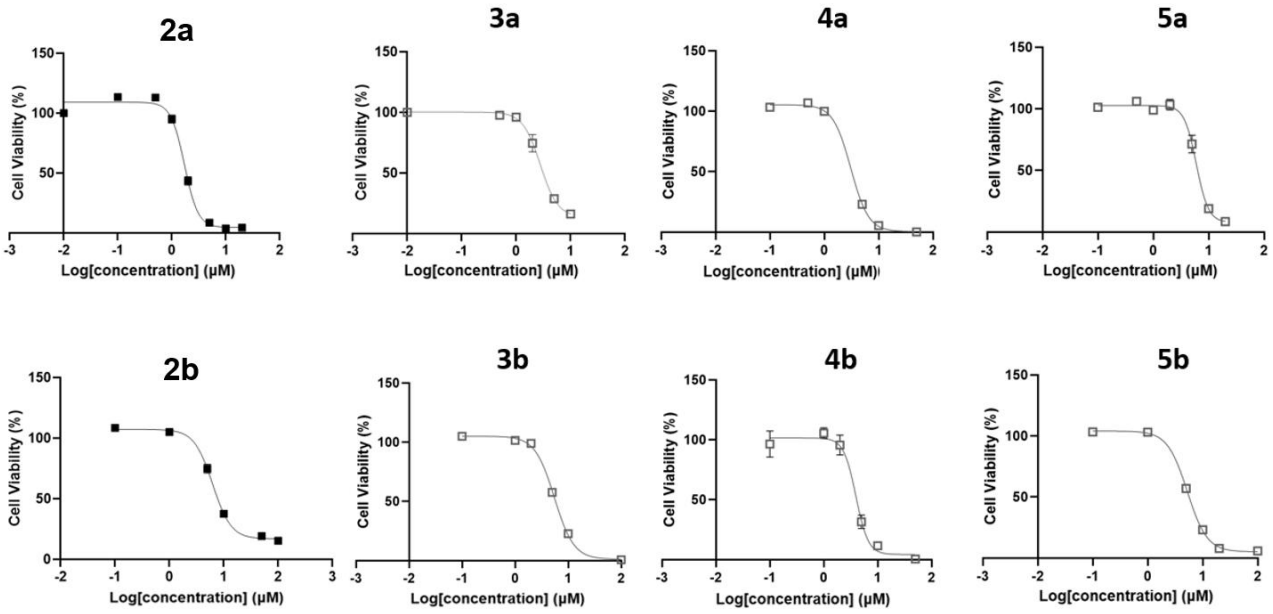

Figure S127. Representative Dose-response curves showing the antiproliferative effects of **2a-5b** in MDA-MB-231 cells in a 48 h MTS cell viability assay. Dose-response curves were constructed using log(inhibitor) vs response, variable slope (4 parameters) nonlinear regressions on GraphPad Prism 8. Absolute IC50 concentrations were interpolated from these normalised curves (data normalised to DMSO vehicle control) with the top constrained to 100%. Equation: Y=Bottom + (Top-Bottom)/(1+10^((LogIC50-X)*HillSlope)).

S4.12 HPTS, JC-1 and MTS Bivariate Analysis

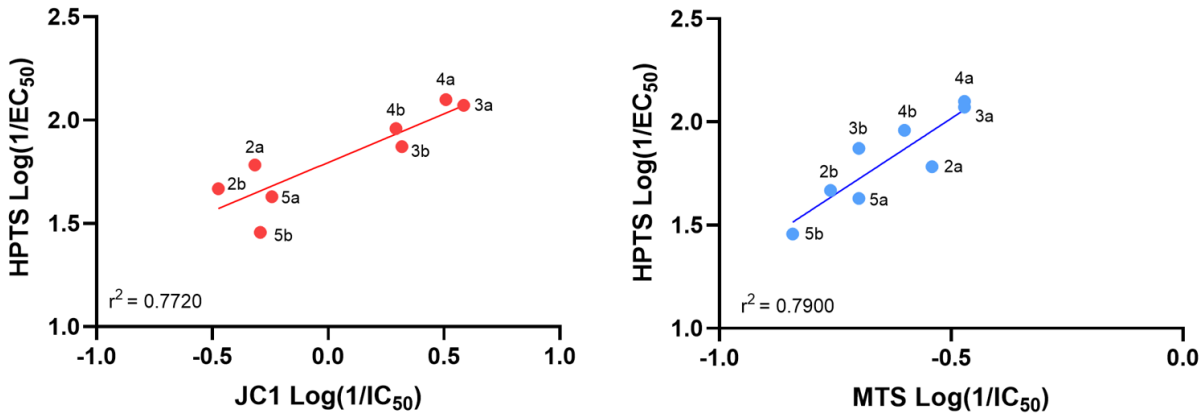

Figure S128. Correlation plot of HPTS Log(1/EC_{50}) against left: JC-1 Log(1/IC_{50}) and right: MTS (Log(1/IC_{50}) for **2a-5b**.

S4.13 LDH release data

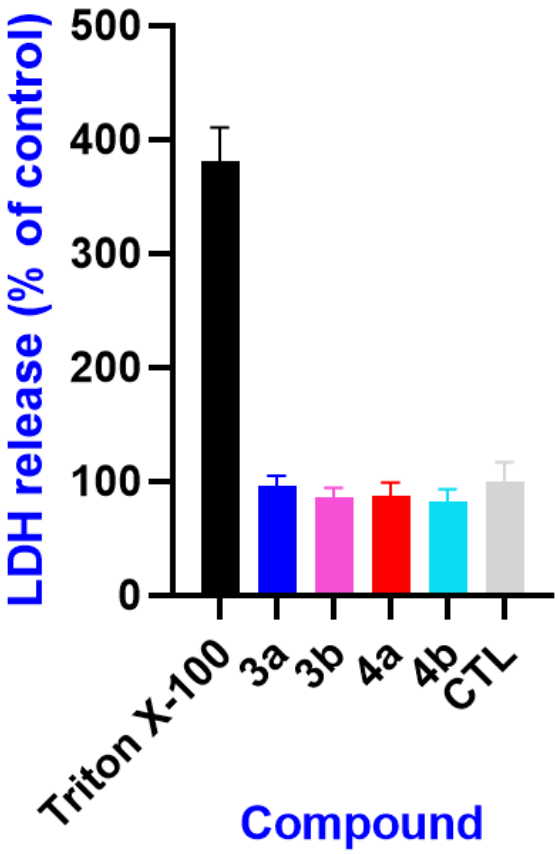

Figure S129. LDH release assay data displaying cytotoxicity of **3a-4b** vs DMSO vehicle control following 6 hours treatment. Maximum LDH release determined from a positive control consisting of cells treated with 0.2% Triton X-100 and incubated for 15 minutes prior to sample collection.

S4.14 Diphenyl Urea intermediate and product ^{1}H NMR and ^{13}C NMR Spectra

3-nitrobenzaldehyde dioxolane acetal (7)

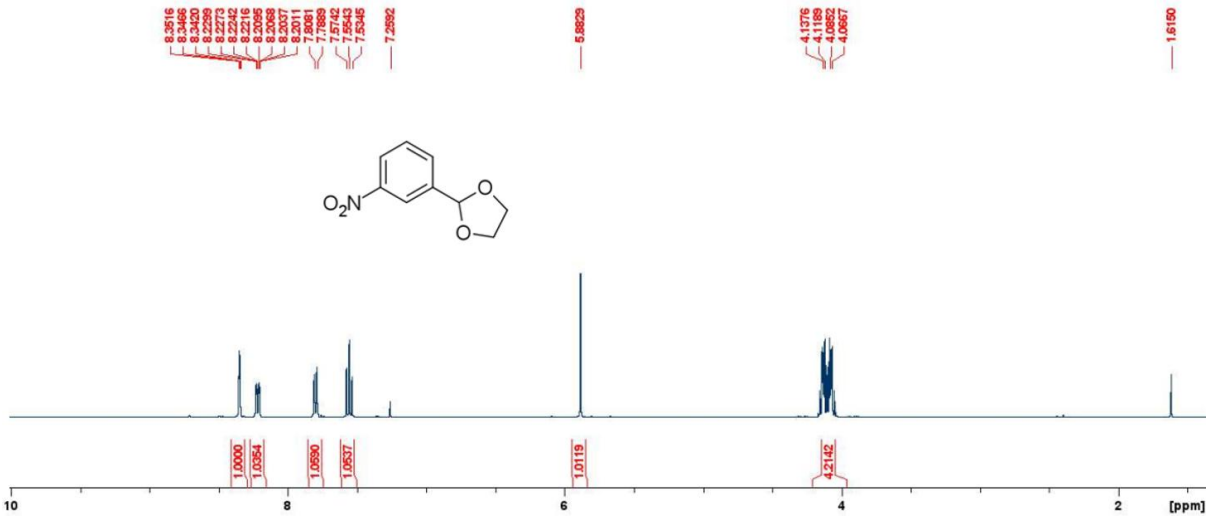

Figure S130. 400 MHz ^{1}H NMR spectrum of **7**

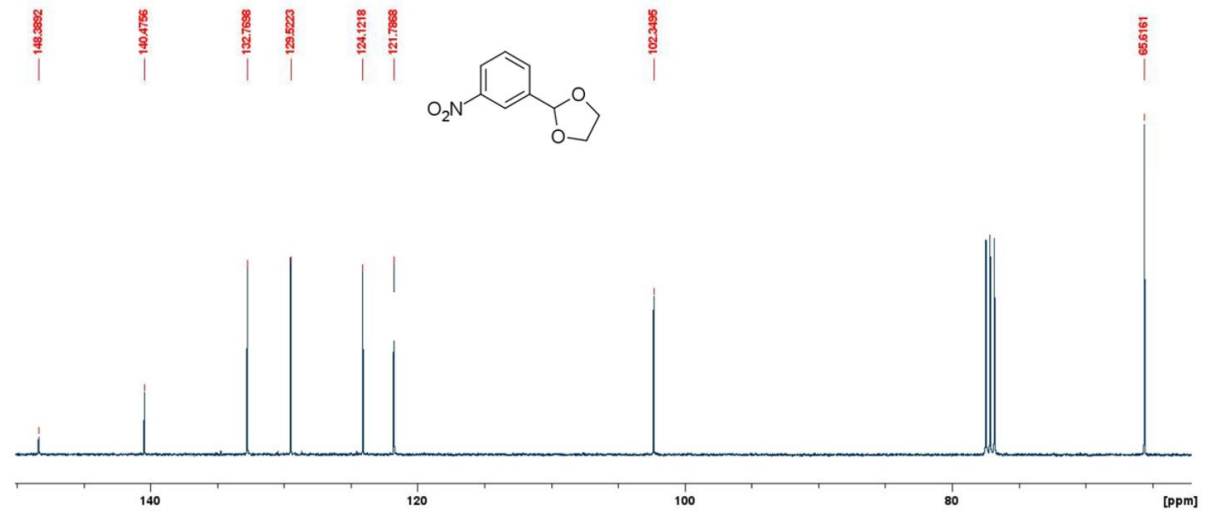

Figure S131. 100 MHz ^{13}C NMR spectrum of **7**

3-aminobenzaldehyde dioxolane acetal (8)

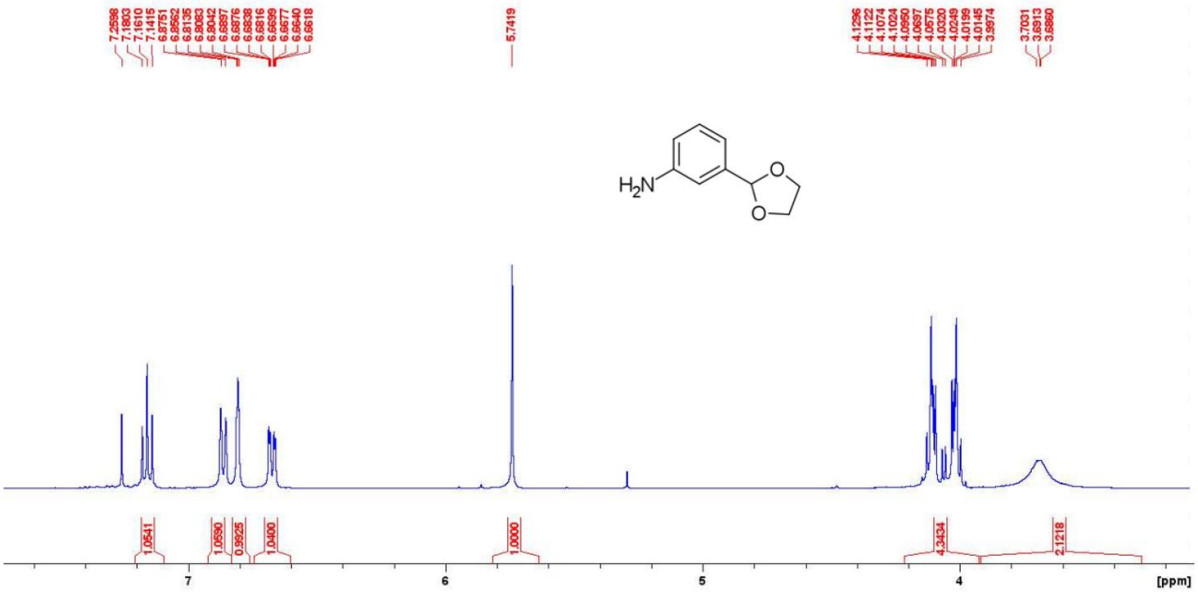

Figure S132. 400 MHz ^{1}H NMR spectrum of **8**

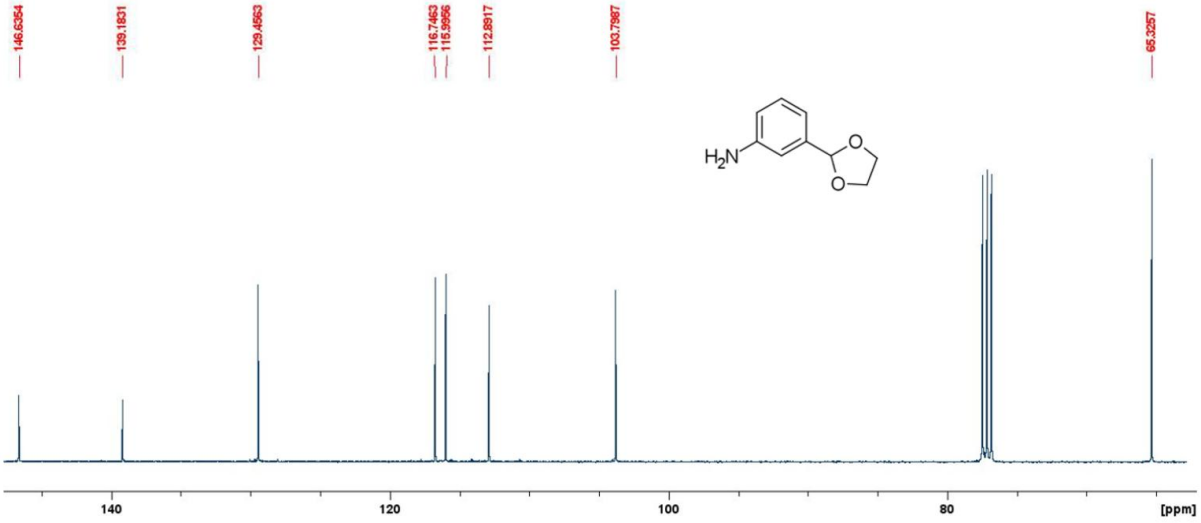

Figure S133. 100 MHz ^{13}C NMR spectrum of **8**

Boc-3-aminobenaldehyde dioxolane acetal (9)

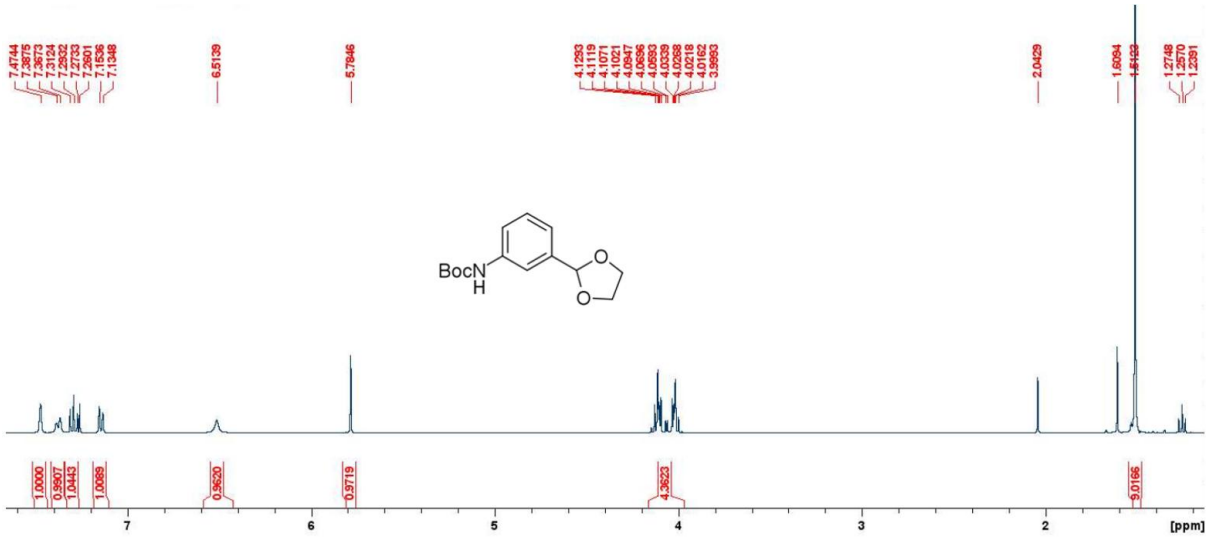

Figure S134. 400 MHz ^{1}H NMR spectrum of **9**

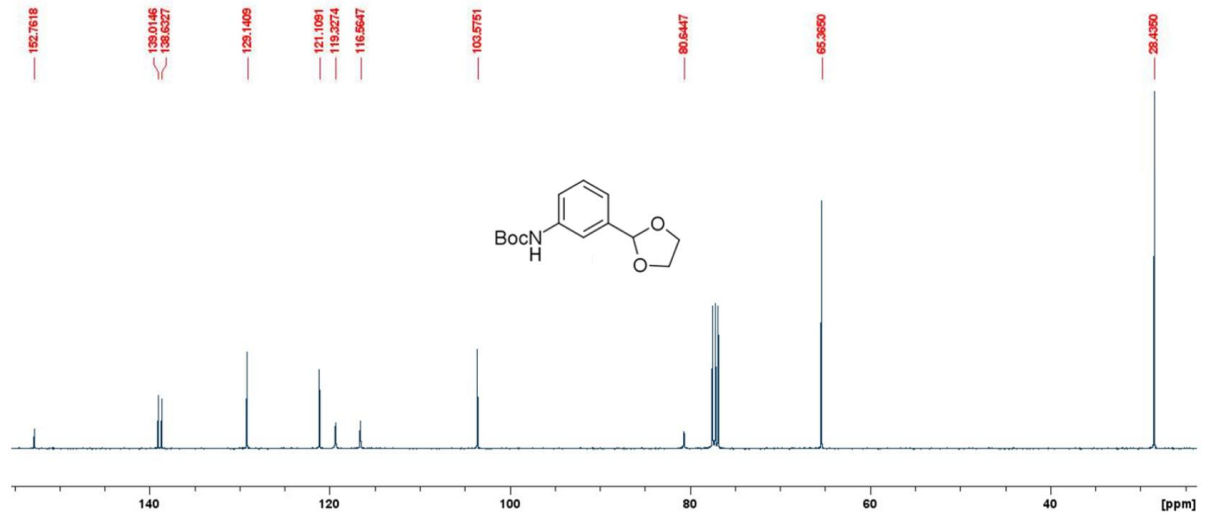

Figure S135. 100 MHz ^{13}C NMR spectrum of **9**

Boc-3-aminobenzaldehyde (10)

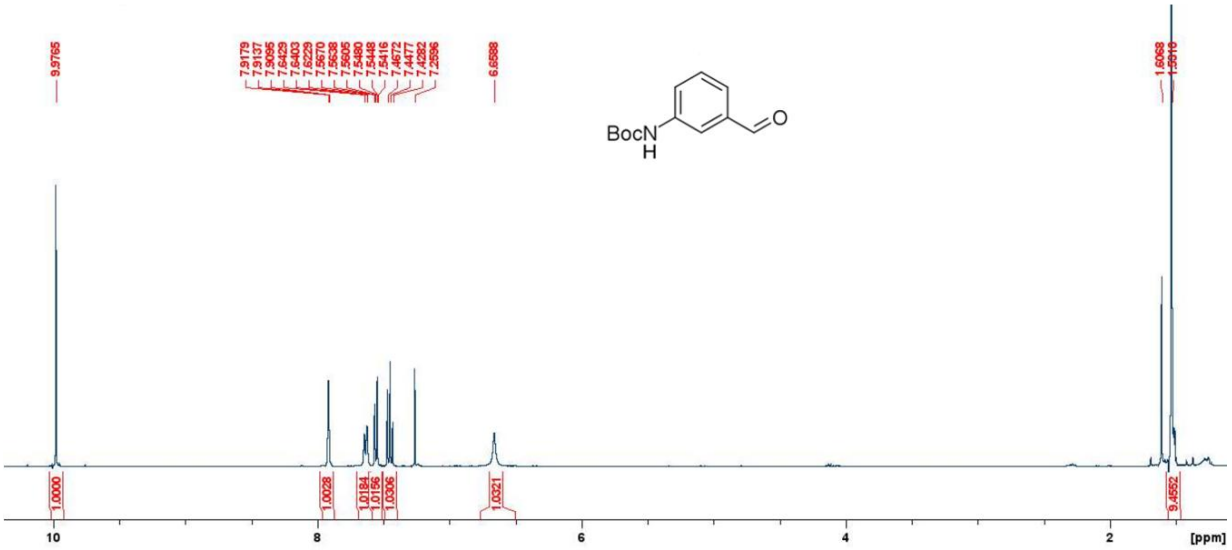

Figure S136. 400 MHz ^{1}H NMR spectrum of **10**

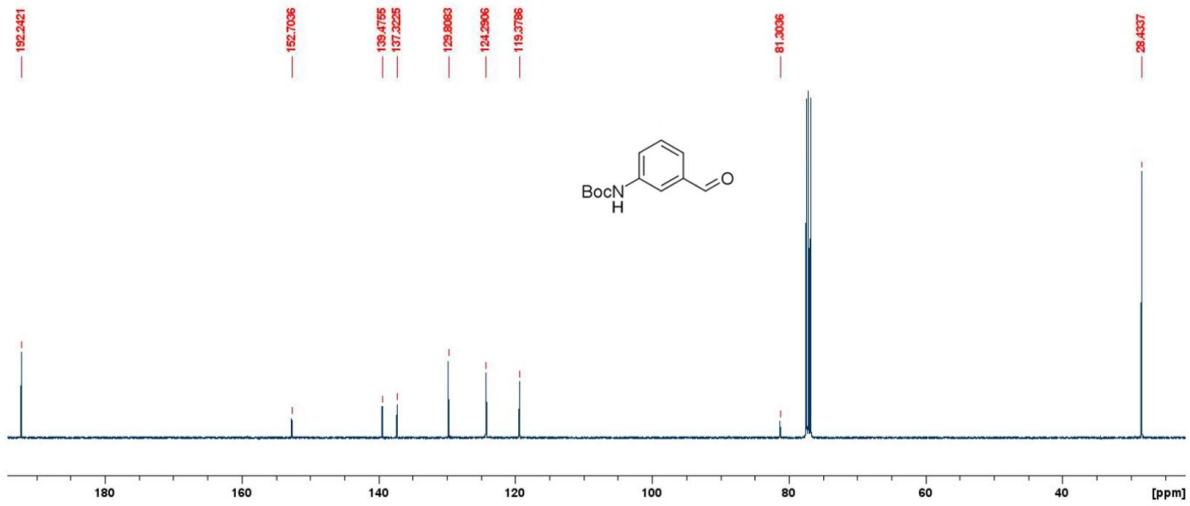

Figure S137. 100 MHz ^{13}C NMR spectrum of **10**

Boc-3-aminophenol (19)

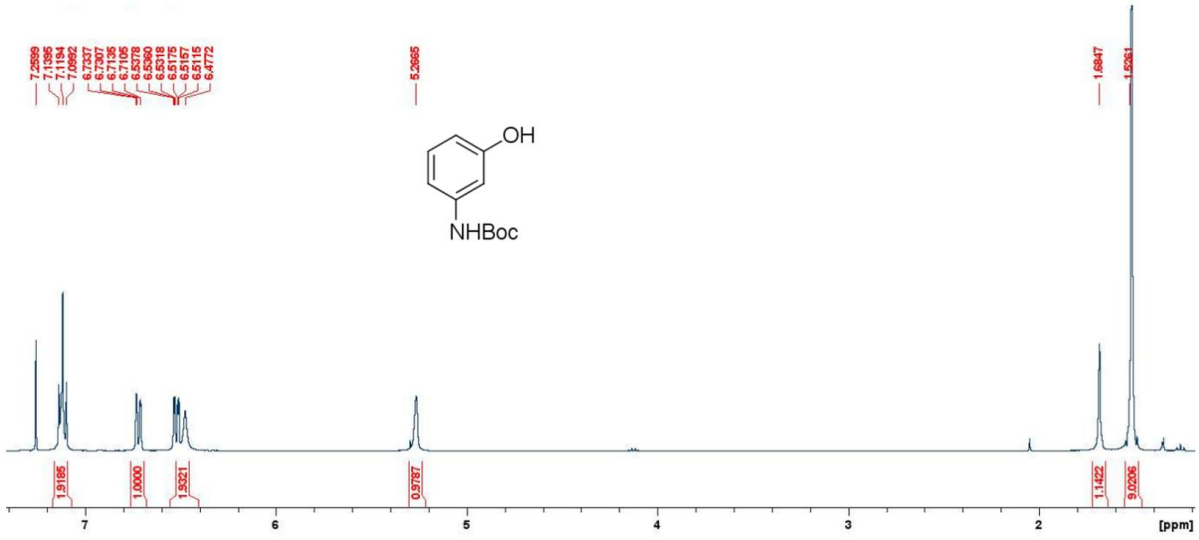

Figure S138. 400 MHz ^{1}H NMR spectrum of **19**

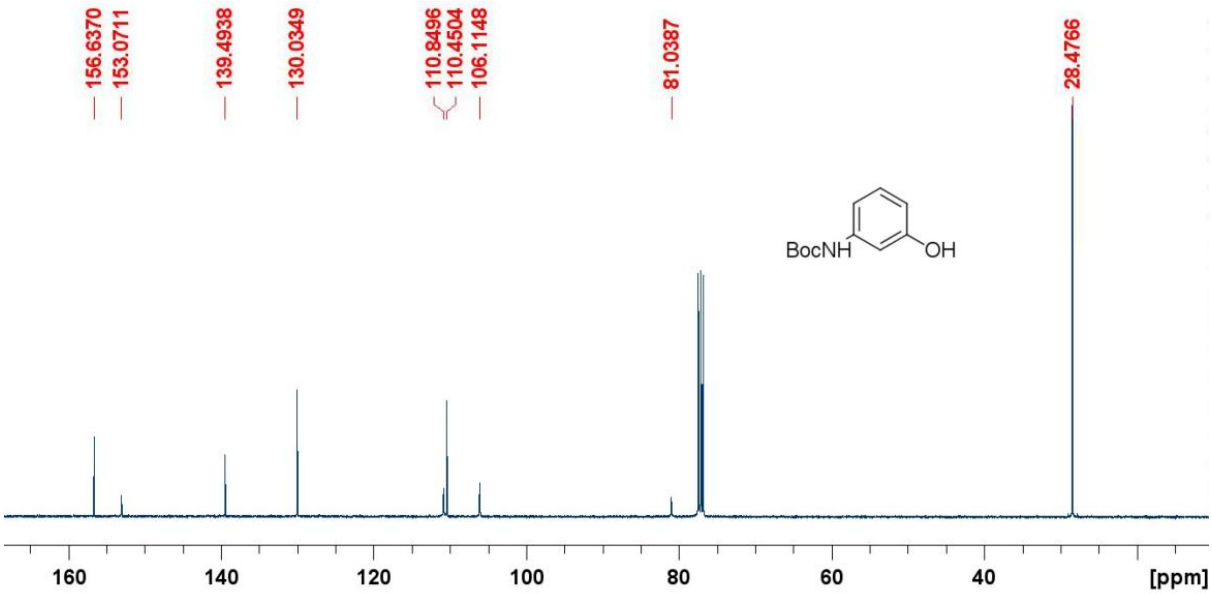

Figure S139. 100 MHz ^{13}C NMR spectrum of **19**

Boc-4-aminophenol (20)

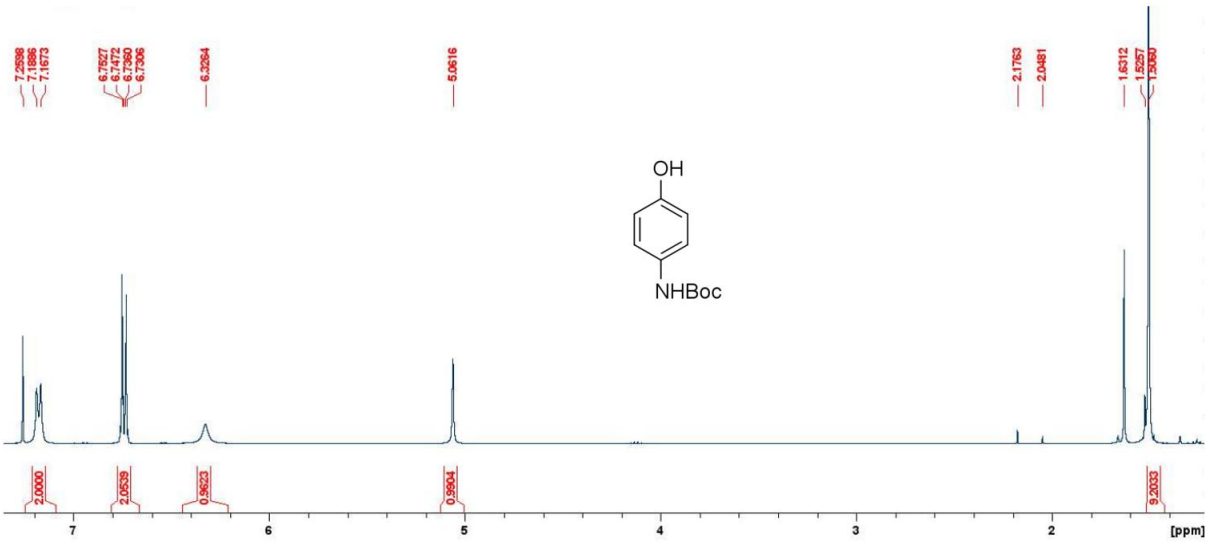

Figure S140. 400 MHz ^{1}H NMR spectrum of **20**

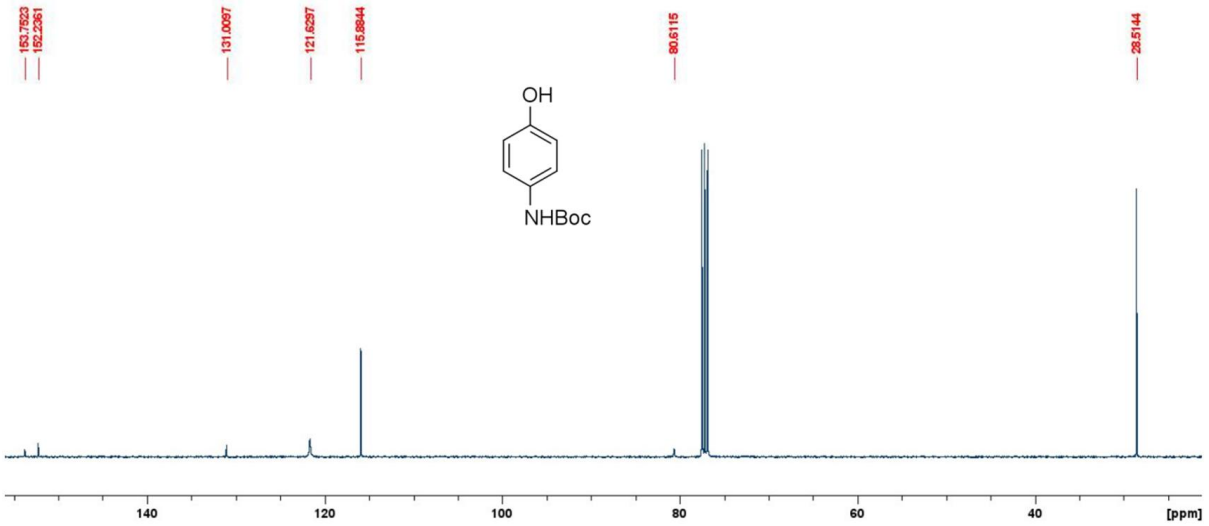

Figure S141. 100 MHz ^{13}C NMR spectrum of **20**

12-bromododecanoic acid (13)

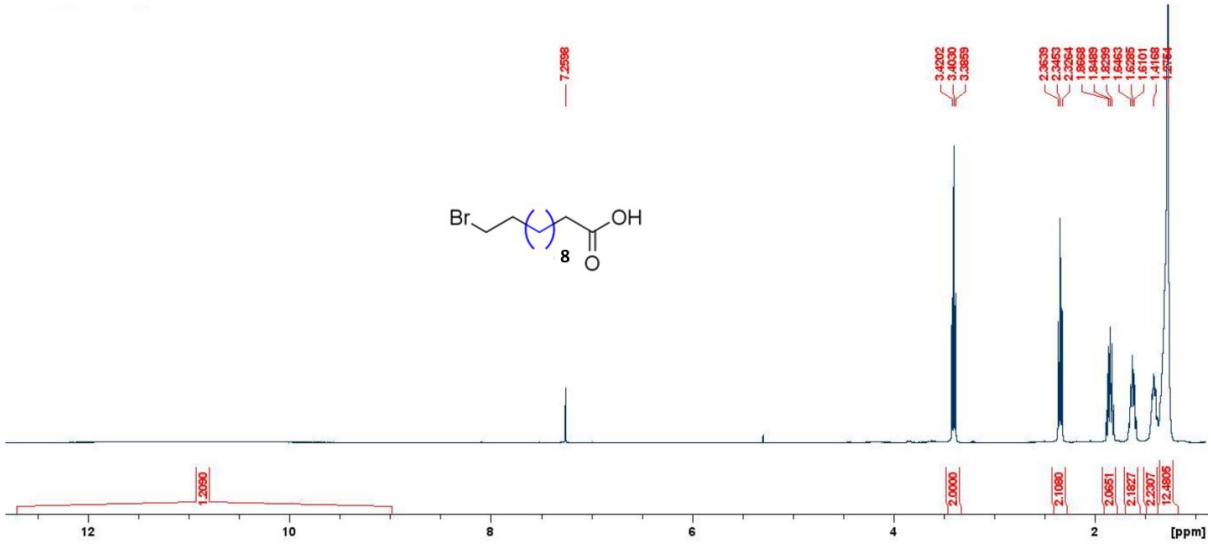

Figure S142. 400 MHz ^{1}H NMR spectrum of **13**

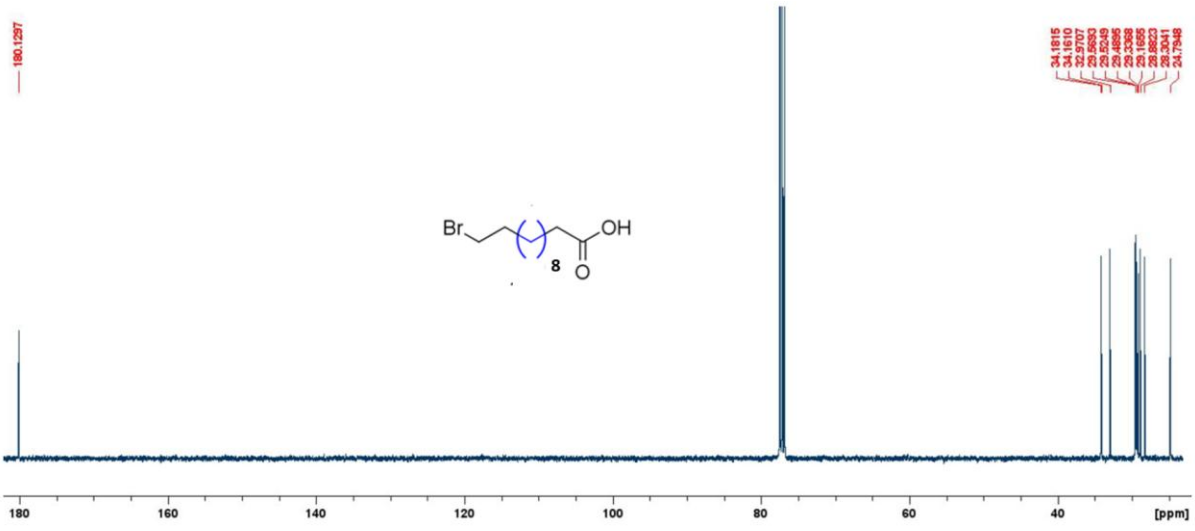

Figure S143. 100 MHz ^{13}C NMR spectrum of **13**

Ethyl 10-bromododecanoate (14)

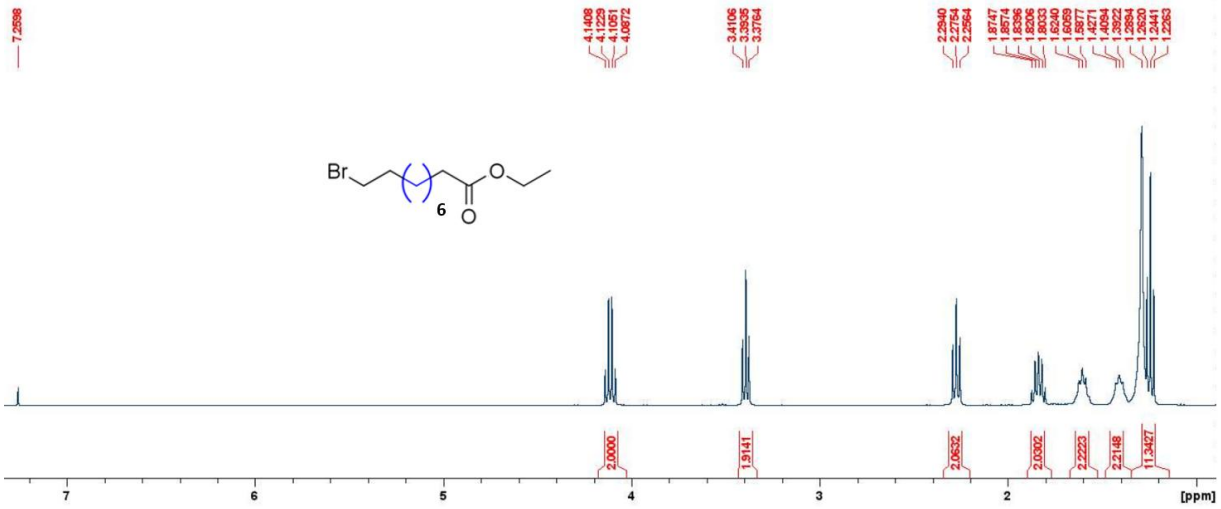

Figure S144. 400 MHz ^{1}H NMR spectrum of **14**

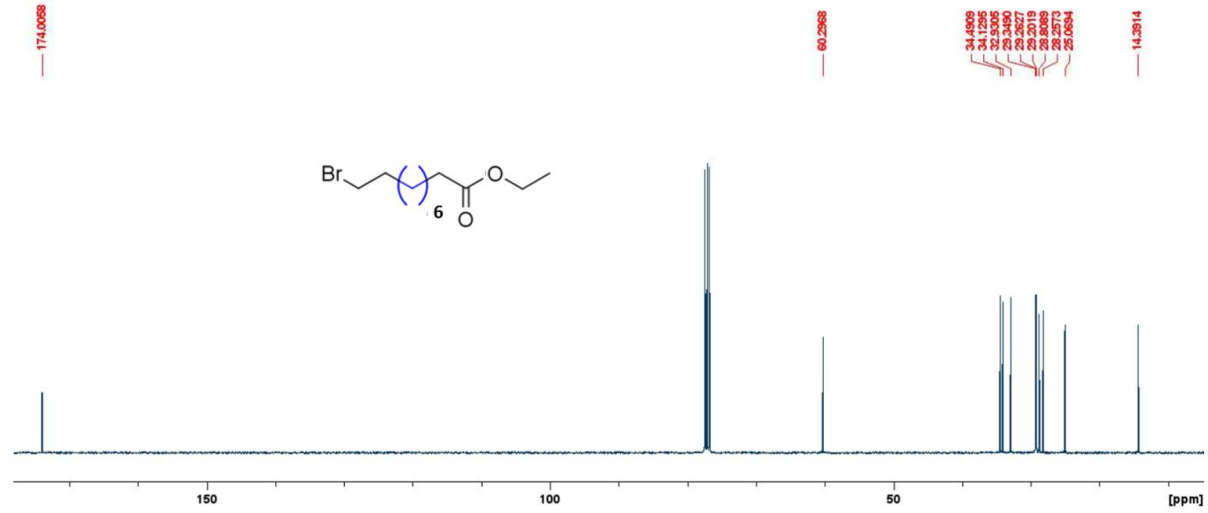

Figure S145. 100 MHz ^{13}C NMR spectrum of **14**

Ethyl 12-bromododecanoate (15)

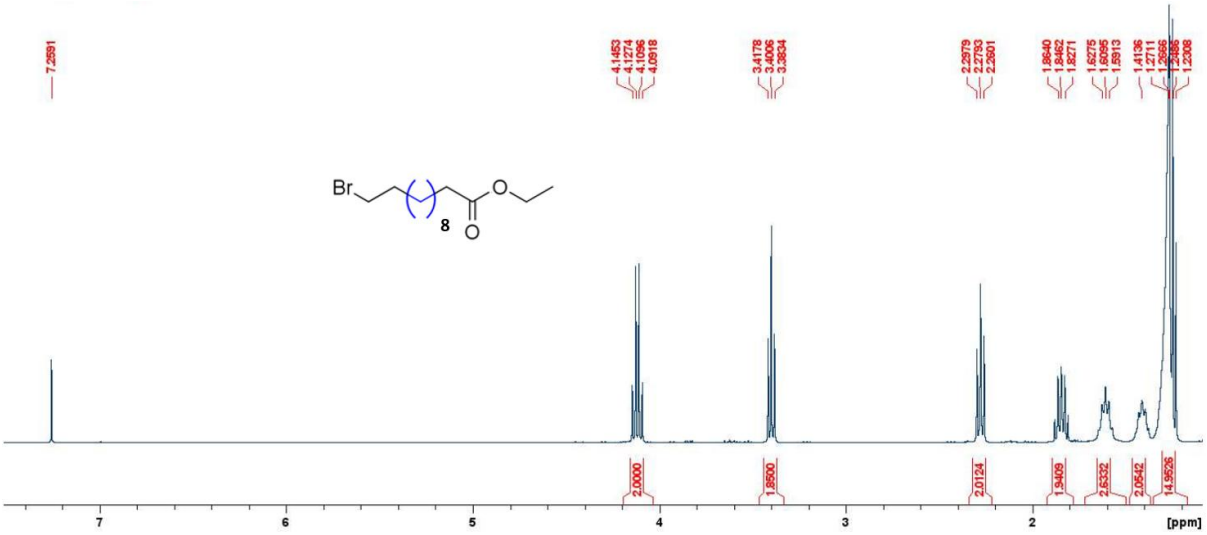

Figure S146. 400 MHz ^{1}H NMR spectrum of **15**

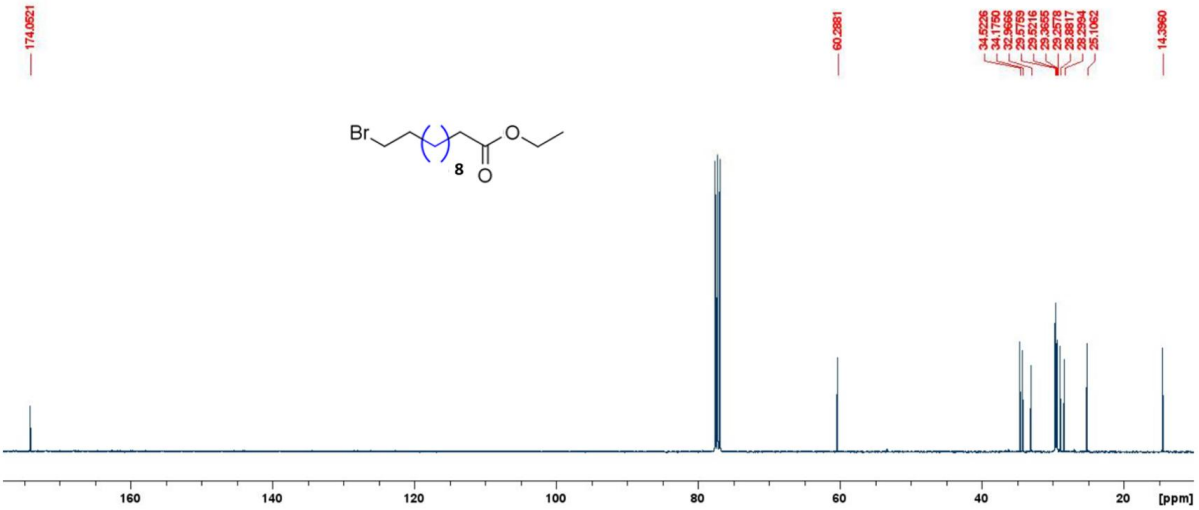

Figure S147. 100 MHz ^{13}C NMR spectrum of **15**

(10-ethoxy-10-oxodecyl)triphenylphosphonium bromide (16)

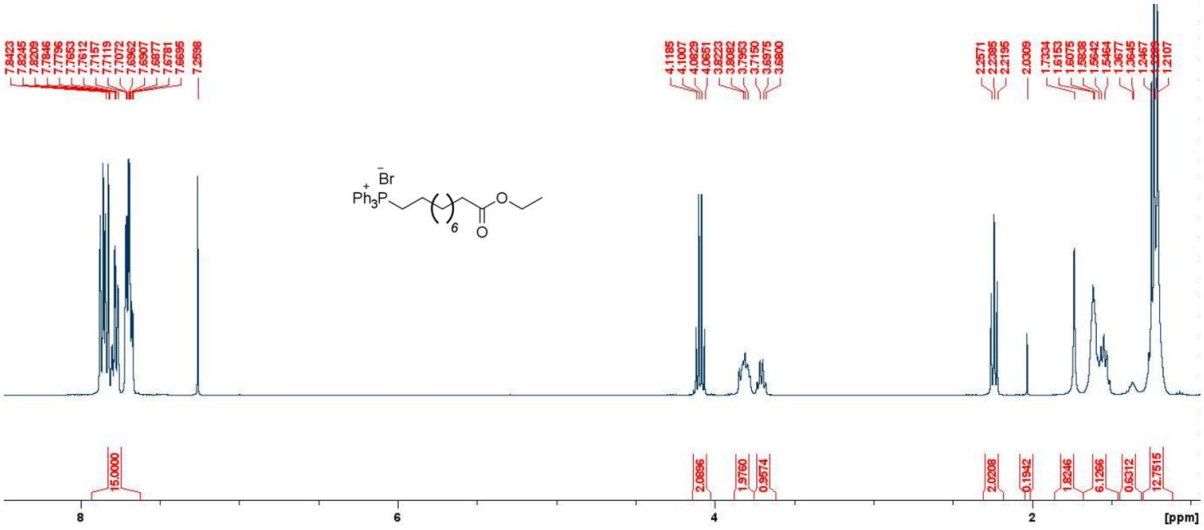

Figure S148. 400 MHz ^{1}H NMR spectrum of **16**

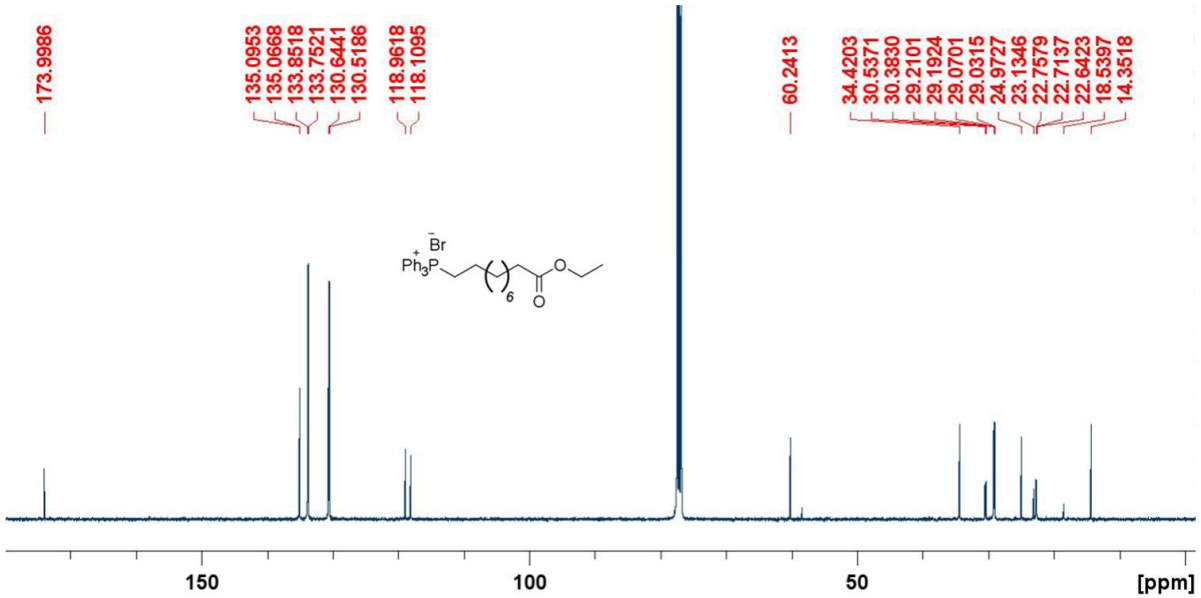

Figure S149. 100 MHz ^{13}C NMR spectrum of **16**

Ethyl(10E)-11-(3-{[(tert-butoxy)carbonyl]amino}phenyl)undec-10-enoate (21)

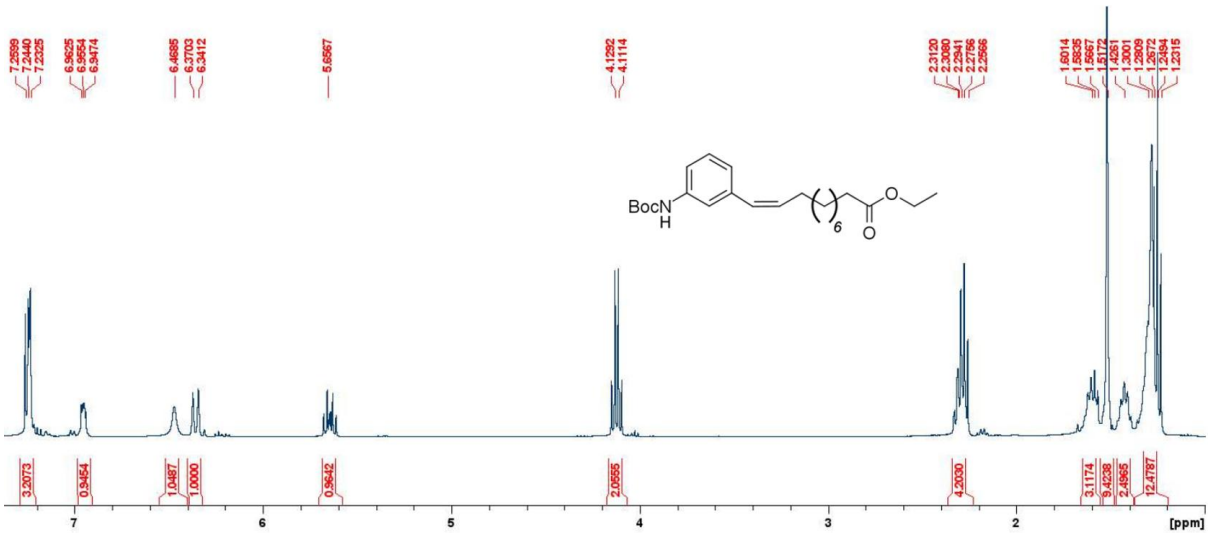

Figure S150. 400 MHz ^{1}H NMR spectrum of **21**

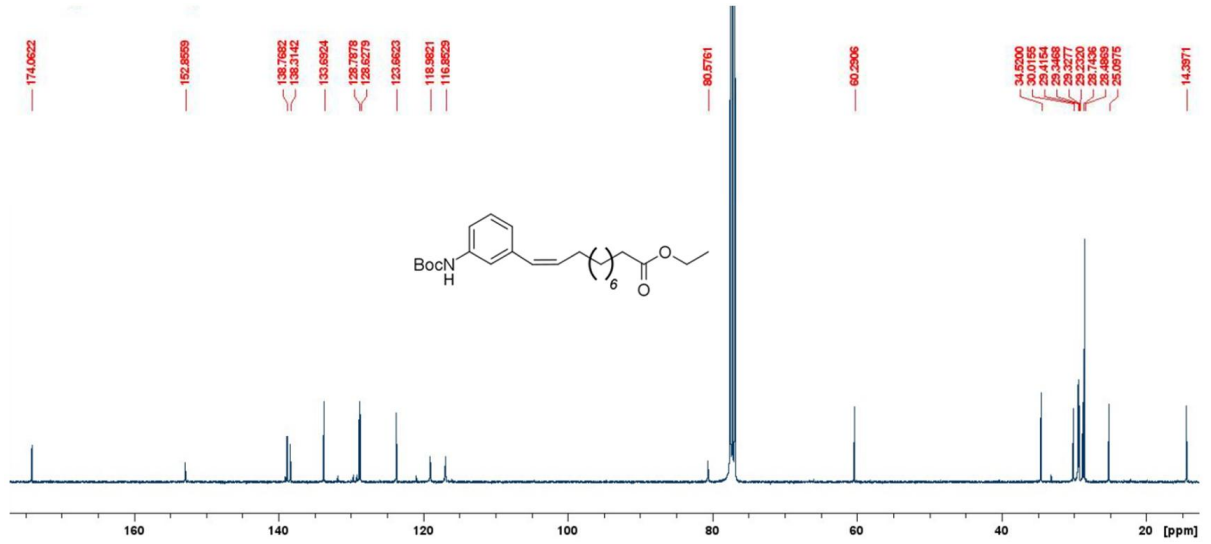

Figure S151. 100 MHz ^{13}C NMR spectrum of **21**

Ethyl 11-(3-{[(tert-butoxy)carbonyl]amino}phenyl)undecanoate (Boc3)

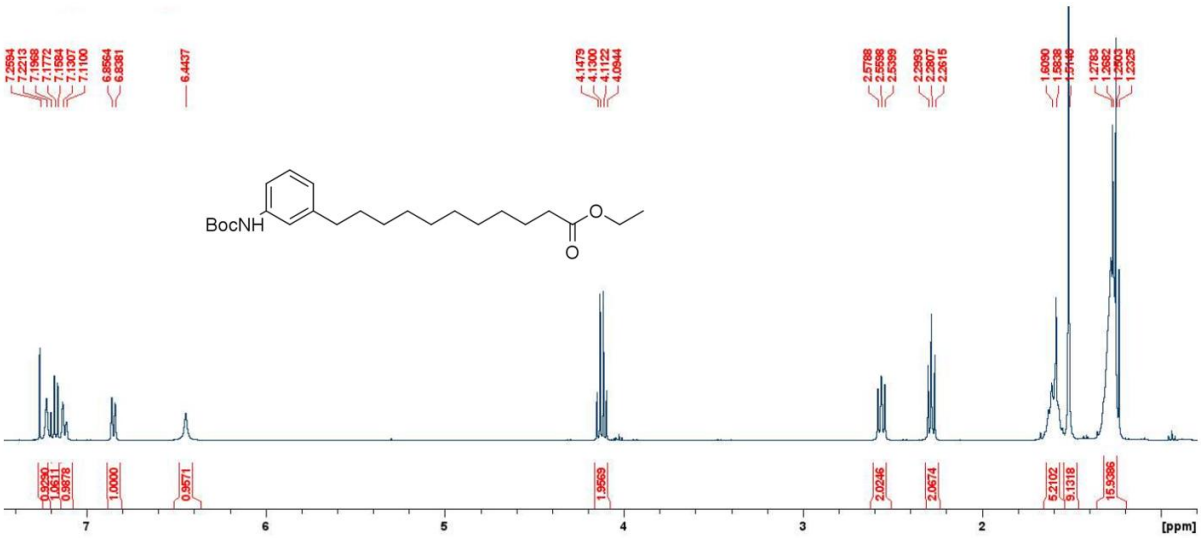

Figure S152. 400 MHz ^{1}H NMR spectrum of **Boc3**

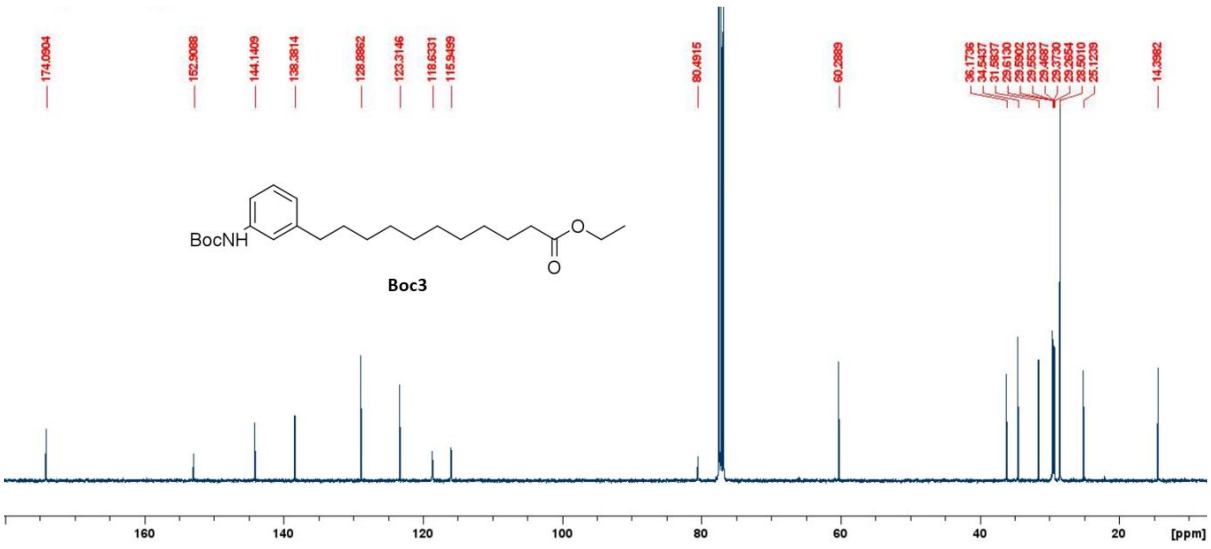

Figure S153. 100 MHz ^{13}C NMR spectrum of **Boc3**

Ethyl 12-(3-{[(tert-butoxy)carbonyl]amino}phenoxy)dodecanoate (Boc4)

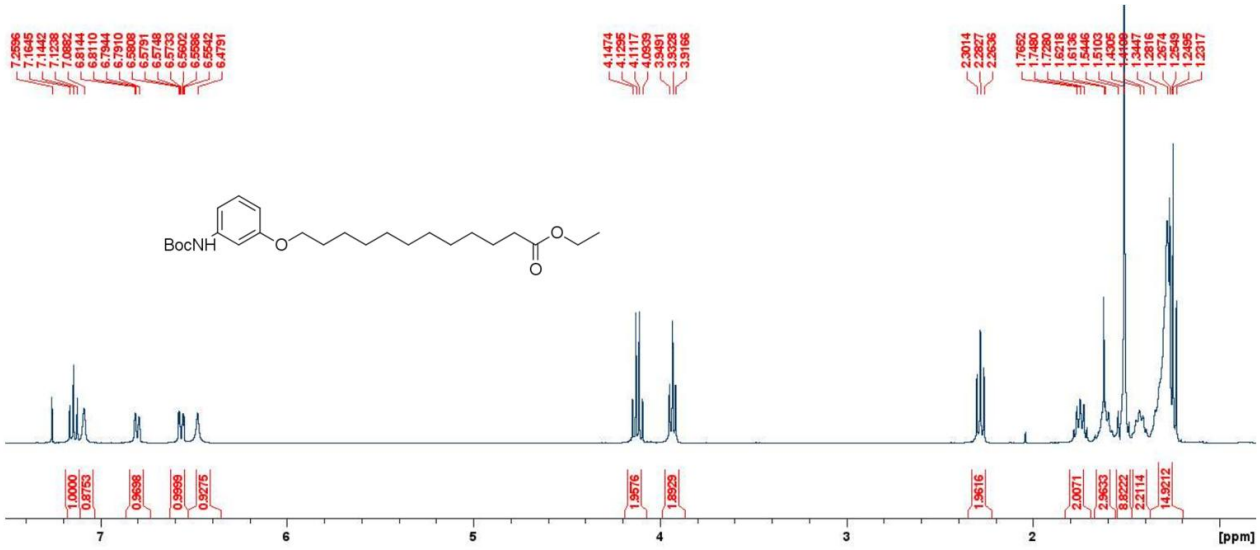

Figure S154. 400 MHz ^{1}H NMR spectrum of **Boc4**

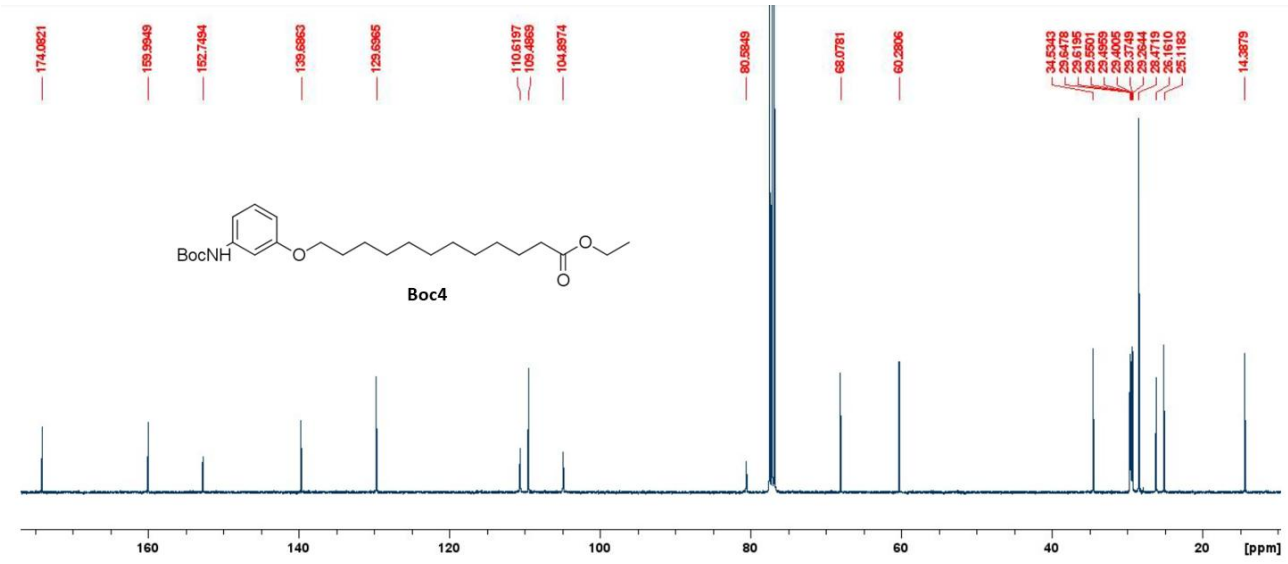

Figure S155. 100 MHz ^{13}C NMR spectrum of **Boc4**

Ethyl 12-(4-{[(tert-butoxy)carbonyl]amino}phenoxy)dodecanoate (Boc5)

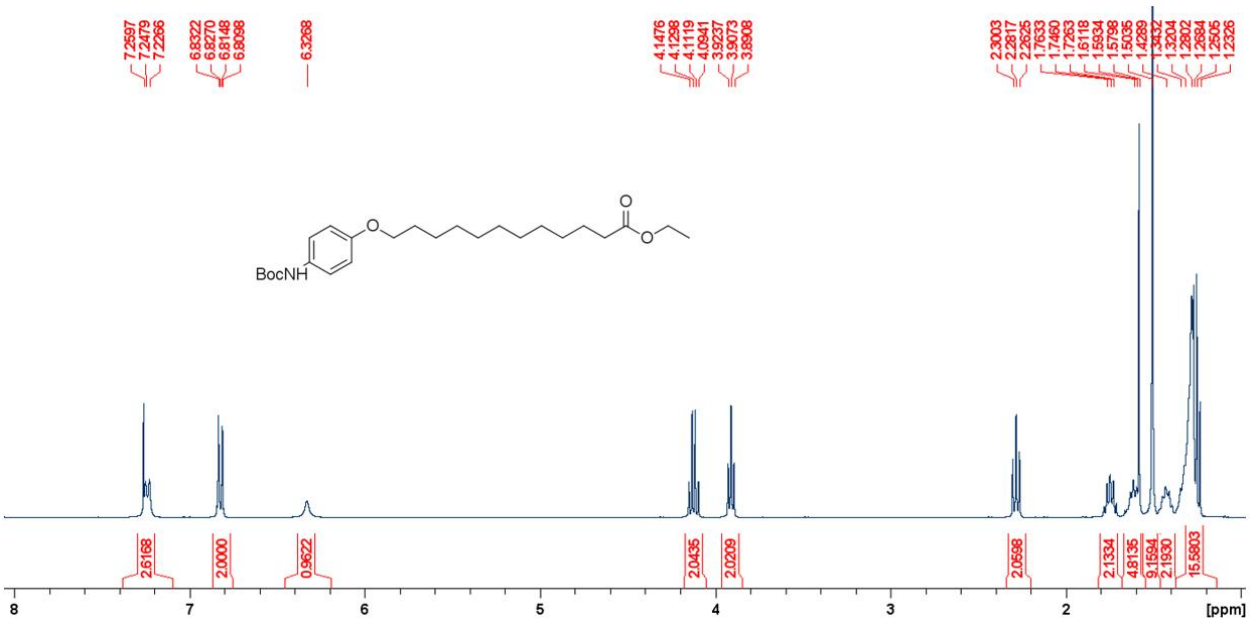

Figure S156. 400 MHz ^{1}H NMR spectrum of **Boc5**

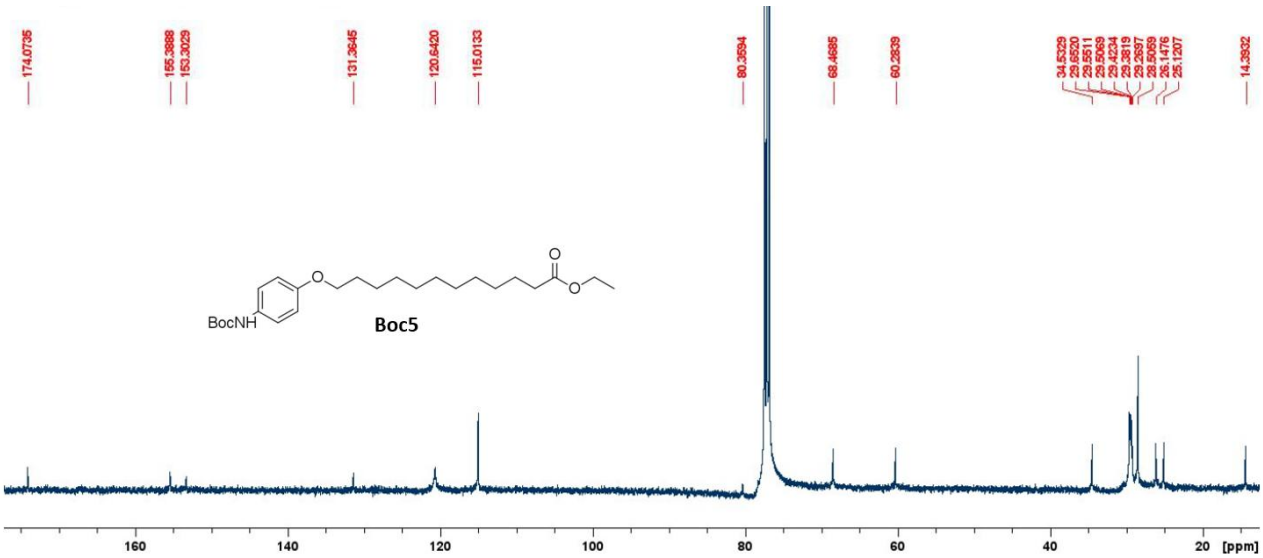

Figure S157. 100 MHz ^{13}C NMR spectrum of **Boc5**

Ethyl 11-(3-aminophenyl)undecanoate (3x)

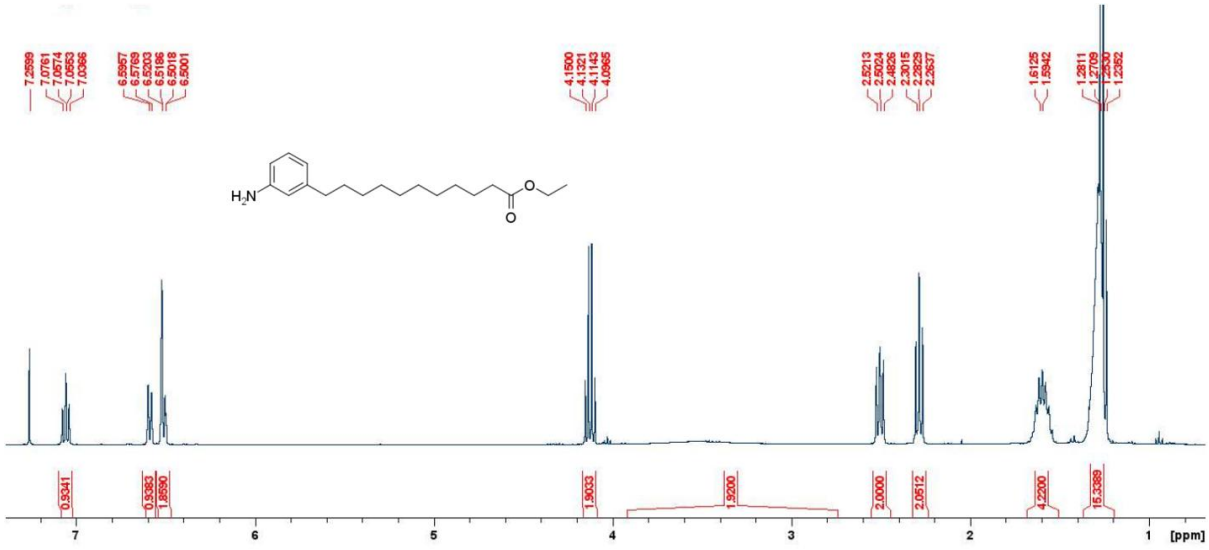

Figure S158. 400 MHz ^{1}H NMR spectrum of **3x**

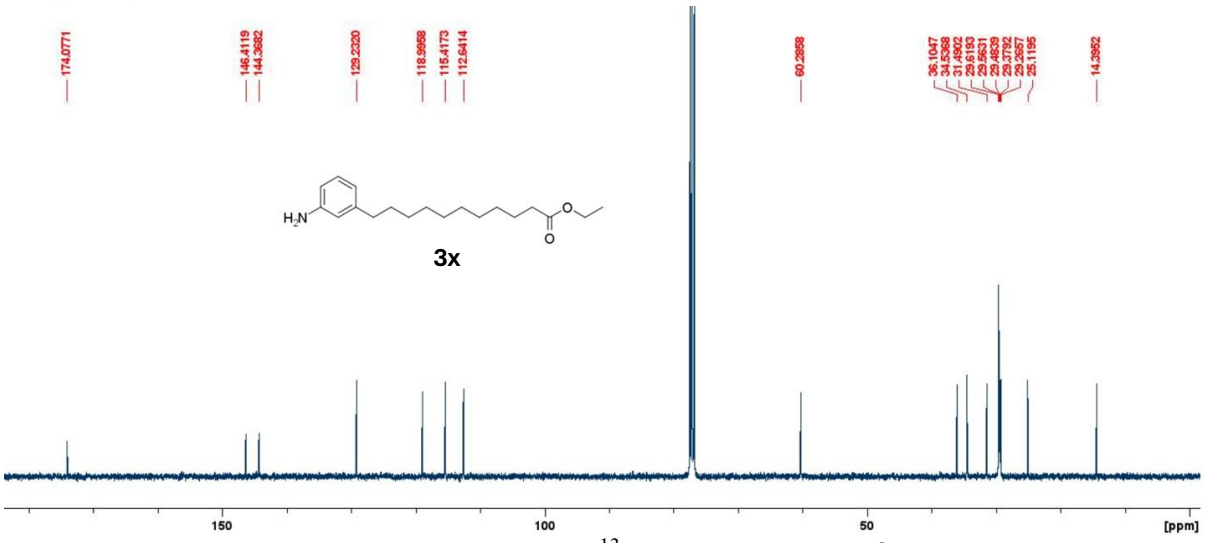

Figure S159. 100 MHz ^{13}C NMR spectrum of **3x**

Ethyl 12-(3-aminophenoxy)dodecanoate (4x)

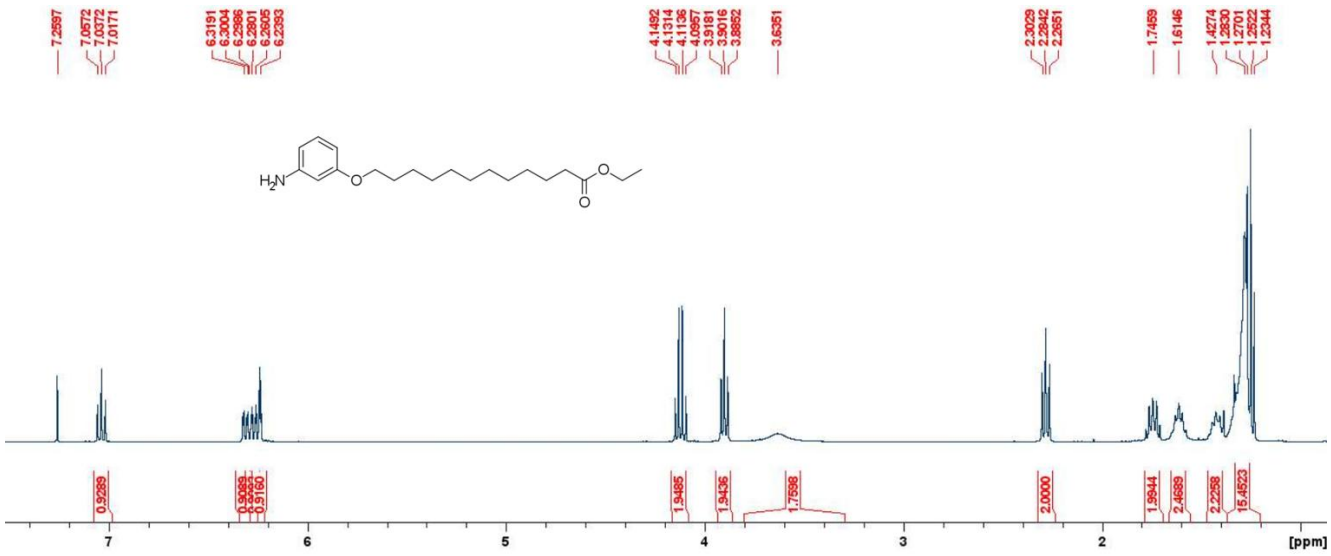

Figure S160. 400 MHz ^{1}H NMR spectrum of **4x**

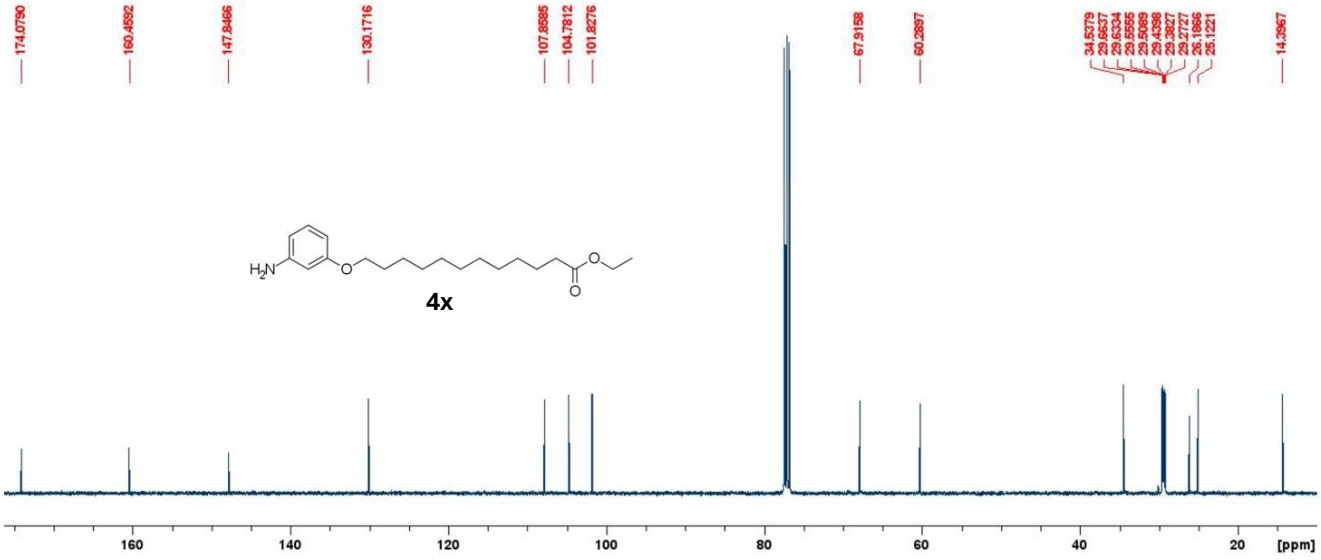

Figure S161. 100 MHz ^{13}C NMR spectrum of **4x**

2-(3-aminophenoxy)dodecanoate (5x)

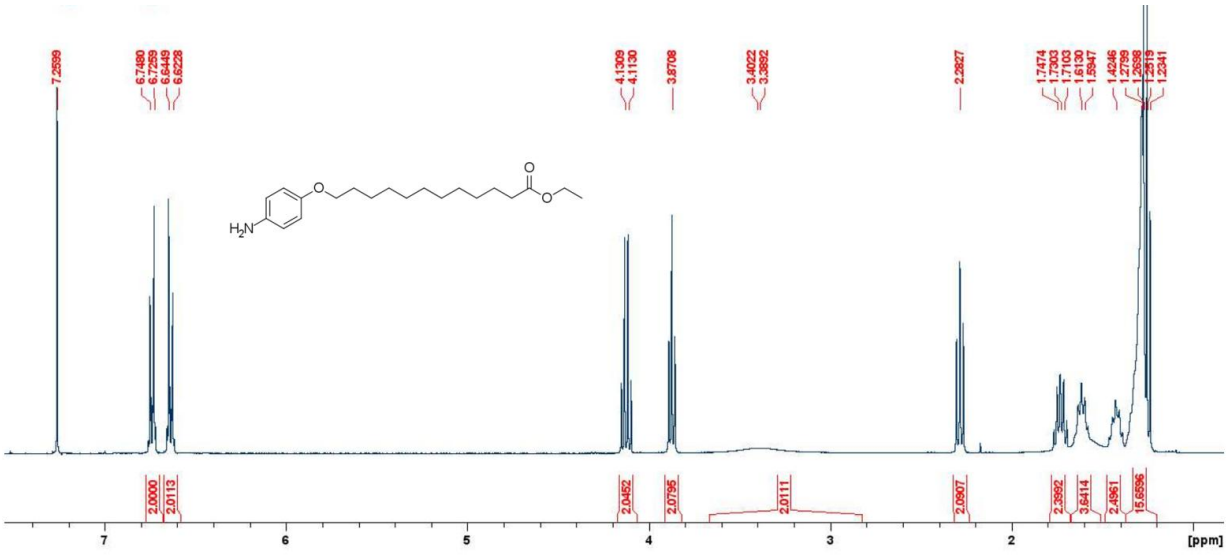

Figure S162. 400 MHz ^{1}H NMR spectrum of **5x**

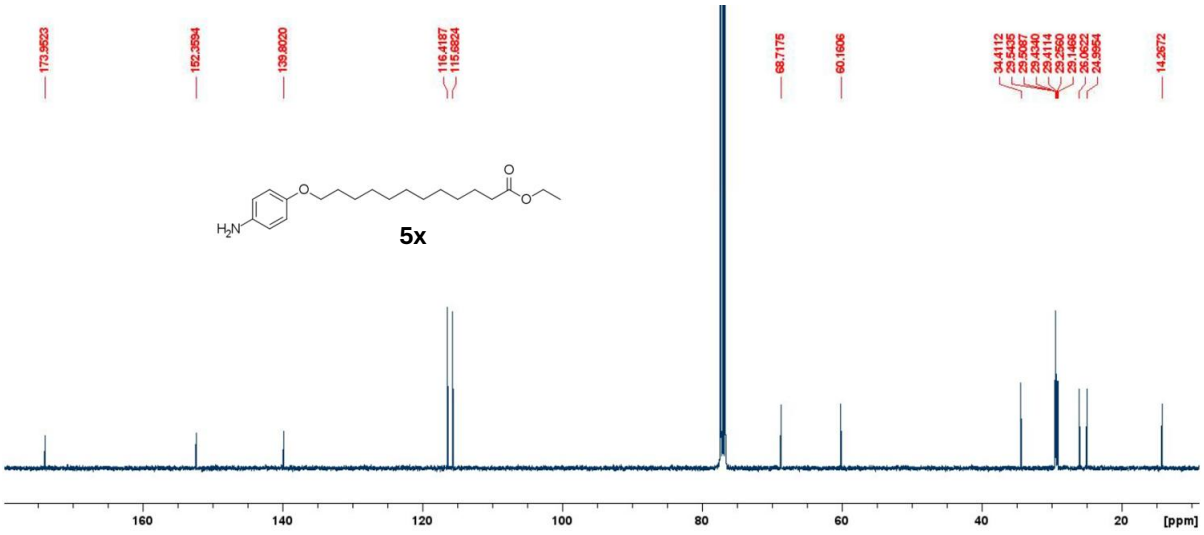

Figure S163. 100 MHz ^{13}C NMR spectrum of **5x**

Ethyl 11-[3-({[3-chloro-5-(trifluoromethyl)phenyl]carbamoyl}amino)phenyl]-undecanoate (3a-Et)

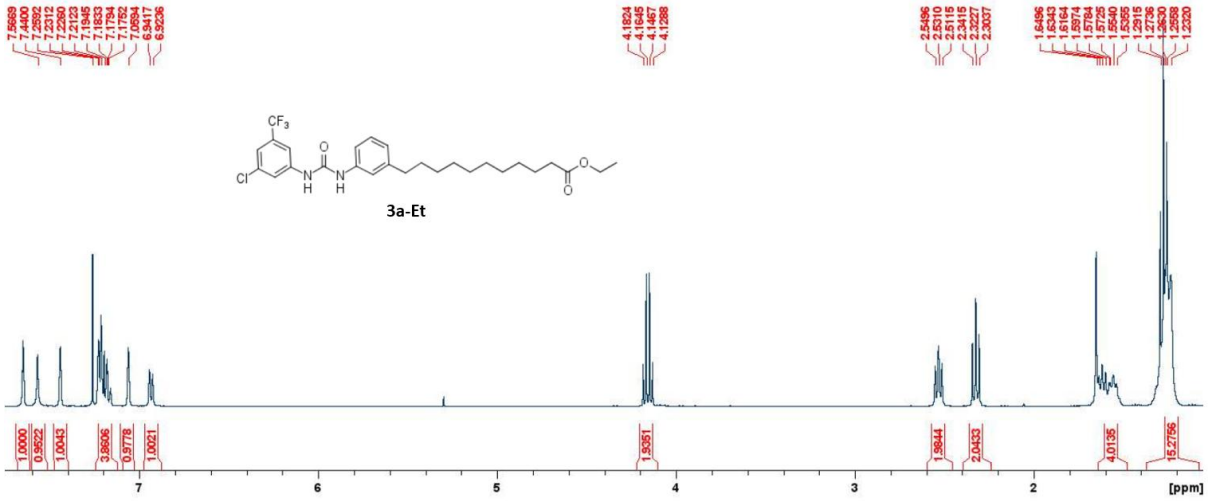

Figure S164. 400 MHz ^{1}H NMR spectrum of **3a-Et**

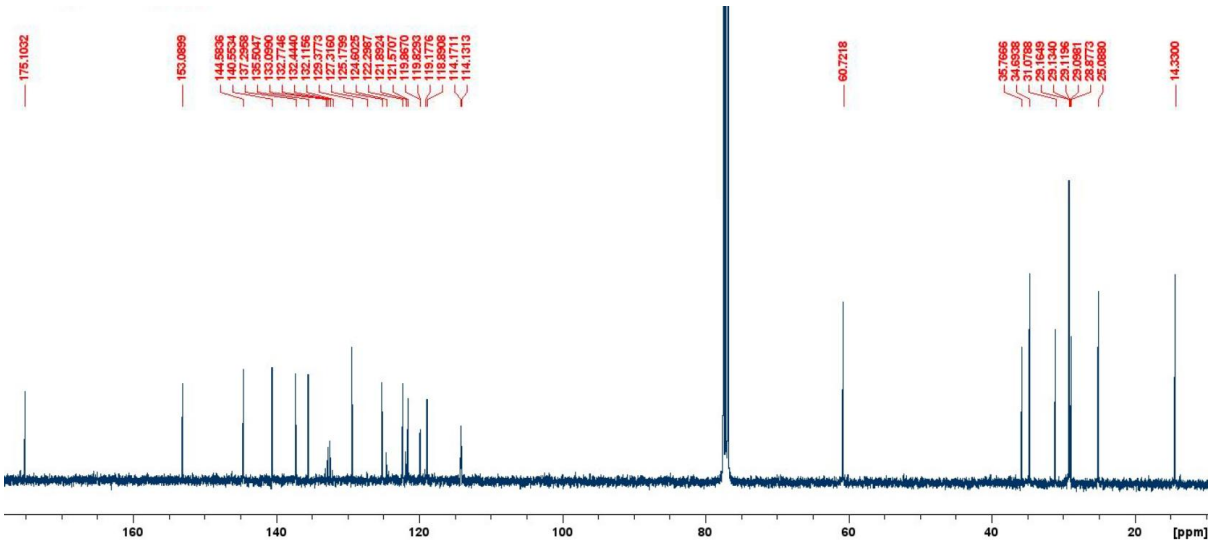

Figure S165. 100 MHz ^{13}C NMR spectrum of **3a-Et**

Ethyl 11-[3-({[4-chloro-3-(trifluoromethyl)phenyl]carbamoyl}amino)phenyl]-undecanoate (3b-Et)

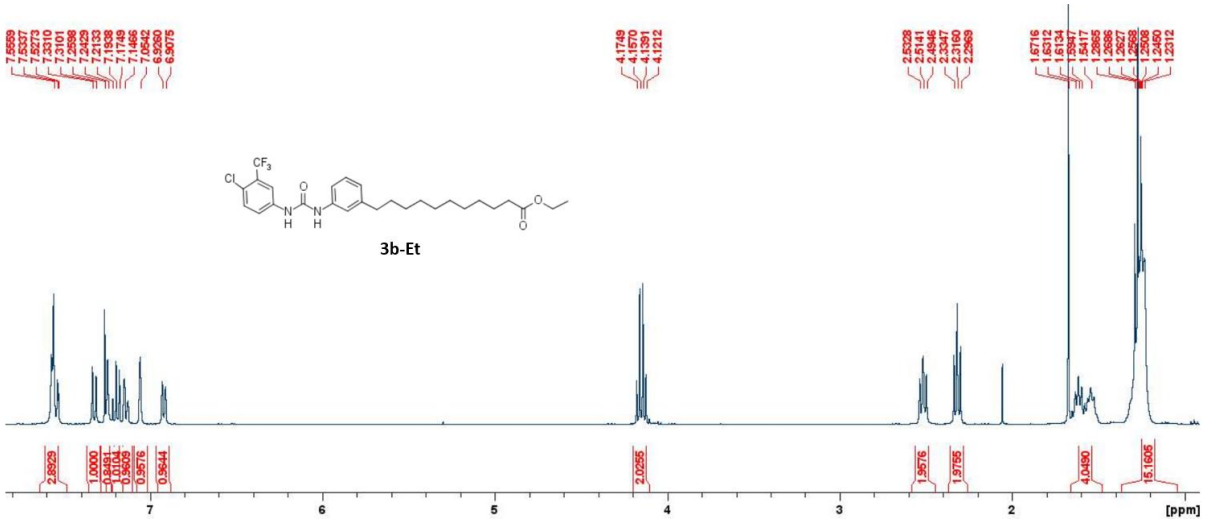

Figure S166. 400 MHz ^{1}H NMR spectrum of **3b-Et**

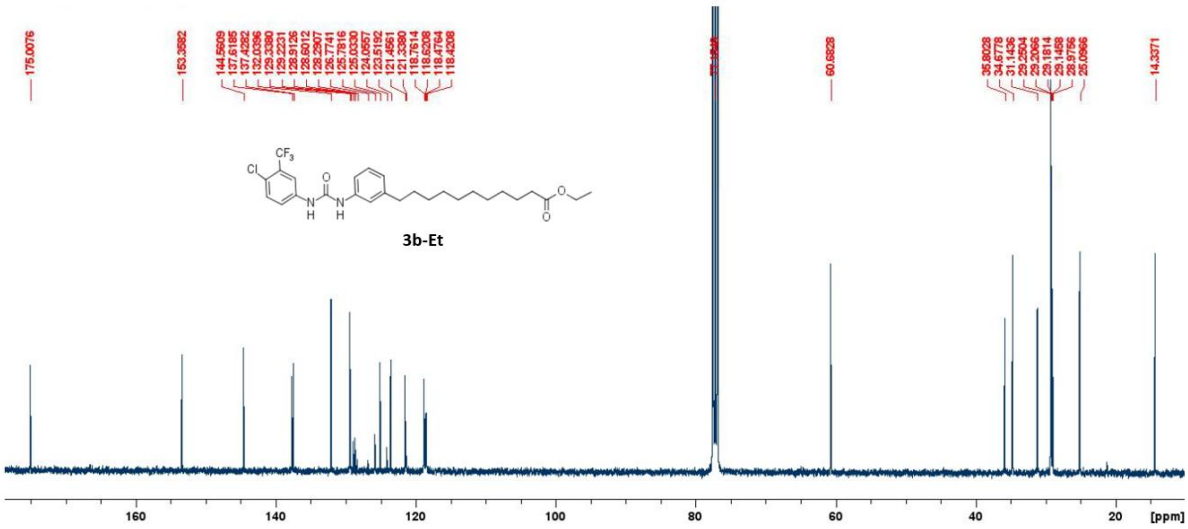

Figure S167. 100 MHz ^{13}C NMR spectrum of **3b-Et**

Ethyl 12-[3-({[3-chloro-5 (trifluoromethyl)phenyl]carbamoyl}amino)phenoxy]dodecanoate (4a-Et)

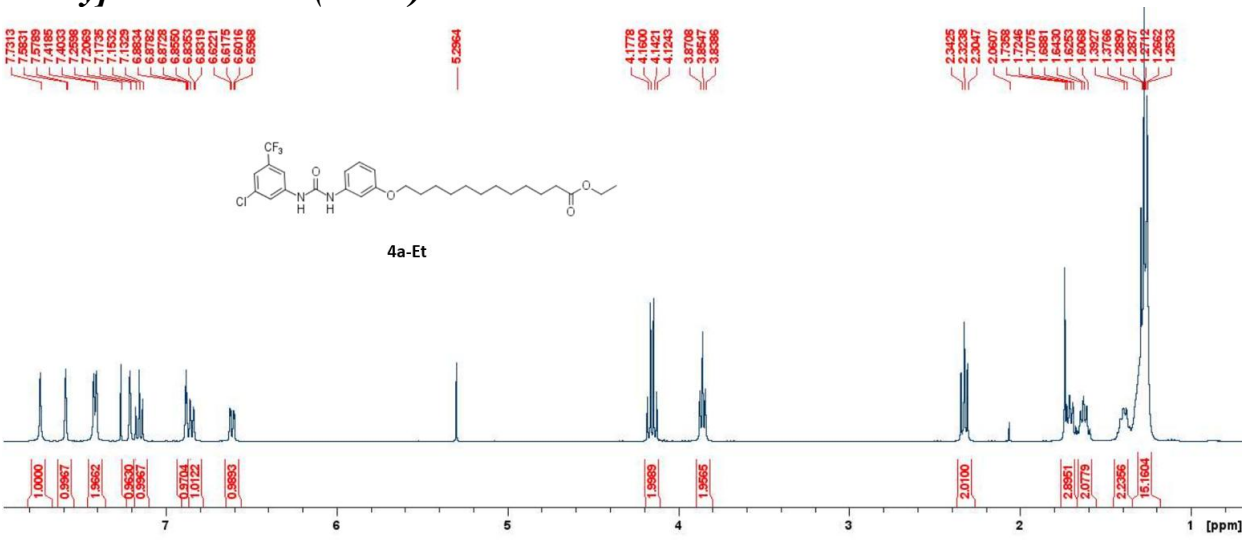

Figure S168. 400 MHz ^{1}H NMR spectrum of **4a-Et**

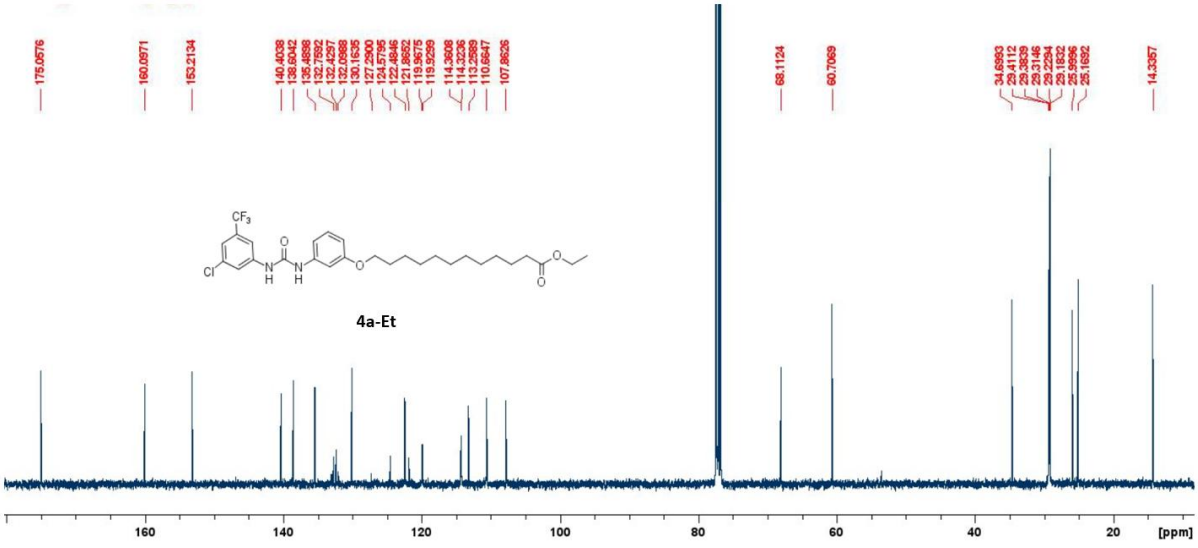

Figure S169. 100 MHz ^{13}C NMR spectrum of **4a-Et**

Ethyl 12-[3-({[4-chloro-3(trifluoromethyl)phenyl]carbamoyl}amino)phenoxy]-dodecanoate (4b-Et)

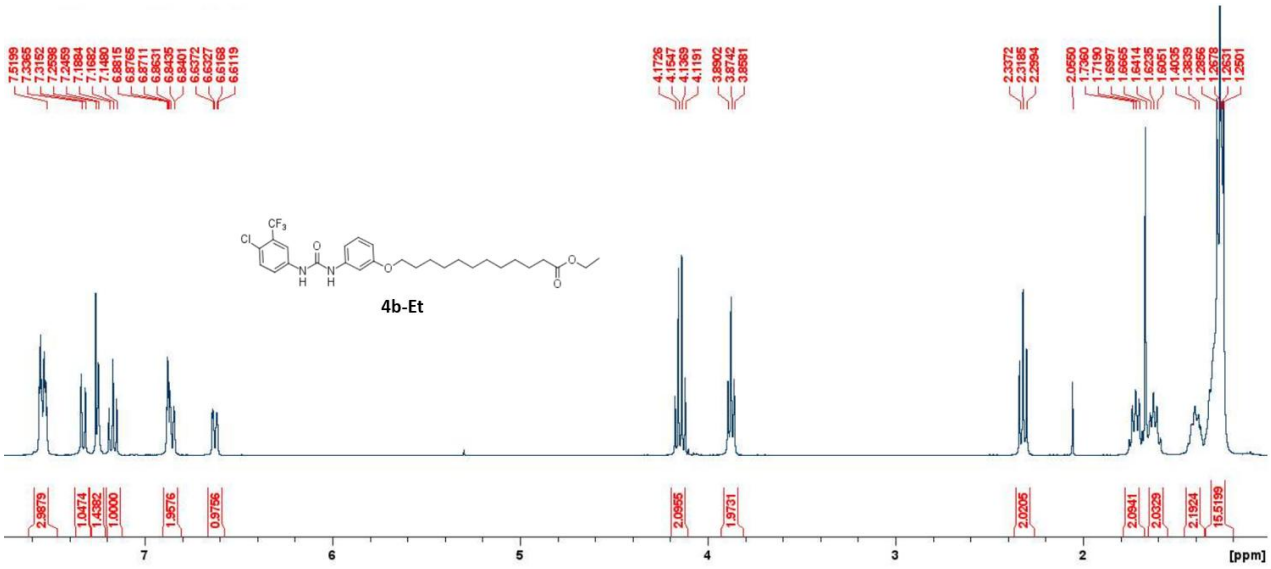

Figure S170. 400 MHz ^{1}H NMR spectrum of **4b-Et**

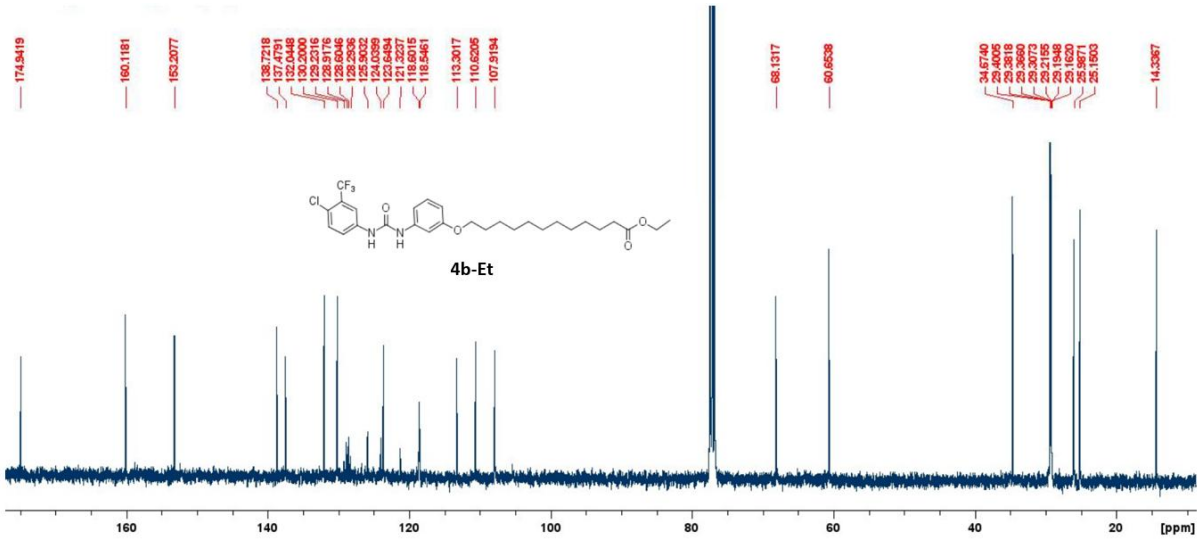

Figure S171. 100 MHz ^{13}C NMR spectrum of **4b-Et**

Ethyl 12-[4-({[3-chloro-5-(trifluoromethyl)phenyl]carbamoyl}amino)phenoxy]dodecanoate (5a-Et)

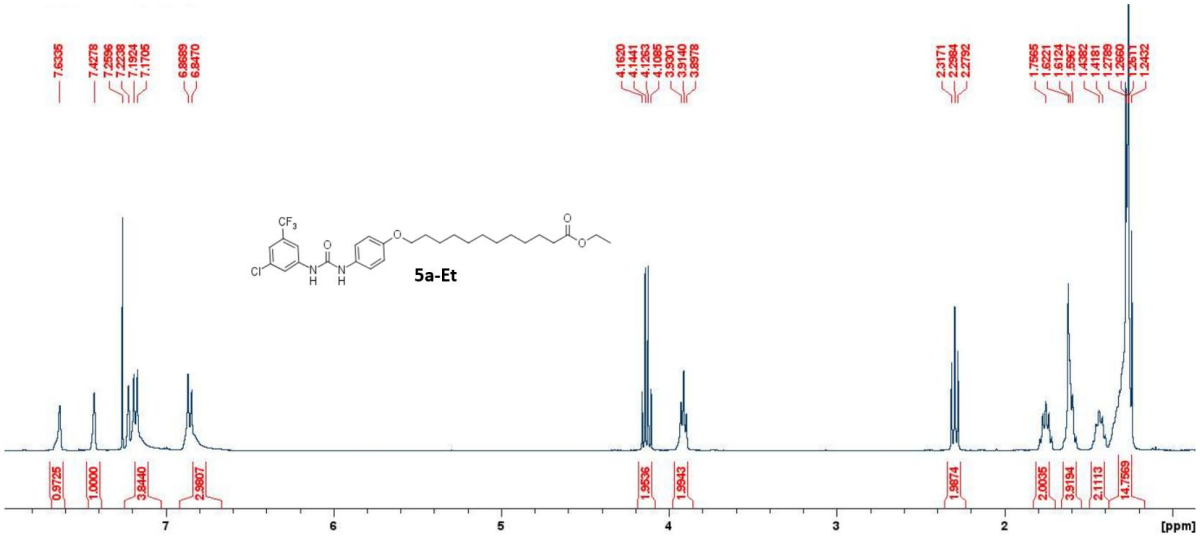

Figure S172. 400 MHz ^{1}H NMR spectrum of **5a-Et**

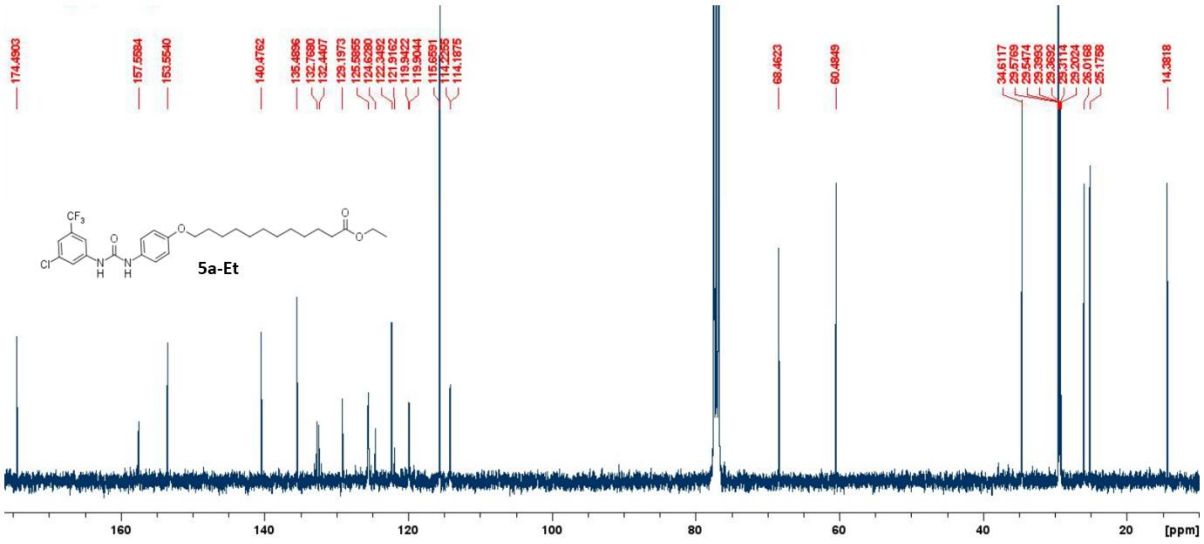

Figure S173. 100 MHz ^{13}C NMR spectrum of **5a-Et**

Ethyl 12-[4-({[4-chloro-3-(trifluoromethyl)phenyl]carbamoyl}amino)phenoxy]dodecanoate (5b-Et)

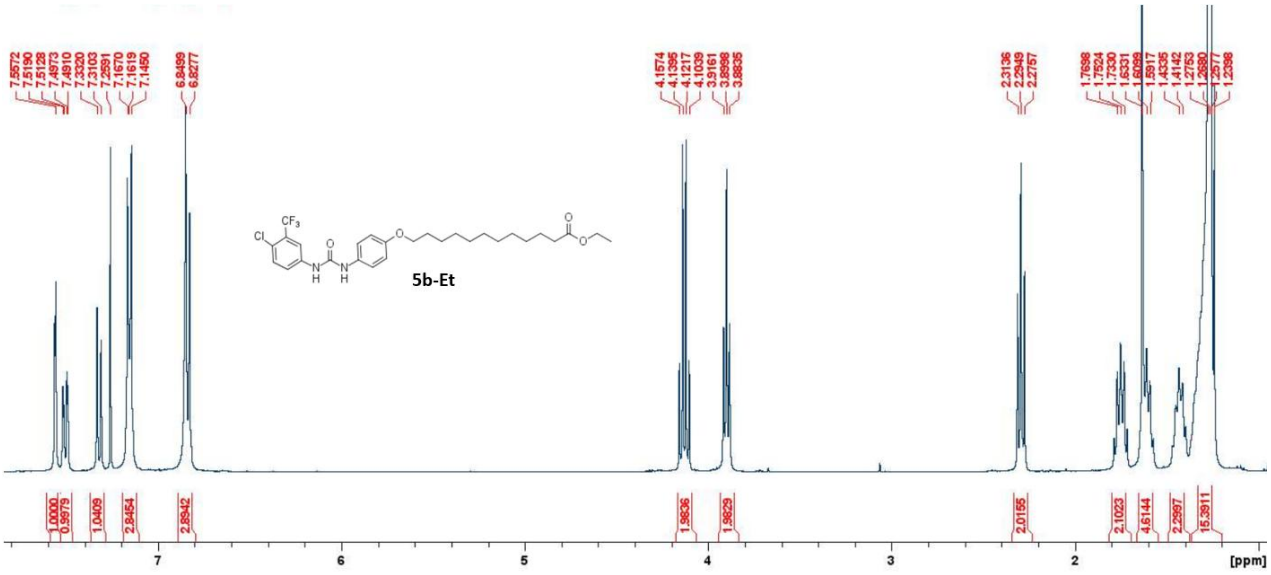

Figure S174. 400 MHz ^{1}H NMR spectrum of **5b-Et**

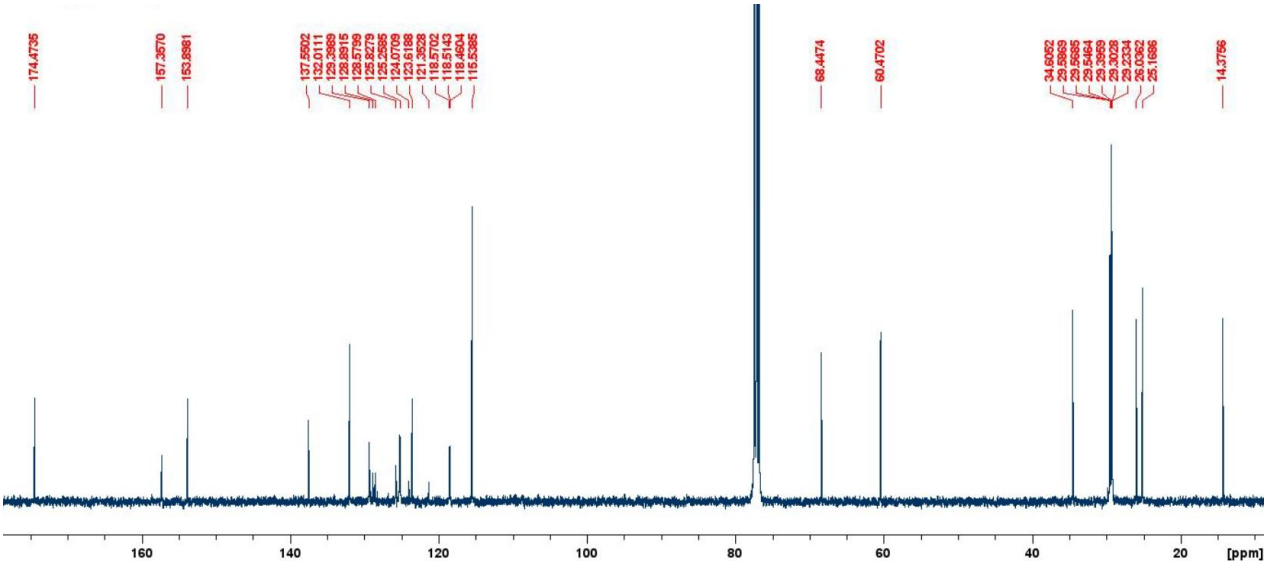

Figure S175. 100 MHz ^{13}C NMR spectrum of **5b-Et**

11-[3-({[3-chloro-5-(trifluoromethyl)phenyl]carbamoyl}amino)phenyl]undecanoic acid (3a)

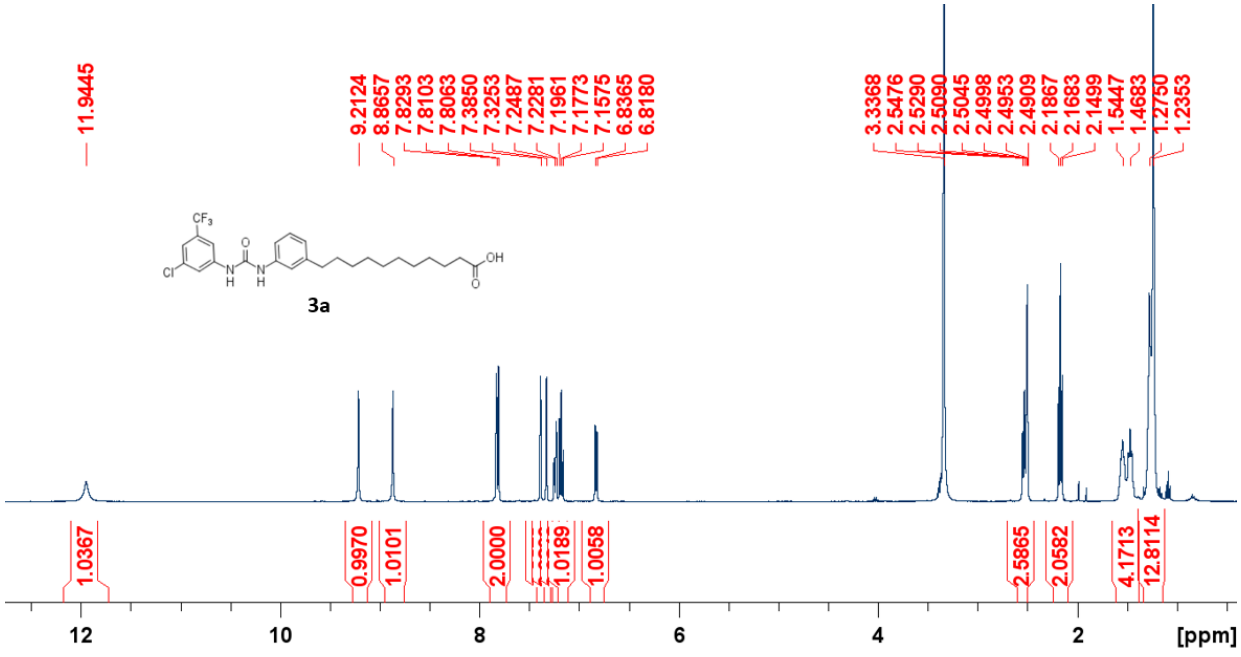

Figure S176. 400 MHz ^{1}H NMR spectrum of **3a**

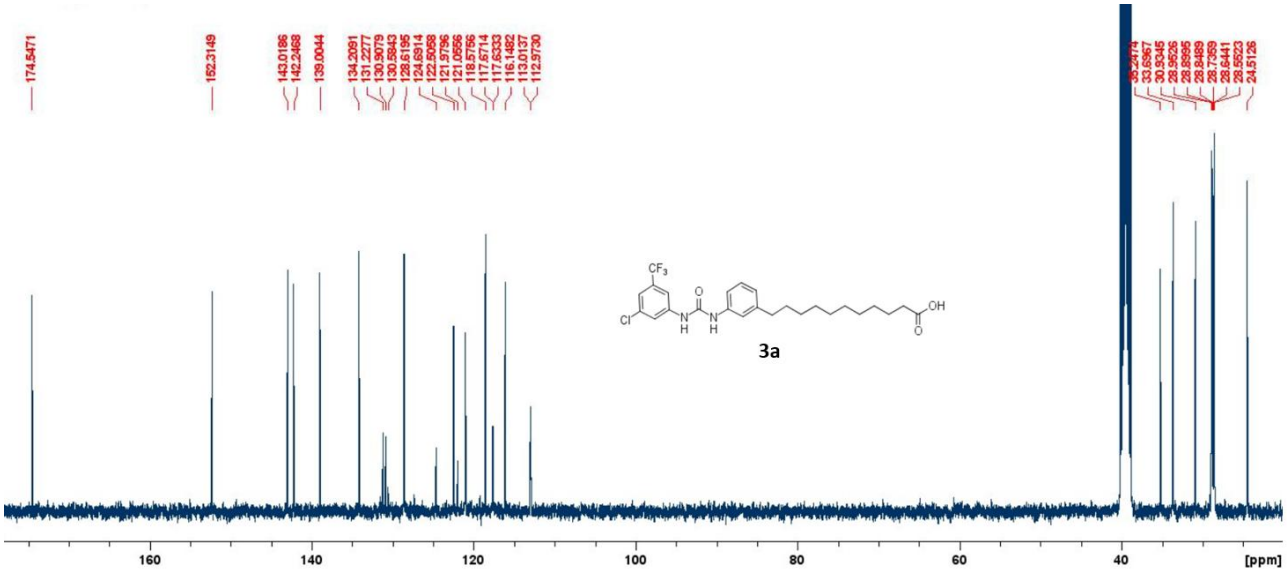

Figure S177. 100 MHz ^{13}C NMR spectrum of **3a**

11-[3-({[4-Chloro-3-(trifluoromethyl)phenyl]carbamoyl}amino)phenyl]undecanoic acid (3b)

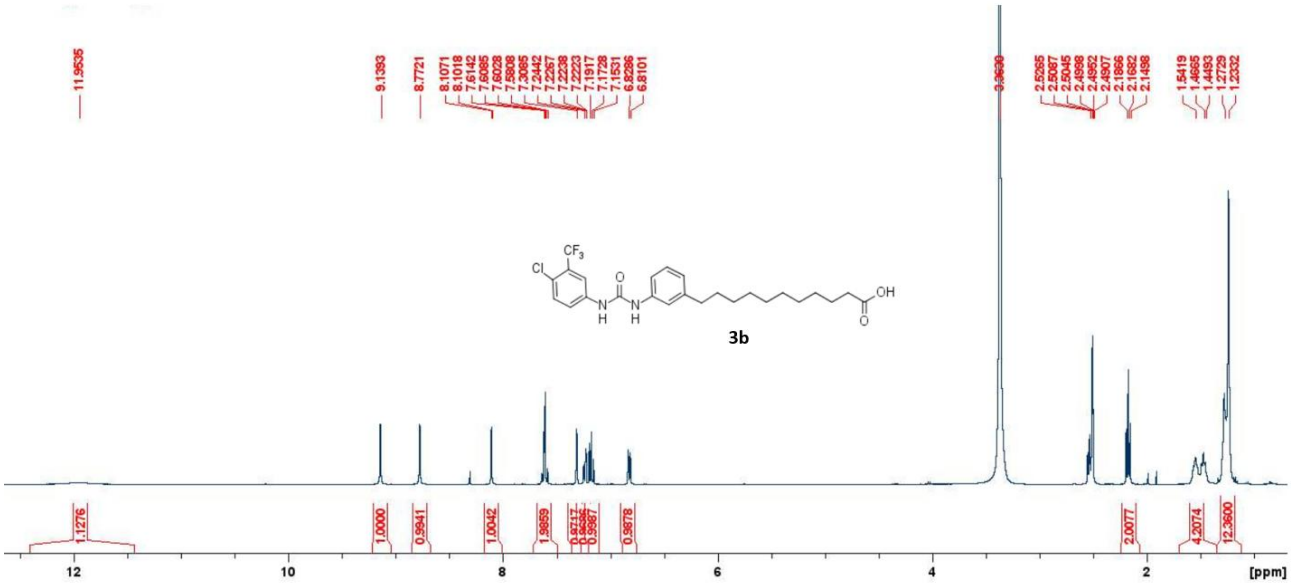

Figure S178. 400 MHz ^{1}H NMR spectrum of **3b**

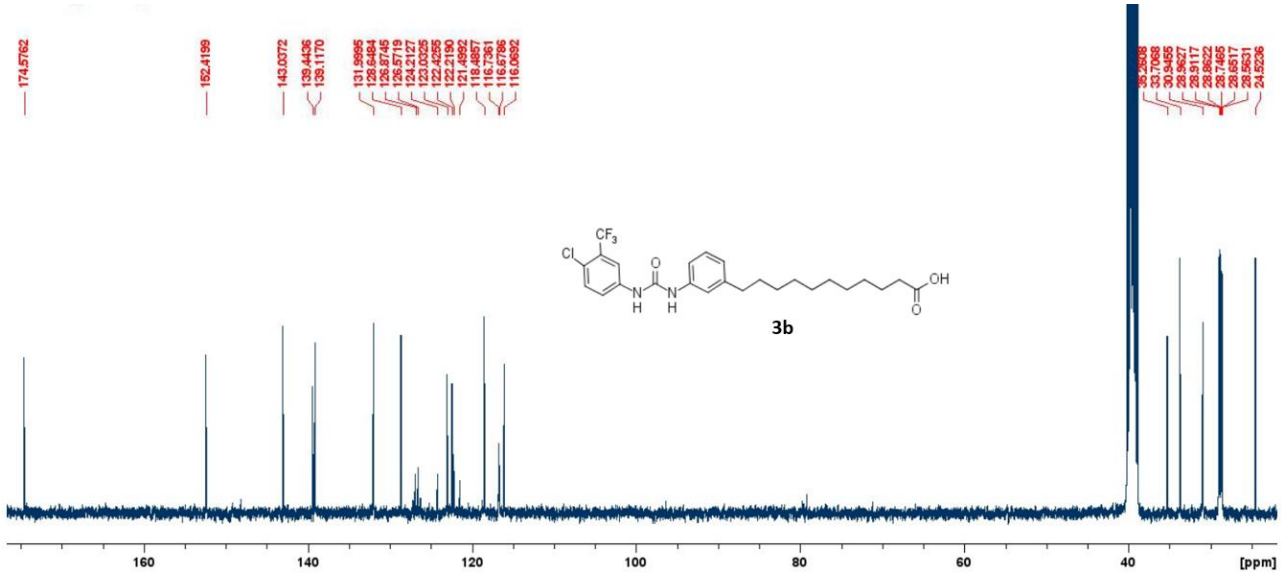

Figure S179. 100 MHz ^{13}C NMR spectrum of **3b**

12-[3-({[3-chloro-5-(trifluoromethyl)phenyl]carbamoyl}amino)phenoxy]dodecanoic acid (4a)

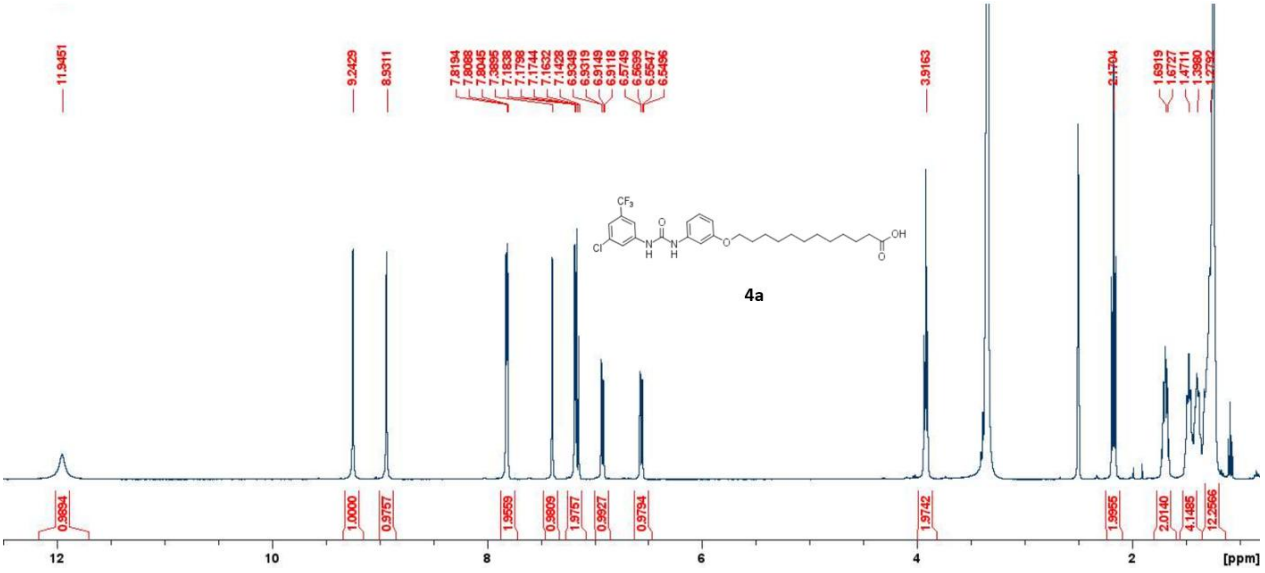

Figure S180. 400 MHz ^{1}H NMR spectrum of **4a**

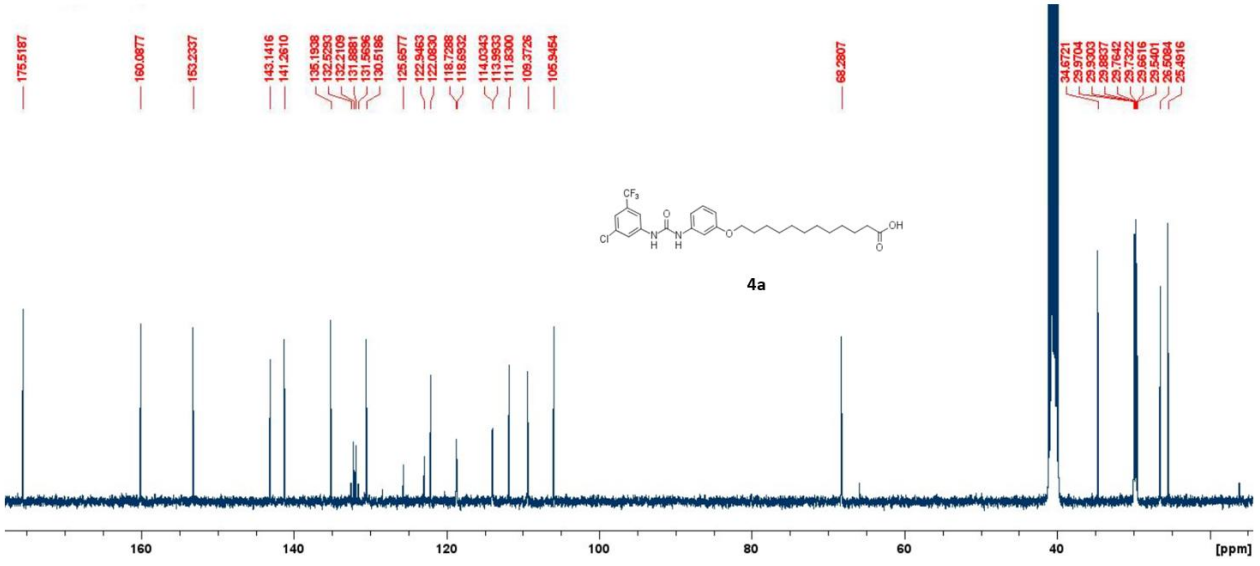

Figure S181. 100 MHz ^{13}C NMR spectrum of **4a**

12-[3-({[4-Chloro-3-(trifluoromethyl)phenyl]carbamoyl}amino)phenoxy]dodecanoic acid (4b)

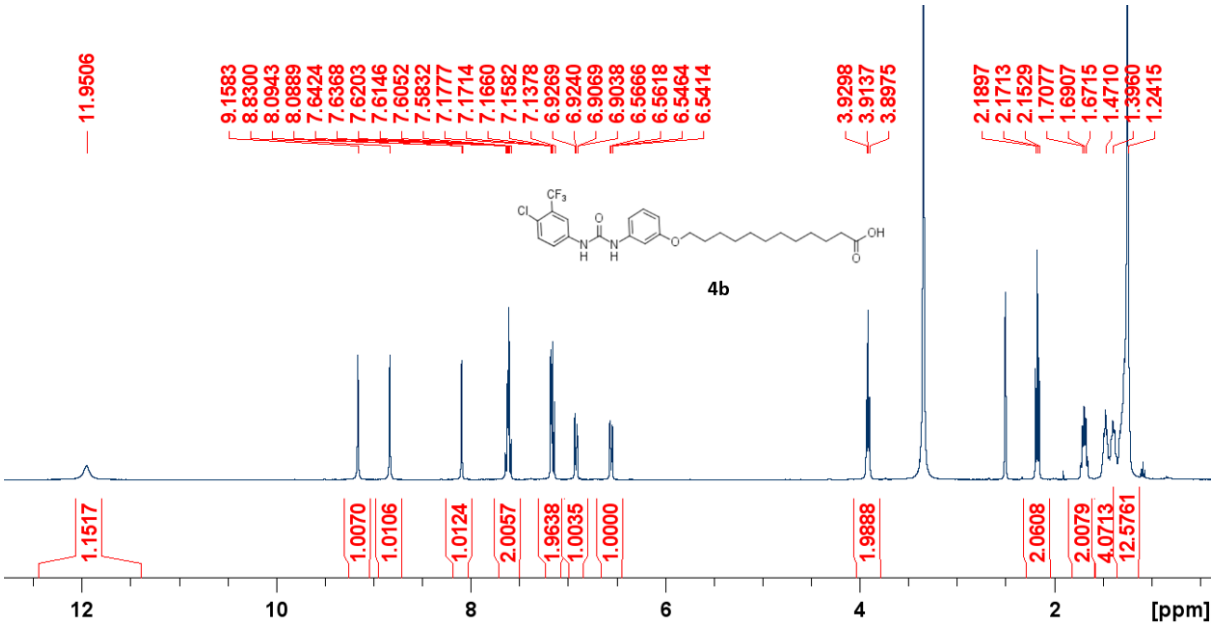

Figure S182. 400 MHz ^{1}H NMR spectrum of **4b**

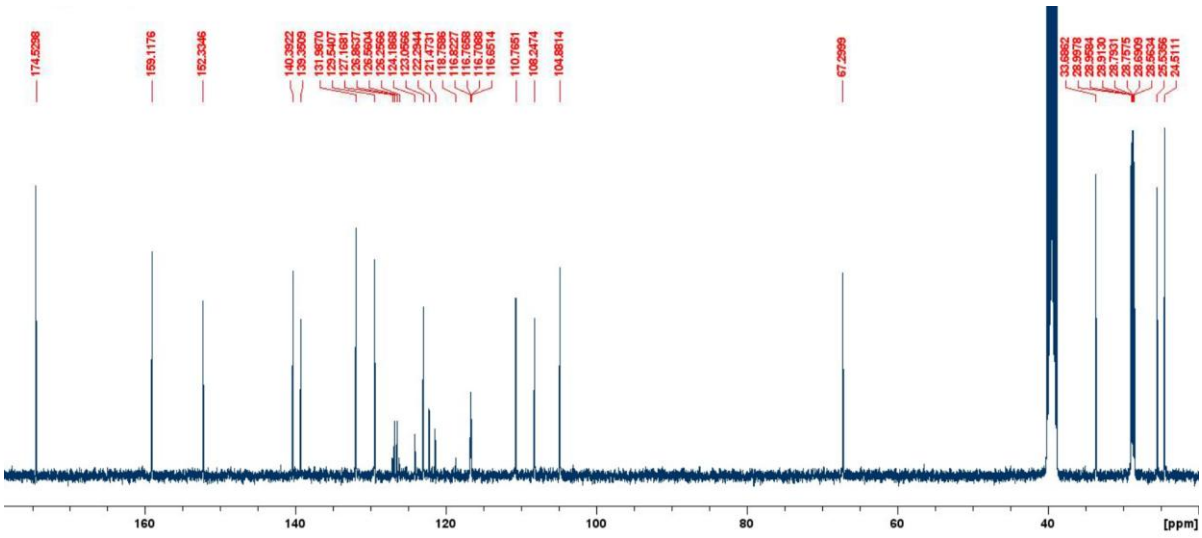

Figure S183. 100 MHz ^{13}C NMR spectrum of **4b**

12-[4-({[3-Chloro-5-(trifluoromethyl)phenyl]carbamoyl}amino)phenoxy]do-decanoic acid (5a)

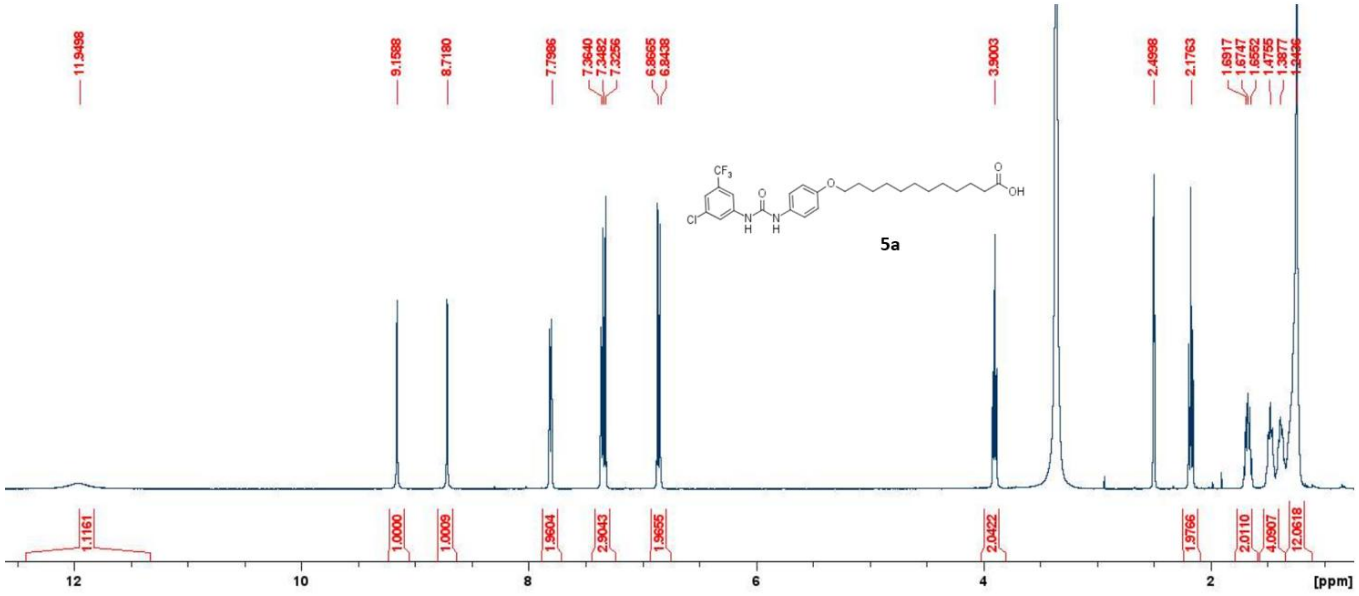

Figure S184. 400 MHz ^{1}H NMR spectrum of **5a**

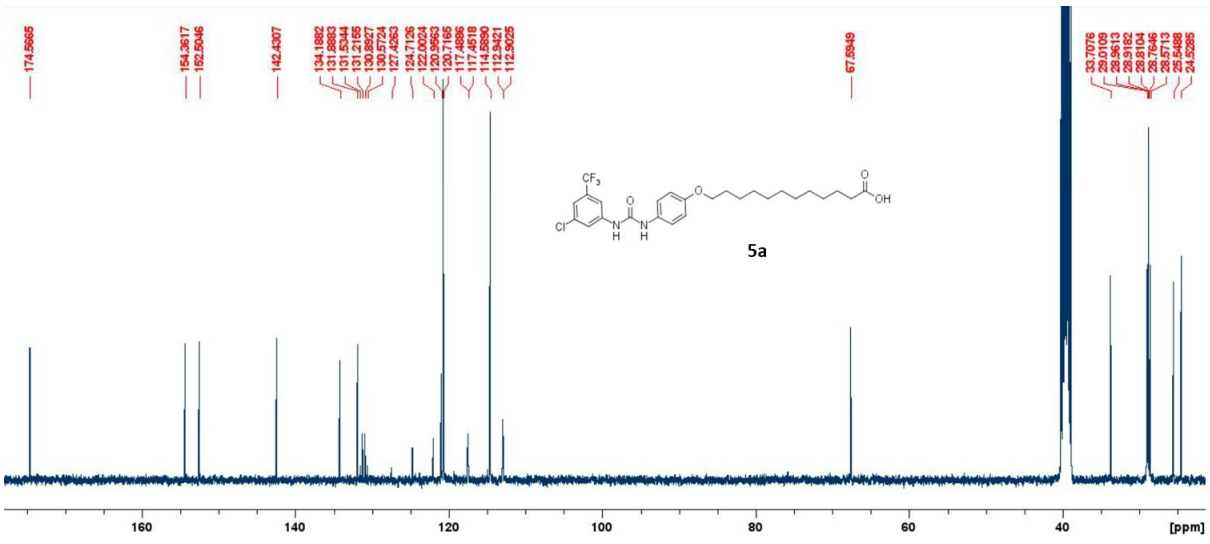

Figure S185. 100 MHz ^{13}C NMR spectrum of **5a**

12-[4-({[4-Chloro-3-(trifluoromethyl)phenyl]carbamoyl}amino)phenoxy]dodecanoic acid (5b)

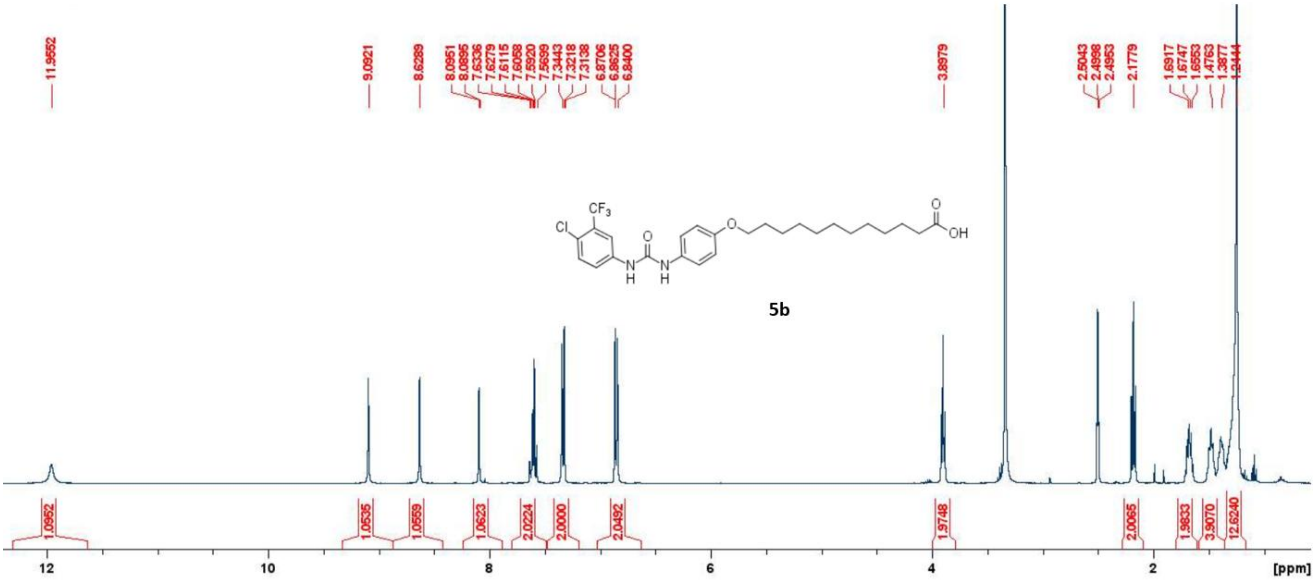

Figure S186. 400 MHz ^{1}H NMR spectrum of **5b**

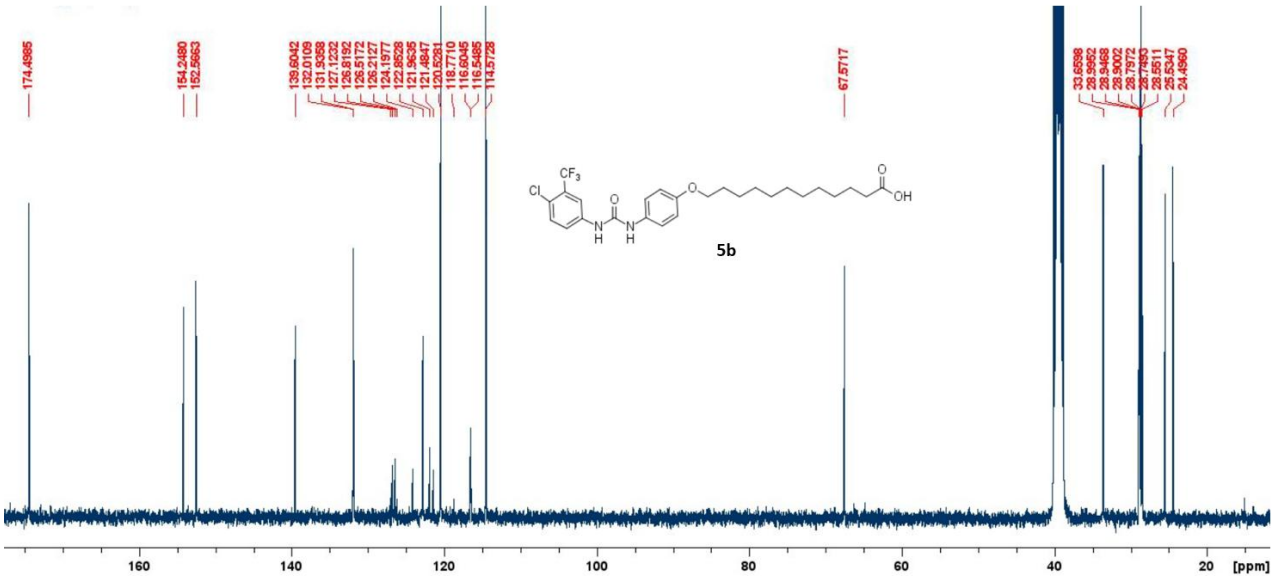

Figure S187. 100 MHz ^{13}C NMR spectrum of **5b**

S4.15 2a-5a Optimised Geometry XYZ Archive

2a Dianionic Dimer

136

Coordinates from ORCA-job /home/hzzeng/Desktop/ORCA/DazCalculations/CTUaDI--/01bb_DI_GeOpt2/CTUaDI--GeOpt2

C	-7.25194706169951	1.38841787876227	1.52161347990418
C	-6.39499053384323	0.29236793329615	1.52957025434917
C	-6.67241441597434	2.63840272902512	1.71409226036181
C	-5.30717988131517	2.81557184383844	1.91128853401182
C	-4.46422125322865	1.69127147267723	1.92206712322479
C	-5.03197366127916	0.41489041320163	1.72196309678192
H	-8.31679329786068	1.27114917558579	1.36511627904710
Cl	-7.07415596599989	-1.30507510934822	1.28100136752805
C	-7.55469226214030	3.85017906748128	1.77298646845205
H	-4.88411966092641	3.80226808324301	2.04164835376855
H	-4.38162580902653	-0.45530260599906	1.71512821560939
N	-3.10730283569061	1.73004146171199	2.14458311482194
C	-2.29589301265585	2.86409806590214	2.16734115479661
O	-2.68421952527212	3.99670223864506	1.88606045829127
N	-1.03185212728264	2.54903287440365	2.53236182659951
C	2.56832803026147	3.36843893192903	1.59916021964624
C	1.22902195465378	2.64214695855129	1.68156525800691
C	0.09722391193542	3.43236677841362	2.34029046564999
H	-0.81616319736508	1.57579621178790	2.80948468199651
H	-2.61426892452532	0.81248425807522	2.06679823762914
C	3.65642948184984	2.44247571869088	1.05512721249785
C	5.05021868627845	3.06210909991246	0.98495023714822
C	6.10603047959649	2.05562574148494	0.52837004742986
H	5.32644037147474	3.45366385624680	1.97414087225493
H	5.04040457335188	3.92331424312722	0.30216581739160
C	7.51738771778758	2.63283593358061	0.44478899152208
H	5.82068438214561	1.65094784957859	-0.45340072547436
H	6.10654867003418	1.20239117912105	1.22152630746477
C	8.56017414023779	1.60096012928620	0.01641930189607
H	7.79874623902136	3.04801760714342	1.42285614133363
H	7.52680833547582	3.47498351530305	-0.26152992156659
C	9.97499980293125	2.17127938948635	-0.06992046597038
H	8.27707181040493	1.18283669634287	-0.96031259033240
H	8.54935742178074	0.75934077202119	0.72401645955681
C	11.01786740523473	1.13782223384848	-0.49207172136587
H	10.25613730857477	2.59337996453519	0.90523322700881
H	9.98518562407167	3.00884450015642	-0.78174494498376
C	12.43211982891754	1.70863402626473	-0.59274848300547
H	10.73054290225460	0.70948968858753	-1.46314361014634
H	11.01256413456780	0.30393172262593	0.22447064337027
C	13.46875895513094	0.67172105087904	-1.02166403953187
H	12.72217613922761	2.13399124289588	0.37839988429662
H	12.43573020814132	2.54368189207080	-1.30765367374116
C	14.88816702950969	1.22768309958974	-1.13820140284278
H	13.17185617999542	0.24318810771171	-1.98975806776353
H	13.46471374569144	-0.16182775970861	-0.30438063723543
C	15.89609847523644	0.16733330680580	-1.57585619608542
H	15.19290091376996	1.65436437276892	-0.17200602521964
H	14.89499335413290	2.05916006425586	-1.85780658596799
C	17.32770794396384	0.68089214129056	-1.72302532828772
H	15.59191061040761	-0.26453856157448	-2.53612646880327
H	15.88442981270842	-0.66035292478495	-0.85158469246268
C	18.27817439511848	-0.43324523118252	-2.19057377195883
H	17.34992113679789	1.48699590025052	-2.46973654511558
H	17.70145301469982	1.09589955325706	-0.78157316855364
O	19.39718212473075	-0.51797140494983	-1.62084101315317
O	17.85280670237466	-1.18337831343654	-3.10618058944054
F	-7.79815493885611	4.23203657251791	3.04043807694190
F	-8.75332565932380	3.63835308328828	1.20203652332182
F	-7.00525716062996	4.90780745016244	1.15710403703888
H	3.36541440881189	2.09323179850157	0.05411092765871
H	3.69751680285349	1.54510757898484	1.68909099153502
H	0.90346059640442	2.34105779337067	0.67677136346797
H	1.35907303481102	1.71149611904804	2.24945985757357
H	0.44175974096724	3.84183931509574	3.30158894357880
H	-0.22571129134907	4.27732958870756	1.72449952544833
H	2.85860835279190	3.71989366403443	2.59933593329707
H	2.48334090499236	4.26237392628804	0.96565945993397

C	24.72351499148692	-2.59598609025434	-0.84719207293761
C	23.88310298829242	-1.49816205202208	-0.98923491776233
C	24.15995531708074	-3.85111299726812	-1.06317717709120
C	22.82577237494290	-4.02925471720282	-1.40725811967422
C	21.99778016455478	-2.90099926475729	-1.55015364164829
C	22.54831409815230	-1.62181986915962	-1.32995148932635
H	25.76774920587985	-2.47787120506591	-0.58501854214240
Cl	24.54417059601426	0.10519904012551	-0.72977027172281
C	25.02205852304508	-5.06054434026977	-0.85254305600192
H	22.41475539841489	-5.01674910644072	-1.56238323230456
H	21.90937166870395	-0.74873450420697	-1.42827435518458
N	20.67566486949073	-2.94383965291499	-1.93076253852916
C	19.85958157987121	-4.07352836062565	-1.97522352253486
O	20.20969705635844	-5.19049496368268	-1.59809972668776
N	18.64048987031035	-3.77722427115435	-2.48401956409147
C	14.99289805500344	-4.56233702134601	-1.70167291657518
C	16.33716868872437	-3.84118178865441	-1.73547948756796
C	17.49104659029975	-4.64408941273071	-2.33805760174107
H	18.44749971430127	-2.81050994921954	-2.79802074021491
H	20.18740077107207	-2.02081619878505	-1.94808218326531
C	13.88655960384238	-3.62825084390581	-1.21154254352302
C	12.49137268079237	-4.24782089895977	-1.17811173838568
C	11.42439341367382	-3.23864400686946	-0.75548086668383
H	12.48236165259089	-5.10472201274983	-0.48989456714810
H	12.24303131357190	-4.64559480534934	-2.17219589333410
C	10.01087084125304	-3.81361024458225	-0.69977585045017
H	11.44032760675850	-2.39015935096306	-1.45408022303599
H	11.68668096436438	-2.82785355389762	0.23015302978042
C	8.96506891766574	-2.78030853288693	-0.28249582745290
H	9.98754585279183	-4.65842219353016	0.00303764880175
H	9.74490412263761	-4.22402958818239	-1.68410847996877
C	7.54765333550522	-3.34607395770495	-0.21367764862400
H	8.98716756596561	-1.93570179172666	-0.98632043011121
H	9.23750881407118	-2.36723506077154	0.69939339573455
C	6.50763082370147	-2.31404988354503	0.21870409027289
H	7.53012741767275	-4.19280315215885	0.48709283849226
H	7.27015656000706	-3.75406444504693	-1.19581893240049
C	5.09273132812588	-2.88283861757772	0.31925066848799
H	6.51318120336551	-1.47281490511813	-0.48931481489813
H	6.79811384922361	-1.89609755443285	1.19337447646044
C	4.06418556760317	-1.85196968286485	0.78056044997171
H	5.09339314563257	-3.73164070235434	1.01778601930045
H	4.79219623610249	-3.28820579029593	-0.65721457667839
C	2.64693752472009	-2.40916705414936	0.91504941266680
H	4.05650544277870	-1.00691315014014	0.07687137957497
H	4.37842338945200	-1.43919641420485	1.75006432559981
C	1.65412498632100	-1.35978713658288	1.40949040848786
H	2.65621108866116	-3.26027082496912	1.61131553538188
H	2.31710392270077	-2.80812495448441	-0.05472155893851
C	0.22665869167462	-1.87398496496730	1.58828791863485
H	1.64559221409763	-0.51307698585232	0.70762524894893
H	1.98831888883317	-0.95449965222021	2.37128288410206
C	-0.69960514618038	-0.77436929158696	2.13224834562556
H	-0.18319773996038	-2.25278880466407	0.64664688668853
H	0.22771337669592	-2.70684955460442	2.30541036881580
O	-1.83888982671390	-0.66334363294306	1.60938199595856
O	-0.23518900207331	-0.06040292249793	3.05803842269830
F	25.02036658967585	-5.46173327737199	0.43199251801643
F	26.30768271919242	-4.82374264010701	-1.17128327906911
F	24.62150585978580	-6.11132809008241	-1.58258061678043
H	13.86735217928721	-2.74083409053112	-1.86039942180596
H	14.14310871100998	-3.26306142937551	-0.20674319982180
H	16.23586092898008	-2.91574769138278	-2.31728644719347
H	16.62174249931571	-3.53258833543601	-0.72050135825487
H	17.77634849985703	-5.48929183713912	-1.70474774379642
H	17.18783698642094	-5.05279179603772	-3.31312798913256
H	15.04870602007597	-5.44973216972690	-1.05580772672394
H	14.74284453658247	-4.92368495249697	-2.70919734172309

3a Dianionic Dimer

126

Coordinates from ORCA-job /home/hzzeng/Desktop/ORCA/DazCalculations/3aDI--/01b_DI_GeOptb/3aDI--b

C	20.79393528339680	-4.54380627938811	-2.99330435387677
C	20.04139739625438	-3.73583547689603	-2.14583014030991
C	20.18030479598477	-4.96337614367339	-4.16713263240101
C	18.87904819255469	-4.60567121295202	-4.50963741284139
C	18.14280776526317	-3.78804969549406	-3.63810240749627
C	18.74594910767207	-3.35470522329970	-2.43756444554088
H	21.80635609855678	-4.83402325968613	-2.74296362013903
Cl	20.76939402183222	-3.18615149402093	-0.64961571443481
C	20.94825856306612	-5.80716924482039	-5.14107638154078
H	18.42854539037020	-4.95827541042034	-5.42697722276824
H	18.17308911798472	-2.73260318498418	-1.75508303829106
N	16.85088250648741	-3.35111143630875	-3.85781395683848
C	16.01765218236451	-3.71361335528400	-4.90304731395508
O	16.32317539840264	-4.51422744121431	-5.78193536454235
N	14.81953442329962	-3.05817255246979	-4.81468032677242
C	13.56642630299036	-4.16635181639993	-6.65059517803810
C	12.34335309985546	-4.30135716224151	-7.30324070183357
C	11.22157212503177	-3.57405512240264	-6.91187482803579
C	11.31649519444266	-2.67872242929820	-5.84211636688508
C	12.53593080193462	-2.53805017688841	-5.18591518408324
H	12.27020417597013	-4.99329489747173	-8.13811125143840
C	13.66726733409332	-3.27536151146513	-5.57096177365134
H	14.43262218486960	-4.73342916934570	-6.96086548111145
H	12.63075646880873	-1.85052811427910	-4.34678608122107
H	14.72115425356751	-2.32686885740673	-4.07811219796101
H	16.43936220870485	-2.80191691536851	-3.06648599301082
C	10.11854169211413	-1.90429650226671	-5.34211897194644
C	9.55962197881616	-2.48102464085000	-4.03440608833321
C	8.43319505374670	-1.63988717288708	-3.43673636608729
H	10.37657619901520	-2.56027609049731	-3.30542388286386
H	9.20612429803560	-3.50512689095273	-4.21564120278279
C	7.86303447301887	-2.24067368016167	-2.15219136982360
H	7.62661597423075	-1.52198783115719	-4.17437964942485
H	8.81226425989643	-0.62922210391388	-3.22846762411070
C	6.80359545949441	-1.36412540626554	-1.48545763049957
H	8.68305710813887	-2.41522802119808	-1.44162002711829
H	7.43334371060064	-3.22787722001863	-2.37366515705212
C	6.18917092650622	-2.00627953880520	-0.24195477868426
H	6.00650775988249	-1.13739104705999	-2.20767231823888
H	7.25442482303822	-0.39927906865930	-1.21321141141016
C	5.20440903245618	-1.09635628738725	0.49140500681322
H	6.99179065115139	-2.29900415044842	0.44945433661575
H	5.67971091443016	-2.93653061655846	-0.53113116773548
C	4.51773737568776	-1.77689766671183	1.67578188429028
H	4.43984664778822	-0.73983948158523	-0.21329215024993
H	5.73562359008740	-0.20076813589277	0.84520060330639
C	3.61655124779791	-0.83236774531637	2.46925579839257
H	5.28216017044593	-2.19764668788278	2.34482795133146
H	3.92983261606512	-2.63088405777264	1.30945456701730
C	2.89337659937642	-1.51473048503250	3.62484517516304
H	2.87638630429688	-0.37184742319042	1.80382735071353
H	4.21625590069121	-0.00289083940804	2.86458202436312
C	2.07548617026817	-0.56050742159754	4.50521229968480
H	3.60548825871134	-2.03183426248620	4.28017059948689
H	2.21372489209540	-2.29279182748764	3.25225912590090
O	1.58500717872268	-1.04435549610535	5.55914564436200
O	1.95794262738115	0.63045413575134	4.11922243127221
F	22.08141951970268	-6.29972367976364	-4.61266897627362
F	21.30467236629367	-5.11002649529665	-6.23450127134957
F	20.22973635117182	-6.85438351261022	-5.57659905456667
H	10.27568409531784	-3.69645458966321	-7.43339984353510
H	10.40509210289090	-0.85879138280756	-5.17021331905568
H	9.33033327181079	-1.89918881696766	-6.10529504950505
C	-2.02291585926569	-1.35985940747820	9.92112268621528
C	-1.36755721890294	-1.95624534564128	8.84713781228050
C	-1.84296405647614	0.00807677522684	10.08345315786517
C	-1.05185336477630	0.77219273401555	9.22947612093668
C	-0.40164449896461	0.14640526378843	8.15443277559067
C	-0.57117129928647	-1.24306927848867	7.97218003386155
H	-2.64154810911179	-1.93885773253869	10.59473674606279
Cl	-1.56262687671149	-3.68047888793948	8.60109035487285
C	-2.50479752363359	0.71831065158148	11.22803994767581
H	-0.92919678846127	1.83443570649888	9.38936625207070
H	-0.06317248888926	-1.73185768657569	7.14516476019885

N	0.39571515093152	0.78716378512634	7.22594098358032
C	0.81144215158633	2.10775643942587	7.26654097830983
O	0.53751518005744	2.88660319151384	8.17490769276892
N	1.56243124552001	2.41410646876772	6.16427230202453
C	2.29517637697473	4.71268537396147	6.75423252578233
C	3.08788225697975	5.80334045406858	6.40506679840004
C	3.87415336468326	5.79719859175932	5.25549653061020
C	3.86971007668538	4.67534187771907	4.42113155191412
C	3.07806579322975	3.58255200420373	4.76253948488648
H	3.08782670644915	6.67731839911279	7.05101681652969
C	2.29071843345375	3.58036423985637	5.92505853628887
H	1.68774336485335	4.72572020219397	7.64791337770911
H	3.06380793409087	2.69679691231416	4.12918453749215
H	1.64075550351345	1.69353755351631	5.41490304619826
H	0.83742681231936	0.15471154757816	6.51675681369520
C	4.74948581348418	4.59178598112788	3.19532820956549
C	5.98226388418212	3.70892622709289	3.43061201126814
C	6.82128302256957	3.49425803265580	2.17260969817327
H	5.65110743012843	2.73482737189555	3.81359598567304
H	6.60000713140477	4.15787703326316	4.22025637276236
C	8.05942703647105	2.63627400016477	2.42880255084825
H	7.12830543806878	4.46590936150767	1.76015570345582
H	6.19906408183877	3.01442626592643	1.40376681819076
C	8.86142319558845	2.32747237452840	1.16561383540982
H	7.75125576870926	1.69128917508367	2.89787038675553
H	8.70743804904422	3.14347169367166	3.15758661019288
C	10.13145874616786	1.52463378828429	1.44409643697503
H	9.12896144076972	3.26649516563213	0.66065601188853
H	8.22546327271291	1.77147388009835	0.46221704116909
C	10.88362182937730	1.11691025275726	0.17854437189185
H	9.87148665974123	0.62190392869848	2.01461978125956
H	10.79686266966439	2.11455429208612	2.09041870779079
C	12.19672795413070	0.38766149634689	0.46163397493556
H	11.08987452259317	2.00925535782226	-0.42928551726776
H	10.23621282836624	0.47243812965417	-0.43385767517945
C	12.89205889951509	-0.10116106282797	-0.80736254078740
H	12.00021140641885	-0.46882069548517	1.12251709980001
H	12.86837441407783	1.05612154262653	1.01941230161691
C	14.22115895436859	-0.79687442989645	-0.53942221223702
H	13.05804478166615	0.73979234413923	-1.49156420633975
H	12.23019694526922	-0.79283953866252	-1.34338319732515
C	14.88020928174751	-1.39224664400372	-1.78987209067408
H	14.09476376109964	-1.61444282006500	0.18171301631852
H	14.93849201564180	-0.10412877983371	-0.07968295569427
O	15.92116719034716	-2.07695150427221	-1.60923359294580
O	14.33473636586023	-1.16357561392775	-2.89935906110810
F	-3.30085628630362	-0.09114022835326	11.94645334609188
F	-3.26473804914881	1.74451911288614	10.80958509680045
F	-1.60702138180206	1.23852080472641	12.08200397725581
H	4.48848652595774	6.65773117686430	5.00284360110221
H	4.17371735276738	4.17558655090909	2.35877294021153
H	5.07180778571134	5.59655686770595	2.89502041928589

4a Dianionic Dimer

134

Coordinates from ORCA-job /home/hzzeng/Desktop/ORCA/DazCalculations/4aDI--/01_DI_GeOpt3/4aDI--GeOpt3

Cl	23.85854855121871	0.06977685321591	-1.32461507639543
C	21.88674597709846	-0.65212081181712	0.38174864876749
C	22.26310149816382	-1.26055149263901	2.69810977596772
C	24.56747665138086	-1.32628128926088	3.62711875242577
C	21.37432183656394	-1.06423883764103	1.62824456955707
H	21.19980049995467	-0.48924738753132	-0.44405465244409
O	19.70658483699905	-1.45494242623549	3.97513681044872
N	20.01017451779371	-1.26619115777418	1.69057604183533
C	19.25513229602947	-1.47720993051021	2.83495686079126
H	21.88420412976757	-1.55965229866380	3.66486959885950
C	16.88699236315478	-1.64262595609897	4.74534165355637
H	17.84311202526066	-1.64525996185482	5.24877246915014
C	15.69368703000120	-1.59833979563328	5.45527446529357
N	17.94775717435191	-1.70641303936427	2.50211195833498
H	19.49095428520938	-1.03434989166969	0.81350134849549
C	16.83468004953430	-1.68343392490955	3.34092664379315
H	15.73166194646112	-1.56923116423222	6.54079985929208
H	12.05338371114221	-0.58179897583652	4.01589876359183
C	14.44661159103733	-1.59036405804693	4.82757903034323
H	17.73399515319594	-1.84778571159981	1.49085443504061
C	15.59242996846867	-1.68436713415345	2.69727927992028
C	14.41038599454416	-1.62918843223127	3.43063422315922
H	13.53882671628773	-1.55503996992825	5.41752182201234
H	9.52975423799534	-0.42003966005676	3.67411907238055
H	15.54858400615691	-1.71202707371267	1.61201088932636
O	13.26783670768822	-1.60479630734608	2.68961966606197
H	11.13913666937164	-0.44247366869930	1.71925352281212
C	12.03453910174123	-1.47007467877876	3.36784189888665
C	10.94170267225861	-1.33717611503802	2.32239048129929
C	9.55490478007562	-1.25114466912384	2.95550842498535
H	7.00990046256260	-0.23742439187780	3.32318432798765
H	8.60116850027386	-0.12386090473030	1.38096912326433
H	11.85601918466686	-2.34760521030146	4.00736591070762
C	8.43668899981257	-1.06061859118755	1.93176291547663
C	7.04993476487995	-1.03858999414215	2.57169012883641
H	4.47942000968843	-0.07648072489395	2.98258912945801
H	9.36180040269681	-2.16523523035540	3.53406155373139
H	6.05489374160706	0.10846584109507	1.03703911291035
H	10.99463122760407	-2.19780879623008	1.64446304981669
C	5.91559579468354	-0.84427114696383	1.56783292624904
C	4.53282563372545	-0.86440649402578	2.21796942954722
H	6.89089225274993	-1.97938265876254	3.11748233044327
H	1.93015393468443	0.04953923559979	2.62692038222295
H	8.48211725022194	-1.86859704506326	1.18795879893017
H	3.52537216250936	0.28120423933947	0.69358455801245
C	3.39645681326069	-0.67712276892757	1.21627285689012
H	4.39711823468486	-1.81756479259003	2.74857122886667
C	2.00407959311910	-0.72019840130920	1.84516314794475
H	5.96773403884269	-1.63268745297366	0.80325588780662
H	-0.64336094784230	0.23853457123093	2.11758184540114
H	1.04389158268138	0.46667966545787	0.32102600388324
C	0.90516990669071	-0.50422403889338	0.80896360180236
H	1.86032580206960	-1.68700947007218	2.34823109115500
C	-0.51761013697057	-0.55210148815304	1.36525248590058
H	3.46340535135062	-1.45612261848786	0.44360735918392
C	-1.53738158812818	-0.32378071547586	0.24287550713402
H	-0.72737709800043	-1.51019611930122	1.85102114256228
O	-2.52559800661441	-1.09719564477368	0.17211784287232
H	1.00488403123521	-1.26079570137797	0.01752367508117
O	-1.28600103028304	0.62226636252581	-0.55117596362809
F	24.01432401258868	-1.09533531686914	4.82615707363333
F	25.68136781189586	-0.57674213934256	3.55185381743499
F	24.97336866659062	-2.60941115892039	3.63271556758551
C	23.62170138523678	-1.04553198604816	2.49683971039561
C	24.14831491005228	-0.64020930059607	1.27418231567590
C	23.24686873086655	-0.45090222709010	0.23270189101298
H	25.20960099081020	-0.47114933288490	1.13950373237653
Cl	-7.39491438581799	-2.64613886274736	0.78457901462493
C	-5.51708687827401	-1.78268348317097	-0.96274179822678
C	-5.76222516980574	-1.89949701036281	-3.37212232392582
C	-7.85000820672175	-2.82780437879031	-4.37441688410735
C	-4.99491578391073	-1.54345039976892	-2.24888424204054
H	-4.91925427736965	-1.52472194157339	-0.09328641701970

O	-3.30424589082644	-1.11435800775486	-4.56189332583064
N	-3.74387195418354	-0.95771034451620	-2.29994849446666
C	-2.96654939970546	-0.77462230316828	-3.43248963101290
H	-5.36960151058835	-1.73650103764421	-4.36474304233242
C	-0.62479664481677	-0.28424112079628	-5.30778947635451
H	-1.54080083458014	-0.52504775844192	-5.82719363314528
C	0.58360867004219	-0.17620929151347	-5.98409267432466
N	-1.77947397155307	-0.17069404575932	-3.11418624504124
H	-3.26998542874162	-0.87343823056997	-1.37184874729221
C	-0.64144392200422	-0.07736227192573	-3.91723687870530
H	0.59742084253391	-0.33075092531216	-7.05950862846329
H	4.23403881115527	1.34270005824552	-4.53504542526876
C	1.78145985233656	0.12394452353284	-5.33385421720330
H	-1.65491207772593	0.17447395952821	-2.13839846989472
C	0.54986347879141	0.23421176700321	-3.25235792514530
C	1.75233330790854	0.32064067891348	-3.94998275906623
H	2.70340371785165	0.19993024173111	-5.89725381648076
H	6.73999472053132	1.48007461754339	-3.94233487103586
H	0.54212795077928	0.38840519762020	-2.17680642992316
O	2.85273923122242	0.58610760574076	-3.19106701051110
H	5.03576200266998	1.49737485015097	-2.14220649329890
C	4.11984783904729	0.51710627929730	-3.81639801459933
C	5.18648517290375	0.58923360950626	-2.73819661055266
C	6.59068247445997	0.57367182463111	-3.33942074562599
H	9.23985016922758	1.44283665597666	-3.45308213998154
H	7.60947008130990	1.29639310121812	-1.57440616475194
H	4.21354906650606	-0.42613475541430	-4.37335229166025
C	7.70160252918229	0.47171378562865	-2.29510158105288
C	9.09471956280326	0.49119956541412	-2.92253718301195
H	11.77453789792975	1.28651356239806	-3.04952473251088
H	6.67941152299131	-0.27463580180505	-4.03277417155823
H	10.17478886314820	1.07328835946566	-1.14403931010763
H	5.05565376666981	-0.26438483175770	-2.06171904101668
C	10.22751174844343	0.29356439937546	-1.91733676173086
C	11.61091050728962	0.31249286727430	-2.56699606708296
H	9.15436482708136	-0.29728141631646	-3.68620300794932
H	14.35720887954044	1.01485768190472	-2.62971418919914
H	7.57323398593977	-0.45654172627395	-1.72056723860760
H	12.72136248311557	0.78087394097177	-0.77667951769389
C	12.74225821154813	0.03209073256833	-1.58100585397900
H	11.63986441961765	-0.43730222468776	-3.37043450895582
C	14.13174386240733	0.02044442342115	-2.21914462200437
H	10.08659738695891	-0.66506277903710	-1.39755305668908
H	16.96254878306839	0.54421286533817	-2.12636974692780
H	15.19024370139326	0.27890564901067	-0.35872440392990
C	15.21030744156099	-0.39896671353786	-1.22408186734788
H	14.13474505008517	-0.67424862673572	-3.07162348656762
C	16.62819870193510	-0.44311954758938	-1.79316041604147
H	12.56489316102838	-0.93897308335977	-1.09726410928998
C	17.61365379162353	-0.98635373625279	-0.74972438618936
H	16.64962024737093	-1.11298185433856	-2.66399700263906
O	18.70863616757568	-0.38913202960499	-0.59449772228107
H	14.97693199245542	-1.39629965898149	-0.83616368217162
O	17.23231489049766	-1.99985055213393	-0.10363870209447
F	-8.80964841400217	-1.90917509173929	-4.59248120760922
F	-8.48548699521787	-4.00296698078160	-4.21283882352299
F	-7.13595809608499	-2.91716603928124	-5.50391946739556
C	-7.00886888729943	-2.48140563349399	-3.18149725280437
C	-7.54436769178117	-2.72352379139902	-1.91906732225242
C	-6.76803916967608	-2.35855752627661	-0.82647601440477
H	-8.51742153726650	-3.18309107425132	-1.79210746682988

5a Dianionic Dimer

134

Coordinates from ORCA-job /home/hzzeng/Desktop/ORCA/DazCalculations/5aDI--/01b_DI_GeOpt2/5aDI--GeOpt2

C	-6.20337895306595	4.53257713388281	1.88696483043405
C	-5.75146142563928	3.44580980489351	2.62664764081917
C	-5.48088332567227	4.86274068151093	0.74437691243654
C	-4.35601212407721	4.15552681695001	0.33401062624122
C	-3.92350659032253	3.05867062223892	1.09762777293313
C	-4.63964756588399	2.70992915202165	2.25974793652593
H	-7.07411628649108	5.09953931150842	2.19255543020174
Cl	-6.62127524443414	2.99858851199353	4.08031580895820
C	-5.98276064175771	5.98424524703411	-0.11712939533659
H	-3.80756864526895	4.44727016136633	-0.55058827730001
H	-4.29759489672987	1.87043953013386	2.85837928000907
N	-2.84585746239954	2.25375026737339	0.78269001269936
C	-1.84447039051660	2.53889372420062	-0.13310583049141
O	-1.76090446843549	3.58879140612007	-0.76120347522482
N	-0.97192278007015	1.48771545115639	-0.23125416082669
C	0.92559018586287	2.60124477312920	-1.38059665741786
C	2.24671853831684	2.50700521282154	-1.81718927216329
C	2.96213494524815	1.32113678603071	-1.68608745873000
C	2.34376536704529	0.20541372472935	-1.12144110227513
C	1.03288045012908	0.28918996107658	-0.67614098357233
H	2.73599542118791	3.36445603332776	-2.26999878177126
C	0.31213976265024	1.49231934897848	-0.78220644035896
H	0.37364519110797	3.52498551030148	-1.48728861520791
H	2.89767239787025	-0.72532541944423	-1.03387598117953
O	4.26733488036133	1.25177117930314	-2.12498780912662
H	-1.23922156591609	0.60346954157387	0.24323250593752
H	-2.63936379783139	1.50653667099610	1.48335859408986
F	24.60327581257313	-2.48410929580817	4.02059918132571
C	5.22240485399722	1.36326707322040	-1.07518757898903
C	6.61179379816212	1.32471024954598	-1.68367989551508
H	13.85823509145927	-1.39081442574705	0.27981090903475
H	5.06368943676962	2.30776139481417	-0.53327923956362
C	7.71454633804912	1.48016105518566	-0.63623470098149
H	6.68570454568478	2.13185022575434	-2.42307199638844
H	6.73497533250356	0.38068037424431	-2.22841901669005
C	9.10781359714679	1.55950543370062	-1.26044776168570
H	7.67367743158322	0.64343796841745	0.07497304985498
H	7.53306602130869	2.39268655472869	-0.05152860478949
C	10.22636819856170	1.81046404586193	-0.24833318090482
H	9.11478130652563	2.37031976460040	-2.00248574605758
H	9.31477449398713	0.63427404176833	-1.81569361913057
C	11.58374599637458	2.02772831017636	-0.91748418270417
H	10.28717064196406	0.96941101339110	0.45668238509979
H	9.97601101089336	2.69799199586078	0.34982620860673
C	12.71140554117351	2.38947004284831	0.04984227079969
H	11.48383332030451	2.83368259858178	-1.65881823913448
H	11.86260433074690	1.12711914005332	-1.48248528607926
C	14.00932892546608	2.74596228234919	-0.67482012770651
H	12.89194145347713	1.55578011910223	0.74259209456745
H	12.39717011710488	3.24267276650416	0.66769172588992
C	15.16070163284515	3.13161202479844	0.25259147794909
H	13.81011721208474	3.57573482179280	-1.36921138436550
H	14.32364098747085	1.89561216305390	-1.29680027393116
C	16.39741087504993	3.60035741298648	-0.51591150083103
H	15.43477686235467	2.27057996927392	0.87425787114283
H	14.83141900583974	3.92771343537238	0.93625667187058
C	17.62201185836394	3.78377683864218	0.37457635712087
H	16.16370683561782	4.54016528595804	-1.03457115146857
H	16.64128768349968	2.85634659072880	-1.28215022989695
C	18.19401034290478	2.46375997497697	0.91244239683058
H	17.39987274465465	4.42713704102363	1.23430217627817
H	18.43116923846358	4.28067445755533	-0.17612829284534
O	17.80765969099819	1.39732851076716	0.36647338383295
O	19.02333545158930	2.54882163987370	1.85452966156800
C	23.82169303810864	0.58284498205758	4.32186195230808
C	23.12195270745609	1.62152418257939	3.71804867234363
H	24.82013492030638	0.72911817752409	4.71534056678259
C	23.17611007322157	-0.64720992888732	4.40169507669013
Cl	23.88950759965174	3.19198982297126	3.59707894939114
C	21.84514160329653	1.46207871222071	3.21119204514596
C	21.89284182896267	-0.85841956286680	3.91100373433675
C	23.92515079573694	-1.81545402971369	4.97171022693249
C	21.20937452998377	0.20712486967422	3.30132418875150

H	21.31778182396420	2.28964053519298	2.74478351432765
O	19.28597952288953	-1.95973959956869	3.50672350185775
N	19.94856853796166	0.11974442888465	2.74742701634922
C	19.07947510008906	-0.95640385712029	2.83046150743119
H	21.41448442550901	-1.82314766474731	4.00117944289427
C	16.53022382532754	-2.60749760533760	2.81751614476889
H	17.27776740349150	-2.95339034273562	3.51771670618542
C	15.29733348312344	-3.25129797308422	2.71666921653972
N	17.97253063566185	-0.73746390741137	2.05823186054979
H	19.57811068117629	1.01084613235051	2.34035826123862
C	16.80242157343331	-1.49580246522329	2.00785808922425
H	15.07573451709352	-4.10913794310204	3.34527388075140
F	-4.99340576448005	6.61482022042199	-0.76498998591143
C	14.33605819231856	-2.81227686929326	1.81336259220679
H	17.99089222644955	0.08050314099452	1.41134375237748
C	15.83060028149463	-1.06796276520744	1.08464545212419
C	14.61077366849386	-1.71935543536630	0.99144909852305
O	13.11299658279319	-3.44178404211160	1.72034452803476
H	9.80015184178712	-1.74166286502152	3.21816310481147
H	16.05529793177253	-0.21176706172885	0.45304649332334
F	24.83263905227321	-1.43700058049924	5.88923028322357
H	10.60278871796182	-2.98276582899409	1.09566786662564
C	12.12934576322359	-2.87323661900523	2.57737826682035
C	10.75946674001724	-3.33620630220664	2.12258673057964
C	9.64694830185749	-2.81379956942410	3.03063870492195
H	7.33902852318901	-1.57800775649316	3.75458492607155
H	8.19760973567389	-2.44191942513062	1.49087144846615
H	12.32419156243138	-3.17127570522521	3.61929953239410
C	8.25790506180190	-3.01221384855239	2.42863223874021
C	7.12103590253434	-2.57727637560261	3.35239239480074
H	4.82268157517481	-1.31402064836432	4.13906279314511
H	9.70461635360726	-3.30951360556786	4.00916084719394
H	5.82670375081750	-1.80123565677257	1.82589165597311
H	10.74067342286624	-4.43221670042283	2.08955484149935
C	5.77283787417072	-2.54239361747495	2.63655127821679
C	4.58707077533322	-2.20450094329539	3.53959718677840
H	7.06998578748736	-3.25380931022390	4.21684715102667
H	2.26467482695925	-0.94062128306867	4.33363041354884
H	8.12114788791502	-4.06739344633136	2.15408918628142
H	3.48766551663156	-1.07450334482379	2.08453333177059
C	3.31658290517963	-1.94582538813249	2.73314011674029
H	4.42147488944269	-3.02384599017125	4.25303357450848
C	2.05747774842126	-1.69753026666437	3.56402029187934
H	5.59042455413138	-3.51114030344370	2.15035117111913
H	-0.33302649049808	-0.38994519030534	4.26234201265483
H	1.20432180530380	-0.28046124814064	2.20156686471886
C	0.90883713305925	-1.22666745288160	2.67593841249912
H	1.77724161198622	-2.61633153635332	4.09844711822937
C	-0.43419392789833	-1.02437375875401	3.37608280687006
H	3.13540658612987	-2.79389811068798	2.05736808760889
C	-1.43259834491275	-0.36825225176624	2.41136846655501
H	-0.83417904391010	-1.99256081861608	3.70622465636778
O	-2.14098427635263	0.57315364322129	2.85029340995647
H	0.76148709794236	-1.93611388790320	1.85333004503241
O	-1.43429088230414	-0.79572478554698	1.22487451335260
F	23.11354086240722	-2.70581007368724	5.55951835681591
F	-6.64581719677156	6.91216329585916	0.59537562882359
F	-6.84059280007041	5.54556290213980	-1.05671225060982
H	12.18934818142227	-1.77622249640930	2.53130748206608
H	5.08765919400390	0.54260989515235	-0.35407768040286
H	0.54518068145514	-0.56646093694167	-0.21595267557199

2a linear monomer

68

Coordinates from ORCA-job /home/hzzeng/Desktop/ORCA/DazCalculations/CTUaDI--/06_MO_GeOpt1/CTUaMO-GeOpt

C	-6.50278681359339	2.74405422999252	-1.68354601901975
C	-6.27249456379017	1.41100916014105	-1.37328761087023
C	-5.58823522871420	3.67690084329883	-1.20342403121482
C	-4.47985472664126	3.32270542010746	-0.44362182824312
C	-4.27036146557748	1.96891656945524	-0.14511008681128
C	-5.18018281206228	1.01267247283141	-0.61881910326942
H	-7.35772711144598	3.04289018304040	-2.27848925599714
Cl	-7.38107418451850	0.19438206261897	-1.95245634318055
C	-5.85753498567248	5.13235954149993	-1.46985969838085
H	-3.78511304419977	4.07066214353113	-0.09035986827819
H	-5.02968948141760	-0.04015886679785	-0.40088135365095
N	-3.20164695148392	1.49651427989888	0.61526744172309
C	-2.12189303790555	2.22171510133614	1.10591562768558
O	-1.97327434937531	3.41911676184485	0.91936850259393
N	-1.26071936847571	1.46151041393947	1.84597514489482
C	2.49181799535062	2.26816662095052	1.85931940479313
C	1.15482776012797	1.76593626564717	1.31823886910963
C	0.00952019413038	2.00410082664512	2.30047746750162
H	-1.33955683395795	0.45396400489278	1.80446980814567
H	-3.22772584871289	0.50714124106183	0.82484536413818
C	3.66508041644000	1.96330333245137	0.92935153659902
C	5.00954749077342	2.42272099675929	1.49092128588513
C	6.19356660741087	2.04876707695092	0.60063032668230
H	5.15452344958481	1.97824850275185	2.48572189885280
H	4.99154392728654	3.51123944569476	1.63986908237002
C	7.54162536202721	2.46779411119384	1.18518623531353
H	6.06577852971914	2.50535730077814	-0.39070256270432
H	6.19346352833476	0.96128989870218	0.44077734215122
C	8.73091646076450	2.03669611012311	0.32839379499733
H	7.64768361697847	2.03601986505100	2.19044504807740
H	7.56065097550460	3.55878566872509	1.31583671424523
C	10.08065568476974	2.41950641542857	0.93368641049089
H	8.64022597903866	2.47982321889635	-0.67319878729782
H	8.69612766453804	0.94727162504421	0.18656770636740
C	11.27145775363226	1.94705400907697	0.10117288258365
H	10.15588075187854	1.99400573537604	1.94442938619667
H	10.12998512121916	3.51068648389487	1.05564343654882
C	12.62247077551682	2.30094838209894	0.72118179571737
H	11.20764653516608	2.38148146206901	-0.90640650868906
H	11.20977627481149	0.85749466088340	-0.03041210473215
C	13.81313298556030	1.80110198210660	-0.09547618992171
H	12.67596535833708	1.87812995664202	1.73460949364968
H	12.69391737939078	3.39145150730687	0.84033454238932
C	15.16729184873626	2.13437950172338	0.53017660693259
H	13.76598055256085	2.22891325384999	-1.10699548133030
H	13.73346714553574	0.71189877601150	-0.22114934033480
C	16.35380774487787	1.61475017973366	-0.28075887160962
H	15.20623325175305	1.71468181951062	1.54642839073413
H	15.25098428826418	3.22477472711286	0.64992243617785
C	17.71003074412008	1.92983212792890	0.33571000844310
H	16.31922353028607	2.02917881563579	-1.29653677603653
H	16.27220477396673	0.52859023566848	-0.40956932796334
C	18.93232038622114	1.37391199176451	-0.46436685014106
H	17.84194675135113	3.01553564574473	0.44481220520928
H	17.76577286645038	1.52438016417575	1.35674477330389
O	20.05017547829599	1.68957731779514	-0.00069219655232
O	18.66176711317934	0.67542961690598	-1.46742658636150
F	-6.71852691746257	5.64434847184934	-0.57532702754882
F	-6.40558054602152	5.31952414532443	-2.68039657985117
F	-4.74493766614722	5.87332117057617	-1.41140104742475
H	3.49245752934869	2.43773204064976	-0.04636451266515
H	3.70390133529482	0.88070711096739	0.74363491515495
H	0.91876979975236	2.26460701390473	0.36992424533948
H	1.22715288591444	0.69032160445394	1.10562071489827
H	0.24271681342490	1.54977032600509	3.26967787044605
H	-0.13967772525697	3.07415004096584	2.46112919252928
H	2.68187115438917	1.80650169158840	2.83864639187260
H	2.43263909041613	3.35096518621187	2.03427164933582

3a linear monomer

63

Coordinates from ORCA-job /home/hzzeng/Desktop/ORCA/DazCalculations/3aDI--/06_MO_GeOpt1/3aMO-GeOpt

C	-6.17877619320122	1.92937852420088	0.10237968480579
C	-5.50235469432721	0.83415799240298	-0.41300650036959
C	-5.41015835446091	2.98758573456104	0.58103187267220
C	-4.02190396310324	2.98020898309861	0.55840341097294
C	-3.36235201935620	1.85946857925641	0.03123825345171
C	-4.11668733980989	0.78347812698197	-0.45468473996153
H	-7.26226059097403	1.95962893548113	0.12995813520727
Cl	-6.41060235801564	-0.52167827468768	-1.02877794147708
C	-6.14904318137902	4.16797507762132	1.14949475529504
H	-3.45670882379602	3.81807275822873	0.93753847319055
H	-3.62178860578065	-0.09114715732172	-0.86563676252533
N	-1.97406455507585	1.73717027127168	-0.05265360903963
C	-1.01718592327932	2.64437128546009	0.38229635028057
O	-1.29301045920235	3.70056920874596	0.92366034905270
N	0.25949536135537	2.20672990612943	0.12948474203350
C	1.56138859907335	4.09795639696744	1.07102511071371
C	2.82151450295412	4.63886032628141	1.30171748786497
C	3.98598904869197	3.98492969167154	0.90398262982103
C	3.90598450103181	2.75180167277691	0.25400617617709
C	2.64242331701625	2.20655272165570	0.02192448472483
H	2.89290630365294	5.59778321885427	1.80617862323992
C	1.47350256966385	2.86087049712258	0.42009207404745
H	0.66735838075834	4.61604896354066	1.38435998785145
H	2.56704599022231	1.24509701042481	-0.48491275708705
H	0.36736283251776	1.31551254116373	-0.33702911506966
H	-1.64858795555472	0.87709972104884	-0.47467006198519
C	5.12620797076529	1.98247063276453	-0.21274095658993
C	6.47880740446678	2.62701654237633	0.07883406096261
C	7.64109432576028	1.77820296069616	-0.43373045059786
H	6.59051674071376	2.78127540707136	1.16028868969418
H	6.52375884920164	3.62115863945425	-0.38528811261027
C	9.00917882245928	2.39677518620487	-0.15245450759101
H	7.52833087074424	1.62437314801081	-1.51605575439583
H	7.59288400519687	0.78094318340829	0.02559723083996
C	10.16785453970086	1.54680877878275	-0.67111849479735
H	9.12426208778965	2.54694491620998	0.93014528640545
H	9.05752045149988	3.39537911384701	-0.60881523507655
C	11.54093547011975	2.15440463114659	-0.38891873771170
H	10.05261398368116	1.39913670830041	-1.75417130142868
H	10.11461941623189	0.54683151497381	-0.21794297129156
C	12.69623797584672	1.30085222648749	-0.90947970811459
H	11.65679369229399	2.30072830273799	0.69443875931983
H	11.59514496212269	3.15497214268437	-0.84098677311478
C	14.07478837720705	1.89553159159467	-0.62362760180980
H	12.58221886111810	1.15798393835869	-1.99344668677406
H	12.63599267471523	0.29862824578266	-0.46177689112704
C	15.22450411548358	1.03600086180040	-1.14768729984655
H	14.18689478357124	2.03848036345705	0.46140556995328
H	14.13386654525380	2.89975450446010	-1.06898101594705
C	16.60580794793150	1.60899035889795	-0.86108774751883
H	15.12269716128785	0.89165036891511	-2.23009969164921
H	15.16057480336351	0.02931561653693	-0.71482139300028
C	17.79099328622024	0.75365005661371	-1.41461929238223
H	16.75477173570496	1.73354416054850	0.22067580651712
H	16.69365273964065	2.61936041627891	-1.28704937217720
O	18.92846389610585	1.17305312071096	-1.10729518172261
O	17.47617670677345	-0.24314311686222	-2.10343892542996
F	-6.86910107890860	3.81789079358816	2.22740899299734
F	-7.01839000903004	4.67373889358799	0.25996387304237
F	-5.33114411533492	5.15873811207950	1.51877283532311
H	4.95111262110470	4.43865645915189	1.10150446110300
H	5.10318997939359	0.98312193935039	0.24275031842288
H	5.03863101018152	1.81533656705279	-1.29494289576383

4a linear monomer

67

Coordinates from ORCA-job /home/hzzeng/Desktop/ORCA/DazCalculations/4aDI--/06_MO_GeOpt1/4aMO-GeOpt

C	-7.35802752613386	1.95644510748626	-0.19554339153921
C	-6.62312737206993	0.79626092250085	-0.39959884837259
C	-6.65258302249802	3.10629306981605	0.14371501229855
C	-5.26919723081239	3.12828265084664	0.28143208556667
C	-4.55190541811393	1.94329973256171	0.07058179976936
C	-5.24335543587673	0.77269336514727	-0.27278317825941
H	-8.43714283815179	1.96194418719230	-0.29222454659089
Cl	-7.45396311266117	-0.67881991120649	-0.82053900204586
C	-7.41643697159771	4.39307786817959	0.29426453680119
H	-4.75535436793095	4.03844709514355	0.55424272032216
H	-4.70204787964444	-0.15436602127844	-0.43508784370194
N	-3.16242242341229	1.84344446021483	0.16311585073121
C	-2.27887848013390	2.80463446436806	0.63506567148609
O	-2.63320670080371	3.89072566057474	1.05710537991488
N	-0.97394949364202	2.37931574320103	0.56828837335054
C	0.15719384609680	4.26463508444436	1.71443978248810
C	1.36846578943842	4.85311208638682	2.05750079084816
C	2.59748081142118	4.31354189319403	1.68078994631831
C	2.60594435152566	3.13782052319806	0.92623282551925
C	1.40030019244010	2.53130009823919	0.56886361697050
H	1.35599608904524	5.76635073395417	2.64457082141825
C	0.18129144032782	3.08472353337199	0.95738527185760
H	-0.78132542769798	4.70276298054411	2.01869012250814
H	1.43896117023116	1.62003335593750	-0.02126404333754
H	3.51878776729852	4.80291647210518	1.97124576723984
H	-0.78950551284077	1.49557690638448	0.11170914384969
H	-2.78478795478799	0.93725616556413	-0.08141126754200
O	3.72271014251308	2.50897236219798	0.49033711889294
C	4.98525133085876	3.07683974809488	0.81472777538824
C	6.05476982009602	2.20414640005585	0.18728196327079
H	5.10466526041966	3.11876733988634	1.90648432559316
H	5.04314974319816	4.10304318887354	0.42597791562297
C	7.46477619668438	2.70567469052568	0.49366998763674
H	5.89294771619472	2.17649458974415	-0.89709875269754
H	5.93331129026912	1.17874975554245	0.55647771965063
C	8.54417538727670	1.85595888010723	-0.17524346425332
H	7.62525074377526	2.70909312052370	1.58045632074590
H	7.56626276382591	3.74797639728959	0.16113085935284
C	9.96470538007731	2.31510968722795	0.14772394250869
H	8.39413475946845	1.87462347243503	-1.26372671488059
H	8.42353664823620	0.80856398557179	0.13430329132618
C	11.03529793568101	1.48316018596970	-0.55652713925157
H	10.12346990321813	2.26795633510442	1.23408184018939
H	10.08018972535440	3.37093542516980	-0.13516158537951
C	12.46153380852994	1.90304366237427	-0.20565654387732
H	10.89118669048949	1.55520604973881	-1.64408587720098
H	10.89819710739496	0.42360269806487	-0.29845145898038
C	13.52764976584856	1.08934430945298	-0.93763643349607
H	12.61302004610876	1.80320409289313	0.87802216146228
H	12.59468729585572	2.96948949484381	-0.43761692894082
C	14.95439364890333	1.46415711159606	-0.54294862027313
H	13.39621406150482	1.21638897737083	-2.02279041516015
H	13.36996303780404	0.02105361071397	-0.73224599016959
C	16.02002779217305	0.66716479847454	-1.29235209629872
H	15.10205965234512	1.28133814105000	0.52732978942984
H	15.10916586001930	2.54010422216319	-0.71680502332955
C	17.42908972744952	0.98377047963305	-0.80407654020129
H	15.92327816784257	0.85443524037305	-2.37292455031239
H	15.83809103702046	-0.39973354186606	-1.11977816605234
C	17.72700220063306	0.49519809357231	0.65225412176038
H	17.62873124500252	2.06266732971900	-0.85169250910327
H	18.17362222345833	0.51155240540451	-1.46043918659801
O	16.91312406687780	-0.32599184981015	1.13804134390281
O	18.76646059935468	0.96511388647713	1.16182052131540
F	-8.65565552163674	4.18244704475350	0.76289093825709
F	-7.54956571258864	5.02099796445513	-0.88534284777688
F	-6.81061583655366	5.24823198615984	1.12715151005808

5a linear monomer

67

Coordinates from ORCA-job /home/hzzeng/Desktop/ORCA/DazCalculations/5aDI--/06_MO_GeOpt1/5aMO-GeOpt

C	-7.20548806328148	-3.26606211326152	2.12040883876250
Cl	-8.15229336967287	-2.07390733244397	1.26775666413172
C	-5.82185122321879	-3.22170572658077	1.99459916536109
C	-5.69598987491301	-5.13841387000638	3.46588779031897
C	-7.75041338365345	-6.22271652963074	4.36604383727915
C	-5.05254478866572	-4.17250445687238	2.67952072469887
H	-5.34719363523128	-2.46699524508938	1.38541743751383
O	-3.19386192599863	-2.36166907279371	1.37159842978394
N	-3.65857520181728	-4.22551064735450	2.62841262654435
C	-2.80225595615956	-3.33002503399452	2.00086708145776
H	-5.11299463665655	-5.87627643581062	4.00883185136521
C	-0.41651765704580	-1.88306484188449	0.80500062126680
H	-1.37038186997532	-1.55002787032692	0.42305807014215
C	0.75125526438842	-1.24866864370560	0.41052288454228
N	-1.48375884186064	-3.66734480404891	2.16651732014346
H	-3.24470078892325	-4.99161764108159	3.14334220331290
C	-0.35357706636298	-2.95359443639975	1.70847058454736
H	0.71384836248180	-0.41659997911537	-0.28490198194759
H	3.01548364779927	-3.07763147546572	2.16942145470633
C	2.00050991447722	-1.65676940601084	0.88851424803215
H	-1.26794984760697	-4.46771629649308	2.74658131673628
C	0.89332157850613	-3.36323139488830	2.18112783886494
C	2.06673699362970	-2.72895307627283	1.77937615002580
O	3.07163081573460	-0.95960874367056	0.43521251155898
H	7.06197297792362	-1.70401118982300	0.44432141850633
H	0.95599710628710	-4.19367963375598	2.88044972535548
F	-8.02172969364067	-7.30274435219249	3.61624607831423
H	5.28134283697374	-0.45645664112233	-0.81082176617362
C	4.35870268207944	-1.32449350399739	0.90977306309961
C	5.36323765993922	-0.37930813246615	0.27995239043005
C	6.79595351924413	-0.67410194229373	0.71936258390016
H	9.52347058635395	-1.00174581731218	0.24394854160740
H	7.73075184001697	0.23634227892747	-0.99602999763928
F	-6.98209092709122	-6.64044594182359	5.38331657337425
C	7.80327343590624	0.29258978594426	0.09890353804514
C	9.24570127768860	0.02431059738815	0.52327304660062
H	11.97480261923414	-0.26754930117270	0.04079913515018
H	6.86467748477640	-0.61681622409290	1.81447018712237
H	10.16357309814057	0.95257262432306	-1.19243995405379
H	5.09212214540774	0.64834800663948	0.55001064583329
C	10.23879243999433	1.00553044471810	-0.09719018380990
C	11.68692726211300	0.75596265250356	0.32016806235809
H	9.31861072407156	0.07627208231071	1.61872562152900
H	14.41650391871074	0.49072687430476	-0.16254796190076
H	7.53062308193642	1.32120614875533	0.37261185742981
H	12.59299825057243	1.69170921771970	-1.39821833894229
C	12.66935747474670	1.74633985701555	-0.30296205407368
H	11.76316270236090	0.80813497721752	1.41561747474642
C	14.12212239173368	1.51493847922858	0.11068966028841
H	9.95450941778441	2.03045770209187	0.17987030218741
H	16.87384307083251	1.28548088183774	-0.37649274244308
H	15.02283146537157	2.46203612476717	-1.61292468690020
C	15.09429478914166	2.51166253986515	-0.51934569101943
H	14.19744648837509	1.56953911948418	1.20688992000817
C	16.54638558135680	2.30184357807259	-0.11344528143095
H	12.37500661415466	2.76912847188570	-0.02778300945097
C	17.55501409271548	3.30902953419611	-0.75518057837657
H	16.65285523865209	2.36888062924079	0.97871278955014
O	18.74263086897308	3.16315742902763	-0.39086742475717
H	14.79777165013364	3.53521642417592	-0.25726838849378
H	-8.94420721321162	-4.21727709970022	2.97812552284091
O	17.07041461303193	4.14038613587430	-1.55599076587269
C	-7.07879860149280	-5.14576612136280	3.56248443349038
F	-8.91370318058496	-5.80519798804981	4.88286863521554
H	4.57743549610118	-2.36679617911542	0.63571860064758
H	4.38782288493608	-1.24901193628189	2.00640265758299
C	-7.86419361772470	-4.21183451975024	2.89360569097484

2a cyclic monomer

68

Coordinates from ORCA-job /home/hzzeng/Desktop/ORCA/DazCalculations/CTUaDI--/06b_MO_GeOpt1_CURVYBOY/CTUaMO-GeOpt_CURVYBOY

C	-7.62062866702694	2.57652978389238	0.18068257899527
C	-6.86873537357269	1.43705452887391	-0.07055444421850
C	-6.92259013185519	3.72035138163181	0.56538497066872
C	-5.54203861061813	3.74997679973443	0.70363370066461
C	-4.80269789227066	2.57899494479745	0.44564261978762
C	-5.48995511775050	1.41412799828157	0.05054333910483
H	-8.69987835541110	2.57606564806218	0.07991346859023
Cl	-7.69861791555493	-0.02798657149604	-0.56002146820762
C	-7.73398575821692	4.95502732702921	0.82647281409534
H	-5.02508633449745	4.65275884848807	0.99470993257252
H	-4.92246058274585	0.51241504602412	-0.16153451274538
N	-3.43599141910660	2.47106347470328	0.57032051259884
C	-2.52786323223489	3.50434164497850	0.78703749384447
O	-2.83778967768500	4.69259104772294	0.86749166813724
N	-1.26243736649277	3.03639433481803	0.88293900382196
C	2.33848914864424	4.08411496393853	0.28740361929913
C	1.06454336118818	3.24607939334042	0.22852320902151
C	-0.11349119377655	3.90932227107408	0.94114017138127
H	-1.08428009829930	2.01599138747180	0.90259768345467
H	-3.03207809129687	1.55368460237979	0.27733074321561
C	3.52778780959998	3.45078384104683	-0.44067276204981
C	4.05108416731121	2.16830290611046	0.21028168776479
C	5.35348860559998	1.68128860480047	-0.43251796321272
H	3.28735801949734	1.38260068991123	0.16731625969390
H	4.23525917891472	2.36265252504737	1.27692401112570
C	6.03486615058523	0.50582838788509	0.28977243738991
H	6.04761275889398	2.53159273740075	-0.45790267376277
H	5.16814020102097	1.41241389928631	-1.48270392114451
C	5.68110728557907	-0.88837399470114	-0.23531241054647
H	5.79798424968285	0.55758433438053	1.36169677337297
H	7.12278537478128	0.62279465277716	0.21447051470246
C	4.20454521649291	-1.27179756646774	-0.13805566601979
H	6.27306076032902	-1.62881934574265	0.32079040199287
H	6.00094153945962	-0.96812029034585	-1.28422409804046
C	3.98047418281924	-2.75312121836438	-0.45724143934308
H	3.61409838968033	-0.64212600185891	-0.81345396409017
H	3.83570647296583	-1.06526223144851	0.87709492052422
C	2.52385717630530	-3.23955059729270	-0.36134752845330
H	4.37172259330383	-2.97064528964630	-1.46250963645281
H	4.60066447573175	-3.33502279725447	0.23733053525295
C	1.75181702191245	-3.21226601540443	-1.68521818643002
H	1.98989004083235	-2.65160652340905	0.39726949114330
H	2.51862365817677	-4.27417455895585	0.00208469326906
C	1.56527874637693	-1.82576597778337	-2.30794090972369
H	2.27675714497861	-3.85510565629642	-2.40525728286564
H	0.76773022355725	-3.67147943577135	-1.52954225960051
C	0.82890192335860	-0.82157141854837	-1.41793924906024
H	2.54665922750040	-1.41640626659350	-2.58478186289262
H	1.01007735294833	-1.94139575181050	-3.24868142993089
C	-0.56985636961239	-1.26727217275191	-0.98809948815812
H	0.74667902754662	0.13186795500953	-1.95666106193037
H	1.40150031339352	-0.60492603631918	-0.50981292706998
C	-1.26513114594480	-0.17110869218013	-0.16912954953159
H	-1.19000610552718	-1.52171710919307	-1.85417013085108
H	-0.49766244428190	-2.16270736317504	-0.35620372899233
O	-2.44888346904956	0.12261728443238	-0.47815891005236
O	-0.58067197715516	0.35631593375037	0.74482820822797
F	-8.65753844932177	4.74988035488921	1.78475622703737
F	-8.41740944701627	5.34141307491973	-0.26741395794133
F	-6.99096833345801	5.99860423832631	1.21409442029300
H	4.34969391744369	4.17883805829682	-0.48015179442740
H	3.24819657377397	3.24365460837136	-1.48326962179251
H	0.78407716836949	3.07098754202318	-0.81877393589070
H	1.22497284906317	2.25573717495081	0.67151540576735
H	0.16513793062712	4.13526935167888	1.98237679689141
H	-0.37517363327049	4.86200404694955	0.46863722226454
H	2.61380729750970	4.26064949525932	1.33703591295912
H	2.13518965729414	5.07150175806336	-0.14826467349787

3a cyclic monomer

63

Coordinates from ORCA-job /home/hzzeng/Desktop/ORCA/DazCalculations/3aDI--/06b_MO_GeOpt1_CURVYBOY/3aMO-GeOpt_CURVYBOY

C	-5.99233970058161	2.69371262553406	-2.17380636059572
C	-5.30623115906777	1.53259440045582	-2.51652033517986
C	-5.30457261509527	3.62496635267249	-1.40505663422866
C	-3.99109250759522	3.43470395589284	-0.98515019924063
C	-3.32166546871722	2.25434960546855	-1.34488261550857
C	-4.00305365570191	1.29435560065855	-2.12325103225047
H	-7.01529456427266	2.85703312494542	-2.48840455799882
Cl	-6.13285920332938	0.32526617588252	-3.48080898744249
C	-5.97676827635024	4.91592019494970	-1.03900369556980
H	-3.48773171809613	4.17660145917445	-0.38157704562241
H	-3.49088691651414	0.37604017595250	-2.39729466482085
N	-2.02179937453689	1.93936346698304	-0.99392520907588
C	-1.16127411560151	2.70384826486076	-0.22599013532550
O	-1.45735872811158	3.79029363969212	0.26265865730312
N	0.05217123416504	2.08498784601891	-0.08661568281799
C	1.23915582563870	3.75569809551087	1.32102318519764
C	2.41460458923293	4.07776912868779	1.99462435262841
C	3.51205934111744	3.21906351061959	2.00422573273345
C	3.43778615138579	1.99789380976700	1.32931081760049
C	2.26391876732442	1.66737067271261	0.65742111002445
H	2.47112894029951	5.02632846682620	2.52190515080252
C	1.15902176561177	2.53247603913277	0.63639674629357
H	0.39498795820508	4.43011851422921	1.31635373720415
H	2.18548297629024	0.72037513057166	0.12579476956433
H	0.21002598594672	1.19274012616140	-0.59999311702901
H	-1.70270635572222	0.99632596663471	-1.31525026173633
C	4.60366609083329	1.03707070388532	1.27220654376395
C	5.19766775335525	0.93578719442776	-0.13814792919540
C	6.25189073151135	-0.16424288508070	-0.27447075043595
H	5.64006066697583	1.90193625864344	-0.41577807765477
H	4.38237328293468	0.76003427419041	-0.84713433393133
C	6.72215137771767	-0.38585404352049	-1.72218183171781
H	5.84829219022020	-1.10664721559788	0.12397945860726
H	7.10840333593638	0.09177574559747	0.36241430361446
C	5.93722972668986	-1.45751683532963	-2.48904923792764
H	7.78025265707011	-0.67397578527631	-1.72614302460246
H	6.66276185434588	0.56645861546463	-2.26757587503569
C	4.42834582464776	-1.22520914263650	-2.58133625038624
H	6.34718658515796	-1.53126320117639	-3.50602364032087
H	6.11527502178444	-2.43419021304571	-2.01657737805579
C	3.73401586475468	-2.20924516074616	-3.52514557685653
H	4.23183669338391	-0.20353573828879	-2.93505295309378
H	3.97986654599863	-1.29388551975357	-1.58168944323732
C	2.20735139024893	-2.07188927216073	-3.52340968679167
H	4.12349482773029	-2.04865401694249	-4.53934319514215
H	4.00887823040563	-3.23886394209964	-3.25081053104829
C	1.53596645538635	-2.73416647644602	-2.31930982071352
H	1.79380345014988	-2.51310841635440	-4.44019537830023
H	1.93935847904319	-1.00808074070380	-3.53201646431129
C	0.04831968553737	-2.41171419867325	-2.22815024276214
H	1.68227518611189	-3.82109485215729	-2.38364904508704
H	2.01457155046450	-2.39420401678634	-1.39504385651885
C	-0.25460531438288	-0.96779992000557	-1.79949797846786
H	-0.44544775940543	-3.06174482174505	-1.49452866771544
H	-0.45925395324100	-2.59483130460148	-3.18309346113453
O	-1.45159754762042	-0.59360879241048	-1.89723225954694
O	0.69789824121898	-0.27700055007168	-1.35601557232896
F	-5.74243764523689	5.26215693718681	0.23626644837949
F	-7.31031703484016	4.85868575683567	-1.19458814508175
F	-5.54448357407518	5.94003687459372	-1.79610251980055
H	4.42131122614422	3.49216477781836	2.53353163396800
H	5.38056810892203	1.34192887482116	1.98432823021068
H	4.26475061819667	0.03840469814982	1.57869278374999

4a cyclic monomer

67

Coordinates from ORCA-job /home/hzzeng/Desktop/ORCA/DazCalculations/4aDI--/06b_MO_CURVYBOY_GeOpt1/4aMO-GeOpt_CURVYBOY

C	-7.89221941665310	2.94436023126926	-0.30349759953345
C	-6.91764649962956	2.10771388237701	-0.83058748345712
C	-7.45212229448068	4.01943260979504	0.46542162839771
C	-6.10835180657470	4.27070051604464	0.71028470489753
C	-5.14171394633886	3.40575698612008	0.16548335326934
C	-5.56596717177656	2.31222246031514	-0.61436957613245
H	-8.94668786717746	2.76660886407018	-0.48110169195618
Cl	-7.41678988731973	0.73689640446245	-1.80067429820303
C	-8.50058359314973	4.94116496461191	1.01562972906953
H	-5.79831489357916	5.11580342517361	1.30666385513214
H	-4.82106815116952	1.64320937974094	-1.03637211790792
N	-3.77703618933193	3.52775656865854	0.34851123395941
C	-3.11450241311600	4.54272412533339	1.01361927463266
O	-3.66748889831453	5.53197145449355	1.48336933169472
N	-1.76777724855262	4.28704014980182	1.07289716956856
C	-0.98690883354643	6.41268051302119	2.07205428870484
C	0.10325745754322	7.14056641394339	2.54800802035900
C	1.38561238395155	6.61387021344796	2.56915085069746
C	1.59272603982521	5.31177610360434	2.09584684750003
C	0.52637280365462	4.56610744970513	1.60411075857823
H	-0.06164274821707	8.14901223267445	2.91734076412463
C	-0.77265041193383	5.11345733177784	1.59495885901492
H	-1.98154198674344	6.83221991633828	2.06769383294896
H	0.65513542342997	3.56056499556090	1.21595160758733
H	2.23322014346619	7.17484986422289	2.94756560500627
H	-1.44398061165811	3.34654495286352	0.76225845368126
H	-3.20581027567620	2.80845768042350	-0.15538332223658
O	2.87833693341483	4.86528912586733	2.17361433452862
C	3.17998376987071	3.53616243903665	1.77801847741696
C	3.40113605047156	3.40362607799647	0.27693217865903
H	2.40396020712718	2.84458703244098	2.12972020444721
H	4.10557474187419	3.28961046530268	2.30889956133931
C	3.82986203546102	1.98637881935519	-0.09931945734133
H	4.17039507185484	4.12611209339758	-0.02324551065456
H	2.48238337670753	3.66832879934825	-0.26025052805062
C	4.08707392742652	1.81127558279291	-1.59489318917008
H	3.04545319358021	1.28101989656252	0.20965017818042
H	4.73392465662502	1.71160985259956	0.46348495046948
C	4.52381232059345	0.38590613634257	-1.95990215712975
H	4.85855404051977	2.52059786073321	-1.92459924141337
H	3.17671577752273	2.08023269388321	-2.14244400277892
C	4.34849690576592	0.03384846597792	-3.44862039462868
H	3.95027549817332	-0.33318895697606	-1.35704479629654
H	5.57126555728403	0.25761326205973	-1.66099483989773
C	3.01485060356911	-0.66364038036976	-3.75178121508747
H	4.42988261900021	0.95019020013852	-4.04998646386448
H	5.16381448546791	-0.62135962525803	-3.77686994068742
C	1.79165465555619	0.13415465909254	-3.30812706893419
H	3.00559471712427	-1.63688457395277	-3.24037294957938
H	2.94764858495529	-0.87781617991397	-4.82685462676114
C	0.44943822912490	-0.56681418360314	-3.51942387786223
H	1.89327071052293	0.36979320846937	-2.24273549543692
H	1.77356911239333	1.10063382643924	-3.83229009818643
C	-0.69112469786286	0.21274871544491	-2.85355002724909
H	0.25943587286154	-0.67680781495645	-4.59503810561772
H	0.49472014068214	-1.58382764157484	-3.10350710416534
C	-0.68089325522646	0.08419872234576	-1.32281186089725
H	-0.59798924548135	1.27124505507910	-3.12967041026784
H	-1.66458832280304	-0.11122610519960	-3.23365089046580
C	-1.37159211911943	1.26476524521492	-0.63910220735474
H	-1.20073723430161	-0.83756501090576	-1.03174791086235
H	0.33837431826938	0.01814489158262	-0.93301861928888
O	-0.75695016974830	1.83520772496641	0.29728847979888
O	-2.50777449941317	1.58324764224778	-1.08103749109212
F	-9.45958550747829	4.26655646371741	1.67707665080953
F	-9.13135857864382	5.61671355295399	0.03688081666654
F	-8.00234359065330	5.84994227147001	1.86239056930797

5a cyclic monomer

67

Coordinates from ORCA-job /home/hzzeng/Desktop/ORCA/DazCalculations/5aDI--/06b_MO_GeOpt1_CURVYBOY/5aMO-GeOpt_CURVYBOY

Cl	24.86010461683699	-3.76495938952028	3.52848260449556
C	22.89035786343496	-1.92267877655570	3.73431839625322
C	23.26222014388582	0.45312287136298	3.42258791385325
C	25.53459280356148	1.32430875681590	2.84633311903988
C	22.38565266230488	-0.61330322547105	3.70638197952861
H	22.23239579327206	-2.75522231507162	3.93764162934431
O	20.05737509564885	-2.34237123697138	3.76074819725480
N	21.07194103304125	-0.27451257330156	3.96940194040143
C	19.98969517740427	-1.14135299920984	4.00024630227664
H	22.86570066998190	1.46359413952838	3.39021965043973
C	17.14567203994334	-2.09917718077975	3.53054658069739
H	17.88879155079736	-2.87220534122108	3.38900859506900
C	15.82062689455372	-2.31643356012661	3.15957112236651
N	18.84518746353221	-0.46800664110396	4.33346079771548
H	20.85079416102246	0.73813595511381	3.83715520836727
C	17.53050361450228	-0.85466099245784	4.05023145426234
H	15.52347795809973	-3.26422365680909	2.72123579637749
H	14.49668174429965	0.68602196207218	4.03453701849193
C	14.85827411077223	-1.31861804247832	3.30432532182025
H	18.94722149658040	0.52885109988049	4.60966626359403
C	16.54410126915605	0.11943861562959	4.25935277429827
C	15.22584726827411	-0.10323272909232	3.88575191219891
O	13.58821051856270	-1.57789327113091	2.85275587335144
H	10.44932898677231	0.86545966518199	1.91979371851354
H	16.84318670050260	1.07587963714365	4.68047509537634
F	25.94860867481899	1.26422125360158	1.56744940668071
H	11.99821931032939	-1.52022743822745	0.75935697673386
C	12.88329167706669	-0.44145013712952	2.37857953311255
C	11.66510844264855	-0.89775849630604	1.59871048042621
C	10.82262002454460	0.27256187559754	1.07301117350325
H	11.52727231594091	3.05826760828252	1.18066797685981
H	10.85583399424911	1.57714871404865	-0.66131587584006
F	24.98015610901183	2.52898164695557	3.02327545630782
C	11.56232266150456	1.19504666317785	0.08662999862503
C	12.27356944821054	2.39290561611620	0.72573802799712
H	14.57741500798581	4.78613244422630	-0.35013694774132
H	9.93791899099613	-0.14920348977682	0.58367694320847
H	13.61895855513202	2.48313765167650	-0.96127750028001
H	11.05384342249303	-1.53414443504984	2.24926824742923
C	13.12057448261233	3.18543728448336	-0.27799938680985
C	14.19617025554417	4.06027059497008	0.37965385629350
H	12.90947859739675	2.05352887774925	1.55001644023001
H	16.01541564340246	4.66037838101090	2.40904566752157
H	12.29872076487866	0.59952435758706	-0.47200543479406
H	14.99633186177341	2.48467164890472	1.62892897777346
C	15.36710382679260	3.23669012668959	0.91829341741340
H	13.74859007913149	4.64574447266403	1.19537861247661
C	16.46209425903749	4.04768138162863	1.61324192077282
H	12.45852854513286	3.79995078139352	-0.90098513287301
H	18.18425259064248	4.49473869121133	3.75768685711934
H	17.01340027975772	2.42326214652768	2.89215654763287
C	17.51910394407011	3.12678959415322	2.22041357955804
H	16.92199119495777	4.74673468700840	0.90084490792854
C	18.63021215086621	3.81888929189660	3.01924114484810
H	15.81326071347639	2.67055456936158	0.08856721603799
C	19.41728597763296	2.72492517367446	3.75112875899356
H	19.28860527114224	4.39067706713379	2.35809016511812
O	20.48981806683680	2.32360174449850	3.23262904007128
H	17.97760361093615	2.51895888371771	1.42868628616670
O	18.86909326992913	2.24350039535285	4.77982667124591
F	26.64752839542684	1.28258792496449	3.60159510109276
H	13.55848017838075	0.14601703461640	1.74243141121361
H	12.56521020226734	0.19804357680243	3.21547221753960
C	25.12518181917764	-1.09330024718777	3.20582314037920
C	24.24313038341370	-2.12438210823634	3.48446610650163
H	26.17571083020256	-1.28184812762585	3.01704832755672
C	24.59967253349628	0.20041154642822	3.18045042058001

2a monoanionic dimer

137

Coordinates from ORCA-job /home/hzzeng/Desktop/ORCA/DazCalculations/CTUa_DIH-/01_DI_GeOpt/CTUa_DIH-_GeOpt

C	-7.25585320584030	1.82310679139588	1.30341220775336
C	-6.57347184231559	0.63771548949643	1.55185023138464
C	-6.53223536468902	3.00420448674175	1.41700298651745
C	-5.18595153081012	3.03245587417286	1.76468108450045
C	-4.52209495044625	1.82444254970918	2.01140566238214
C	-5.23312793601028	0.61817717879181	1.89871899907882
H	-8.30345077920245	1.82186943611348	1.02962475787494
Cl	-7.43092872771803	-0.87855216891858	1.41689878296886
C	-7.22045328201872	4.32312019757761	1.20969720432260
H	-4.65163327091068	3.97005440201595	1.83173783325322
H	-4.72992334490579	-0.32711703933046	2.07803660785788
N	-3.19058311168457	1.74078216437310	2.40033493754703
C	-2.23197367654426	2.74308910381724	2.28363551180088
O	-2.44142083920814	3.83270815390527	1.77063683871476
N	-1.03022604611326	2.36445688935191	2.80136230953336
C	2.61040338815946	3.03344105274113	1.84770200170394
C	1.28967295369872	2.29322071554418	2.03536880730353
C	0.17654323405489	3.14892057750468	2.63418254655878
H	-0.96159464092817	1.49846835584212	3.32196016707092
H	-2.83046779674304	0.80173902440654	2.55405560581760
C	3.69427086213482	2.12062076603561	1.27611942540822
C	5.05083433949249	2.80023235269327	1.10407248469545
C	6.11690282990944	1.85192309053293	0.55830765409857
H	5.38192113384828	3.20114511403617	2.07207261094944
H	4.94608116774589	3.66239425862870	0.43120904374302
C	7.49087691542715	2.50017184292359	0.39826406298165
H	5.78740298008937	1.45637481080155	-0.41332380406453
H	6.20404407904473	0.98492419355271	1.22959252445898
C	8.55114589745867	1.52248956664468	-0.10524327417598
H	7.81063626565008	2.91627469132641	1.36380556098930
H	7.41604288984539	3.34968783237292	-0.29468754555654
C	9.93622453844645	2.14727133724616	-0.26310827158898
H	8.23010668722957	1.10349093576265	-1.06979994699408
H	8.61687592114875	0.67465621188576	0.59171962715121
C	10.98839885466681	1.14515828711270	-0.73499604062456
H	10.25107328656826	2.57872348097894	0.69739527558332
H	9.88168578526093	2.98356255462575	-0.97399583380310
C	12.38587199570955	1.74582908056425	-0.88030520907702
H	10.67584700044409	0.71808602941045	-1.69874118033360
H	11.02851392177351	0.30546975314492	-0.02607343940089
C	13.43052735107634	0.72044198116809	-1.31735881860848
H	12.69143758922940	2.18951323582466	0.07772203624749
H	12.35520533590171	2.57059330570897	-1.60615878202009
C	14.84005436408029	1.29414109073945	-1.46112219268909
H	13.12408523439137	0.27544728091138	-2.27496988877951
H	13.45063473162377	-0.10367661491399	-0.58957770788677
C	15.86198532593558	0.23380435086010	-1.86473966439788
H	15.14269175186714	1.75627631612170	-0.51071921539005
H	14.83183995762834	2.10152045056753	-2.20746706286688
C	17.28794160098364	0.76117152268732	-2.01933391281330
H	15.56747925924149	-0.23137709548439	-2.81255901867878
H	15.85735982552776	-0.57086694739359	-1.11485311994341
C	18.25656220943108	-0.36677879967235	-2.40964481728025
H	17.30985300025826	1.52578698893904	-2.80809326245672
H	17.63991202217110	1.22972367607119	-1.09482929686676
O	19.34510159880102	-0.43695482751036	-1.78238645930900
O	17.87159913947490	-1.14265545370914	-3.32127714591476
F	-7.41160085525630	4.96490154611714	2.37429615549701
F	-8.42401659378423	4.18446699869770	0.63566396364048
F	-6.49761822172794	5.14335242042316	0.43365505677427
H	3.35946424078599	1.72860306015420	0.30466106934492
H	3.81180341265337	1.24709520808473	1.93523234564344
H	0.94169157884618	1.89467928981779	1.07287272361949
H	1.45772465344025	1.42679570617606	2.69095672757149
H	0.49833955150929	3.56874895370004	3.59643782209982
H	-0.07406810803153	3.98546270915383	1.97769522559519
H	2.94513453078467	3.43987643274169	2.81190363610650
H	2.46129576344938	3.89328387288011	1.18114048261127
C	24.50068200828661	-2.47055312935082	-0.26853449516607
C	23.68602653912328	-1.38142443723705	-0.56013625417862
C	23.97212270940727	-3.73321337008136	-0.51607014118770
C	22.69515697574667	-3.92893542437199	-1.03167199333688
C	21.89381439659669	-2.81180789155069	-1.32141845340072
C	22.41002444594267	-1.52272555814259	-1.07255354196095

H	25.49932233930779	-2.33796580820198	0.12803029171243
Cl	24.30671486838324	0.23204724304731	-0.26831491641707
C	24.78656415922754	-4.94513597212573	-0.17104302734199
H	22.31065748328795	-4.92404492883829	-1.20809666393550
H	21.78960562573665	-0.65631684975154	-1.28345352830726
N	20.63247059182469	-2.87201744919645	-1.87328804454418
C	19.82462364876789	-4.00222597253385	-1.97422245180798
O	20.12652529734612	-5.10610382087401	-1.52452873941914
N	18.67110316461506	-3.72841359747180	-2.63325319834208
C	14.99270342321471	-4.51654691223442	-1.98082459706089
C	16.33475126452952	-3.79019383111616	-1.97061413096380
C	17.50625277522955	-4.58408861103075	-2.55106665427902
H	18.49895988890808	-2.76472702104477	-2.96642597721036
H	20.15256119606284	-1.95129428009862	-1.98145195403030
C	13.87202625581279	-3.59388912123424	-1.50253239590763
C	12.48206922987991	-4.22574984894960	-1.48369178154482
C	11.40848700034362	-3.23015885076969	-1.04633294492514
H	12.47855745146376	-5.09199159358622	-0.80726520816065
H	12.23897433571706	-4.61125326462983	-2.48375687160277
C	9.99922140508022	-3.81528570693158	-0.98317641792615
H	11.41331988318277	-2.37374212983918	-1.73547074012671
H	11.67430687144861	-2.82799580199874	-0.05803992625486
C	8.96120169182808	-2.79152409592195	-0.52574804044337
H	9.99083378017902	-4.67302777232692	-0.29599629143322
H	9.71868802968341	-4.20710358555293	-1.97082065881363
C	7.54615495757369	-3.35657353165836	-0.41695625175978
H	8.96079813301256	-1.93964395678928	-1.22055916468837
H	9.26299236502544	-2.38897732685963	0.45200724015103
C	6.54041174210014	-2.33512242595732	0.11183133632366
H	7.55547231646761	-4.23084814591830	0.24906669656645
H	7.21861685201273	-3.72077096480003	-1.40057898466099
C	5.12554665140559	-2.89154958760782	0.25953207767475
H	6.52146267798196	-1.46119256073801	-0.55471431557733
H	6.88494072176162	-1.96848149820530	1.08957447919020
C	4.15707485955919	-1.88508897227208	0.87819149604117
H	5.15531400046365	-3.79398552068799	0.88609606549512
H	4.74962732156994	-3.20872233750908	-0.72279749436805
C	2.74650534107204	-2.44082435625213	1.06583948727571
H	4.11417904421009	-0.98255412187007	0.25216967023992
H	4.55054982763049	-1.56473322832233	1.85380846689959
C	1.81974324036250	-1.44599609915301	1.76179072060803
H	2.79299728491886	-3.36627111567931	1.65607033478091
H	2.32209020447381	-2.71244284096624	0.09056452465103
C	0.41304379004578	-2.02047144751390	1.97967379250535
H	1.75361809225083	-0.52400252928017	1.17082782656261
H	2.27878828953926	-1.16735720461443	2.72228284950231
C	-0.54818048750466	-1.04602149452597	2.61657987449337
H	-0.03050861272707	-2.32872203061809	1.03084435431511
H	0.46903890686162	-2.90656189226265	2.62604940488140
O	-1.64677826391159	-0.78075319937343	2.19251596433322
O	-0.13464088092036	-0.44410795123459	3.75207060992441
F	24.41475709831397	-5.48435337162148	1.00368769419340
F	26.09754460901279	-4.66633851881094	-0.06584998412037
F	24.66285991467556	-5.91474181860634	-1.09088049134711
H	13.85220686484525	-2.70456245976301	-2.14869458029041
H	14.11439393263637	-3.22941724533920	-0.49389869288064
H	16.24798947010139	-2.85744502319942	-2.54289862366559
H	16.59050855449538	-3.49580810814655	-0.94374923243764
H	17.76128871367587	-5.44744367569494	-1.92980476515887
H	17.23832720467878	-4.96270236489518	-3.54781646915576
H	15.03722665030435	-5.41224637429868	-1.34560352423329
H	14.76792490898853	-4.86531185342246	-2.99865356236364
H	0.77186513485675	-0.71063453597982	3.98166423118146

3a monoanionic dimer

127

Coordinates from ORCA-job /home/hzzeng/Desktop/ORCA/DazCalculations/3a_DIH-/01_DI_GeOpt/3a_DIH-_GeOpt

C	20.98197769548646	-4.36757166795647	-4.53879934297502
C	20.44096017173430	-3.78190572628727	-3.39779748530091
C	20.10966983573099	-4.61234941775504	-5.59224374803638
C	18.75494115143212	-4.29662321500709	-5.53899060664462
C	18.23451955419652	-3.70749089784023	-4.37678830020368
C	19.10291065343941	-3.45161463060407	-3.29524820728952
H	22.03307988143578	-4.61963373030379	-4.59744888689352
Cl	21.50107040109457	-3.45236305106450	-2.04213957295214
C	20.62624129937382	-5.22406893903367	-6.86177805757211
H	18.10595896339417	-4.49473871188375	-6.38077141528275
H	18.70482630199555	-2.99107640220508	-2.39523648673175
N	16.90801054100629	-3.36892416463546	-4.18706429962086
C	15.91213104344049	-3.36116609700561	-5.15200962351782
O	16.09897101044646	-3.61931553257343	-6.33657321300994
N	14.70878980843437	-3.02195082582417	-4.59635250683111
C	13.29076270427564	-2.87761745953524	-6.62692128172056
C	12.07660024117613	-2.46207192850373	-7.16755030608385
C	11.10318628392235	-1.84371373988813	-6.38600915964735
C	11.33911516363341	-1.63029365465636	-5.02433525435603
C	12.54672695954503	-2.05293653100463	-4.47626695469710
H	11.89205513103903	-2.62370033428039	-8.22618162439954
C	13.53411862123029	-2.66997558133224	-5.26084106594379
H	14.04575948835624	-3.35037312632689	-7.23938310921616
H	12.75742886960228	-1.89512103831982	-3.41978427696696
H	14.66229445529907	-2.96175084597097	-3.55524893732267
H	16.69875108334676	-2.90802931244249	-3.27470513347220
C	10.31813745482027	-0.94865930924417	-4.14167501611034
C	9.64130543567736	-1.89655939513249	-3.14464204707069
C	8.64839458464143	-1.17183854073915	-2.23729526427173
H	10.41148169065201	-2.38274832647596	-2.53145823433307
H	9.12868479665990	-2.69737956757836	-3.69430675963144
C	7.95378228982535	-2.09517408426149	-1.23781617122420
H	7.88887433138098	-0.66978801039497	-2.85328159479800
H	9.17512533777615	-0.37553896206943	-1.69140081532413
C	7.03547055531860	-1.34551541821906	-0.27302519222592
H	8.71093888081259	-2.64658677078986	-0.66356989200689
H	7.37152961360789	-2.84946682918241	-1.78566831915938
C	6.23140788814812	-2.26686706576619	0.64172045365274
H	6.34272709260661	-0.71266837739172	-0.84614190235992
H	7.63925970443221	-0.66339285889012	0.34237616126443
C	5.32506268300219	-1.50717781826193	1.60955377777111
H	6.91857956599328	-2.90782988854612	1.21115579283167
H	5.61849289325450	-2.94087165115093	0.02686087693877
C	4.47641953496680	-2.43357737208383	2.47857844139576
H	4.66360775058071	-0.84002753317361	1.03893061225828
H	5.93692380463407	-0.85962593687773	2.25357565383783
C	3.52982564245667	-1.67655192238727	3.40788153329985
H	5.13538457906319	-3.08147176086749	3.07279799406804
H	3.89051848414655	-3.09948334950177	1.82978743253280
C	2.68327228012544	-2.62507800731526	4.24882059737501
H	2.86683197594633	-1.03218153488350	2.81892623986352
H	4.10159848595285	-1.01750635431033	4.07170402764222
C	1.69656675115559	-1.91559918871998	5.14180599555310
H	3.31796296713066	-3.25687442643807	4.88503033970354
H	2.11316227834373	-3.31017441680658	3.60621291451724
O	0.92339144063788	-2.68632696337432	5.91740693824668
O	1.55760385874004	-0.71382894558114	5.19731109607960
F	21.90519862950545	-5.62171171458317	-6.75684508848365
F	20.56969770651274	-4.36433949902665	-7.89291350847223
F	19.90853267767802	-6.29880927070385	-7.22708320671686
H	10.16658945233429	-1.51714537306337	-6.83063532270177
H	10.80793945392930	-0.14483164139641	-3.57551257942767
H	9.55142543738707	-0.47414449060421	-4.76679303018070
C	-3.32149930847383	-0.18772714031876	9.38078031475394
C	-2.58459544651684	-1.08551358120998	8.61584145177107
C	-2.95585607985217	1.15053385267384	9.31195094931460
C	-1.90419534377030	1.60594417107843	8.52017056567360
C	-1.17997366260981	0.68077278452478	7.75790622137610
C	-1.53241037491974	-0.67913315394501	7.81521428167693
H	-4.14152696998704	-0.52227410737263	10.00354782991643
Cl	-2.99815669974855	-2.78228622678803	8.66624203474757
C	-3.73124182193382	2.17485995955759	10.09382139385709
H	-1.64574992947240	2.65534523095435	8.49414743505235
H	-0.97609675640220	-1.40913821492861	7.23422175931267

N	-0.11114985222218	1.00441475877059	6.92778684406743
C	0.42030722592072	2.26199317137144	6.69115813608485
O	0.01231255643107	3.28212366024160	7.22243078524412
N	1.45726901689400	2.20893449581327	5.79031272242620
C	2.21341440423779	4.56727144105154	5.86002082264207
C	3.04511264145060	5.54215477913579	5.31441121771854
C	3.88995472744561	5.26278302692738	4.24497512847098
C	3.91309741537843	3.97931552159477	3.69136564805857
C	3.08342140184052	3.00169299499713	4.23471125619640
H	3.02676760691442	6.54150392354438	5.73909652220433
C	2.23316890027741	3.27849596190370	5.31356017339241
H	1.55843840181282	4.79557627218789	6.68803655378701
H	3.08866866826328	2.00039608045270	3.80681113904735
H	1.66962891056821	1.30673518065171	5.37822006810613
H	0.32010566637342	0.22265507174487	6.43936405636722
C	4.84922182944344	3.63769830620944	2.55731336864943
C	6.18176407368171	3.05521874989575	3.04731441206294
C	7.14075050975599	2.74482709703115	1.90008577864632
H	5.98368999337323	2.14150605096706	3.62469258769009
H	6.65108829520008	3.76485987935458	3.74153186704054
C	8.46945911641008	2.14858819246125	2.36263626329191
H	7.33400858682639	3.66509939096100	1.33138404939230
H	6.65705574834922	2.04796447929383	1.19982974461630
C	9.41625484931108	1.84714492256555	1.20281470153051
H	8.27517079288029	1.22149601540539	2.92097901019552
H	8.95578992719843	2.83700074065509	3.06782025030513
C	10.73707543998386	1.20467056546900	1.62672093813620
H	9.62382322203674	2.77299864343154	0.64881602283158
H	8.90773922081121	1.17888954834632	0.49298146031212
C	11.53327960707810	0.68708871031216	0.43081386304170
H	10.53411779069880	0.36819164205270	2.31034668439455
H	11.33636039637379	1.92991512853534	2.19438770127663
C	12.90088901815041	0.09779477966011	0.77583331453374
H	11.66282867591829	1.49616167647704	-0.30214902563134
H	10.93627810462058	-0.08679030742041	-0.07451132287061
C	13.52229973952696	-0.60033291365657	-0.43123520561820
H	12.79200443187485	-0.62597257177620	1.59644143934543
H	13.56416333216042	0.89118759043590	1.14734382293723
C	14.89832321949931	-1.21977772710046	-0.19312350831103
H	13.58706283328673	0.11009399454690	-1.26815832693711
H	12.85509788269647	-1.40368238706300	-0.76207388361944
C	15.33088602747822	-2.06219611501419	-1.40251399884014
H	14.85218106684675	-1.88520949474615	0.68028324406695
H	15.65875280136264	-0.45983409541741	0.01047825556402
O	16.51315478626788	-1.95817752985651	-1.81206152325327
O	14.44009493391353	-2.80123073258888	-1.90344254310104
F	-4.59183205685777	1.61238624991889	10.95511409690474
F	-4.44764962674731	2.97292840847889	9.28664064475822
F	-2.92137746253945	2.97347245982435	10.80431718688017
H	4.52955166643896	6.03825330844275	3.83202972525159
H	4.37067979882275	2.91386659086088	1.88570121913467
H	5.04967673130352	4.53845405782068	1.96469615283758
H	1.12379609475070	-3.62896908135454	5.78568014364160

4a monoanionic dimer

135

Coordinates from ORCA-job /home/hzzeng/Desktop/ORCA/DazCalculations/4a_DIH-/01_DI_GeOpt/4a_DIH-_GeOpt

Cl	23.93839977236183	0.63935085356070	-1.05667323180400
C	21.94779569045238	-0.19169747039025	0.57564530277389
C	22.24432036247990	-0.65949516800447	2.93481537919518
C	24.46311644062894	-0.44153206693172	4.00843262148843
C	21.40448479601934	-0.59621850404916	1.81274336848680
H	21.29700947833300	-0.13087248359525	-0.29218904300678
O	19.65328459216441	-1.07450941973317	4.07808270717285
N	20.06101800830226	-0.91968511222372	1.80902085343282
C	19.26442113963561	-1.15723310349807	2.91802656007113
H	21.84228825711174	-0.95285362526238	3.89465697040059
C	16.83288754256976	-1.48032894334570	4.72098906407148
H	17.76418633935462	-1.41395695151004	5.26477630200953
C	15.61034905850456	-1.51400574310958	5.37934361489826
N	17.99386170070369	-1.48957006404527	2.52846311245653
H	19.57669716232452	-0.75890003857121	0.89795249491042
C	16.84500992827693	-1.53413494983499	3.31579534756372
H	15.59990232404454	-1.47669653867961	6.46521187941165
H	11.99486493671575	-0.73471593966108	3.78916085759903
C	14.39368373296657	-1.59478562316958	4.69917279658732
H	17.84054869585527	-1.66683460583600	1.51189516767501
C	15.63362202249300	-1.62304813715004	2.62002937927930
C	14.42025065607046	-1.64292103496495	3.30249618516627
H	13.46145803365790	-1.61958123270143	5.25026417220625
H	9.49640636640002	-0.67421393302774	3.35046812100504
H	15.63832335817061	-1.66119924492444	1.53426116339294
O	13.30836522922950	-1.69764803032856	2.51437168557814
H	11.17415304821710	-0.63321202759656	1.45904036157328
C	12.04431290554693	-1.62219895582141	3.14164400707562
C	10.98841289492328	-1.53624253663286	2.05304713108190
C	9.57655299000202	-1.50360232729774	2.63379094037545
H	7.02674676278360	-0.52529786869796	2.92687606841743
H	8.64542201456317	-0.42143721942613	1.01413811863244
H	11.88025576463836	-2.50762917544958	3.77425682401598
C	8.48307321922668	-1.35201069534288	1.57572832526171
C	7.08583710608394	-1.34114947930879	2.19256929570150
H	4.57137095368843	-0.36318210356739	2.62533575909705
H	9.39708460540284	-2.42384549072852	3.20690050657085
H	6.07183051153096	-0.25522864347097	0.62012885221941
H	11.10294338892846	-2.39404734852216	1.37916429914657
C	5.94243785116605	-1.18688862263347	1.18874800599257
C	4.58536778870605	-1.18115015957181	1.89110837434721
H	6.93827628049362	-2.27157218307813	2.75900372619728
H	2.11092863954008	-0.25666058494222	2.53776432083287
H	8.56042621449675	-2.17211438980081	0.84814574108782
H	3.42818008655827	-0.10663988141156	0.40527092401801
C	3.36685684640666	-1.04234448044056	0.97744795374985
H	4.48582134320528	-2.10968228704328	2.47120074954410
C	2.07717125045968	-1.06819783104679	1.79737228163871
H	5.97912600127233	-2.00730671874454	0.45832921530976
H	-0.39210401481512	-0.19568652466827	2.65366887424678
H	0.77653785210057	0.00028942305981	0.43192082422571
C	0.78704976390048	-0.94497795362551	0.98772239011082
H	2.04457114363772	-2.00354436965128	2.37360300015161
C	-0.41921403400493	-1.00864270364917	1.91708463605873
H	3.35593783885954	-1.85694126556275	0.24037930511396
C	-1.75269204622239	-0.93211009016258	1.23234270312713
H	-0.41545697083524	-1.93667041071323	2.50221688302660
O	-2.76218199601823	-1.03084213111687	2.09833174539934
H	0.72618869719117	-1.75173733718450	0.24736966693681
O	-1.93859658632936	-0.79788932564116	0.03748500512476
F	23.90689471114215	0.13292242249147	5.08647628303397
F	25.66496059397076	0.13151001327436	3.83092497888605
F	24.69166621222754	-1.72498785548530	4.33799522529318
C	23.58796379192570	-0.32358703783410	2.79516595906867
C	24.14335319033714	0.07583529709056	1.58557295445758
C	23.28830011632770	0.13213809546120	0.48882895036257
H	25.19017205330223	0.33738790348911	1.49740093823480
Cl	-8.08050838769326	-0.77342891890659	0.55509285018729
C	-5.90855942289782	-0.80448652866547	-1.04948507895878
C	-5.98351151945691	-1.21047751706373	-3.43157493555795
C	-8.17374021200612	-1.56779933648120	-4.57358467949186
C	-5.23765789089552	-0.94211806434337	-2.27373707770546
H	-5.35123676652409	-0.58059975304761	-0.14546654044632
O	-3.37803210304551	-0.76985615022744	-4.49057263407749

N	-3.85127023154241	-0.82072366640128	-2.24313621051975
C	-2.99617419079020	-0.73519593422575	-3.33270263618394
H	-5.48785479964783	-1.32102641877455	-4.38479118735303
C	-0.60447833106131	-0.40885744838702	-5.16225689129240
H	-1.55028319993788	-0.45541230090917	-5.67971371116023
C	0.58912793360546	-0.27672854151476	-5.86043613529114
N	-1.68702600610050	-0.60609445523997	-2.93877643373518
H	-3.43090159383540	-0.75166276989718	-1.32074543675780
C	-0.55560746099865	-0.48173359162618	-3.76159420119597
H	0.55495167699926	-0.21900957048755	-6.94422235024367
H	4.24173735025924	0.80842870985806	-4.36066245783764
C	1.82741748939281	-0.21407332633145	-5.22369356551002
H	-1.49450060903672	-0.61277708893631	-1.94158586231882
C	0.67583248174737	-0.42179977719171	-3.10758501087641
C	1.86244320576667	-0.28961999342012	-3.82889804435701
H	2.73321565239336	-0.10947544180936	-5.80718156212715
H	6.77128446787982	0.93662682916460	-3.98471611775325
H	0.73424157091174	-0.47853503649008	-2.02421130233337
O	2.99701019491618	-0.24470312321205	-3.08593608367258
H	5.19757780302213	0.69963745834091	-2.05395403954546
C	4.23102132959916	-0.12358370279293	-3.77796445723866
C	5.35083450577231	-0.12875919162843	-2.75647511177776
C	6.71882681416837	-0.00703214310261	-3.42449658516688
H	9.31285244956326	1.00871076498749	-3.62294630877827
H	7.76227994336097	0.73251176629824	-1.68599679605613
H	4.34815233346050	-0.96205890219800	-4.47873841713792
C	7.87504228463910	-0.06962126103358	-2.42912156366461
C	9.24371019273656	0.04598952043200	-3.09743794252815
H	11.87744938305241	0.99723887863186	-3.26360917610862
H	6.83702655583069	-0.81237018894793	-4.16256858767132
H	10.31001316910431	0.69244992313493	-1.33635273711608
H	5.29572029912729	-1.05914932060761	-2.17782052540627
C	10.40230259938406	-0.08179826811199	-2.11166642066537
C	11.77861692918175	0.02171867030720	-2.76706019882545
H	9.33698896539990	-0.73305538167621	-3.86704826801437
H	14.49226990945390	0.88185195711950	-2.81410098650101
H	7.82088985495601	-1.01631165124589	-1.87272886651889
H	12.83968317392388	0.59895378289506	-0.98107846738647
C	12.91607389901039	-0.16609399974804	-1.76664913509110
H	11.86071283590335	-0.73764603616732	-3.55747131495268
C	14.31444714910834	-0.11263724805185	-2.38129324820253
H	10.32588700786526	-1.04789565612074	-1.59209491470801
H	17.11687659552974	0.55972447758641	-2.22844647522554
H	15.30496650923875	0.25935936051566	-0.50467953522203
C	15.38663691522057	-0.44266382353199	-1.34694424273942
H	14.37634739851932	-0.82950981789744	-3.21275366986489
C	16.82279815899405	-0.43087462210083	-1.86833543362112
H	12.79000498638720	-1.13347800742424	-1.25974651715924
C	17.79012528088578	-0.87786229323707	-0.76392046835120
H	16.91188425343669	-1.13281946355025	-2.70882067856354
O	18.83521544983944	-0.20633825299783	-0.57746879322643
H	15.19368324380417	-1.43837697737207	-0.93363849204642
O	17.43958247306838	-1.89223469253185	-0.10157754834355
F	-8.62907687978623	-0.41298488449639	-5.08490763182285
F	-9.25079489192636	-2.33048090915575	-4.32725127688643
F	-7.46584005792460	-2.17115390065015	-5.53580035020724
C	-7.36378017233229	-1.33657894801282	-3.32739324059537
C	-8.04498204469090	-1.21067454913780	-2.12001619029688
C	-7.28585940829234	-0.94293127964673	-0.98979143832562
H	-9.12117301346254	-1.32165793977196	-2.06166268649562
H	-3.60112389190849	-0.98243106074071	1.60438809785743

5a monoanionic dimer

135

Coordinates from ORCA-job /home/hzzeng/Desktop/ORCA/DazCalculations/5a_DIH-/01_DI_GeOpt/5a_DIH-_GeOpt

C	-3.81212267892701	4.43867083347262	5.10372346719466
C	-4.14865438953664	3.20833644706858	4.54734436904340
C	-2.61146408916510	5.00591237037141	4.69382361282043
C	-1.76659120680184	4.39901321858992	3.76913979192610
C	-2.13128900602142	3.16040474233254	3.22113370903612
C	-3.34353198156830	2.56507033544600	3.62657677991562
H	-4.45515930457319	4.92481728953310	5.82638019568879
Cl	-5.64674028291897	2.44589018259813	5.04056751322036
C	-2.20825172964048	6.35033525859262	5.22341907413687
H	-0.83286895719449	4.86303130810720	3.48308496431549
H	-3.61965642261662	1.59784871429650	3.21663187717687
N	-1.39697603750560	2.46558503944609	2.27820094560549
C	-0.07534676464145	2.69891689940875	1.93259181153380
O	0.62240627174378	3.57868508413547	2.42734857229453
N	0.33808673537054	1.81563366360207	0.97227555293085
C	2.78698044695747	2.21793514076410	1.03831383918325
C	4.05704421723571	1.85435372994897	0.57954453887164
C	4.20852161534995	0.85033465960571	-0.37420754611650
C	3.06886003585558	0.21040538170537	-0.87474100647649
C	1.81074359553462	0.56605026392954	-0.42191064987758
H	4.91876496473678	2.37289763144253	0.98388372174022
C	1.64892152292620	1.57252585070633	0.54939848150163
H	2.68257937919442	2.99913507117320	1.77836284731024
H	3.19210970570084	-0.57033799718316	-1.61964866471071
O	5.40882414220585	0.42620751944539	-0.87719447403339
H	-0.37912120877099	1.20160971559987	0.54166086871040
H	-1.79121488939785	1.53292451363302	2.02391573659948
F	18.66323895701399	3.53836480182265	8.03694441393666
C	6.56907317617140	1.09263391457136	-0.42427890139957
C	7.76733015521286	0.50430008897500	-1.14482030620811
H	14.00719886732571	-2.61561953682449	-0.05085657849265
H	6.49037832910090	2.17081568060020	-0.63006192062193
C	9.07365457384841	1.16214268291394	-0.70527991081641
H	7.62632638203411	0.62620940857716	-2.22555309251149
H	7.80501478813807	-0.57492384609572	-0.94749935145153
C	10.30232417764246	0.54722753534485	-1.37231917931753
H	9.17119481807233	1.08229780550879	0.38731172684235
H	9.03710711867554	2.23718299767855	-0.92958040625606
C	11.61955305360321	1.16950904621345	-0.91716822063036
H	10.20779140439269	0.64684791121259	-2.46282490641962
H	10.33453556085604	-0.53036217546942	-1.16213271752456
C	12.83334254515915	0.55087660266669	-1.60617874149138
H	11.72627962854741	1.04604369864502	0.17089315150070
H	11.60195691199205	2.25261970317328	-1.10421170537373
C	14.15704854567815	1.12581704045745	-1.10875083975174
H	12.75114762930450	0.69813882011603	-2.69272723956813
H	12.82281486514057	-0.53480821144810	-1.43542422879143
C	15.37511209712588	0.50720752832372	-1.79078272389234
H	14.23135595885153	0.96758235584573	-0.02373626521891
H	14.16552955562675	2.21384967720975	-1.26691969943253
C	16.69526453669169	1.06117962029947	-1.25893850906609
H	15.31867244837677	0.68115971412848	-2.87479238636361
H	15.35279435660377	-0.58194827001746	-1.64860643835990
C	17.91744592541328	0.41202611982910	-1.90723525228703
H	16.73465202662879	0.91796374062364	-0.16960775093864
H	16.72672076161659	2.14641170787343	-1.43149440531181
C	19.23125756069821	1.05426178415109	-1.46794588296542
H	17.84354701569742	0.49600512713758	-2.99734770363929
H	17.94495750115792	-0.65719948469300	-1.66928554995967
C	19.54417879202553	0.80729711237043	-0.01093320284301
H	19.21229343887692	2.13453288708637	-1.65642701098433
H	20.07889455237849	0.64770663845919	-2.03570982594853
O	19.13494221436840	-0.13718657098751	0.62953810605635
O	20.36573886797196	1.67543295388259	0.59387252535325
C	21.02931618629121	3.58630639245179	5.67210052427922
C	21.53137171019524	2.80012184092245	4.64076243278202
H	21.67899779276387	4.21907613926102	6.26355693087305
C	19.66119773493906	3.52502628131321	5.90389242519358
Cl	23.24371023514634	2.84363470704198	4.29629100299531
C	20.71802863715266	1.98609803098061	3.87256528836555
C	18.80371469113862	2.72307193049169	5.15528382150269
C	19.06022276408552	4.32594931383938	7.02551186641559
C	19.33560563441941	1.93961130275151	4.12365913412702
H	21.14388211201598	1.39284031118307	3.06996466124018

O 16.47003374338654 1.42990636379501 4.15187641585371
N 18.58461595146982 1.10179443979921 3.30348853879193
C 17.21461553825191 0.88263751814877 3.35420538348883
H 17.74293580996184 2.70539553875193 5.36211003802365
C 14.34597350032652 0.06827614647711 2.72085424837667
H 14.42846568940590 0.81679533875031 3.49607900190000
C 13.08480102651291 -0.39035724894685 2.32810970836553
N 16.80996021953293 -0.01727885388490 2.40220946590161
H 19.10777117024842 0.60417699551363 2.58801591893723
C 15.49653393182448 -0.43401723089780 2.11137359802446
H 12.20834952350777 0.02296226268516 2.81425493776938
F -0.92302789231400 6.37383637977347 5.60936467434062
C 12.95617701347035 -1.35135207741368 1.32562651476841
H 17.52218307989833 -0.39543158517215 1.78699067805837
C 15.36015636278274 -1.40892017044042 1.11046038044327
C 14.11214276152949 -1.86167490228349 0.72297997936772
O 11.77723346798646 -1.84778580228294 0.86663634964355
H 7.89869345999167 -0.87443154078091 1.40343108990945
H 16.24949302555854 -1.81377854048406 0.63188251207878
F 19.92695400278535 5.21351271564994 7.53434079178750
H 9.43224138133621 -2.17388787748690 -0.11155088127609
C 10.58670748440376 -1.48686095099416 1.55357495626539
C 9.45295052676073 -2.31293019771814 0.97654264301805
C 8.09074007144508 -1.94536852357130 1.56224196730785
H 5.35120424680189 -1.35699398363574 1.20679429441420
H 6.99548439839386 -2.63327760881746 -0.16051958050917
H 10.70249750646295 -1.68468004690675 2.62868427622079
C 6.96644815066008 -2.76463872144730 0.93071740564643
C 5.56819646648539 -2.41081677501630 1.43252584971846
H 2.82501513445731 -1.97629562918675 1.08030168518683
H 8.09532304323575 -2.10151369009293 2.64952335293255
H 4.52725035330493 -3.16199531292973 -0.29388688870263
H 9.66542818422923 -3.37425670327971 1.15438209058391
C 4.49783801207436 -3.29716250562141 0.79705251263321
C 3.08006304082909 -3.02218361387210 1.29349179691445
H 5.53076387748954 -2.51470862610074 2.52598996471123
H 0.56483989684276 -3.97130302614190 2.21953020605809
H 7.15803814095313 -3.83142027013809 1.11490842762848
H 2.07609260437498 -3.80370552722171 -0.44111280940154
C 2.05316429434646 -3.95492018104417 0.64787402090571
H 3.04227011650885 -3.13768715611169 2.38652643028812
C 0.61775868213786 -3.75523046921769 1.14318907060683
H 4.74911844744070 -4.35179747482399 0.98300194063650
H -1.66887812837085 -2.50468755530831 2.15155677985220
H 0.65268999489201 -1.62255098611508 1.48205056559629
C 0.09309647479673 -2.34731953022887 0.87534508738666
H -0.03684025400673 -4.48588228813567 0.64852843730698
C -1.40118735558456 -2.15852707643901 1.14837462241003
H 2.36041569752701 -4.99538585177140 0.82233364148438
C -1.74216399756211 -0.66942386374298 1.02269727997279
H -1.98477409795008 -2.73596021532720 0.41979063956379
O -2.29972203426942 -0.11063406414578 2.00111517992236
H 0.28603195084636 -2.07732386455283 -0.16955669171609
O -1.36520464732484 -0.09525541470202 -0.03518594102289
F 17.97855273943172 5.00842528405772 6.62266087645061
F -2.94566026411200 6.72770363856124 6.28072382014865
F -2.34229527999433 7.31303361936727 4.29390176855045
H 10.39391877158648 -0.41174705011338 1.42628341383076
H 6.67515024253154 0.97093303778508 0.66525176321140
H 0.92239745362286 0.06480887163495 -0.79790034485185
H 20.61038900713184 2.40454270562393 -0.00067794288519

2a linear monomer

69

Coordinates from ORCA-job /home/hzzeng/Desktop/ORCA/DazCalculations/CTUa_DIH-/07_MOH_GeOpt/CTUa_MOH_GeOpt

C	24.14185526688765	-2.44563325582181	-1.17626836825332
C	22.94047398736207	-3.75156871895473	0.39634355571778
C	21.82648306193959	-3.79045187137204	-0.43606533856295
C	21.88164876918228	-3.13482274313046	-1.67133599104455
C	23.05593616672282	-2.45783361451937	-2.03614403683749
H	24.96957086634554	-3.07313684185589	0.71793285587465
Cl	25.58823249887217	-1.59765768642624	-1.65963300531438
C	22.82784195704609	-4.42154155736418	1.73727440784596
H	20.93483446030953	-4.32577442893446	-0.14216453820198
H	23.11746419522096	-1.94482902502174	-2.99111050826748
N	20.82305986011328	-3.09830089115110	-2.57888058428486
C	19.60843933774900	-3.76611178558771	-2.48366051990688
O	19.31352638676489	-4.50873230684455	-1.56016093583121
N	18.77965232255617	-3.53394470339079	-3.54602245696563
C	15.05620252289102	-3.88058831193566	-2.66358577259779
C	16.46571848058493	-3.29380561763920	-2.63144527750817
C	17.42712677346196	-4.07101064972140	-3.52845632983993
H	18.95041700657313	-2.72432122718657	-4.12767087885526
H	21.01039730730128	-2.60830698806449	-3.44414044593830
C	14.07819325879447	-3.13749593647394	-1.75525970420356
C	12.66320454220492	-3.71090280081717	-1.80518193826101
C	11.67991241495820	-2.96574784287320	-0.90439898945211
H	12.68972257521753	-4.77115580319022	-1.51760481958017
H	12.29759974336986	-3.68184429232985	-2.84126921036139
C	10.25789172513273	-3.51886033186560	-0.98069932504521
H	11.66921649680016	-1.90245187848088	-1.18233346714228
H	12.03301673917131	-3.00857979053609	0.13529706752156
C	9.26855482696627	-2.75621768729177	-0.10141522775405
H	10.26252388188706	-4.57895204404075	-0.69117013331451
H	9.91329475051017	-3.48619659581575	-2.02383738198973
C	7.83906170384134	-3.28532601155989	-0.20434390228550
H	9.28083341792034	-1.69376866963612	-0.38249917095530
H	9.60001435320263	-2.80127511317911	0.94534441433076
C	6.84551291535158	-2.49562050608714	0.64579378197857
H	7.81781692317420	-4.34245272664955	0.09508868165696
H	7.51815731170503	-3.25633688958694	-1.25508220186492
C	5.40932528287035	-3.00117595466098	0.52062706583009
H	6.88177619928176	-1.43709330809374	0.35247158419759
H	7.15519696048452	-2.53368596454387	1.69948700563061
C	4.41518378576433	-2.18252239768278	1.34225008144786
H	5.36304673460849	-4.05375051445211	0.83284683522292
H	5.10903266495789	-2.97937879179113	-0.53621159966491
C	2.97466973232704	-2.66998867405147	1.19967361872720
H	4.47188742915242	-1.12956355546782	1.03348052209070
H	4.70696251509254	-2.20987720178562	2.40132809491028
C	1.98349107153741	-1.82110186907122	1.99309244834553
H	2.90495751976476	-3.71608267814386	1.52834538705516
H	2.68889103495355	-2.65781395224456	0.13939271100767
C	0.54027665166413	-2.31964661211649	1.83430268264844
H	2.04342162345976	-0.77803604633647	1.65857319267644
H	2.27875023857689	-1.82587204273248	3.05150147967914
C	-0.46676461378511	-1.40888595806892	2.50466961019012
H	0.26972233092631	-2.37193791080020	0.77764448188012
H	0.44493928673929	-3.32833134464283	2.25726988314272
O	-1.35426157035869	-0.83213565554894	1.93533911309532
O	-0.31024436039639	-1.24616874366586	3.83698883091970
F	22.07125288292062	-3.70118791737925	2.58030072418065
F	24.02248084613755	-4.58648510957403	2.32127658563031
F	22.25531619562816	-5.62953743513651	1.64173448112258
H	14.04988097207777	-2.07712385923910	-2.04255850225847
H	14.44879117757062	-3.16761506894038	-0.72154321394320
H	16.43888154373887	-2.24353408455717	-2.95168297744520
H	16.85599320317705	-3.31146287049119	-1.60703032852168
H	17.49319805824968	-5.10828612073577	-3.18957936268730
H	17.06557208018224	-4.08065543800111	-4.56164295754042
H	15.09625816792938	-4.93733658664128	-2.36564740085947
H	14.67669780926035	-3.86411820939800	-3.69506633538881
H	0.43349366137439	-1.78036382865722	4.15857984343921
C	24.11259307603789	-3.08787815001089	0.05606411073287

3a linear monomer

64

Coordinates from ORCA-job /home/hzzeng/Desktop/ORCA/DazCalculations/3a_DIH-/07_MOH_GeOpt/3a_MOH_GeOpt

C	20.90000554265966	-4.92032797657775	-4.69884646718174
C	20.50127012554506	-4.32513041769797	-3.50881515607887
C	19.98765554625388	-4.91873363577359	-5.74750829464115
C	18.72046867409270	-4.35524145239023	-5.64342841754189
C	18.34283045667943	-3.76354062597705	-4.43195327536058
C	19.24806187845321	-3.75285631367031	-3.36058917955139
H	21.88435694632644	-5.36016377977162	-4.80434329495298
Cl	21.60638440534265	-4.29168570971928	-2.16012048928667
C	20.36073232666205	-5.60302401530623	-7.03367725174621
H	18.04077095765615	-4.36678782993040	-6.48263274895180
H	18.97177940886956	-3.29577957900727	-2.41522286479263
N	17.10220272854029	-3.16130440173307	-4.20816506600283
C	16.03004410568833	-3.09152967507767	-5.08571477369283
O	16.05407278515404	-3.55573966427273	-6.21183011651093
N	14.95205850745963	-2.43999206034307	-4.53529697162269
C	13.34846886084922	-2.59831019650487	-6.41984679371892
C	12.06896024277898	-2.31142324990946	-6.88954664051503
C	11.13613853509388	-1.64670554677395	-6.10107206169827
C	11.47528424447572	-1.24752642115238	-4.80533023547883
C	12.75302127101653	-1.53376824644447	-4.33045844037402
H	11.80363478771956	-2.61501537535120	-7.89771364327694
C	13.69335306508915	-2.20568585996916	-5.12167542673646
H	14.06507158912834	-3.11252076126463	-7.04258143376281
H	13.02666385948619	-1.22640411228848	-3.32186598047528
H	15.04036324247508	-2.10284177782851	-3.58561895433220
H	16.98680631419801	-2.75432334882604	-3.28911507799621
C	10.46303992480036	-0.57575303212180	-3.90965473032885
C	9.71169730221394	-1.58208355159142	-3.02793108242361
C	8.65490847514002	-0.92054605348231	-2.14576170150323
H	10.43593481570116	-2.11826849880266	-2.39980918634744
H	9.23889079233551	-2.33793150224393	-3.66874780238240
C	7.94002563859215	-1.90953244099852	-1.22666825766720
H	7.91637454221431	-0.41420358042437	-2.78261564669424
H	9.12660231960554	-0.13633233207377	-1.53721370077542
C	6.85797929834389	-1.25669069157669	-0.36773778272864
H	8.67857188705507	-2.39518036513623	-0.57365856868105
H	7.49092785016900	-2.70946617653057	-1.83148506768711
C	6.17111655170624	-2.23796054736557	0.58045005532163
H	6.10535805951229	-0.79413812993263	-1.02121815758472
H	7.30191115607314	-0.43918658417670	0.21733256379965
C	5.07933671369354	-1.58838746187860	1.42916699120462
H	6.92408000361709	-2.69005219664640	1.24116218856009
H	5.73720213849420	-3.06303989230493	-0.00148707756328
C	4.41044697797587	-2.56481162986404	2.39489188350830
H	4.31742889254504	-1.15023804268153	0.76995537729300
H	5.50971826284665	-0.75392982300342	1.99983161866833
C	3.31955453521318	-1.90720603571661	3.23711318703365
H	5.17280428955341	-2.99938202920818	3.05657007440957
H	3.98171161461403	-3.40210217054324	1.82667957745208
C	2.66488571718651	-2.88453021226491	4.20471606774843
H	2.54867799471600	-1.47933192690643	2.58611528067471
H	3.73844643458928	-1.06979418028772	3.80674834826718
C	1.58791420056607	-2.23482462126624	5.04991753416978
H	3.41201823981583	-3.32195321913695	4.88116215831052
H	2.21146590449261	-3.72555813171449	3.66223171908286
O	0.97444685697209	-3.05027506657773	5.93444882134952
O	1.26260349171009	-1.08034280344208	4.97635747412804
F	21.68666654940338	-5.59801768751048	-7.23403737374207
F	19.78864193622367	-5.01745272539101	-8.09348291281932
F	19.97065047538515	-6.88704547304009	-7.03898678628814
H	10.14362727193424	-1.43138147739303	-6.48739981727188
H	10.96285138284515	0.15923008444171	-3.26675043710769
H	9.73987068390386	-0.02478318787133	-4.52278353746638
H	1.34069241054506	-3.94745356977332	5.87521876236119

4a linear monomer

68

Coordinates from ORCA-job /home/hzzeng/Desktop/ORCA/DazCalculations/4a_DIH-/07_MOH_GeOpt/4a_MOH_GeOpt

C	24.03473609435366	-0.43900337080941	3.57850062204674
Cl	24.77497780673019	1.43833029346109	0.14374008657281
C	22.62204843070950	0.33555535903166	1.34093376920597
C	22.67443141127033	-0.72876268903606	3.51144842356606
C	24.76989758187541	-0.88363490834482	4.81302640248684
C	21.95534926785121	-0.33623440819118	2.37797483001913
H	22.08044428650220	0.64675483815966	0.45273197253499
O	20.07565269396755	-1.68917526994487	4.13057481332627
N	20.58905271993597	-0.56456721695084	2.19721942140794
C	19.72404049803763	-1.21104175334214	3.06701126553169
H	22.18189396405811	-1.24795181997077	4.32134944908158
C	17.35704319604734	-2.59095065378498	4.36519193487696
H	18.30483529586450	-2.82368043271679	4.82578165399604
C	16.16630690787190	-3.07338029400932	4.89292630037060
N	18.43691974912940	-1.24892682431873	2.58383554384652
H	20.20953643079665	-0.21675238215676	1.32627062902184
C	17.30083965035012	-1.78623020673393	3.21793814863876
H	16.20478144291078	-3.69618185421286	5.78138871557096
H	12.41819953142474	-1.70569042269921	4.10976030432111
C	14.92589247100373	-2.79067501654946	4.32347842628874
H	18.24382429752876	-0.76183794020814	1.71835964660385
C	16.06914410758936	-1.49378673662069	2.63276326843933
C	14.88489743909722	-1.99141187303539	3.17862376603656
H	14.02202117113868	-3.18829669223358	4.76726293114847
H	9.92348815803374	-1.52626847879520	3.79193584536251
H	16.00479745785745	-0.86927974851622	1.74620623318515
O	13.74864581136947	-1.63939392150910	2.52732777377566
H	11.49098944127822	-0.42314120801405	2.17208357513572
C	12.51179788463240	-2.06943262845551	3.07676308489922
C	11.39446884046805	-1.51458826493292	2.21466863338403
C	10.02166072488516	-1.89936363140192	2.76316264750869
H	7.42600828754013	-1.32467883413767	3.52385953814890
H	8.95454631554800	-0.26544850909190	1.84517709026181
H	12.47452400617099	-3.16765669131124	3.09929441933734
C	8.86704277645075	-1.35792080545680	1.92220588897008
C	7.49927550286275	-1.71714584491652	2.49991980516063
H	4.91505037978701	-1.12227909308255	3.29701118581746
H	9.94367122358740	-2.99370586972590	2.82217295060921
H	6.41985031342399	-0.09322841818699	1.57742078175113
H	11.51341089011089	-1.88985297390344	1.19120308780827
C	6.33073230902505	-1.18434466137376	1.67295603980303
C	4.97074342454850	-1.52925911356064	2.27762929927007
H	7.41612210644448	-2.80985152034782	2.58299429196034
H	2.39442871899427	-0.92344839363103	3.09989980576869
H	8.94695624381956	-1.74796233524292	0.89827860679456
H	3.88087603042623	0.08694578455905	1.35329308000347
C	3.79244177074121	-1.00300377000493	1.46054439513310
H	4.88452079394223	-2.62036548739880	2.37731458913084
C	2.43927908707202	-1.34042635788114	2.08409021927924
H	6.39031580961556	-1.58922155486053	0.65315153794509
H	-0.15452173426931	-0.73162528585765	2.92024710355383
H	1.33914016803299	0.27011606688705	1.15110732107754
C	1.25996287319867	-0.81714760842789	1.26771987913377
H	2.35240143750264	-2.43036333123572	2.19487002217130
C	-0.07840989756277	-1.15544828263940	1.91124753675248
H	3.83833064208214	-1.41774281986515	0.44411584337388
C	-1.25230772802709	-0.64930163143893	1.11352214005708
H	-0.20092762998152	-2.23907665088466	2.03113642707870
O	-2.42408745862569	-0.95642685712570	1.70001768931810
H	1.28978573676065	-1.23674636061752	0.25534471724893
O	-1.19128182827677	-0.04021014454264	0.07350667310788
F	24.23393834662981	-0.35260162465217	5.92196069435523
F	24.71722734758263	-2.21581133080910	4.96067553921981
F	26.06265741941554	-0.53483666983152	4.78699665494344
C	24.71368371694822	0.22509239474901	2.56599240692786
C	23.97584885162628	0.60294219335150	1.44918414361883
H	25.77224130720287	0.44131877655137	2.63772580573783
H	-3.12778832492091	-0.59843722721274	1.12845567117919

5a linear monomer

68

Coordinates from ORCA-job /home/hzzeng/Desktop/ORCA/DazCalculations/5a_DIH-/07_MOH_GeOpt/5a_MOH_GeOpt

C	23.20379788159270	-1.68309295980270	4.79236758062721
Cl	25.28351070402072	1.47542340837415	3.53396712705011
C	22.76562172208436	0.54829985821883	3.22979949172573
C	21.94512752297213	-1.49553396856916	4.23084353236609
C	23.44019187603812	-2.92622677861688	5.60606086074255
C	21.71998867474103	-0.36275681860428	3.43922314234029
H	22.60719496366684	1.43226842826584	2.61958733376246
O	19.33356952411872	-2.00498124710862	3.21986534360579
N	20.48841211382108	-0.05208888133112	2.85842687165550
C	19.36042974645360	-0.85870434939471	2.80901818394625
H	21.15127393728733	-2.20734382412323	4.40523432627786
C	16.74439594074788	-2.12803306231154	1.94970835333979
H	17.57201823184825	-2.82367940518246	1.92464487013940
C	15.44310259877846	-2.58886971941166	1.83286947135176
N	18.28832472065065	-0.22032504445657	2.23073277533135
H	20.45427334491541	0.83260748774809	2.36798822608820
C	16.98542960228863	-0.75821650117246	2.12118911531537
H	15.24301528232276	-3.64821173809795	1.71047429330817
H	11.97716876400928	-0.66346983990822	1.11859382227058
C	14.35732804530556	-1.70674824692312	1.86851310665054
H	18.34992466211624	0.78141792147354	2.10151858732502
C	15.90500346794422	0.12054893410924	2.14697547394738
C	14.59584847360845	-0.33999875840295	2.01655902136587
O	13.12574808645416	-2.26634597730620	1.75404745419094
H	9.40906972302468	-0.66592814024217	1.37542603673084
H	16.08211015836096	1.18523265007421	2.27759634849829
F	24.45582871017207	-2.77285071185184	6.46747350307568
F	23.74198899149951	-3.97638705027761	4.82702401300572
H	10.70005429594980	-2.78003515473692	0.88695902048966
C	11.99779162449267	-1.42120586626171	1.91514943650879
H	13.78068304682537	0.37303440839291	2.04116931797149
C	10.75297991021645	-2.28654459430043	1.86476305464387
C	9.48571450606567	-1.47212035737654	2.11792936043873
H	6.86310104474698	-0.67725862066739	1.71734088622176
H	8.10905841978088	-2.76875202374210	1.07846709973649
H	12.06258675338943	-0.89638504595852	2.87937802529137
C	8.21545421786277	-2.32015876971354	2.07558812004417
C	6.95794682198390	-1.52172031745973	2.41421693010903
H	4.33698622894367	-0.68964568128543	2.11283258219029
H	9.55924150270803	-0.98365736467508	3.09940377909793
H	5.54395361661210	-2.76440228230774	1.35948610463216
H	10.84744124189677	-3.07605003604003	2.61971708026566
C	5.67984100060717	-2.35755104705083	2.37113118923354
C	4.43691342729066	-1.56425282694522	2.77078708863487
H	7.06942488181959	-1.08330341926755	3.41583218482797
H	1.82684811273628	-0.69473278888824	2.50505272896473
H	8.31469533375706	-3.15576593956082	2.78195530552728
H	3.00249649524474	-2.76285065643627	1.69394191088564
C	3.14959977070363	-2.38494719458580	2.71512469210896
H	4.57184777374574	-1.17033143563321	3.78784662775054
C	1.91915266378219	-1.58595822800294	3.14085745712860
H	5.78853980541421	-3.22277844493031	3.03983892290702
H	-0.67998913746801	-0.65952265224082	2.89112377102184
H	0.47533248877928	-2.75163129044156	2.03959644189473
C	0.62587384264155	-2.39437555909768	3.06634125065956
H	2.05969409850242	-1.22049573880584	4.16758274727388
C	-0.58921413302958	-1.56371447710909	3.49755261154251
H	3.25136963081598	-3.26848808928649	3.36029843178139
C	-1.88411364522148	-2.32130727554592	3.36601476132887
H	-0.47449792632105	-1.26440919004143	4.54635625272457
O	-2.83212664616993	-1.99143174799308	2.69586891476068
H	0.70260924183707	-3.28231802070666	3.70371393735038
O	-1.88145945187384	-3.45352664447935	4.09542035200163
F	22.35752587152154	-3.26854140649336	6.31681371591861
C	24.25331255803802	-0.79220610743188	4.59959139437178
C	24.00458292855660	0.32176146332873	3.80744396180266
H	25.22478734957678	-0.95367149874022	5.05071545082081
H	-2.74439903760808	-3.88296374264991	3.94976083309987

2a cyclic monomer

69

Coordinates from ORCA-job /home/hzzeng/Desktop/ORCA/DazCalculations/CTUa_DIH-/09_MOH_CURVED_GeOpt/CTUa_MOH_CURVED_GeOpt

C	-7.80853577892836	2.73820545904444	0.87088813393769
C	-7.15307336304709	1.52058007427226	0.76517425282165
C	-7.02001516191304	3.88724755763842	0.86791801052813
C	-5.63733841163025	3.85034803010497	0.76219911676739
C	-4.99808096747967	2.60478779248348	0.65477956062180
C	-5.77249297114647	1.43589116121174	0.65905067595151
H	-8.88836143791261	2.79195035073903	0.95135110596583
Cl	-8.08679071818240	0.04491695121045	0.76150996519767
C	-7.72431885425032	5.20836923761530	1.00459506318188
H	-5.05477488972757	4.75942081784451	0.75310207451664
H	-5.29425064106417	0.46425986572031	0.58152632296418
N	-3.62007418165848	2.45059053519320	0.56077273871864
C	-2.66664898608198	3.45269956914092	0.39815463143578
O	-2.93569595583973	4.63917560063044	0.28108277072699
N	-1.39905826535741	2.95676104677579	0.35278735672757
C	2.22067328311085	3.94449231098482	-0.25599123783348
C	0.97779405260803	3.06291472401073	-0.16083815702724
C	-0.25664610560730	3.84877879086388	0.26670605188219
H	-1.22219586073263	2.02507772386862	0.71655014024458
H	-3.28925575148066	1.49632196109624	0.46238399310682
C	3.47831212057162	3.19108360690837	-0.69639617938888
C	3.94065865966849	2.11694580800116	0.29023193489453
C	5.33698376007222	1.58183338950505	-0.03926441421453
H	3.21884292177790	1.29038890765364	0.31723377364986
H	3.95645997068373	2.54169007496666	1.30434192389285
C	5.83730976644313	0.48224740186121	0.91586478386506
H	6.03239123122038	2.43002420360488	-0.02073497881799
H	5.35056929188873	1.20589557012692	-1.07301429602639
C	5.66333002041006	-0.94486545267265	0.38732913093357
H	5.31902098528579	0.57734393198656	1.88018209106826
H	6.90127343718741	0.63738393102590	1.12702226450059
C	4.21747102323383	-1.33873689482556	0.09026679113204
H	6.08375345293931	-1.65136216378402	1.11535355058782
H	6.25705394631647	-1.05856509478571	-0.53085247775993
C	4.09680417705587	-2.79013776200845	-0.38421908602976
H	3.80907578256613	-0.65465790560957	-0.66206908562497
H	3.60833268859045	-1.20257783568566	0.99627310414575
C	2.66457705843763	-3.29985853407572	-0.61483970337318
H	4.68200180180907	-2.92176901443543	-1.30617273286013
H	4.57854591346791	-3.42495786498320	0.37044404263863
C	2.10030068676416	-3.05628466301068	-2.02025673091280
H	1.99766463046914	-2.86720686506629	0.14399392018119
H	2.64547865055384	-4.38238240117110	-0.44343205656407
C	1.98006061614913	-1.58979609762171	-2.44867608983787
H	2.74081873295493	-3.57319646672265	-2.74618081080579
H	1.11786401563892	-3.54115375401784	-2.09294050926896
C	1.15181872889083	-0.71555642722721	-1.50559988167910
H	2.98152283172757	-1.15414774234983	-2.54180273666137
H	1.54093612941988	-1.54983176739821	-3.45426998914742
C	-0.31426838424731	-1.14291577480080	-1.42910134409627
H	1.19743645936376	0.32774868809906	-1.83996747276588
H	1.56723239135715	-0.73293925904634	-0.49321226519706
C	-1.07535472478826	-0.31485599794434	-0.42153912771825
H	-0.79004452861076	-1.08240150026659	-2.41513007695508
H	-0.39876142717882	-2.18657299223491	-1.09760850206646
O	-2.38296591509634	-0.09074224938023	-0.66867470404293
O	-0.59662074327397	0.13269188321289	0.59205324765433
F	-8.33528911864915	5.31597497996914	2.19612898349009
F	-8.68060121474200	5.35098636012215	0.07218573996562
F	-6.89314935186541	6.24940135422926	0.88847196897043
H	4.29222806695068	3.91518249760404	-0.83291659052573
H	3.30627050935527	2.73208141428013	-1.68061669854363
H	0.77777192749349	2.59466102088941	-1.13443811151124
H	1.14513383768630	2.24515214888344	0.55206705206664
H	-0.07182591994268	4.34847239154727	1.22850789773366
H	-0.49181627582061	4.63097406475899	-0.46076520490517
H	2.40769962035892	4.41272330256343	0.72020118433189
H	2.02281624653955	4.76314093418711	-0.95967112493963
H	-2.65131852076311	-0.45914494531160	-1.52705197389855

3a cyclic monomer

64

Coordinates from ORCA-job /home/hzzeng/Desktop/ORCA/DazCalculations/3a_DIH-/09_MOH_CURVED_GeOpt/3a_MOH_CURVED_GeOpt

C	-5.93058789301388	2.80218162664644	-2.22723975510119
C	-5.14922274466435	1.84704339370308	-2.86814936642133
C	-5.31690337822925	3.55859665265997	-1.23707326690602
C	-3.98266604183393	3.39087229371541	-0.87683785109504
C	-3.21925307243576	2.42021706658439	-1.53644249110467
C	-3.81865330455830	1.64684603728469	-2.54503278595432
H	-6.96998082357060	2.94850616824247	-2.49316864762268
Cl	-5.86673047507754	0.86410243052681	-4.12140183151148
C	-6.11309710516454	4.58394529528476	-0.47865331122125
H	-3.53974158251436	4.00114781878752	-0.10258391271060
H	-3.23996203670971	0.89043517407618	-3.06508267634692
N	-1.88067803435840	2.15328258251288	-1.25863924129685
C	-1.07150254274189	2.79964071456568	-0.33484244585980
O	-1.44361380152484	3.72831357487746	0.36318852731786
N	0.19041060110683	2.26095269444164	-0.31177106247203
C	1.29897497093576	3.76401910700435	1.32170551535201
C	2.43733083510549	4.01308595413745	2.08305130749798
C	3.53567449350517	3.15607248306872	2.05802539001823
C	3.50660435404429	2.01135749802362	1.25939615108037
C	2.36581986809163	1.75616339248650	0.50090916927106
H	2.46412929311476	4.90180134484671	2.70653206509904
C	1.26431742755257	2.61753880830515	0.51780991193790
H	0.45357647697380	4.43643961932058	1.34518757839254
H	2.32549536266178	0.86398005952044	-0.12357188463309
H	0.36046473085154	1.45897152005482	-0.90871500621219
H	-1.45965849168439	1.39769892815673	-1.79254736479376
C	4.67479064865092	1.05657893138721	1.17276673985589
C	5.29893257394576	1.02780226021741	-0.22732774848877
C	6.36830780012785	-0.05433138039689	-0.39461223298868
H	5.73249964289670	2.01019736621238	-0.45463815217255
H	4.50277914915219	0.87432127736359	-0.96359447639687
C	6.74115680489064	-0.30789996171653	-1.86502078350141
H	6.01290360262592	-0.99332028504843	0.05462745241952
H	7.25735609649162	0.23600410741574	0.17781657639291
C	5.94234603138186	-1.43878202520077	-2.52507640391284
H	7.80524223385535	-0.55771973813897	-1.94238085362262
H	6.60249804246891	0.61999711433671	-2.43696051420106
C	4.42107839014065	-1.27895839901891	-2.48464574195325
H	6.26055727633865	-1.53415641995009	-3.57177992531040
H	6.20542195870230	-2.38758487800205	-2.03641007237846
C	3.70233106510051	-2.38642349194355	-3.25708797655451
H	4.13681476927633	-0.30492500203719	-2.90791904683406
H	4.08425076957602	-1.27567673384970	-1.43935966068806
C	2.17490250862101	-2.27703207951430	-3.23825349893577
H	4.04732240284415	-2.36719090778794	-4.29856163253872
H	3.99924235845008	-3.36452258398731	-2.85244381796937
C	1.56273483410896	-2.54411926496174	-1.86183430174046
H	1.75619511170400	-3.00050359529292	-3.95028877739575
H	1.87387094186078	-1.28062837789062	-3.58582780121920
C	0.03668888696424	-2.54933954529858	-1.87952751409627
H	1.90332534225346	-3.52080144746240	-1.49908759189117
H	1.90109822783601	-1.79785099565256	-1.13570018584046
C	-0.56435521767050	-1.17626810474081	-2.06300624951924
H	-0.36641680064865	-2.93778171809144	-0.93448497284199
H	-0.34457120945266	-3.20408208040580	-2.67404321278674
O	-1.88862731806320	-1.11992083861367	-2.26405888377714
O	0.05282189570763	-0.13531035989133	-2.01411640113947
F	-6.32653791376374	4.19994893610342	0.78996657400637
F	-7.31395521643410	4.80379141303402	-1.03219287480060
F	-5.47599220988508	5.76222351538314	-0.42053044151542
H	4.41466265233314	3.37299351293714	2.65840596594576
H	5.43359701580867	1.32453313368054	1.91716913549984
H	4.33197482667227	0.04285501369555	1.42160480372045
H	-2.28494306073070	-2.00817960570693	-2.27646821553301

4a cyclic monomer

68

Coordinates from ORCA-job /home/hzzeng/Desktop/ORCA/DazCalculations/4a_DIH-/09_MOH_CURVED_GeOpt/4a_MOH_CURVED_GeOpt

C	-7.50265167255545	3.02569337743743	-1.24738240618421
C	-6.46310169038737	2.36587966530235	-1.89420662889823
C	-7.15445785474149	3.92424341845902	-0.24759027111890
C	-5.83430972466876	4.17644744631419	0.11556728970167
C	-4.80613148279664	3.49841867474544	-0.54977791443574
C	-5.13686941851331	2.58573130886252	-1.56595700318547
H	-8.53594775280191	2.84321971701605	-1.51439015243108
Cl	-6.83789072503169	1.22118818085661	-3.15801551978780
C	-8.22382471201819	4.68253984660953	0.48938187350922
H	-5.60413519784860	4.88325757874382	0.90009064092637
H	-4.35274813327459	2.05212278650241	-2.09441186232129
N	-3.45033329495818	3.65805473418289	-0.27304331017430
C	-2.88541673256927	4.46296037039490	0.70700152739008
O	-3.53900117768582	5.17758332998184	1.44851733985884
N	-1.51781653877741	4.34750656539016	0.73106096563477
C	-1.00008830542541	5.85960159784800	2.62273811079427
C	-0.00185720737795	6.43184692610228	3.41297126252293
C	1.34251402029000	6.17329690591730	3.20078162886753
C	1.71649410706399	5.31458098820020	2.15970141383666
C	0.74020362105144	4.73200224673495	1.35623488667585
H	-0.29262924518489	7.09990546070129	4.21804089376856
C	-0.61877798406654	5.00194356050114	1.58859539929918
H	-2.04306093190780	6.06937184382396	2.80371474008914
H	1.00527602518183	4.05748552304330	0.54920140458258
H	2.11741052114418	6.61969821818255	3.81393146851755
H	-1.09552786971726	3.70122849296906	0.06924598228019
H	-2.81882500736319	3.09807237441197	-0.83687286170491
O	3.05287067145357	5.12331608970786	2.00679910160035
C	3.51464852352985	4.27050718446347	0.96845652703469
C	3.39453393761101	2.79579860942679	1.33468751415115
H	4.56886591299139	4.53440930118948	0.83688125241166
H	2.99590006512542	4.50995445053113	0.03226199480926
C	4.06450165697666	1.87847548323322	0.30949434343485
H	2.33842130647681	2.52115431977994	1.43972092696802
H	3.85991072445773	2.66022303640352	2.31756201895031
C	3.48051103075035	1.98185655062801	-1.10156428959680
H	3.97199957929498	0.84106980279783	0.65665969898437
H	5.14148151802149	2.09271815458173	0.27098314825408
C	4.05518419238088	0.91826964952524	-2.04078365996276
H	3.69423353876649	2.97150598062968	-1.52604632477255
H	2.38549134096456	1.90232062090561	-1.04831294976836
C	3.49454293513107	0.95157316485413	-3.47368846571650
H	3.88717327922184	-0.07868831537482	-1.60707849680335
H	5.14384945458138	1.05156027239037	-2.06862391935077
C	2.34973895692509	-0.03475281476727	-3.72435539655583
H	3.15645869435650	1.96978788200261	-3.71037622084994
H	4.29674611561564	0.72464269886545	-4.18450912612939
C	1.10754067797008	0.20632364714481	-2.86859002866635
H	2.71410912180651	-1.05617331362555	-3.54511723143895
H	2.06152035699011	0.00894480331779	-4.78256049086605
C	0.00112577728582	-0.81356529263974	-3.14119033258220
H	1.39194585970509	0.15695765372326	-1.80746624793513
H	0.73150899589497	1.22403521015210	-3.04417604348882
C	-1.31948415838390	-0.51430960391538	-2.42715909922519
H	-0.18966082030217	-0.86237464536526	-4.22025827820138
H	0.35583403586791	-1.81005959573293	-2.84395963558010
C	-1.16272613786667	-0.33007625576102	-0.91338858058957
H	-1.77104543225175	0.39544378651581	-2.83720686026271
H	-2.02363507873757	-1.33175266048939	-2.60763172652248
C	-0.69304163842944	1.05996443816711	-0.54559524720994
H	-2.13429757330812	-0.44562570440148	-0.41596630784606
H	-0.49433035815546	-1.09107452923848	-0.49379907619426
O	-1.08122196356989	2.06517100550270	-1.10558717391663
O	0.15238834001791	1.19004970577809	0.48206358958573
F	-9.45708567087142	4.31911888276674	0.11125635410257
F	-8.11758587602915	6.00434959413548	0.28646074105654
F	-8.13854991988737	4.48948234687725	1.81418734428914
H	0.40043239256208	0.32324026607819	0.84587475638667

5a cyclic monomer

68

Coordinates from ORCA-job /home/hzzeng/Desktop/ORCA/DazCalculations/5a_DIH-/09_MOH_CURVED_GeOpt/5a_MOH_CURVED_GeOpt

Cl	24.86835962394155	-3.85847552194598	3.24608301993327
C	23.00134165384860	-1.97126278053822	3.73967531849412
C	23.50990891161321	0.39323896519264	3.85402838085967
C	25.85317429811807	1.21702293293277	3.52152355584376
C	22.57438877080687	-0.65090132727687	3.92641108532604
H	22.29710941673372	-2.78910141626052	3.78650454348707
O	20.16173230630642	-2.23297247682717	3.60048421718093
N	21.25654243394355	-0.29855926489659	4.21006400411660
C	20.13416489794491	-1.09143556011720	4.02849490382636
H	23.18451912865662	1.41913185175904	3.99458585956584
C	17.26461226456689	-2.02281444063987	3.59771992461246
H	17.97048886973019	-2.84165276264401	3.60570876481947
C	15.95956652048809	-2.22389293287785	3.16989233223187
N	18.98729303305739	-0.42906613739202	4.40253766351496
H	21.08859044933635	0.69787979298425	4.33116743591717
C	17.67644564801226	-0.74410480867827	3.99853089372666
H	15.63563050064989	-3.20656170966140	2.84275956864851
H	14.74357523466692	0.92790842914620	3.57501969924010
C	15.03658000550192	-1.17465377196824	3.13518387124998
H	19.10631046826747	0.51420595543963	4.75493873356344
C	16.74333482447140	0.29417053315183	3.99858180830418
C	15.43438008141897	0.09212861609076	3.56782919559347
O	13.78880811307820	-1.46720293122291	2.67560699364413
H	10.40664800822993	0.75673568616964	2.10797148453781
H	17.04574599038252	1.28449548947875	4.33476394894481
F	26.48827655550278	1.22228277955489	2.33891027003558
H	12.02836060334132	-1.45496184744935	0.72644065482390
C	12.98637197878172	-0.36225822645686	2.29156406617871
C	11.73323639309021	-0.88183074173842	1.61358028334662
C	10.76237038386112	0.23501623029904	1.20880524523675
H	11.27545429828173	3.04007181411391	1.43808942598991
H	10.55933608811577	1.62884452197074	-0.44249732101803
F	25.30104846481235	2.42673709955498	3.68340502646618
C	11.35014084106492	1.25825963906525	0.22138137140221
C	12.02575232320837	2.46419380403053	0.88067716647787
H	14.14649501155022	5.04459054785536	-0.07946611183267
H	9.88165806381934	-0.23920199454731	0.76341806723613
H	13.14793833013905	2.78617913337282	-0.94315518354253
H	11.23494645403177	-1.57869183971490	2.29691990914697
C	12.73891656432725	3.38606261398511	-0.11795818289882
C	13.88780188145252	4.16992061619578	0.52936789212231
H	12.74882577310968	2.12334941535183	1.63064260554012
H	15.78825102960645	4.09093834164666	2.60422726377225
H	12.07679683264061	0.75074665998483	-0.42961832104985
H	14.85602323957165	2.33166336353126	1.14473435953226
C	15.13634035267955	3.30270166495774	0.71058409151238
H	13.55949885102065	4.55601436509084	1.50477179012285
C	16.20446768989205	3.93559592867270	1.59952229196303
H	12.01201224739524	4.07096545926307	-0.56912562808231
H	17.94520672313188	3.90104781074208	3.65916628523462
H	17.15319754449405	2.04562092291642	1.99789536736603
C	17.45346699798582	3.06082080092010	1.71010234768879
H	16.47738281170821	4.92842505745835	1.21720385580851
C	18.45448967485689	3.60996042473370	2.73733980204251
H	15.56112832681363	3.08130094833506	-0.27809936601928
C	19.52102408562104	2.61760711821864	3.13492533581250
H	18.95421933357673	4.50528199425898	2.34498672531361
O	20.11362275529244	1.92401377780179	2.15799920315846
H	17.91957344282002	2.98483993614822	0.71735688111138
O	19.86439153815649	2.41454256891162	4.28231498112796
F	26.80047785557509	1.08157663848834	4.46250348743389
H	13.56988972087338	0.27087201629608	1.60928202284592
H	12.71737080547762	0.24029339829063	3.17198594394647
C	25.28922373685863	-1.19454341962823	3.40319698602978
C	24.34754591588403	-2.20872811882599	3.48090340490668
H	26.33242388508381	-1.40791216056500	3.19877727568208
C	24.84037093488431	0.11087674770923	3.59742687801359
H	19.73944020583587	2.14900577980095	1.28907234283173

Figure S188. An emblematic schema of calcination from The Book with Seven Seals c.a. 1760.[157] Calcination or "The First Death" is the first cleansing of the base matter to ash, in pursuit of the Great Work.

Bibliography

1. Mitchell, P. (2011). Chemiosmotic coupling in oxidative and photosynthetic phosphorylation. 1966. *Biochimica Et Biophysica Acta, 1807*(12), 1507-1538. https://doi.org/10.1016/j.bbabio.2011.09.018
2. Papa, S., Martino, P. L., Capitanio, G., Gaballo, A., De Rasmo, D., Signorile, A., & Petruzzella, V. (2012). The oxidative phosphorylation system in mammalian mitochondria. *Advances in Experimental Medicine and Biology, 942*, 3-37. https://doi.org/10.1007/978-94-007-2869-11
3. Schultz, B. E., & Chan, S. I. (2001). Structures and proton-pumping strategies of mitochondrial respiratory enzymes. *Annual Review of Biophysics and Biomolecular Structure, 30*, 23-65. https://doi.org/10.1146/annurev.biophys.30.1.23
4. Lodish, H., Berk, A., Zipursky, S. L., Matsudaira, P., Baltimore, D., & Darnell, J. (2000). Electron Transport and Oxidative Phosphorylation. *Molecular Cell Biology. 4th edition*.
5. Cooper, G. M. (2000). The Mechanism of Oxidative Phosphorylation. *The Cell: A Molecular Approach. 2nd edition*.
6. Bagkos, G., Koufopoulos, K., & Piperi, C. (2014). A new model for mitochondrial membrane potential production and storage. *Medical Hypotheses, 83*(2), 175-181. https://doi.org/10.1016/j.mehy.2014.05.001
7. Heaton, G. M., Wagenvoord, R. J., Kemp, A., Jr., & Nicholls, D. G. (1978). Brown-adipose-tissue mitochondria: photoaffinity labelling of the regulatory site of energy dissipation. *European Journal of Biochemistry, 82*(2), 515-521. https://doi.org/10.1111/j.1432-1033.1978.tb12045.x
8. Demine, S., Renard, P., & Arnould, T. (2019). Mitochondrial Uncoupling: A Key Controller of Biological Processes in Physiology and Diseases. *Cells, 8*(8). https://doi.org/10.3390/cells8080795
9. Amorim, J. A., Coppotelli, G., Rolo, A. P., Palmeira, C. M., Ross, J. M., & Sinclair, D. A. (2022). Mitochondrial and metabolic dysfunction in ageing and age-related diseases. *Nature Reviews: Endocrinology, 18*(4), 243-258. https://doi.org/10.1038/s41574-021-00626-7
10. Childress, E. S., Alexopoulos, S. J., Hoehn, K. L., & Santos, W. L. (2018). Small Molecule Mitochondrial Uncouplers and Their Therapeutic Potential. *Journal of Medicinal Chemistry, 61*(11), 4641-4655. https://doi.org/10.1021/acs.jmedchem.7b01182
11. Ozaki, S., Kano, K., & Shirai, O. (2008). Electrochemical elucidation on the mechanism of uncoupling caused by hydrophobic weak acids. *Physical chemistry chemical physics: PCCP, 10*(30), 4449-4455. https://doi.org/10.1039/b803458c
12. Ripoll, C., Roldan, M., Contreras-Montoya, R., Diaz-Mochon, J. J., Martin, M., Ruedas-Rama, M. J., & Orte, A. (2020). Mitochondrial pH Nanosensors for Metabolic Profiling of Breast Cancer Cell Lines. *International journal of molecular sciences, 21*(10), 3731. https://doi.org/10.3390/ijms21103731
13. Benz, R., & McLaughlin, S. (1983). The molecular mechanism of action of the proton ionophore FCCP (carbonylcyanide p-trifluoromethoxyphenylhydrazone). *Biophysical Journal, 41*(3), 381-398. https://doi.org/10.1016/S0006-3495(83)84449-X
14. Azzu, V., & Brand, M. D. (2010). The on/off switches of the mitochondrial uncoupling proteins. *Trends in biochemical sciences, 35*(5), 298-307. https://doi.org/10.1016/j.tibs.2009.11.001

15. Mookerjee, S. A., Divakaruni, A. S., Jastroch, M., & Brand, M. D. (2010). Mitochondrial uncoupling and lifespan. *Mechanisms of ageing and development, 131*(7-8), 463-472. https://doi.org/10.1016/j.mad.2010.03.010
16. Hirschenson, J., Melgar-Bermudez, E., & Mailloux, R. J. (2022). The Uncoupling Proteins: A Systematic Review on the Mechanism Used in the Prevention of Oxidative Stress. *Antioxidants (Basel), 11*(2). https://doi.org/10.3390/antiox11020322
17. Ramsden, D. B., Ho, P. W., Ho, J. W., Liu, H. F., So, D. H., Tse, H. M., Chan, K. H., & Ho, S. L. (2012). Human neuronal uncoupling proteins 4 and 5 (UCP4 and UCP5): structural properties, regulation, and physiological role in protection against oxidative stress and mitochondrial dysfunction. *Brain and Behavior, 2*(4), 468-478. https://doi.org/10.1002/brb3.55
18. Andreyev, A., Bondareva, T. O., Dedukhova, V. I., Mokhova, E. N., Skulachev, V. P., Tsofina, L. M., Volkov, N. I., & Vygodina, T. V. (1989). The ATP/ADP-antiporter is involved in the uncoupling effect of fatty acids on mitochondria. *European Journal of Biochemistry, 182*(3), 585-592. https://doi.org/10.1111/j.1432-1033.1989.tb14867.x
19. Skulachev, V. P. (1991). Fatty acid circuit as a physiological mechanism of uncoupling of oxidative phosphorylation. *Federation of European Biochemical Societies Letters, 294*(3), 158-162. https://doi.org/10.1016/0014-5793(91)80658-p
20. Garlid, K. D., Jabůrek, M., & Ježek, P. (1998). The mechanism of proton transport mediated by mitochondrial uncoupling proteins. *Federation of European Biochemical Societies Letters, 438*(1-2), 10-14. https://doi.org/10.1016/s0014-5793(98)01246-0
21. Berardi, M. J., & Chou, J. J. (2014). Fatty acid flippase activity of UCP2 is essential for its proton transport in mitochondria. *Cell Metabolism, 20*(3), 541-552. https://doi.org/10.1016/j.cmet.2014.07.004
22. Pohl, E. E., Rupprecht, A., Macher, G., & Hilse, K. E. (2019). Important Trends in UCP3 Investigation. *Frontiers in Physiology, 10*, 470. https://doi.org/10.3389/fphys.2019.00470
23. Hoang, T., Smith, M. D., & Jelokhani-Niaraki, M. (2012). Toward Understanding the Mechanism of Ion Transport Activity of Neuronal Uncoupling Proteins UCP2, UCP4, and UCP5. *Biochemistry, 51*(19), 4004-4014. https://doi.org/10.1021/bi3003378
24. Mironova, G. D., & Pavlov, E. V. (2021). Mitochondrial Cyclosporine A-Independent Palmitate/Ca(2+)-Induced Permeability Transition Pore (PA-mPT Pore) and Its Role in Mitochondrial Function and Protection against Calcium Overload and Glutamate Toxicity. *Cells, 10*(1). https://doi.org/10.3390/cells10010125
25. Divakaruni, A. S., & Brand, M. D. (2011). The regulation and physiology of mitochondrial proton leak. *Physiology (Bethesda), 26*(3), 192-205. https://doi.org/10.1152/physiol.00046.2010
26. Kreiter, J., Škulj, S., Brkljača, Z., Bardakji, S., Vazdar, M., & Pohl, E. E. (2023). FA Sliding as the Mechanism for the ANT1-Mediated Fatty Acid Anion Transport in Lipid Bilayers. *International journal of molecular sciences, 24*(18). https://doi.org/10.3390/ijms241813701
27. Brunaldi, K., Miranda, M. A., Abdulkader, F., Curi, R., & Procopio, J. (2005). Fatty acid flip-flop and proton transport determined by short-circuit current in planar bilayers. *Journal of Lipid Research, 46*(2), 245-251. https://doi.org/10.1194/jlr.M400155-JLR200
28. Kang, Y., & Chen, L. (2023). Structural basis for the binding of DNP and purine nucleotides onto UCP1. *Nature, 620*(7972), 226-231. https://doi.org/10.1038/s41586-023-06332-w
29. Grundlingh, J., Dargan, P. I., El-Zanfaly, M., & Wood, D. M. (2011). 2,4-dinitrophenol (DNP): a weight loss agent with significant acute toxicity and risk of death. *Journal of Medical Toxicology, 7*(3), 205-212. https://doi.org/10.1007/s13181-011-0162-6

30. Roger, G. P. (1919). A Study of the Munitions Intoxications in France. *Public Health Reports (1896-1970), 34*(43), 2335-2374. https://doi.org/10.2307/4575357
31. Budd, S. L., & Nicholls, D. G. (1996). A reevaluation of the role of mitochondria in neuronal Ca2+ homeostasis. *Journal of Neurochemistry, 66*(1), 403-411. https://doi.org/10.1046/j.1471-4159.1996.66010403.x
32. Peng, T. I., & Greenamyre, J. T. (1998). Privileged access to mitochondria of calcium influx through N-methyl-D-aspartate receptors. *Molecular Pharmacology, 53*(6), 974-980.
33. Maragos, W. F., & Korde, A. S. (2004). Mitochondrial uncoupling as a potential therapeutic target in acute central nervous system injury. *Journal of Neurochemistry, 91*(2), 257-262. https://doi.org/10.1111/j.1471-4159.2004.02736.x
34. De Felice, F. G., & Ferreira, S. T. (2006). Novel neuroprotective, neuritogenic and anti-amyloidogenic properties of 2,4-dinitrophenol: the gentle face of Janus. *International Union of Biochemistry and Molecular Biology Life, 58*(4), 185-191. https://doi.org/10.1080/15216540600702198
35. Jin, Y., McEwen, M. L., Nottingham, S. A., Maragos, W. F., Dragicevic, N. B., Sullivan, P. G., & Springer, J. E. (2004). The mitochondrial uncoupling agent 2,4-dinitrophenol improves mitochondrial function, attenuates oxidative damage, and increases white matter sparing in the contused spinal cord. *Journal of Neurotrauma, 21*(10), 1396-1404. https://doi.org/10.1089/neu.2004.21.1396
36. Brown, J. S., Amend, S. R., Austin, R. H., Gatenby, R. A., Hammarlund, E. U., & Pienta, K. J. (2023). Updating the Definition of Cancer. *Molecular Cancer Research, 21*(11), 1142-1147. https://doi.org/10.1158/1541-7786.Mcr-23-0411
37. Stratton, M. R., Campbell, P. J., & Futreal, P. A. (2009). The cancer genome. *Nature, 458*(7239), 719-724. https://doi.org/10.1038/nature07943
38. *Australian Institute of Health and Welfare (2019), Cancer in Australia 2019. Canberra: Australian Institute of Health and Welfare . Cancer series no.119. Cat. no. CAN 123.* https://www.aihw.gov.au/reports/cancer/cancer-in-australia-2019/data (*Accessed: 29 May 2024)*.
39. *Changing Patterns of Mortality in Australia in Australia since 1900* (Vol. Chapter 4). ((2022)). https://www.aihw.gov.au/reports/australias-health/australias-health-2022-data-insights/about *(Accessed: 29 May 2024)*.
40. *Australian Government | Cancer Australia (2024), Breast cancer in Australia statistics, Available at: https://www.canceraustralia.gov.au/cancer-types/breast-cancer/statistics (Accessed: 29 May 2024)*.
41. Jin, X., & Mu, P. (2015). Targeting Breast Cancer Metastasis. *Breast Cancer : Basic and Clinical Research, 9*(Suppl 1), 23-34. https://doi.org/10.4137/BCBCR.S25460
42. Dagogo-Jack, I., & Shaw, A. T. (2018). Tumour heterogeneity and resistance to cancer therapies. *Nature Reviews Clinical Oncology, 15*(2), 81-94. https://doi.org/10.1038/nrclinonc.2017.166
43. Debela, D. T., Muzazu, S. G., Heraro, K. D., Ndalama, M. T., Mesele, B. W., Haile, D. C., Kitui, S. K., & Manyazewal, T. (2021). New approaches and procedures for cancer treatment: Current perspectives. *SAGE Open Medicine, 9*, 20503121211034366. https://doi.org/10.1177/20503121211034366
44. Marupudi, N. I., Han, J. E., Li, K. W., Renard, V. M., Tyler, B. M., & Brem, H. (2007). Paclitaxel: a review of adverse toxicities and novel delivery strategies. *Expert Opinion on Drug Safety, 6*(5), 609-621. https://doi.org/10.1517/14740338.6.5.609

45. Potter, M., Newport, E., & Morten, K. J. (2016). The Warburg effect: 80 years on. *Biochemical Society Transactions, 44*(5), 1499-1505. https://doi.org/10.1042/BST20160094
46. Wallace, D. C. (2012). Mitochondria and cancer. *Nature reviews Cancer, 12*(10), 685-698. https://doi.org/10.1038/nrc3365
47. Fulda, S., Galluzzi, L., & Kroemer, G. (2010). Targeting mitochondria for cancer therapy. *Nature Reviews Drug Discovery, 9*(6), 447-464. https://doi.org/10.1038/nrd3137
48. Gogvadze, V., Orrenius, S., & Zhivotovsky, B. (2008). Mitochondria in cancer cells: what is so special about them? *Trends in Cell Biology, 18*(4), 165-173. https://doi.org/https://doi.org/10.1016/j.tcb.2008.01.006
49. Vander Heiden, M. G., Cantley, L. C., & Thompson, C. B. (2009). Understanding the Warburg Effect: The Metabolic Requirements of Cell Proliferation. *Science (New York), 324*(5930), 1029-1033. https://doi.org/10.1126/science.1160809
50. Sancho, P., Barneda, D., & Heeschen, C. (2016). Hallmarks of cancer stem cell metabolism. *British Journal of Cancer, 114*(12), 1305-1312. https://doi.org/10.1038/bjc.2016.152
51. Hirpara, J., Eu, J. Q., Tan, J. K. M., Wong, A. L., Clement, M. V., Kong, L. R., Ohi, N., Tsunoda, T., Qu, J., Goh, B. C., & Pervaiz, S. (2019). Metabolic reprogramming of oncogene-addicted cancer cells to OXPHOS as a mechanism of drug resistance. *Redox Biology, 25*, 101076. https://doi.org/10.1016/j.redox.2018.101076
52. Guerra, F., Arbini, A. A., & Moro, L. (2017). Mitochondria and cancer chemoresistance. *Biochimica et Biophysica Acta Bioenergetics, 1858*(8), 686-699. https://doi.org/10.1016/j.bbabio.2017.01.012
53. Lunt, S. Y., & Vander Heiden, M. G. (2011). Aerobic Glycolysis: Meeting the Metabolic Requirements of Cell Proliferation. *Annual review of cell and developmental biology, 27*(1), 441-464. https://doi.org/10.1146/annurev-cellbio-092910-154237
54. Locasale, Jason W., & Cantley, Lewis C. (2011). Metabolic Flux and the Regulation of Mammalian Cell Growth. *Cell Metabolism, 14*(4), 443-451. https://doi.org/10.1016/j.cmet.2011.07.014
55. Chen, X., Qian, Y., & Wu, S. (2015). The Warburg effect: evolving interpretations of an established concept. *Free radical biology & medicine, 79*, 253-263. https://doi.org/10.1016/j.freeradbiomed.2014.08.027
56. Bonnet, S., Archer, S. L., Allalunis-Turner, J., Haromy, A., Beaulieu, C., Thompson, R., Lee, C. T., Lopaschuk, G. D., Puttagunta, L., Bonnet, S., Harry, G., Hashimoto, K., Porter, C. J., Andrade, M. A., Thebaud, B., & Michelakis, E. D. (2007). A Mitochondria-K+ Channel Axis Is Suppressed in Cancer and Its Normalization Promotes Apoptosis and Inhibits Cancer Growth. *Cancer Cell, 11*(1), 37-51. https://doi.org/https://doi.org/10.1016/j.ccr.2006.10.020
57. Bernal, S. D., Lampidis, T. J., McIsaac, R. M., & Chen, L. B. (1983). Anticarcinoma activity in vivo of rhodamine 123, a mitochondrial-specific dye. *Science, 222*(4620), 169. https://doi.org/10.1126/science.6623064
58. Houston, M. A., Augenlicht, L. H., & Heerdt, B. G. (2011). Stable Differences in Intrinsic Mitochondrial Membrane Potential of Tumor Cell Subpopulations Reflect Phenotypic Heterogeneity. *International Journal of Cell Biology, 2011*, 978583. https://doi.org/10.1155/2011/978583
59. Heerdt, B. G., Houston, M. A., & Augenlicht, L. H. (2005). The intrinsic mitochondrial membrane potential of colonic carcinoma cells is linked to the probability of tumor progression. *Cancer research (Chicago), 65*(21), 9861-9867. https://doi.org/10.1158/0008-5472.CAN-05-2444

60. Heerdt, B. G., Houston, M. A., & Augenlicht, L. H. (2006). Growth properties of colonic tumor cells are a function of the intrinsic mitochondrial membrane potential. *Cancer research (Chicago), 66*(3), 1591-1596. https://doi.org/10.1158/0008-5472.CAN-05-2717
61. Fantin, V. R., St-Pierre, J., & Leder, P. (2006). Attenuation of LDH-A expression uncovers a link between glycolysis, mitochondrial physiology, and tumor maintenance. *Cancer Cell, 9*(6), 425-434. https://doi.org/10.1016/j.ccr.2006.04.023
62. Boyle, J. (2008). Molecular biology of the cell, 5th edition by B. Alberts, A. Johnson, J. Lewis, M. Raff, K. Roberts, and P. Walter. *Biochemistry and Molecular Biology Education, 36*(4), 317-318. https://doi.org/https://doi.org/10.1002/bmb.20192
63. Alpert, N. M., Guehl, N., Ptaszek, L., Pelletier-Galarneau, M., Ruskin, J., Mansour, M. C., Wooten, D., Ma, C., Takahashi, K., Zhou, Y., Shoup, T. M., Normandin, M. D., & El Fakhri, G. (2018). Quantitative in vivo mapping of myocardial mitochondrial membrane potential. *PlOS One, 13*(1), e0190968-e0190968. https://doi.org/10.1371/journal.pone.0190968
64. Heerdt, B. G., Houston, M. A., Anthony, G. M., & Augenlicht, L. H. (1998). Mitochondrial Membrane Potential (ΔΨM) in the Coordination of p53-independent Proliferation and Apoptosis Pathways in Human Colonic Carcinoma Cells. *Cancer Research, 58*(13), 2869.
65. Heerdt, B. G., Houston, M. A., Mariadason, J. M., & Augenlicht, L. H. (2000). Dissociation of Staurosporine-induced Apoptosis from G2-M Arrest in SW620 Human Colonic Carcinoma Cells: Initiation of the Apoptotic Cascade Is Associated with Elevation of the Mitochondrial Membrane Potential (ΔψM). *Cancer Research, 60*(23), 6704.
66. Heiskanen, K. M., Bhat, M. B., Wang, H.-W., Ma, J., & Nieminen, A.-L. (1999). Mitochondrial Depolarization Accompanies Cytochrome C Release During Apoptosis in PC6 Cells *. *Journal of Biological Chemistry, 274*(9), 5654-5658. https://doi.org/10.1074/jbc.274.9.5654
67. Ren, X., Duan, L., He, Q., Zhang, Z., Zhou, Y., Wu, D., Pan, J., Pei, D., & Ding, K. (2010). Identification of Niclosamide as a New Small-Molecule Inhibitor of the STAT3 Signaling Pathway. *American Chemical Society Medicinal Chemistry Letters, 1*(9), 454-459. https://doi.org/10.1021/ml100146z
68. Alasadi, A., Chen, M., Swapna, G. V. T., Tao, H., Guo, J., Collantes, J., Fadhil, N., Montelione, G. T., & Jin, S. (2018). Effect of mitochondrial uncouplers niclosamide ethanolamine (NEN) and oxyclozanide on hepatic metastasis of colon cancer. *Cell Death and Disease, 9*(2), 1-14. https://doi.org/10.1038/s41419-017-0092-6
69. Yu, J., Yang, K., Zheng, J., Zhao, W., & Sun, X. (2021). Synergistic tumor inhibition of colon cancer cells by nitazoxanide and obeticholic acid, a farnesoid X receptor ligand. *Cancer Gene Therapy, 28*(6), 590-601. https://doi.org/10.1038/s41417-020-00239-8
70. Senkowski, W., Zhang, X., Olofsson, M. H., Isacson, R., Höglund, U., Gustafsson, M., Nygren, P., Linder, S., Larsson, R., & Fryknäs, M. (2015). Three-Dimensional Cell Culture-Based Screening Identifies the Anthelmintic Drug Nitazoxanide as a Candidate for Treatment of Colorectal Cancer. *Molecular Cancer Therapeutics, 14*(6), 1504-1516. https://doi.org/10.1158/1535-7163.Mct-14-0792
71. Alasadi, A., Cao, B., Guo, J., Tao, H., Collantes, J., Tan, V., Su, X., Augeri, D., & Jin, S. (2021). Mitochondrial uncoupler MB1-47 is efficacious in treating hepatic metastasis of pancreatic cancer in murine tumor transplantation models. *Oncogene, 40*(12), 2285-2295. https://doi.org/10.1038/s41388-021-01688-7
72. Qian, K., Chen, H., Qu, C., Qi, J., Du, B., Ko, T., Xiang, Z., Kandawa-Schulz, M., Wang, Y., & Cheng, Z. (2020). Mitochondria-targeted delocalized lipophilic cation complexed with human serum albumin for tumor cell imaging and treatment. *Nanomedicine: Nanotechnology, Biology, and Medicine, 23*, 102087. https://doi.org/10.1016/j.nano.2019.102087

73. Jara, J. A., Castro-Castillo, V., Saavedra-Olavarría, J., Peredo, L., Pavanni, M., Jaña, F., Letelier, M. E., Parra, E., Becker, M. I., Morello, A., Kemmerling, U., Maya, J. D., & Ferreira, J. (2014). Antiproliferative and uncoupling effects of delocalized, lipophilic, cationic gallic acid derivatives on cancer cell lines. Validation in vivo in singenic mice. *Journal of Medicinal Chemistry, 57*(6), 2440-2454. https://doi.org/10.1021/jm500174v
74. Peredo-Silva, L., Fuentes-Retamal, S., Sandoval-Acuña, C., Pavani, M., Maya, J. D., Castro-Castillo, V., Madrid-Rojas, M., Rebolledo, S., Kemmerling, U., Parra, E., & Ferreira, J. (2017). Derivatives of alkyl gallate triphenylphosphonium exhibit antitumor activity in a syngeneic murine model of mammary adenocarcinoma. *Toxicology and applied pharmacology, 329*, 334-346. https://doi.org/10.1016/j.taap.2017.06.017
75. Park, Y. S., Choi, S. E., & Koh, H. C. (2018). PGAM5 regulates PINK1/Parkin-mediated mitophagy via DRP1 in CCCP-induced mitochondrial dysfunction. *Toxicology Letters, 284*, 120-128. https://doi.org/10.1016/j.toxlet.2017.12.004
76. Figarola, J. L., Singhal, J., Tompkins, J. D., Rogers, G. W., Warden, C., Horne, D., Riggs, A. D., Awasthi, S., & Singhal, S. S. (2015). SR4 Uncouples Mitochondrial Oxidative Phosphorylation, Modulates AMP-dependent Kinase (AMPK)-Mammalian Target of Rapamycin (mTOR) Signaling, and Inhibits Proliferation of HepG2 Hepatocarcinoma Cells. *The Journal of Biological Chemistry, 290*(51), 30321-30341. https://doi.org/10.1074/jbc.M115.686352
77. Figarola, J. L., Singhal, J., Singhal, S., Kusari, J., & Riggs, A. (2018). Bioenergetic modulation with the mitochondria uncouplers SR4 and niclosamide prevents proliferation and growth of treatment-naïve and vemurafenib-resistant melanomas. *Oncotarget, 9*(97). https://doi.org/10.18632/oncotarget.26421
78. Rawling, T., MacDermott-Opeskin, H., Roseblade, A., Pazderka, C., Clarke, C., Bourget, K., Wu, X., Lewis, W., Noble, B., Gale, P. A., O'Mara, M. L., Cranfield, C., & Murray, M. (2020). Aryl urea substituted fatty acids: a new class of protonophoric mitochondrial uncoupler that utilises a synthetic anion transporter. *Chemical Science, 11*(47), 12677-12685. https://doi.org/10.1039/D0SC02777D
79. Rawling, T., Choucair, H., Koolaji, N., Bourget, K., Allison, S. E., Chen, Y. J., Dunstan, C. R., & Murray, M. (2017). A Novel Arylurea Fatty Acid That Targets the Mitochondrion and Depletes Cardiolipin To Promote Killing of Breast Cancer Cells. *Journal of Medicinal Chemistry, 60*(20), 8661-8666. https://doi.org/10.1021/acs.jmedchem.7b00701
80. Serasinghe, M. N., Gelles, J. D., Li, K., Zhao, L., Abbate, F., Syku, M., Mohammed, J. N., Badal, B., Rangel, C. A., Hoehn, K. L., Celebi, J. T., & Chipuk, J. E. (2018). Dual suppression of inner and outer mitochondrial membrane functions augments apoptotic responses to oncogenic MAPK inhibition. *Cell Death and Disease, 9*(2), 29. https://doi.org/10.1038/s41419-017-0044-1
81. Gao, Z. x., Cui, Z. l., Zhou, M. r., Fu, Y., Liu, F., Zhang, L., Ma, S., & Chen, C. y. (2022). The new mitochondrial uncoupler BAM15 induces ROS production for treatment of acute myeloid leukemia. *Biochemical Pharmacology, 198*, 114948-114948. https://doi.org/10.1016/j.bcp.2022.114948
82. Gedaly, R., Galuppo, R., Daily, M. F., Shah, M., Maynard, E., Chen, C., Zhang, X., Esser, K. A., Cohen, D. A., Evers, B. M., Jiang, J., & Spear, B. T. (2014). Targeting the Wnt/β-catenin signaling pathway in liver cancer stem cells and hepatocellular carcinoma cell lines with FH535. *PlOS One, 9*(6), e99272. https://doi.org/10.1371/journal.pone.0099272
83. Turcios, L., Chacon, E., Garcia, C., Eman, P., Cornea, V., Jiang, J., Spear, B., Liu, C., Watt, D. S., Marti, F., & Gedaly, R. (2019). Autophagic flux modulation by Wnt/β-catenin pathway

inhibition in hepatocellular carcinoma. *PlOS One, 14*(2), e0212538-e0212538. https://doi.org/10.1371/journal.pone.0212538
84. Figarola, J. L., & Rahbar, S. (2013). Smallmolecule COH-SR4 inhibits adipocyte differentiation via AMPK activation. *Int J Mol Med, 31*(5), 1166-1176. https://doi.org/10.3892/ijmm.2013.1313
85. Figarola, J. L., Weng, Y., Lincoln, C., Horne, D., & Rahbar, S. (2012). Novel dichlorophenyl urea compounds inhibit proliferation of human leukemia HL-60 cells by inducing cell cycle arrest, differentiation and apoptosis. *Investigational New Drugs, 30*(4), 1413-1425. https://doi.org/10.1007/s10637-011-9711-8
86. Singhal, S. S., Figarola, J., Singhal, J., Leake, K., Nagaprashantha, L., Lincoln, C., Gabriel Gugiu, B., Horne, D., Jove, R., Awasthi, S., & Rahbar, S. (2012). 1,3-Bis(3,5-dichlorophenyl) urea compound 'COH-SR4' inhibits proliferation and activates apoptosis in melanoma. *Biochemical Pharmacology, 84*(11), 1419-1427. https://doi.org/10.1016/j.bcp.2012.08.020
87. Ho, J., Zwicker, V. E., Yuen, K. K. Y., & Jolliffe, K. A. (2017). Quantum Chemical Prediction of Equilibrium Acidities of Ureas, Deltamides, Squaramides, and Croconamides. *J Org Chem, 82*(19), 10732-10736. https://doi.org/10.1021/acs.joc.7b02083
88. Jakab, G., Tancon, C., Zhang, Z., Lippert, K. M., & Schreiner, P. R. (2012). (Thio)urea organocatalyst equilibrium acidities in DMSO. *Organic Letters, 14*(7), 1724-1727. https://doi.org/10.1021/ol300307c
89. Davis, J. T., Gale, P. A., & Quesada, R. (2020). Advances in anion transport and supramolecular medicinal chemistry. *Chemical Society Reviews, 49*(16), 6056-6086. https://doi.org/10.1039/C9CS00662A
90. Yu, X.-H., Hong, X.-Q., Mao, Q.-C., & Chen, W.-H. (2019). Biological effects and activity optimization of small-molecule, drug-like synthetic anion transporters. *European Journal of Medicinal Chemistry, 184*, 111782. https://doi.org/https://doi.org/10.1016/j.ejmech.2019.111782
91. Li, H., Valkenier, H., Thorne, A. G., Dias, C. M., Cooper, J. A., Kieffer, M., Busschaert, N., Gale, P. A., Sheppard, D. N., & Davis, A. P. (2019). Anion carriers as potential treatments for cystic fibrosis: transport in cystic fibrosis cells, and additivity to channel-targeting drugs. *Chemical Science, 10*(42), 9663-9672. https://doi.org/10.1039/c9sc04242c
92. Busschaert, N., Park, S.-h., Baek, K.-h., Choi, Y. P., Park, J., Howe, E. N. W., Hiscock, J. R., Karagiannidis, L. E., Marques, I., Félix, V., Namkung, W., Sessler, J. L., Gale, P. A., & Shin, I. (2017). A synthetic ion transporter that disrupts autophagy and induces apoptosis by perturbing cellular chloride concentrations. *Nature Chemistry, 9*(7), 667-675. https://doi.org/http://dx.doi.org/10.1038/nchem.2706
93. Ko, S.-K., Kim, S. K., Share, A., Lynch, V. M., Park, J., Namkung, W., Van Rossom, W., Busschaert, N., Gale, P. A., Sessler, J. L., & Shin, I. (2014). Synthetic ion transporters can induce apoptosis by facilitating chloride anion transport into cells. *Nature Chemistry, 6*(10), 885-892. https://doi.org/10.1038/nchem.2021
94. Gale, P. A., Davis, J. T., & Quesada, R. (2017). Anion transport and supramolecular medicinal chemistry. *Chemical Society Reviews, 46*(9), 2497-2519. https://doi.org/10.1039/C7CS00159B
95. Blažek Bregović, V., Basarić, N., & Mlinarić-Majerski, K. (2015). Anion binding with urea and thiourea derivatives. *Coordination Chemistry Reviews, 295*, 80-124. https://doi.org/https://doi.org/10.1016/j.ccr.2015.03.011
96. Amendola, V., Fabbrizzi, L., & Mosca, L. (2010). Anion recognition by hydrogen bonding: urea-based receptors. *Chemical Society Reviews, 39*(10), 3889-3915. https://doi.org/10.1039/B822552B

97. Antonenko, Y. N., Avetisyan, A. V., Cherepanov, D. A., Knorre, D. A., Korshunova, G. A., Markova, O. V., Ojovan, S. M., Perevoshchikova, I. V., Pustovidko, A. V., Rokitskaya, T. I., Severina, I. I., Simonyan, R. A., Smirnova, E. A., Sobko, A. A., Sumbatyan, N. V., Severin, F. F., & Skulachev, V. P. (2011). Derivatives of rhodamine 19 as mild mitochondria-targeted cationic uncouplers. *The Journal of Biological Chemistry, 286*(20), 17831-17840. https://doi.org/10.1074/jbc.M110.212837
98. Penzo, D., Tagliapietra, C., Colonna, R., Petronilli, V., & Bernardi, P. (2002). Effects of fatty acids on mitochondria: implications for cell death. *Biochimica et Biophysica Acta - Bioenergetics, 1555*(1), 160-165. https://doi.org/https://doi.org/10.1016/S0005-2728(02)00272-4
99. Weinberg, S. E., & Chandel, N. S. (2015). Targeting mitochondria metabolism for cancer therapy. *Nat Chem Biol, 11*(1), 9-15. https://doi.org/10.1038/nchembio.1712
100. Shrestha, R., Johnson, E., & Byrne, F. L. (2021). Exploring the therapeutic potential of mitochondrial uncouplers in cancer. *Molecular metabolism (Germany)*, 101222-101222. https://doi.org/10.1016/j.molmet.2021.101222
101. Di Paola, M., & Lorusso, M. (2006). Interaction of free fatty acids with mitochondria: coupling, uncoupling and permeability transition. *Biochimica et Biophysica Acta, 1757*(9-10), 1330-1337. https://doi.org/10.1016/j.bbabio.2006.03.024
102. Wojtczak, L., Wieckowski, M. R., & Schönfeld, P. (1998). Protonophoric activity of fatty acid analogs and derivatives in the inner mitochondrial membrane: a further argument for the fatty acid cycling model. *Archives of Biochemistry and Biophysics, 357*(1), 76-84. https://doi.org/10.1006/abbi.1998.0777
103. Singhal, S. S., Figarola, J., Singhal, J., Nagaprashantha, L., Berz, D., Rahbar, S., & Awasthi, S. (2013). Novel compound 1,3-bis (3,5-dichlorophenyl) urea inhibits lung cancer progression. *Biochemical Pharmacology, 86*(12), 1664-1672. https://doi.org/10.1016/j.bcp.2013.09.022
104. Wu, X., & Gale, P. A. (2016). Small-Molecule Uncoupling Protein Mimics: Synthetic Anion Receptors as Fatty Acid-Activated Proton Transporters. *Journal of the American Chemical Society, 138*(50), 16508-16514. https://doi.org/10.1021/jacs.6b10615
105. Gilchrist, A. M., Wang, P., Carreira-Barral, I., Alonso-Carrillo, D., Wu, X., Quesada, R., & Gale, P. A. (2021). Supramolecular methods: the 8-hydroxypyrene-1,3,6-trisulfonic acid (HPTS) transport assay. *Supramolecular Chemistry*, 1-20. https://doi.org/10.1080/10610278.2021.1999956
106. Hansch, C., Leo, A., Unger, S. H., Kim, K. H., Nikaitani, D., & Lien, E. J. (1973). Aromatic substituent constants for structure-activity correlations. *Journal of Medicinal Chemistry, 16*(11), 1207-1216. https://doi.org/10.1021/jm00269a003
107. Saggiomo, V., Otto, S., Marques, I., Félix, V., Torroba, T., & Quesada, R. (2012). The role of lipophilicity in transmembrane anion transport. *Chemical Communications, 48*(43), 5274-5276. https://doi.org/10.1039/C2CC31825C
108. Knight, N. J., Hernando, E., Haynes, C. J. E., Busschaert, N., Clarke, H. J., Takimoto, K., García-Valverde, M., Frey, J. G., Quesada, R., & Gale, P. A. (2016). QSAR analysis of substituent effects on tambjamine anion transporters. *Chemical Science, 7*(2), 1600-1608. https://doi.org/10.1039/C5SC03932K
109. Plitzko, B., & Loesgen, S. (2018). Measurement of Oxygen Consumption Rate (OCR) and Extracellular Acidification Rate (ECAR) in Culture Cells for Assessment of the Energy Metabolism. *Bio-protocol, 8*(10), e2850-e2850. https://doi.org/10.21769/BioProtoc.2850

110. Beyer, R. E., & Macdonald, J. E. (1970). Inhibition of respiration in submitochondrial particles by uncouplers of oxidative phosphorylation. *Archives of Biochemistry and Biophysics, 137*(1), 38-50. https://doi.org/https://doi.org/10.1016/0003-9861(70)90408-X
111. Ricci, A., Carra, A., Rolli, E., Bertoletti, C., Morini, G., Incerti, M., & Vicini, P. (2004). Effect of Cl-Substitution on Rooting- or Cytokinin-like Activity of Diphenylurea Derivatives. *Journal of Plant Growth Regulation, 23*(4), 261-268. https://doi.org/10.1007/s00344-004-0016-4
112. Marshall, S. R., Singh, A., Wagner, J. N., & Busschaert, N. (2020). Enhancing the selectivity of optical sensors using synthetic transmembrane ion transporters. *Chemical Communications, 56*(92), 14455-14458. https://doi.org/10.1039/D0CC06437H
113. Denoyelle, S., Chen, T., Chen, L., Wang, Y., Klosi, E., Halperin, J. A., Aktas, B. H., & Chorev, M. (2012). In vitro inhibition of translation initiation by N,N'-diarylureas—potential anti-cancer agents. *Bioorganic and Medicinal Chemistry Letters, 22*(1), 402-409. https://doi.org/https://doi.org/10.1016/j.bmcl.2011.10.126
114. Busschaert, N., Kirby, I. L., Young, S., Coles, S. J., Horton, P. N., Light, M. E., & Gale, P. A. (2012). Squaramides as potent transmembrane anion transporters. *Angewandte Chemie International Edition, 51*(18), 4426-4430. https://doi.org/10.1002/anie.201200729
115. Guan, Z.-H., Lei, H., Chen, M., Ren, Z.-H., Bai, Y., & Wang, Y.-Y. (2012). Palladium-Catalyzed Carbonylation of Amines: Switchable Approaches to Carbamates and N,N'-Disubstituted Ureas. *Advanced Synthesis & Catalysis, 354*(2-3), 489-496. https://doi.org/https://doi.org/10.1002/adsc.201100545
116. Wang, M., Han, J., Si, X., Hu, Y., Zhu, J., & Sun, X. (2018). Effective approach to ureas through organocatalyzed one-pot process. *Tetrahedron Letters, 59*(17), 1614-1618. https://doi.org/https://doi.org/10.1016/j.tetlet.2017.11.030
117. Pfeifer, L., Engle, K. M., Pidgeon, G. W., Sparkes, H. A., Thompson, A. L., Brown, J. M., & Gouverneur, V. (2016). Hydrogen-Bonded Homoleptic Fluoride–Diarylurea Complexes: Structure, Reactivity, and Coordinating Power. *Journal of the American Chemical Society, 138*(40), 13314-13325. https://doi.org/10.1021/jacs.6b07501
118. Zhou, S., Yao, T., Yi, J., Li, D., & Xiong, J. (2013). A Simple and Efficient Synthesis of Diaryl Ureas with Reduction of the Intermediate Isocyanate by Triethylamine. *Journal of Chemical Research, 37*(5), 315-319. https://doi.org/10.3184/174751913X13663925002708
119. Lim, M. L., Minamikawa, T., & Nagley, P. (2001). The protonophore CCCP induces mitochondrial permeability transition without cytochrome c release in human osteosarcoma cells. *Federation of European Biochemical Societies Letters, 503*(1), 69-74. https://doi.org/10.1016/s0014-5793(01)02693-x
120. Chen, H., Wang, J., Feng, X., Zhu, M., Hoffmann, S., Hsu, A., Qian, K., Huang, D., Zhao, F., Liu, W., Zhang, H., & Cheng, Z. (2019). Mitochondria-targeting fluorescent molecules for high efficiency cancer growth inhibition and imaging. *Chemical Science, 10*(34), 7946-7951. https://doi.org/10.1039/C9SC01410A
121. York, E., McNaughton, D. A., Roseblade, A., Cranfield, C. G., Gale, P. A., & Rawling, T. (2022). Structure–Activity Relationship and Mechanistic Studies of Bisaryl Urea Anticancer Agents Indicate Mitochondrial Uncoupling by a Fatty Acid-Activated Mechanism. *ACS Chemical Biology, 17*(8), 2065-2073. https://doi.org/10.1021/acschembio.1c00807
122. Schenkel, L. C., & Bakovic, M. (2014). Formation and Regulation of Mitochondrial Membranes. *International Journal of Cell Biology, 2014, 709828*. https://doi.org/10.1155/2014/709828
123. Park, S.-H., Park, S.-H., Howe, E. N. W., Hyun, J. Y., Chen, L.-J., Hwang, I., Vargas-Zuñiga, G., Busschaert, N., Gale, P. A., Sessler, J. L., & Shin, I. (2019). Determinants of Ion-Transporter

Cancer Cell Death. *Chem, 5*(8), 2079-2098. https://doi.org/https://doi.org/10.1016/j.chempr.2019.05.001
124. Andrews, N. J., Haynes, C. J. E., Light, M. E., Moore, S. J., Tong, C. C., Davis, J. T., Harrell Jr, W. A., & Gale, P. A. (2011). Structurally simple lipid bilayer transport agents for chloride and bicarbonate. *Chemical Science, 2*(2), 256-260. https://doi.org/10.1039/C0SC00503G
125. Cushman, M., Georg, G., Holzgrabe, U., & Wang, S. (2014). Absolute Quantitative 1H NMR Spectroscopy for Compound Purity Determination. *Journal of Medicinal Chemistry, 57*(22), 9219-9219. https://doi.org/10.1021/jm501683w
126. Amendola, V., Fabbrizzi, L., Mosca, L., & Schmidtchen, F.-P. (2011). Urea-, Squaramide-, and Sulfonamide-Based Anion Receptors: A Thermodynamic Study. *Chemistry – A European Journal, 17*(21), 5972-5981. https://doi.org/10.1002/chem.201003411
127. Sheetal, Sharma, A. K., Shaifali, Bhattacherjee, D., Sharma, N., Giri, K., & Das, P. (2021). Supported-Pd catalyzed tandem approach for N-arylbenzamides synthesis. *Molecular Catalysis, 516*, 111948. https://doi.org/https://doi.org/10.1016/j.mcat.2021.111948
128. Skrylkova, A. S., Egorov, D. M., & Tarabanov, R. V. (2022). Reaction of Hexamethylene Diisocyanate with Amines. *Russian Journal of General Chemistry, 92*(10), 2033-2041. https://doi.org/10.1134/S1070363222100176
129. Bao, X., Wu, X., Berry, S. N., Howe, E. N. W., Chang, Y.-T., & Gale, P. A. (2018). Fluorescent squaramides as anion receptors and transmembrane anion transporters. *Chemical Communications, 54*(11), 1363-1366. https://doi.org/10.1039/C7CC08706C
130. Marques, I., Costa, P. M. R., Q. Miranda, M., Busschaert, N., Howe, E. N. W., Clarke, H. J., Haynes, C. J. E., Kirby, I. L., Rodilla, A. M., Pérez-Tomás, R., Gale, P. A., & Félix, V. (2018). Full elucidation of the transmembrane anion transport mechanism of squaramides using in silico investigations. *Physical Chemistry Chemical Physics, 20*(32), 20796-20811. https://doi.org/10.1039/C8CP02576B
131. Howe, E. N. W., & Gale, P. A. (2019). Fatty Acid Fueled Transmembrane Chloride Transport. *Journal of the American Chemical Society, 141*(27), 10654-10660. https://doi.org/10.1021/jacs.9b02116
132. Rostami, A., Colin, A., Li, X. Y., Chudzinski, M. G., Lough, A. J., & Taylor, M. S. (2010). N,N'-Diarylsquaramides: General, High-Yielding Synthesis and Applications in Colorimetric Anion Sensing. *The Journal of Organic Chemistry, 75*(12), 3983-3992. https://doi.org/10.1021/jo100104g
133. MacMillan, D. S., Murray, J., Sneddon, H. F., Jamieson, C., & Watson, A. J. B. (2013). Evaluation of alternative solvents in common amide coupling reactions: replacement of dichloromethane and N,N-dimethylformamide. *Green Chemistry, 15*(3), 596-600. https://doi.org/10.1039/C2GC36900A
134. Gensure, R. H., Zeidel, M. L., & Hill, W. G. (2006). Lipid raft components cholesterol and sphingomyelin increase H+/OH- permeability of phosphatidylcholine membranes. *The Biochemical journal, 398*(3), 485-495. https://doi.org/10.1042/BJ20051620
135. van Hoogevest, P., & Wendel, A. (2014). The use of natural and synthetic phospholipids as pharmaceutical excipients. *European Journal of Lipid Science and Technology, 116*(9), 1088-1107. https://doi.org/https://doi.org/10.1002/ejlt.201400219
136. Amendola, V., Bergamaschi, G., Boiocchi, M., Fabbrizzi, L., & Milani, M. (2010). The Squaramide versus Urea Contest for Anion Recognition. *Chemistry – A European Journal, 16*(14), 4368-4380. https://doi.org/https://doi.org/10.1002/chem.200903190
137. MacDermott-Opeskin, H., Clarke, C., Wu, X., Roseblade, A., York, E., Pacchini, E., Roy, R., Cranfield, C., Gale, P. A., O'Mara, M. L., Murray, M., & Rawling, T. (2022). Protonophoric and

mitochondrial uncoupling activity of aryl-carbamate substituted fatty acids. Organic and Biomolecular Chemistry, *21*(1), 132-139. https://doi.org/10.1039/d2ob02049a
138. Jahani, F., Tajbakhsh, M., Khaksar, S., & Azizi, M. R. (2011). An efficient and highly chemoselective N-Boc protection of amines, amino acids, and peptides under heterogeneous conditions. *Monatshefte für Chemie - Chemical Monthly, 142*(10), 1035. https://doi.org/10.1007/s00706-011-0534-2
139. Rawling, T., Duke, C. C., Cui, P. H., & Murray, M. (2010). Facile and stereoselective synthesis of (Z)-15-octadecenoic acid and (Z)-16-nonadecenoic acid: monounsaturated omega-3 fatty acids. *Lipids, 45*(2), 159-165. https://doi.org/10.1007/s11745-009-3378-3
140. Rawling, T., McDonagh, A. M., Tattam, B., & Murray, M. (2012). Synthesis of unsymmetrical biaryl ureas from N-carbamoylimidazoles: kinetics and application. *Tetrahedron, 68*(30), 6065-6070. https://doi.org/10.1016/j.tet.2012.05.002
141. Wu, X., Judd, Luke W., Howe, Ethan N. W., Withecombe, Anne M., Soto-Cerrato, V., Li, H., Busschaert, N., Valkenier, H., Pérez-Tomás, R., Sheppard, David N., Jiang, Y.-B., Davis, Anthony P., & Gale, Philip A. (2016). Nonprotonophoric Electrogenic Cl− Transport Mediated by Valinomycin-like Carriers. *Chem, 1*(1), 127-146. https://doi.org/https://doi.org/10.1016/j.chempr.2016.04.002
142. Boiocchi, M., Del Boca, L., Gómez, D. E., Fabbrizzi, L., Licchelli, M., & Monzani, E. (2004). Nature of Urea−Fluoride Interaction: Incipient and Definitive Proton Transfer. *Journal of the American Chemical Society, 126*(50), 16507-16514. https://doi.org/10.1021/ja045936c
143. Zhao, Y., & Truhlar, D. G. (2008). The M06 suite of density functionals for main group thermochemistry, thermochemical kinetics, noncovalent interactions, excited states, and transition elements: two new functionals and systematic testing of four M06-class functionals and 12 other functionals. *Theoretical Chemistry Accounts, 120*(1), 215-241. https://doi.org/10.1007/s00214-007-0310-x
144. Sivandzade, F., Bhalerao, A., & Cucullo, L. (2019). Analysis of the Mitochondrial Membrane Potential Using the Cationic JC-1 Dye as a Sensitive Fluorescent Probe. *Bio-protocol, 9*(1), e3128. https://doi.org/10.21769/BioProtoc.3128
145. Divakaruni, A. S., Paradyse, A., Ferrick, D. A., Murphy, A. N., & Jastroch, M. (2014). Analysis and interpretation of microplate-based oxygen consumption and pH data. *Methods in Enzymology, 547*, 309-354. https://doi.org/10.1016/b978-0-12-801415-8.00016-3
146. Pauli, G. F., Jaki, B. U., & Lankin, D. C. (2005). Quantitative 1H NMR: development and potential of a method for natural products analysis. *Journal of Natural Products, 68*(1), 133-149. https://doi.org/10.1021/np0497301
147. Neese, F. (2022). Software update: The ORCA program system—Version 5.0. *Wiley Interdisciplinary Reviews: Computational Molecular Science, 12*(5), e1606. https://doi.org/https://doi.org/10.1002/wcms.1606
148. Boys, S. F., & Bernardi, F. (1970). The calculation of small molecular interactions by the differences of separate total energies. Some procedures with reduced errors. *Molecular Physics, 19*(4), 553-566. https://doi.org/10.1080/00268977000101561
149. Simon, S., Duran, M., & Dannenberg, J. J. (1996). How does basis set superposition error change the potential surfaces for hydrogen-bonded dimers? *The Journal of Chemical Physics, 105*(24), 11024-11031. https://doi.org/10.1063/1.472902
150. Huang, M., Myers, C. R., Wang, Y., & You, M. (2021). Mitochondria as a Novel Target for Cancer Chemoprevention: Emergence of Mitochondrial-targeting Agents. *Cancer Prevention Research (Philadelphia), 14*(3), 285-306. https://doi.org/10.1158/1940-6207.Capr-20-0425

151. Plášek, J., Babuka, D., & Hoefer, M. (2017). H+ translocation by weak acid uncouplers is independent of H+ electrochemical gradient. *Journal of bioenergetics and biomembranes, 49*(5), 391-397. https://doi.org/10.1007/s10863-017-9724-x
152. Kanicky, J. R., & Shah, D. O. (2003). Effect of Premicellar Aggregation on the pKa of Fatty Acid Soap Solutions. *Langmuir, 19*, 2034-2038.
153. Lund, M., & Jönsson, B. (2013). Charge regulation in biomolecular solution. *Quarterly Reviews of Biophysics, 46*(3), 265-281. https://doi.org/10.1017/s003358351300005x
154. Škulj, S., & Vazdar, M. (2019). Calculation of apparent pKa values of saturated fatty acids with different lengths in DOPC phospholipid bilayers. *Physical Chemistry Chemical Physics, 21*(19), 10052-10060. https://doi.org/10.1039/C9CP01204D
155. Monaco, M. E. (2017). Fatty acid metabolism in breast cancer subtypes. *Oncotarget, 8*(17), 29487-29500. https://doi.org/10.18632/oncotarget.15494
156. Vecchi, L., Araújo, T. G., Azevedo, F., Mota, S. T. S., Ávila, V. M. R., Ribeiro, M. A., & Goulart, L. R. (2021). Phospholipase A(2) Drives Tumorigenesis and Cancer Aggressiveness through Its Interaction with Annexin A1. *Cells, 10*(6). https://doi.org/10.3390/cells10061472
157. Hall, M. P. (1500). Manly Palmer Hall collection of alchemical manuscripts, circa 1500-1825. In J. Böhme, S. Bacstrom, A. Cagliostro, M. Maier, & G. Ripley (Eds.), (pp. (7.5 linear ft.).).